TRANSITION METAL COMPLEXES OF AMBIPHILIC LIGANDS

Ph.D. Thesis
Bradley E. Cowie
Department of Chemistry and Chemical Biology
McMaster University

LATE TRANSITION METAL COMPLEXES OF GROUP 13 LEWIS ACID-CONTAINING AMBIPHILIC LIGANDS

By BRADLEY E. COWIE, H.B.Sc

A Thesis Submitted to the School of Graduate Studies in Partial Fulfillment of the Requirements for the Degree Doctor of Philosophy

McMaster University

McMaster University DOCTOR OF PHILOSOPHY (2015)
Hamilton, Ontario (CHEMISTRY)

TITLE: Late transition Metal Complexes of Group 13 Lewis Acid-Containing Ambiphilic Ligands

AUTHOR: Bradley E. Cowie

SUPERVISOR: Prof. David J. H. Emslie

NUMBER OF PAGES: lii, 380

Ph.D. Thesis
Bradley E. Cowie
Department of Chemistry and Chemical Biology
McMaster University

Lay Abstract

Ambiphilic ligands are defined as ligands which contain both conventional Lewis basic donors and unconventional Lewis acidic moieties, and the focus of this thesis is to expand the transition metal chemistry of Group 13 Lewis acid-containing ambiphilic ligands. This work expands the knowledge base of fundamental coordination and organometallic chemistry by exploring the effects of ambiphilic ligands on the structures, stability and reactivity of the resulting late transition metal complexes. Three different ambiphilic ligand systems have been employed in this research (TXPB, FcPPB and FcPPAl), which vary either by the structural rigidity of the ligand backbone (TXPB = thioxanthene; FcPPB and FcPPAl = ferrocene), the donor groups available to bind to the metal centre (TXPB = phosphine/thioether; FcPPB and FcPPAl = phosphine/phosphine), or the identity of the appended Lewis acid (TXPB and FcPPB = aryldiphenylborane; FcPPAl = aryldimethylalane). These ligands have provided access to a wide variety of metal–Lewis acid and metal–co-ligand–Lewis acid bonding interactions and novel reaction pathways with small molecules, some of which are relevant to the future development of unique cooperative and catalytic reactivity.

Ph.D. Thesis
Bradley E. Cowie
Department of Chemistry and Chemical Biology
McMaster University

Abstract

The coordination chemistry of a structurally rigid phosphine–thioether–borane ligand, TXPB (TXPB = 2,7-di-*tert*-butyl-5-diphenylboryl-4-diphenylphosphino-9,9-dimethylthioxanthene), as well as the Group 13 Lewis acid-appended analogues of 1,1'-bis(phosphino)ferrocene, FcPPB (FcPPB = [Fe(η^5-$C_5H_4PPh_2$){η^5-$C_5H_4P^tBu(C_6H_4BPh_2$-*o*)}]) and FcPPAl (FcPPAl = [Fe(η^5-$C_5H_4PPh_2$){η^5-$C_5H_4P^tBu(C_6H_4AlMe_2$-*o*)}]) has been explored with a range of transition metal pre-cursors.

Previously reported [Rh(μ-Cl)(CO)(TXPB)] (**1**) reacted with Me_3SiBr, Me_3SiI, $[NMe_4]F$, $Tl[PF_6]$ and $NaBH_4$ to provide [Rh(μ-Br)(CO)(TXPB)] (**2**), [RhI(CO)(TXPB)] (**3**), [Rh(CO)(TXPB-F)] {(**4**); TXPB-F = {5-(2,7-di-*tert*-butyl-4-diphenylphosphino-9,9-dimethylthioxanthenyl)}diphenylfluoroborate]}, $[Rh(CO)(TXPB)][PF_6]$ (**5**) and [Rh(μ-H)(CO)(TXPB)] (**6**), respectively; the rhodium–borane and rhodium–co-ligand–borane coordination modes within these complexes are dependant on the co-ligand bound to rhodium (co-ligand = Cl, Br, I, F, H, or none in the case of cationic **5**).

Additionally, previously reported [(TXPB)Rh(μ-$CO)_2$Fe(CO)Cp] (**7**) reacted with various isonitriles (CNR; R = C_6H_4Cl-*p*, 2,6-Me_2-C_6H_3, ^{n}Bu) to yield the bridging borataaminocarbyne complexes [(TXPB)Rh(μ-CO)(μ-CNR)Fe(CO)Cp] (**8**–**10)**. The borane-free analogue of (**7**), [(TXPH)Rh(μ-$CO)_2$Fe(CO)Cp] (**11**; TXPH = 2,7-di-*tert*-butyl-4-diphenylphosphino-9,9-dimethylthioxanthene), was synthesized for comparison, and reacted with CNC_6H_4Cl-*p* to yield [(TXPH)Rh(CO)(μ-CNC_6H_4Cl-*p*)$_2$Fe(CO)Cp] (**12**), featuring two bridging isonitrile ligands.

The TXPB ligand reacted with $[PtMe_2(cod)]$ (cod = 1,5-cyclooctadiene), forming [PtMePh(TXPB')] (**13**; TXPB' = 2,7-di-*tert*-butyl-5-methylphenylboryl-4-diphenylphosphino-9,9-dimethylthioxanthene), which exists in equilibrium with zwitterionic [PtMe(TXPB-Me)] (**13'**) in solution. When heated, [PtMePh(TXPB')] (**13**) was converted to [$PtPh_2$(TXPB")] (**14**; TXPB" = 2,7-di-*tert*-butyl-5-dimethylboryl-4-diphenylphosphino-9,9-dimethylthioxanthene) as an 86:14 equilibrium mixture with **13**. Moreover, [PtMePh(TXPB')] (**13**) reacted with PPh_3 and $P(OPh)_3$ to provide neutral

[PtMePh(PR_3)(TXPB')] [R = Ph (**15**), OPh (**16**)], or with CNXyl to yield zwitterionic [PtMe(CNXyl)$_2$(TXPB-Me)] (**17**; TXPB-Me = {5-(2,7-di-*tert*-butyl-4-diphenylphosphino-9,9-dimethylthioxanthenyl)}methyldiphenylborate).

To address several limitations with the TXPB ligand, a new borane-containing ambiphilic ligand, FcPPB (**26**), was prepared in a seven step convergent synthesis from commercially available ferrocene and 1,2-dibromobenzene. The FcPPB ligand reacted with the Group 10 metal pre-cursors [Ni(cod)$_2$], [Pd$_2$(dba)$_3$] (dba = *trans,trans*-dibenzylideneacetone) and [Pt(nb)$_3$] (nb = norbornene), yielding co-ligand free [M(FcPPB)] complexes [M = Ni (**28**), Pd (**29**), Pt (**30**)] exhibiting κ^2*PP*- and η^3*BCC*-coordination of the FcPPB ligand. Alternatively, a trisphosphine-analogue of FcPPB, FcPPP (FcPPP = [Fe(η^5-$C_5H_4PPh_2$){η^5-$C_5H_4P^tBu(C_6H_4PPh_2$-*o*)}]) (**25**), reacted with [Ni(cod)$_2$] and [Pd$_2$(dba)$_3$] to form [{Ni(FcPPP)}$_2$(μ-N_2)] (**33**) and [Pd(η^2-dba)(FcPPP)] (**34**), respectively.

Platinum complex **30** reacted with CO, CNXyl and H_2, providing [Pt(CO)(FcPPB)] (**35**), [Pt(CNXyl)(FcPPB)] (**36**) and [PtH(μ-H)(FcPPB)] (**37**), in which the borane is no longer η^3*BCC*-coordinated; the arylborane in FcPPB is now engaged in η^2*BC*-, η^1*B*- and bridging Pt–H–B coordination, respectively. Moreover, [Pt(FcPPB)] (**30**) reacted with PhC_2H to provide [Pt(C_2Ph)(μ-H)(FcPPB)] (**38**), which rapidly isomerized to the vinylborane complex, [Pt(FcPPB')] (**39**; FcPPB' = [Fe(η^5-$C_5H_4PPh_2$)(η^5-$C_5H_4P^tBu${C_6H_4BPh(CPh=CHPh-*Z*)-*o*})]).

The FcPPB ligand also reacted with [Au(PPh_3)][$GaCl_4$] to yield [{Au(FcPPB)}$_2$][$GaCl_4$] (**40**) as a diastereomeric mixture, or with [W(CO)$_6$] and [Ru$_3$(CO)$_{12}$] under photochemical and thermal conditions, respectively, to yield [W(CO)$_4$(FcPPB*)] (**41**; FcPPB* = [Fe(η^5-$C_5H_4PPh_2$){η^5-$C_5H_3P(^tBu)C_6H_4BPh$-*o*}]) and [Ru$_3$(μ-H)(CO)$_{10}$(FcPPB**)] (**42**; FcPPB** = [Fe(η^5-$C_5H_4PPh_2$){η^5-$C_5H_3P(^tBu)C_6H_4BPh_2$-*o*}]$^-$), respectively. Both [W(CO)$_4$(FcPPB*)] (**41**) and [Ru$_3$(μ-H)(CO)$_{10}$(FcPPB**)] (**42**) are products of intramolecular attack of the borane on the adjacent cyclopentadienyl-ring. Free FcPPB did not undergo any reaction under similar conditions. However, FcPPB reacted with $B(C_6F_5)_3$ and $BF_3{\cdot}OEt_2$ to yield

FcPPB{$B(C_6F_5)_3$} (**43**; [$Fe(\eta^5\text{-}C_5H_4PPh_2\{B(C_6F_5)_3\})\{\eta^5\text{-}C_5H_4P^tBu(C_6H_4BPh_2\text{-}o)\}$]) and [$FcPPB^{\text{-Ph}}$][$BF_4$] (**44**; [$Fe(\eta^5\text{-}C_5H_4PPh_2)\{\eta^5\text{-}C_5H_4P^tBu(C_6H_4BPh\text{-}o)\}]^+$), respectively; the former is a phosphine–borane adduct, whereas the latter is a bisphosphine-stabilized boronium cation.

The coordination chemistry of a dimethylalane-appended analogue of FcPPB, FcPPAl (**27**), was also investigated; reaction with [$Pt(nb)_3$] provided [$Pt(\eta^2\text{-nb})$(FcPPAl)] (**45**), which readily reacted with C_2H_4, C_2Ph_2, H_2, and CO to provide [$Pt(\eta^2\text{-}C_2H_4)$(FcPPAl)] (**47**), [$Pt(\eta^2\text{-}C_2Ph_2)$(FcPPAl)] (**48**), [$PtH_2$(FcPPAl)] (**49**) and [Pt(CO)(FcPPAl)] (**50**), respectively. Alternatively, heating a benzene solution of [$Pt(\eta^2\text{-nb})$(FcPPAl)] (**45**) yielded co-ligand free [$\{Pt(FcPPAl)\}_2$] (**46**). All of the isolated platinum-FcPPAl complexes feature κ^3*PPAl*-coordination of the FcPPAl ligand to platinum, and are the first unambiguous examples of η^1*Al*-coordinated alkylalane complexes.

Acknowledgments

Firstly, I'd like to thank my supervisor, Dr. David J. H. Emslie, whom in my opinion is the greatest supervisor a graduate student can have the pleasure to work for. Your relentless enthusiasm towards chemistry, your ability to help any student at any time of the day regardless of your personal schedule and agenda, and your drive for innovation and success are an inspiration, and I hope to become half the supervisor you are some day. Additionally, I am extremely grateful for the countless reference letters sent on my behalf, and your willingness to proofread through any piece of work I have completed, whether it is for a publication or for a conference presentation. Furthermore, having a friend to enjoy a few beers with, along with the occasional wrestling match is something that I will always cherish, and this thesis would not be possible without you.

I would like to thank all of the Emslie group members I have had the opportunity to work with over the years, which consists of Matt Ray, Jordan Thomson, Velislava Bacharova, Adam Pantaleo, Lilly Vo, Tara Dickie, Judy Tsao, Meera Mehta, Terry Chu, Katarina Paskaruk, Aathith Vasanthakumar, Kris Kolpin, Kelly Motolko, Jeffrey Price, Nick Andreychuk, Dr. Venkat Ramalingam, Dr. Preeti Chadha, Dr. Sougandi Ilango, Dr. Bala Vidjayacoumar, Dr. Carlos Cruz, Dr. Edwin Wong and Dr. Todd Whitehorne. More specifically, I would like to thank Dr. Bala Vidjayacoumar and Dr. Carlos Cruz for showing me what it meant to be an effective and productive graduate student, as well as an Emslie group member; I will always cherish the fb and "two pizzas" jokes. Additionally, I would like to extend a special thank you to Nick Andreychuk as a colleague and as a friend; having a lab mate to share a few beers with and discuss the challenges of life as a grad student is truly priceless, and I am very grateful for having the opportunity to work alongside a friend like you.

I would also like to thank my Ph.D. committee members, Dr. Gary Schrobilgen and Dr. Ignacio Vargas-Baca, for the guidance they provided not only with respect to research, but also pertaining to mentoring and educating the younger generations of future chemists. In addition, I would like to extend my gratitude to Dr. Joshua Figueroa and Dr.

Luis Branda for acting as the external examiner and the examination Chair for my Ph.D. thesis defence, respectively.

I would like to thank the members of the facilities staff that have provided an enormous amount of help and guidance over the years, which includes Dr. Jim Britten and Dr. Hilary Jenkins in the McMaster Analytical X-ray Diffraction Facility, Dr. Bob Berno and Dr. Dan Sorensen in the Nuclear Magnetic Resonance Facility, Dr. Steve Kornic for assistance with elemental analysis, Raman, IR and NMR spectroscopy, Megan Fair for assistance with elemental analysis, and Dr. Kirk Green in the McMaster Regional Centre for Mass Spectrometry.

I would also like to extend my gratitude to the office staff of the Department of Chemistry and Chemical Biology: Jane Garneau for assistance with submitting expense reports for conferences, Linda Spruce for assistance with conference room bookings, Christine Cosgrove for assistance with thesis and defence requirements, as well as for the plentiful Thursday seminar reminders, and Connie Carrabs for the endless help with the financial errors/discrepancies that have risen over the past couple of years. For whatever reason, as scientists we tend to get surprisingly bogged down whenever an administrative task arises, and you four made completing those tasks infinitely easier every time.

Additionally, I would like to thank Karen Neumann, whom I've had the pleasure of working with as both an undergraduate student working through the undergraduate program, and as a graduate student TAing the younger generations of undergraduate chemistry students. Your organization and limitless patience is admirable, and you are a cornerstone in the undergraduate chemistry program.

I would also like to extend my gratitude to the Department of Chemistry and Chemical Biology at McMaster University, the Natural Sciences and Engineering Research Council of Canada and the Government of Ontario for their generous financial support throughout my graduate career.

I will forever be grateful to the countless friends I have made during the time I have attended graduate school at McMaster University, such as Vinodh Rajendra, Patricia Edem, Aimen Zlitni, Dave McLeod, Greg Bahun and Lucia Lee. More specifically, the

countless wrestling matches with Vinodh Rajendra, including the infamous CPPBA grab, and having a solid crew of friends to hang out with and participate in non-chemistry discussions.

I would like to thank my parents, Ian and Sue Cowie, as well as my brother and sister-in-law, Aaron and Marlena Cowie, and my grandparents, for being there for me every step of the way through this journey. At times graduate school can get exceedingly difficult, and you were always there to pick me up and help me out.

Lastly and most importantly, I'd like to thank my girlfriend, Nikki Banko, for all the love and support, especially over the past year and a half throughout the course of the writing and defence process. Your unwavering up-beat and positive attitude, and your never ending laughter are a few of the attributes I look most forward to seeing every day, and were quintessential for me to get over the final hurdles of graduate school. I look forward to our journey in Edinburgh together with the greatest anticipation; without you none of it would be possible.

Table of Contents

List of Figures

Hydrogen atoms have been omitted for clarity.

List of Schemes

List of Tables

List of Compounds

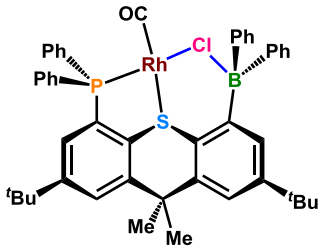 (1)	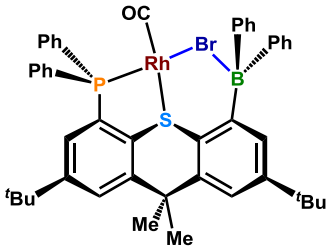 (2)	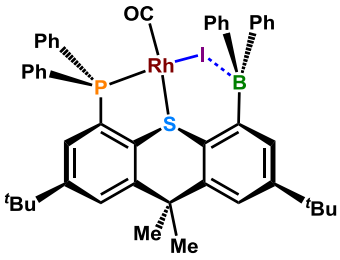 (3)
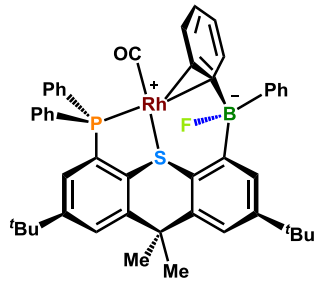 (4)	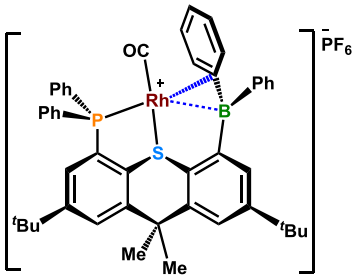 (5)	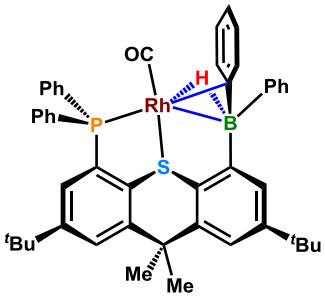 (6)
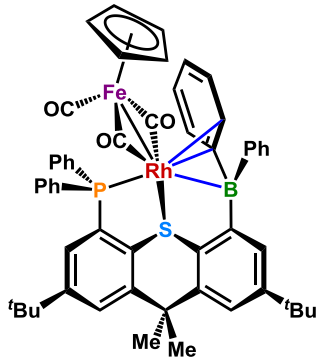 (7)	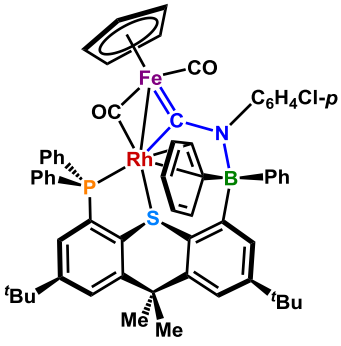 (8)	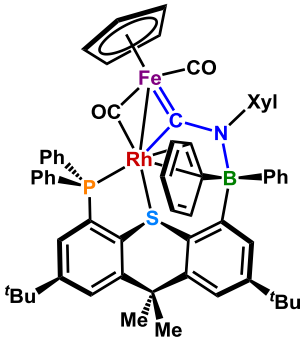 (9)
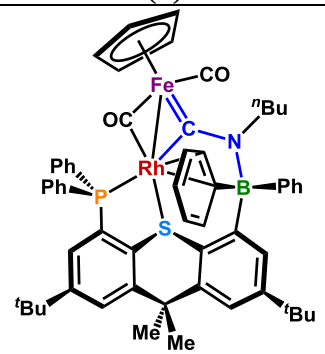 (10)	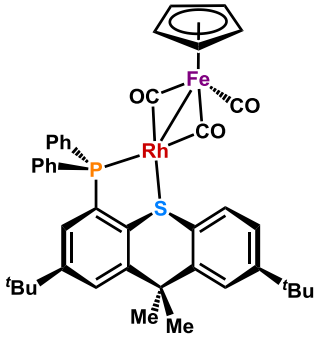 (11)	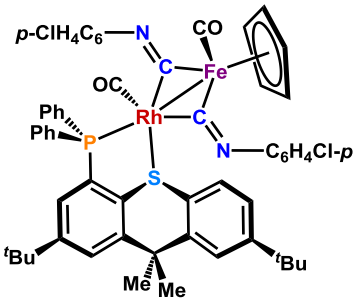 (12)

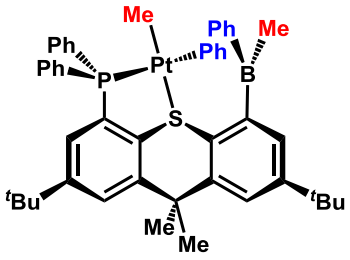 (13)	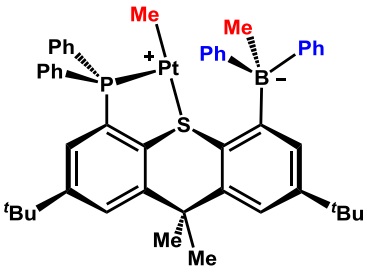 (13')	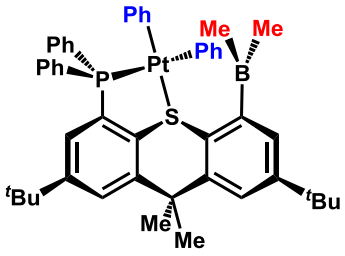 (14)
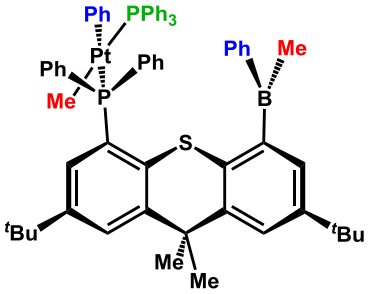 (15)	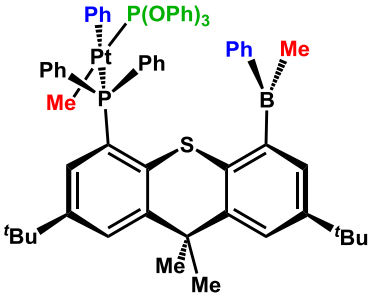 (16)	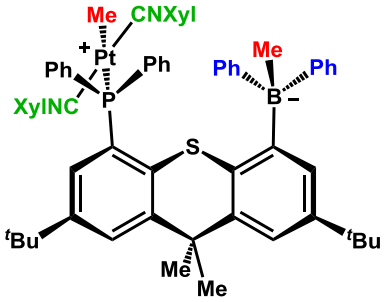 (17)
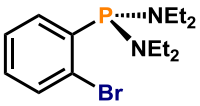 (18)	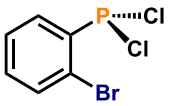 (19)	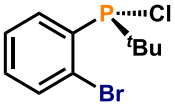 (20)
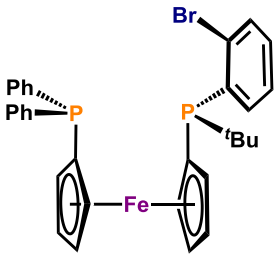 (21)	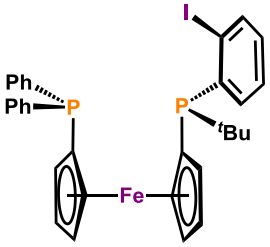 (21-I)	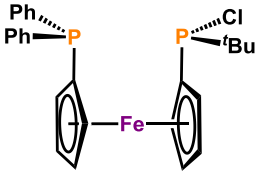 (22)
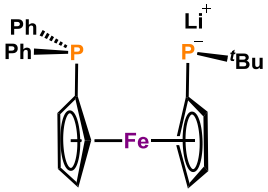 (23)	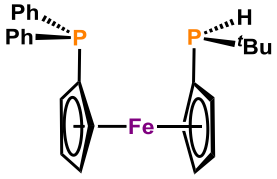 (24)	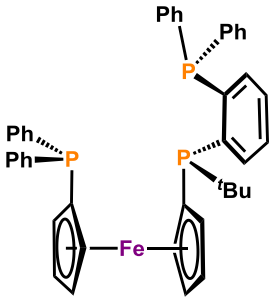 (25)

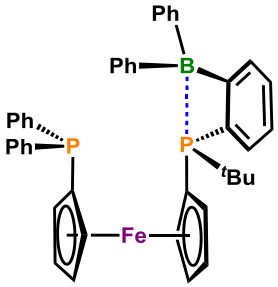

(26)

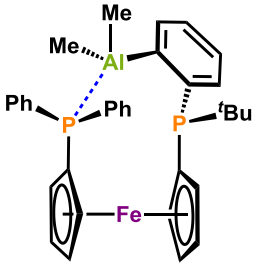

(27)

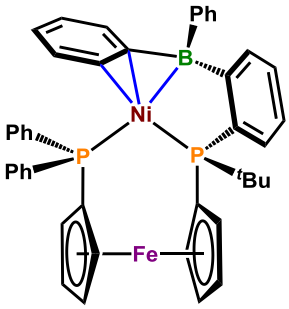

(28)

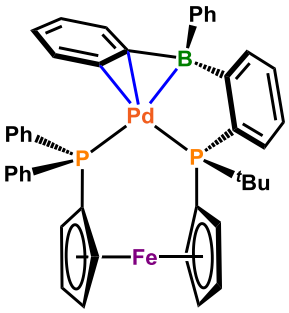

(29)

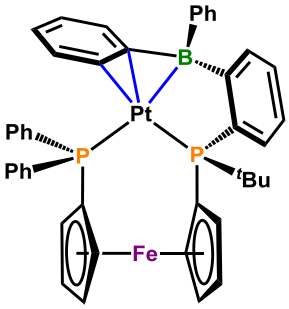

(30)

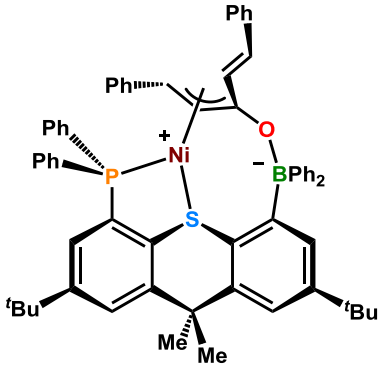

(31)

“Ni(FcPPP)”
(32)

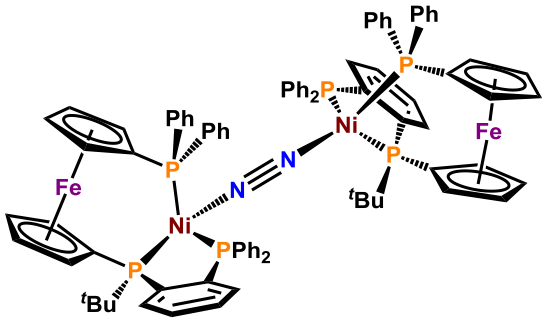

(33)

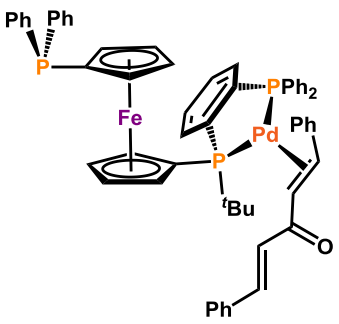

(34)

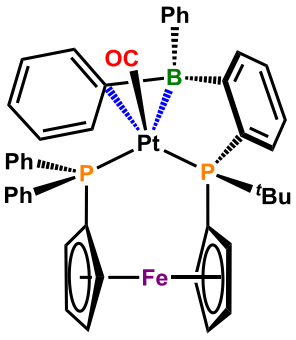

(35)

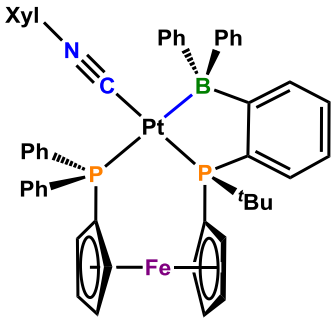

(36)

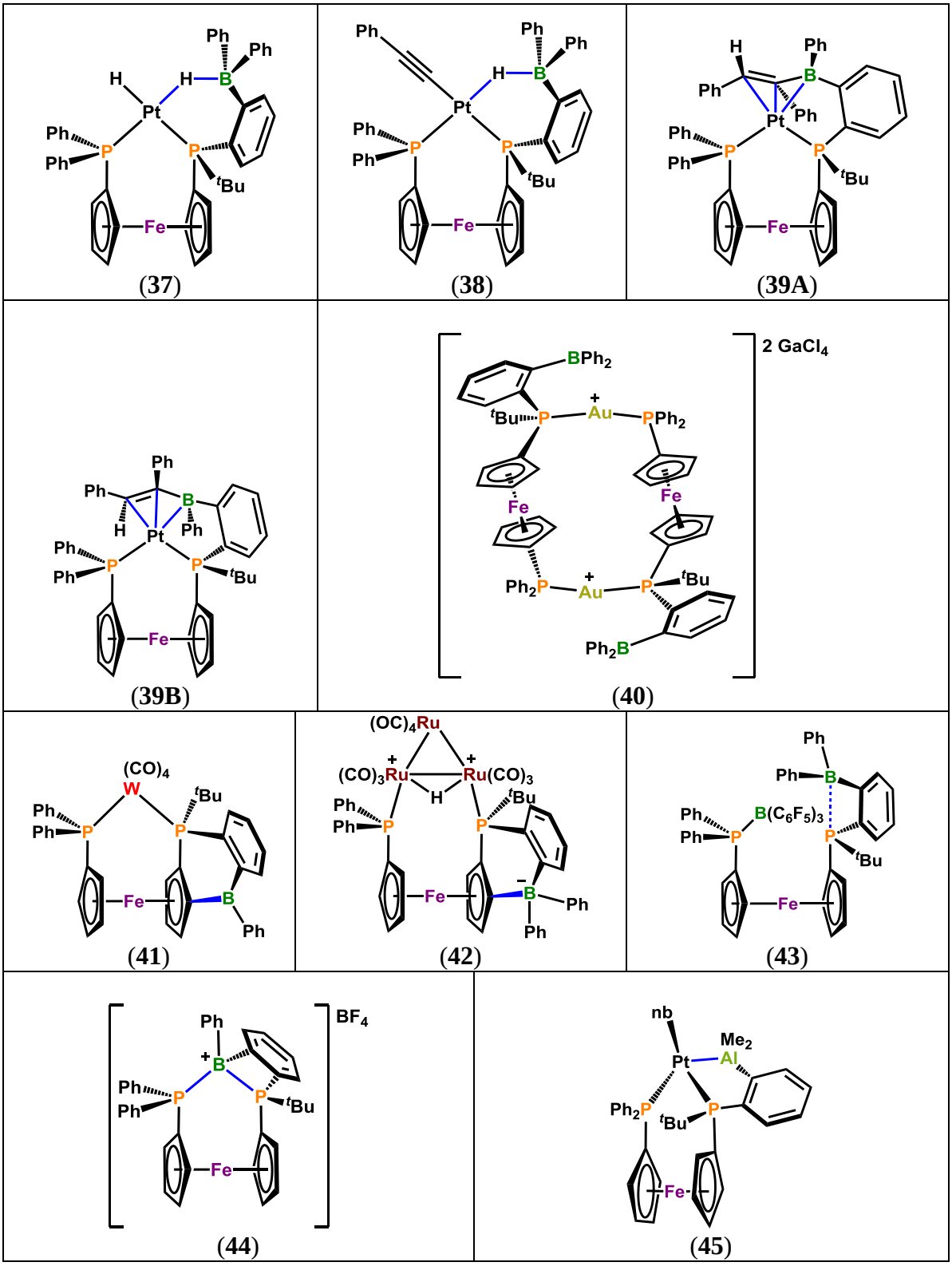
(37)
(38)
(39A)
(39B)
2 GaCl4
(40)
(41)
(42)
(43)
BF4
(44)
(45)

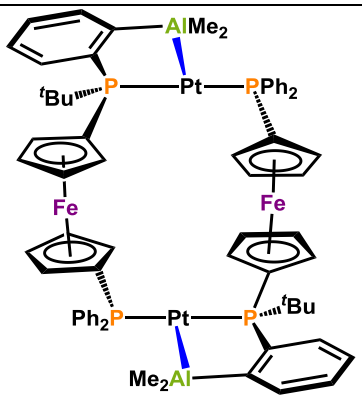
AlMe2
tBu
P
Pt
PPh2
Fe
Fe
Ph2P
Pt
P
tBu
Me2Al

(**46**)

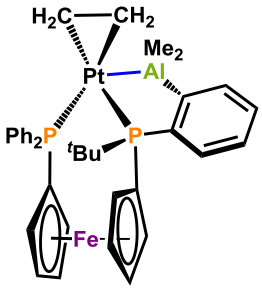
H2C
CH2
Me2
Al
Pt
Ph2P
tBu
P
Fe

(**47**)

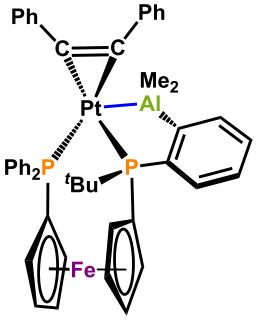
Ph
Ph
C
C
Me2
Pt
Al
Ph2P
tBu
P
Fe

(**48**)

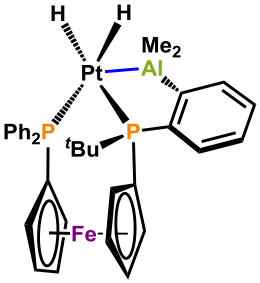
H
H
Me2
Pt
Al
Ph2P
tBu
P
Fe

(**49**)

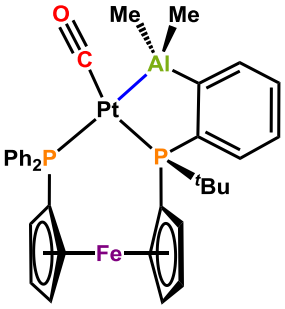
O
C
Me
Me
Al
Pt
Ph2P
P
tBu
Fe

(**50**)

List of Abbreviations

General:

° – degree(s)

η^n – denotes the hapticity of the ligand, which is the coordination of a ligand to a metal centre via delocalized charge distribution over a series of n atoms.

κ^n – denotes the denticity of the ligand, which refers to the number of donor groups in a single ligand, n, that bind to a central metal in a coordination complex.

μ_n – refers to a ligand that is bridging between n atoms.

avg – average

C – Celcius

cent – centroid

Collidinium – 2,4,6-trimethylpyridinium [2,4,6-Me_3-C_5H_2NH]$^+$

D – deuterium

DME – 1,2-dimethoxyethane

DMSO – dimethylsulfoxide (Me_2SO)

g – grams

K – Kelvin

LA – Lewis acid

m – meta

M – molarity (mol L^{-1})

MAO – methylaluminoxane

mL – millilitre(s)

mmol – millimole

mol – moles

o – ortho

p – para

rac – racemic

tetraglyme – tetraethylene glycol dimethylether

THF – tetrahydrofuran

TMEDA – *N*,*N*,*N*′,*N*′-tetramethylethane-1,2-diamine

Substituents:

2-picolyl – 2-methylpyridinyl (2-CH_2-NC_5H_4)

Ac – acetyl {$H_3CC(O)$}

Ace – acenaphthyl

Ad – 1-adamantyl

Ant – 9-anthracenyl ($C_{14}H_9$)

Ar – aryl

Ar^F – 3,5-bis(trifluoromethyl)phenyl {3,5-$(CF_3)_2$-C_6H_3}

azaind – 7-azaindolyl

B(cat) – catecholboranyl ($C_6H_4BO_2$)

BFlu – 9-borafluorenyl

Cy – cyclohexyl

Dipp – 2,6-di-*iso*-propylphenyl (2,6-$^iPr_2$-C_6H_3)

Et – ethyl

Fu – 2-furyl

Ind – indenyl

^{i}Pr – *iso*-propyl

Me – methyl

Mes – mesityl, 2,4,6-trimethylphenyl

mp – 2-sulfanylpyridyl

mt^{Me} – 2-sulfanyl-1-methylimidazolyl

mt$^{t\mathrm{Bu}}$ – 2-sulfanyl-1-*tert*-butylmethylimidazolyl

^{n}Bu – *n*-butyl (*n* = normal)

Ph – phenyl

pn^{Me} – 6-methyl-3-sulfanylpyridazinyl

pn^{Ph} – 6-phenyl-3-sulfanylpyridazinyl

pn^{tBu} – 6-*tert*-butyl-3-sulfanylpyridazinyl

py – 2-pyridyl (*o*-NC_5H_4)

pz – pyrazolyl

pz^{Me2} – 3,5-dimethylpyrazolyl

taz – 5-sulfanyl-4-ethyl-3-methyl-1,2,4-triazolyl

^{t}Bu – *tert*-butyl (*tert* = tertiary)

Tf – triflyl, trifluoromethylsulfonyl (SO_2CF_3)

Tip – 2,4,6-tri-*iso*-propylphenyl (2,4,6-$^i Pr_2$-C_6H_2)

TMS – trimethylsilyl ($SiMe_3$)

Tol – tolyl, methylphenyl

Xyl – xylyl, 2,6-dimethylphenyl

Ligands and Compounds:

[2.2.2]-cryptand – 4,7,13,16,21,24-hexaoxa-1,10-diazabicyclo[8.8.1]hexacosane

9-BBN – 9-borabicyclo[3.3.1]nonanyl ($C_8H_{14}B$)

12-crown-4 – 1,4,7,10-tetraoxacyclododecane

18-crown-6 – 1,4,7,10,13,16-hexaoxacyclooctadecane

acac – acetylacetonato $\{OC(Me)CHC(Me)O\}^-$

Allyl – $C_3H_5^-$

bai^{Ph} – $PhB(azaind)_2$

Benzyl – phenylmethyl (CH_2Ph)

BINAP – 2,2'-bis(diphenylphosphino)-1,1'-binaphthyl

bipy – 2,2'-bipyridine

Borataalkene – $R_2C{=}BR'_2^-$

cod – 1,5-cyclooctadiene

Cp – cyclopentadienyl (η^5-C_5H_5)

Cp* – pentamethylcyclopentadienyl (η^5-C_5Me_5)

dba – *trans,trans*-dibenzylideneacetone

diop – 2-(diphenylphosphino)-2'-methoxy-1,1'-binaphthyl

dmpe – 1,2-bis(dimethylphosphino)ethane {$Me_2P(CH_2)_2PMe_2$}

dppf – 1,1'-bis(diphenylphosphino)ferrocene, [$Fe(\eta^5$-$C_5H_4PPh_2)_2$]

dvds – 1,3-divinyltetramethyldisiloxane

FcPP – 1,1'-bis(phosphino)ferrocene

FcPPAl – 1'-{(*ortho*-dimethylalanylphenyl)-*tert*-butylphosphino}-1-diphenylphosphinoferrocene

FcPPAl^{Ph} – 1'-{(*ortho*-diphenylalanylphenyl)-*tert*-butylphosphino}-1-diphenylphosphinoferrocene

FcPPB – 1'-{(*ortho*-diphenylborylphenyl)-*tert*-butylphosphino}-1-diphenylphosphinoferrocene

FcPPB^{Me} – 1'-{(*ortho*-dimethylborylphenyl)-*tert*-butylphosphino}-1-diphenylphosphinoferrocene

FcPPB^{-Ph} – A bisphosphine-stabilized boronium cation derived from FcPPB; see Scheme 7.6.

FcPPB' – 1'-{(*ortho*-{(*Z*-1,2-diphenylvinyl)phenylboryl}phenyl)-*tert*-butylphosphino}-1-diphenylphosphinoferrocene

FcPPB* – A neutral bisphosphine ligand derived from FcPPB; see Scheme 7.2.

FcPPB –** An anionic bisphosphine ligand derived from FcPPB; see Scheme 7.3.

FcPPP – 1'-{(*ortho*-diphenylphosphinophenyl)-*tert*-butylphosphino}-1-diphenylphosphinoferrocene

ma – maleic anhydride

^{Mes}BQuin – 8-(dimesitylboryl)quinoline

nb – norbornene (C_7H_{10})

nbd – 1,4-norbornadiene (C_7H_8)

***p*-cymene –** 1-methyl-4-*iso*-propylbenzene (1-Me-4-^{i}Pr-C_6H_4)

POPheph –$PPh_2POCH(Ph)CH(Me)NMe\{CH(Ph)(\eta^2$-Ph)}

^{R}DPB$^{R'}$ – {(o-R_2P)C_6H_4}$_2$BR'

^{R}MPB$^{R'}$ – (o-R_2P)C_6H_4BR'$_2$

^{R}TPB – {(o-R_2P)C_6H_4}$_3$B

silox – OSi^{t}Bu$_3$

SIR – C{N(R)(CH)}$_2$; R = Mes, ^{t}Bu

tai – B(7-azaindolyl)$_3$

tht – tetrahydrothiophene

Tpy – terpyridine

TXPB – 2,7-di-*tert*-butyl-5-diphenylboryl-4-diphenylphosphino-9,9-dimethylthioxanthene

TXPB' – 2,7-di-*tert*-butyl-5-methylphenylboryl-4-diphenylphosphino-9,9-dimethylthioxanthene

TXPB'' – 2,7-di-*tert*-butyl-5-dimethylboryl-4-diphenylphosphino-9,9-dimethylthioxanthene

TXPB-F – {5-(2,7-di-*tert*-butyl-4-diphenylphosphino-9,9-dimethylthioxanthenyl)}diphenylfluoroborate

TXPB-Me – {5-(2,7-di-*tert*-butyl-4-diphenylphosphino-9,9-dimethylthioxanthenyl)}diphenylmethylborate

TXPH – 2,7-di-*tert*-butyl-4-diphenylphosphino-9,9-dimethylthioxanthene

Spectroscopy, Diffraction and Analytical Techniques:

Å – angstrom

α, β, γ – unit cell angles

δ – chemical shift (ppm)

λ – wavelength

μ – absorption coefficient

θ – angle of reflection; used to measure the unit cell in degrees.

$\omega_{1/2}$ – signal width at half intensity

1D – one dimensional

{^{1}H} – proton decoupled

2D – two dimensional

***a, b, c* –** unit cell lengths

app. – apparent

COSY – correlation spectroscopy

Cryst. Syst. – crystal system

d – doublet

DEPT – distortionless enhancement by polarization transfer

EA – elemental analysis

EXSY – exchange spectroscopy

***F*(000) –** The expression for a structure factor evaluated in the zeroth-order case h = k = l = 0, *F*(000). For X-ray diffraction, non-dispersive *F*(000) is a positive number and counts the effective number of electrons in the unit cell.

GOF – goodness of fit

HMBC – heteronuclear multiple bond correlation

HSQC – heteronuclear single quantum coherence

Hz – hertz

Indep – independent

IR – infrared

***J* –** symbol for coupling constant

m – multiplet

MHz – megahertz

$^{n}J_{X,Y}$ – coupling constant between nuclei X and Y; n = the number of bonds separating nuclei X and Y

NMR – nuclear magnetic resonance

No. – number

ppm – parts per million

PXRD – powder X-ray diffraction

q – quartet

r_α **–** ratio between a specified bond length and the sum of the covalent radii for the atoms involved.

Reflns – reflections

ROESY – rotating-frame Overhauser effect spectroscopy

s – singlet

t – triplet

T_c **–** coalescence temperature

uDEFT – uniform driven equilibrium Fourier transform

UV – ultraviolet

wt – weight

***Z* –** number of chemical formula units per unit cell

Thermodynamics and Kinetics:

$\Delta G^{\ddagger}$ **–** Gibbs free energy of activation

$\Delta H^{\ddagger}$ **–** enthalpy of activation

$\Delta S^{\ddagger}$ **–** entropy of activation

***h* –** Planck's constant (6.626×10^{-34} m^2 kg s^{-1})

J – joule(s)

***k* –** rate of reaction

k_B **–** Boltzmann constant (1.38×10^{-23} m^2 kg s^{-2} K^{-1})

KJ – kilojoule(s)

max – maximum

min – minimum

R – molar gas constant (8.314 m^2 kg s^{-2} K^{-1} mol^{-1})

s – second(s)

T – temperature

t – time

$[X]_{eq}$ – Equilibrium concentration of compound X

$[X]_o$ – Original concentration of compound X

$[X]_t$ – Concentration of compound X at time t

Calculations:

ζ – zeta, used to represent the exponent of a Slater-type orbital basis function

ADF – Amsterdam density functional

D3-BJ – D3(Becke-Johnson) dispersion correction

DFT – density functional theory

DZ – double-zeta basis set

DZP – double-zeta basis set with 1 polarization function

GUI – graphical user interface

MO – molecular orbital

NBO – natural bond order

NLMO – natural localized molecular orbital

NM – Nalewajski Mrozek bond orders

PBE – Perdew-Burke-Ernzerhof

QZ4P – quadruple-zeta basis set with 4 polarization functions

SCF – self-consistent field method

SCFDD – self-consistent field deformation density

SZ – single-zeta basis set

TZP – triple-zeta basis set with 1 polarization function

TZ2P – triple-zeta basis set with 2 polarization functions

ZORA – zero-order regular approximation

Ph.D. Thesis
Bradley E. Cowie
Department of Chemistry and Chemical Biology
McMaster University

Declaration of Academic Achievement

Prof. D. J. H. Emslie was responsible for the synthesis and characterization of [Rh(CO)(TXPB)][PF_6] (**5**), as well as performing DFT calculations for the geometry optimization of [PtH(μ-H)(FcPPB)] (**37**), and for computational evaluation of the bonding in [PtH_2(FcPPAl)] (**49**) and [Pt(CO)(FcPPAl)] (**50**). Natalie Huk, a former M.Sc. student in the Emslie group, was responsible for the initial synthesis of [PtMePh(TXPB')] (**13**). Judy Tsao, a former 4th year undergraduate thesis student in the Emslie group, was responsible for the initial synthesis of the FcPPAl ligand, and for obtaining an X-ray crystal structure for the FcPPAl ligand. Kristopher B. Kolpin, a current Ph.D. student in the Emslie group, was responsible for the synthesis of $B(C_6F_5)_3$. Jeffrey S. Price, a current Ph.D. student in the Emslie group, was responsible for performing PXRD experiments. Dr. Kirk Green was responsible for performing mass spectrometry experiments. Dr. Steve Kornic was responsible for performing elemental analysis for all samples for which it was required, as well as performing Raman spectroscopy experiments on *rac*-[{Ni(FcPPP)}$_2$(μ-N_2)] (**33**), [Pt(η^2-C_2H_4)(FcPPAl)] (**47**) and [Pt(η^2-C_2Ph_2)(FcPPAl)] (**48**). Hilary A. Jenkins was responsible for crystal mounting, data acquisition and data processing for single crystal X-ray diffraction experiments. All other results were obtained by myself, Bradley E. Cowie.

Ph.D. Thesis
Bradley E. Cowie
Department of Chemistry and Chemical Biology
McMaster University

Chapter 1

Introduction

1.1 – Coordination Chemistry

1.1.1 – L-, X- and Z-Type Ligands

Monodentate σ-donating ligands, with or without the possibility for π-donation or π-acceptance, are ubiquitous in transition metal chemistry. Such ligands are divided into two general categories according to Covalent Bond Classification (CBC), which are L- and X-type ligands. Ligands of L-type are neutral Lewis bases that σ-donate two electrons to an empty orbital on the metal centre upon coordination, forming a ligand→metal dative bond (Figure 1.1, left); examples of these ligands are amines (NR_3), phosphines (PR_3) and carbon monoxide (CO). Ligands of X-type are anionic ligands that σ-donate two electrons to the metal. Alternatively, they can be described as neutral ligands with an unpaired electron which can engage in a covalent interaction with an unpaired electron on a neutral metal centre (Figure 1.1, middle). Examples of X-type ligands are halides (F^-, Cl^-, Br^-, I^-), amido (NR_2^-) and hydride (H^-) ligands.[2,3]

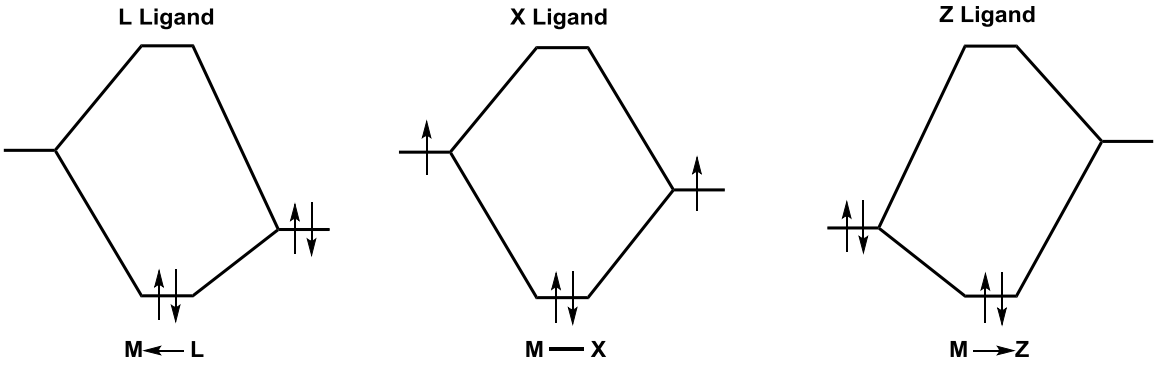

Figure 1.1. Three fundamental classes of ligands in coordination chemistry, based on the supply of electrons within the metal–ligand covalent bond if the ligand is considered to be neutral.

The third class of ligand in coordination chemistry, Z-type ligands, are Lewis acids, and coordination to a metal centre requires two electron σ-donation from the metal to the ligand, resulting in a dative metal→ligand bond (Figure 1.1, right). Group 13 elements bound to three substituents, for example, boranes (BR_3) and alanes (AlR_3), possess an empty p orbital capable of electron acceptance, rendering them Lewis acidic and thus Z-type ligands.[2,3] The coordination chemistry of this class of ligands has primarily been developed in combination with less electropositive late transition metals (in particular those of Groups 8-11) in low oxidation states.

1.1.2 – Coordination Complexes of Unsupported Group 13 Lewis Acids

Transition metal complexes featuring metal–alane, –gallane and –indane coordination have been known for over 30 years. In 1979, Burlich and co-workers described the synthesis of the transition metal→alane adducts $[NMe_4][Co(CO)_4(AlPh_3)]$, $[NEt_4][CpW(CO)_3(AlPh_3)]$ (Cp = η^5-C_5H_5) and $[NEt_4][CpFe(CO)_2(AlPh_3)]$; the latter anionic iron–alane complex was the first structurally authenticated transition metal complex bearing a coordinated alane.[4] In addition, Mayer and Calabrese explored the reactivity of various trialkylalanes and alkylhaloalanes with cyclopentadienyl-rhodium fragments bearing phosphine co-ligands, and reported the crystallographic characterization of $[CpRh(PMe_3)_2(Al_2Me_4Cl_2)]$.[5] Additionally, Bergman and Andersen reported the synthesis and structure of $[Cp^*IrH_2(PMe_3)(AlPh_3)]$ (Cp^* = η^5-C_5Me_5), which exhibits η^1*Al*-coordination of $AlPh_3$ to iridium, and most recently Braunschweig and co-workers have reported the synthesis and structural characterization of a series of transition metal→AlX_3 (X = Cl or Br) adducts involving rhodium,[6] palladium[7] and platinum.[8,9] In 1999, Fischer and co-workers published the synthesis and solid-state structure of $K[Co(CO)_4(GaCl_3)]$,[10] and in 2005 $[(p\text{-cymene})Ru(GaCp^*)_2(GaCl_3)]$,[11] $[Cp^*Rh(GaCp^*)_2(GaCl_2Cp^*)]$ and $[Cp^*Rh(GaCp^*)_2(GaCl_3)]$[12] were reported, all of which are transition metal→gallane adducts featuring η^1*Ga*-coordination of the gallane. Furthermore, Scheer and co-workers reported the synthesis and solid-state structure of

$[Na(OEt_2)]_2[Fe(CO)_4(GaCl_3)_2]$,[13] Aldridge *et al*. reported the synthesis and X-ray crystal structure of $[tmpH_2][Cp^*Fe(CO)_2(GaX_3)]$ (tmp = tetramethylpiperamide, $N\{C(Me)_2(CH_2)_3C(Me)_2\}$; X = Cl, Br)[14] and $[HNEt_3][CpFe(CO)_2(GaBrI_2)]$,[15] and recently Braunschweig and co-workers reported the synthesis of the first platinum→gallane adduct, $[Pt(PCy_3)_2(GaCl_3)]$.[16]

In the case of transition metal→indane complexes, in 1990 Ziegler reported the synthesis and structural authentication of $[Cp_3Mo_3(\mu\text{-}CO)_3(CO)_3(\mu_3\text{-}O)][CpMo(CO)_3(InCl_3)]$,[17] Neumüller and Petz reported the synthesis and X-ray crystal structure of $[C(NMe_2)_3]_2[Fe(CO)_4(InCl_3)]$,[18] Sandhöfner and co-workers reported the synthesis and characterization of $[PPh_4]_2[M(CO)_5(InX_3)]$ (M = Cr, X = Cl, Br; M = Mo, X = Cl; M = W, X = Cl),[19] and Aldridge and co-workers reported the synthesis of $[Cp^*Fe(\eta^6\text{-}C_6H_5Me)][Cp^*Fe(CO)_2(InI_3)]$.[15]

In contrast to the chemistry of alanes, gallanes and indanes, unsupported transition metal→borane adducts have evaded crystallographic authentication to-date. In the 1960s, Shriver and co-workers reported on the reactions of BF_3 and BCl_3 with $[Cp_2MoH_2]$, $[Cp_2WH_2]$ and $[Cp_2ReH]$, and concluded that BF_3 and BCl_3 formed 1:1 adducts with tungsten and rhenium, providing $[Cp_2WH_2(BX_3)]$ and $[Cp_2ReH(BX_3)]$ (X = F, Cl), respectively, while BF_3 reacted with $[Cp_2MoH_2]$ to yield $[Cp_2MoH_2(BF_3)]$.[20] Additionally, Parshall reported reactions of B_2H_6 with salts of $[Re(CO)_5]^-$, $[Mn(CO)_5]^-$ and $[Mn(CO)_4(PPh_3)]^-$, claiming the formation of 1:1 adducts exhibiting metal→BH_3 bonding interactions; the diborane complexes $[NEt_4][Re(CO)_5(BH_3)_2]$ and $[P^nBu_4][Re(CO)_5(BH_3)_2]$ were also claimed to have been isolated.[21] Burlitch and co-workers in 1979 also reported that BPh_3 reacted with $[NEt_4][CpFe(CO)_2]$ to provide $[NEt_4][CpFe(CO)_2(BPh_3)]$ containing a Fe–B bond, which spontaneously isomerized in dilute THF solutions to form $[NEt_4][(\eta^5\text{-}C_5H_4BPh_3)Fe(CO)(\mu\text{-}CO)_2Fe(CO)Cp]$ and $[NEt_4][HBPh_3]$.[22] However, due to the lack of structural authentication of the aforementioned complexes, in addition to contradicting structural data provided in the 1990s by Braunschweig and co-workers, these reports came under high scrutiny. For example, in 1994 Braunschweig and co-workers provided the X-ray crystal structure of

zwitterionic [(η^5-$C_5H_4B^tBuCl_2$)$CpWH_3$], obtained via reaction of $^tBuBCl_2$ with [Cp_2WH_2], which was unambiguously found not to form a 1:1 tungsten→borane adduct.[23] In addition, Braunschweig reported the reaction of [Cp_2WH_2] with $^iPr_2BCl$, BCl_3 and BF_3 resulted in the formation of [Cp_2WH_3][$^iPr_2BCl_2$] and [Cp_2WH_3][BX_4] (X = Cl, F) salts (the former complex was structurally characterized by X-ray diffraction),[24] and reactions of $B(C_6F_5)_3$ and $Me_2NB(CF_3)_2$ with [Cp_2WH_2] lead to the formation of zwitterionic [{η^5-$C_5H_4B(C_6F_5)_3$}$CpWH_3$] and [{η^5-$C_5H_4B(NMe_2)(CF_3)_2$}$CpWH_3$], respectively, while reactions of $B(C_6F_5)_3$ and $^tBuBCl_2$ with [$Cp^*_2WH_2$] provided [$Cp^*_2WH_3$][$B(C_6F_5)_4$] and [$Cp^*_2WH_3$][$^tBuBCl_3$], respectively.[25] Most recently, Wolczanski and co-workers reported the reactions of [$Ta(silox)_3$] (silox = $^tBu_3SiO$) with $PhBCl_2$ and BH_3, forming [Ta(η^2*BCl*-Cl_2BPh)$(silox)_3$] and [$Ta(BH_3)(silox)_3$], respectively. The former complex was crystallographically characterized, whereas the latter was not, and while there is no unambiguous evidence of the exact structure of the Ta–BH_3 complex, DFT calculations suggest an equilibrium between η^1*B*- and η^2*HB*-coordination modes, while IR spectroscopy in combination with simulated IR spectra suggest that the identity of the ground state structure is [Ta(η^2*BH*-BH_3)$(silox)_3$].[26]

1.1.3 – The Emergence of Ambiphilic Ligands

The first report of a structurally characterized transition metal–borane complex by single crystal X-ray diffraction was produced in 1999 when Hill and co-workers utilized an *in situ* generated tris(2-sulfanyl-1-methylimidazolyl)borane ligand to encourage η^1*B*-coordination to ruthenium (Section 1.2.1, *vide infra*). Since this initial report by Hill, tris(azolyl)borane and bis(azolyl)borane ligands have been utilized extensively to isolate late transition metal complexes featuring η^1*B*-coordination. However, a paradigm shift occurred in 2006 towards the deployment of isolable phosphine/borane-containing ligand systems to study metal–borane coordination chemistry (Section 1.3, *vide infra*). Such ligand systems, generated *in situ* or pre-formed, are called ambiphilic ligands, and are defined as ligands that contain both conventional Lewis base donors and Lewis acidic

moieties. While nearly all of the research published to-date pertaining to the coordination chemistry of boranes with transition metals involves the use of ambiphilic ligands, unsupported alanes have dominated the area of metal–alane coordination. Additionally, while borane-containing ambiphilic ligands have proven successful as a means to promote metal–borane coordination, most reactions involving alane-containing ambiphilic ligands have not provided examples of metal–alane bonding, instead engaging in alternate reactivity with co-ligands in the primary coordination sphere of the metal. These reactions include halide or alkyl coordination and abstraction,[27-32] neutral ligand (NEt_3 and DMSO) abstraction,[27,28,33] and acyl or formyl ligand (formed through 1,1-insertion) coordination to form η^2*CO*-coordinated five-membered CR-O-AlR_2-N^{t}Bu-PR_2 rings in preference to metal–alane bonding.[34-37] Only recently have alane-containing ambiphilic ligands been employed to prepare complexes featuring η^1*Al*-coordination.[38,39]

While initial transition metal–Group 13 Lewis acid chemistry focused on exploring the nature of the metal–Lewis acid bonding interactions, research conducted as of late has focused more on investigating the reactivity of ambiphilic ligand transition metal complexes. This is largely due to their potential to promote unique reactivity as a consequence of their:

1) High *trans* influence.[40-43]

2) Ability to reduce the number of d-electrons in a complex by two units (i.e. the number of electrons in the frontier orbitals) without changing the overall electron count.

3) Propensity to yield compounds with unusual coordination geometries.[3,44]

4) Ability to stabilise complexes in a range of oxidation states by modulating the amount of electron density at the metal centre through metal–Lewis acid interactions of varying strength.[45,46]

5) Potential to engage in Lewis acid–substrate or metal–co-ligand–Lewis acid bridging interactions.[47-49]

6) Potential to form zwitterions through anionic ligand abstraction, in some cases resulting in substituent exchange between boron and the metal centre.[50-60]

7) Potential to promote 1,1-insertion reactions.[61-64]

The focus of this introductory chapter is the isolation of transition metal complexes bearing novel borane- and alane-containing ambiphilic ligands, and the reactivity of such complexes under stoichiometric conditions with small molecule substrates, or in catalysis. Despite the dominance of poly(azolyl)borane-containing ambiphilic ligands between 1999-2006, primarily to prepare complexes featuring η^1*B*-coordination, the focus of this chapter will be the deployment of phosphine/borane-containing ligands, as well as other emerging examples of effective ambiphilic ligands. The majority of this chemistry involves the use of isolable ambiphilic ligands. However, key examples of *in situ* generated borane-containing ligands will also be discussed.

1.2 – Transition Metal Complexes of Borane-Containing Ambiphilic Ligands

1.2.1 – The First Structural Authentication of a Metal–Borane Bonding Interaction

Early ambitions in the realm of metal–borane chemistry were directed towards the synthesis and characterization of transition metal complexes bearing direct η^1*B*-coordination of a borane to the metal centre. Such complexes are of interest given the fundamentally counterintuitive nature of a metal–Group 13 Lewis acid bonding interaction – the requirement for σ-electron donation from the metal centre to the ligand. However, the first structurally authenticated example of a transition metal complex bearing an η^1*B*-coordinated borane ligand was not reported until 1999, when Hill and co-workers capitalized upon an *in situ* generated ambiphilic ligand framework to promote metal–borane coordination.[65] This ligand contained three conventional Lewis basic donors in addition to the borane, which was positioned as the central buttress in the ligand framework, allowing it to take advantage of the chelate effect and promote close approach

of the Lewis acid to the metal upon coordination of the peripheral donor atoms, akin to Brown's azoboratrane, $N(CH_2CH_2O)_3B$, displayed in Figure 1.2 below.[66]

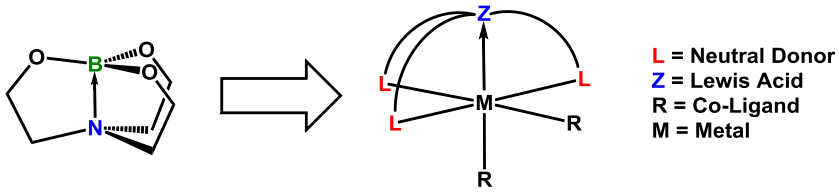

Figure 1.2. Conceptual progression from an azoboratrane $N(CH_2CH_2O)_3B$ (left) to the borane-containing ambiphilic ligand (right) utilized by Hill and co-workers.

The reaction used by Hill *et al.* to prepare the first η^1*B*-borane complex involved treatment of $[RuCl(R)(CO)(PPh_3)_2]$ (R = $CH{=}CHCPh_2OH$, $CH{=}CH_2$, $CH{=}CH(p\text{-}MeC_6H_4)$ or Ph) with $Na[HB(mt^{Me})_3]$ (mt^{Me} = 2-sulfanyl-1-methylimidazole) (**A** in Scheme 1.1),[65,67] affording $[Ru(CO)(PPh_3)\{B(mt^{Me})_3\}]$ via *in situ* RH elimination from initially formed $[Ru(R)(CO)(PPh_3)\{HB(mt^{Me})_3\}]$ (**B** in Scheme 1.1).

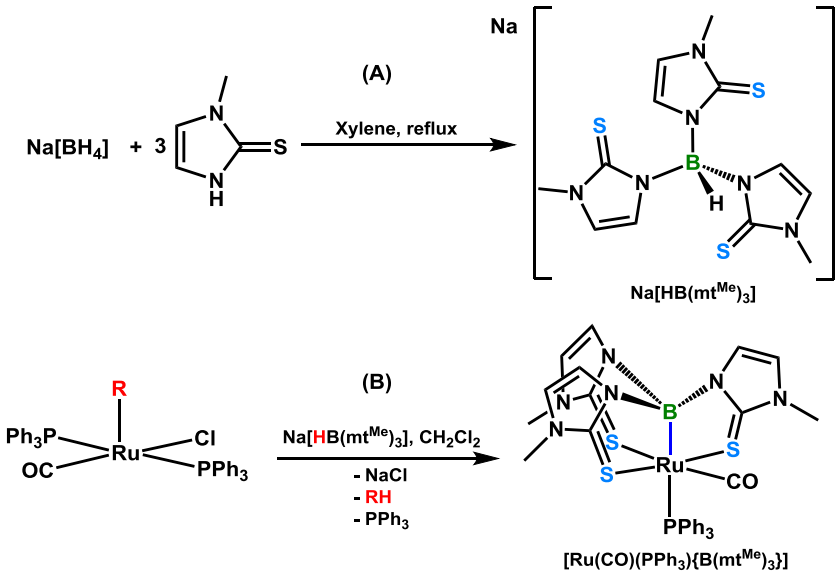

Scheme 1.1. A. Synthesis of the $Na[HB(mt^{Me})_3]$ (mt^{Me} = 2-sulfanyl-1-methylimidazolyl) ligand, and **B.** synthesis of $[Ru\{B(mt^{Me})_3\}(CO)(PPh_3)]$, the first crystallographically characterized transition metal complex featuring direct η^1*B*-coordination of a borane to the metal centre.

In order to gauge the extent and strength of metal–borane coordination, several metrics are typically utilized, which are: (1) The metal–boron bond length and the ratio between the metal–boron bond length and the sum of the covalent radii[68] (denoted as r_α; typical values range from ~0.9–1.2), (2) the degree of pyramidalization of boron, indicated as the sum of the R–B–R angles (R = initial substituent bound to boron prior to coordination to the metal), and denoted as Σ(R–B–R) (close approach of Σ(R–B–R) to 328.5° is indicative of tetrahedral, four-coordinate boron, and strong metal–boron coordination), and (3) the ^{11}B NMR chemical shift (a shift of the ^{11}B chemical shift to lower frequency relative to the free borane indicates an increase in electron density at boron, therefore the greater the shift the stronger the bonding interaction).[45] Close approach of the borane in [Ru(CO)(PPh$_3$){B(mt^{Me})$_3$}] to ruthenium was evidenced by a Ru–B bond distance of 2.161(5) Å (r_α = 0.94), near tetrahedral geometry of boron with N–B–N angles ranging from 105.5(4)–113.9(4)°, and a low frequency chemical shift for the ^{11}B NMR signal (17.1 ppm).[68] At the time, the only comparable structurally authenticated ruthenium complex bearing a ruthenium–boron bonding interaction was the ruthenium–boryl complex [(η^5-C$_5$H$_5$)Ru{B(NMe$_2$)BBr(NMe$_2$)}(CO)$_2$], which possessed a Ru–B bond length of 2.173(3) Å.[69] Given that boryl ligands are viewed as 2-electron σ-donor ligands and boranes are considered 0-electron σ-acceptor ligands, the comparable metal–boron bond distances in the borane and boryl complexes indicated that a strong Ru–B bonding interaction was present in [Ru(CO)(PPh$_3$){B(mt^{Me})$_3$}].

1.2.2 – Coordination Chemistry of Poly(azolyl)borane Ligands

Hill and co-workers have been able to exploit the Na[HB(mt^{Me})$_3$] hydroborate for *in situ* generation of complexes featuring η^1*B*-coordination of the central borane buttress for a wide variety of transition metals, which include ruthenium,[65,70] osmium,[71] rhodium,[72-74] iridium[75] and platinum.[76] The most important structural and spectroscopic features of these complexes are listed in Table 1.1 below, which includes the metal–boron bond distance, ratio of metal–boron (or co-ligand–boron) bond distance to the sum of the

covalent radii (r_α), the degree of pyramidalization of boron and the ^{11}B NMR chemical shifts. In all cases, initial coordination of the tris(methylimidazolyl)borate was proposed to take place via coordination of at least two of the sulfanyl-arms with concomitant NaCl elmination and B–H bond addition to the metal centre (to yield a borane-coordinated metal hydride complex). This was followed by reductive elimination of an RH hydrocarbon, or was accompanied by dissociation of a co-ligand (either a neutral phosphine or an anionic chloride or hydride ligand), facilitating association of the third sulfanyl-donor, as shown in Scheme 1.2 below. These metal complexes are referred to as metallaboratranes, and their name stems from the azoboratrane prepared by Brown and co-workers in 1951 (Figure 1.2).[66]

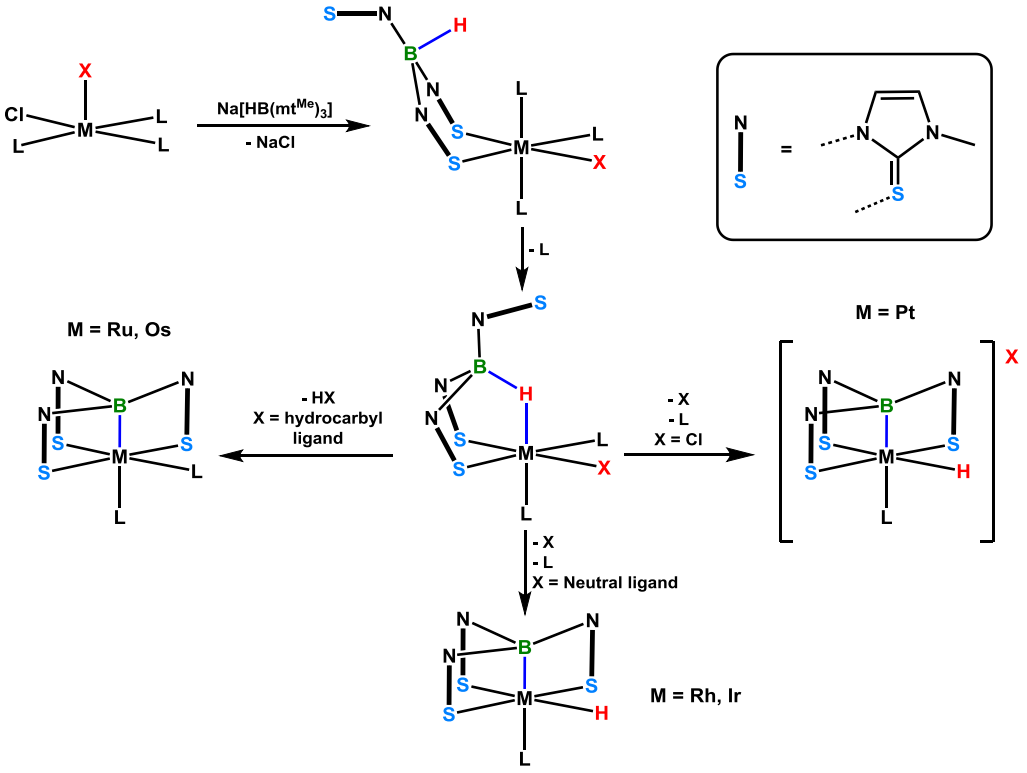

Scheme 1.2. Potential avenues for κ^4*SSSB*-coordination of the B(mt^{Me})$_3$ ligand.

Hill and co-workers have expanded this work to bis(2-sulfanyl-1-methylimidazolyl)borane complexes, proving that a tripodal donor array was not required

to promote η^1*B*-coordination to a metal. The $Li[H_2B(mt^{Me})_2]$ borate was originally reported by Parkin *et al*. in 1997 and was prepared from reaction of 2-sulfanyl-1-methylimidazole with $Li[BH_4]$.[77] Hill and co-workers utilized the sodium salt, which was prepared via reaction of 2-sufanyl-1-methylimidazole with $Na[BH_4]$, and addition of $Na[H_2B(mt^{Me})_2]$ to $[IrCl(CO)_2(PPh_3)_2]$ lead to the formation of $[IrH(CO)(PPh_3)\{HB(mt^{Me})_2\}]$ which exhibited κ^3*SSB*-coordination of the ambiphilic ligand.[78] In addition, Hill and co-workers have made efforts to explore the reactivity of their metallaboratrane complexes; whereas the addition of $Na[H_2B(mt^{Me})_2]$ to $[MCl(CO)(PPh_3)_2]$ (M = Rh, Ir) lead to the formation of $[MH(CO)(PPh_3)\{HB(mt^{Me})_2\}]$ complexes, $Na[H_2B(mt^{Me})_2]$ reacted with $[RhCl(CS)(PPh_3)_2]$ to provide $[RhH(PPh_3)\{\eta^2CS{:}\kappa^2S',S''\text{-}SC(PPh_3)BH(mt^{Me})_2\}]$, the product of 1,1-insertion of η^2-coordinated CS into the Rh–B bond, in addition to migration of PPh_3 from rhodium to the C_{CS}-carbon atom (**A** in Scheme 1.3).[61] Additionally, Hill and co-workers found that oxidative addition of MeI, Cl_2, Br_2 and I_2 to $[Pt(PPh_3)\{B(mt^{Me})_3\}]$ yielded $[PtI(Me)\{B(mt^{Me})_3\}]$ and $[PtX_2\{B(mt^{Me})_3\}]$ (X = Cl, Br, I) complexes, which retain platinum–borane coordination (**B** in Scheme 1.3).[76]

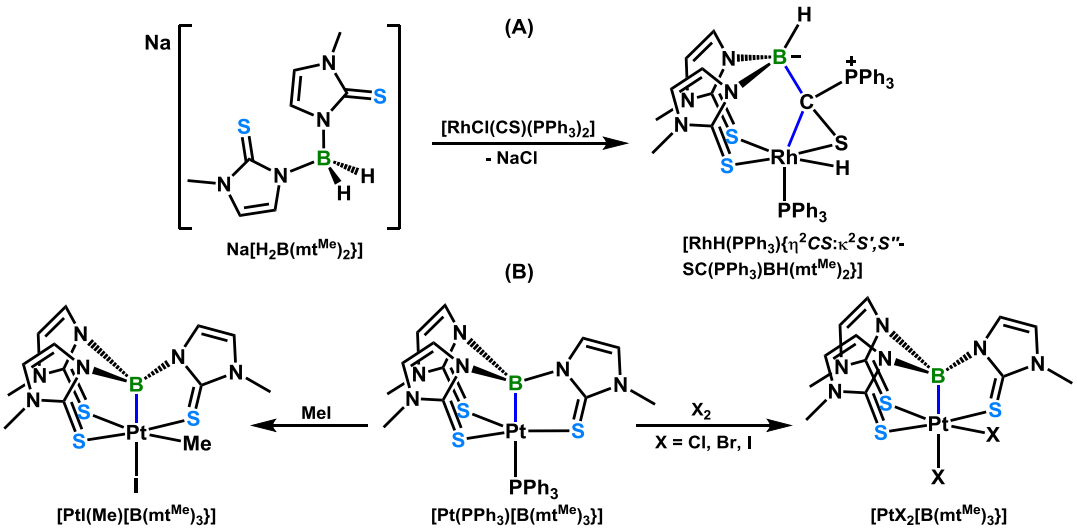

Scheme 1.3. A. Reaction of $Na[H_2B(mt^{Me})_2]$ with $[RhCl(CS)(PPh_3)_2]$ to yield $[RhH(PPh_3)\{\eta^2CS{:}\kappa^2S',S''\text{-}SC(PPh_3)BH(mt^{Me})_2\}]$, and **B.** oxidative addition of either X_2 (X = Cl, Br or I) or MeI to $[Pt(PPh_3)\{B(mt^{Me})_3\}]$, forming $[PtXY\{B(mt^{Me})_3\}]$ (X = Y = Cl, Br or I; X = Me, Y = I) products.

Table 1.1. Important crystallographic and spectroscopic metrics of all poly(azolyl)borane-containing metallaboratrane complexes published to-date exhibiting η^1*B*-coordination to a transition metal.

Complex	M–B [Å]	r_a [a]	Σ(R–B–R) [°]	^{11}B NMR [ppm]	Reference
		Hill			
[IrH(CO)(PPh$_3$){B(mt^{Me})$_3$}]	2.193(6)	0.98	321.5(7)	3.19	[75]
[IrH(CO)(PPh$_3$){HB(mt^{Me})$_2$}]	2.210(5)	0.98	330.5	–4.5	[75]
[Ru(CO)(CN^{t}Bu){B(mt^{Me})$_3$}]	2.176(7)	0.95	325.8(8)	14.6	[70]
[Ru(CS)(PPh$_3$){B(mt^{Me})$_3$}]	2.154(5)	0.94	324.9(7)	–	[70]
[Ru(CO)(CNMes){B(mt^{Me})$_3$}]	2.146(4)	0.93	325.2(5)	–	[70]
[Ru(CO)(PPh$_3$){M(mt^{Me})$_3$}]	2.161(5)	0.94	328.5[45]	17.1	[65]
[RhCl(PPh$_3$){B(mt^{Me})$_3$}] [c]	2.132(6), 2.122(7)	0.94, 0.94	327.1[45]	1.7	[72]
[Os(CO)(PPh$_3$){B(mt^{Me})$_3$}]	2.171(8)	0.95	323(1)	12.4	[71]
[Rh$_2$\{B(mt^{Me})$_3$\}$_2$\{κ^2*SS*-B(mt^{Me})$_3$\}]Cl	2.098(6)	0.93	328.5, 330.6[b]	–	[73]
[Rh(PPh$_3$)(CN^{t}Bu){B(mt^{Me})$_3$}]Cl	2.155(7)	0.95	329.6(9)	9.0	[74]
[Rh(PPh$_3$)(CNXyl){B(mt^{Me})$_3$}]Cl	2.146(3)	0.95	329.6(4)	8.7	[74]
[Rh(PMe$_3$)$_2$\{B(mt^{Me})$_3$\}]Cl [c]	2.15(1), 2.15(1)	0.95	329(1), 328(1)	9.5	[74]
[PtI$_2$\{B(mt^{Me})$_3$\}]	2.119(4)	0.96	332.8(5)	5.05	[76]
[PtH(PPh$_3$){B(mt^{Me})$_3$}]Cl	2.157(4)	0.98	330.7(5)	1.6[45]	[76]
		Parkin			
[{Pd\{B(mt^{tBu})$_3$\}\}$_2$]	2.073(4)	0.93	325.0(5)	–	[79]
[Pd(PMe$_3$){B(mt^{tBu})$_3$}]	2.050(8)	0.92	321.2(9)	4.4	[79]
[Fe(CO)$_2$\{B(mt^{tBu})$_3$\}]	2.108(6)	0.98	326.9(7)	20.3	[51]
[IrH(CO)(PPh$_3$){B(mt^{tBu})$_3$}]	2.178(4)	0.97	321.0(5)	–	[80]
[IrH(CO)(PPh$_3$){B(mt^{Ph})$_3$}]	2.186(3)	0.97	320.7(4)	–	[80]
[RhCl(PPh$_3$){B(mt^{tBu})$_3$}]	2.095(3)	0.93	324.9(3)	–	[80]
[IrCl(PPh$_3$){B(mt^{tBu})$_3$}]	2.15(2)	0.96	328(2)	–	[80]
[NiCl{B(mt^{tBu})$_3$}]	2.110(8)	1.01	330.6(5)	–	[50]
[Ni(N$_3$){B(mt^{tBu})$_3$}]	2.092(5)	1.01	331.3(5)	–	[50]
[Ni(NCS){B(mt^{tBu})$_3$}]	2.08(1)	1.00	332(2)	–	[50]
[Ni(OAc)({B(mt^{tBu})$_3$}]	2.112(3)	1.02	330.2(4)	–	[50]

Tatsumi					
[NiCl{B(mt$^{t\text{Bu}}$)$_3$}]	2.108(4)	1.01	325.1(5)	–	[81]
Rabinovich					
[Co(PPh$_3$){B(mt$^{t\text{Bu}}$)$_3$}]BPh$_4$	2.132(4)	1.02	328.4 [b]	–	[82]
Connelly					
[Rh(PPh$_3$){B(mt$^{\text{Me}}$)$_3$}][PF$_6$]	2.077(4)	0.92	332.8(5)	–	[83]
[Rh{B(taz)$_2$(pz$^{\text{Me}}$)}{HB(taz)$_2$(pz$^{\text{Me}}$)}]	2.136(7)	0.95	324.5(9)	–	[84]
[Rh(CO)(PCy$_3$){B(taz)$_3$}][PF$_6$]	2.173(5)	0.96	332.1(7)	7.79	[85]
[Rh(CO){P(NMe$_2$)$_3$}{B(taz)$_3$}][PF$_6$]	2.176(2)	0.96	333.1(3)	7.58	[85]
[Rh$_2$(PCy$_3$){B(taz)$_3$}$_2$][PF$_6$]$_2$	2.084(5)	0.92	333.9(5)	–	[85]
[RhI(PPh$_3$){B(taz)$_3$}]	2.117(5)	0.94	331.1(6)	–	[85]
[Rh(CO)(PPh$_3$){B(taz)$_3$}][PF$_6$]	2.153(5)	0.95	332.3 [b]	7.52	[86]
[IrH(cod){B(mt$^{\text{Me}}$)$_2$(pz$^{\text{Me2}}$)}]	2.156(3)	0.96	317.9(4)	–1.01	[87]
[IrH(CO)$_2${B(mt$^{\text{Me}}$)$_2$(pz$^{\text{Me2}}$)}]	2.222(6)	0.99	322.8(7)	2.41	[87]
[IrH(CO)(PPh$_3$){B(mt$^{\text{Me}}$)$_2$(pz$^{\text{Me2}}$)}]	2.220(5)	0.99	321.7(6)	1.56	[87]
[IrH(CO)(PPh$_3$){B(mt$^{\text{Me}}$)$_2$(pz)}]	2.195(3)	0.98	320.8(3)	1.99	[87]
[(cod)HIr{μ-B(mt)$_3$}IrCl(cod)]	2.166(4)	0.96	317.9(5)	–	[87]
Owen					
[Ir(CO)(C$_8$H$_{13}$){κ^3*NNB*-(tai)}]	2.196(6)	0.98	334.1 [b]	–9.3	[88]
[Ir(CO)(CNXyl)(C$_8$H$_{13}$){κ^3*NNB*-(tai)}]	2.222(3)	0.99	326.9 [b]	4.3	[88]
[{Rh{κ^3*NNB*-(tai)}}$_2$(μ-H)(μ-azaind)] [c]	2.171(4),	0.96,	336.3(5),	3.3, 3.7	[89]
	2.148(2)	0.95	331.3(2)		
[Rh(C$_7$H$_9$){κ^4*N$_3$B*-(tai)]	2.064(4)	0.91	340.3(5)	5.00	[90]
[Pt(PPh$_3$){κ^3*SSB*-HB(mp)$_2$}] [c]	2.098(4),	0.95,	324(3), 328(3)	15.2	[91]
	2.104(4)	0.96			
[Pd(PPh$_3$){κ^3*SSB*-HB(mp)$_2$}] [c]	2.091(3),	0.94,	326(2), 327(2)	12.5	[91]
	2.094(3)	0.94			
[Pd(PPh$_3$){B(mp)$_3$}]	2.065(3)	0.93	323.9(4)	–	[91]
[Ir(CO)(C$_8$H$_{13}$){P(OCH$_2$)$_3$CEt}{κ^3*NNB*-(tai)}] [c]	2.240(4), 2.245(5)	1.00, 1.00	326.8, 327.9	4.2	[92]
[IrH(CO){κ^3*NNB*-(bai$^{\text{Ph}}$)}]	2.248(3)	1.00	331.5	–2.6	[92]
[Ru(CO)(PPh$_3$){B(mt$_2$)(mp)}]	2.146(5)	0.93	322.9(7)	21.3	[93]
[Ru(CO)(PPh$_3$){B(mp)$_3$}]	2.093(5)	0.91	318.6(5)	32.5	[93]
[Rh(η^3-C$_8$H$_{13}$){HB(mp)$_2$}]	2.054(2)	0.91	320(2)	8.0	[94]
[IrCl(cod){HB(mp)2}]	2.20(1)	0.98	320(6)	–	[94]

Mösch-Zanetti					
[NiCl{B(Pn^{Me})$_3$}]	2.016(3)	0.97	327.0(5)	–	[95]
[NiCl{B(pn^{tBu})$_3$}]	2.034(2)	0.98	331.2(3)	–	[95]
[CoCl{B(pn^{tBu})$_3$}]	2.068(3)	0.99	326.7(4)	–	[95]
[Co{B(pn^{tBu})$_3$}(pn^{tBu})]	2.004(2)	0.95	326.4(2)	–	[95]
[Co{B(pn^{Ph})$_3$}(pn^{Ph})]	1.984(3)	0.95	325.9(3)	–	[95]
[CuCl{B(pn^{tBu})$_3$}]	2.060(3)	0.95	330.4(4)	–	[96]

mt^{Me} = 2-sulfanyl-1-methylimidazolyl; mt^{tBu} = 2-sulfanyl-1-*tert*-butylmethylimidazolyl; taz = 5-sulfanyl-4-ethyl-3-methyl-1,2,4-triazolyl; pz = pyrazolyl; pz^{Me2} = 3,5-dimethylpyrazolyl; tai = B(7-azaindolyl)$_3$; azaind = 7-azaindolyl; bai^{Ph} = PhB(azaind)$_2$; mp = 2-sulfanylpyridyl; pn^{Me} = 6-methyl-3-sulfanylpyridazinyl; pn^{tBu} = 6-*tert*-butyl-3-sulfanylpyridazinyl; pn^{Ph} = 6-phenyl-3-sulfanylpyridazinyl; r_α = ratio of metal–boron bond distance to the sum of the covalent radii; [a] Covalent radii were obtained from Alvarez and co-workers;[68] [b] Calculated from the published cif using Mercury; [c] Two crystallographically independent molecules were found in the unit cell.

In addition to the coordination chemistry of the B(mt^{Me})$_3$ and HB(mt^{Me})$_2$ ligands investigated by Hill and co-workers, many other researchers have dipped into the realm of metal–borane bonding interactions through the preparation of poly(azolyl)borane-containing metallaboratranes. These researchers include Parkin, Owen, Connelly, Tatsumi, Rabinovich and Mösch-Zanetti, and the important spectroscopic and crystallographic parameters for the η^1*B*-coordinated borane complexes prepared by these Research Groups are summarized above in Table 1.1. Parkin and co-workers have been able to prepare iron, rhodium, iridium, nickel and palladium complexes featuring η^1*B*-coordination through introduction of *tert*-butyl and phenyl substituted B(mt^{R})$_3$ (R = ^{t}Bu, Ph) borane ligands to metal pre-cursors via their respective potassium borate salts.[50,51,97] [NiCl{B(mt^{tBu})$_3$}], featuring κ^4*SSSB*-coordination of the tris(*tert*-butylimidazolyl)borane ligand, reacted cleanly with TlOAc, KSCN and NaN_3 to form [NiX{B(mt^{tBu})$_3$}] (X = OAc, SCN, N_3) substitution products with retention of nickel–borane coordination. Additionally, [NiCl{B(mt^{tBu})$_3$] reacted with $CHCl_3$ and $CHBr_3$ to form [NiX{κ^3*SSS*-ClB(mt^{tBu})$_3$}] (X = Cl, Br), with XeF_2 to form [NiCl{κ^3*SSS*-FB(mt^{tBu})$_3$}], or with I_2 to provide [NiI{κ^3*SSS*-ClB(mt^{tBu})$_3$]; [NiR{B(mt^{tBu})$_3$}] (R = NCS, N_3) also reacted with I_2, to yield [NiI{κ^3*SSS*-RB(mt^{tBu})$_3$] (R = NCS, N_3) complexes (Scheme 1.4).[50] The

aforementioned nickelboratrane reactivity highlights the application of hard-soft acid-base theory,[98] as the hardest co-ligand migrated towards the hard Lewis acid. Parkin and co-workers have also demonstrated this concept through the reactivity of the ferraboratrane $[Fe(CO)_2\{B(mt^{tBu})_3\}]$ with $CHCl_3$ and $CHBr_3$, forming $[FeX\{\kappa^3SSS\text{-}XB(mt^{tBu})_3\}]$ (X = Cl or Br, respectively), with benzoyl peroxide to provide $[Fe(O_2CPh)\{\kappa^3SSS\text{-}(PhCO_2)B(mt^{tBu})_3\}]$, or with $CHCl_3/I_2$ to yield $[FeI\{\kappa^3SSS\text{-}ClB(mt^{tBu})_3\}]$ (Scheme 1.5).[51]

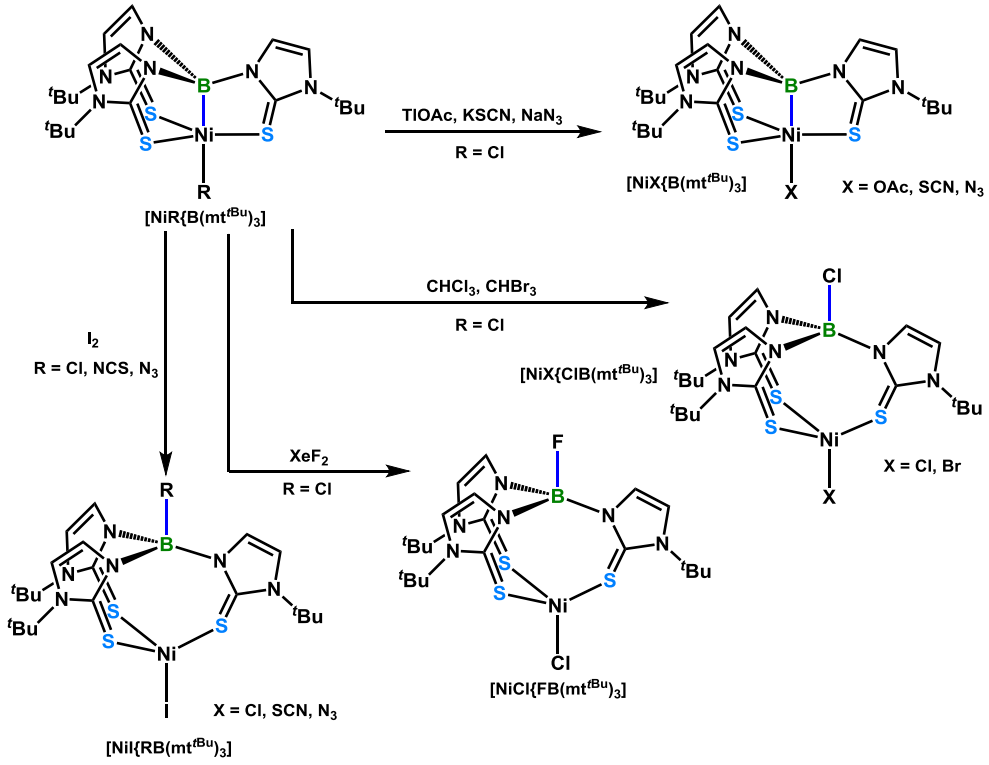

Scheme 1.4. Reactions of the nickelboratrane, $[NiR\{B(mt^{tBu})_3\}]$ (R = Cl, NCS, N_3), with various substrates.

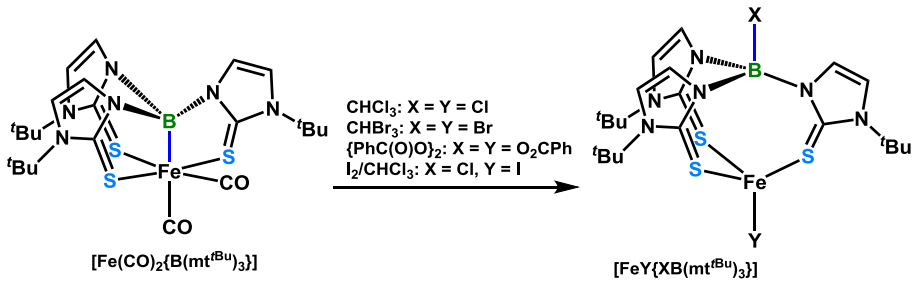

Scheme 1.5. Reactions of the ferraboratrane, $[Fe(CO)_2\{B(mt^{tBu})_3\}]$, with $CHCl_3$, $CHBr_3$, benzoyl peroxide and $I_2/CHCl_3$.

Connelly, Owen and Mösch-Zanetti embarked on the preparation of metallaboratrane complexes featuring alternative polyazolyl-donor groups flanking the central borane. Connelly utilized 5-sulfanyl-4-ethyl-3-methyl-1,2,4-triazolyl (taz) substituents (**A** in Figure 1.3), as well as a mixture of taz and 3,5-dimethylpyrazolyl (pz^{Me2}) substituents (**B** in Figure 1.3), and 2-sulfanyl-1-methylimidazolyl (mt^{Me}) and pz^{Me2} substituents (**C** in Figure 1.3) bound to boron; these ligands were used to prepare rhodium and iridium complexes exhibiting η^1*B*-coordination.[83-85,87,99] The $Na[HB(taz)_3]$ salt, which was used to access coordination of $B(taz)_3$, was prepared via reaction of 5-sulfanyl-4-ethyl-3-methyl-1,2,4-triazole with $Na[BH_4]$ in the melt at 175 °C to reduce the amount of $Na[H_2B(taz)_2]$ obtained.[85,100] Alternatively, $K[HB(taz)_2(pz^{Me2})]$ was prepared by reaction of $K[HB(pz^{Me2})_3]$ salt with 5-sulfanyl-4-ethyl-3-methyl-1,2,4-triazole in a sealed reaction vessel under static vacuum to a temperature of 125 °C for 90 minutes; the reaction was driven by sublimation of 3,5-dimethylpyrazole onto the colder portions of the reaction vessel.[84] $K[HB(mt^{Me})_2(pz^{Me2})]$ was prepared in a similar manner, except with the addition of 2-sulfanyl-1-methylimidazole, and with heating to 130 °C.[87] In all cases, the anionic borate was introduced to a chloride-containing metal pre-cursor, resulting in elimination of MCl (M = Na or K). The heteroscorpionate ligands $B(mt^{Me})_2(pz^{Me2})$ and $B(taz)_2(pz^{Me2})$ coordinated to the rhodium and iridium, respectively, via κ^3*SSB*-coordination of boron and the 2-sulfanyl-1-methylimidazolyl (mt^{Me}) and the 5-sulfanyl-4-ethyl-3-methyl-1,2,4-triazolyl (taz) substituents, respectively; the 3,5-dimethylpyrazolyl (pz^{Me}) subsitituent of each ligand remained uncoordinated to the metal.[84,87] Direct η^1*B*-coordination to the metal has also been achieved following oxidation of metal-

polyazolylborate complexes using $[FeCp_2][PF_6]$; treatment of $[Rh(CO)(PR_3)\{HB(taz)_3\}]$ (R = Ph, Cy, NMe_2) or $[Rh(CO)(PPh_3)\{HB(mt^{Me})_3\}]$ with $[FeCp_2][PF_6]$ in the presence of NEt_3 and NH^iPr_2, respectively, lead to the formation of κ^4*SSSB*-coordinated complexes $[Rh(CO)(PR_3)\{B(taz)_3\}]$ and $[Rh(PPh_3)\{B(mt^{Me})_3\}]$, respectively.[83,85,99] Alternatively, reaction of $K[HB(mt^{Me})_2(pz)]$ and $K[HB(mt^{Me})_2(pz^{Me2})]$ with $[\{Ir(\mu\text{-}Cl)(cod)\}_2]$ provided $[IrH(cod)\{B(mt^{Me})_2(pz)\}]$ and $[IrH(cod)\{B(mt^{Me})_2(pz^{Me2})\}]$, respectively, featuring κ^3*SSB*-coordination of boron and the 2-sulfanyl-1-methylimidazolyl substituents (the pyrazolyl substituent of each ligand remained uncoordinated to iridium). Treatment with CO lead to substitution of the cod ligand for two CO ligands, and subsequent addition of PR_3 (R = Ph, Cy) resulted in substitution of the CO ligand *trans* to boron for a PR_3 ligand.[87] Furthermore, reaction of $K[HB(taz)_2(pz^{Me2})]$ with $[\{Rh(\mu\text{-}Cl)(nbd)\}_2]$ provided $[Rh\{B(taz)_2(pz^{Me2})\}\{HB(taz)_2(pz^{Me2})\}]$ featuring κ^3*SSB*-coordination.[84]

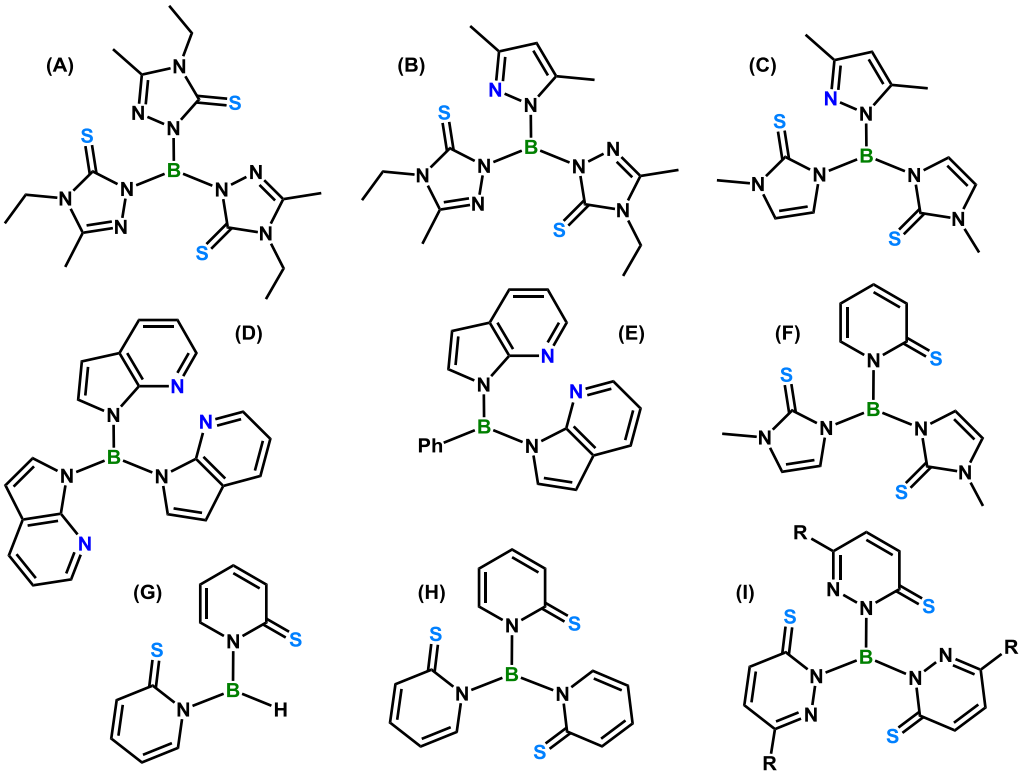

Figure 1.3. Various poly(azolyl)boranes deployed for the synthesis of transition metal complexes featuring η^1*B*-coordination. **A.** $B(taz)_3$, **B.** $B(taz)_2(pz^{Me2})$, **C**. $B(mt^{Me})_2(pz^{Me2})$, **D.** tai, **E.** bai^{Ph}, **F.** $B(mt^{Me})_2(mp)$, **G.** $HB(mp)_2$, **H.** $B(mp)_3$, **I.** $B(pn^R)$ (R = Me, ^{t}Bu, Ph).

Owen and co-workers initially utilized a polyazolylborane ligand derived from 7-azaindole, and introduced it to metal pre-cursors via the potassium borate salt, K[Htai] (tai = B(7-azaindolyl)$_3$; **D** in Figure 1.3). The K[Htai] salt was originally reported by Wang and co-workers, and was obtained via reaction of K[BH_4] with 7-azaindole at 180 °C in the melt.[101] In particular, Owen and co-workers examined hydride migration between the tris(7-azaindolyl)borate and a coordinated cod or nbd (nbd = 1,4-norbornadiene) ligand in novel iridaboratrane and rhodaboratrane complexes bearing the B(7-azaindolyl)$_3$ ligand.[88-90,92] The bis(7-azaindolyl)borane ligand, PhB(7-azaindolyl)$_2$ (bai^{Ph}, **E** in Figure 1.3), was also utilized by Owen *et al*. for this purpose, and was accessed via Li[Hbai^{Ph}] from reaction of lithium phenylborate, Li[$PhBH_3$], with 7-azaindole in refluxing toluene.[90]

Owen and co-workers also explored the utility of 2-sulfanylpyridyl substituents bound to boron; the B(mt^{Me})$_2$(mp) (mp = 2-sulfanylpyridyl; **F** in Figure 1.3) ligand was accessed from the Na[HB(mt^{Me})$_2$(mp)] salt, which was prepared by reaction of Na[H_2B(mt^{Me})$_2$] with 2-sulfanylpyridine in refluxing xylene;[93] reaction of Na[HB(mt^{Me})$_2$(mp)] with [RuRCl(CO)(PPh_3)$_2$] (R = H, CH=CH_2, CH=CHPh_2OH, CH=CH(C_6H_4Me-4) provided the ruthenaboratrane [Ru(CO)(PPh_3){B(mt^{Me})$_2$(mp)}] via alkene reductive elimination,[93] in a reaction analogous to that used by Hill *et al*. to prepare [Ru(CO)(PPh_3){B(mt^{Me})$_3$}] (Scheme 1.1, *vide supra*).[65]

Bis- and tris(2-sulfanylpyridyl)borane ligands have also been accessed from the corresponding sodium borate salts, Na[H_2B(mp)$_2$] (**G** in Figure 1.3) and Na[HB(mp)$_3$] (**H** in Figure 1.3), respectively; Na[H_2B(mp)$_2$] was prepared by reacting Na[BH_4] with 2-sulfanylpyridine in refluxing toluene for 12 hours, whereas Na[HB(mp)$_3$] was prepared via reaction of Na[BH_4] with 2-sulfanylpyridine in refluxing xylene for 48 hours.[102] The HB(mp)$_2$ ligand has been utilized to prepare rhodaboratrane, iridaboratrane, palladaboratrane and platinaboratrane complexes possessing κ^3*SSB*-coordination,[91,94] whereas the HB(mp)$_3$ ligand has been employed to prepare a novel palladaboratrane complex featuring κ^4*SSSB*-coordination.[91]

Finally, Mösch-Zanetti and co-workers published the synthesis of potassium tris(6-hydrocarbyl-3-sulfanylpyridazolyl)borate salts (**I** in Figure 1.3), in which the hydrocarbyl substituent is either a methyl, *tert*-butyl or a phenyl group. These salts were prepared by reacting $K[BH_4]$ with each respective sulfanylpyridazine between 150 and 170 °C in diphenylmethane,[95] and were deployed for the synthesis of cobalt, nickel[95] and copper[96] complexes featuring η^1*B*-coordination.

1.3 – Non-Poly(azolyl)borane-Containing Ambiphilic Ligands

Despite the success of the bis and tris(azolyl)borane ligands utilized above for the synthesis of transition metal–borane complexes, the requirement for *in situ* generation of the borane-containing ligand impacts the generality of this approach to metal–borane complex synthesis. Between 2006 and 2007, Bourissou and co-workers reported the synthesis and isolation of three phosphine/borane-containing ambiphilic ligand classes, displayed in Figure 1.4.[47,103,104] A large percentage of the recent research on transition metal phosphine/borane-containing ambiphilic ligand complexes has featured these three particular ligand classes with variations in the R and R' substituents bound to phosphorus and boron, respectively. These three classes of phosphine/borane ligand are defined as bidentate (**A** in Figure 1.4), tridentate (**B** in Figure 1.4) and tetradentate (**C** in Figure 1.4) phosphine/borane-containing ligands. Here-in, an overview of the use of phosphine/borane-containing ambiphilic ligands that fall under these three classes of ligand systems, and their use in the coordination chemistry of transition metals will be presented. Additionally, select examples of *in situ* generated phosphine/borane- and alternative Lewis base/borane-containing ligands will be discussed.

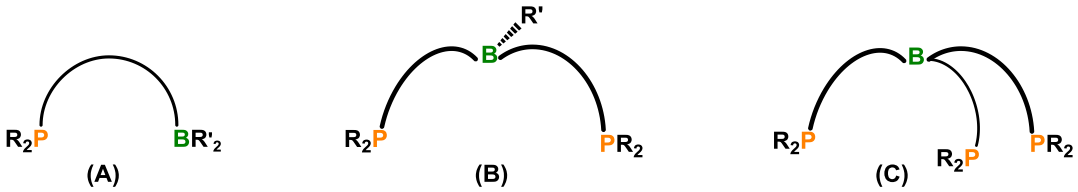

Figure 1.4. Schematic representation of a family of isolable phosphine/borane-containing ambiphilic ligands that has been prevalent in the literature from 2006 to-date.

1.3.1 – Transition Metal Complexes Featuring Bidentate Borane-Containing Ambiphilic Ligands

1.3.1.1 – Complexes of the (*o*-R_2P)$C_6H_4BR'_2$ (R = ^{i}Pr, Ph; BR'_2 = BCy_2, BFlu, $BMes_2$; BFlu = 9-borafluorenyl) Ligand

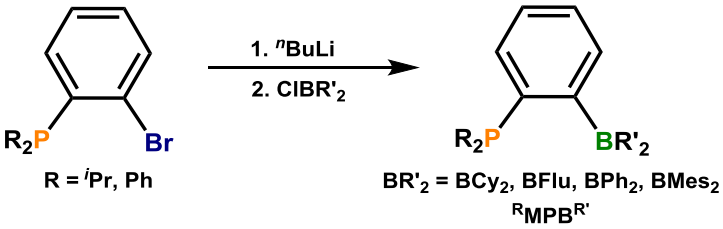

Scheme 1.6. Synthesis of the ^{R}MPB$^{R'}$ (^{R}MPB$^{R'}$ = (*o*-R_2P)$C_6H_4BR'_2$; R = ^{i}Pr, Ph; BR'_2 = BCy_2, BFlu, BPh_2, $BMes_2$) ligand.

Bourissou and co-workers in 2006 demonstrated the feasibility of preparing metal complexes featuring metal–borane coordination through the use of a κ^2*PB*-coordinated phosphine/borane ligand containing only a single donor group, (*o*-^{i}Pr$_2$P)$C_6H_4BR'_2$ (^{iPr}MPB$^{R'}$; BR'_2 = BCy_2, BFlu, BPh_2; Scheme 1.6). The ^{iPr}MPB$^{R'}$ ligand was prepared through reaction of one equivalent of (*o*-^{i}Pr$_2$P)C_6H_4Li with $ClBR'_2$, as shown in Scheme 1.6 above.[47] While the ^{iPr}MPB$^{R'}$ (BR'_2 = BCy_2, BFlu, $BMes_2$) ligands exist as monomers with no intramolecular P→B adduct formation in solution, the ^{iPr}MPB^{Ph} ligand does demonstrate intramolecular P→B adduction formation, as evidenced by ^{31}P and ^{11}B chemical shifts of 28.5 and 13.0 ppm, respectively;[105] the ^{31}P signal is shifted to higher frequency relative to free and uncoordinated aryldialkylphosphines, and the ^{11}B signal is shifted to lower frequency relative to triarylboranes. Bourissou and co-workers reported

on the reactivity of the $^{i\text{Pr}}$MPB$^{\text{Cy}}$ ligand with [AuCl(SMe$_2$)], which provided [AuCl($^{i\text{Pr}}$MPB$^{\text{Cy}}$)], and features κ^2*PB*-coordination of the MPB ligand (**A** in Scheme 1.7). Despite an Au–B bond length of 2.90 Å (r_α = 1.32),[68] which is shorter than the sum of the van der Waals radii (~3.7 Å),[68] a shift to higher frequency for the ^{11}B NMR signal relative to the free ligand (80 ppm vs. 76 ppm for the free ligand) and only marginal pyramidalization of boron [Σ(C–B–C) = 358.6°] indicate that the bonding interaction between gold(I) and boron is rather weak when the R' groups bound to boron are cyclohexyl substituents. However, when the Lewis acidity of the borane was increased through the use of 9-borafluorenyl group, a contraction in the Au–B bond length (2.66 Å; r_α = 1.21),[68] a shift to lower frequency for the ^{11}B NMR signal (55 ppm vs. 64.5 ppm in the free ligand) and an increase in the pyramidalization of boron [Σ(C–B–C) = 355.8°] was observed, indicating the presence of a stronger Au–B bonding interaction.[47]

Alternatively, reaction of $^{i\text{Pr}}$MPB$^{\text{Cy}}$ with half an equivalent of [{PdCl(η^3-allyl)}$_2$] provided [Pd(μ-Cl)(η^3-allyl)($^{i\text{Pr}}$MPB$^{\text{Cy}}$)], in which a chloride ligand is bridging between the metal and the pendant borane (**B** in Scheme 1.7); at the time this was the first report of a bridging M–Cl–B interaction involving the borane of an ambiphilic ligand. A B–Cl bond distance of 2.16 Å (r_α = 1.16)[68] in the solid-state structure of [Pd(μ-Cl)(η^3-allyl)($^{i\text{Pr}}$MPB$^{\text{Cy}}$)] indicates close approach of the chloride ligand to boron, and an ^{11}B chemical shift of 47 ppm verifies the presence of a B–Cl interaction in solution. Moreover, boron is substantially pyramidalized in the solid-state, with the sum of the C–B–C angles equal to 349.1°.[47]

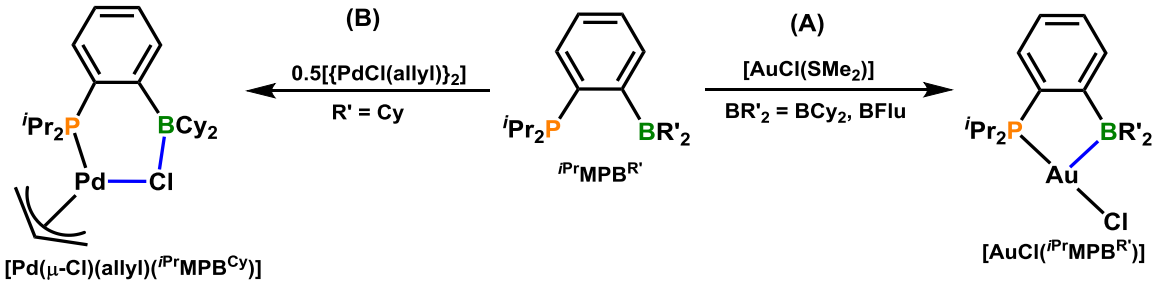

Scheme 1.7. Reaction of $^{i\text{Pr}}$MPB$^{\text{R}'}$ (BR'$_2$ = BCy$_2$, BFlu) with [AuCl(SMe$_2$)], or with [{PdCl(η^3-allyl)}$_2$] (R' = Cy) to form complexes that feature η^1*B*- and μ-Pd–Cl–B coordination, respectively.

Bourissou *et al*. also found that reaction of [Pd(μ-Cl)(η^3-allyl)($^{i\text{Pr}}$MPB$^{\text{Cy}}$)] with HCl afforded [{PdCl(μ-Cl)($^{i\text{Pr}}$MPB$^{\text{Cy}}$)}$_2$] (**A** in Figure 1.5), and subsequent reaction with PPh_3 provided monomeric *trans*-[PdCl(μ-Cl)(PPh_3)($^{i\text{Pr}}$MPB$^{\text{Cy}}$)] (**B** in Figure 1.5). Further, reaction of $^{i\text{Pr}}$MPB$^{\text{Cy}}$ with [{Rh(μ-Cl)(nbd)}$_2$] provided [Rh(μ-Cl)(nbd)($^{i\text{Pr}}$MPB$^{\text{Cy}}$)] (**C** in Figure 1.5); all three complexes feature κ^1*P*-coordination of the MPB ligand, in addition to a bridging M–Cl–$BArCy_2$ (M = Pd, Rh) bonding interaction. The [{PdCl(μ-Cl)($^{i\text{Pr}}$MPB$^{\text{Cy}}$)}$_2$] dimer possesses a B–Cl bond length of 2.334(7) Å (r_α = 1.26),[68] which is significantly elongated relative to the B–Cl bond length in [Pd(μ-Cl)(η^3-allyl)($^{i\text{Pr}}$MPB$^{\text{Cy}}$)]. In addition, boron is only slightly pyramidalized, with the sum of the C–B–C angles equal to 353.7°, indicating that Cl–$BArCy_2$ coordination is significantly weaker in [{PdCl(μ-Cl)($^{i\text{Pr}}$MPB$^{\text{Cy}}$)}$_2$]. On the other hand, *trans*-[PdCl(μ-Cl)(PPh_3)($^{i\text{Pr}}$MPB$^{\text{Cy}}$)] bears much tighter Cl–$BArCy_2$ coordination, with a B–Cl bond length of 2.109(4) Å (r_α = 1.13) and a Σ(C–B–C) value of 343.5°. The B–Cl bond length in [Rh(μ-Cl)(nbd)($^{i\text{Pr}}$MPB$^{\text{Cy}}$)] [2.117(2) Å; r_α = 1.14][68] more closely resembles that found in *trans*-[PdCl(μ-Cl)(PPh_3)($^{i\text{Pr}}$MPB$^{\text{Cy}}$)], and displays similar pyramidalization of boron [Σ(C–B–C) = 342.6°]. All three complexes evaded observation by solution-state ^{11}B NMR spectroscopy, however, *trans*-[PdCl(μ-Cl)(PPh_3)($^{i\text{Pr}}$MPB$^{\text{Cy}}$)] and [Rh(μ-Cl)(nbd)($^{i\text{Pr}}$MPB$^{\text{Cy}}$)] gave rise to signals at 22 and 26 ppm in their solid-state ^{11}B NMR spectra, respectively, corroborating the notion of strong Cl–$BArCy_2$ coordination as suggested from the X-ray crystallographic data.[49]

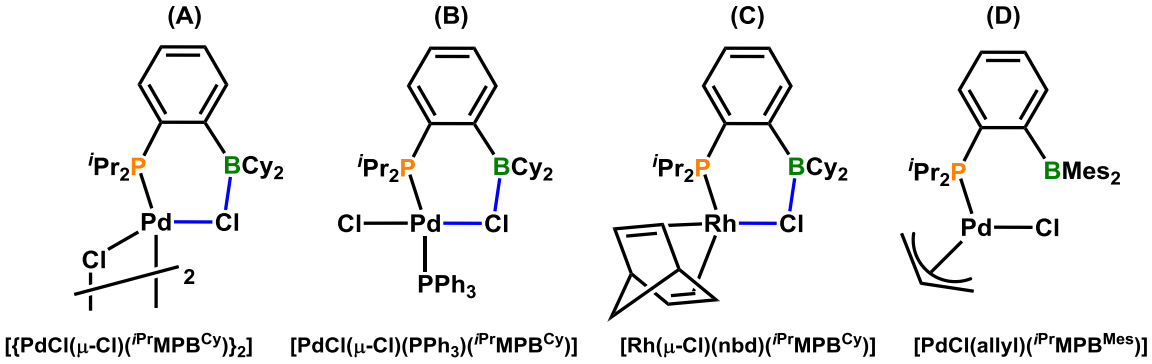

Figure 1.5. Palladium and rhodium complexes featuring μ-M–Cl–B coordination, or when the appended borane is $–BMes_2$, the non-existence of a μ-M–Cl–B interaction.

Alternatively, when the $^{i\text{Pr}}$MPB$^{\text{Mes}}$ ligand was deployed, which possesses mesityl groups bound to boron, as opposed to cyclohexyl substituents, no reaction occurred between $^{i\text{Pr}}$MPB$^{\text{Mes}}$ and [{Rh(μ-Cl)(nbd)}$_2$], and reaction with [{PdCl(η^3-allyl)}$_2$] lead to isolation of [PdCl(η^3-allyl)($^{i\text{Pr}}$MPB$^{\text{Mes}}$)] (**D** in Figure 1.5), which features κ^1*P*-coordination of the phosphine/borane ligand and a 3-coordinate pendant borane [B–Cl = 4.381(5) Å, Σ(C–B–C) = 358.9°, ^{11}B NMR solution-state = 73 ppm]. The lack of Cl–BAr$_3$ coordination was attributed to the greater steric hindrance imparted by mesityl substituents relative to cyclohexyl substituents.[49]

Aside from generating late transition metal complexes with bridging metal–chloride–borane interactions while utilizing bidentate phosphine/borane-containing ambiphilic ligands, Bourissou and co-workers found that reaction of the $^{i\text{Pr}}$MPB$^{\text{Ph}}$ ligand with CuCl provided [{CuCl($^{i\text{Pr}}$MPB$^{\text{Ph}}$)}$_2$], exhibiting κ^1*P*-coordination, in addition to η^3*BCC*-coordination of boron, *ipso*- and *ortho*-carbon atoms of a *B*-phenyl ring to copper (**A** in Scheme 1.8). At the time, metal complexes exhibiting η^n*BC*$_{n-1}$-interactions between a *B*-aryl group and the metal were rare, with the only prior reports stemming from the work of Emslie and co-workers in 2006 and 2008 in the synthesis of [(TXPB)Rh(μ-CO)$_2$Fe(CO)Cp], [Ni(TXPB)] and [Pd(TXPB)] (TXPB = 2,7-di-*tert*-butyl-5-diphenylboryl-4-diphenylphosphino-9,9-dimethylthioxanthene), and [CuCl($^{\text{Ph}}$DPB$^{\text{Ph}}$)] ($^{\text{Ph}}$DPB$^{\text{Ph}}$ = {(*o*-Ph$_2$P)C$_6$H$_4$}$_2$BPh) reported in 2010 by Bourissou (Sections 1.3.2.4 and 1.3.2.5).

[{CuCl($^{i\text{Pr}}$MPB$^{\text{Ph}}$)}$_2$] is a dimer that possesses two bridging Cu–Cl–Cu interactions between each copper centre. The Cu–B bond distance is 2.555(2) Å (r_α = 1.18),[68] and [{CuCl($^{i\text{Pr}}$MPB$^{\text{Ph}}$)}$_2$] gave rise to an ^{11}B NMR signal located at 58 ppm, which is shifted to significantly higher frequency relative to free $^{i\text{Pr}}$MPB$^{\text{Ph}}$ (5 ppm), however this was attributed to intramolecular adduct formation in free $^{i\text{Pr}}$MPB$^{\text{Ph}}$; the computed ^{11}B NMR chemical shift for free, non-adducted $^{i\text{Pr}}$MPB$^{\text{Ph}}$ is 61.8 ppm. The Cu–C$_{ipso}$ and Cu–C$_{ortho}$ bond distances are 2.339(2) (r_α = 1.14)[68] and 2.596(2) Å (r_α = 1.27),[68] but the ^{1}H and ^{13}C NMR spectra show equivalence of the –*B*Ph$_2$ groups, indicating that the *B*-phenyl rings are rapidly exchanging on the NMR time scale, either by dissociation

and re-coordination, or by η^n-slippage of copper. Alternatively, when the $^{i\text{Pr}}$MPB$^{\text{Cy}}$ ligand was employed, reaction with CuCl yielded [{Cu(μ-Cl)($^{i\text{Pr}}$MPB$^{\text{Cy}}$)}$_2$] (**B** in Scheme 1.8), in which the $^{i\text{Pr}}$MPB$^{\text{Cy}}$ ligand is κ^1*P*-coordinated to copper, and the two copper centres are bridged by chloro ligands. However, in this case there was no apparent bonding interaction involving the pendant borane and the copper centre, as evidenced by an ^{11}B NMR chemical shift of 82.5 ppm and a Cu–B bond distance of 3.05 Å.[105]

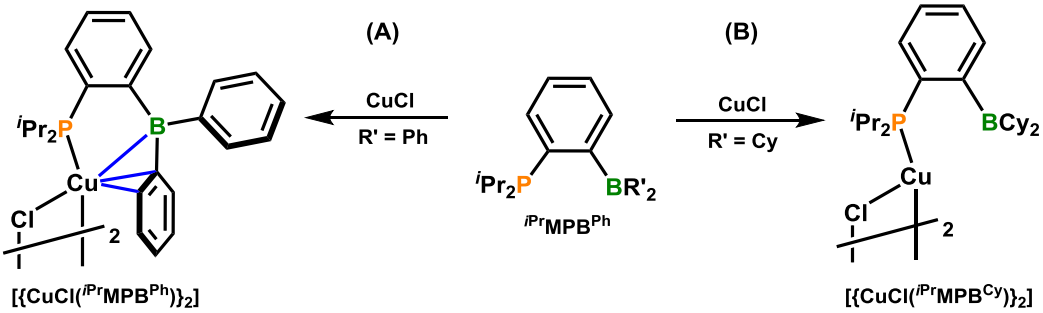

Scheme 1.8. Reactions of $^{i\text{Pr}}$MPB$^{\text{R'}}$ (R' = Ph, Cy) with CuCl.

Echavarren and Smirnova have also explored the coordination chemistry of the $^{\text{Ph}}$MPB$^{\text{R'}}$ ($^{\text{Ph}}$MPB$^{\text{R'}}$ = (*o*-Ph$_2$P)C$_6$H$_4$BR'$_2$; BR'$_2$ = B(OCH$_2$CMe$_2$CH$_2$O), BMes$_2$) ligand motif by preparing gold(I) complexes exhibiting coordination of the P/B-ligands.[106]

1.3.1.2 – Complexes Bearing the (2-picolyl)BCy$_2$ (2-picolyl = CH$_2$-py; py = *o*-NC$_5$H$_4$) Ligand

Bourissou and co-workers have also observed a metal–chloride–borane interaction in a ruthenium complex bearing the pyridine-borane ligand, (2-picolyl)BCy$_2$. The (2-picolyl)BCy$_2$ ligand was prepared by lithiation of 2-methylpyridine with ^{n}BuLi, followed with the addition of Cl–BCy$_2$, and exists as both a monomer and dimer in solution, with the dimer being the major species at room temperature and the monomer being the major species at elevated temperatures (**A** in Scheme 1.9).[48] Reaction of {(2-picolyl)BCy$_2$}$_2$ with [{RuCl(μ-Cl)(*p*-cymene)}$_2$] (*p*-cymene = 1-^{i}Pr-4-Me-C$_6$H$_4$) resulted in the formation of [RuCl(μ-Cl)(*p*-cymene){(2-picolyl)BCy$_2$}], which features κ^1*N*-coordination of the

pyridine-borane ligand and a bridging Ru–Cl–BR_3 interaction (R = alkyl substituent; **B** in Scheme 1.9). The B–Cl bond length is 2.103(9) Å (r_α = 1.13),[68] and the ^{11}B chemical shift is 22.2 ppm, which is in good agreement with the palladium and rhodium complexes *trans*-[PdCl(μ-Cl)(PPh$_3$)(^{iPr}MPB^{Cy})] and [Rh(μ-Cl)(nbd)(^{iPr}MPB^{Cy})], which exhibit strong chloride–borane interactions.[48]

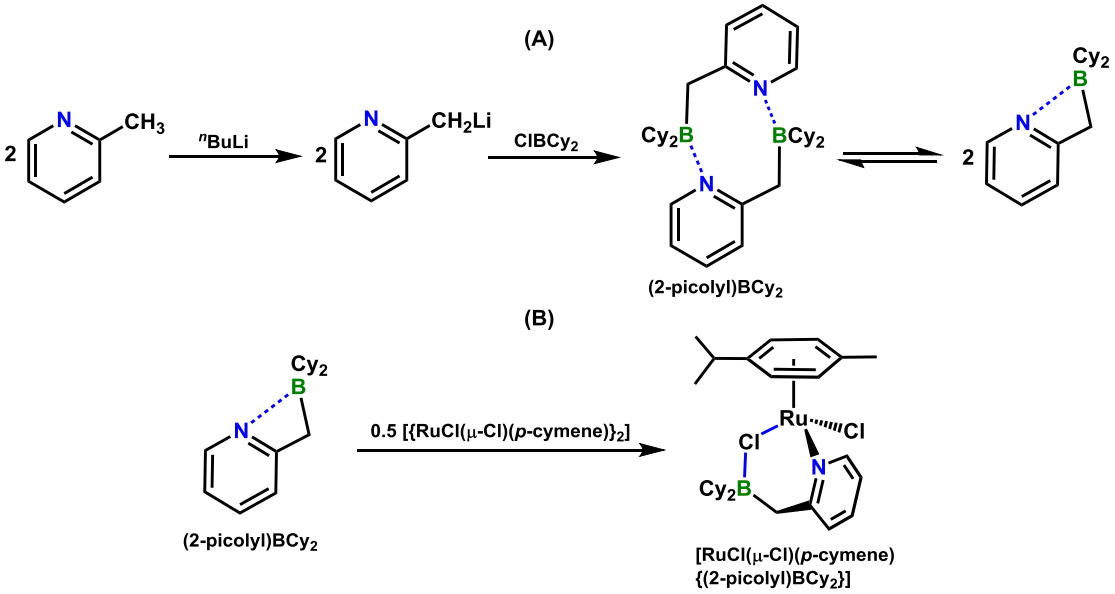

Scheme 1.9. A. Synthesis of the (2-picolyl)BCy_2 ligand, and **B.** reaction of (2-picolyl)BCy_2 with [{RuCl(μ-Cl)(*p*-cymene)}$_2$] to yield [RuCl(μ-Cl)(*p*-cymene){(2-picolyl)BCy_2}].

1.3.1.3 – Copper(I), Silver(I) and Palladium(II) Complexes of a 8-Quinolinylborane Ligand

Hoefelmeyer and co-workers reported the synthesis and coordination chemistry of 8-(dimesitylboryl)quinoline (^{Mes}BQuin) with Group 10 and 11 metals. The ^{Mes}BQuin ligand was prepared by lithiation of either 8-bromoquinoline or 8-iodoquinoline, followed with the addition of F–$BMes_2$ (Scheme 1.10).[107] Reaction of ^{Mes}BQuin with CuCl or AgOTf resulted in the formation of [{CuCl(^{Mes}BQuin)}$_2$] and [{AgOTf(^{Mes}BQuin)}$_2$], respectively (Scheme 1.10). Both complexes are dimers with bridging chloride or triflate ligands between the two metal centres, respectively, and also feature κ^1*N*- and η^3*BCC*-

coordination of the ^{Mes}BQuin ligand. Approach of boron and the *ipso*- and *ortho*-carbon atoms of a *B*-mesityl ring to copper and silver in [{CuCl(^{Mes}BQuin)}$_2$] and [{AgOTf(^{Mes}BQuin)}$_2$] was evidenced by Cu–B and Ag–B bond lengths of 2.660(3) (r_α = 1.23)[68] and 2.902(3) Å (r_α = 1.27),[68] Cu–C_{ipso} and Ag–C_{ipso} bond lengths of 2.126(2) (r_α = 1.04)[68] and 2.359(3) Å (r_α = 1.08),[68] and Cu–C_{ortho} and Ag–C_{ortho} bond lengths of 2.422(2) (r_α = 1.18)[68] and 2.596(3) Å (r_α = 1.19),[68] respectively. In addition, both complexes experience slight shifts in the ^{11}B NMR signal to lower frequency (69 and 72 ppm for the Cu and Ag complexes, respectively) relative to the free ligand (75 ppm), indicative of weak metal–borane coordination. Alternatively, the ^{Mes}BQuin ligand reacted with [$PdCl_2(PhCN)_2$], yielding monomeric [PdCl(^{Mes}BQuin^{CH2})] (^{Mes}BQuin^{CH2} = 8-{(2,4-Me_2-6-CH_2-C_6H_2)MesB}C_9H_6N), in which the quinoline backbone is κ^1*N*-coordinated to palladium, and a methyl group in one of the *B*-mesityl rings has undergone cyclometallation at palladium with loss of HCl, resulting in η^4*BCCC*-coordination of boron, the *ipso*- and *ortho*-carbon atoms, and the deprotonated –CH_2 group to palladium (Scheme 1.10). Significantly stronger metal–borane coordination is observed in the palladium(II) complex relative to the copper(I) and silver(I) complexes, as evidenced by a greater shift of the ^{11}B NMR signal to lower frequency (49 ppm) relative to the free ligand (75 ppm), and closer approach of boron to palladium (2.379(5) and 2.363(5) Å for two crystallographically independent molecules within the unit cell; r_α = 1.07 and 1.06, respectively).[68] Based on the C–C and B–C bond lengths within the coordinated *B*-mesityl ring, the observed η^4*BCCC*-coordination in [PdCl(^{Mes}BQuin^{CH2})] is consistent with η^3*CCC*-allyl coordination with a Pd–B dative bond.[107]

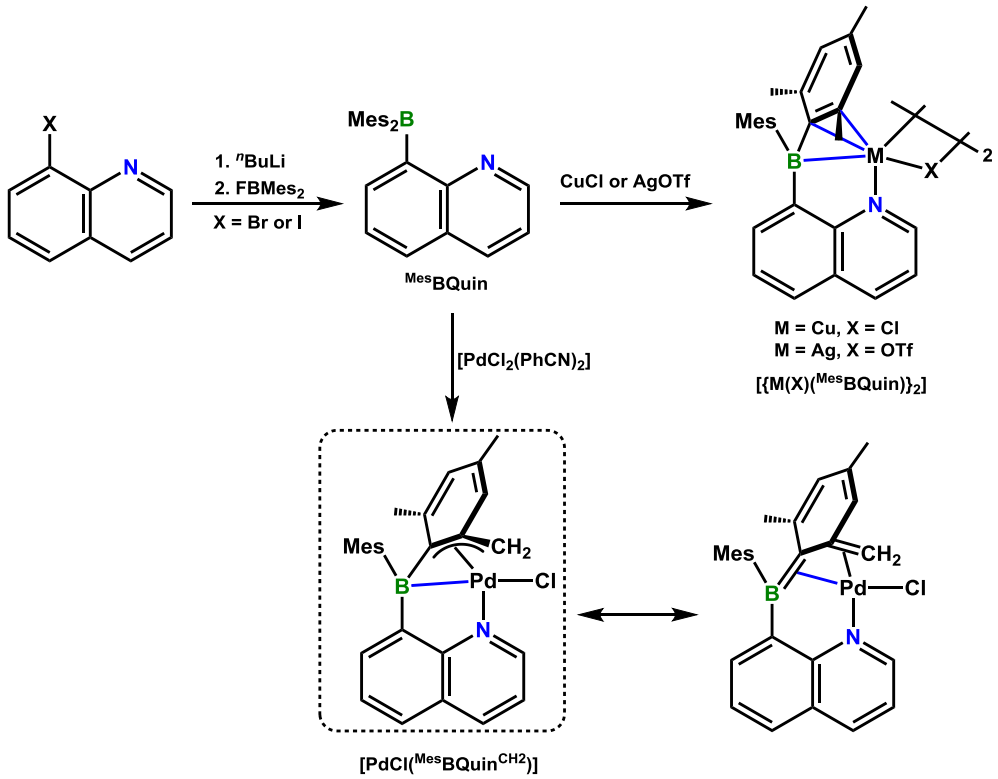

Scheme 1.10. Synthesis of the ^{Mes}BQuin ligand and subsequent reactivity with CuCl, AgOTf and $[PdCl_2(PhCN)_2]$.

1.3.1.4 – Complexes Bearing $Ph_2P(CH_2)_2BR'_2$ (BR'_2 = BCy_2, 9-BBN, $B(C_6F_5)_2$) Ligands

Bourissou and Tilley sought to explore the coordination chemistry of phosphine/borane-containing bidentate ligands that possess increased ligand flexibility relative to the *ortho*-phenylene linker that has been utilized in the $(o\text{-}R_2P)C_6H_4BR'_2$ (R = ^{i}Pr, Ph; BR'_2 = BCy_2, BFlu, $BMes_2$; *vide supra*) ligands, and simultaneously reported on the synthesis of $Ph_2P(CH_2)_2BR'_2$ (BR'_2 = BCy_2, 9-BBN; 9-BBN = 9-borabicyclo[3.3.1]nonanyl) (Scheme 1.11). Bourissou and co-workers were able to isolate the $Ph_2P(CH_2)_2BCy_2$ and $Ph_2P(CH_2)_2$-9-BBN ligands by regioselective hydroboration of vinyldiphenylphosphine with $\{HBCy_2\}_2$ or $\{H\text{-}9\text{-}BBN\}_2$ after one hour in THF at room temperature, or after 10 hours in THF at 60 °C, respectively. Reaction of $Ph_2P(CH_2)_2BR'_2$ (BR'_2 = BCy_2, 9-BBN) with $[\{RuCl(\mu\text{-}Cl)(p\text{-cymene})\}_2]$ provided $[RuCl_2(p\text{-}$

cymene){$Ph_2P(CH_2)_2BR'_2$}] complexes, in which only κ^1*P*-coordination of the phosphine/borane ligand was observed (Scheme 1.11); the pendant borane remained free and uncoordinated to either the metal or a metal co-ligand, as evidenced by ^{11}B chemical shifts of 81.7 and 86.3 ppm for the $–CH_2BCy_2$ and $–CH_2$-9-BBN boranes, respectively. In attempts to abstract chloride co-ligands from ruthenium, Bourissou and co-workers reacted [$RuCl_2$(*p*-cymene){$Ph_2P(CH_2)_2BR'_2$}] with $AgBF_4$ and AgOAc; in both cases chloride abstraction was achieved, forming AgCl. Reaction with $AgBF_4$ in acetonitrile provided the expected cationic product, [RuCl(MeCN)(*p*-cymene){$Ph_2P(CH_2)_2BR'_2$}][BF_4], whereas reaction with AgOAc yielded [RuCl(κ^2*PC*-$CH_2CH_2PPh_2$)(*p*-cymene)], the product of borane elimination to form the four-membered metallocycle (Scheme 1.11). Addition of $Cl–BCy_2$ to [RuCl(κ^2*PC*-$CH_2CH_2PPh_2$)(*p*-cymene)] regenerated [$RuCl_2$(*p*-cymene){$Ph_2P(CH_2)_2BCy_2$}] either by σ-bond metathesis, or by electrophilic addition of $Cl–BCy_2$ to ruthenium with concomitant cleavage of the Ru–C bond and transfer of chloride to ruthenium. Alternatively, heating a mixture of $Cl–AlEt_2$ and [RuCl(κ^2*PC*-$CH_2CH_2PPh_2$)(*p*-cymene)] to 50 °C for 24 hours resulted in substitution of the chloride ligand for an ethyl ligand to afford [RuEt(κ^2*PC*-$CH_2CH_2PPh_2$)(*p*-cymene)] (Scheme 1.11).[108]

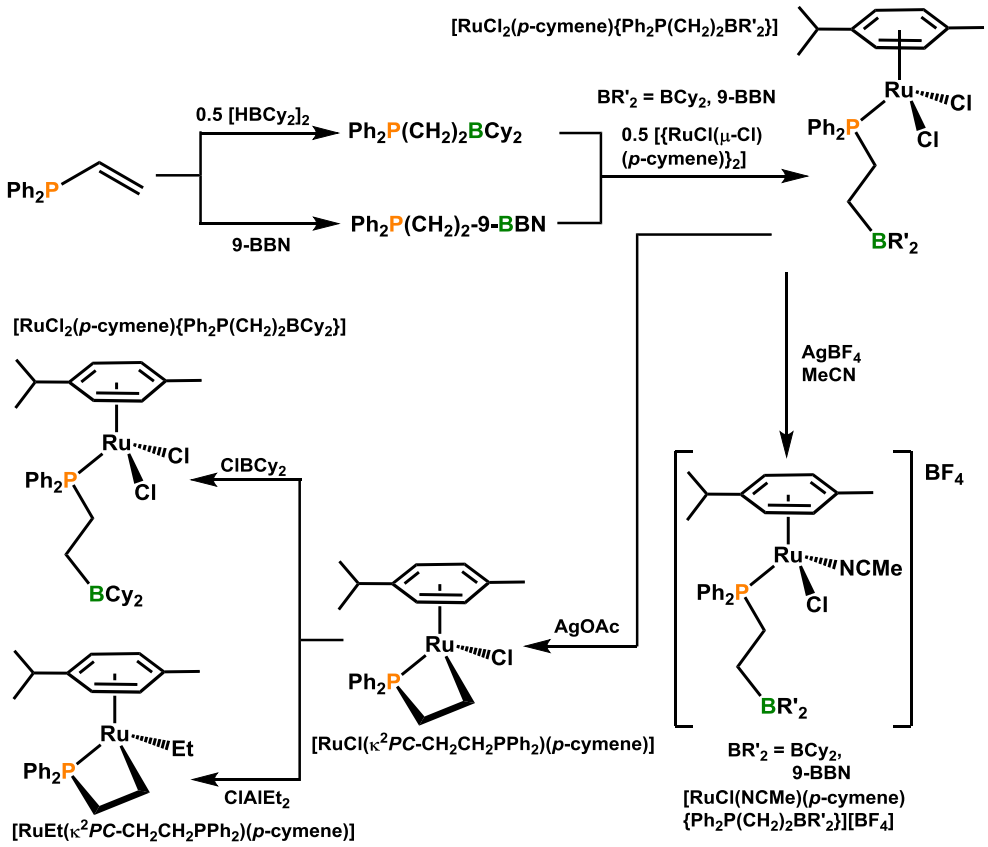

Scheme 1.11. Synthesis of the $Ph_2P(CH_2)_2BR'_2$ (BR'_2 = BCy_2, 9-BBN) ligands, reported by Bourissou, and subsequent reactivity stemming from $[RuCl_2(p\text{-cymene})\{Ph_2P(CH_2)_2BR'_2\}]$.

Contrary to the procedure reported by Bourissou *et al.* for the synthesis of the $Ph_2P(CH_2)_2BR'_2$ (BR'_2 = BCy_2, 9-BBN) ligands, Tilley and co-workers performed the hydroborations in toluene due to undesired side reactions that took place during the hydroboration of vinyldiphenylphosphine with $\{H\text{-}9\text{-}BBN\}_2$ in THF, generating P–B bonded compounds with loss of ethylene. Moreover, Tilley was able to achieve hydroboration of vinyldiphenylphosphine with $\{H\text{-}9\text{-}BBN\}_2$ in a much shorter period of time, requiring only 3 hours at 60 °C.[54]

As opposed to exploring the reactivity of these ligands with halide-containing transition metal pre-cursors, Tilley chose to explore their reactivity with $[NiMe_2(dmpe)]$ (dmpe = 1,2-bis(dimethylphosphino)ethane). Reaction of the $Ph_2P(CH_2)_2BR'_2$ ligands with $[NiMe_2(dmpe)]$ provided zwitterionic $[NiMe\{Ph_2P(CH_2)_2BR'_2Me\}(dmpe)]$, in which

the $Ph_2P(CH_2)_2BR'_2$ ligand was κ^1*P*-coordinated to nickel, and the pendant borane has abstracted a methyl ligand from nickel, generating a cationic metal centre (Scheme 1.12). While the addition of a second equivalent of $Ph_2P(CH_2)_2BR'_2$ ligand did not result in displacement of dmpe with abstraction of the second methyl ligand, addition of $B(C_6F_5)_3$ to [NiMe{$Ph_2P(CH_2)_2BR'_2Me$}(dmpe)] provided cationic [NiMe{$Ph_2P(CH_2)_2BCy_2$}(dmpe)][$MeB(C_6F_5)_3$], in which the more Lewis acidic borane has abstracted the methyl group from the less Lewis acidic $–CH_2BCy_2$ borane (Scheme 1.12).[54]

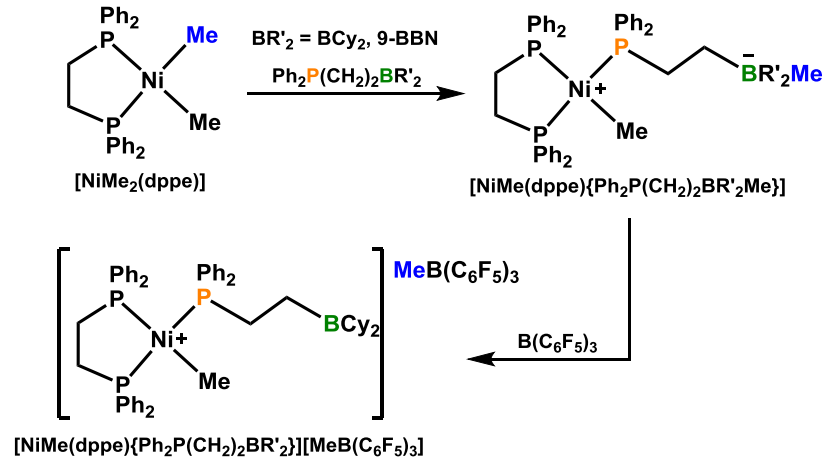

Scheme 1.12. Reaction of $Ph_2P(CH_2)_2BR'_2$ (BR'_2 = BCy_2, 9-BBN) with [$NiMe_2$(dppe)], followed by reaction with $B(C_6F_5)_3$.

Erker and co-workers have also shown that the $Mes_2P(CH_2)_2B(C_6F_5)_2$ ligand, previously reported by Stephan *et al.*, was capable of alkyl group abstraction from a metal centre; $Mes_2P(CH_2)_2B(C_6F_5)_2$ was prepared via hydroboration of vinyldimesitylphosphine (prepared from chlorodimesitylphosphine and vinylmagnesium bromide) with $HB(C_6F_5)_2$.[109] Reaction of $Mes_2P(CH_2)_2B(C_6F_5)_2$, which exists as an intramolecular P→B adduct in solution,[109] with [Cp_2ZrMe_2] provided zwitterionic [Cp_2ZrMe{$Mes_2P(CH_2)_2B(C_6F_5)_2Me$}], in which the pendant borane has abstracted a methyl ligand and the resulting phosphine/borate ligand is κ^1*P*-coordinated to zirconium. Alternatively, reaction of $Mes_2P(CH_2)_2B(C_6F_5)_2$ with [$Cp^*_2ZrMe_2$] yielded the tight ion pair [Cp^*_2ZrMe][$Me(C_6F_5)_2B(CH_2)_2PMes_2$], which possesses a bridging $Zr---CH_3–B$

interaction (Scheme 1.13). The discrepancy in coordination modes of the $Mes_2P(CH_2)_2B(C_6F_5)_2$ ligand to the two different zirconium fragments is attributed to the additional steric bulk provided by the Cp*-rings, which deters coordination of the sterically bulky dimesitylphosphine group.[56]

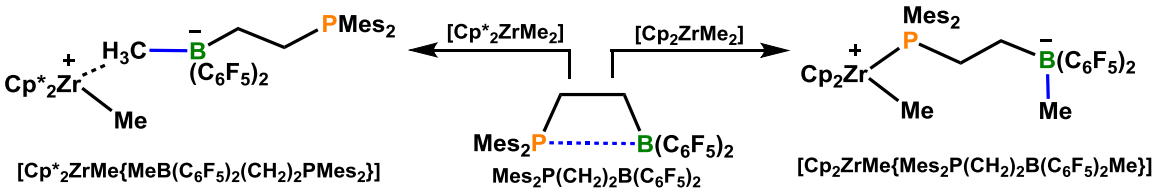

Scheme 1.13. Reactivity of $Mes_2P(CH_2)_2B(C_6F_5)_2$ with $[Cp_2ZrMe_2]$ and $[Cp^*_2ZrMe_2]$.

Bercaw and co-workers sought to utilize the $Ph_2P(CH_2)_2$-9-BBN ligand to effect functionalization of carbonyl co-ligands bound to transition metal pre-cursors. More specifically, Bercaw and co-workers targeted the potential for hydride and/or alkyl migration onto CO, thus forming new C–H and C–C bonds. *In situ* hydroboration was required in order to install the $Ph_2P(CH_2)_2$-9-BBN ligand onto a rhenium centre; reaction of $[ReBr(CO)_3(Ph_2PC_2H_3)_2]$ with $AgBF_4$ under a CO atmosphere provided cationic $[Re(CO)_4(Ph_2PC_2H_3)_2][BF_4]$, which readily reacted with $\{H\text{-}9\text{-}BBN\}_2$ to provide the target complex, $[Rh(CO)_3\{Ph_2P(CH_2)_2\text{-}9\text{-}BBN\}_2][BF_4]$ (**I**) (Scheme 1.14).[64]

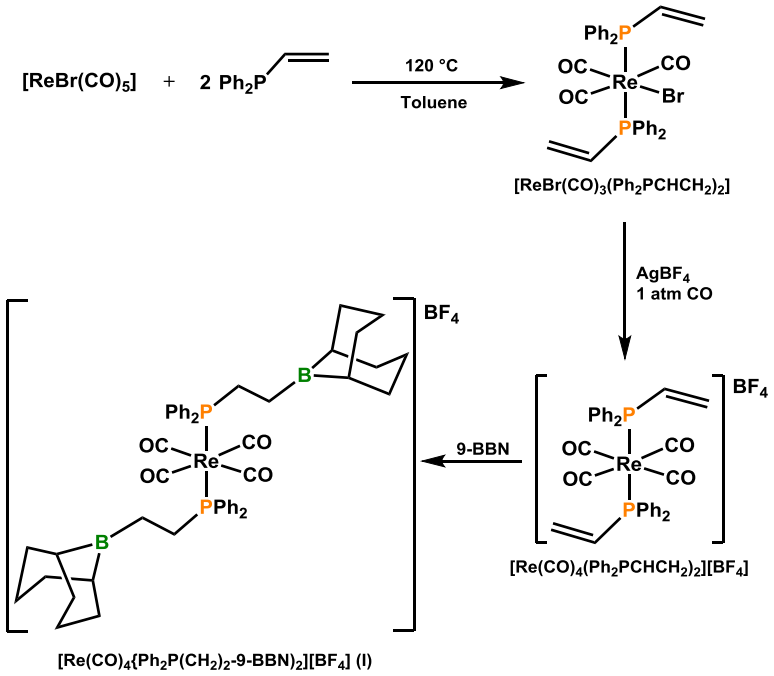

Scheme 1.14. Synthesis of $[Re(CO)_4\{Ph_2P(CH_2)_2\text{-}9\text{-}BBN\}_2][BF_4]$ (**I**) from $[Re(CO)_4(Ph_2PC_2H_3)_2][BF_4]$ and H-9-BBN via *in situ* hydroboration.

Complex **I** reacted with $[HPt(dmpe)_2][PF_6]$ (dmpe = 1,2-bis(dimethylphosphino)ethane) to provide $[Re(CO)_3\{C(H)\text{-}O\text{-}(9\text{-}BBN)\text{-}(CH_2)_2PPh_2\}\{Ph_2P(CH_2)_2\text{-}9\text{-}BBN\}]$ (**II**), the product of 1,1-insertion of one hydride equivalent onto CO, and formation of a boratoxycarbene (Scheme 1.15). The reactivity stands in stark contrast to the lack of reactivity observed between $[Re(CO)_4(PPh_3)_2]^+$ and $[HPt(dmpe)_2][PF_6]$ in the presence of BEt_3. Complete conversion of **I** to **II** was also achieved through the use of $NaHBEt_3$ in place of $[HPt(dmpe)_2][PF_6]$.[64]

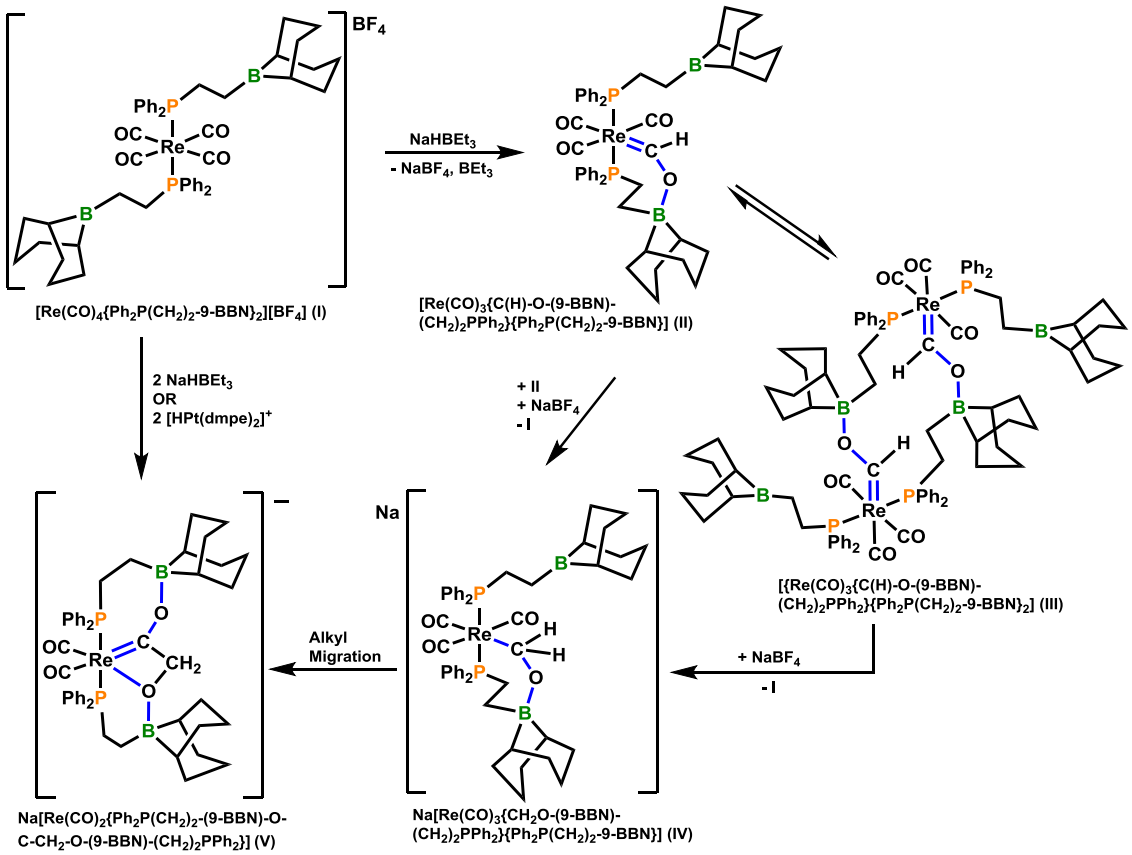

Scheme 1.15. Reactivity of complex **I** with either $[HPt(dmpe)_2][PF_6]$ or $NaHBEt_3$, resulting in hydride and alkyl migration onto CO.

When left for days at room temperature, or when complex **I** was treated with $NaHBEt_3$ in CD_2Cl_2, decomposition of **II** and formation of the dimerized complex, $[\{Re(CO)_3\{C(H)\text{-}O\text{-}(9\text{-}BBN)\text{-}(CH_2)_2PPh_2\}\{Ph_2P(CH_2)_2\text{-}9\text{-}BBN\}_2]$ (**III**) occurred, which features C–O–B boratoxycarbene linkages, this time involving the pendant borane of another rhenium unit (Scheme 1.15). All attempts to obtain X-ray quality crystals provided $[Re(CO)_2\{Ph_2P(CH_2)_2\text{-}(9\text{-}BBN)\text{-}O\text{-}C\text{-}CH_2\text{-}O\text{-}(9\text{-}BBN)\text{-}(CH_2)_2PPh_2\}]^-$ (**V**), a boratoxy(boratoxymethyl)carbene complex generated via 1,1-insertion of an alkyl group onto CO (Scheme 1.15). Bercaw *et al.* proposed that formation of **V** takes place through migratory insertion of an alkyl ligand in unobserved intermediate **IV**, $Na[Re(CO)_3\{CH_2O\text{-}(9\text{-}BBN)\text{-}(CH_2)_2PPh_2\}\{Ph_2P(CH_2)_2\text{-}9\text{-}BBN\}]$, which possesses boratoxymethyl-coordination to rhenium (Scheme 1.15). The formation of complex **IV**

could occur via conversion of **III** into **IV** and **I** by intramolecular hydride transfer. Complex **V** may also be accessed more straightforwardly by reaction of **I** with either two equivalents of $NaHBEt_3$ or $[PtH(dmpe)_2][PF_6]$; the latter is particularly intriguing since $[PtH(dmpe)_2][PF_6]$ is pre-formed via reaction of $[Pt(dmpe)_2]^{2+}$ with H_2 in the presence of either KOPh or tetramethylguanidine, thus enabling the synthesis of a new C_2-unit coordinated to rhenium from CO and H_2, the components of syngas.[64] Unfortunately, $[HPt(dmpe)_2][PF_6]$ is typically formed in acetonitrile, which forms a strong adduct with the pendant borane moiety of the $Ph_2P(CH_2)_2$-9-BBN ligand, shutting down insertion reactivity. However, it was hypothesized that a base of sufficient basicity and steric bulk to allow for the formation of $[HPt(dmpe)_2][PF_6]$ but not participate in strong adduct formation with the borane moiety could enable the aforementioned platinum complex to be used as a catalyst in the presence of H_2 to provide complex **V**, as shown in Scheme 1.16 below.[110]

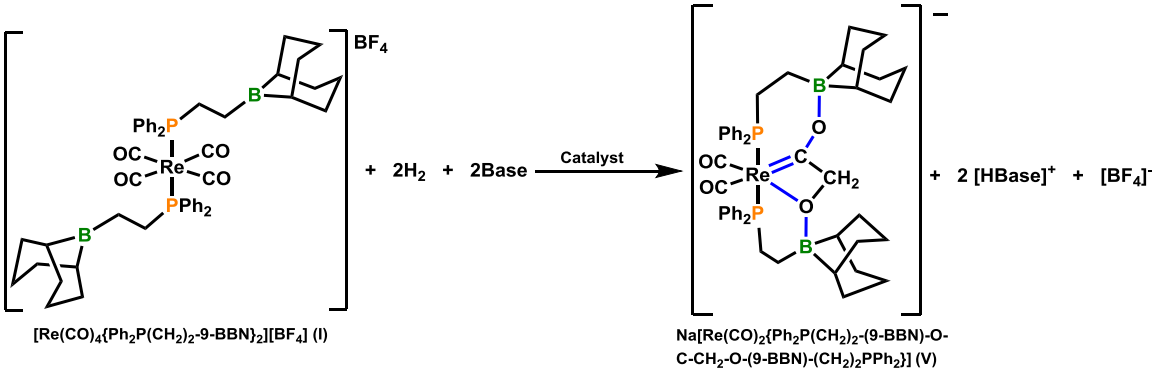

Scheme 1.16. Potential formation of **V** from **I** and H_2 under catalytic conditions.

Bercaw and co-workers opted for ^{t}BuNP(pyrrolidinyl)$_3$ (pyrrolidinyl = NC_4H_8) as an appropriate base, as well as swapping out the typically used $[PF_6]^-$ anion with $[Pt(dmpe)_2]^{2+}$ for the $[BAr^F{}_4]^-$ anion (Ar^F = 3,5-$(CF_3)_2$-C_6H_3) to ensure solubility of regenerated $[Pt(dmpe)_2][BAr^F{}_4]_2$. However, they determined that the high solubility of $[Pt(dmpe)_2][BAr^F{}_4]_2$ inhibited catalytic reactivity, and rather, FLP chemistry involving ^{t}BuNP$(NC_4H_8)_3$ and the pendant borane in **I** was the culprit for heterolytic H_2 cleavage,

generating $[Re(CO)_4\{Ph_2P(CH_2)_2\text{-}9\text{-}BBN\}\{Ph_2P(CH_2)_2\text{-}H\text{-}9\text{-}BBN\}]$ (**VI**) and $[^tBu(H)NP(NC_4H_8)_3]^+$ (Scheme 1.17); prior observation of the synthesis of **V** from $[HPt(dmpe)_2][PF_6]$ was driven by precipitation of $[Pt(dmpe)_2][PF_6]_2$ from solution. Complex **VI** then engages in hydride transfer to a CO co-ligand, generating **III**, which may undergo ligand redistribution to yield complex **V** and regenerate **I**, or undergo a second FLP-mediated hydride transfer process involving the second appended borane, generating $2[^tBu(H)NP(NC_4H_8)_3][\mathbf{V}]$ (Scheme 1.17). Increasing the concentration of $^tBuNP(NC_4H_8)_3$ resulted in an increase in reaction rate for the formation of **V**, and the C–C coupling reactivity observed in the formation of **V** did not occur in the absence of an appended borane within rhenium complex **I**.[110] Bercaw and co-workers have also explored the reactivity of rhenium complexes bearing the $Ph_2P(CH_2)_n$-9-BBN (n = 1 and 3) ligand motif, as well rhenium complexes coordinated by either one or two equivalents of $Ph_2P(CH_2)_n$-9-BBN (n = 1-3) for hydride/alkyl migration to CO co-ligands.[63]

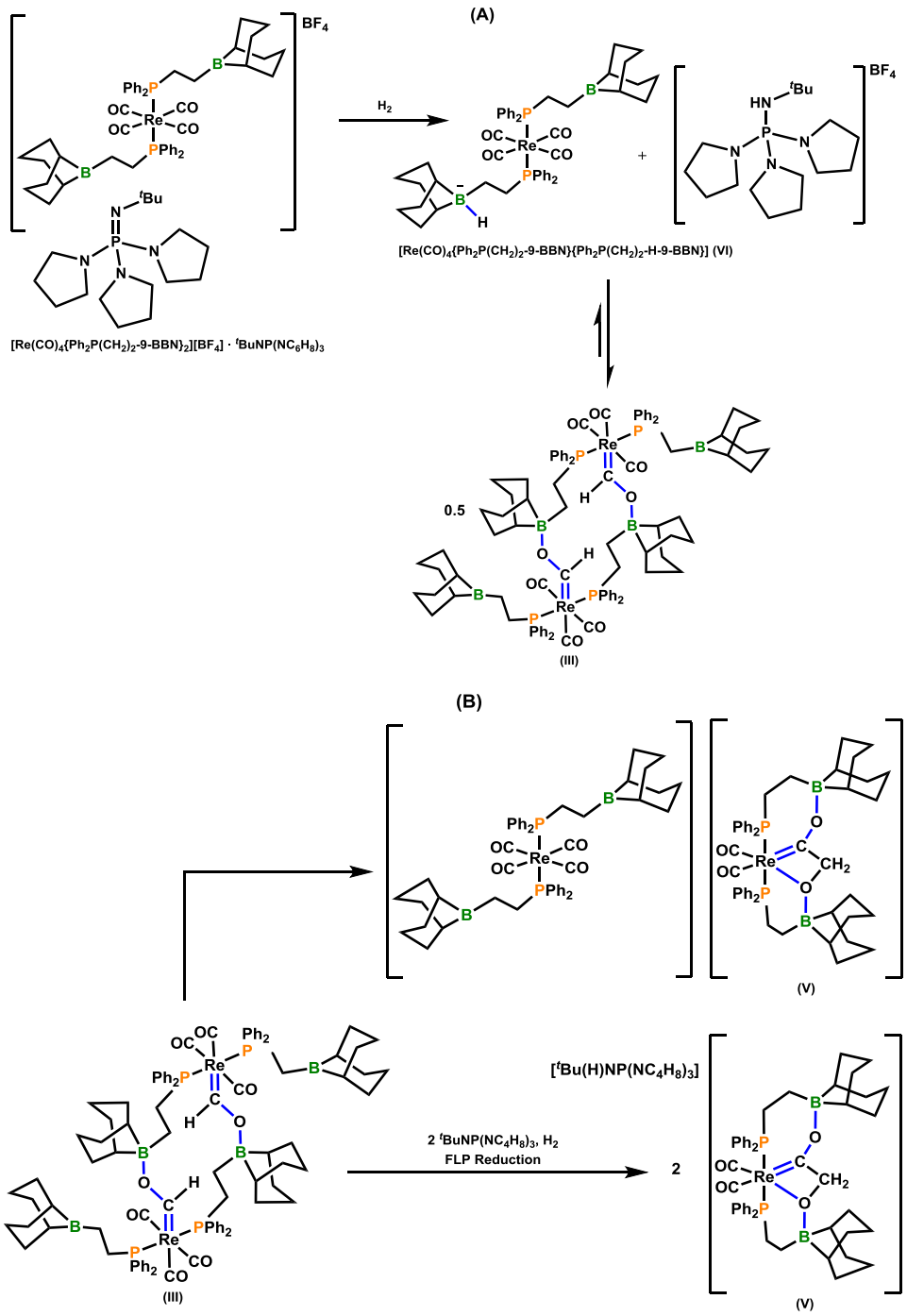

Scheme 1.17. Formation of **V** by FLP reduction brought about by **I** and ^{t}BuNP(NC$_4$H$_8$)$_3$.

Klankermayer and co-workers have utilized the $Ph_2P(CH_2)_2BR'_2$ (BR'2 = 9-BBN, $B(C_6F_5)_2$) ligands in ruthenium chemistry, but with the objective being to from bridging Ru–H–B bridging interactions;[111] The $Ph_2P(CH_2)_2$-9-BBN ligand was isolated according to the literature procedures of Bourissou and Tilley, and reaction with *in situ* generated $[CpRuH(CO)_2]$ in refluxing *n*-heptane provided $[CpRuH(CO)\{Ph_2P(CH_2)_2\text{-9-BBN}\}]$ (Scheme 1.18). The solid-state structure of $[CpRuH(CO)\{Ph_2P(CH_2)_2\text{-9-BBN}\}]$ verified the presence of a bridging Ru–H–B interaction, with B–H and Ru–H bond distances of 1.52(6) and 1.59(5) Å (r_α = 1.32 and 0.90),[68] respectively. However, in the solution-state the bridging Ru–H–B bonding interaction is only apparent below –50 °C, since at higher temperatures the sharp hydride signals at –13.88 and –13.90 ppm in the ^{1}H NMR spectrum converge into a broad singlet at –16.2 ppm ($\omega_{1/2}$ = 47 Hz). Klankermayer and co-workers were unable to utilize the isolated $Ph_2P(CH_2)_2B(C_6F_5)_2$ ligand due to very strong P→B adduct formation, so they generated the ligand on ruthenium via the reaction of $HB(C_6F_5)_2$ with $[(\eta^5\text{-}C_5R_5)Ru(CO)(Ph_2P\text{–}CH{=}CH_2)]$ (R = H, Me). The resulting $[(\eta^5\text{-}C_5R_5)Ru(\mu\text{-}H)(CO)\{Ph_2P(CH_2)_2B(C_6F_5)_2\}]$ (R = H, Me) complexes possessed bridging Ru–H–B bonding interactions that were maintained at room temperature in the solution-state, giving rise to broadened hydride signals at –15.4 and –13.9 ppm in their respective ^{1}H NMR spectra, and singlets located at –4.2 and –4.1 ppm in their respective ^{11}B NMR spectra (Scheme 1.18). The B–H and Ru–H bond lengths in $[(\eta^5\text{-}C_5R_5)Ru(\mu\text{-}H)(CO)\{Ph_2P(CH_2)_2B(C_6F_5)_2\}]$ (R = H, Me) are 1.43(6) (r_α = 1.24)[68] and 1.60(6) Å, and 1.41(3) (r_α = 1.23)[68] and 1.68(2) Å, respectively.[111]

Baker and co-workers were also able isolate complexes featuring a bridging M–H–BR_3 interaction via treatment of an η^2*PC*-coordinated $Me_2PCH_2^-$ ligand (bound to ruthenium or osmium) with thexylborane $[\{BH(\mu\text{-}H)(CMe_2CHMe_2)\}_2]$ or $\{H\text{-}9\text{-}BBN\}_2$.[112]

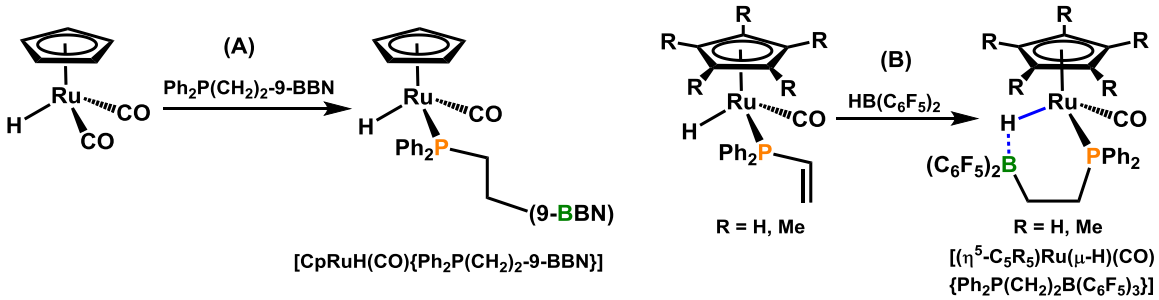

Scheme 1.18. A. Reaction of *in situ* generated $[CpRuH(CO)_2]$ with $Ph_2P(CH_2)_2$-9-BBN, and **B.** reaction of $[(\eta^5\text{-}C_5R_5)RuH(CO)(Ph_2PCHCH_2)]$ (R = H, Me) with $HB(C_6F_5)_2$ for *in situ* generation of the PB-ligand.

Berke and co-workers have also utilized the $Ph_2P(CH_2)_2$-9-BBN ligand, in addition to the tridentate bisphosphine/borane ligands $Ph_2PCH(PPh_2)CH_2$-9-BBN and $Ph_2PCH_2CH(9\text{-BBN})PPh_2$, to prepare tungsten complexes featuring bridging W–H–BR_3 (R = alkyl substituents) interactions.[113] Additionally, Crossley and co-workers expanded the coordination chemistry of the $Ph_2P(CH_2)_2$-9-BBN and $Fu_2P(CH_2)_2$-9-BBN (Fu = 2-furyl) ligands to rhodium(I), iridium(III), palladium(II) and platinum(II), but were only able to isolate complexes in which the pendant borane remained uncoordinated to both the metal and the co-ligands.[114]

1.3.1.5 – Nickel Complexes Featuring a Phosphino-Alkynyl-Borane Ligand

In 2010, Stephan and co-workers reported the synthesis and coordination chemistry of the phosphino-alkynyl-borane ligand, $^t Bu_2P\text{–}C\equiv C\text{–}B(C_6F_5)_2$, which was prepared from the phosphinoalkyne $^t Bu_2PC\equiv CH$ according to Scheme 1.19 below. Although isolation of $^t Bu_2P\text{–}C\equiv C\text{–}B(C_6F_5)_2$ proved troublesome due to its proclivity for decomposition, *in situ* generation followed by the addition of $[Ni(cod)_2]$ resulted in the formation of $[Ni(cod)\{^t Bu_2P\text{–}C\equiv C\text{–}B(C_6F_5)_2\}]$ (Schemes 1.19 and 1.20).[43]

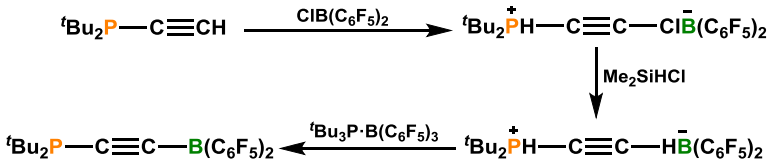

Scheme 1.19. Synthesis of the $^{t}Bu_2PC{\equiv}CB(C_6F_5)_2$ ligand.

X-ray diffraction on the nickel complex elucidated the coordination mode of the phosphino-alkynyl-borane ligand as η^3*BCC*-coordination via boron and the α- and β-carbon atoms of the alkyne fragment. The C≡C bond length was 1.254(4) Å, which is elongated relative to a carbon–carbon triple bond, and the C≡C stretching band was located at 1881 cm^{-1}, down from 2125 cm^{-1} in the free ligand; both pieces of data indicate significant π-backdonation into the alkynyl fragment. [Ni(cod){$^{t}Bu_2P$–C≡C–$B(C_6F_5)_2$}] also possessed a short Ni–B bond distance [2.358(3) Å; r_α = 1.13],[68] and nickel–borane coordination was made apparent by elongation of the Ni–C bond lengths for the η^2*CC*-coordinated cod ligand *trans* to the coordinated borane, highlighting the strong *trans* influence of boranes. Noteworthy of [Ni(cod){$^{t}Bu_2P$–C≡C–$B(C_6F_5)_2$}] was the significantly shortened B–C bond length [1.486(4) Å] relative to the free ligand and other alkynylboranes in the literature, rendering the BCC-unit as borataallene/boratapropargyl-like.[115] [Ni(cod){$^{t}Bu_2P$–C≡C–$B(C_6F_5)_2$}] also reacted with acetonitrile to generate the dimeric nickel complex [{Ni(NCMe)(μ*P*-$^{t}Bu_2P$–C≡C–$B(C_6F_5)_2$}$_2$], in which a MeCN ligand has displaced the η^2:η^2-coordinated cod ligand, and the phosphine of the phosphino-alkynyl-borane ligand was bridging between two nickel centres, each maintaining η^3*BCC*-coordination of the alkynylborane fragment (Scheme 1.20). The Ni–B bond distance in [{Ni(NCMe)(μ-$^{t}Bu_2P$–C≡C–$B(C_6F_5)_2$}$_2$] is 2.324(2) Å (r_α = 1.12)[68] and the C≡C stretch was located at 1838 cm^{-1}; reduction in both the Ni–B bond length and C≡C stretching frequency in [{Ni(NCMe)(μ*P*-$^{t}Bu_2P$–C≡C–$B(C_6F_5)_2$}$_2$] relative to [Ni(cod){$^{t}Bu_2P$–C≡C–$B(C_6F_5)_2$}] is indicative of tighter η^3*BCC*-coordination of the alkynylborane to nickel, which is a consequence of increased electron density at nickel.[43]

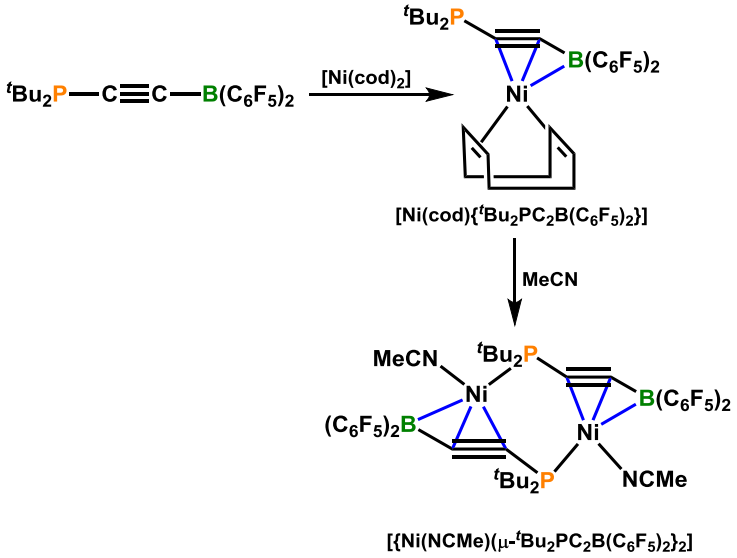

Scheme 1.20. Reaction of $^{t}Bu_2PC{\equiv}CB(C_6F_5)_2$ with $[Ni(cod)_2]$, followed by subsequent reactivity with acetonitrile.

1.3.1.6 – Platinum Complexes of a (Boryl)iminomethane Ligand

Figueroa and co-workers have reported the synthesis of a platinum(0) (boryl)iminomethane complex, $[Pt(\kappa^2\textit{NB}\text{-}^{Cy2}BIM)(CNAr^{Dipp2})]$ (^{Cy2}BIM = $Cy_2B(H)C{=}NAr^{Dipp2}$; Ar^{Dipp2} = 2,6-(2,6-$^{i}Pr_2$-C_6H_3)-C_6H_3), prepared via initial oxidative addition of $HBCy_2$ to $[Pt(CNAr^{Dipp2})_2]$, forming $[PtH(BCy_2)(CNAr^{Dipp2})_2]$, followed by α-hydride migration (i.e. 1,1-insertion) and B–C bond forming reductive elimination (Scheme 1.21). $[Pt(\kappa^2\textit{NB}\text{-}^{Cy2}BIM)(CNAr^{Dipp2})]$ features a 3-coordinate Pt(0) centre with T-shaped geometry, with a Pt–B bond distance of 2.314(6) Å (r_α = 1.05)[68] and an acute B–Pt–N bite angle [66.0(2)°]. Additionally, a significant low frequency shift was observed for $[Pt(\kappa^2\textit{NB}\text{-}^{Cy2}BIM)(CNAr^{Dipp2})]$ (18 ppm) relative to free ^{Cy2}BIM (prepared through hydroboration of free $CNAr^{Dipp2}$; 74 ppm), and boron is significantly pyramidalized [Σ(C–B–C = 348.4°] indicating that the pendant borane is strongly coordinated to platinum.[116]

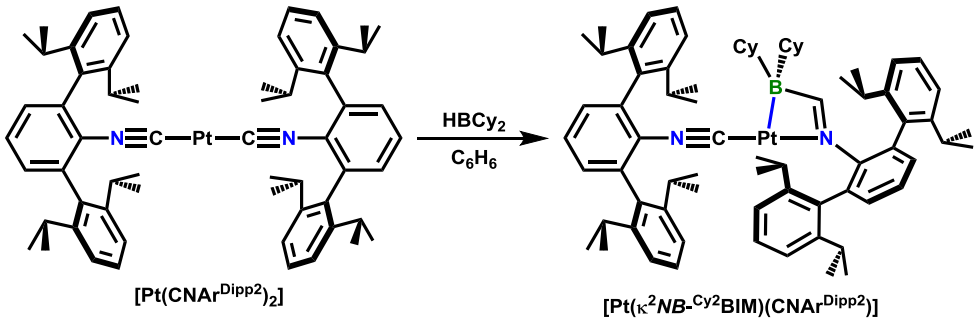

Scheme 1.21. Synthesis of [Pt(κ^2*NB*-^{Cy2}BIM)(CNAr^{Dipp2})] by reaction of $HBCy_2$ with [Pt(CNAr^{Dipp2})$_2$].

[Pt(κ^2*NB*-^{Cy2}BIM)(CNAr^{Dipp2})] reacted with H_2, *p*-$O_2NC_6H_4NH_2$, ROH (R = H, Me) and PhC_2H by initial oxidative addition across an E–H bond (E = H, N, O, or C) followed by insertion into the Pt–B bond, yielding complexes featuring a bridging H, $N(H)C_6H_4NO_2$-*p*, OR (R = H, Me) or C_2Ph unit between platinum and the borane, respectively (Scheme 1.22). Alternatively, [Pt(κ^2*NB*-^{Cy2}BIM)(CNAr^{Dipp2})] reacted with acetone and benzaldehyde by 1,2-insertion of the R_1R_2C=O unit (R^1 = R^2 = Me; R^1 = Ph, R^2 = H) into the Pt–B bond, accompanied with 1,2-cyclohexyl migration from boron to the adjacent carbon atom (Scheme 1.22).[116]

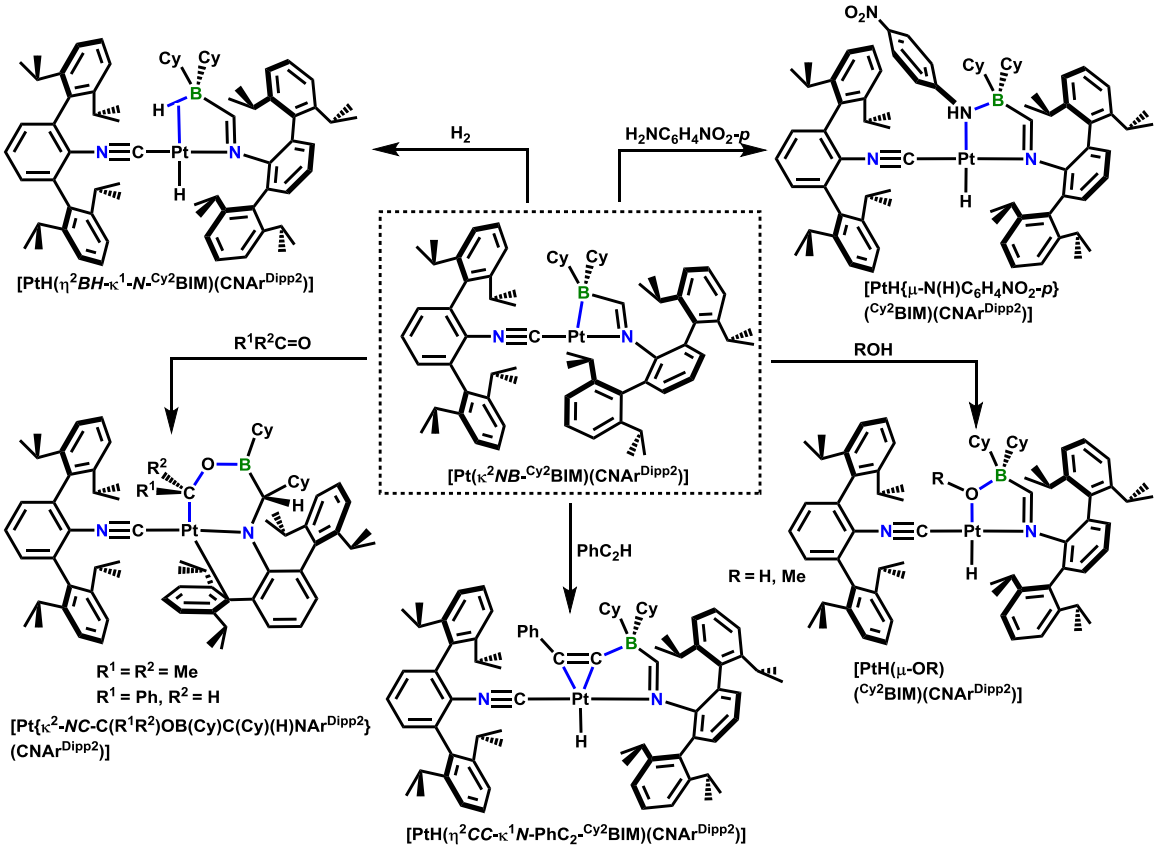

Scheme 1.22. Reactivity of [Pt(κ^2*NB*-^{Cy2}BIM)(CNAr^{Dipp2})] with H_2, $H_2NC_6H_4NO_2$-*p*, ROH (R = H, Me), PhC_2H, acetone and benzaldehyde.

1.3.1.7 – Catalytic Application of Bidentate Phosphine/Borane-Containing Ambiphilic Ligands

Bourissou and co-workers developed the synthesis of a ferrocene-based P/B-ambiphilic ligand, [Fe(η^5-$C_5H_4PPh_2$)(η^5-$C_5H_4BMes_2$)] (FcPB), which was obtained by lithiation of [Fe(η^5-C_5H_4Br)(η^5-$C_5H_4PPh_2$)], providing [Fe(η^5-$C_5H_4PPh_2$)(η^5-C_5H_4Li)] followed with the addition of F–$BMes_2$, as shown in Scheme 1.23 below. Bourissou *et al.* directed the application of the FcPB ligand towards catalytic hydroformylation of 1-octene, utilizing [Rh(acac)$(CO)_2$] (acac = acetylacetonato) as the pre-catalyst. The catalytic trials were performed in a toluene solution containing [Rh(acac)$(CO)_2$], 20 equivalents FcPB and a 1-octene:Rh ratio of ~4000, heated to 90 °C under ~40 atm of

syngas. The rhodium concentration was fixed at 0.5 mM, and complete conversion was reached in ~45 minutes with 72 % selectivity for the linear isomer (TOF = 6400 h^{-1}). However, utilizing diphenylphosphinoferrocene as the ligand ([Fe(η^5-$C_5H_4PPh_2$)(η^5-C_5H_5)]) resulted in the same catalytic rate and product distribution within error, indicating the presence of a –$BMes_2$ group did not play any role. To evaluate the role of the flexible ferrocene linker in the FcPB ligand, Bourissou and co-workers sought to explore the catalytic reactivity of rhodium bearing the structurally more rigid $^{Ph}MPB^{Mes}$ ligand, (*o*-$Ph_2P)C_6H_4BMes_2$. Under the same reaction conditions, however containing a 1 mM solution of Rh, and a 1-octene:Rh ratio of ~2000, a 54:46 ratio of linear and branched aldehydes was obtained in ~150 minutes. Similar results were obtained when employing 1-(PPh_2)-2-(2,4,6-$^{i}Pr_3$-C_6H_2)C_6H_4 as the ligand, indicating that again, the presence of a Lewis acid did not play a role in the catalysis, but rather the steric bulk provided by either mesityl or 2,4,6-tri-*iso*-propylphenyl groups did. In addition, the decreased ligand flexibility resulted in reduced activity and selectivity.[117]

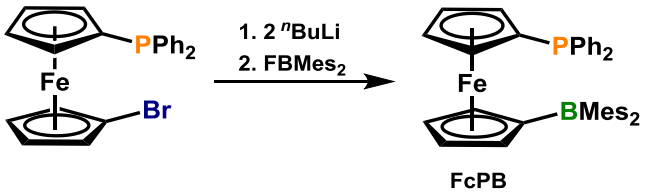

Scheme 1.23. Synthesis of the FcPB ligand.

Bourissou and Gómez aimed to extend the catalytic relevance of the (*o*-$R_2P)C_6H_4BMes_2$ ($^{R}MPB^{Mes}$, R = Ph, ^{i}Pr) ligands to C–C cross-coupling reactivity utilizing palladium(II)-based catalysts. As a model reaction, Bourissou and Gómez studied the coupling of phenylboronic acid with 4-bromoanisole in Suzuki-Miyaura cross-coupling, and utilizing $Pd(OAc)_2$ as the pre-catalyst. The Pd-$^{Ph}MPB^{Mes}$ system proved to be sensitive to the steric bulk of the reactants, providing 75 % of the cross-coupled product for 2-methylphenylboronic acid and 4-bromoanisole compared to less than 20 % for 2-methylphenylboronic acid and 2,4,6-tri-*iso*-propylbromobenzene, and this system was also capable of activating C–Cl bonds, accommodating 4-chloroanisole when

coupling with phenylboronic acid, however in significantly reduced yields (27 %). Additionally, the presence of more Lewis basic phosphines did not enhance the catalytic activity; a Pd/PPh_3 system exhibited lower catalytic activity with similar chemoselectivity as the Pd-^{R}MPB^{Mes} (R = Ph, ^{i}Pr) systems, indicating that while the presence of the –$BMes_2$ group decreased catalytic activity in hydroformylation catalysis (*vide supra*), it enhanced catalytic activity in C–C Suzuki-Miyaura coupling reactions.[118]

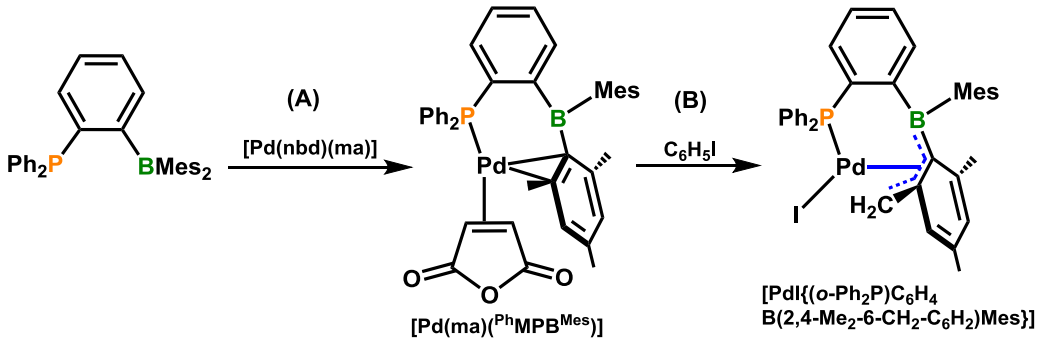

Scheme 1.24. A. Synthesis of [Pd(ma)(^{Ph}MPB^{Mes})], which was hypothesized to be a potential model for the catalytically active species in C–C cross-coupling catalysis, and **B.** subsequent reactivity with PhI to yield [PdI{(*o*-Ph_2P)C_6H_4B(2,4-Me_2-6-CH_2-C_6H_2)Mes}], which was hypothesized to be a potential intermediate in the degradation pathway of the catalyst.

To gather insight into the structure of the catalytically active species bearing the ^{Ph}MPB^{Mes} ligand, Bourissou and Gómez pursued isolation of a palladium(II) species coordinated to by the P/B-ligand. Reaction of ^{Ph}MPB^{Mes} with [Pd(nbd)(ma)] (nbd = 1,4-norbornadiene; ma = maleic anhydride) at 65 °C in THF for one hour provided [Pd(ma)(^{Ph}MPB^{Mes})] (**A** in Scheme 1.24). X-ray crystallography elucidated that the connectivity to palladium entailed η^2*CC*-coordination of a maleic anhydride ligand, in addition to bidentate coordination of ^{Ph}MPB^{Mes} via phosphorus and an η^2*CC*-bonding interaction involving the *ipso*- and *ortho*-carbon atoms of a *B*-mesityl ring, with the absence of any Pd–B bonding interaction. Biarylphosphine ligands are prominent in catalytic systems in C–C coupling reactivity that possess high activity. Indeed, the 1-(Ph_2P)-2-(2,4,6-$^{i}Pr_3$-C_6H_2)C_6H_4 ligand designed by Buchwald's group out-performed the ^{R}MPB^{Mes} (R = Ph, ^{i}Pr) ligands, providing higher activity with greater chemoselectivity in

the Suzuki-Miyaura cross-coupling of phenylboronic acid with 4-bromoanisole. The presence of η^2*CC*-arene coordination in [Pd(ma)(^{Ph}MPB^{Mes})] hints at the notion that the –$BMes_2$ group acts as a biaryl substituent coordinated to phosphorus, and η^nC_n-arene stabilization of the active palladium species is important for the high activity of these catalytic systems. To verify that such an η^nC_n-interaction is operative in the active catalytic species in the Pd-^{R}MPB^{Mes} (R = Ph, ^{i}Pr) systems, [Pd(ma)(^{Ph}MPB^{Mes})] was subject to the same catalytic conditions, producing the cross-coupled product in 82 % yield.[118]

Bourissou and Gómez have also utilized palladium-^{R}MPB^{Mes} (R = Ph, ^{i}Pr) systems for Suzuki-Miyaura C–C cross-coupling of chloro-*N*-heterocycles with arylboronic acids, as well as double cross-coupling reactivity, which was the case for 2,6-dichloro-3-nitropyridine, which allowed access to unsymmetrical 2,6-diarylpyridines. While investigating this particular avenue of catalytic C–C coupling reactivity, Bourissou and Gómez found that their previously reported [Pd(ma)(^{Ph}MPB^{Mes})] reacted with iodobenzene in toluene after one hour at 100 °C to form [PdI{(*o*-Ph_2P)C_6H_4B(2,4-Me_2-6-CH_2-C_6H_2)Mes}] (**B** in Scheme 1.24). Oxidative addition of iodobenzene presumably led to dissociation of the previously coordinated maleic anhydride ligand, at which point reductive elimination of benzene rendered a *B*-mesityl ring η^4*BCCC*-coordinated via an anionic borabutadiene coordination mode to palladium through boron, the *ipso*- and *ortho*-carbon atoms, as well as the deprotonated –CH_2 group that was previously a methyl substituent in the 6-position of the mesityl ring (**B** in Scheme 1.24). Due to the significantly reduced activity of [PdI{(*o*-Ph_2P)C_6H_4B(2,4-Me_2-6-CH_2-C_6H_2)Mes}] towards the coupling of 4-amino-2-chloropyridine with phenylboronic acid, Bourissou and Gómez reasoned that this complex may represent an intermediate present within the deactivation pathway of their catalytic systems.[119]

1.3.2 – Transition Metal Complexes Featuring Tridentate Phosphine/Borane Ligands

1.3.2.1 – Synthesis of the {(*o*-$R_2P)C_6H_4\}_2BR'$ ($^{R}DPB^{R'}$; R = ^{i}Pr, Ph; R' = Ph, Mes) Ligand

The first tridentate phosphine/borane ligand reported was the {(*o*-$^{i}Pr_2P)C_6H_4\}_2BPh$ ($^{iPr}DPB^{Ph}$; Scheme 1.25) ligand, prepared by Bourissou and co-workers, which was obtained via lithiation of two equivalents of (*o*-$^{i}Pr_2P)C_6H_4Br$ followed by the addition of Cl_2B–Ph. The ligand was designed to feature a phenyl group as a rigid two-carbon linker between phosphorus and boron to discourage intramolecular P→B adduct formation. However, $^{iPr}DPB^{Ph}$ gave rise to solution ^{31}P and ^{11}B NMR signals at 11 and 43 ppm, respectively,[103] and a solid-state ^{11}B chemical shift of 71.0 ppm, indicating that an equilibrium existed between P→B adducted and non-adducted forms of the $^{iPr}DPB^{Ph}$ ligand in the solution-state.[104]

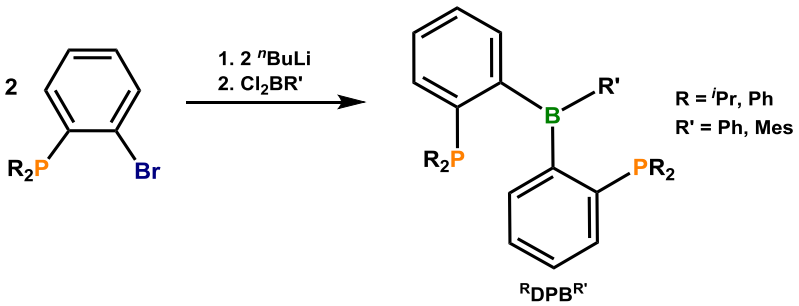

Scheme 1.25. Synthesis of the $^{R}DPB^{R'}$ ($^{R}DPB^{R'}$ = {(*o*-$R_2P)C_6H_4\}_2BR'$; R = ^{i}Pr, Ph; R' = Ph, Mes) ligand.

1.3.2.2 – Initial Coordination Chemistry of the $^{iPr}DPB^{Ph}$ Ligand: Complexes Bearing κ^3*PPB*-Coordination

The reactivity of $^{iPr}DPB^{Ph}$ with square planar metal pre-cursors was targeted given that the occupied d_z^2-orbital of the metal centre makes for an excellent match for the σ-accepting borane, which would ideally be situated in the z-axis upon coordination of the phosphine arms. Its reactivity was surveyed with the rhodium(I) pre-cursor [{Rh(μ-

Cl)(nbd)$_2$}$_2$], which was indeed found to react successfully to form *cis*-[{RhCl($^{i\text{Pr}}$DPB$^{\text{Ph}}$)}$_2$], and subsequent addition of *N*,*N*-dimethylaminopyridine (DMAP) provided the monomeric complex *cis*-[RhCl(DMAP)($^{i\text{Pr}}$DPB$^{\text{Ph}}$)] (Scheme 1.26). The Rh–B bond lengths and ^{11}B NMR chemical shifts for *cis*-[{RhCl($^{i\text{Pr}}$DPB$^{\text{Ph}}$)}$_2$] and *cis*-[RhCl(DMAP)($^{i\text{Pr}}$DPB$^{\text{Ph}}$)] are 2.306(3) (r_α = 1.02)[68] and 2.295(5) Å (r_α = 1.02),[68] respectively, and 20 ppm for both complexes. In addition, the sum of the C–B–C angles of boron is equal to 338.8(5) and 340.2(7)°, respectively, indicating that there is a significant bonding interaction between rhodium and boron.[103]

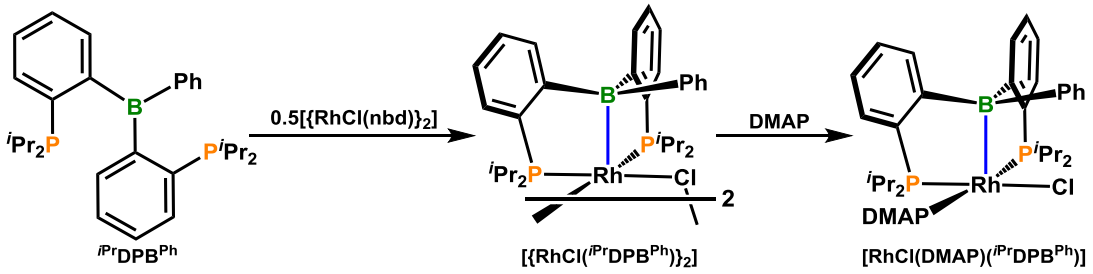

Scheme 1.26. Rhodium(I) complexes featuring κ^3*PPB*-coordination of the $^{i\text{Pr}}$DPB$^{\text{Ph}}$ ligand.

Reaction of $^{i\text{Pr}}$DPB$^{\text{Ph}}$ with 0.5 equivalents of [{Rh(μ-Cl)(CO)$_2$}$_2$] lead to the formation of *trans*-[RhCl(CO)($^{i\text{Pr}}$DPB$^{\text{Ph}}$)]; this complex was isolated as a 80:20 mixture with CO residing *syn* to the *B*-Ph ring 80% of the time, and Cl residing *syn* to the *B*-Ph ring 20% of the time. The degree of Rh–B bonding in *trans*-[RhCl(CO)($^{i\text{Pr}}$DPB$^{\text{Ph}}$)] appeared to be less than in *cis*-[{RhCl($^{i\text{Pr}}$DPB$^{\text{Ph}}$)}$_2$] and *cis*-[RhCl(DMAP)($^{i\text{Pr}}$DPB$^{\text{Ph}}$)], given an increase in Rh–B bond length (2.374 Å; r_α = 1.05),[68] decrease in pyramidalization of boron [Σ(C–B–C) = 342.6°] and a shift to higher frequency for the ^{11}B NMR signal (26.7 ppm). DFT calculations revealed that the difference in Rh–B bonding was attributable to the presence of a π-accepting CO co-ligand. Bourissou *et al.* also utilized IR spectroscopy to probe whether borane coordination resulted in electron density depletion at the rhodium centre; the CO stretching band for *trans*-[RhCl(CO)($^{i\text{Pr}}$DPB$^{\text{Ph}}$)] was located at 2001.8 cm^{-1} versus 1966.7 cm^{-1} for *trans*-[RhCl(CO)(^{i}Pr$_2$PPh)$_2$], indicating rhodium–borane coordination does indeed deplete

electron density at rhodium. For comparison with equivalent Group 10 metal complexes, Bourissou and co-workers surveyed the reactivity of $^{i\text{Pr}}$DPB$^{\text{Ph}}$ with [MCl_2(cod)] (M = Pd, Pt), isolating *cis*-[MCl_2($^{i\text{Pr}}$DPB$^{\text{Ph}}$)] complexes. Despite the absence of π-accepting co-ligands in the Pd(II) and Pt(II) complexes, the degree of metal–borane coordination decreased such that Rh(I) > Pt(II) > Pd(II), as evidenced by decreases in the pyramidalization of boron, and ^{11}B chemical shifts located at much higher frequency relative to the Rh(I) complex. This trend adheres to the degree of basicity of each metal; a decrease in basicity resulted in a decrease in the strength of metal–Lewis acid coordination.[120]

Reaction of $^{i\text{Pr}}$DPB$^{\text{Ph}}$ with [AuCl(SMe_2)] yielded square planar *trans*-[AuCl($^{i\text{Pr}}$DPB$^{\text{Ph}}$)], which possesses a shorter Au–B bond distance (2.309 Å; r_α = 1.05),[68] greater pyramidalization of boron [Σ(C–B–C) = 341.2°] and a shift to lower frequency for the ^{11}B NMR signal (24.6 ppm) relative to [AuCl($^{i\text{Pr}}$MDP$^{\text{R'}}$)] complexes (BR'_2 = BCy_2, BFlu). Replacing the *iso*-propyl substituents on phosphorus with phenyl groups resulted in the formation of an analogous square planar complex, albeit with a slightly elongated Au–B bond length (2.335 Å; r_α = 1.06)[68] and decreased degree of pyramidalization of boron [Σ(C–B–C) = 343.8°] owing to the decrease in donor ability of triarylphosphines versus aryldialkylphosphines.

A remarkable feature of the *trans*-[AuCl($^{\text{R}}$DPB$^{\text{Ph}}$)] (R = ^{i}Pr, Ph) complexes is their square planar geometry; tetra-coordinate Au(I) d^{10}-complexes tend to adopt tetrahedral geometries, whereas tetra-coordinate Au(III) d^8-complexes are likely to adopt square planar geometries.[121] The square planar geometry of [AuCl($^{\text{R}}$DPB$^{\text{Ph}}$)] (R = ^{i}Pr, Ph) is suggestive of two-electron oxidation of the metal centre upon coordination of boron. DFT calculations revealed a three-centre four-electron bonding interaction involving the $d_{x2\text{-}y2}$ orbital of gold, and p_y orbitals on boron and chlorine; Parkin *et al.* reported a similar interaction in the iridaboratrane [IrCl(PH_3){B(mt^{H})$_3$}], which served as a computational model for the isolated iridaboratrane, [IrCl(PPh_3){B($mt^{t\text{Bu}}$)$_3$}].[80] However, second-order perturbative NBO analyses revealed only a marginal increase in the charge of gold upon coordination of boron (from +0.30 in T-shaped [AuCl(PMe_3)$_2$] to +0.64 in *trans*-

[AuCl(^{R}DPB^{Ph})]), and ^{197}Au Mössbauer spectroscopy revealed an isomer shift/quadrupole splitting relationship diagnostic of Au(I) complexes as opposed to Au(III) complexes, which was presented as unambiguous evidence that *trans*-[AuCl(^{R}DPB^{Ph})]) is a gold(I) d^{10}-complex.[44]

1.3.2.3 – Emergence of a New Tridentate P/S/B-Ligand, 2,7-di-*tert*-butyl-5-diphenylboryl-4-diphenylphosphino-9,9-dimethylthioxanthene (TXPB)

Shortly following Bourissous report of the $^{i\text{Pr}}$DPB^{Ph} ligand was the 2006 report by Emslie *et al.* of a tridentate phosphine/thioether/borane-containing ligand, known as TXPB (Scheme 1.27). The TXPB ligand contains phosphine and thioether donors which readily bind to late transition metals, and incorporates the structurally rigid thioxanthene ligand backbone to place the pendant Lewis acid in close proximity to the metal centre or metal co-ligands. The synthesis of TXPB is a five-step process beginning with commercially available thioxanthone, as shown below in Scheme 1.27; initial reaction of thioxanthone with excess $AlMe_3$ provided 9,9-dimethylthioxanthene. Next, a Friedel-Crafts alkylation installed *tert*-butyl substituents in the 2- and 7-positions of the ligand backbone, which served a two-fold purpose: (1) The C*Me*$_3$ substituents, in combination with the C*Me*$_2$ group, provided an excellent ^{1}H NMR handle when evaluating the reactivity of the TXPB ligand, and (2) the presence of ^{t}Bu-protection groups in the 2- and 7-positions of the ligand backbone enabled selective bromination in the 4- and 5-positions of the ligand backbone. The diphenylphosphino moiety was then installed by selective monolithiation with one equivalent of ^{n}BuLi, followed with the addition of Cl–PPh$_2$. In the final step of the synthesis of TXPB the Lewis acid was appended via lithiation of the remaining bromo-substituent on the ligand backbone through the use of two equivalents of ^{t}BuLi, followed with the addition of Br–BPh$_2$. Further purification of the ligand entailed recrystallization from acetonitrile (MeCN), which precipitated the MeCN–TXPB adduct as a white powder, followed by removal of coordinated MeCN under dynamic vacuum. The TXPB ligand gave rise to ^{11}B and ^{31}P NMR signals at 69 and –12.2 ppm, respectively,[59] and differs from the $^{i\text{Pr}}$DPB^{Ph} ligand in that: (1) The ligand backbone is

much more rigid, being a derivative of thioxanthene, (2) the phosphine/thioether donor set in TXPB is less electron donating than the bisphosphine donor set in the $^{i\text{Pr}}$DPB$^{\text{Ph}}$ ligand, and (3) the pendant borane is positioned on the periphery of the ligand framework in TXPB, rather than as the central buttress as in $^{i\text{Pr}}$DPB$^{\text{Ph}}$ and the poly(azolyl)borane ligands.

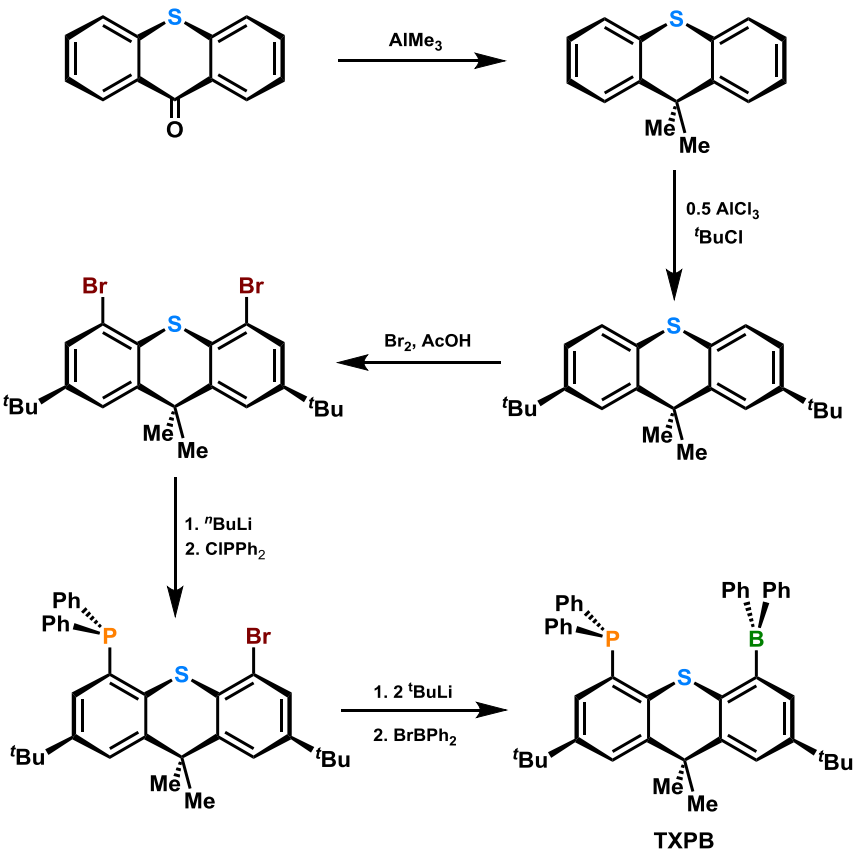

Scheme 1.27. Synthetic scheme for the preparation of the TXPB ligand.

1.3.2.4 – Development of Complexes Featuring κ^2*PS*:η^3*BCC*- and κ^2*PS*:μ-M–L–BR$_3$ (M = Metal, L = Co-Ligand) Coordination of the TXPB Ligand

Conversely to the $^{i\text{Pr}}$DPB$^{\text{Ph}}$ ligand, which displayed a propensity to coordinate to various metals via η^1*B*-coordination of the pendant borane, the TXPB ligand did not. In the initial reports of the TXPB ligand in 2006, Emslie and co-workers surveyed its

reactivity with palladium(0) and rhodium(I) pre-cursors. Reaction of TXPB with 0.5 equivalents of $[Pd_2(dba)_3]$ resulted in the formation of [Pd(μ-dba)(TXPB)], which featured κ^2*PS*-coordination of the TXPB ligand, with one equivalent of dba remaining coordinated to the metal centre in a bridging position between the metal and the pendant borane. Two canonical structures of [Pd(μ-dba)(TXPB)] can potentially exist, which are a zwitterionic palladium(II) η^3-boratoxypentadienyl complex, or a palladium(0) alkene complex with intramolecular ketone-borane adduct formation (Scheme 1.28). X-ray crystallography and $^{13}C\{^1H\}$ NMR spectroscopy revealed: (1) Bond length contraction for C_α–C_β (C_α = *C*–O, C_β = coordinated alkene carbon atom), similar to that observed for an allyl group, (2) an increase in C_α–O bond length relative to ketone–borane adducts, (3) the Pd–C_α bond length was only slightly longer than that observed in palladium–allyl complexes, and (4) a $^2J_{13C,31P}$ coupling constant of 10 Hz for the α-carbon atom, verifying persistence of Pd–C_α coordination in the solution-state. The aforementioned findings indicated that the appropriate description of [Pd(μ-dba)(TXPB)] was a zwitterionic palladium(II) η^3-boratoxypentadienyl complex, and highlighted the unique cooperative structural activation of an enone between a metal centre and the pendant Lewis acid of an ambiphilic ligand.[59]

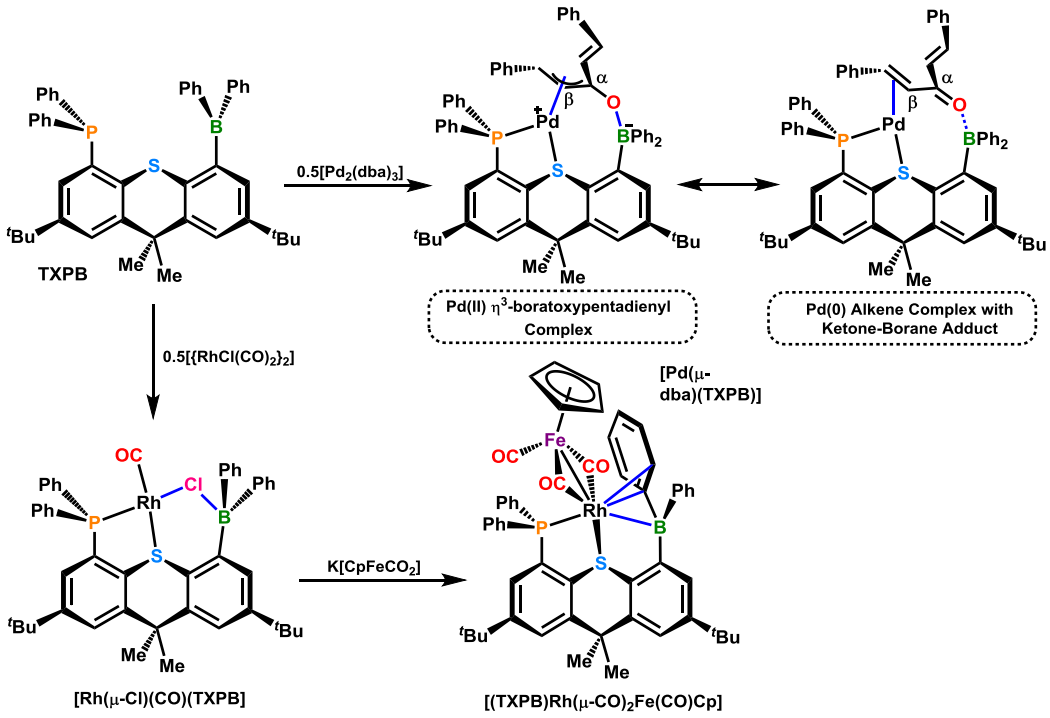

Scheme 1.28. Reaction of the TXPB ligand with $[Pd_2(dba)_3]$ to form [Pd(μ-dba)(TXPB)], or with $[\{RhCl(CO)_2\}_2]$ to form [Rh(μ-Cl)(CO)(TXPB)], followed with subsequent reaction with $K[CpFe(CO)_2]$ to form [(TXPB)Rh(μ-$CO)_2$Fe(CO)Cp].

The reaction of TXPB with 0.5 equivalents of $[\{Rh(\mu\text{-}Cl)(CO)_2\}_2]$ lead to the formation of [Rh(μ-Cl)(CO)(TXPB)], in which a chloride ligand resided in a bridging position between rhodium and boron; similarly to [Pd(μ-dba)(TXPB)], the TXPB ligand was κ^2*PS*-coordinated to rhodium (Scheme 1.28). This divergent reactivity relative to Bourissou's *trans*-[RhCl(CO)($^{i\text{Pr}}$DPB$^{\text{Ph}}$)] complex highlighted the differences in steric and electronic properties of the two ligands (*vide supra*). The B–Cl bond length in the solid-state structure of [Rh(μ-Cl)(CO)(TXPB)] is 1.995(9) Å (r_α = 1.07),[68] which is only slightly elongated relative to anionic chloroborates, and significant pyramidalization of boron was observed [Σ(C–B–C) = 340(1)°]. Moreover, the ^{11}B chemical shift is 11.5 ppm, which is shifted 57.5 ppm to lower frequency relative to free TXPB. Subsequent reaction of [Rh(μ-Cl)(CO)(TXPB)] with $K[CpFe(CO)_2]$ provided [(TXPB)Rh(μ-$CO)_2$Fe(CO)Cp], a heterobimetallic complex in which κ^2*PS*-coordination of TXPB to rhodium was maintained, but with a [Cp(CO)Fe(μ-$CO)_2$]-unit bound to rhodium via a

Rh–Fe bond and two bridging carbonyl ligands. In addition, a *B*-phenyl ring of TXPB was coordinated to rhodium via boron and the *ipso*- and *ortho*-carbon atoms, rendering the borane of TXPB η^3*BCC*-coordinated to rhodium. This novel coordination mode was evidenced by: (1) An ^{11}B chemical shift of 39 ppm, which is shifted 30 ppm to lower frequency of free TXPB (69 ppm, *vide supra*), indicative of bonding between rhodium and boron, (2) inequivalence of all five aromatic protons of a *B*-phenyl ring in the ^{1}H NMR spectrum collected at –75 °C, and (3) a Rh–B bond distance of 2.63(2) Å (r_α = 1.16).[68] The η^3*BCC*-bonding interaction between the *B*-phenyl unit and rhodium may be described as either η^2-arene/η^1*B*-coordination, or η^3-borataallyl-like coordination of the three-atom unit; DFT calculations (ADF 2005.01, TZP, VWN, PW91, ZORA) were utilized, and an examination of the relevant molecular orbitals following application of the Boys Foster localization method concluded that the bonding interaction was intermediate between the two descriptions.[1]

Since the early reports of the TXPB ligand in 2006, Emslie and co-workers have expanded its versatility in the coordination chemistry of late transition metals by surveying its reactivity with other Group 10 metal pre-cursors. Reaction of TXPB with [$PdCl_2$(cod)] provided [PdCl(μ-Cl)(TXPB)], which similarly to [Rh(μ-Cl)(CO)(TXPB)], contained a chloride co-ligand bridging between the metal and boron;[122] the TXPB ligand has also shown promising reactivity with the platinum(II) pre-cursors [PtX_2(cod)] (X = Cl, I), forming [PtX(μ-X)(TXPB)] complexes with a chloride or iodide residing in a bridging position between platinum and boron, albeit with chloride interacting much more strongly with boron than the iodide (Scheme 1.29).[123] Subsequent reaction of [Pd(Cl(μ-Cl)(TXPB)] with one equivalent of either magnesium or zinc powder afforded the palladium(I)–palladium(I) dimer, [{Pd(μ-Cl)(TXPB)}$_2$], or with two equivalents of magnesium powder yielded the palladium(0) complex, [Pd(TXPB)]; the TXPB ligand was κ^2*PS*-coordinated in both cases, with additional η^3*BCC*-coordination of the borane in [Pd(TXPB)]. An alternate route to [Pd(TXPB)] was via reaction of [Pd(μ-dba)(TXPB)] with either $LiNEt_2$ or $LiN(SiMe_3)_2$, and [{Pd(μ-Cl)(TXPB)}$_2$] may also be accessed via comproportionation reactions involving [Pd(TXPB)] and [PdCl(μ-Cl)(TXPB)], or [Pd(μ-

dba)(TXPB)] and [PdCl(μ-Cl)(TXPB)]. The analogous nickel(0) complex, [Ni(TXPB)], was prepared through the reaction of TXPB with [Ni(cod)$_2$] (Scheme 1.29).[122]

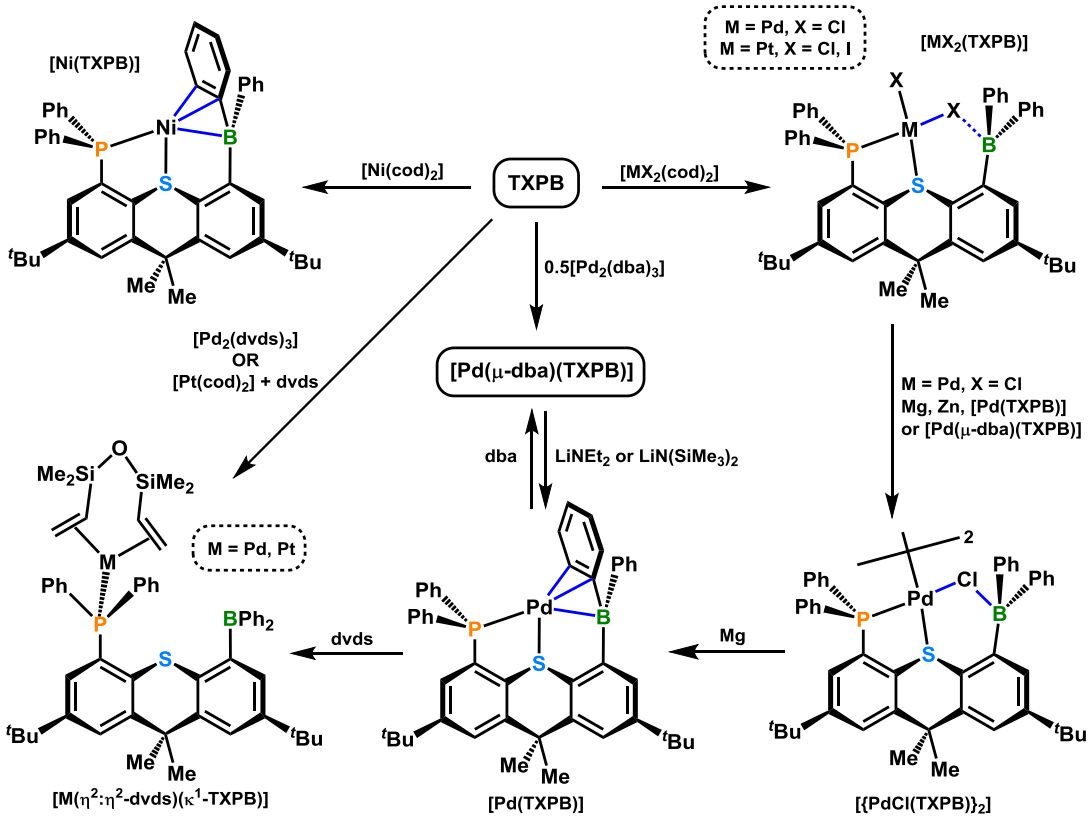

Scheme 1.29. Reactivity of TXPB and Group 10 metal-TXPB complexes.

One of the major drawbacks of the Emslie group's TXPB ligand is the ease of displacement of the metal centre from the central binding pocket in the presence of other neutral donors, converting the κ^3*PSB*-ligand into a monodentate κ^1*P*-ligand. For example, the addition of dvds to [Pd(TXPB)] (or addition of dvds to [Pt(cod)$_2$], followed with the addition of TXPB) provided [M(η^2:η^2-dvds)(κ^1*P*-TXPB)] (M = Pd, Pt) in which coordination of palladium and platinum to the diene co-ligand was preferred over the thioether of TXPB, thus limiting potential for metal–borane coordination; [Pd(η^2:η^2-dvds)(κ^1*P*-TXPB)] may also be accessed directly via reaction of TXPB with [Pd$_2$(dvds)$_3$] (Scheme 1.29).[122]

1.3.2.5 – Complexes Exhibiting κ^2*PP*:η^n*BC*$^{n-1}$ and κ^2*PP*:μ-M–L–BR_3 (M = Metal, L = Co-Ligand) Coordination of the DPB Ligand, and Associated Reactivity

Aside from the copper(I) complex [{CuCl($^{i\text{Pr}}$MPB$^{\text{Ph}}$)}$_2$] reported by Bourissou *et al.* featuring η^3*BCC*-coordination of a *B*-phenyl ring, analogous to the bonding situation in Emslie's Ni(0), Pd(0) and Rh(I) complexes (*vide supra*), Bourissou has also prepared [CuCl($^{\text{Ph}}$DPB$^{\text{Ph}}$)] via reaction of $^{\text{Ph}}$DPB$^{\text{Ph}}$ with CuCl. This complex features κ^2*PP*- as well as η^2*BC*-coordination of the $^{\text{Ph}}$DPB$^{\text{Ph}}$ ligand involving boron and the *ipso*-carbon atom of a *B*-phenyl ring. The solid-state geometry of [CuCl($^{\text{Ph}}$DPB$^{\text{Ph}}$)] is pseudo-tetrahedral with a Cu–B bond distance [2.396(5) Å; r_α = 1.11][68] that is much shorter than in [{CuCl($^{i\text{Pr}}$MPB$^{\text{Ph}}$)}$_2$] (*vide supra*) and [CuCl(TPB)] (*vide infra*). The Cu–C_{ipso} bond length is 2.364(4) Å (r_α = 1.15),[68] which compares well with that found in [{CuCl($^{i\text{Pr}}$MPB$^{\text{Ph}}$)}$_2$]. However, no other carbon atoms of the *B*-phenyl ring experience close approach to copper, indicating that the η^nBC_{n-1}-interaction is limited to an η^2*BC*-interaction. When the phenyl substituents on phosphorus were replaced with *iso*-propyl groups in $^{i\text{Pr}}$DPB$^{\text{Ph}}$, similar coordination to the [CuCl] fragment was observed, however four crystallographically independent molecules were located within the unit cell; one shows striking resemblance to [CuCl($^{\text{Ph}}$DPB$^{\text{Ph}}$)], with Cu–B and Cu–C_{ipso} bond lengths of 2.379(5) (r_α = 1.10)[68] and 2.414(4) Å (r_α = 1.18),[68] supporting η^2*BC*-coordination to Cu, while the other three are nearly identical and exhibit average Cu–B and Cu–C_{ipso} bond lengths of 2.49 (r_α = 1.15)[68] and 2.66 Å (r_α = 1.30),[68] respectively. These features of the solid-state structure of [CuCl($^{i\text{Pr}}$DPB$^{\text{Ph}}$)] indicate that for three out of four independent molecules in the unit cell, coordination of the borane unit to copper is intermediate between η^1*B*- and η^2*BC*-coordination. The [CuCl($^{\text{R}}$DPB$^{\text{Ph}}$)] (R = ^{i}Pr, Ph) complexes gave rise to ^{11}B NMR signals at 56 and 55 ppm, respectively, which are in good agreement with [{CuCl($^{i\text{Pr}}$MPB$^{\text{Ph}}$)}$_2$] (*vide supra*).[105]

Nakazawa and Kameo have also investigated the chemistry of the $^{\text{Ph}}$DPB$^{\text{Ph}}$ ligand by exploring its reactivity with [MH(CO)(PPh_3)$_3$] (M = Rh, Ir) pre-cursors. The $^{\text{Ph}}$DPB$^{\text{Ph}}$ ligand reacted with [RhH(CO)(PPh_3)$_3$] to form [Rh(μ-H)(CO)(PPh_3)($^{\text{Ph}}$DPB$^{\text{Ph}}$)], which features a bridging Rh–H–B bonding interaction in addition to κ^2*PP*-coordination of the

DPB backbone, or with [IrH(CO)(PPh_3)$_3$] to provide [IrH(CO)(PPh_3)(^{Ph}DPB^{Ph})], in which the DPB ligand is κ^3*PPB*-coordinated (Scheme 1.30). The ^{1}H NMR spectrum of [Rh(μ-H)(CO)(PPh_3)(^{Ph}DPB^{Ph})] contained a broadened resonance at –11.61 ppm, representing the Rh*H* hydride, and the ^{11}B chemical shift is 11.5 ppm, indicating the bridging Rh–H–B interaction is maintained in solution. Furthermore, the solid-state structure exhibits Rh–H and B–H bond lengths of 1.76 and 1.24 Å (r_α = 1.08),[68] respectively, and substantial pyramidalization of boron, with the sum of the C–B–C angles equal to 341.2°. The Ir–*H* resonance for [IrH(CO)(PPh_3)(^{Ph}DPB^{Ph})] was observed as a sharp doublet of triplets at –9.07 ppm, indicating that a bridging Ir–H–B interaction is not present in solution, and the ^{11}B NMR signal is located at 21.9 ppm. In addition, the Ir–B bond length in [IrH(CO)(PPh_3)(^{Ph}DPB^{Ph})] is 2.444 Å (r_α = 1.09).[68] The divergent reactivity of rhodium and iridium pre-cursors with respect to positioning of the hydride co-ligand may be attributed to the greater basicity of iridium relative to rhodium, which produces stronger Ir–B coordination and deters formation of an Ir–H–B bonding interaction.[124]

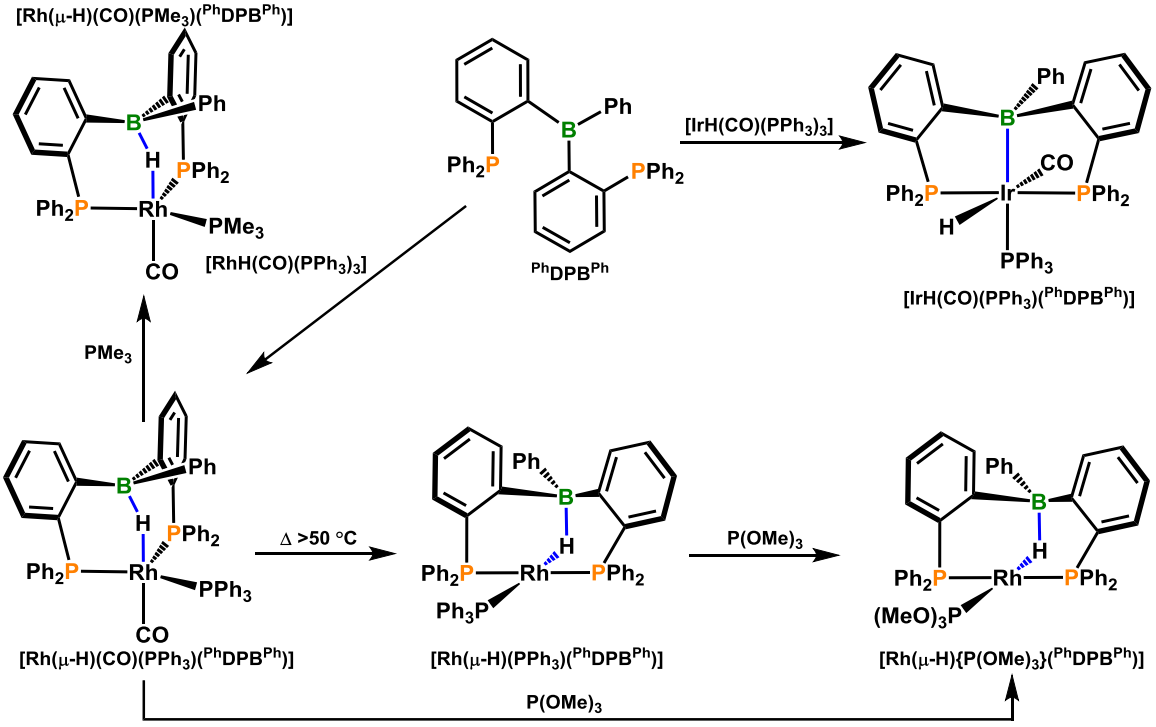

Scheme 1.30. Reaction of $^{Ph}DPB^{Ph}$ with $[MH(CO)(PPh_3)_3]$ (M = Rh, Ir) to form $[Rh(\mu\text{-}H)(CO)(PPh_3)(^{Ph}DPB^{Ph})]$ and $[IrH(CO)(PPh_3)(^{Ph}DPB^{Ph})]$, respectively, and reactivity of $[Rh(\mu\text{-}H)(CO)(PPh_3)(^{Ph}DPB^{Ph})]$.

Both $[MH(CO)(PPh_3)(^{Ph}DPB^{Ph})]$ (M = Rh, Ir) complexes reported by Nakazawa and Kameo give rise to carbonyl stretching bands at significantly higher stretching frequency than their respective $[MH(CO)(PPh_3)_3]$ pre-cursors, indicating that both bridging Rh–H–B and direct Ir–B coordination results in significant depletion in electron density at the metal centre. This was further corroborated by the unusual thermal dissociation of CO when $[Rh(\mu\text{-}H)(CO)(PPh_3)(^{Ph}DPB^{Ph})]$ was heated to 50 °C or higher, providing square planar *trans*-$[Rh(\mu\text{-}H)(PPh_3)(^{Ph}DPB^{Ph})]$; heating $[RhH(CO)(PPh_3)_3]$ resulted in the formation of $[\{Rh(CO)\}_3(\mu\text{-}PPh_2)_3(PPh_3)_2]$, suggesting that the presence of a Rh–H–B interaction is responsbile for CO displacement. Moreover, addition of PMe_3 to $[Rh(\mu\text{-}H)(CO)(PPh_3)(^{Ph}DPB^{Ph})]$ resulted in facile substitution of the PPh_3 ligand for PMe_3, indicating that substitution of PPh_3 is more favourable than substitution of CO. Alternatively, addition of $P(OMe)_3$ to $[Rh(\mu\text{-}H)(CO)(PPh_3)(^{Ph}DPB^{Ph})]$ resulted in

displacement of both the CO and PPh_3 co-ligands yielding square planar *trans*-[Rh(μ-H){$P(OMe)_3$}(^{Ph}DPB^{Ph})] (Scheme 1.30). The addition of σ-donating PMe_3 did not result in displacement of CO because it provides additional electron density for π-backdonation to the CO ligand, whereas the addition of π-accepting $P(OMe)_3$ depletes electron density at rhodium, promoting displacement of CO.[124]

Britovsek and co-workers have attempted to utilize rhodium carbonyl complexes bearing the ^{Ph}DPB^{Ph} ligand to achieve methyl acetate carbonylation, forming acetic anhydride (Scheme 1.31). Britovsek and co-workers were able to isolate square pyramidal [RhCl(CO)(^{Ph}DPB^{Ph})] bearing κ^3*PPB*-coordinated ^{Ph}DPB^{Ph}. This compound exists as a mixture of three isomers: *cis*-[RhCl(CO)(^{Ph}DPB^{Ph})] (65%), *trans*-[RhCl(CO)(^{Ph}DPB^{Ph})] with CO *syn* to the *B*-Ph group (29%) and *trans*-[RhCl(CO)(^{Ph}DPB^{Ph})] with chloride *syn* to the *B*-Ph group (6 %). Additionally, reaction of [RhCl(CO)(^{Ph}DPB^{Ph})] with Ag[SbF_6] under a CO atmosphere provided *cis*-[$Rh(CO)_2$(^{Ph}DPB^{Ph})][SbF_6], which reacted with acetonitrile to yield *cis*-[$Rh(NCMe)_2$(^{Ph}DPB^{Ph})][SbF_6]. However, neither *cis*-[RhL_2(^{Ph}DPB^{Ph})][SbF_6] (L = CO, MeCN) complexes reacted with methyl acetate or methyl iodide, which is required for catalytic carbonylation of methanol, likely owing to the strength of rhodium–borane coordination.[125]

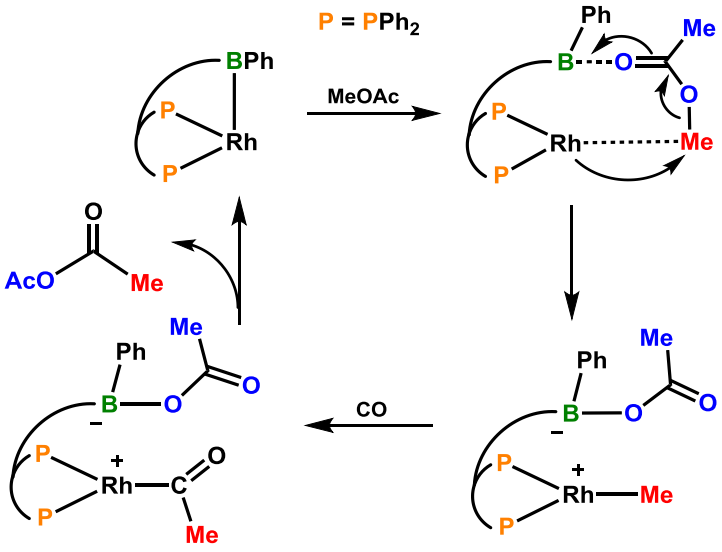

Scheme 1.31. Hypothetical catalytic cycle for the carbonylation of methyl acetate using a rhodium(I) complex bearing the ^{Ph}DPB^{Ph} ligand.

Stephan and Boone have also reported on the use of Bourissou's ^{Ph}DPB^{Ph} ligand; reaction of ^{Ph}DPB^{Ph} with $[RuCl_2(PPh_3)_3]$ provided zwitterionic $[RuCl\{(\eta^6\text{-}C_6H_5)BCl(C_6H_4PPh_2)_2\}]$, in which the borane has abstracted a chloride co-ligand from ruthenium. Subsequent reaction of $[RuCl\{(\eta^6\text{-}C_6H_5)BCl(C_6H_4PPh_2)_2\}]$ with $K[B(C_6F_5)_4]$ resulted in abstraction of chloride from boron, forming KCl, and isolation of the cationic Ru(II) complex $[RuCl\{(\eta^6\text{-}C_6H_5)B(C_6H_4PPh_2)_2\}][B(C_6F_5)_4]$. Both ruthenium complexes feature κ^2*PP*-coordination of the DPB backbone to ruthenium, and η^6-coordination of a *B*-phenyl ring to ruthenium; boron remains uncoordinated to ruthenium, with Ru–B distances of 3.221(5) and 2.647(2) Å, respectively.[126] The addition of PCy_3,[126] PMe_3, $PHCy_2$, PPh_3, $[Fe(\eta^5\text{-}C_5H_4P^iPr_2)_2]$, $Ph_2P(CH_2)_2PPh_2$, $P\{(CH_2)_2PPh_2\}_3$ or $Ph_2P(CH_2)_2(o\text{-}C_5H_4N)$ to $[RuCl\{(\eta^6\text{-}C_6H_5)B(C_6H_4PPh_2)_2\}][B(C_6F_5)_4]$ resulted in formation of $[RuCl\{(\eta^5\text{-}C_6H_5\text{-}o\text{-}PR_3)B(C_6H_4PPh_2)_2\}][B(C_6F_5)_4]$ complexes which now contain an η^5-coordinated *B*-cyclohexadienyl ring (**A** in Scheme 1.32). Alternatively, the addition of *N*-heterocyclic carbenes SIMes and SI^{t}Bu (SIR = $C\{N(R)(CH)\}_2$; R = Mes, ^{t}Bu) resulted in nucleophilic attack at either the *ortho*- or the *para*-positions of the η^6-coordinated *B*-phenyl ring, yielding $[RuCl\{(\eta^5\text{-}C_6H_5\text{-}o\text{-}SIR)B(C_6H_4PPh_2)_2\}][B(C_6F_5)_4]$ and $[RuCl\{(\eta^5\text{-}C_6H_5\text{-}p\text{-}SIR)B(C_6H_4PPh_2)_2\}][B(C_6F_5)_4]$ (R = Mes, ^{t}Bu) complexes featuring η^5-coordination of the *B*-phenyl ring, similarly to the phosphine-substituted complexes (**B** in Scheme 1.32). In contrast, the addition of the isonitriles AdNC and ^{t}BuNC resulted in coordination to boron yielding the isonitrile–borane adducts $[RuCl\{(\eta^6\text{-}C_6H_5)B(CNR)(C_6H_4PPh_2)_2\}][B(C_6F_5)_4]$ (R = Ad, ^{t}Bu; **C** in Scheme 1.32).[127]

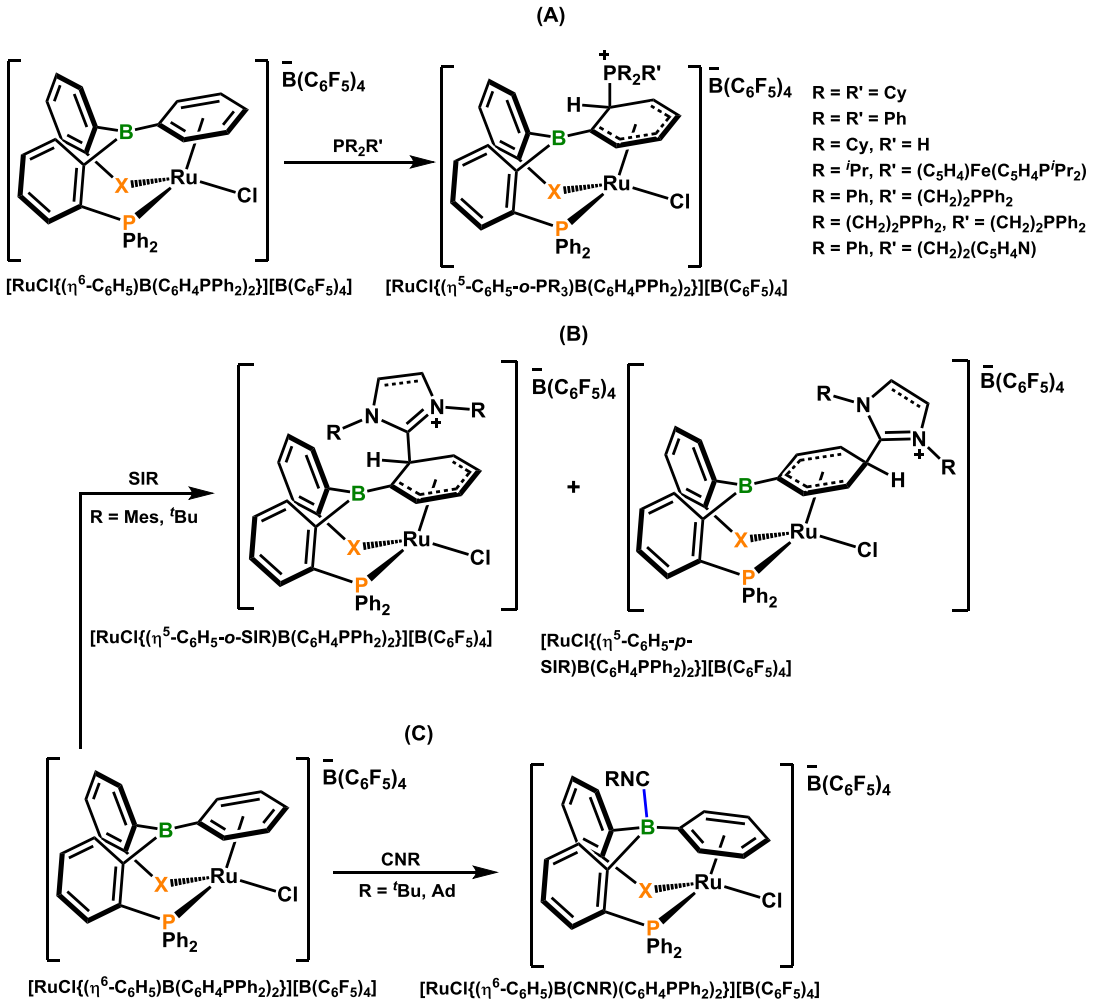

Scheme 1.32. Reactivity of $[RuCl\{(\eta^6\text{-}C_6H_5)B(C_6H_4PPh_2)_2\}][B(C_6F_5)_4]$ with various phosphines (**A**), *N*-heterocyclic carbenes (**B**) and isonitriles (**C**); $[RuCl\{(\eta^6\text{-}C_6H_5)B(C_6H_4PPh_2)_2\}][B(C_6F_5)_4]$ was formed via reaction of $^{Ph}DPB^{Ph}$ with $[RuCl_2(PPh_3)_3]$, followed with the addition of $K[B(C_6F_5)_4]$.

1.3.2.6 – Coordination Chemistry and Reactivity of Nickel and Iron Complexes of the DPB Ligand: Stabilization of a Variety of Oxidation States

The utility of Bourissous $^{R}DPB^{R'}$ ligand framework and its ability to stabilize transition metals in a variety of oxidation states was further expanded by Peters and co-workers, who explored the redox chemistry of nickel and iron complexes bearing the $^{R}DPB^{R'}$ (R = Ph, ^{i}Pr; R' = Ph, Mes) ligand and their reactivity towards H_2 and other small molecules. Reaction of $^{Ph}DPB^{Ph}$ with of 0.5 equivalents of both $NiBr_2$ and $[Ni(cod)_2]$

provided [NiBr(^{Ph}DPB^{Ph})] via comproportionation; the ^{Ph}DPB^{Ph} ligand is κ^2*PP*- and η^2*BC*-coordinated to nickel. Subsequent reduction of [NiBr(^{Ph}DPB^{Ph})] with Na/Hg amalgam produced the nickel(0) species [Ni(THF)(^{Ph}DPB^{Ph})], in which a *B*-phenyl ring is again η^2*BC*-coordinated to nickel (Scheme 1.33). Unfortunately, [Ni(THF)(^{Ph}DPB^{Ph})] did not react with H_2, owing to the strength of η^2*BC*-coordination as well as the difficulty in THF displacement. Alternatively, reduction of [NiBr(^{Ph}DPB^{Mes})] (^{Ph}DPB^{Mes} = {(*o*-$Ph_2P)C_6H_4\}_2$BMes) with Na/Hg amalgam afforded THF-free [Ni(^{Ph}DPB^{Mes})], which features η^3*BCC*-coordination. This complex readily reacted with H_2 (1 atm) at room temperature to provide a 5:1 equilibrium mixture of [NiH(μ-H)(^{Ph}DPB^{Mes})] and unreacted [Ni(^{Ph}DPB^{Mes})]; the addition of 4 atm H_2 pushed the equilibrium between [NiH(μ-H)(^{Ph}DPB^{Ph})] and [Ni(^{Ph}DPB^{Ph})] to 95:5. [NiH(μ-H)(^{Ph}DPB^{Mes})] is the product of oxidative addition of H_2, and possesses one terminal hydride ligand bound *trans*- to a hydride ligand bridging between nickel and boron, as evidenced by hydride signals located at –6.16 ppm (broad singlet) and –15.5 ppm (sharp triplet of doublets). However, [NiH(μ-H)(^{Ph}DPB^{Mes})] evaded structural characterization by single crystal X-ray diffraction due to its propensity to revert back to [Ni(^{Ph}DPB^{Ph})] in the absence of an H_2 atmosphere.[128]

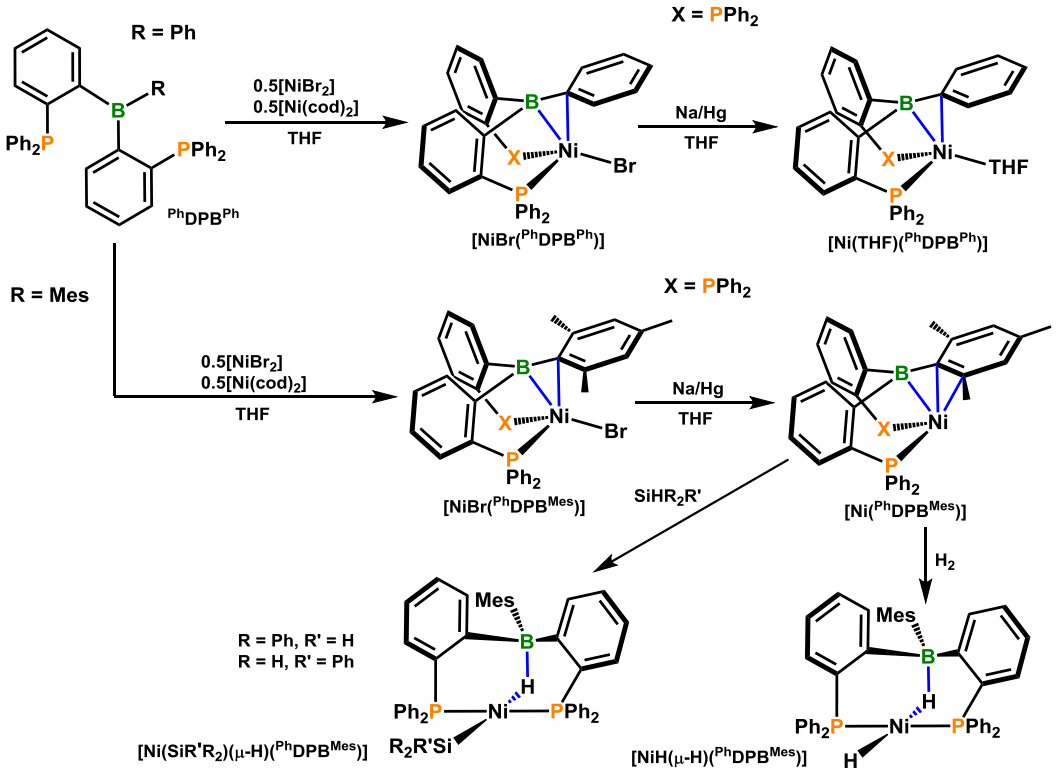

Scheme 1.33. Synthesis of [NiBr(^{Ph}DPB^{R})] (R = Ph, Mes) complexes, and subsequent reactivity with Na/Hg, H_2 and $HSiR_2R'$ (R = Ph, R' = H; R = H, R' = Ph).

Peters and co-workers embarked on tuning the electronics of the nickel centre in an attempt to isolate the non-classical [Ni(η^2-H_2)(DPB)] complex, which at the time would have been the first report of a d^{10}-transition metal–H_2 adduct characterized in solution. By changing the phenyl substituents on phosphorus to *iso*-propyl substituents, and by changing the mesityl groups on boron to phenyl groups, the DPB ligand possessed increased donor ability in conjunction with increased Lewis acidity of the pendant borane. Reduction of [NiBr(^{iPr}DPB^{Ph})] with Na/Hg amalgam in THF, analogous to [NiBr(^{Ph}DPB^{R})] (R = Ph, Mes) complexes above (*vide supra*), lead to isolation of [Ni(N_2)(^{iPr}DPB^{Ph})] (Scheme 1.34). A solution of [Ni(N_2)(^{iPr}DPB^{Ph})] in THF evolved from brick-red to a deep blue-green under vacuum, indicating N_2 displacement and THF coordination, and subsequent addition of 1 atm of H_2 produced a cherry-red solution, attributed to the formation of [Ni(η^2-H_2)(^{iPr}PDB^{Ph})]. Over several hours, [Ni(η^2-H_2)(^{iPr}DPB^{Ph})] underwent oxidative addition of H_2 to yield [NiH(μ-H)(^{iPr}DPB^{Ph})], and

unlike [NiH(μ-H)(^{Ph}DPB^{Mes})], the ^{iPr}DPB^{Ph} complex does not exist in equilibrium with [Ni(^{iPr}DPB^{Ph})]. Peters and co-workers utilized DFT calculations (M06L/6-31+G*) to identify the transition state for oxidative addition of H_2, and found that a transition state in which B–H bond formation occurs in concert with H–H bond cleavage across Ni is 9 kcal mol^{-1} lower in energy compared to a transition state in which H–H bond cleavage provides a Ni(II)-dihydride, from which boron abstracts one of the hydride ligands. On the basis of these calculations, Peters *et al.* favoured the mechanism in which both boron and nickel interact with H_2 to effect H–H bond cleavage.[40]

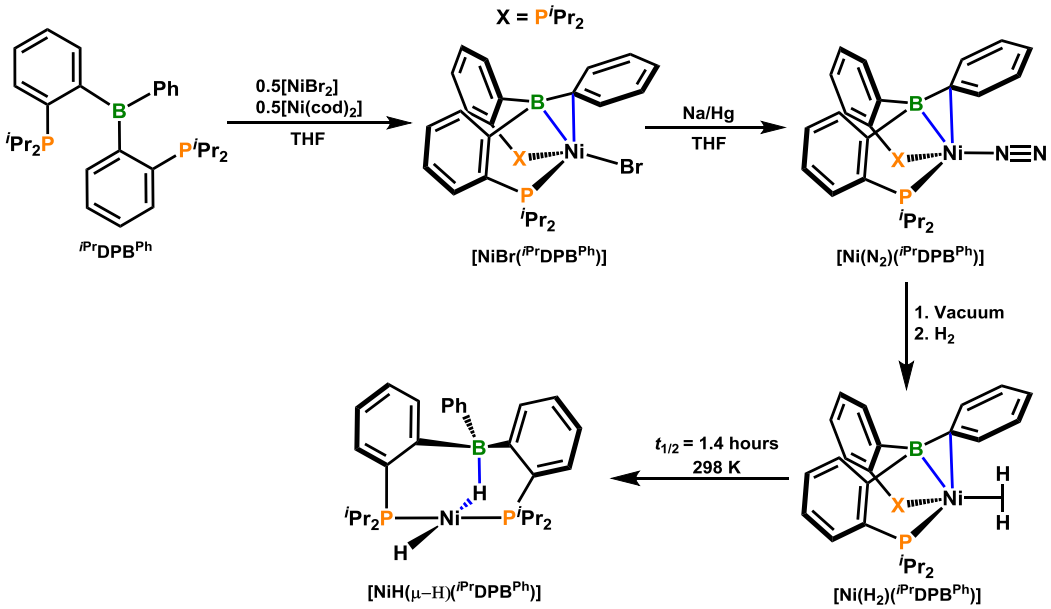

Scheme 1.34. Synthesis of [NiBr(^{iPr}DPB^{Ph})] and subsequent reactivity with Na/Hg and H_2.

As a means to exploit the ability for the DPB ligand framework to stabilize a rare two-electron redox process for a first row transition metal (i.e. to promote oxidative addition of H_2 to nickel) Peters and Harman added 20 equivalents of styrene to [Ni(^{Ph}DPB^{Mes})] under an H_2 atmosphere, and found complete conversion to ethylbenzene; prior to the addition of H_2, styrene reacted with [Ni(^{Ph}DPB^{Ph})] to form [Ni(η^2-H_2C=CHPh)(^{Ph}DPB^{Ph})], and during the course of catalysis, only [Ni(η^2-H_2C=CHPh)(^{Ph}DPB^{Ph})] was observed in solution. Overall, [Ni(^{Ph}DPB^{Ph})] was capable of

hydrogenating styrene under 1 atm H_2 at room temperature with 1 % catalyst loading.[128] In addition, Peters and co-workers sought to explore the reactivity of [Ni(^{Ph}DPB^{Ph})] with various $HSiR_2R'$ silanes (R = Ph, R' = H; R = H, R' = Ph) and were able to achieve successful oxidative addition, providing [Ni($SiR'R_2$)(μ-H)(^{Ph}DPB^{Mes})] complexes possessing a hydride ligand bridging between nickel and boron, verified by NMR spectroscopy and single crystal X-ray crystallography. Peters and co-workers sought to explore the effectiveness of [Ni($SiHPh_2$)(μ-H)(^{Ph}DPB^{Ph})] for the hydrosilylation of *para*-substituted benzaldehydes, and found that [Ni($SiHPh_2$)(μ-H)(^{Ph}DPB^{Ph})] was an effective catalyst. Similarly to the reactivity of [Ni(^{Ph}DPB^{Mes})] with styrene, stoichiometric addition of benzaldehyde to [Ni(^{Ph}DPB^{Ph})] resulted in the formation of [Ni(η^2-O=CHPh)(^{Ph}DPB^{Mes})].[129]

Peters also explored the potential functionalization of N_2 through the use of an iron complex bearing the DPB ligand framework. By generating iron-aminoimide complexes from N_2, functionalization at the N_α-atom with either hydrogen or silanes was hypothesized to be possible via reactivity similar to that observed (for alkenes and aldehydes) with the nickel complexes described above (*vide supra*). Peters and Suess were able to isolate [FeBr(^{R}DPB^{Ph})] (R = ^{i}Pr, Ph), which exhibits κ^2*PP*- and η^2*BC*-coordination of the DPB ligand, via reaction of ^{R}DPB^{Ph} with $FeBr_2$, followed with the addition of one equivalent of Na/Hg amalgam. Further reduction of [FeBr($^{i\text{Pr}}$DPB^{Ph})] with one equivalent of Na/Hg amalgam under an atmosphere of N_2 provided [Fe_2(μ-N_2)($^{i\text{Pr}}$DPB^{Ph})$_2$], in which one molecule of N_2 bridges between two iron centres, and is end-on coordinated to each (Scheme 1.35). In addition, a *B*-phenyl ring on one $^{i\text{Pr}}$DPB^{Ph} ligand is η^3*BCC*-coordinated, whereas the other is η^2*BC*-coordinated, owing to the flexibility of η^n-borane coordination in the DPB ligand framework. Alternatively, reduction of [FeBr(^{Ph}DPB^{Ph})] with one equivalent of Na/Hg under an atmosphere of N_2 provided co-ligand free [Fe(^{Ph}DPB^{Ph})], which exhibits κ^2*PP*-coordination in addition to a very unusual η^7*BPh*-coordination mode of a *B*-phenyl unit to iron (Scheme 1.35); η^7*BPh*-coordination is maintained in solution, as evidenced by significant shifts of the *B*-phenyl ^{13}C and ^{1}H NMR signals to lower frequency in the NMR spectra.[130]

Generation of iron-aminoimide complexes was achieved via the addition of 1.1 equivalents of 1,2-bis(chlorodimethylsilyl)ethane and 3.1 equivalents of Na/Hg amalgam to [FeBr(^{R}DPB^{Ph})] (R = ^{i}Pr, Ph) under an N_2 atmosphere, which ultimately resulted in clean formation of [Fe{N_2(Me_2SiCH_2)$_2$}(^{R}DPB^{Ph})], featuring κ^2*PP*- and η^3*BCC*-coordination, in addition to a Fe≡N triple bond between iron and the aminoimide ligand (Scheme 1.35). Similarly to the reduction of [FeBr(^{R}DPB^{Ph})] (R = ^{i}Pr, Ph), divergent reactivity was observed with [Fe{N_2(Me_2SiCH_2)$_2$}(^{R}DPB^{Ph})] possessing either *iso*-propyl or phenyl substituents on phosphorus. The addition of $PhSiH_3$ to [Fe{N_2(Me_2SiCH_2)$_2$}(^{iPr}DPB^{Ph})] produced the iron-trisilylhydrazido(–) product [Fe(μ-H){N(SiH_2Ph)–N(Me_2SiCH_2)$_2$}(^{iPr}DPB^{Ph})] (Scheme 1.35), formed by hydrosilylation of the Fe–N bond (resulting in attachment of SiH_2Ph to the N_α-atom and formation of a bridging Fe–H–B interaction), which at the time of report was the first example of an iron-hydrazido(–) complex derived from N_2. Alternatively, the addition of H_2 to [Fe{N_2(Me_2SiCH_2)$_2$}(^{Ph}DPB^{Ph})] yielded [Fe(μ-H)(κ^2*NN*-N(H)Si(Me_2)(CH_2)$_2$Si(Me_2)N={(PPh_2-*o*)C_6H_4}BPh{C_6H_4(*o*-Ph_2P)}] (Scheme 1.35). The initial step in this reaction is presumably analogous to the observed hydrosilylation of [Fe{N_2(Me_2SiCH_2)$_2$}(^{Ph}DPB^{Ph})] (*vide supra*), likely followed by hydrazine rearrangement to provide the six-membered (HN–Si(Me_2)–CH_2–CH_2–Si(Me_2)–N)–Fe unit, and either direct N–N cleavage and transfer to phosphorus, providing the phosphinimine in the final product, or N–N bond cleavage to yield an iron(IV)–imido complex, followed by transfer of the NR unit to phosphorus.[130]

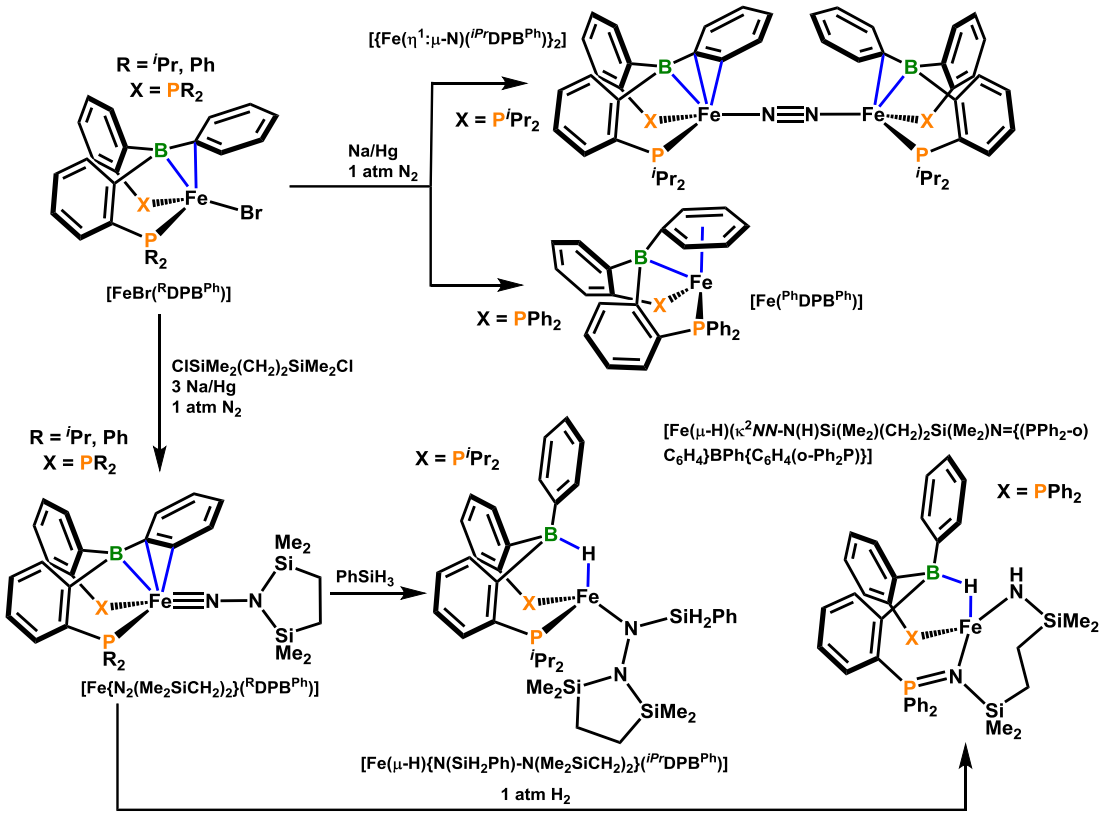

Scheme 1.35. Reactivity of [FeBr(^{R}DPB^{Ph})] (R = ^{i}Pr, Ph) with Na/Hg under N_2 in the presence and absence of 1,2-bis(chlorodimethylsilyl)ethane, as well as the reactivity of [Fe{N_2(Me$_2$SiCH$_2$)$_2$}(^{R}DPB^{Ph})] (R = ^{i}Pr, Ph) with PhSiH$_3$ and H_2, respectively.

Peters and Suess continued to explore the reduction chemistry of their Fe-DPB system for potential in reductive coupling of CO-containing fragments. Using [Fe$_2$(μ-N_2)(^{iPr}DPB^{Ph})$_2$] as their starting material, addition of two equivalents of CO yielded [Fe(CO)$_2$(^{iPr}DPB^{Ph})], which further reacted with an additional equivalent of CO to provide [Fe(CO)$_3$(^{iPr}DPB^{Ph})] (Scheme 1.36). While the latter complex features κ^3*PPB*-coordination of the DPB ligand, the former entails κ^2*PP*- and unusual η^2*BC*-coordination involving boron and the *ipso*-carbon atom of the phenylene linker between boron and one of the phosphine donors. Peters and Suess were also able to isolate monoanionic and dianionic analogues of [Fe(CO)$_2$(^{iPr}DPB^{Ph})] through reaction of [Fe(CO)$_2$(^{iPr}DPB^{Ph})] with either one equivalent of potassium and two equivalents of benzo-15-crown-5 (benzo-15-c-5), or with excess potassium and four equivalents of benzo-15-c-5, yielding [K(benzo-

15-c-5)$_2$][Fe(CO)$_2$($^{i\text{Pr}}$DPB$^{\text{Ph}}$)] and [K(benzo-15-c-5)$_2$]$_2$[Fe(CO)$_2$($^{i\text{Pr}}$DPB$^{\text{Ph}}$)], respectively (Scheme 1.36). Both the monoanionic and dianionic complexes are κ^3*PPB*-coordinated by the DPB ligand, and in moving from neutral to dianionic [Fe(CO)$_2$($^{i\text{Pr}}$DPB$^{\text{Ph}}$)]$^{2-}$ the following structural and spectroscopic features are observed: (1) A decrease in Fe–CO bond length, (2) a decrease in Fe–P bond length, (3) an increase in Fe–B bond length, (4) increased pyramidalization of boron, (5) a shift of the ^{11}B NMR signal to higher frequency, and (6) a decrease in CO stretching frequency. These data suggest that upon reduction of iron, increased π-backbonding to CO and phosphorus occurs rather than increased σ-backbonding to boron. Given the high electron density presumed to be centred in the carbonyl co-ligands of dianionic [Fe(CO)$_2$($^{i\text{Pr}}$DPB$^{\text{Ph}}$)]$^{2-}$, the authors hypothesized that functionalization of the oxygen atoms using an electrophilic reagent could provide the respective iron-dicarbyne complex; treatment of neutral [Fe(CO)$_2$($^{i\text{Pr}}$DPB$^{\text{Ph}}$)] with excess potassium and 2.2 equivalents of trimethylsilyltriflate resulted in silylation of both oxygen atoms and generation of the iron-dicarbyne species [Fe(COSiMe$_3$)$_2$($^{i\text{Pr}}$DPB$^{\text{Ph}}$)] (Scheme 1.36). Peters and Suess also sought to investigate the ease of reductive coupling of the two carbyne fragments upon the addition of H_2, and indeed, room temperature addition of 1 atm H_2 to [Fe(COSiMe$_3$)$_2$($^{i\text{Pr}}$DPB$^{\text{Ph}}$)] provided *Z*-(Me$_3$SiO)CH=CH(OSiMe$_3$) in an average yield of 43 %.[131]

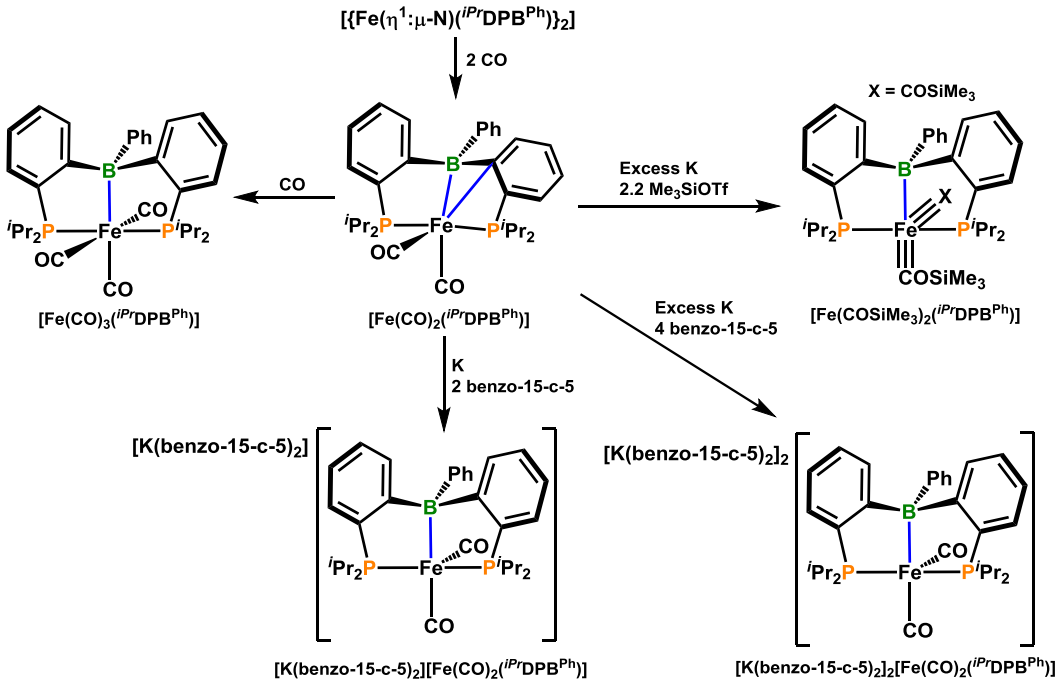

Scheme 1.36. Reactivity of $[Fe_2(\mu\text{-}N_2)(^{iPr}DPB^{Ph})_2]$ with CO, in addition to reduction of $[Fe(CO)_2(^{iPr}DPB^{Ph})]$ to $[Fe(CO)_2(^{iPr}DPB^{Ph})]^{x-}$ (x = 1 or 2), and reduction of $[Fe(CO)_2(^{iPr}DPB^{Ph})]$ in the presence of Me_3SiOTf to yield $[Fe(COSiMe_3)_2(^{iPr}DPB^{Ph})]$.

1.3.3 – Transition Metal Complexes Featuring Tetradentate Phosphine/Borane Ligands

1.3.3.1 – The $\{(o\text{-}R_2P)C_6H_4\}_3B$ (^{R}TPB; R = ^{i}Pr, Ph) Ligands

The $\{(o\text{-}^{i}Pr_2P)C_6H_4\}_3B$ ligand (^{iPr}TPB, Scheme 1.37) was the missing piece of the series of phosphine/borane ligands prepared by Bourissou and co-workers, and was obtained via lithiation of three equivalents of $(o\text{-}^{i}Pr_2P)C_6H_4Br$ followed with the addition of BCl_3 (Scheme 1.37). The ^{iPr}TPB ligand, similarly to the $^{iPr}DPB^{Ph}$ ligand, exists in the solution-state in an equilibrium between P→B adducted and non-adducted forms; at room temperature the ^{31}P and ^{11}B chemical shifts are 4.9 and 50.1 ppm, respectively. However, when cooled to –100 °C the ^{iPr}TPB ligand gives rise to two ^{31}P NMR signals in the solution-state located at 26.1 and –2.9 ppm that integrate in a 1:2 ratio, and the solid-state ^{11}B chemical shift is 13.0 ppm, which is shifted to significantly lower frequency relative

to the solution-state ^{11}B chemical shift at room temperature, indicating that the $^{i\text{Pr}}$TPB ligand exists as in intramolecular P→B adduct in the solid-state and at low temperatures in the solution-state. This is further corroborated by a P(1)–B bond distance of 2.154 Å (r_α = 1.13)[68] compared to P(2)–B and P(3)–B bond distances of 3.307 and 3.267 Å observed in the solid-state structure of $^{i\text{Pr}}$TPB.[104]

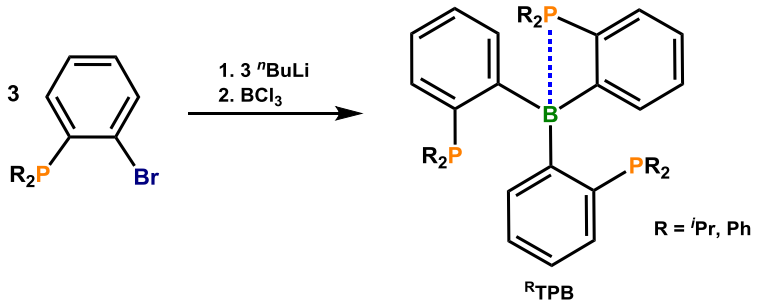

Scheme 1.37. Synthesis of the ^{R}TPB ligand (R = ^{i}Pr, Ph).

1.3.3.2 – Group 10 and Group 11 Metal Coordination Complexes of $^{i\text{Pr}}$TPB

Reaction of the $^{i\text{Pr}}$TPB ligand with either [Pt(P^tBu_3)$_2$] or [AuCl(SMe_2)] lead to platinum(0) and gold(I) complexes featuring κ^4*PPPB*-coordination of the trisphosphine/borane ligand, possessing trigonal pyramidal and trigonal bipyramidal geometries, respectively (Scheme 1.38). The Au–B bond length in [AuCl($^{i\text{Pr}}$TPB)] is 2.318(8) Å (r_α = 1.05),[68] and the ^{11}B chemical shift and sum of the C–B–C angles are equal to 27.7 ppm and 339.3°, respectively, indicating that coordination of the trisphosphine/borane ligand $^{i\text{Pr}}$TPB to gold yields a much stronger bonding interaction between the gold and boron than is achieved using the $^{i\text{Pr}}$MDP$^{R'}$ ligands (R' = Cy, Flu; *vide supra*). Similarly, [Pt($^{i\text{Pr}}$TPB)] exhibits close approach of boron to the metal centre, with the Pt–B bond distance, ^{11}B chemical shift and sum of the C–B–C angles equal to 2.224(4) Å (r_α = 1.01),[68] 18.2 ppm and 337.2°, respectively. These data are indicative of stronger metal–borane coordination for the Pt(0) complex relative to the Au(I) complex, likely due to the greater basicity of Pt(0) compared with Au(I).[132]

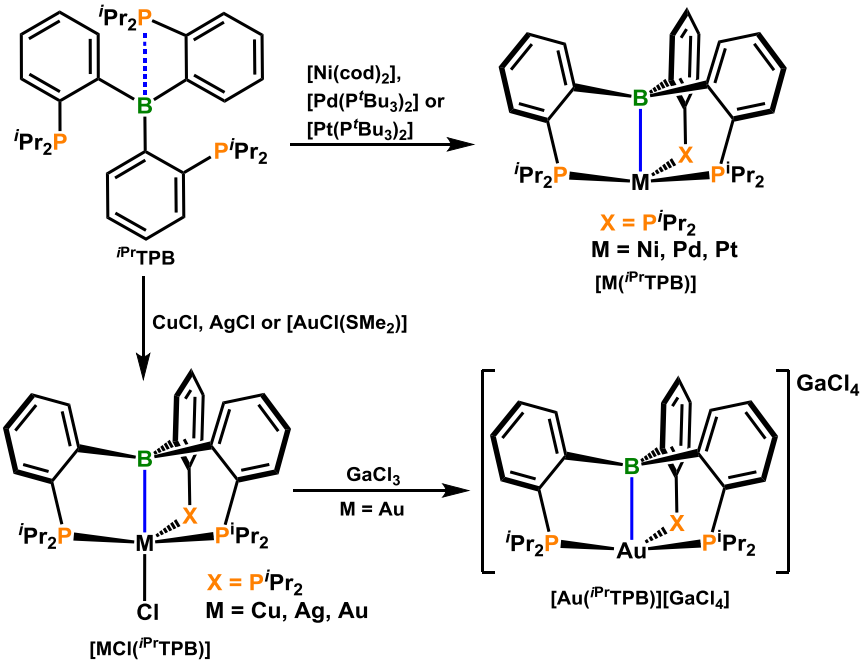

Scheme 1.38. Reaction of ^{iPr}TPB with [Ni(cod)$_2$], [Pd(P^{t}Bu$_3$)$_2$], [Pt(P^{t}Bu$_3$)$_2$], AgCl and [AuCl(SMe$_2$)], and subsequent reactivity of [AuCl(^{iPr}TPB)] with GaCl$_3$ to generate cationic [Au(^{iPr}TPB)][GaCl$_4$].

Bourissou and Ozerov have extended the coordination chemistry of the ^{iPr}TPB ligand to the remainder of the Group 10 and Group 11 metals. Reaction of ^{iPr}TPB with either [Ni(cod)$_2$] with heating to 80 °C, or [Pd(P^{t}Bu$_3$)$_2$] at room temperature provided co-ligand free [M(^{iPr}TPB)] (M = Ni, Pd) complexes that possess κ^4*PPPB*-coordination of the P$_3$B-ligand and trigonal pyramidal geometry (Scheme 1.38). Alternatively, reaction of ^{iPr}TPB with CuCl or AgCl yielded [MCl(^{iPr}TPB)] (M = Cu, Ag) complexes isostructural with the gold(I) complex displayed in Scheme 1.38 above. In addition, Bourissou and Ozerov generated the gold(I) cationic complex, [Au(^{iPr}TPB)][GaCl$_4$], via reaction of [AuCl(^{iPr}TPB)] with GaCl$_3$ (Scheme 1.38).

For the nickel and palladium complexes of ^{iPr}TPB, close approach of boron to the metal centre is evidenced by Ni–B and Pd–B bond lengths of 2.168(2) (r_α = 1.04)[68] and 2.254(2) Å (r_α = 1.01),[68] respectively, in conjunction with ^{11}B chemical shifts and Σ(C–B–C) values of 15.9 ppm and 339.1° for [Ni(^{iPr}TPB)], and 27.3 ppm and 341.8° for [Pd(^{iPr}TPB)]. In light of the equivalent values reported for the isostructural platinum

complex (*vide supra*), the strength of metal–borane coordination appears to be greater for nickel and platinum than for palladium, as opposed to increasing with increasing basicity of the Group 10 metals. These values have been further substantiated by DFT calculations, and the progression in metal–borane coordination strength is attributed to: (1) The covalent radius of nickel presents itself as a more appropriate fit into the binding pocket of the TPB ligand, giving rise to tighter coordination to the borane than palladium, and (2) the superior basicity of platinum allows for the strongest metal–borane coordination of the Group 10 metals.

A similar trend is observed for the Group 11 metal complexes of $^{i\text{Pr}}$TPB; close approach of copper and silver are evidenced by M–B (M = Cu, Ag) bond lengths of 2.508(2) (r_α = 1.16)[68] and 2.540(2) Å (r_α = 1.17),[68] which are well within the sum of the van der Waals radii, but the ^{11}B chemical shifts for [CuCl($^{i\text{Pr}}$TPB)] and [Ag($^{i\text{Pr}}$TPB)] are 53.8 ppm for both complexes, which is shifted to lower frequency relative to the expected chemical shift for a free triarylborane, and the sum of the C–B–C angles are 347.0 and 347.4°, respectively, demonstrating that copper– and silver–borane coordination is weaker than gold–borane coordination. Similarly to the Group 10 analogs, these values have been further corroborated by DFT calculations, and support the notion that Group 11 metal–borane coordination strength increases as the basicity of the metal increases. Relative to the Group 10 metals, the Group 11 metals display weaker coordination to boron, which is attributed to the higher oxidation state of the metals (+1 versus neutral). However, the gold–borane coordination strength is similar to that involving platinum due to destabilization of the 5d orbitals by relativistic effects. Furthermore, in moving from neutral [AuCl($^{i\text{Pr}}$TPB)] to cationic [Au($^{i\text{Pr}}$TPB)][$GaCl_4$], the Au–B bond length increases from 2.318(8) to 2.448(8) Å (r_α = 1.11),[68] the ^{11}B chemical shift increases from 27.7 to 56.6 ppm, and the sum of the C–B–C angles increases from 339.3 to 351.3°, indicating that gold–borane coordination is weaker in the cationic complex relative to the neutral complex.[133]

1.3.3.3 – Coordination Chemistry and Reactivity of Iron, Copper and Cobalt Complexes of the $^{i\mathrm{Pr}}$TPB Ligand

Aside from exploring the chemistry of the DPB ligand framework, the Peters Group have burrowed into the rich chemistry made accessible through the use of the TPB ligand scaffold. Peters and co-workers moved towards surveying the coordination chemistry of the TPB ligand with iron, cobalt and copper, and began exploring the redox chemistry of these metal complexes, and their reactivity towards small molecules.

In 2011, Peters and Moret reported the comproportionation reaction of $^{i\mathrm{Pr}}$TPB with a 1:1 mixture of 0.5 equivalents $FeBr_2$ and iron powder, which provided [FeBr($^{i\mathrm{Pr}}$TPB)] as a complex with a geometry intermediate between trigonal bipyramidal and pseudotetrahedral, with a κ^4*PPPB*-coordinated TPB ligand (Scheme 1.39). Evans magnetic measurements indicated there are three unpaired electrons in [FeBr($^{i\mathrm{Pr}}$TPB)], and the solid-state structure possesses an Fe–B bond length of 2.459 Å (r_α = 1.14)[68] with the sum of the C–B–C angles equalling 341.9°. From the iron(I) bromide complex, reaction with either 1 or 2.5 equivalents of sodium naphthalenide under an N_2 atmosphere provided the neutral and anionic iron complexes [Fe(N_2)($^{i\mathrm{Pr}}$TPB)] and Na[Fe(N_2)($^{i\mathrm{Pr}}$TPB)] (or [Na(12-crown-4)$_2$][Fe(N_2)($^{i\mathrm{Pr}}$TPB)] if the latter complex is treated with two equivalents of 12-crown-4; Scheme 1.39). In both complexes the $^{i\mathrm{Pr}}$TPB ligand is κ^4*PPPB*-coordinated to iron, the N_2 ligand is bound end-on and the coordination geometry of iron is trigonal bipyramidal. The N_2 ligand in neutral [Fe(N_2)($^{i\mathrm{Pr}}$TPB)] was labile and could be removed *in vacuo*. The solid-state structures of Na[Fe(N_2)($^{i\mathrm{Pr}}$TPB)] and [Na(12-crown-4)$_2$][Fe(N_2)($^{i\mathrm{Pr}}$TPB)] featured similar Fe–B bond lengths (2.311 and 2.293 Å, respectively; r_α = 1.07 and 1.06)[68] and similar pyramidalization of boron [Σ(C–B–C) = 329.8 and 331.0°, respectively]; shorter Fe–B bond lengths and greater pyramidalization of boron were observed for the anionic complex, consistent with expectations for a more basic metal centre. Neutral [Fe(N_2)($^{i\mathrm{Pr}}$TPB)] was then subject to reaction with CO, resulting in displacement of N_2 and coordination of CO forming [Fe(CO)($^{i\mathrm{Pr}}$TPB)]. Furthermore, [Fe(N_2)($^{i\mathrm{Pr}}$TPB)] reacted with *p*-methoxyphenylazide to yield the iron(II) imide complex [Fe(NC_6H_4OMe-*p*)($^{i\mathrm{Pr}}$TPB)] (Scheme 1.39). The former

complex contained a CO ligand coordinated *trans* to the borane, and in addition to κ^2*PP*-coordination, boron, the *ipso*- and *ortho*-carbon atoms of one of the phenylene linkers and phosphorus are engaged in rare η^4*BCCP*-coordination to iron. The Fe–B bond length in [Fe(CO)(^{iPr}TPB)] (2.227 Å; r_α = 1.03)[68] is shorter than in the anionic N_2 complexes, and the sum of the C–B–C angles is 352.0°. In the case of [Fe(NC$_6$H$_4$OMe-*p*)(^{iPr}TPB)], iron possesses pseudotetrahedral geometry with only a weak bonding interaction with boron. The Fe–B bond length is the longest of the series of iron complexes (2.608 Å; r_α = 1.21),[68] although boron is still significantly pyramidalized [Σ(C–B–C) = 338.3°].[46]

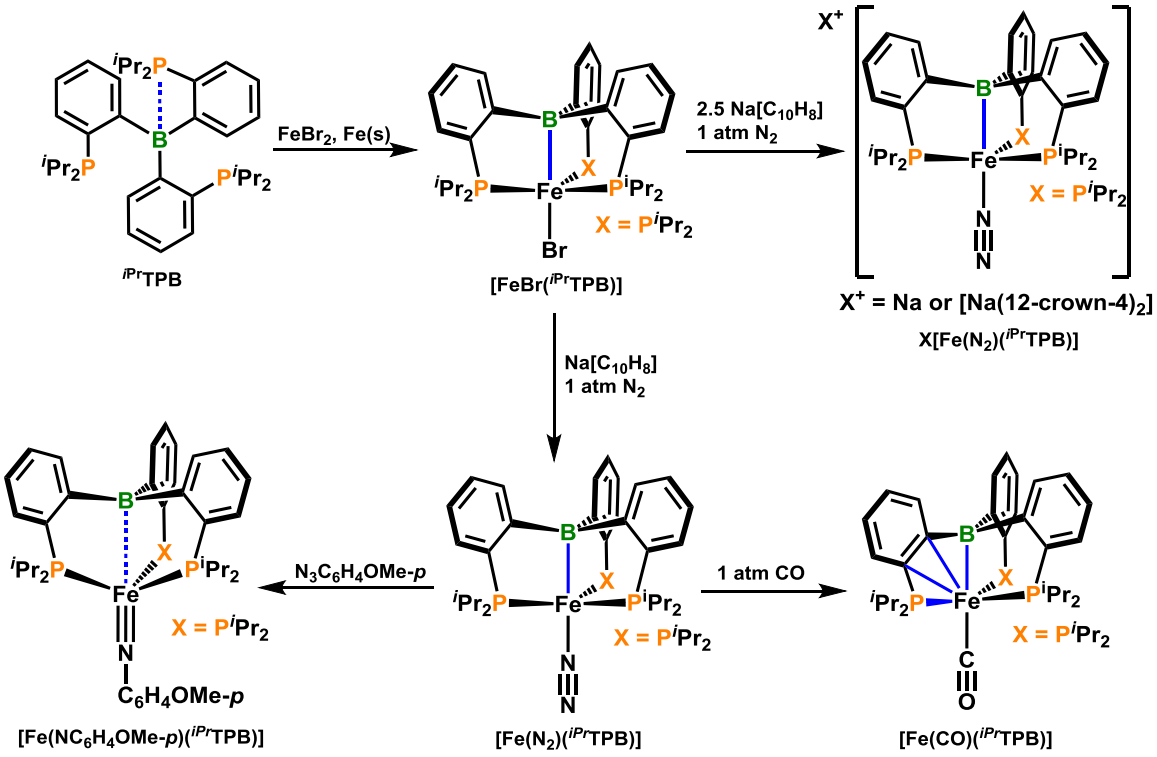

Scheme 1.39. Coordination of ^{iPr}TPB to Fe(–1), Fe(0), Fe(I) and Fe(II).

Given the progress made in accessing iron complexes in a range of oxidation states and coordinated to by a variety of small molecule ligands, all while retaining the TPB ligand, Peters and Moret turned their attention towards functionalization of N_2 coordinated to iron, analogous to efforts made while utilizing the ^{R}DPB^{Ph} (R = ^{i}Pr, Ph)

ligand (Section 1.3.2.6). Starting from anionic Na[Fe(N_2)($^{i\text{Pr}}$TPB)], treatment with trimethylsilyl chloride (TMSCl) yielded the iron(I) silyldiazenido complex, [Fe(N_2SiMe$_3$)($^{i\text{Pr}}$TPB)], which is paramagnetic and contains one unpaired electron (Scheme 1.40). [Fe(N_2SiMe$_3$)($^{i\text{Pr}}$TPB)] exhibits intermediate geometry between trigonal bipyramidal and pseudotetrahedral, as it contains an elongated Fe–B bond length [2.4350(9) Å; r_α = 1.13][68] relative to anionic Na[Fe(N_2)($^{i\text{Pr}}$TPB)]. Addition of either excess Na/Hg amalgam to [Fe(N_2SiMe$_3$)($^{i\text{Pr}}$TPB)], or excess Na/Hg amalgam and excess TMSCl to [FeBr($^{i\text{Pr}}$TPB)] provided the diamagnetic iron(II) complex, [Na(THF)][Fe(N_2SiMe$_3$)($^{i\text{Pr}}$TPB)], in which the $^{i\text{Pr}}$TPB ligand is κ^2*PP*-coordinated by two of the three phosphine donors, and the borane unit is η^3*BCC*-coordinated via boron and the *ipso*- and *ortho*-carbon atoms of a phenylene linker. The Fe–B bond length in [Na(THF)][Fe(N_2SiMe$_3$)($^{i\text{Pr}}$TPB)] is 2.319(3) Å (r_α = 1.07),[68] and the former N=N double bond is significantly elongated from 1.222(2)/1.227(2) Å in [Fe(N_2SiMe$_3$)($^{i\text{Pr}}$TPB)] (the β-nitrogen atoms is disordered over two positions) to 1.260(3) Å in the monoanion, in conjunction with a decrease in N–N–Si angle from 161.3(2)/166.6(2) to 131.3(2)°, indicative of population of the π*-orbitals of the N–N linkage. The β-nitrogen atom of coordinated N_2 may also be functionalized by treatment of [FeBr($^{i\text{Pr}}$TPB)] with 1,2-bis(chloridimethylsilyl)ethane in the presence of excess Na/Hg amalgam under an N_2 atmosphere, providing the diamagnetic iron(II) disilylhydrazide complex [Fe{N_2(Si(Me$_2$)CH$_2$CH$_2$Si(Me$_2$))}($^{i\text{Pr}}$TPB)] (Scheme 1.40), which gave rise to an ^{11}B NMR signal at 27 ppm and calculated Fe–B and N–N bond lengths of 2.785 (r_α = 1.29)[68] and 1.349 Å, respectively. Despite only obtaining crystals that suffered from severe disorder, the addition of either CO or CN^{t}Bu to [Fe{N_2(Me$_2$SiCH$_2$CH$_2$SiMe$_2$)}($^{i\text{Pr}}$TPB)] resulted in the formation of the crystalline adducts, [FeL{N_2(Si(Me$_2$)CH$_2$CH$_2$Si(Me$_2$))}($^{i\text{Pr}}$TPB)] (L = CO, CN^{t}Bu). The solid-state structures of both complexes indicated the TPB ligand is only κ^2*PP*-coordinated to iron by two of the three phosphine donors, with Fe–B bond distances of 2.943 (r_α = 1.36)[68] and 2.863 Å (r_α = 1.33)[68] for L = CO and CN^{t}Bu, respectively. Futhermore, the disilylhydrazido ligand remains intact, with CO or CN^{t}Bu terminally bound to the iron centre (Scheme 1.40). In

addition, the N–N bond length is 1.3273(7) and 1.351(3) Å when L = CO or CN^{t}Bu, respectively, consistent with an N–N single bond.[134]

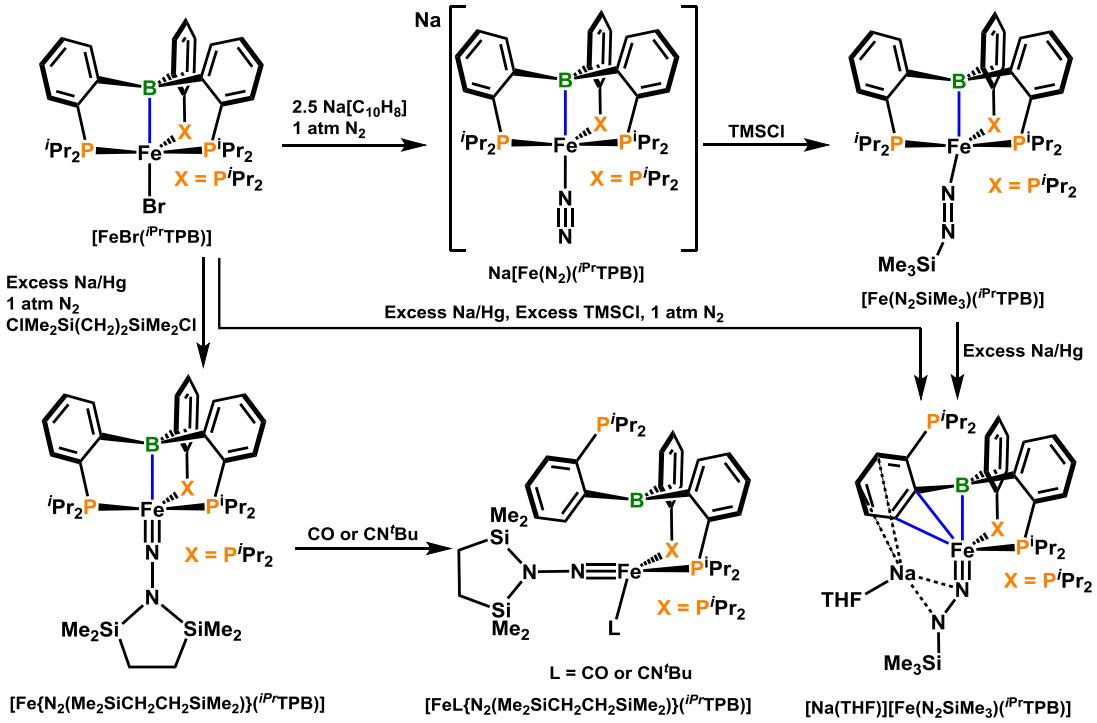

Scheme 1.40. Fe(–1), Fe(0), Fe(I) and Fe(II) complexes bearing the $^{i\text{Pr}}$TPB ligand, and a progression of Fe–N bond contraction in combination with N–N bond elongation upon reduction and functionalization of a N_2 ligand.

Throughout the series of Fe–N_2, Na[Fe–N_2], Fe–N=NR, Na[Fe≡N–NR], Fe≡N–NR_2 and LFe≡N–NR_2 (L = CO or CN^{t}Bu; R = silyl substituents) complexes, a noticeable decrease in Fe–N bond length and increase in N–N bond length is observed due to population of the π*(N–N) orbitals. Such a progression may be viewed analogously to the iron-based Chatt cycle for nitrogen fixation, in which Fe–N bond contraction and N–N bond elongation is suggested upon the addition of protons to the β-nitrogen atom;[135] in this case, silyl cations are being added as opposed to protons. In terms of the influence of the pendant borane in the TPB ligand system, the hemilabile nature of the Fe–B bonding interaction and its ability to adjust the Fe–B bond distance and accommodate varying

coordination geometries at iron as a function of the reactivity taking place at the iron centre (ie. oxidation/reduction, functionalization of N_2) appears quintessential during these transformative processes.[134]

In 2012 and 2013, Peters and co-workers published two separate reports on the production and release of NH_3 from an iron–TPB complex. Initial efforts were geared towards generating the co-ligand-free Fe–TPB complex; first by reaction of [FeBr($^{i\text{Pr}}$TPB)] with MeLi, yielding [FeMe($^{i\text{Pr}}$TPB)], followed by protonation using $[H(OEt_2)_2][BAr^F{}_4]$ (Ar^F = 3,5-$(CF_3)_2$-C_6H_3) to liberate methane and generate [Fe($^{i\text{Pr}}$TPB)][$BAr^F{}_4$] as a distorted trigonal pyramid (Scheme 1.41). The Fe–B bond length in [Fe($^{i\text{Pr}}$TPB)][$BAr^F{}_4$] [2.217(2) Å; r_α = 1.03][68] is shorter than in [FeBr($^{i\text{Pr}}$TPB)] [2.459(5) Å; r_α = 1.14],[68] which is unexpected given that removal of a σ-donor ligand and generation of a cation should reduce the basicity of iron, thus decreasing the Fe–B bond strength, as was observed by Bourissou and co-workers upon conversion of [AuCl($^{i\text{Pr}}$TPB)] to [Au($^{i\text{Pr}}$TPB)][$GaCl_4$] (*vide supra*). However, the sum of the C–B–C angles in [Fe($^{i\text{Pr}}$TPB)][$BAr^F{}_4$] is 347.3° (versus 341.2° in [FeBr($^{i\text{Pr}}$TPB)]) indicating that despite a shorter Fe–B distance in the co-ligand free cation, the iron–borane bonding interaction is likely weaker. Treatment of [Fe($^{i\text{Pr}}$TPB)][$BAr^F{}_4$] with excess hydrazine provided [Fe(N_2H_4)($^{i\text{Pr}}$TPB)][$BAr^F{}_4$], which was stable to vacuum, but converted to the cationic ammonia complex [Fe(NH_3)($^{i\text{Pr}}$TPB)][$BAr^F{}_4$] over several hours at room temperature (Scheme 1.42). The Fe–N bond distances in the hydrazine and ammonia complexes were 2.205(2) and 2.280(3) Å, respectively, and the Fe–B bond lengths were 2.392(2) Å (r_α = 1.11)[68] [Σ(C–B–C) = 339°] and 2.433(3) Å (r_α = 1.13)[68] [Σ(C–B–C) = 341°], respectively. Furthermore, treatment of [Fe($^{i\text{Pr}}$TPB)][$BAr^F{}_4$] with either excess $NaNH_2$ or NaOH generated [Fe(NH_2)($^{i\text{Pr}}$TPB)] and [Fe(OH)($^{i\text{Pr}}$TPB)], respectively (Scheme 1.42).[136]

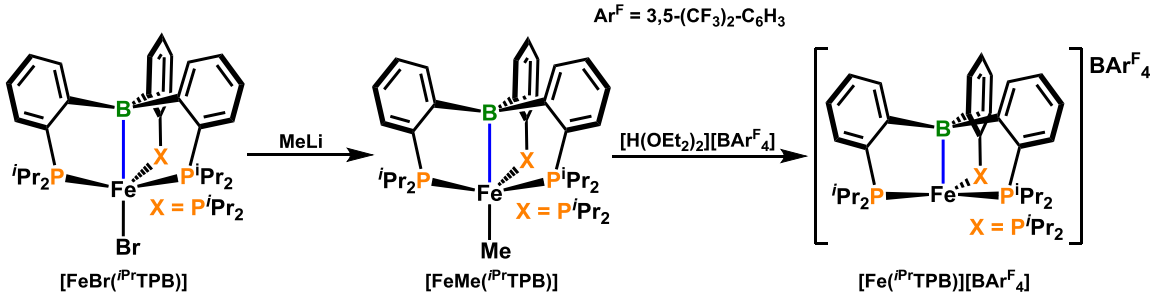

Scheme 1.41. Synthesis of [FeMe(^{iPr}TPB)] and [Fe(^{iPr}TPB)][BAr^F_4] (Ar^F = 3,5-$(CF_3)_2$-C_6H_3).

Peters and co-workers also attempted to form cationic [Fe(NH_3)(^{iPr}TPB)][BAr^F_4] from [Fe(NH_2)(^{iPr}TPB)], followed by generation of the Fe–N_2 complex, [Fe(N_2)(^{iPr}TPB)], with release of NH_3 via the addition of a proton source in the presence of a reductant. Indeed, both endeavours were achieved via reaction of [Fe(NH_2)(^{iPr}TPB)] with [$H(OEt_2)_2$][BAr^F_4], followed by reduction with potassium graphite under an atmosphere of N_2 (Scheme 1.42).[136] Furthermore, the addition of excess [$H(OEt_2)_2$][BAr^F_4] and excess potassium graphite to either [Na(12-crown-4)$_2$][Fe(N_2)(^{iPr}TPB)] or [Fe(^{iPr}TPB)][BAr^F_4] in diethyl ether at –78 °C under an atmosphere of N_2 catalytically produced an average of 7.0 equivalents of NH_3 per iron atom after 16 trials, indicating that 44 % of the added protons were reliably transferred to N_2 to produce NH_3; the maximum yield was 8.5 equivalents of NH_3. Moreover, the addition of potassium graphite to [$H(OEt_2)_2$][BAr^F_4] under an atmosphere of N_2 only produced H_2 and not NH_3, indicating the iron centre is essential for the transfer of protons to nitrogen, and the silyl-containing analogue, [Na(12-crown-4)$_2$][Fe(N_2)(^{iPr}TPSi)] (^{iPr}TPSi = {(*o*-^{i}Pr$_2$P)C_6H_4}$_3$$Si^-$) only produced 0.7 ± 0.5 equivalents of ammonia when subject to the same reaction conditions, indicating that hemilabile iron–borane coordination made possible through the use of the TPB ligand framework is extremely important in this catalytic process.[137]

Peters and co-workers have also explored the propensity for [Fe(N_2)(^{iPr}TPB)] to react with H_2 (1 and 2 equivalents), acetone, CO, CN^tBu, C_2H_4 and aryl acetylenes (aryl = phenyl, tolyl).[60]

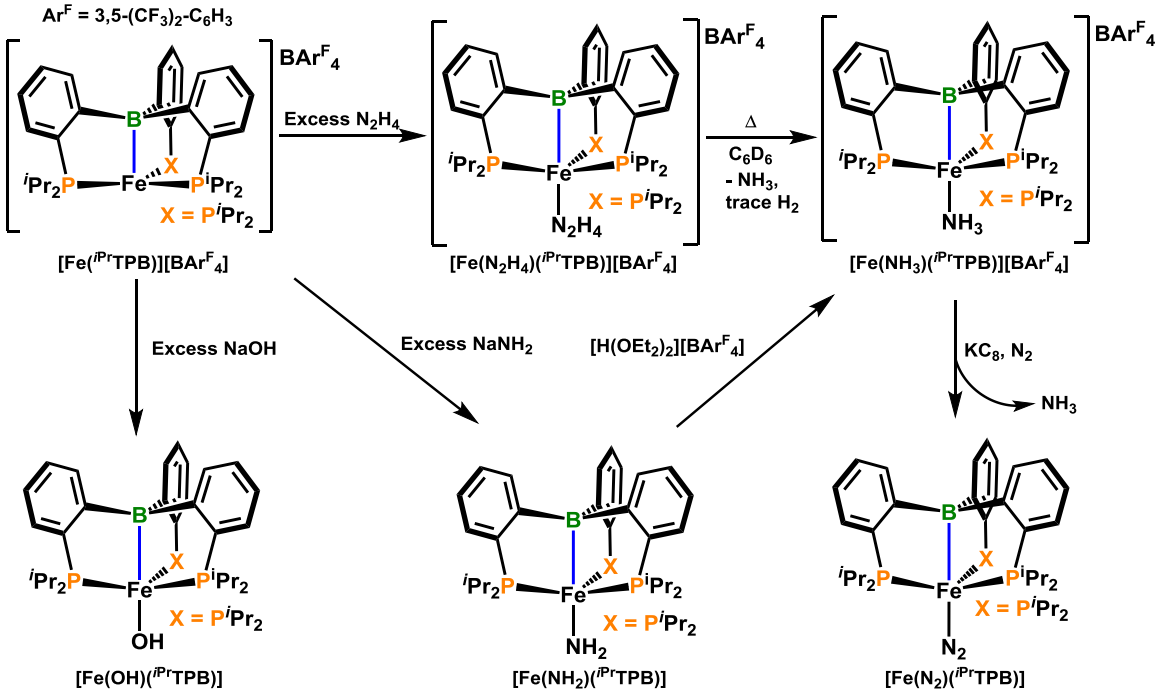

Scheme 1.42. Generation of [Fe(NH$_3$)($^{i\text{Pr}}$TPB)][BAr$^F_4$] (Ar^F = 3,5-(CF$_3$)$_2$-C$_6$H$_3$) from [Fe(N$_2$H$_4$)($^{i\text{Pr}}$TPB)][BAr$^F_4$] or [Fe(NH$_2$)($^{i\text{Pr}}$TPB)], followed with generation of [Fe(N$_2$)($^{i\text{Pr}}$TPB] and liberation of NH$_3$.

Moving from iron to copper, reaction of $^{i\text{Pr}}$TPB with CuBr in THF with excess Na/Hg amalgam provided the copper(0) complex [Cu($^{i\text{Pr}}$TPB)], while the reaction of $^{i\text{Pr}}$TPB with CuBr in the presence of Na[BAr$^F_4$] (Ar^F = 3,5-(CF$_3$)$_2$-C$_6$H$_3$) resulted in the formation of the copper(I) complex, [Cu($^{i\text{Pr}}$TPB)][BAr$^F_4$] (Scheme 1.43). Alternatively, the anionic copper(–1) complex was isolated as either the sodium salt or the potassium salt by stirring [Cu($^{i\text{Pr}}$TPB)] with either alkali metal in excess (Scheme 1.43). All three complexes possess trigonal pyramidal geometry, and single crystal X-ray diffraction revealed a contraction in Cu–B bond length and an increase in pyramidalization of boron in moving from cationic [Cu($^{i\text{Pr}}$TPB)][BAr$^F_4$] (Cu–B = 2.495 Å, r_α = 1.16;[68] Σ(C–B–C) = 355.0°) to neutral [Cu($^{i\text{Pr}}$TPB)] (Cu–B = 2.289 Å, r_α = 1.06;[68] Σ(C–B–C) = 347.1°) to anionic M[Cu($^{i\text{Pr}}$TPB)] (M = Na or K; Cu–B = 2.198 Å, r_α = 1.02;[68] Σ(C–B–C) = 338.9°), indicating an increase in copper–boron bond strength occurs as the electron density at

copper is increased. A shift in the ^{11}B chemical shift from 67 ppm for the cationic complex to 6.7 ppm for the anionic complex is also observed. Neutral [Cu(^{iPr}TPB)] is a stable radical, and its EPR spectrum at 77 K indicates the unpaired electron is in an orbital of σ symmetry delocalized over boron and copper. Furthermore, a natural atomic orbital population analysis of the spin density obtained from DFT calculations indicated that much of the spin population was on boron rather than copper, and the spin population that was on copper was largely contained in the 4p orbital, indicating that the bonding interaction between copper and boron was a one electron bond. Given the increase in copper–boron bond strength observed in moving from the cationic copper complex to the anionic copper complex, it may be concluded that the bonding interaction between copper and boron progresses from non-bonding in the cationic complex to a one electron bonding interaction in the neutral complex, and then to a two electron bonding interaction in the anionic complex; the latter two cases were thought of as $R_3B\cdot^-$ Cu^+ and $R_3B:^{2-}$ Cu^+ bonding interactions, respectively, given the distribution of spin population in each bonding interaction.[138]

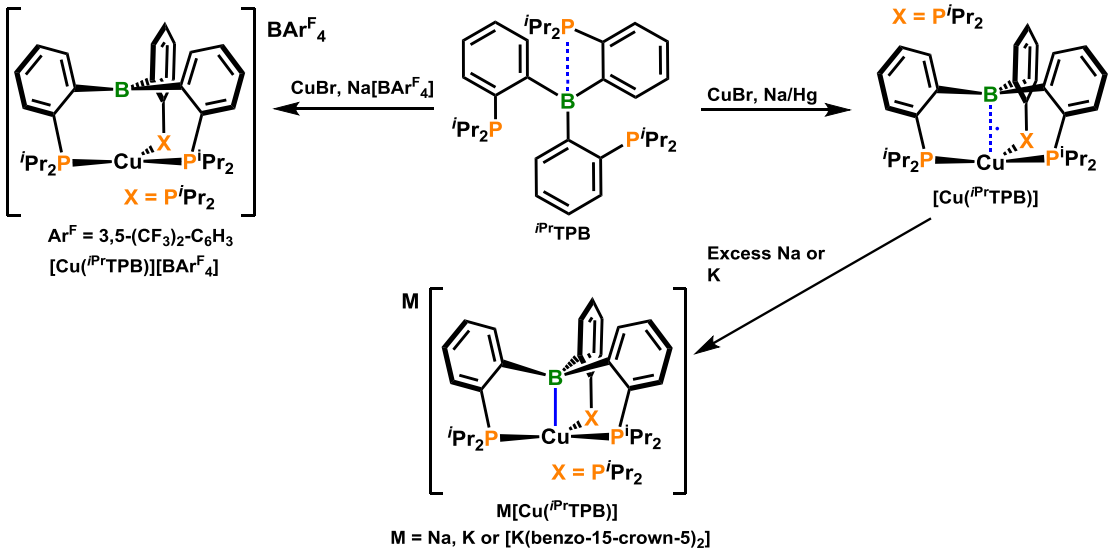

Scheme 1.43. Synthesis of [Cu(^{iPr}TPB)][BAr$^F_4$] (Ar^F = 3,5-(CF$_3$)$_2$-C$_6$H$_3$), [Cu(^{iPr}TPB)] and M[Cu(^{iPr}TPB)] (M = Na, K or [K(benzo-15-crown-5)$_2$]).

Peters and co-workers have also extended the coordination chemistry of the $^{i\text{Pr}}$TPB ligand to cobalt, isolating the cobalt(I) complex [CoBr($^{i\text{Pr}}$TPB)] via reaction of $^{i\text{Pr}}$TPB with 0.5 equivalents of both Co powder and $CoBr_2$. [CoBr($^{i\text{Pr}}$TPB)] features κ^4*PPPB*-coordination of the TPB ligand, and reduction with sodium naphthalenide provided [Co(N_2)($^{i\text{Pr}}$TPB)], analogous to [Fe(N_2)($^{i\text{Pr}}$TPB)] displayed above in Scheme 1.42, which reacts with H_2 to yield the side-on coordined H_2 complex [Co(η^2-H_2)($^{i\text{Pr}}$TPB)]. Both [Co(N_2)($^{i\text{Pr}}$TPB)] and [Co(η^2-H_2)($^{i\text{Pr}}$TPB)] are κ^4*PPPB*-coordinated by the TPB ligand.[139]

1.3.3.4 – Rhodium Complexes of the $^{\text{Ph}}$TPB Ligand

Nakazawa and co-workers prepared {(*o*-Ph_2P)C_6H_4}$_3$B ($^{\text{Ph}}$TPB) by reaction of three equivalents of (*o*-Ph_2P)C_6H_4Li with BCl_3 at 100 °C, and investigated its coordination chemistry with rhodium either by reaction with [RhH(CO)(PPh_3)$_3$] at 50 °C, generating neutral [RhH(CO)($^{\text{Ph}}$TPB)], or through subsequent isolation of cationic and anionic rhodium complexes via reaction with [H(OEt_2)$_2$][BF_4] and KH/18-crown-6, respectively (Scheme 1.44). Neutral [RhH(CO)($^{\text{Ph}}$TPB)] possesses κ^4*PPPB*-coordination of the $^{\text{Ph}}$TPB ligand and a distorted octahedral geometry with a Rh–B bond distance of 2.370 Å (r_α = 1.07).[68] The sum of the C–B–C angles is equal to 332.5°, and the ^{11}B NMR chemical shift is –7.5 ppm.[42]

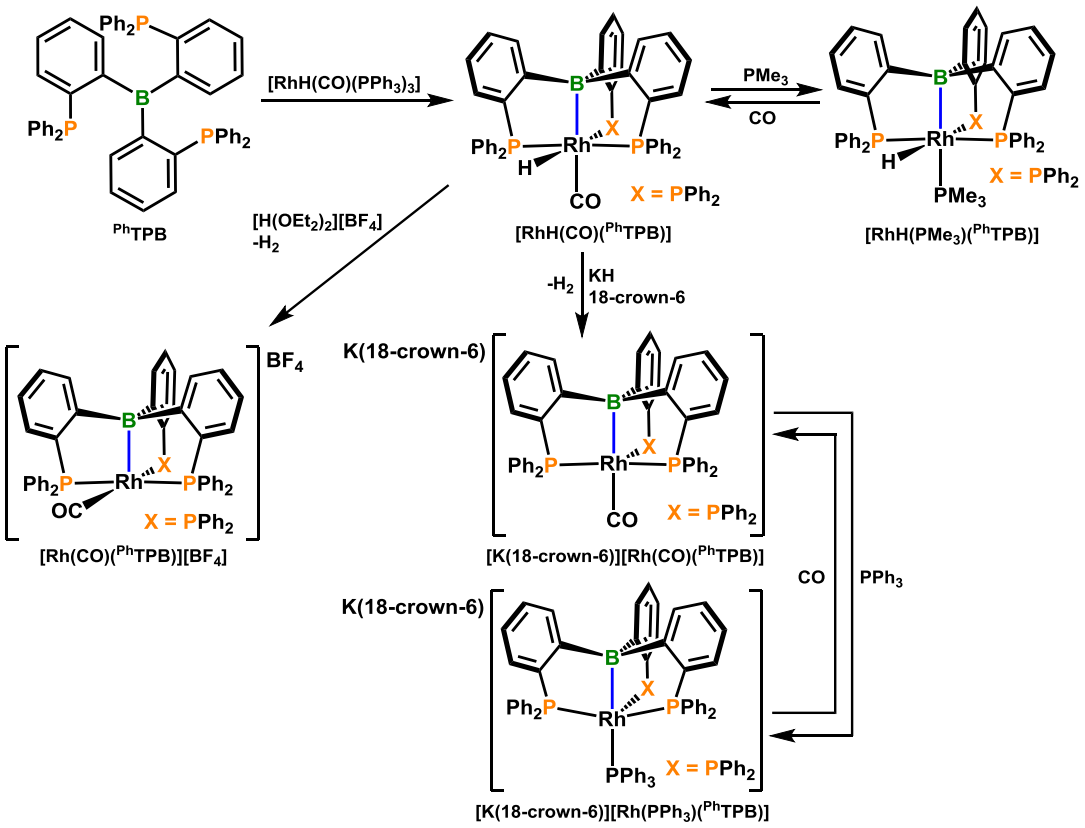

Scheme 1.44. Synthesis of [RhH(CO)(^{Ph}TPB)], and subsequent cation/anion generation and reactivity with phosphines.

Reaction of [RhH(CO)(^{Ph}TPB)] with [H(OEt$_2$)$_2$][BF$_4$] provided cationic [Rh(CO)(^{Ph}TPB)][BF$_4$] with concomitant H$_2$ evolution (Scheme 1.44). The geometry of [Rh(CO)(^{Ph}TPB)][BF$_4$] is square pyramidal with κ^4*PPPB*-coordination of ^{Ph}TPB to rhodium, and the CO co-ligand resides in the square plane as opposed to *trans* to boron, which is the case in neutral [RhH(CO)(^{Ph}TPB)]. Reaction of [RhH(CO)(^{Ph}TPB)] with KH/18-crown-6 generated anionic [K(18-crown-6)][Rh(CO)(^{Ph}TPB)], with loss of H$_2$, also featuring κ^4*PPPB*-coordination of the ^{Ph}TPB ligand, albeit with trigonal bipyramidal geometry and the CO co-ligand residing in the apical position *trans* to boron (Scheme 1.44). The observed deviations in the coordination site for the π-accepting CO ligand were proposed to be related to the strong *trans*-influence of borane ligands, in combination with the amount of electron density at rhodium; the cationic rhodium

complex possesses less electron density for π-backdonation to CO, therefore coordination of CO *trans* to boron is discouraged. Cationic [Rh(CO)(^{Ph}TPB)][BF_4] exhibits a Rh–B bond distance of 2.286(6) Å (r_α = 1.03),[68] the sum of the C–B–C angles is equal to 341.7°, and the ^{11}B chemical shift is 0.0 ppm, suggestive of weaker rhodium–borane coordination relative to neutral [RhH(CO)(^{Ph}TPB)]. X-ray quality crystals of anionic [K(18-crown-6)][Rh(CO)(^{Ph}TPB)] evaded isolation, but the ^{11}B chemical shift was located at –7.6 ppm, indicative of stronger Rh–BR_3 coordination than in the cationic analogue. The labilizing ability of a coordinated borane has also been highlighted by reacting [RhH(CO)($^{i\text{Pr}}$TPB)] with PMe_3, or [K(18-crown-6)][Rh(CO)($^{i\text{Pr}}$TPB)] with PPh_3, which resulted in displacement of the CO ligand bound *trans* to boron, and coordination of PMe_3 and PPh_3, respectively; exposure of [K(18-crown-6)][Rh(PPh_3)($^{i\text{Pr}}$TPB)] to CO regenerated [K(18-crown-6)][Rh(CO)($^{i\text{Pr}}$TPB)].[42]

1.4 – Vanadium Complexes of a Potentially Pentadentate Borane-Containing Ambiphilic Ligand

Szymczak and co-workers developed a structurally rigid *NNN*-terpyridine donor ligand, Tpy^{BN}, which is flanked with a Lewis basic morpholino group and a Lewis acidic boronic acid pinacol ester (Scheme 1.45). The design criteria described for the Tpy^{BN} ligand are as follows: (1) Lewis base and Lewis acid moieties were positioned on the periphery of the central donor system to interact with ligands in the secondary coordination sphere of the metal, (2) a rigid ligand backbone was utilized to avoid Lewis acid–metal coordination and Lewis base→Lewis acid adduct formation, and (3) a synthetic route that allowed for fine tuning of the Lewis base and Lewis acid groups was required. The synthesis of Tpy^{BN} is displayed below in Scheme 1.45; the ligand was prepared in 4 steps from commercially available 2-acetyl-6-bromopyridine. In the second to last step, a Kröhnke condensation was used to assemble the central pyridine ring, and in the final step the boronic pinacol ester was installed via a palladium catalyzed Miyaura coupling reaction.[140]

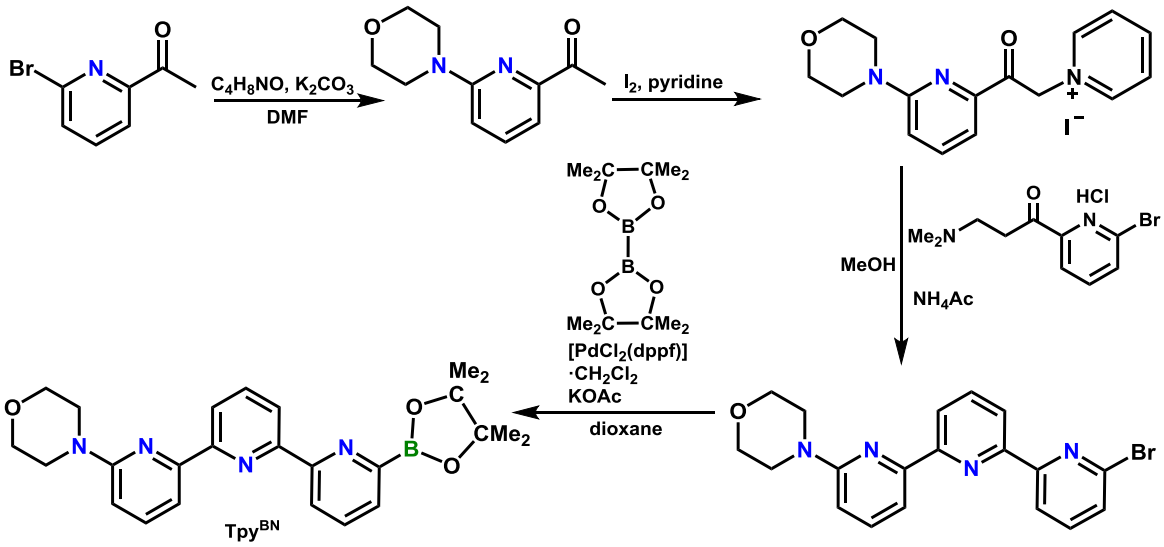

Scheme 1.45. Synthetic scheme for the preparation of the Tpy^{BN} ligand.

The Tpy^{BN} ligand reacted cleanly with $[VCl_3(THF)_3]$ to afford $[VCl_3(Tpy^{BN})]$ (Scheme 1.46). The X-ray crystal structure revealed κ^3*NNN*-coordination of the terpyridine ligand backbone, with a chloride co-ligand weakly interacting with the pendant borane, as evidenced by a B–Cl bond distance of 2.410(9) Å (r_α = 1.30),[68] which is elongated relative to complexes reported by Emslie and Bourissou containing metal–Cl–borane interactions (r_α for B–Cl = 1.07–1.26; *vide supra*). Additionally, the sum of the C–B–C angles is equal to 350(1)°, indicating that boron is only slightly pyramidalized and thus the B–Cl bonding interaction is rather weak.[140]

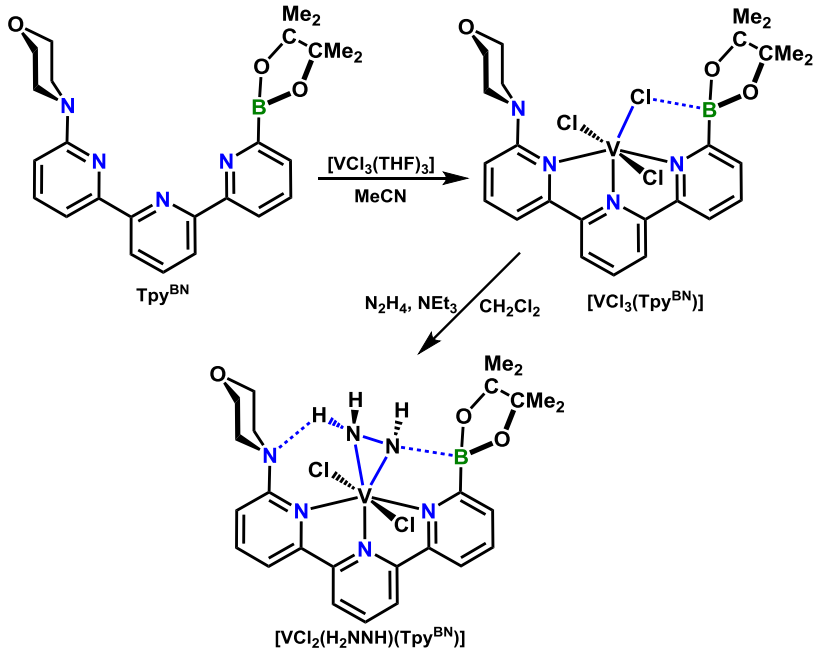

Scheme 1.46. Reaction of Tpy^{BN} with $[VCl_3(THF)_3]$, providing $[VCl_3(Tpy^{BN})]$, and subsequent reaction with hydrazine to yield $[VCl_2(\eta^2\text{-}H_2NNH)(Tpy^{BN})$.

Further reaction of $[VCl_3(Tpy^{BN})]$ with hydrazine in the presence of NEt_3 provided $[VCl_2(\eta^2\text{-}H_2NNH)(Tpy^{BN})]$, in which one of the chloride co-ligands has been eliminated as HCl, and the monoanionic H_2NNH^- ligand is η^2*NN*-coordinated to vanadium (Scheme 1.46). X-ray diffraction revealed that one of the hydrogen atoms of the H_2NNH^- ligand is interacting with the nitrogen atom of the morpholino group (N–H = 2.68(4) Å), and one of the nitrogen atoms is interacting with the pendant borane (B–N = 1.623(4) Å; r_α = 1.05),[68] providing the first example of a crystallgraphically characterized vanadium complex bearing an η^2*NN*-coordinated H_2NNH^- ligand. Given that vanadium-hydrazine and vanadium-hydrazine complexes are suspected intermediates in N_2 reduction, treatment of $[VCl_2(\eta^2\text{-}H_2NNH)(Tpy^{BN})]$ with $[CoCp^*_2]$ and collidinium chloride was investigated, resulting in 0.6 ± 0.2 equivalents of NH_3, or 1.8 ± 0.2 equivalents of NH_3 in the presence of excess hydrazine (10 equivalents).[140]

1.5 – Transition Metal Complexes of Alane-Containing Ambiphilic Ligands

The coordination chemistry of alane-containing ambiphilic ligands is significantly less developed than that of ambiphilic ligands containing boranes. The successful isolation and characterization of transition metal complexes featuring η^1*Al*-coordination of unsupported alanes has proven to be much more facile than with their borane counterparts, and has been extensively studied (Section 1.1.2). Additionally, the high sensitivity of alane-containing ambiphilic ligands towards protonolysis and redistribution of Al–C bonds,[29,141] and the potential pyrophoricity of such ligands[27] has restricted their synthetic utility, and introduces additional constraints in potential ligand design. However, their increased Lewis acidity relative to their borane analogues provides intrigue into their potential reactivity with transition metal pre-cursors, as well as the reactivity of such complexes with external substrates.[31] Presented here-in Section 1.5 is a summary of the progress made to-date pertaining to the coordination chemistry of alane-containing ambiphilic ligands.

1.5.1 – M–CO Activation in Iron and Manganese Carbonyl Complexes of a PNAl-Ligand

Similarly to Bercaw and co-workers, who employed a P/B-ligand for 1,1-migratory insertion of hydride and alkyl groups into a metal-bound CO ligand (Section 1.3.1.4), Labinger and co-workers envisioned that reduction of CO with hydrogen, as shown in Scheme 1.47 below, may be achieved through the use of an alane-containing ambiphilic ligand via simultaneous activation of both the carbon and oxygen atoms of a CO co-ligand through transition metal–carbon and aluminum–oxygen interactions, respectively.[34]

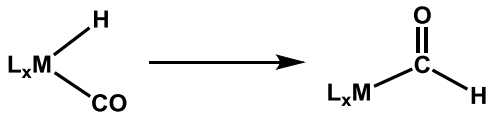

Scheme 1.47. Reduction of a carbonyl co-ligand via 1,1-insertion of a metal-bound hydride.

Labinger and co-workers selected the P/Al-ligand $Ph_2P–N(^tBu)–AlEt_2$ ($PNAl^{Et}$) as the ambiphilic ligand because of its monomeric nature in solution, and it was prepared via reaction of $Cl–PPh_2$ with $^tBuNH_2$, providing $Ph_2P–N(^tBu)H$, followed by reaction with $X–AlEt_2$ (X = Cl or I). The addition of $PNAl^{Et}$ to $[CpFe(CO)_2Me]$ initially formed $[CpFe(CO)\{\eta^2CO\text{-}(Me)C\text{-}PNAl^{Et}\text{-}O\}]$ (Scheme 1.48), in which the Fe–Me group has undergone 1,1-insertion onto a CO co-ligand, yielding a COMe ligand which is η^2CO-coordinated to iron, and is bound to the $PNAl^{Et}$ ligand via P–C and Al–O interactions. After approximately one day $[CpFe(CO)\{\kappa^2CP\text{-}(Me)CO\text{-}^{Et}AlNP\}]$ was isolated, in addition to $[CpFe(CO)\{\kappa^2OP\text{-}(H_2CCH)O\text{-}^{Et}AlNP\}]$ and unreacted $[CpFe(CO)_2Me]$ (Scheme 1.48); the former complex is formed by $R_3P–C$ dissocation followed by $Fe–PR_3$ coordination, providing an alane adduct of an acetyl ligand coordinated to iron, and the latter complex, which contains an ethenolate ligand, is formed by acetyl group rearrangement via a hydrogen shift. Although the mechanism for the formation of these complexes was not determined, Labinger and co-workers hypothesized their formation to occur via undetected $[CpFeMe(CO)(CO\text{-}^{Et}AlNP)]$, in which the $PNAl^{Et}$ ligand is coordinated only to the oxygen atom of the carbonyl ligand, allowing for rapid 1,1-insertion of the Fe–Me ligand at carbon.[34,36]

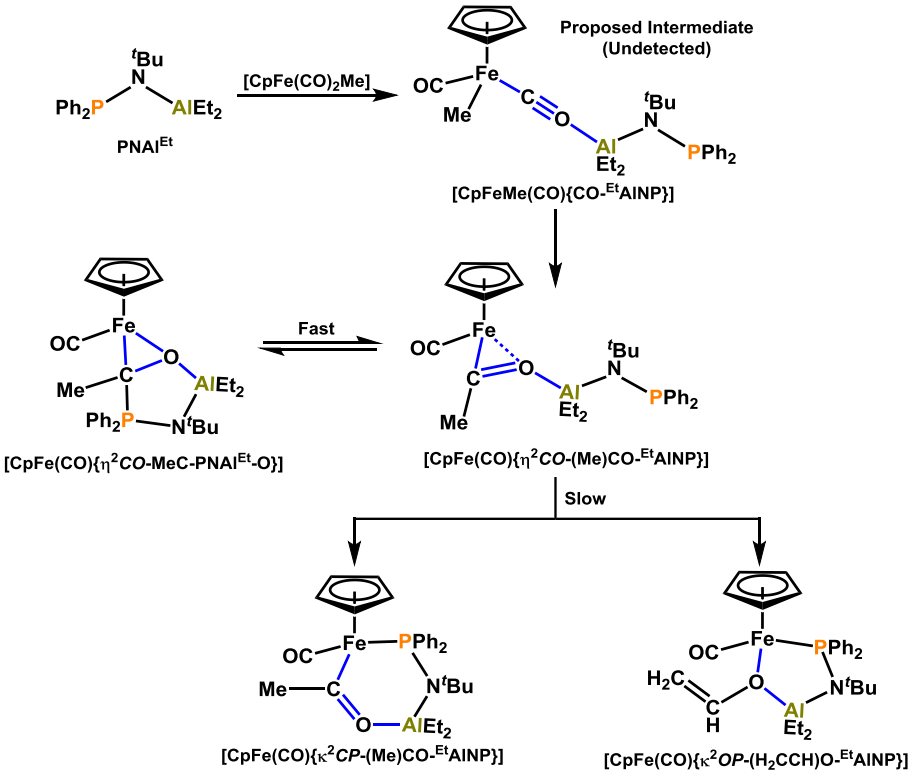

Scheme 1.48. Insertion and re-arrangement of a CO co-ligand on iron facilitated by CO–AlR_3 coordination of an ambiphilic ligand.

Labinger and co-workers have also surveyed the reactivity of $PNAl^R$ (R = Me, Et) ligands with $[HMn(CO)_5]$; reaction with one equivalent of $PNAl^{Et}$ resulted in the formation of $[Mn(CO)_4\{\eta^2\textit{CO}\text{-C(H)-}PNAl^{Et}\text{-O}\}]$, which is the product of 1,1-insertion of Mn–*H* into CO, in conjunction with O–Al and C–P bond formation (Scheme 1.49). This complex was found to react with one equivalent of $P(OPh)_3$ to provide $[Mn(CO)_3\{P(OPh)_3\}\{\eta^2\textit{CO}\text{-C(H)-}PNAl^{Et}\text{-O}\}]$, in which $P(OPh)_3$ has displaced one of the CO ligands.[35]

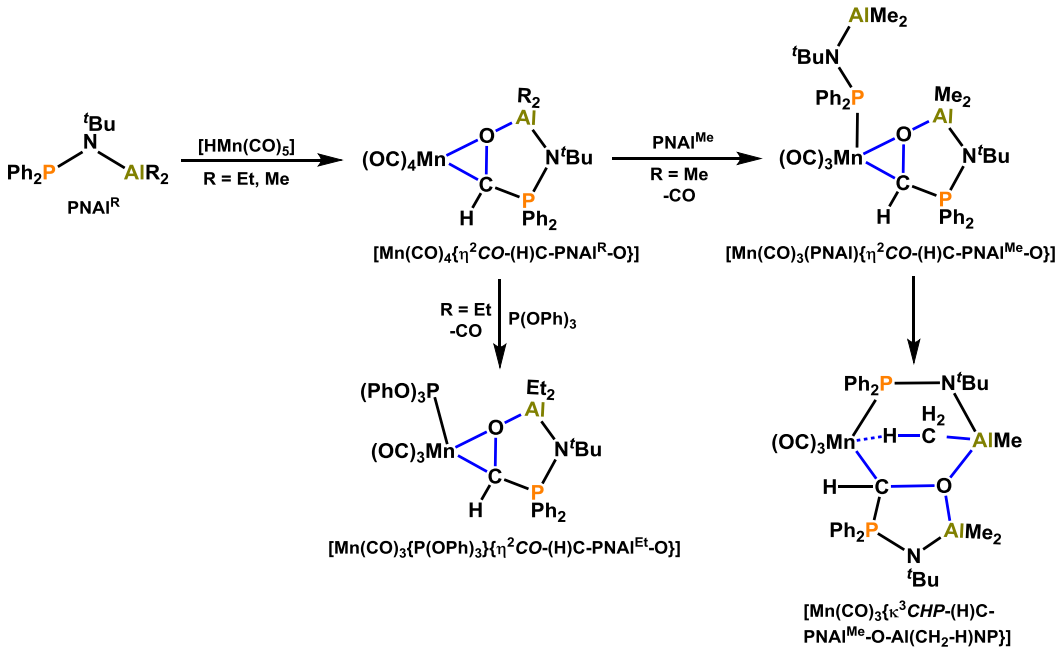

Scheme 1.49. Reactivity of the PNAl^{R} (R = Me, Et) ligands with [HMn(CO)$_5$].

Alternatively, PNAl^{Me}, which contains an –AlMe$_2$ moiety rather than an –AlEt$_2$ group, reacted readily with [HMn(CO)$_5$] to provide [Mn(CO)$_3${κ^3*CHP*-C(H)-PNAl^{Me}-O-Al(CH$_2$-H)NP}]. This reaction presumably proceeds via the intermediate [Mn(CO)$_3$(PNAl^{Me}){η^2*CO*-C(H)-PNAl^{Me}-O}], followed by reaction of a second equivalent of PNAl^{Me} with [Mn(CO)$_4${η^2*CO*-C(H)-PNAl^{Me}-O}] to displace a CO ligand and coordinate a second PNAl^{Me} ligand to manganese via phosphorus (Scheme 1.49). [Mn(CO)$_3${κ^3*CHP*-C(H)-PNAl^{Me}-O-Al(CH$_2$-H)NP}] possesses an aluminoxyphosphinomethyl ligand, which is derived from the reduction of CO. Additionally, this complex contains a bridging Mn–H–CH$_2$–AlMe interaction, formed via interaction of hydrogen from an Al-*Me* group with manganese. The formation of [Mn(CO)$_3${κ^3*CHP*-C(H)-PNAl^{Me}-O-Al(CH$_2$-H)NP}] likely occurs through interaction of the pendant alane group of the second PNAl^{Me} equivalent with the oxygen atom of the η^2*CO*-coordinated unit, generating a vacant coordination site, which becomes occupied by the bridging Mn–H–CH$_2$–AlMe interaction. While the PNAl^{Me} ligand readily reacted with [HMn(CO)$_5$] to form [Mn(CO)$_3${κ^3*CHP*-C(H)-PNAl^{Me}-O-Al(CH$_2$-H)NP}], PNAl^{Et}

only reacted in a similar fashion with [$HMn(CO)_5$] if a second equivalent of $PNAl^{Et}$ was introduced into the reaction mixture.[35]

During the reaction of $PNAl^{Et}$ with [$HMn(CO)_5$] an unisolable intermediate was observed en route to the formation of [$Mn(CO)_4\{\eta^2$*CO*-C(H)-$PNAl^{Et}$-O}], which seemed to possess a P–H moiety. Reactions of $PNAl^{R}$ (R = Me, Et) with other [$CpMH(CO)_3$] precursors (M = Cr, Mo, W) involved a similar P–H functionality, in addition to other NMR spectroscopic features that indicated the formation of the ion pair, [R_2Al–N(^{t}Bu)–PPh_2H][$CpM(CO)_3$], had occurred. Therefore, it was proposed that insertion of a metal-bound hydride into CO in the Fe–$PNAl^{R}$ and Mn–$PNAl^{R}$ systems does not occur via direct metal→CO migration, but rather, initial transfer of H^+ to phosphorus, followed by subsequent transfer to the carbon atom of a CO ligand.[35,37]

1.5.2 – *In Situ* Generation of a PPAl-Ligand, and Formation of an η^2*NAl*-Iridium Complex

Fryzuk and co-workers explored the reactions of $AlMe_3$ and $AlEt_3$ with the iridium(I) vinylidene complex, [Ir=C=CH_2(PNP)] (PNP = $(Ph_2PCH_2SiMe_2)_2N$), which was obtained via reaction of [Ir(η^2-C_8H_{14})(PNP)] with acetylene. The addition of AlR_3 (R = Me, Et) yielded [Ir{C(R)=CH_2}{κ^3*PPN*-$(Ph_2PCH_2SiMe_2)_2N(\mu$-$AlR_2)$}] (R = Me, Et) (Scheme 1.50), presumably through initial oxidative addition of AlR_3, providing the iridium(III) vinylidene complex [Ir=C=CH_2(R)(AlR_2)(PNP)], followed by 1,1-insertion of the vinylidene ligand into the Ir–R bond, generating an isopropenyl ligand, and concomitant N–Al bond forming reductive elimination.[142]

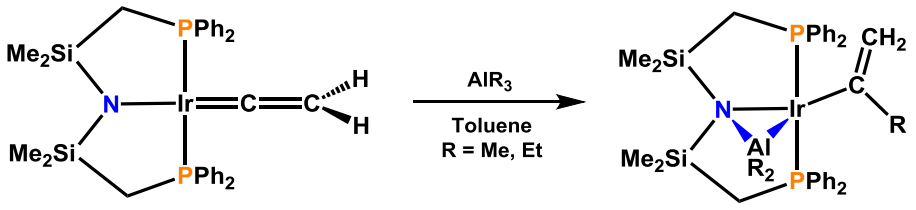

Scheme 1.50. Formation of [Ir{C(R)=CH_2}{κ^3*PPN*-$(Ph_2PCH_2SiMe_2)_2N(\mu$-$AlR_2)$}] (R = Me, Et) from [Ir=C=CH_2(PNP)] (PNP = $(Ph_2PCH_2SiMe_2)_2N$) and AlR_3.

The [Ir{C(R)=CH_2}{κ^3*PPN*-($Ph_2PCH_2SiMe_2)_2$N(μ-AlR_2)}] (R = Me, Et) complexes features η^2*NAl*-coordination to iridium, in addition to bisphosphine coordination of the diphenylphosphine moieties. An X-ray crystal structure was obtained for the methyl complex, which exhibits distorted square pyramidal geometry with the coordinated alane occupying the apical position. The Ir–Al bond distance is 2.411(2) Å (r_α = 0.92), which is suggestive of stronger metal–alane bonding interaction than in metal–aluminatrane complexes reported by Lu and co-workers which feature η^1*Al*-coordination to iron, cobalt and nickel (Section 1.5.5, *vide infra*). However, this is likely due to bridging nature of the –AlR_2 unit between iridium and the coordinated amide, or alkene-like bonding of the R'$_2$NAlR_2 unit.[142]

1.5.3 – Nickel(II)-Catalyzed Dehydrogenative Coupling of Silanes Utilizing the $Me_2PCH_2AlMe_2$ Ligand

Methylaluminoxane (MAO) has been utilized with [NiCl(PPh_3)(1-Me-Ind)] (Ind = indenyl) for the dehydrogenative coupling of silanes. It was found that in the absence of MAO, the [NiMe(PPh_3)(1-Me-Ind)] and [NiMe(PMe_3)(1-Me-Ind)] species either oligomerize phenylsilane ($PhSiH_3$) to trimers and tetramers, or form linear $(PhSiH)_n$ oligomers with n~16, respectively, whereas the [NiCl(PPh_3)(1-Me-Ind)]/MAO system can form linear $(PhSiH)_n$ chains with n between 20 and 50. Additionally, silane polymerization reactions are performed with a Ni:MAO concentration ratio of 1:10. Zargarian and Fontaine proposed that [NiCl(PPh_3)(1-Me-Ind)] is converted to [NiMe(PPh_3)(1-Me-Ind)] during catalysis, and the presence of MAO not only generates the Ni–Me species present during catalysis, but potentially activates neutral Ni–R species (R = growing polymeric chain) during the catalytic cycle, forming Ni···R···Al(MAO) interactions as opposed to generating cationic species. Furthermore, utilizing $AlMe_3$ rather than MAO, which is known to convert [NiCl(PPh_3)(1-Me-Ind)] to [NiMe(PPh_3)(1-Me-Ind)], suppresses the catalytic properties of the [NiMe(PPh_3)(1-Me-Ind)] system, likely due to the formation of [Ni{(μ-$Me)_2AlMe_2$}(PPh_3)(1-Me-Ind)] units that inhibit approach of the silane substrate (as determined by spin saturation transfer NMR

experiments, which indicate exchange between Ni*Me* and Al*Me* groups). Given the aforementioned observations, Zargarian and Fontaine sought to exploit an ambiphilic ligand coordinated to a Ni–Me species to mimic the catalytic capabilites of the Ni/MAO system, but to avoid the presence of either bridging Ni–Me–Al bonding interactions or nickel cation generation, both of which have been shown to suppress catalytic reactivity.[32]

As the ambiphilic ligand to incorporate with {NiMe(1-Me-Ind)}, Zargarian and Fontaine selected previously reported $\{Me_2PCH_2AlMe_2\}_2$, which was prepared via reaction of $Cl–AlMe_2$ with $LiCH_2PMe_2$.[143] Addition of 200 equivalents of $PhSiH_3$ to a 2:1 mixture of [NiMe(PPh_3)(1-Me-Ind)] and $\{Me_2PCH_2AlMe_2\}_2$ resulted in rapid formation of linear oligomeric $(PhSiH)_n$ (n = 3-6) within the first 60 minutes, which was converted to cyclic oligomers if the reaction was left for 10-24 hours (Scheme 1.51). The turnover frequency (TOF) of the [NiMe(PPh_3)(1-Me-Ind)]/$Me_2PCH_2AlMe_2$ system was 554 h^{-1}, which is approximately 50 times greater than that of [NiMe(PPh_3)(1-Me-Ind)] alone. Additionally, experiments were performed to determine if [NiMe(1-Me-Ind)($Me_2PCH_2AlMe_2$)], formed via displacement of PPh_3 upon introduction of 0.5 equivalents of $\{Me_2PCH_2AlMe_2\}_2$ to [NiMe(PPh_3)(1-Me-Ind)], was the catalytically active species, but it was found that the P/Al-ligand did not displace PPh_3 from nickel to a detectable extent. It was thus reasoned that very small quantities of monomeric $Me_2PCH_2AlMe_2$ produced in the $2Me_2PCH_2AlMe_2/\{Me_2PCH_2AlMe_2\}_2$ equilibrium is able to displace PPh_3 (however not in high enough quantities to be observed by NMR spectroscopy) to provide [NiMe(1-Me-Ind)($Me_2PCH_2AlMe_2$)] (Scheme 1.51).[32]

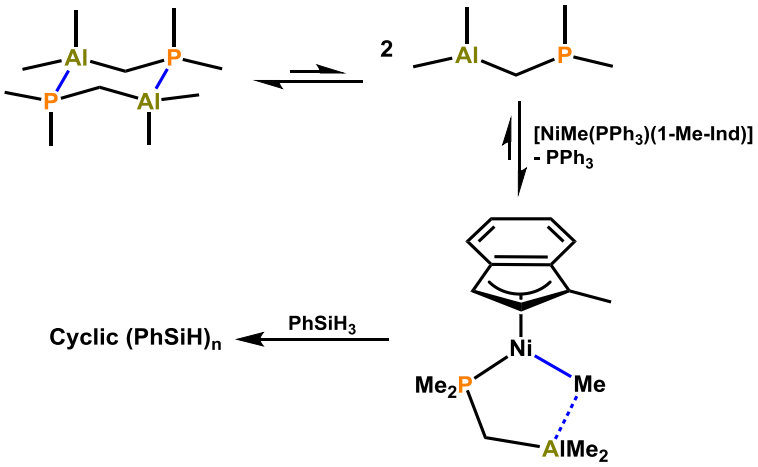

Scheme 1.51. Formation of [NiMe(1-Me-Ind)($Me_2PCH_2AlMe_2$)] and subsequent dehydrogenative cyclization of $PhSiH_3$, forming cyclic $(PhSiH)_n$ (n = 3-6) units.

In order to promote generation of monomeric $Me_2PCH_2AlMe_2$ and aid in isolating [NiMe(1-Me-Ind)($Me_2PCH_2AlMe_2$)], triethylamine (NEt_3) was added to the reaction mixture; the addition of 5 equivalents NEt_3 to a mixture of $\{Me_2PCH_2AlMe_2\}_2$ and [NiMe(PPh_3)(1-Me-Ind)] resulted in an 85:15 ratio of [NiMe(1-Me-Ind)($Me_2PCH_2AlMe_2$)]:[NiMe(PPh_3)(1-Me-Ind)]/$\{Me_2PCH_2AlMe_2\}_2$. Moreover, a 2:1:10 ratio of [NiMe(PPh_3)(1-Me-Ind)]:$\{Me_2PCH_2AlMe_2\}_2$:NEt_3 resulted in a TOF of 1760 h^{-1} for the dehydrogenative coupling of $PhSiH_3$, which is 3 times greater than 2:1 [NiMe(PPh_3)(1-Me-Ind)]/$\{Me_2PCH_2AlMe_2\}_2$ and 150 times greater than [NiMe(PPh_3)(1-Me-Ind)] alone. Overall, the presence of a pendant Lewis acid alane within an ambiphilic ligand resulted in rate enhancements in dehydrogenative coupling of $PhSiH_3$, however, preferentially forming cyclic $(PhSiH)_n$ units (n = 3-6) as opposed to the linear $(PhSiH)_n$ polymers (n = 20-50) formed with Ni/MAO systems (*vide supra*). The $–CH_2–$ linker was hypothesized to provide the appropriate steric restraints to deter strong bridging Ni–Me–Al interactions which could shut down potential coordination sites at the metal centre, or remove the methyl ligand, thus ionizing the metal centre. Furthermore, it was suggested that weak Al···Me or Al···co-ligand (co-ligand = hydride, silyl) interactions (as evidenced by slow exchange of the Ni(CD_3) and Al(CH_3) groups observed between

[Ni(CD_3)(1-Me-Ind)(PPh_3)] and {$Me_2PCH_2AlMe_2$}$_2$, which was monitored over the course of 12 hours by ^{1}H NMR spectroscopy) likely play in important role during the catalysis.[32]

Aside from its use in catalytic dehydrogenative coupling of silanes, Fontaine and co-workers have also investigated the reactivity of {$Me_2PCH_2AlMe_2$}$_2$ with a series of rhodium(III) hydrocarbyl complexes.[27,28]

1.5.4 – Transition Metal Complexes of the {(*o*-^{i}Pr$_2$P)C$_6$H$_4$}$_2$AlCl and {(*o*-^{i}Pr$_2$P)C$_6$H$_4$}$_3$Al Ligands

In 2008, Bourissou and co-workers expanded the coordination chemistry of Group 13 Lewis acid-containing ambiphilic ligands by replacing the borane in their {(*o*-$R_2P)C_6H_4\}_2BR'$ (^{R}DPB$^{R'}$) and {(*o*-$R_2P)C_6H_4\}_3B$ (^{R}TPB) ligands with an alane. The {(*o*-^{i}Pr$_2$P)C$_6$H$_4$}$_2$AlCl ($^{i\text{Pr}}$DPAl$^{\text{Cl}}$) ligand was prepared via lithium-bromide exchange of two equivalents of (*o*-^{i}Pr$_2$P)C$_6$H$_4$Br followed by the addition of $AlCl_3$ (Scheme 1.52). Although an X-ray crystal structure of the PPAl-ligand was never obtained, a ^{31}P chemical shift of 24 ppm was in good agreement with related phosphine/borane ligands exhibiting intramolecular P→B adduct formation, indicating that intramolecular P→Al adduct formation is likely present in the $^{i\text{Pr}}$DPAl$^{\text{Cl}}$ ligand.[29]

Reaction of $^{i\text{Pr}}$DPAl$^{\text{Cl}}$ with [AuCl(SMe_2)] provided zwitterionic [Au($^{i\text{Pr}}$DPAl$^{\text{Cl}}$-Cl] (Scheme 1.52), in which the PPAl-ligand is κ^2*PP*-coordinated to gold, and the chloride co-ligand has been abstracted by the alane. The Al–Cl bond length is 2.21 Å (r_α = 0.99),[68] whereas the Au–Cl distance is 3.04 Å.[29] Alternatively, $^{i\text{Pr}}$DPAl$^{\text{Cl}}$ reacted with CuCl to produce polymeric [{Cu(μ-Cl)($^{i\text{Pr}}$DPAl$^{\text{Cl}}$)}$_n$], in which zwitterionic units are connected via Cl–Al–Cu bridges. Aluminum possesses two short Al–Cl bonds [2.204(1) and 2.241(1) Å; r_α = 0.99, 1.01, respectively],[68] and copper possesses two elongated Cu–Cl bonds, one with a chloride coordinated to aluminum within the same molecule [2.582(1) Å] and one with a chloride on a neighbouring molecule [2.540(1) Å]. The propensity for copper to maintain coordination to a chloride ligand is attributed to the greater electrophilicity of cationic copper relative to cationic gold.[30]

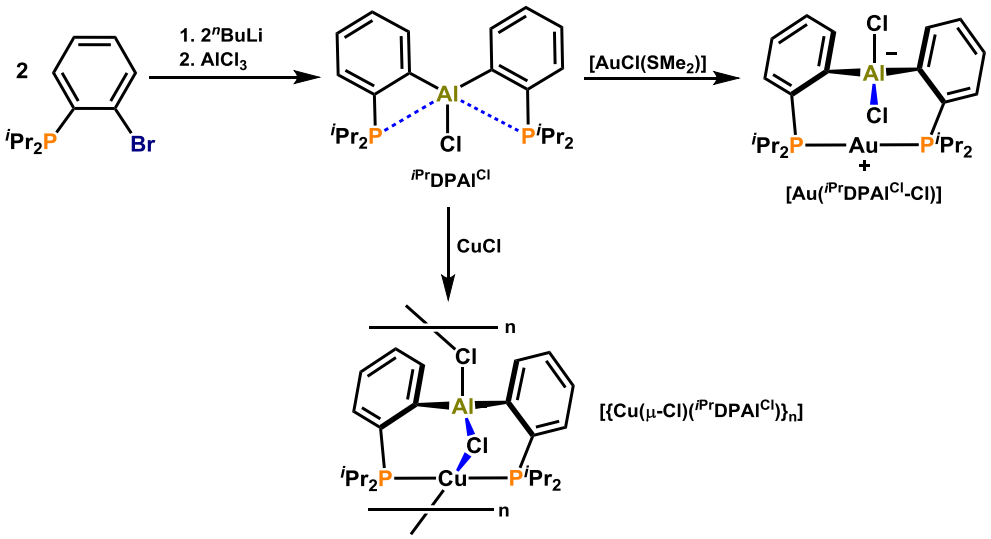

Scheme 1.52. Synthesis of the ^{iPr}DPAl^{Cl} ligand, and reactivity with [AuCl(SMe$_2$)] and CuCl.

The {(*o*-^{i}Pr$_2$P)C$_6$H$_4$}$_3$Al (^{iPr}TPAl) ligand was prepared in an analogous fashion to ^{iPr}DPAl^{Cl}, via initial bromide-lithium exchange using three equivalents of (*o*-^{i}Pr$_2$P)C$_6$H$_4$Br (Scheme 1.53). The ^{iPr}TPAl ligand reacted with both [AuCl(SMe$_2$)] and CuCl to provide zwitterionic [M(^{iPr}TPAl-Cl)] (M = Au, Cu) complexes (Scheme 1.53); the ^{iPr}TPAl ligand is κ^3*PPP*-coordinated to the metal in both complexes. The Al–Cl bond lengths in [Au(^{iPr}TPAl-Cl)] and [Cu(^{iPr}TPAl-Cl)] are 2.266(2) (r_α = 1.02)[68] and 2.255(3) Å (r_α = 1.01),[68] respectively, and aluminum is slightly pyramidalized with the sum of the C–Al–C angles equal to 354.3 and 352.3°, respectively. In both complexes, aluminum is pyramidalized away from the metal centre, but is still within the sum of the van der Waals radii of the elements (Au–Al = 3.026(1) Å, r_α = 1.18; Cu–Al = 3.044(2) Å, r_α = 1.20),[68] and indeed, NBO analysis indicated that a weak M→Al (M = Au, Cu) interaction was present.[30]

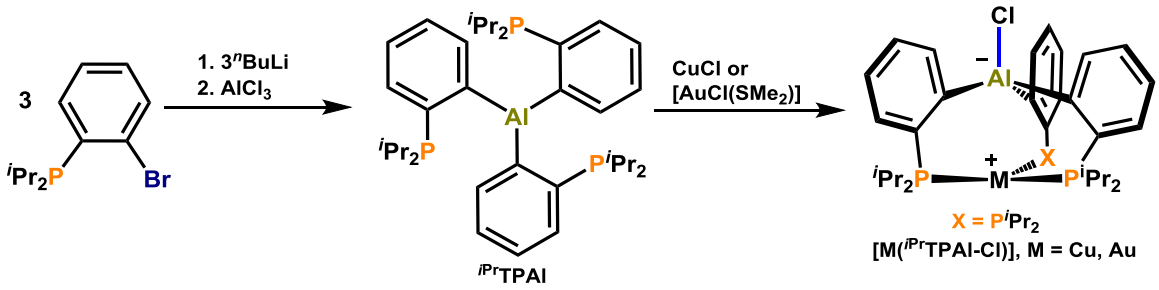

Scheme 1.53. Synthesis of ^{iPr}TPAl, and reactivity with [AuCl(SMe$_2$)] and CuCl.

The geminally substituted PAl-ligand, PhC(H)=C(Al^{t}Bu$_2$)(PMes$_2$) (PCAl), was first reported by Lammertsma and Uhl, and was prepared via hydroalumination of Mes$_2$PC≡CPh with di-*tert*-butylaluminum hydride.[144] Since this report, Bourissou and co-workers have explored the coordination chemistry of PCAl with chloride-containing late transition metal pre-cursors. The PCAl ligand reacted with [{Pd(μ-C)l(η^3-allyl)}$_2$] and [{Rh(μ-Cl)(nbd)$_2$}] to provide [Pd(μ-Cl)(η^3-allyl)(PCAl)] and [Rh(μ-Cl)(nbd)(PCAl)], respectively (Scheme 1.54). In both cases, the PCAl ligand is κ^1*P*-coordinated to the metal, and the alane is involved in a bridging Al–Cl–M (M = Pd, Rh) bonding interaction. Alternatively, PCAl reacted with [AuCl(L)] (L = PMe$_3$, tht) to provide zwitterionic [Au(L)(PCAl-Cl)] (L = PMe$_3$, tht), in which the PCAl ligand is κ^1*P*-coordinated to gold and the chloride co-ligand has been completely abstracted by aluminum (Scheme 1.54). Noteworthy is that coordination of PCAl to gold is initiated by chloride abstraction, as opposed to PMe$_3$ or tht displacement, demonstrating the propensity for aluminum to engage in anionic ligand abstraction. The addition of an extra equivalent of PCAl to [Au(tht)(PCAl-Cl)] resulted in the formation of [Au(PCAl)(PCAl-Cl)], in which two PCAl units are κ^1*P*-coordinated to gold, and the chloride is bound to one of two pendant alanes.[31]

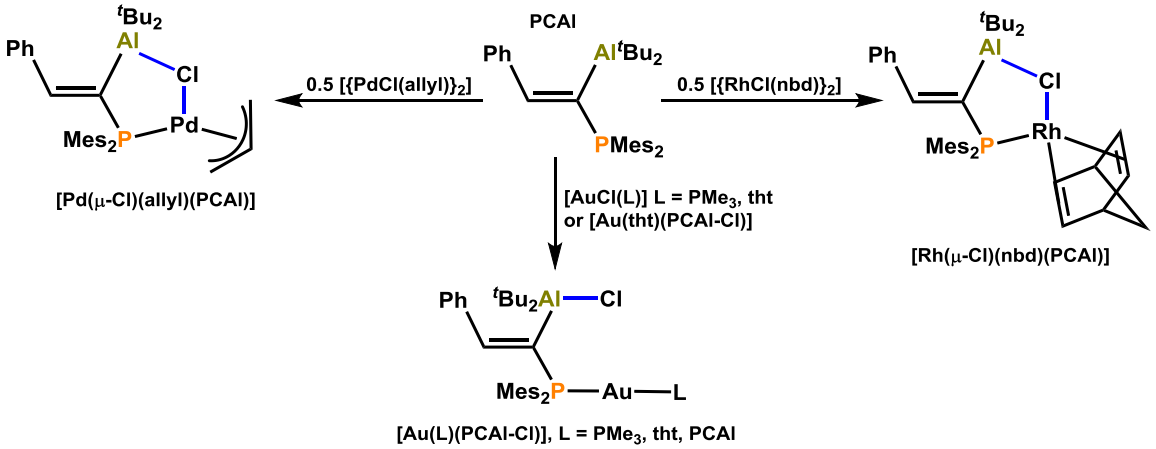

Scheme 1.54. Reactivity of the PCAl ligand with [{Pd(μ-Cl)(allyl)}$_2$], [{Rh(μ-Cl)(nbd)}$_2$] and [AuCl(L)] (L = PMe$_3$, tht, PCAl).

1.5.5 – Metallalumatrane Complexes of a PPPAl-Ligand

Lu and co-workers provided the first examples of metallalumatrane complexes, which are metal complexes exhibiting η^1*Al*-coordination through the use of a tripodal tris-donor ligand framework in which the alane is positioned as the central buttress. In order to accomplish this, the AltraPhos ligand, depicted in Scheme 1.55 below, was prepared via deprotonation of 2,2',2''-tris(diisopropylphosphinomethylamino)triphenylamine using ^{n}BuLi, and quenching with AlCl$_3$. The AltraPhos ligand is a base stabilized P$_3$Al-ligand that is capable of κ^4*PPPAl*-coordination to metal centres.[38]

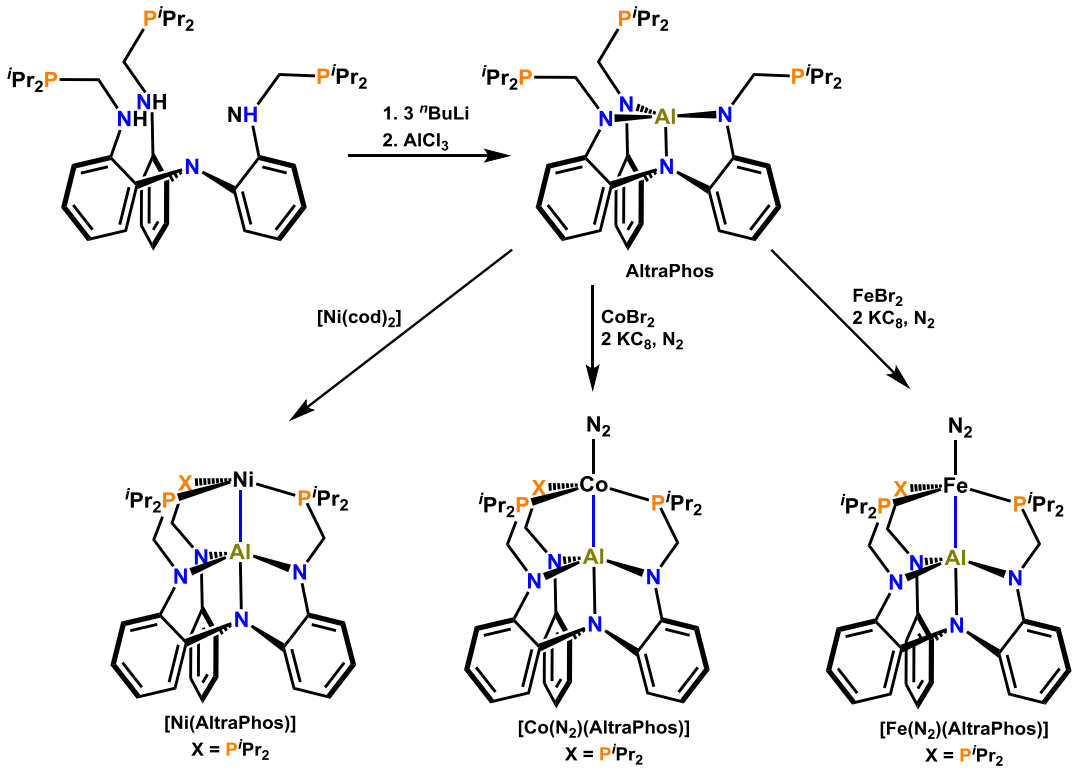

Scheme 1.55. Synthesis of the AltraPhos ligand, and reactivity with either $[Ni(cod)_2]$ or $CoBr_2$ and $FeBr_2$ in the presence of KC_8 in an N_2 atmosphere.

The AltraPhos ligand reacted with $[Ni(cod)_2]$ to provide [Ni(AltraPhos)], and with $CoBr_2$ and $FeBr_2$ in the presence of KC_8 to yield $[M(N_2)(AltraPhos)]$ (M = Co, Fe) complexes; in all three complexes the AltraPhos ligand is κ^4*PPPAl*-coordinated to the metal (Scheme 1.55). The Ni–Al bond length in [Ni(AltraPhos)] is 2.450(1) Å (r_α = 1.00),[68] and the sum of the N–Al–N angles is 354.5(1)°. The N–N stretching frequencies for the $[M(N_2)(Altraphos)]$ complexes (M = Co, Fe) were 2081 cm^{-1} and 2010 cm^{-1}, respectively, diagnostic of end-on N_2 coordination. While $[Co(N_2)(AltraPhos)]$ crystallized as the monomeric complex coordinated η^1-end-on by an N_2 ligand, the analogous iron complex crystallized as the dimer, $[Fe_2(\mu\text{-}N_2)(AltraPhos)_2]$. The Co–Al and Fe–Al bond lengths are 2.6202(9) (r_α = 1.06)[68] and 2.809(2) Å (r_α = 1.11),[68] respectively, and the sum of the N–Al–N angles are 351.5(2) and 351.56(9)°, respectively. Additionally, amongst all three complexes the Al–N_{apical} bond length (N_{apical} = central alane-stabilizing nitrogen atom) increases from 2.060(3) Å in an

MeCN→AltraPhos adduct to 2.099(2), 2.187(2) and 2.176(4) Å in the nickel, cobalt and iron complexes, respectively. The geometry of [Ni(AltraPhos)] and [M(N_2)(AltraPhos)] (M = Co, Fe) progresses from trigonal bipyramidal in the nickel complex, in which the sum of the P–Ni–P angles is equal to 349.5°, towards pseudo-tetrahedral in the iron complex, where Σ(P–Fe–P) is equal to 335.0°, resulting in an elongated metal–alane bond length in the iron complex. The progression in metal coordination geometry and metal–alane bond length may also be a result of a decrease in bond strength between iron and aluminum relative to nickel and aluminum, given the decreased basicity of iron relative to nickel.[38]

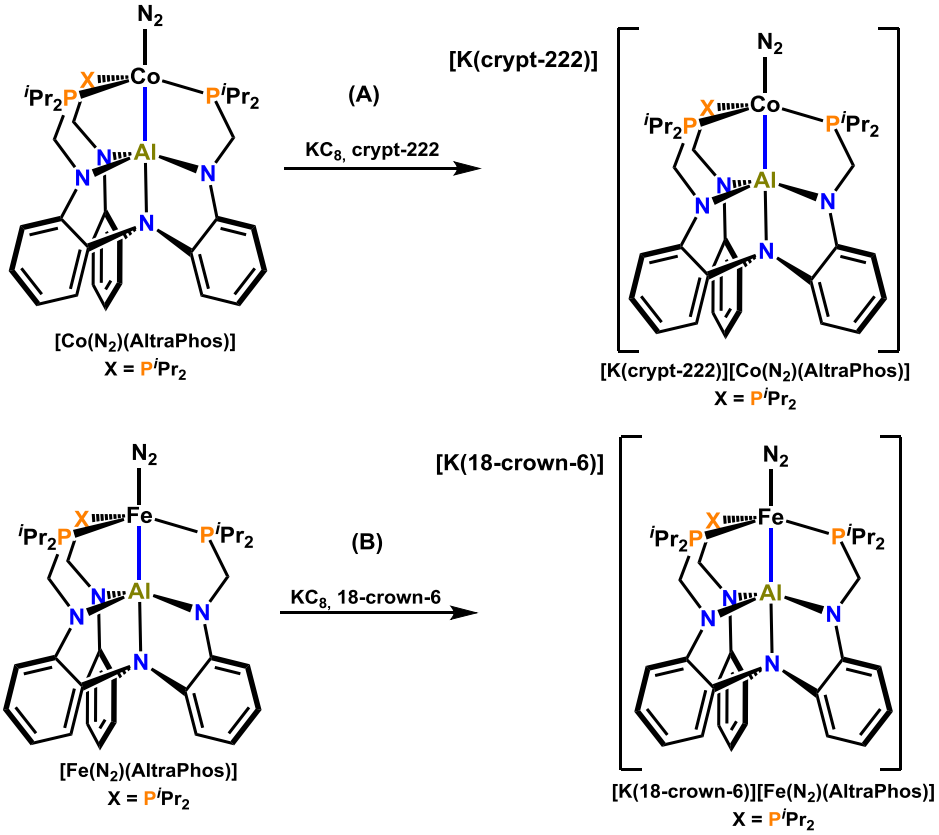

Scheme 1.56. Reduction of [M(N_2)(AltraPhos)] (M = Co, Fe) with KC_8, yielding their respective anionic complexes [M(N_2)(AltraPhos)]$^-$ (M = Co, Fe).

Lu and co-workers have also been able to prepare the anionic cobalt and iron complexes, [K(crypt-222)][Co(N_2)(AltraPhos)] and [K(18-crown-6)][Fe(N_2)(AltraPhos)],

via reaction of the neutral complexes with KC_8 (Scheme 1.56); both crystallized as monomeric complexes with an η^1-end-on coordinated N_2 molecule, however, short $K\cdots N_2$ contacts were observed in the iron complex. The anionic cobalt and iron complexes were prepared in order to investigate whether an increase in the reducing ability of the metal centres would result in a weaker N–N bond strength within coordinated N_2, potentially allowing for functionalization. Indeed, reduction of the cobalt and iron complexes resulted in a decrease in the N–N stretching frequency by 83 and 88 cm^{-1}, respectively (KBr pellet). However, only a modest increase in N–N bond length was observed in the X-ray crystal structure for the anionic cobalt complex (N–N = 1.110(8) Å vs. 1.107(4) Å in the neutral complex; the N–N bond length in anionic $[Co(N_2)(Altraphos)]^-$ is an average of three cyrstallographically independent molecules within the unit cell), and a decrease in N–N bond length was observed for the anionic iron complex (N–N = 1.135(4) Å vs. 1.146(7) Å in the neutral complex); the decrease may be attributed to the difference in the N_2 coordination mode in the neutral and anionic iron complexes; bridging in the former and terminal in the latter. Upon reduction, decreases in M–N bond length (~0.06 Å) and M–Al bond length (0.12 and 0.23 Å for Co and Fe, respectively; r_α = 1.02 for both metals)[68] were observed, in conjunction with increased $Al–N_{apical}$ bond lengths, an increase in the pyramidalization of aluminum, and progression towards trigonal bipyramidal geometry.[39]

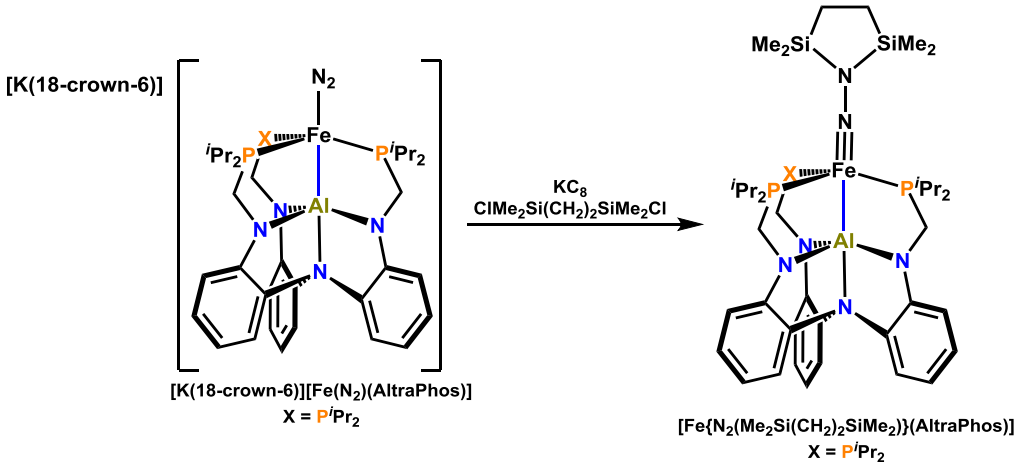

Scheme 1.57. Reaction of [K(18-crown-6)][Fe(N_2)(AltraPhos)] with KC_8 and 1,2-bis(chlorodimethylsilyl)ethane to yield the iron(II) disilylhydrazido complex, [Fe{N_2($Me_2Si(CH_2)_2SiMe_2$)}(AltraPhos)].

With respect to the above structural changes in metal–N_2 bonding parameters, Lu and co-workers sought to functionalize the distal nitrogen atom of the coordinated N_2 molecule via reaction with 1,2-bis(chlorodimethylsilyl)ethane in the presence of KC_8. While the anionic cobalt complex, [K(crypt-222)][Co(N_2)(AltraPhos)], did not react cleanly, at –78 °C, [K(18-crown-6)][Fe(N_2)(AltraPhos)] was converted to the diamagnetic iron(II) disilylhydrazido complex, [Fe{N_2($Me_2Si(CH_2)_2SiMe_2$)}(AltraPhos)] (Scheme 1.57). The solid-state structure of [Fe{N_2($Me_2Si(CH_2)_2SiMe_2$)}(AltraPhos)] features a shortened Fe–N bond length [1.661(2) vs. 1.783(3) Å], a lengthened N–N bond length [1.351(3) vs. 1.135(4) Å], and a lengthened Fe–Al bond length [2.8237(8) vs. 2.574(1) Å; r_α = 1.12 vs. 1.02][68] relative to the anionic iron–N_2 complex. Similar structural changes were observed by Peters and co-workers upon distal-nitrogen atom functionalization utilizing the borane-containing ^{iPr}TPB ligand scaffold (*vide supra*).[39]

1.6 – Thesis Goals

Outlined in the previous sections of this Chapter is the literature reported to-date pertaining to the coordination chemistry of borane- and alane-containing ambiphilic ligands. With respect to borane-containing ligands, much of the early chemistry was

dominated by attempts to isolate complexes featuring new metal–borane and metal–co-ligand–borane coordination modes, which stemmed from the first structurally characterized example of a transition metal complex featuring η^1*B*-coordination, reported by Hill and co-workers in 1999.[65] Recently such complexes have been shown to possess a diverse array of potential reactivity, both stoichiometrically towards small molecules, and catalytically. In terms of metal–alane chemistry, the synthesis of complexes featuring η^1*Al*-coordination of an unsupported alane proved facile, with the first example being reported in 1979.[4] Since alane-containing ambiphilic ligands were not required to promote metal–alane coordination, early work in this realm was geared towards the reactivity of the pendant alane in the secondary coordination sphere of the metal, and only very recently has this class of ligand been utilized to obtain complexes exhibiting η^1*Al*-coordination.

Prior to the onset of this Ph.D. research, the Emslie Group had utilized a phosphine–thioether–borane ligand, TXPB (2,7-di-*tert*-butyl-5-diphenylboryl-4-diphenylphosphino-9,9-dimethylthioxanthene), to prepare transition metal complexes featuring a variety of metal–borane and metal–co-ligand–borane coordination modes. However, the potential for such complexes to exhibit productive reactivity towards external substrates had yet to be realized. Additionally, the TXPB ligand was the only Group 13 Lewis acid-containing ambiphilic ligand to be utilized within the Emslie Group. Thus, the following objectives were proposed for this Ph.D. research:

1. Probe the reactivity of previously prepared transition metal complexes bearing the TXPB ligand (Chapters 2–4).
2. Design and prepare a new borane-containing ambiphilic ligand that is consistent with the donors–donor–acceptor motif of the TXPB ligand, however offers variability in the ligand backbone and the ligand donor functionalities (Chapter 5).

3. Explore the coordination chemistry of the newly synthesized borane-containing ambiphilic ligand with late transition metal pre-cursors (Chapters 6 and 7).
4. Utilize the newly designed ligand backbone for installation of an alane, and explore the coordination chemistry of the alane-containing ambiphilic ligand with late transition metal pre-cursors (Chapter 8).

Here-in, a discussion of the progress made towards accomplishing the aforementioned thesis objectives is presented.

Ph.D. Thesis
Bradley E. Cowie
Department of Chemistry and Chemical Biology
McMaster University

Chapter 2

Diversity of Metal–Halide–Borane (Halide = F, Cl, Br, I), Metal–Hydride–Borane and Metal–Borane Interactions in Ambiphilic Ligand Rhodium(I) Complexes

Adapted with permission from: Cowie, B. E.; Emslie, D. J. H.; Jenkins H. A.; Britten J. F. *Inorg. Chem.* **2010**, *49*, 4060-4072.

2.1 – Introduction

The chemistry of ambiphilic borane-containing ligands has seen a burst of activity over the past 10 years, providing a diverse range of complexes, including those containing direct metal-borane interactions (Chapter 1). In this area, our early research has focused on 2,7-di-*tert*-butyl-5-diphenylboryl-4-diphenyl-phosphino-9,9-dimethylthioxanthene (TXPB), a rigid phosphine/thioether/borane ligand,[59] and complexes exhibiting a range of metal-TXPB bonding modes have been prepared (Section 1.3.2.4). Metal–chloride–borane bridging interactions such as those in [Rh(μ-Cl)(CO)(TXPB)] (**1**),[1] [{PdCl(TXPB)}$_2$] and [PdCl(μ-Cl)(TXPB)][122] are rare, and most other early examples were reported by Bourissou *et al.* These complexes include: [RuCl(μ-Cl)(*p*-cymene){(2-picolyl)BCy$_2$}] [*p*-cymene = 1-Me-4-^{i}Pr-C$_6$H$_4$; (2-picolyl)BCy$_2$ = 2-(Cy$_2$BCH$_2$)C$_5$H$_4$N],[48] [Pd(μ-Cl)(η^3-allyl)($^{i\text{Pr}}$MPB$^{\text{Cy}}$)] ($^{i\text{Pr}}$MPB$^{\text{Cy}}$ = (*o*-^{i}Pr$_2$P)C$_6$H$_4$BCy$_2$),[47] [Rh(μ-Cl)(nbd)($^{i\text{Pr}}$MPB$^{\text{Cy}}$)] (nbd = norbornadiene), [{(PdCl(μ-Cl)($^{i\text{Pr}}$MPB$^{\text{Cy}}$)}$_2$], and [PdCl(μ-Cl)(PPh$_3$)($^{i\text{Pr}}$MPB$^{\text{Cy}}$)] (Figure 2.1).[49] Additional complexes containing a metal–chloride–borane interaction are Bochmann *et al.*'s [{η^5-C$_5$H$_4$B(C$_6$F$_5$)$_2$}TiCl(μ-Cl)(L)] (L = Cp, C$_5$H$_4$SiMe$_3$, indenyl, and C$_9$H$_6$NMe$_2$ {2-(dimethylamino)indenyl}),[145] Mayer *et al.*'s [(κ^3-Tp)OsCl(μ-Cl)(NPhBPh$_2$)],[146] Fontaine *et al.*'s [(IMes)$_2$PtH(μ-Cl){BC$_5$H$_4$(SiMe$_3$)-*o*}],[147] and Otero *et al.*'s [(η^5-C$_5$H$_4$SiMe$_3$)$_2$Nb(μ-Cl)(L){B(C$_6$F$_5$)$_3$}] (L = CNXyl, CNCy, CO) (Figure 2.1).[148]

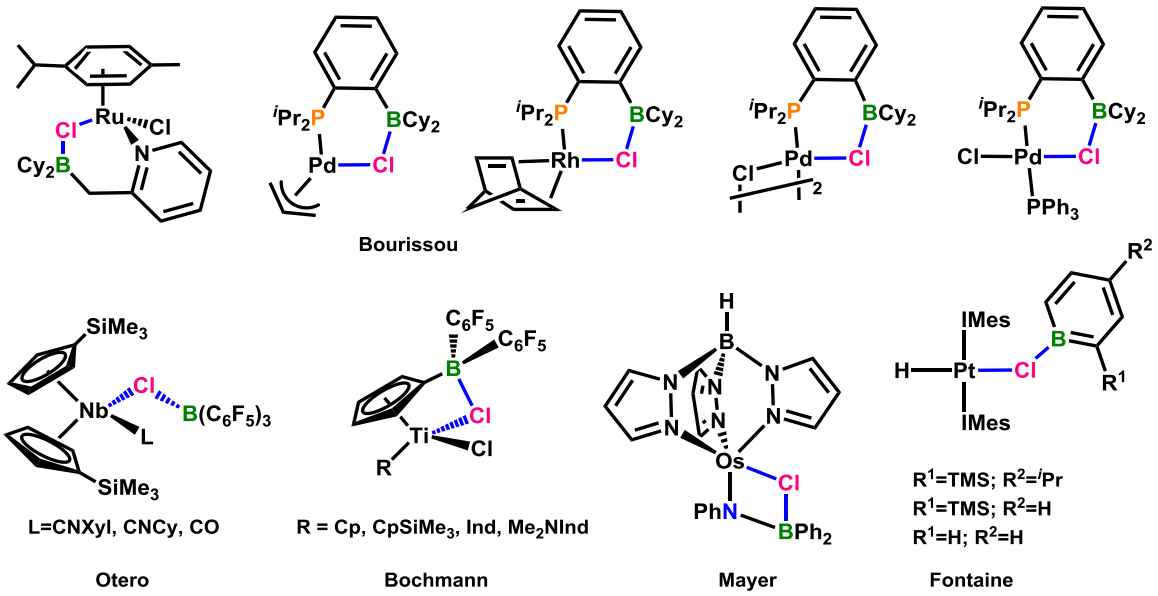

Figure 2.1. Complexes exhibiting a metal–halide–borane bridging interaction, not including TXPB complexes. Xyl = 2,6-dimethylphenyl; $C_9H_6NMe_2$ = 2-(dimethylamino)indenyl; IMes = 1,3-di(2,4,6-trimethylphenyl)imidazolin-2-ylidene.

A wide range of complexes in which a fluoroborate anion interacts with a cationic metal centre via a M–F–B bridge have also been prepared.[149] However, complexes containing a metal–bromide–borane or metal–iodide–borane interaction appeared to be unknown, presumably because of a decrease in B–X bond energies in the order F > Cl > Br > I. This order was demonstrated in the reactivity of a series of late transition metal tris(2-sulfanyl-1-*tert*-butylimidazolyl)borane complexes; [NiCl{κ^4-B(mt$^{t\text{Bu}}$)$_3$}] reacts with I_2 or $CHBr_3$ to form [NiX{κ^3-ClB(mt$^{t\text{Bu}}$)$_3$}] (X = I or Br) and with XeF_2 to form [NiCl{κ^3-FB(mt$^{t\text{Bu}}$)$_3$}], [NiY{κ^4-B(mt$^{t\text{Bu}}$)$_3$}] (Y = NCS or N_3) reacts with I_2 to form [NiI{κ^3-IB(mt$^{t\text{Bu}}$)$_3$}],[50] and [Fe(CO)$_2${κ^4-B(mt$^{t\text{Bu}}$)$_3$}] reacts with I_2 in $CHCl_3$ to form [FeI(CO){κ^3-ClB(mt$^{t\text{Bu}}$)$_3$}] (Section 1.2.2).[51] Furthermore, simple boron halides have considerable precedent as reagents for halide metathesis, for example, [$AuCl_3${C(OEt)(NMe$_2$)}] reacts with BBr_3 to yield [$AuBr_3${C(OEt)(NMe$_2$)}], which reacts with BI_3 to form [AuI_3{C(OEt)(NMe$_2$)}].[150]

An interesting but as of yet unrealized possibility for complexes exhibiting metal–halide–borane bridging interactions is their application in C–X bond activation chemistry,

for example, in C–C bond forming catalysis. A typical cycle for C–C bond formation at palladium (e.g. Suzuki-Miyaura, Stille, or Negishi coupling) involves oxidative addition of an aryl-halide substrate, followed by transmetalation and reductive elimination. For C–X bond oxidative addition, the order of reactivity is generally Ar–I > Ar–Br > Ar–Cl > Ar–F, consistent with substantial increases in Ar–X bond strength as group 17 is ascended (fluorine forms the strongest of all single bonds to carbon).[151,152,§] A mismatch between hard fluoride ligands (resulting from Ar–F oxidative addition) and a soft palladium(II) metal centre may also conspire to reduce the thermodynamic driving force for Ar–F oxidative addition, especially in the absence of strong π-acceptor co-ligands.[152,153] Strong M–X–BR_3 interactions may provide a mechanism to i[1]ncrease the thermodynamic favourability of aryl-chloride and aryl-fluoride oxidative addition, with potential applications in C–C bond forming catalysis.[¶]

Beyond C–X bond activation, ambiphilic ligands offer a more general possibility for cooperative reactivity involving both a metal and a pendant borane. Rare examples of this type of reactivity include: (1) CO insertion reactions at iron or manganese promoted by the pendant alane group of an Ph_2P-N^{t}Bu-AlR_2 (R = Me or Et) ligand,[34,36,37] (2) rate enhancements for the dehydrogenative coupling of $PhSiH_3$ by [NiMe(PPh_3)(1-Me-Ind)] in the presence of $Me_2PCH_2AlMe_2$ (the proposed intermediate in this reactivity is [NiMe{$Me_2PCH_2AlMe_2$}(1-Me-Ind)], and a related rhodium complex, [Cp*$RhMe_2$(κ^1-

§ For a recent example of aryl-fluoride reductive elimination from palladium(II), see ref 151g.

¶ In addition to thermodynamic challenges associated with C–F bond oxidative addition, theoretical studies have in several cases identified substantial kinetic barriers for this process (see refs 151a-e and 152). Recently, phosphine-assisted aryl fluoride oxidative addition has been reported as an alternative pathway for C–F bond activation, involving a four-centred transition state containing the metal, *ipso*-carbon, fluorine and phosphorus atoms (see: (a) Nova, A.; Erhardt, S.; Jasmin, N. A.; Perutz, R. N.; Macgregor, S. A.; McGrady, J. E.; Whitwood, A. C. *J. Am. Chem. Soc.* **2008**, *130*, 15499. (b) Erhardt, S.; Macgregor, S. A. *J. Am. Chem. Soc.* **2008**, *130*, 15490). The borane group of an ambiphilic ligand could in principle assume a similar role [differing in the absence of a metal–ER_3 (E = B or P) interaction], also leading to reduced kinetic barriers for Ar–F oxidative addition.

$Me_2PCH_2AlMe_2$-$OSMe_2$)], has also been prepared),[27,32] and (3) reaction of $Na[H_2B(mt^{Me})_2]$ with $[RhCl(CS)(PPh_3)_2]$ to form $[RhH(L)(PPh_3)]$ [L = $\{H(mt^{Me})_2B\}(Ph_3P)C=S$], presumably via the intermediate $[RhH(CS)(PPh_3)\{\kappa^3$-$HB(mt^{Me})_2\}]$.[61] Reactions of this type rely on the availability of a free pendant Group 13 Lewis acid, so we were interested to probe whether like chloride, the heavier halides (bromide and iodide) engage in metal–halide–borane bridging. Such interactions would be deleterious to cooperative activation reactivity in ambiphilic ligand complexes, and are of broad significance given the ubiquitous nature of halide ligands in organometallic chemistry.

We report here a series of rhodium(I) halide complexes, [RhX(CO)(TXPB)] (X = Cl, Br, I and F), as well as halide-free $[Rh(CO)(TXPB)][PF_6]$ and a rhodium(I) hydride complex, [Rh(μ-H)(CO)(TXPB)], all of which have been investigated by X-ray crystallography and NMR and IR spectroscopy. [RhX(CO)(TXPB)] complexes were chosen for study in this work, rather than [PdX(μ-X)(TXPB)] complexes, for the following reasons: (1) Neutral rhodium(I) complexes contain only one halide co-ligand; in dihalide complexes, halide substitution/abstraction reactions may be complicated by reactivity at different sites, coupled with the presence of only one pendant borane in TXPB to coordinate or abstract a halide from the metal, (2) the products of aryl halide oxidative addition at palladium(0) also contain only one halide ligand, (3) rhodium-103 is 100% abundant with a nuclear spin of 1/2, so can provide an additional NMR handle to probe the strength of metal-phosphine and/or metal-fluoride interactions, and (4) carbonyl stretching frequencies provide valuable insight into electronic changes occurring at rhodium because of halide substitution or abstraction.

2.2 – Rhodium Chloride, Bromide and Iodide Complexes Bearing the TXPB Ligand

In 2006, the Emslie group communicated the synthesis of [Rh(μ-Cl)(CO)(TXPB)] (**1**) (Scheme 2.1) as a pre-cursor to $[(TXPB)Rh(\mu\text{-}CO)_2Fe(CO)Cp]$.[1] Complex **1** adopts a distorted square planar geometry [S–Rh–CO = 171.3(3)°; P–Rh–Cl = 172.64(8)°] and

contains an uncommon metal–halide–borane bridging interaction.[1] The Rh–Cl bond length of 2.381(2) Å is in good agreement with the Rh–Cl distances in related $[RhCl(CO)(PAr_3)(SR_2)]$[154] complexes, indicating that the Rh–Cl bond is not substantially weakened by triarylborane coordination. However, the B–Cl bond length of 1.995(9) Å does indicate a strong bonding interaction between boron and the bridging chloride, since this distance is only 0.10–0.13 Å longer than that in chloroborate anions[155] and chloroborane Lewis base adducts.[156] The presence of a strong B–Cl interaction in **1** is also supported by considerable pyramidalization at boron [Σ(C–B–C) = 340(1)°] and a broad singlet in the ^{11}B NMR spectrum at 12 ppm ($\omega_{1/2}$ ~ 700 Hz), characteristic of 4-coordinate boron. The B–Cl bond length in **1** is 0.1–0.3 Å shorter than those in Bourissou's metal–chloride–borane complexes (*vide supra*), consistent with the enhanced Lewis acidity of the $ArBPh_2$ acceptor in TXPB relative to an $ArBCy_2$ group (see Table 2.1 for key spectroscopic and crystallographic data for complexes **1**–**6**).

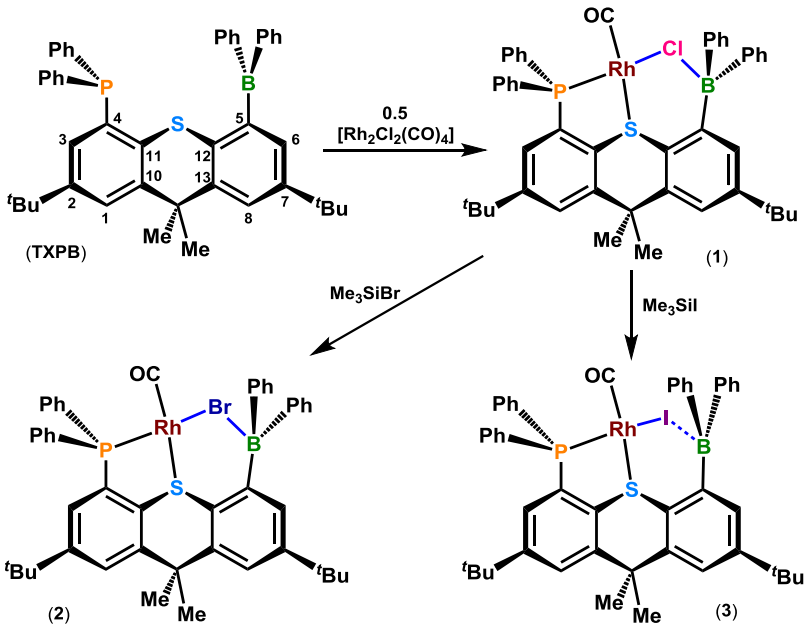

Scheme 2.1. Synthesis of [RhX(CO)(TXPB)] (X = Cl (**1**), Br (**2**), I (**3**)) complexes.

Substitution of the chloride co-ligand in **1** to form [Rh(μ-Br)(CO)(TXPB)] (**2**) was achieved using bromotrimethylsilane in CH_2Cl_2 (Scheme 2.1), providing complex **2** as an

orange powder in 74% isolated yield. A doublet was observed in the ^{31}P NMR spectrum at 64.5 ppm ($^{1}J_{31P,103Rh}$ = 164 Hz), shifted 4.5 ppm to higher frequency of complex **1**. The CO stretching frequency is 2013 cm^{-1} in Nujol and 2008 cm^{-1} in CH_2Cl_2 by IR spectroscopy; very similar values were reported for complex **1** [2010 cm^{-1} (Nujol); 2013 cm^{-1} (CH_2Cl_2)].[1] Complex **2**, like complex **1**, is fluxional in solution, giving a single resonance in the room temperature ^{1}H NMR spectrum for the C*Me*$_2$ group. However, at low temperature these methyl substituents became inequivalent with a coalescence temperature (T_c) of 211(2) K for **2** ($\Delta G^{\ddagger}$ at T_c = 39.7(5) KJ mol^{-1}).[157] For comparison, the T_c for **1** is 254(2) K, leading to a value of 47.7(6) KJ mol^{-1} for $\Delta G^{\ddagger}$ at this temperature. The ^{1}H NMR spectrum of **2** is displayed below in Figure 2.2; numbered protons refer to the positions of the thioxanthene backbone in the TXPB ligand, as shown in Scheme 2.1 above.

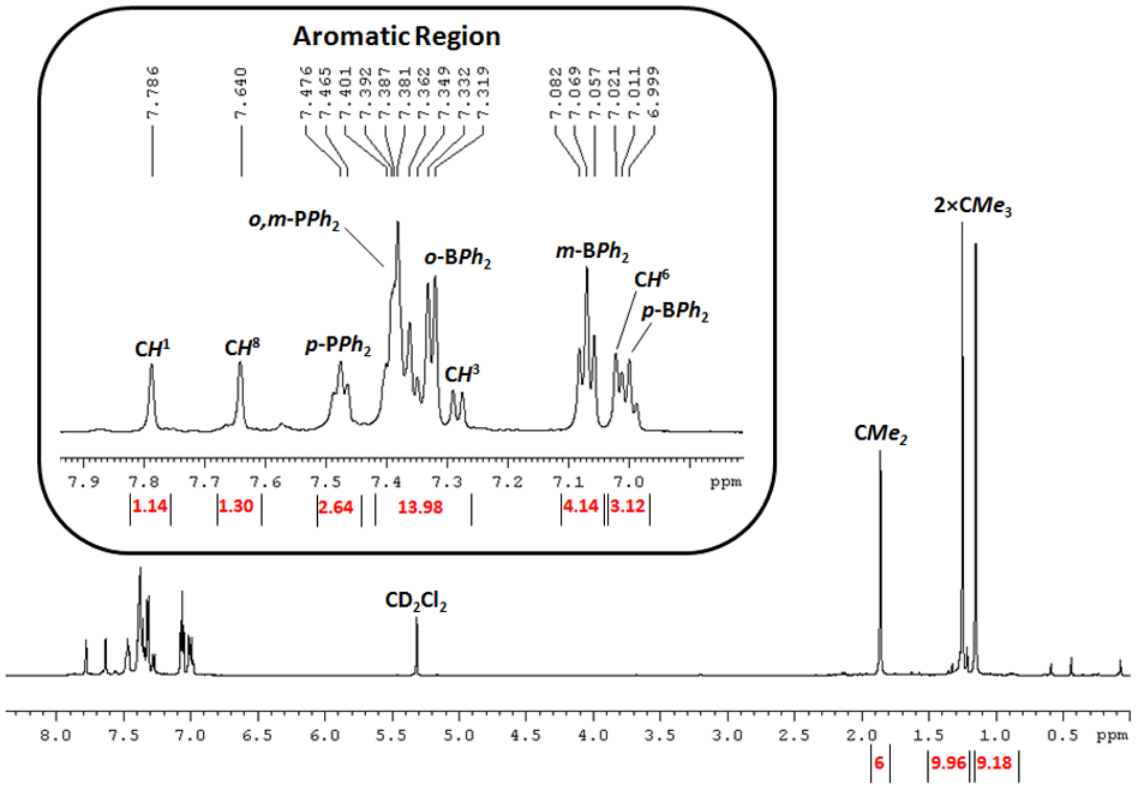

Figure 2.2. ^{1}H NMR spectrum of [Rh(μ-Br)(CO)(TXPB)] (**2**; 600 MHz, 298 K. CD_2Cl_2).

X-ray quality crystals of **2**·hexane were grown from a saturated solution of **2** in hexanes cooled to –30 °C for several days (Figure 2.3, Tables 2.1). The X-ray crystal structure contains two independent molecules of **2** (**A** and **B**) within the unit cell. For both molecules, the geometry at rhodium is distorted square planar with S–Rh–CO and P–Rh–Br angles of 173.4(3)° and 176.34(6)° for **2A**, and 176.0(3)° and 169.56(5)° for **2B**; closely analogous S–Rh–CO and P–Rh–X angles were observed for complex **1**. In addition, **2A** and **2B** exhibit a unique metal–bromide–borane interaction. However, **2A** and **2B** differ in the position of the bromide anion with respect to the thioxanthene backbone; the C(12)–C(5)–B–Br torsion angle is 76.9(7)° in **2A**, and –43.3(9)° in **2B** [cf. 78.7(8)° in **1**]. Only one isomer was observed in the solution ^{1}H and ^{31}P NMR spectra of **2** down to –70 °C, and only one carbonyl stretch was observed in the IR spectrum of **2** in CH_2Cl_2 and Nujol. However, different orientations of the metal–halide bond relative to the TXPB ligand backbone must be involved in the fluxional process responsible for C*Me*$_2$ methyl group exchange.

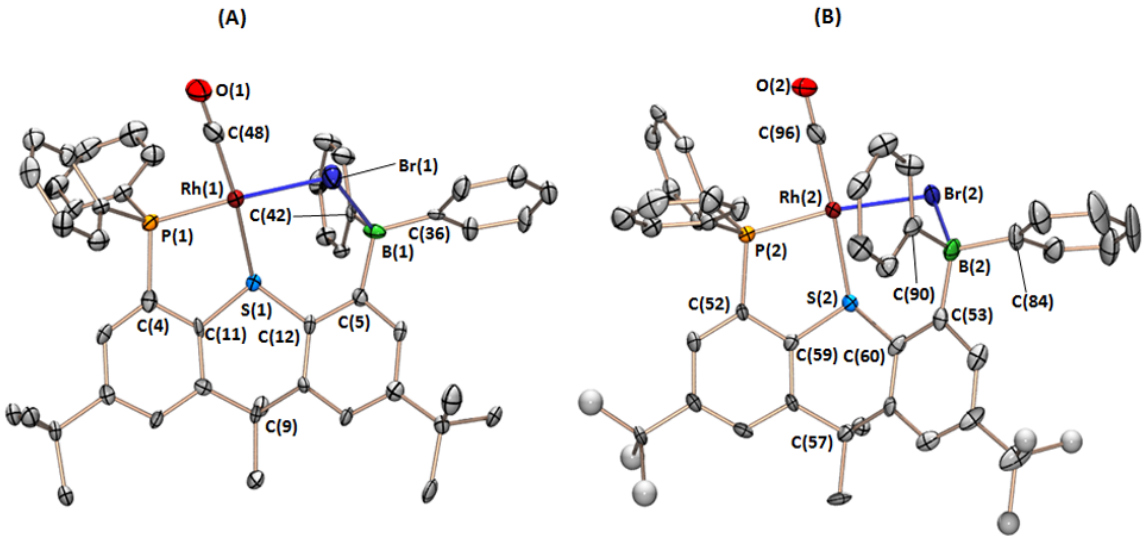

Figure 2.3. Solid-state structure for [Rh(μ-Br)(CO)(TXPB)]·hexane (**2**·hexane) with ellipsoids drawn at 50 % probability; hydrogen atoms and lattice solvent have been omitted for clarity. Two crystallographically independent molecules crystallized within the unit cell, which have been labelled as **2A** and **2B** are depicted in **A** and **B** above, respectively. The *tert*-butyl substituents in **2B**·hexane are positionally disordered over two positions; only one position is displayed for each. Additionally, both *tert*-butyl substituents of **2B**·hexane were unstable to anisotropic refinement, therefore they were refined isotropically.

Because of the inequivalent metal-TXPB binding modes in **2A** and **2B**, key bond lengths and angles in the two molecules are significantly different. For example, the B–Br distance in **2A** is 2.190(8) Å while that in **2B** is 2.267(9) Å. These distances are appreciably different from one another (see below for discussion), but are both approximately 0.2–0.3 Å longer than B–Br in the neutral Lewis acid–Lewis base adducts Ph_3PBBr_3 (1.978–2.013 Å),[158] $PyBBr_3$ (1.96–2.01 Å),[159] and $XBBr_2$, where X = 2-(dimethylaminomethyl)phenyl (2.01 and 2.02 Å),[160] highlighting the presence of a significant B–Br interaction in both **2A** and **2B**. The ^{11}B NMR signal for **2** (δ 27 ppm; $\omega_{1/2}$ ~ 900 Hz) is also closer to that of **1** (12 ppm) than free TXPB (69 ppm),[59] substantiating the presence in solution of a significant B–Br interaction in **2**.

The Rh–Br and Rh–S distances in **2A** and **2B** are also notably different; Rh–Br is 2.452(1) Å in **2A** and 2.516(1) Å in **2B**, while Rh–S is 2.380(2) Å in **2A** and 2.304(2) Å in **2B**. The shorter Rh–Br distance in **2A** is similar to those in closely related

[RhBr(CO)(PPh_3)$_2$] (2.453 Å)[161] and [^{n}Bu$_4$N][RhBr(nbd){^{i}Pr$_2$P(C_6H_4)BPh_3-*p*}] (nbd = norbornadiene) (2.465 Å).[162] However, Rh–Br in **2B** is more comparable with that in [RhBr(CO)(Me$_2$carbox)] [Me$_2$carbox = 1-(4,4-dimethyl-4,5-dihydrooxazol-2-yl)-3-mesity-limidazol-2-ylidene] (2.507 Å)[163] in which the bromo-ligand experiences the high *trans*-influence of an *N*-heterocyclic carbene. By contrast, the Rh–S distance in **2B** is more similar to that in closely related borane-free complexes, while that in **2A** is significantly longer; Rh–S distances of 2.293 and 2.286 Å were reported for [(nacnac^{Xyl})Rh(κ^1*S*-dbt)$_2$] [nacnac^{Xyl} = CH{C(Me)NXyl}$_2$; Xyl = 2,6-Me$_2$-C_6H_3; dbt = dibenzo[*b*,*d*]thiophene],[164] and Pd–S distances of 2.290 and 2.300 Å were reported for [$PdCl_2$(L)] [L = 6-(4-hydroxy-2-phenylsulfanylphenoxy)-5,7-dioxa-6-phosphadibenzo[*a*,*c*]cycloheptene][165] and [$PdCl_2${κ^2-PhS(C_6H_4)CH_2PPh_2-*o*}],[166] respectively (note: the covalent radius of Pd is 1.39 Å versus 1.42 Å for Rh).[68]

A final key structural parameter in the description of complex **2** is the Rh–Br–B angle, which is 103.4(2)° in **2A**, but only 87.6(2)° in **2B** (cf. 104.6(3)° in **1**). Both the acute Rh–Br–B angle and the short Rh–S distance in **2B** are likely a consequence of the alternative binding mode of the rigid TXPB ligand. Elongation of both the Rh–Br and the B–Br bonds in **2B** may perhaps be attributed to increased p-character in Rh–Br and B–Br coordination because of a Rh–Br–B angle constrained to less than 90°. For Al_2X_6 (X = Cl or Br), calculations have shown an ~0.01 Å increase in the bridging Al–X bond lengths upon narrowing of the Al–X–Al angle by only 4–5° (from close to 90° by bending of the Al($X_{terminal}$)$_2$ groups out of the plane with the two bridging halide ligands).[167]

Treatment of complex **1** with iodotrimethylsilane provided [RhI(CO)(TXPB)] (**3**) (Scheme 2.1) as a rust-red powder in 83 % yield. The ^{31}P NMR spectrum of **3** consists of a doublet at 67.2 ppm ($^1J_{31P,103Rh}$ = 166.8 Hz), shifted 7.2 ppm to higher frequency of complex **1**. A very broad singlet at 56 ppm ($\omega_{1/2}$ ~ 1800 Hz) was observed in the ^{11}B NMR spectrum, which is shielded by only 13 ppm relative to free TXPB, consistent with a weak B···I interaction. As with **2**, complex **3** is fluxional in solution, evidenced by chemically equivalent C*Me*$_2$ methyl substituents in the ^{1}H NMR spectrum at room temperature (coalescence temperature = 210(2) K). The $\Delta G^{\ddagger}$ value for C*Me*$_2$ methyl

group exchange at T_c is 39.5(5) KJ mol^{-1}, which is equal within error to $\Delta G^{\ddagger}$ for complex **2** (39.7(5) KJ mol^{-1} at 211(2) K). The ^{1}H NMR spectrum of **3** is displayed below in Figure 2.4.

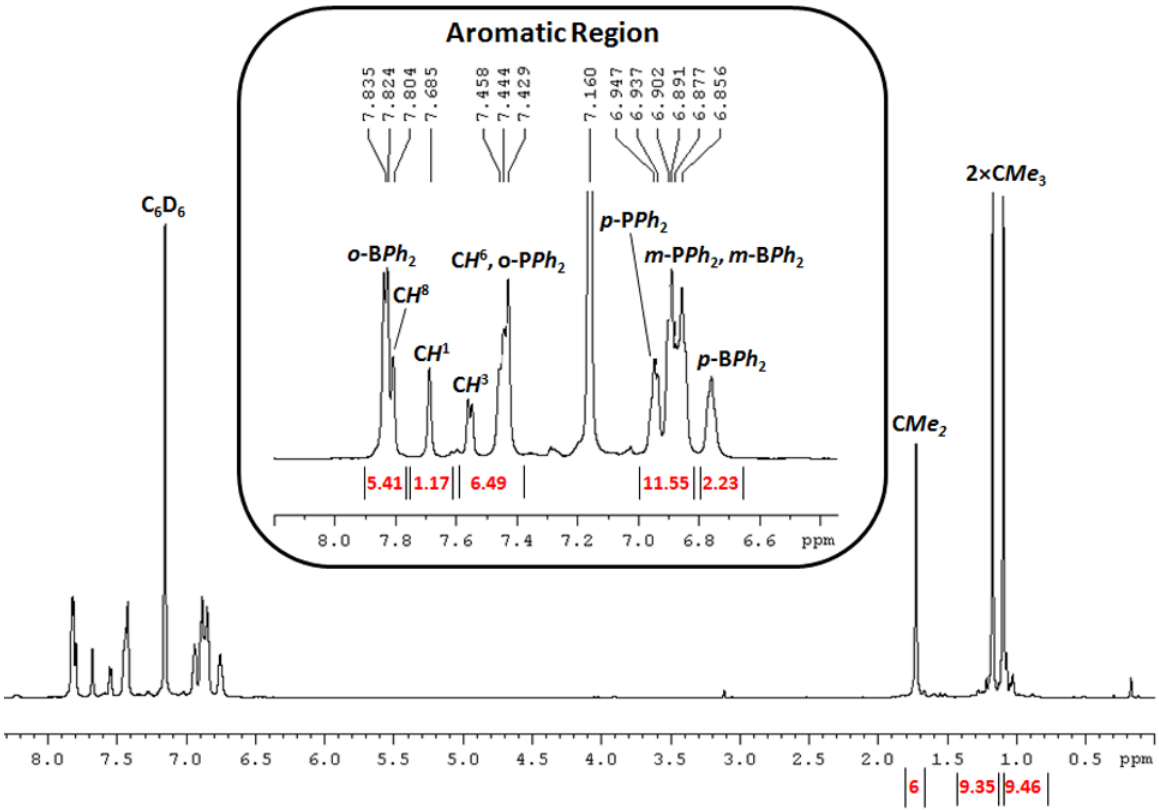

Figure 2.4. ^{1}H NMR spectrum of [RhI(CO)(TXPB)] (**3**; 600 MHz, 298 K, C_6D_6).

X-ray quality crystals of **3**·3hexane were obtained by cooling a saturated solution of **3** in hexanes to –30 °C for several days (Figure 2.5, Table 2.1). The S–Rh–CO and P–Rh–I bond angles are 163.8(2) and 169.58(4)°, respectively, highlighting a substantially distorted square planar geometry. The Rh–P and Rh–CO bond distances are 2.224(1) and 1.855(7) Å, respectively; Rh–P is slightly longer in **3** than in **1** and **2** (Table 2.1), consistent with the higher *trans*-influence of iodide relative to chloride and bromide,[168] and the absence of a strong halide–borane interaction in **3**. The orientation of iodide relative to the thioxanthene backbone of **3** is analogous to that in **2B**, with a C(12)–C(5)–B–I torsion angle of –53.1(6)°. As a consequence, the Rh–S distance is 2.300(1) Å, which

is similar to that in **2B**, but much shorter than those in complex **1** and **2A** (Table 2.1). The Rh–I–B bond angle in **3** is also extremely acute [74.0(1)°]. A similar situation was observed in **2B** [Rh–Br–B = 87.6(2)°], while the Rh–X–B angles are 103–105° in complex **1** and **2A**. The more acute Rh–X–B angle in **3**, relative to that in **2B**, is likely the result of a longer Rh–X bond and the absence of a strong halide–borane interaction in **3**.

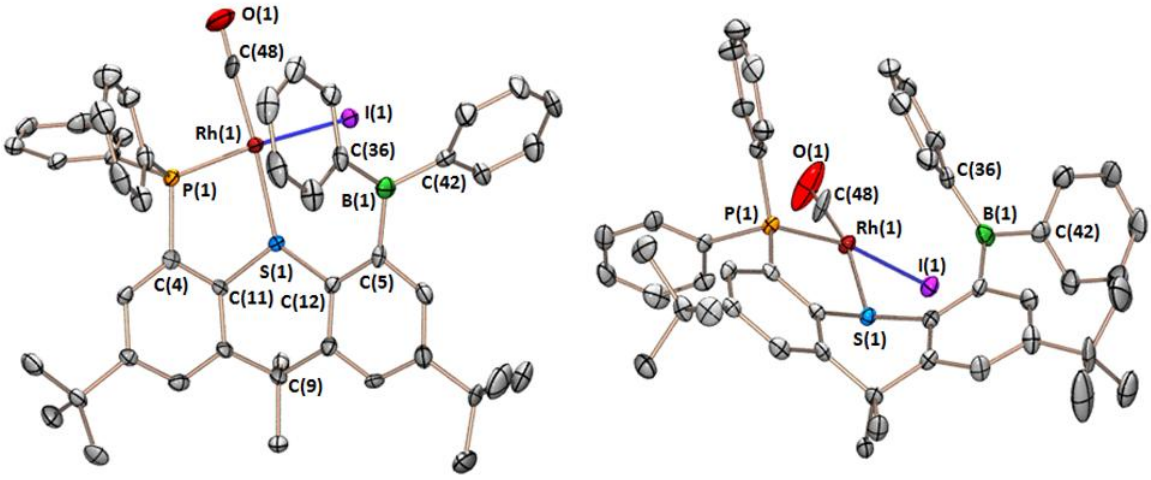

Figure 2.5. Two different views of the solid-state structure for [RhI(CO)(TXPB)]·hexane (**3**·hexane) with ellipsoids drawn at 50 % probability. Hydrogen atoms and lattice solvent have been omitted for clarity.

The Rh–I bond distance of 2.6640(7) Å compares well to those in similar rhodium compounds, where an iodide is bound *trans* to a phosphine. These compounds include [RhI(PPh_3){(*S*)-diop}] [(*S*)-diop = (*S*)-2-(diphenylphosphino)-2'-methoxy-1,1'-binaphthyl][169] and [RhI(CO)(BINAP)] [BINAP = 2,2'-bis(diphenylphosphino)-1,1'-binaphthyl],[170] with Rh–I bond distances of 2.704 and 2.686 Å, respectively. However, a key feature of complex **3** is the extremely long B···I distance of 3.125(7) Å, which is approximately 0.8–0.9 Å longer than B–I distances in the Lewis acid–Lewis base adducts Me_2NCHO–BI_3 (2.224–2.262 Å),[171] (IEtC=CEt)BI_2–Py (2.275, 2.294 Å)[172] and Me_3P–BI_3 (2.237–2.272 Å).[173] The long B···I distance in **3** may be attributed to the incompatibility of a hard borane Lewis acid with a soft iodide anion (B–X bond strengths

decrease in the order F > Cl > Br > I), in combination with an extremely acute Rh–I–B angle. However, recently Stephan and Tsao reported on a bridging tellurium–iodide–borane interaction in [TeI(μ-I){$(CH_2)_2$Ph}{(Ph)C=C(C_6F_5)B(C_6F_5)$_2$}], giving rise to a B–I bond distance of 2.462(4) Å and a Te–I–B bond angle of 75.62(9)°.[174] In keeping with the long B···I distance and the high frequency ^{11}B NMR chemical shift (*vide supra*), boron in this rhodium complex is very nearly planar [Σ(C–B–C) = 356.8(9)°].

The CO stretching frequency for **3** (2004 cm^{-1} in Nujol and 2002 cm^{-1} in CH_2Cl_2) is significantly lower than those in complexes **1** and **2**, indicating increased electron density at the metal. In related series of d^8-complexes with *cis*-disposed halide and carbonyl ligands, the CO stretching frequency is effectively unchanged after substitution of chloride for iodide; see for example [RhX(CO)(BINAP)] (X = Cl or I)[170] and [RhX(CO)(DTBPMB)] [X = Cl or I; DTBPMB = 1,2-(^{t}Bu$_2$PCH$_2$)$_2$C$_6$H$_4$].[175] The lower CO stretching frequency for **3** relative to **1** and **2** is therefore consistent with less effective donation from the halide to the metal centre in **1** and **2** as a result of halide–borane coordination. However, all or part of the shift in ν(CO) could also be due to predominance of a different TXPB bonding mode in complex **3** with a shorter Rh–S distance (as observed in the solid-state structure). It is therefore not possible to draw any definite conclusions from this data.

Table 2.1. Spectroscopic and Crystallographic Data for Complexes **1**–**6**.

Complex	**1**	**2**	**3**	**4**	**5**[a]	**6**
Metal and co-ligands	Rh Cl CO	Rh Br CO	Rh I CO	Rh F CO	Rh CO +	Rh H CO
^{31}P NMR [δ, ppm]	60.0	64.5	67.2	52.2	64.9	57.9
^{11}B NMR [δ, ppm]	12	27	56	4	57	3
^{19}F NMR [δ, ppm]	---	---	---	-186	---	---
$^1J_{P,Rh}$ [Hz]	161.3	164.0	166.8	166.2	166.8	144
$^1J_{13C,103Rh}$ / $^2J_{13C,31P}$ for *C*O [Hz]	77/18	77/15	74/14	75/19	72/13	77/16
$^2J_{P,F}$ [Hz]	---	---	---	6.2	---	---
ν(CO)(CH_2Cl_2/ Nujol) [cm^{-1}]	2013/2010	2008/2013	2002/2004	2011/2008	2038/2028	2006/1984
T_c for C*Me*$_2$	254(2)	211(2)	210(2)	274(2)	312(2)	---

exchange (K)[b]						
$\Delta G^{\ddagger}$ at T_c (KJmol^{-1})[b]	47.7(6)	39.7(5)	39.5(5)	51.5(7)	61.2(8)	---
Rh–X [Å]	2.381(2)	2.452(1) 2.516(1)	2.6640(7)	3.261(3)	---	1.84(5)
Rh–C_{ortho} [Å]	---	---	---	2.564(5)	2.797(3)	3.213(5)
Rh–C_{ipso} [Å]	---	---	---	2.336(4)	2.362(2)	2.568(5)
Rh···B [Å]	3.470	3.647(9) 3.316(9)	3.502(7)	3.231(5)	2.557(3)	2.456(6)
Rh–CO [Å]	1.82(1)	1.829(8) 1.841(7)	1.855(7)	1.816(5)	1.870(3)	1.853(6)
Rh–P [Å]	2.205(2)	2.202(2) 2.196(2)	2.224(1)	2.218(1)	2.2394(7)	2.261(2)
Rh–S [Å]	2.379(2)	2.380(2) 2.305(2)	2.300(1)	2.405(1)	2.3234(6)	2.289(1)
B–X [Å]	1.995(9)	2.190(8) 2.267(9)	3.125(7)	1.445(6)	---	1.59(6)
Rh–X–B [deg]	104.6(3)	103.4(2) 87.6(2)	74.0(1)	76.0(2)	---	92(2)
S–Rh–CO [deg]	171.3(3)	173.4(3) 176.0(3)	163.8(2)	168.0(2)	172.48(9)	157.7(2)
P–Rh–X [deg]	172.64(8)	176.34(6) 169.56(5)	169.58(4)	---	--	162(2)
P–Rh–$CC_{(cent)}$/$BC_{(cent)}$ [c]	---	---	---	160.5(2)	154.20(9)	131.0(2)
Rh–(PCCSplane) [Å][d]	1.023	0.988 0.271	0.144	1.226	0.531	0.976
∑(C-B-C) [deg]	340(1)	342(1) 339(1)	356.8(9)	331.2(7)	358.6(4)	337.1(8)
B–(CCCplane) [Å][e]	0.426	0.397 0.437	0.164	0.518	0.110	0.458
S–C(12)–C(5)–B [deg][f,g]	–13(1)	–14.8(9) 13(1)	16.6(8)	1.1(6)	4.9(3)	20.3(7)
C(12)–C(5)–B–X [deg][f,g]	78.7(8)	76.9(7) –43.3(9)	–53.1(6)	–46.5(6)	---	–56.6[j]
Ligand Bend [deg][g]	42.8	42.4 47.9	52.9	41.6	54.1	56.0

(a) NMR spectroscopic data for complex **5** is for the cation only. (b) T_c is the coalescence temperature and $\Delta G^{\ddagger}$ is for CMe_2 methyl exchange. (c) $CC_{(cent)}$ and $BC_{(cent)}$ represent the centroid position between C(42)–C(43) and B(1)–C(42), respectively. (d) PCCSplane = P(1)–C(4)–C(11)–S(1). (e) CCCplane = C(5)–C(36)–C(42). (f) Torsion angles are for the molecules as shown in Figures 2.3, 2.5, 2.6, 2.8 and 2.11. (g) Positive torsion angles indicate that boron or the B–X bond is oriented up into the fold of the thioxanthene

backbone. (h) Ligand Bend = the angle between the C(1)–C(2)–C(3)–C(4)–C(10)–C(11) and C(5)–C(6)–C(7)–C(8)–C(12)–C(13) planes (an angle of 0° would correspond to a planar thioxanthene backbone). (i) Molecule **B** of complex **2** uses a different numbering scheme; substitute B(1), P(1), C(1)-C(13),C(36), C(42) and C(43) for B(2), P(2), C(49)-C(61), C(84), C(90) and C(91). (j) Calculated using Mercury 3.3.

2.3 – A TXPB Rhodium Fluoride Complex

Treatment of **1** with $[NMe_4]F$ in CH_2Cl_2 gave [Rh(CO)(TXPB-F)] (**4**) [TXPB-F = {5-(2,7-di-*tert*-butyl-4-diphenylphosphino-9,9-dimethylthioxanthenyl)}diphenylfluoro-borate] as an orange-red powder in an isolated yield of 72 % (Scheme 2.2). Reaction of **1** with $[NBu_4][Ph_3SiF_2]$ provided an alternative route to complex **4**, but because of the formation of similarly soluble Ph_3SiF as a reaction byproduct, isolation of pure **4** via this method proved problematic. Complex **4**, unlike **1**–**3** is not thermally stable at room temperature, being substantially decomposed after 24 hours in solution (CH_2Cl_2). A key spectroscopic feature for complex **4** is a singlet in the ^{11}B NMR spectrum at 4 ppm ($\omega_{1/2}$ ~ 350 Hz), characteristic of 4-coordinate boron, and shifted 8 ppm to lower frequency of **1**, indicating the presence of a very strong B–F interaction. Moreover, a broad singlet was observed in the ^{19}F NMR spectrum at –186 ppm ($\omega_{1/2}$ ~ 180 Hz), characteristic of fluorine bound to quadrupolar boron. These NMR data compare well with the related triarylfluoroborate compounds $[FB(C_6F_5)_2\{C_6F_4(P^iPr_3)\text{-}p\}]$ (^{11}B NMR δ –0.89 ppm; ^{19}F NMR δ –191.37 ppm),[176] $[F(Tip)B(C_6H_4\text{-}o)_2PMe_2]$ (Tip = 2,4,6-triisopropylphenyl) (^{11}B NMR δ 3.7 ppm; ^{19}F NMR δ –162.44 ppm),[177] and $[K\{[2.2.2]\text{-cryptand}\}][FB(Ant)_3]$ (Ant = 9-anthracenyl) (^{11}B NMR δ 6.04 ppm; ^{19}F NMR δ –133.32 ppm).[178]

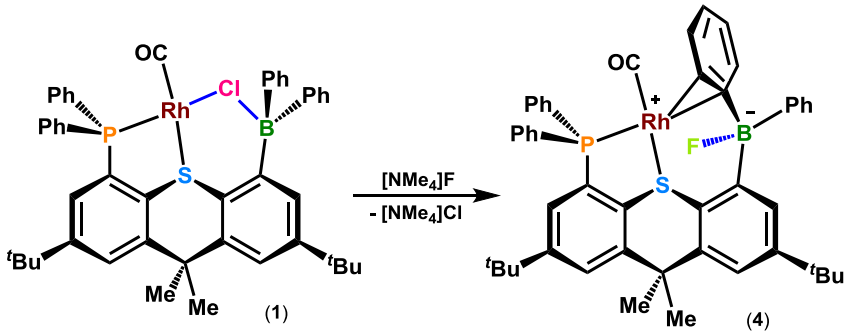

Scheme 2.2. Synthesis of [Rh(CO)(TXPB-F)] (**4**).

X-ray quality crystals of **4**·1.5CH_2Cl_2 were grown by slow diffusion of hexanes into a solution of **4** in CH_2Cl_2 at –30 °C. In the solid-state, as was observed spectroscopically in solution, the fluoride ligand does not form a strong interaction with the metal centre (Figure 2.6, Table 2.1). Rather, it binds preferentially to boron producing a zwitterionic complex containing a 4-coordinate anionic borate and a cationic rhodium centre. The B–F bond distance in **4** is 1.445(6) Å, which lies at the shorter end of the range for B–F bond distances in fluoroborates such as [CPh_3][FB{$C_6F_4(C_6F_5)$-*o*}$_3$] (1.472 Å),[179] [$FB(Mes)_2Ar$] [Ar = 1-(8-(trimethylammonio)methylnaphthalene)] (1.486 Å),[180] and K[$FB(Ph)(CF_3)_2$] (1.452 Å).[181] Boron in **4** also exhibits a greater degree of pyramidalization [Σ(C–B–C) = 331.2(7)°] than that in compounds **1**–**3** (Table 2.1). The Rh···F distance of 3.261(3) Å in complex **4** is well outside of the sum of the covalent radii for the two elements (1.99 Å),[68] and approaches the sum of the van der Waals radii (3.51 Å).[182]

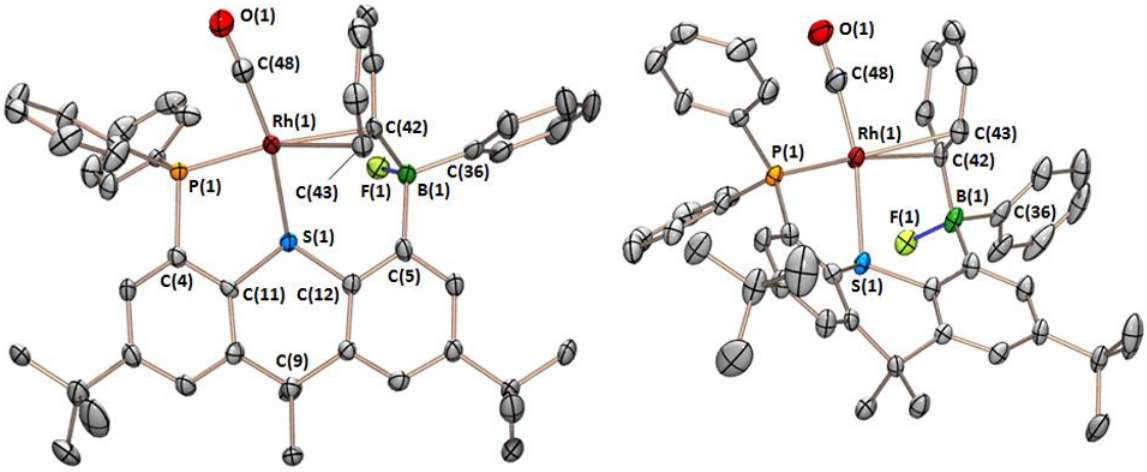

Figure 2.6. Two different views of the solid-state structure for [Rh(CO)(TXPB-F)]·1.5(CH_2Cl_2) [**4**·1.5(CH_2Cl_2)] with ellipsoids drawn at 50 % probability. Hydrogen atoms and lattice solvent have been omitted for clarity. One of the *tert*-butyl substituents [C(16)–C(19)] was positionally disordered over two positions; only one orientation is depicted above.

To complete a highly distorted square planar geometry at rhodium [S–Rh–CO = 168.0(2)°, P–Rh–cent = 160.5(2)°; cent = the centroid position between C_{ipso} and C_{ortho}], a phenyl ring in the $FBAr_3$ unit is η^2-bound to rhodium via the *ipso*- and *ortho*-carbon atoms. The Rh–C_{ipso} distance of 2.336(4) Å in **4** is comparable with those in other rhodium(I) complexes featuring an η^2-bound aryl ring, including [Rh(CO)(POPheph)][ClO_4] [POPheph = κ^1-$PPh_2POCH(Ph)CH(Me)NMe\{CH(Ph)(\eta^2$-Ph)}] (2.334 Å)[183] and [Rh(PEt_3)$_2$\{κ^1-$OC(Ph_2)(\eta^2$-Ph)}] (2.350 Å).[184] By contrast, the Rh-C_{ortho} distance of 2.564(5) Å in **4** is significantly longer (cf. 2.449 Å and 2.398 Å, respectively, in the literature complexes above), indicative of a weaker interaction.

2.4 – Fluxional Behaviour of [Rh(CO)(TXPB-F)]

Despite η^2-arene coordination in the solid-state, complex **4** is fluxional in solution at room temperature; the C*Me*$_2$ methyl groups of the thioxanthene backbone are equivalent [although a coalescence temperature of 274(2) K ($\Delta G^{\ddagger}$ at T_c = 51.5(7) KJ mol^{-1}) for C*Me*$_2$ methyl group exchange does suggest a higher activation barrier for this process in **4**, compared with complexes **1**–**3** (assuming that $\Delta S^{\ddagger}$ is not large and negative)], and the phenyl rings on both boron and phosphorus undergo pair wise exchange. At –50 °C, two distinct *B*-phenyl and *P*-phenyl rings are observed, but the *ortho*- and *meta*-C*H* positions of each ring remain equivalent down to –80 °C. Given the complexity of the aryl region in complex **4**, this assignment was verified by low-temperature 2D COSY and DEPT-135 NMR spectroscopy of d_{10}-**4** in which both *P*-phenyl rings are perdeuterated (Figure 2.7). The exchange process responsible for equivalence of the *ortho*- and *meta*-positions on each of the two *B*-phenyl rings (while maintaining inequivalence of the C*Me*$_2$ methyl, *B*-phenyl and *P*-phenyl groups) in **4** must involve rotation around the B–C bonds. This would require loss of any η^2-arene interaction, presumably with pivoting about B(1)–C(5) to position the previously coordinated *B*-phenyl ring further from rhodium and bring fluorine into closer proximity with the metal. The η^2-arene interactions in [Rh(CO)(POPheph)][ClO_4] and

[$Rh(PEt_3)_2\{\kappa^1$-$OCPh_2(\eta^2$-$Ph)\}$] (*vide supra*) also are not maintained on the NMR time scale in solution at room temperature.[183,184]

Table 2.2. Crystallographic Data Collection and Refinement Parameters for Complexes **2**–**6**.

Structure	**2 · hexane**	**3 · hexane**	**4 · 2(C_6H_{14})**	**5 · 1.5CH_2Cl_2**	**6 · CH_2Cl_2**
Formula	$C_{54}H_{62}BBrOPRhS$	$C_{54}H_{62}BIOPRhS$	$C_{60}H_{77}BOPRhS$	$C_{49.5}H_{51}BCl_3FOPRhS$	$C_{49}H_{50}BCl_2F_6OP_2RhS$
Formula wt	983.70	1030.69	990.96	964.00	1047.51
T (K)	100(2)	100(2)	100(2)	100(2)	173(2)
Cryst. Syst.	Triclinic	Monoclinic	Triclinic	Triclinic	Triclinic
Space Group	*P*–1	*P*2(1)/*c*	*P*–1	*P*–1	*P*–1
a (Å)	13.784(4)	20.985(5)	10.907(2)	10.480(2)	13.7285(11)
b (Å)	16.784(4)	10.931(2)	13.536(3)	14.606(3)	13.7787(10)
c (Å)	22.340(6)	21.318(4)	16.766(4)	15.417(3)	14.0510(11)
α [deg]	78.308(5)	90	96.447(4)	84.035(4)	69.0590(10)
β [deg]	72.860(5)	94.691(4)	93.892(5)	81.671(4)	84.6330(10)
γ [deg]	87.227(5)	90	91.612(6)	76.197(4)	83.8570(10)
Volume [$Å^3$]	4836(2)	4873.7(18)	2452.3(9)	2261.7(8)	2463.7(3)
Z	4	4	2	2	2
μ (mm^{-1})	1.293	1.097	0.464	0.677	0.620
F(000)	2040	2112	996	994	1072
Crystal Size (mm^3)	0.28×0.13× 0.05	0.17×0.10× 0.04	0.20×0.08×0.02	0.22×0.16×0.03	0.58×0.22×0.08
θ Range for Collection [deg]	1.55–26.57	1.92–25.64	1.87–25.44	1.34–26.5	1.55–30.51
No. of Reflns Collected	42443	37759	26269	26414	36404
No. of Indep Reflns	19853	9041	8972	9232	14662
Completeness to θ Max (%)	98.2	98.2	98.8	98.4	97.5
Absorption Correction	Numerical	Numerical	Numerical	Numerical	Numerical
Max and Min Transmission	0.9382, 0.7135	0.9575, 0.8355	0.9908, 0.9129	0.9800, 0.8653	1.000, 0.712
GOF on F^2	0.885	0.936	0.841	0.970	1.049
Final R_1 [$I > 2\sigma(I)$] (%)	7.22	4.86	6.08	5.69	4.53

2.5 – ^{31}P-^{19}F Coupling and CO Stretching Frequency in [Rh(CO)(TXPB-F)]

Interestingly, despite the long P···F distance of 4.830(3) Å in the X-ray crystal structure of **4**, ^{31}P-^{19}F coupling is observed in the solution ^{31}P{^{1}H} NMR spectrum at room temperature (52.2 ppm; $^{1}J_{31P,103Rh}$ = 166Hz, $J_{31P,19F}$ = 6.2 Hz; Figure 2.7). This small coupling could potentially occur via a through-bond or a through-space mechanism. For comparison, the *trans*-$^{2}J_{31P,19F}$ coupling constants in borane-free rhodium(I) fluoride complexes such as [RhF(PPh$_3$)$_3$], [RhF(PPh$_3$)$_2$(PPh$_2$F)], and [Rh$_2$(μ-F)$_2$(PPh$_3$)$_4$] are 172, 217, and 196 Hz, respectively, and the *cis*-$^{2}J_{31P,19F}$ coupling constants for [RhF(PPh$_3$)$_3$] and [RhF(PPh$_3$)$_2$(PPh$_2$F)] are 28.5 and 27 Hz, respectively.[185]

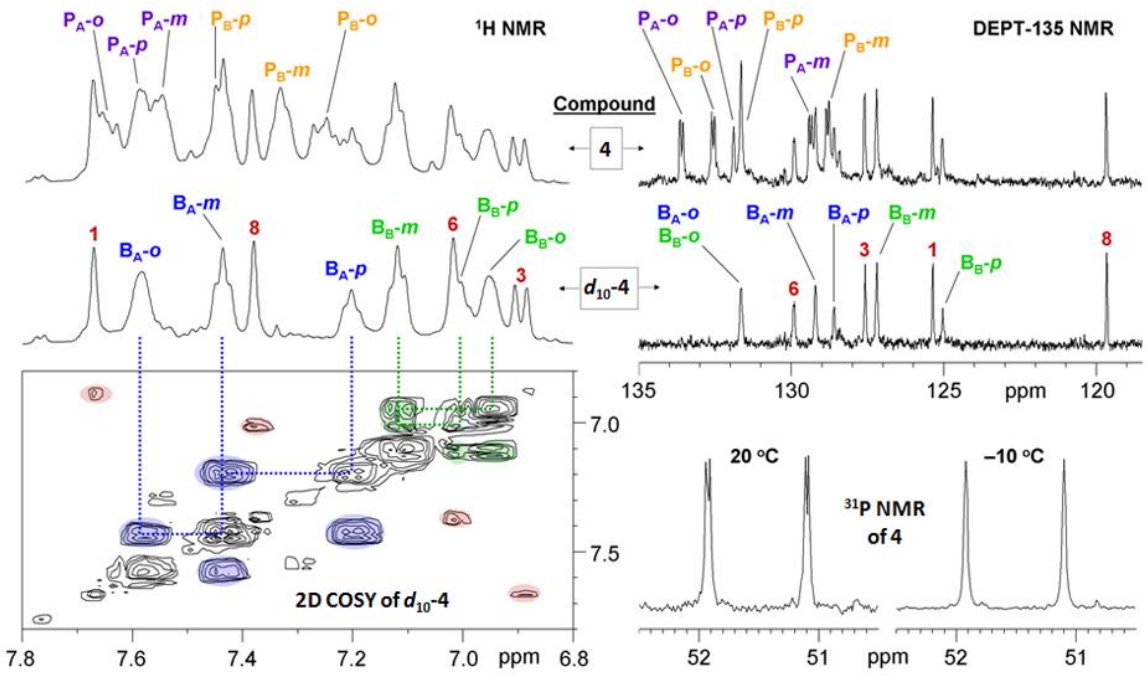

Figure 2.7. Aromatic regions of the ^{1}H and DEPT-135 NMR spectra of **4** and ***d*$_{10}$-4** at –50 °C. Aromatic region of the 2D COSY NMR spectrum for ***d*$_{10}$-4** at –50 °C, and ^{31}P NMR spectra for **4** at 20 and –10 °C. All NMR spectra are in CD_2Cl_2.

Through-space coupling in solution (direct spin-spin coupling) is a result of non-bonding interactions between lone pairs, and decreases in strength rapidly as the distance between coupling nuclei exceeds the sum of the van der Waals radii.[186] For example, in

various tetrakis(diphenylphosphino)ferrocene ligands, ^{31}P-^{31}P through-space coupling was observed only at P···P distances of 4.9 Å and below.[187,188] In addition, for a range of rigid fluorine-containing compounds, ^{19}F-^{19}F through-space coupling was found to decay exponentially with increasing F···F distance, falling to 2 Hz at an F···F distance of 4.2 Å.[189] Similarly, in triflone-bearing phosphoramidite ligands, through-space ^{19}F-^{31}P coupling was calculated (using $Me_2NP(OH)_2\cdots F_4C$ as a model) to be significant only at distances below 4.0–4.9 Å,[§] depending on the angle between the interacting phosphorus lone pair and the trifluoromethyl group.[190]

These couplings represent an ideal situation involving lone pair-lone pair interactions, but in compound **4**, the lone pair on phosphorus is bound to rhodium. Hierso *et al*. have reported that in $[(\kappa^2P_1P_2\text{-L})MX_2]$ (M = Ni and Pd; L = 1,1',2,2'-tetrakis(diphenylphosphino)-4,4'-di-*tert*-butylferrocene; X = Cl or Br), through-space coupling can be transmitted via an interaction between a free phosphine lone pair and the metal-phosphine bonding pair. However, the *trans*-annular through-space $J_{31P,31P}$ couplings in $[(\kappa^2P_1P_2\text{-L})PdCl_2]$ are only 24.0 and 6.4 Hz, despite relatively short P···P distances of 3.8 and 4.4 Å, respectively. On the basis of these and other *trans*-annular $J_{31P,31P}$ coupling constants, Hierso *et al*. concluded that lone pair-bonding pair interactions are less effective for transmission of through-space coupling than lone pair-lone pair interactions.[188]

On the basis of the long P···F distance in the X-ray crystal structure of **4**, the strong angular dependence of through-space coupling,[190,191] and the requirement for coupling to occur via a lone pair-bonding pair interaction rather than a lone pair-lone pair interaction, through-space coupling in **4** seems unlikely. However, it is interesting to note that the magnitude of the $J_{31P,19F}$ coupling decreases with decreasing temperature ($J_{31P,19F}$ = 6.2, 5.1, 4.3, 3.5, 2.7, 1.4, and 0 Hz at 25, 15, 10, 5, 0, –5, and –15 °C, respectively). Significant temperature dependencies (positive and negative) have been observed for

[§] CF_3 rotation averaged $J_{31P,19F}$ values were calculated as a function of P···C distance. This was converted to a closest-approach P···F distance by subtraction of 1.32 Å (the C–F distance in CF_4).

through-space couplings in molecules of intermediate rigidity, where the observed coupling is a time-averaged value from all accessible solution conformations. For example, positive temperature dependencies were reported for through-space coupling in a triflone-bearing phosphoramidite ($J_{31P,19F}$ = 6.5 Hz at 100 °C and 1.7 Hz at –58 °C),[190] $P(C_6H_4CF_3\text{-}o)_xPh_{(3-x)}$ (x = 1–3; for x = 2, $J_{31P,19F}$ = 54.5 Hz at 117 °C and 51.1 Hz at –43 °C),[192] $C_6H_4F(CF_3)$-*o* ($J_{19F,19F}$ = 13.7 Hz at 97 °C and 11.2 Hz at –62 °C)[193] and $C_6H_4(CF_3)(SeCN)$-*o* ($J_{19F,77Se}$ ~ 51 Hz at 80 °C and 42 Hz at –40 °C),[194] while a large negative temperature dependency was reported for through-space coupling in $C_6H_4(CH_2F)(SeCN)$-*o* ($J_{19F,77Se}$ ~ 77 Hz at 20 °C and 104 Hz at –90 °C).[194,195] The $J_{31P,19F}$ coupling in **4** could therefore be assigned as a through-space coupling facilitated by solution conformations with P···F distances significantly shorter than that in the X-ray crystal structure of **4**. However, an alternative explanation is tighter (entropically favoured) η^2-arene binding to rhodium at lower temperatures, leading to an increase in the average Rh···F distance (due to rotation about the C(5)–B bond) and a reduction in the magnitude of through-bond $^2J_{31P,19F}$ coupling.

A final important spectroscopic parameter for **4** is the CO stretching frequency, which is 2008 cm^{-1} in Nujol and 2011 cm^{-1} in CH_2Cl_2. Zwitterionic **4** might be expected to exhibit a significantly higher carbonyl stretching frequency than neutral **1** and **2**, but instead the frequencies are comparable (Table 2.1). The following factors must therefore compensate for the increase in positive charge at rhodium: (1) the η^2-interaction between rhodium and a phenyl ring of the fluoroborate group in TXPB-F, and (2) enhanced electron donor properties of an anionic TXPB-F ligand relative to neutral TXPB. Substantially more effective electron-donation has previously been reported for anionic $R_2B(CH_2PR'_2)_2^-$ and *m*-$Ph_3B(C_6H_4)P^iPr_2^-$ ligands relative to neutral $R_2Si(CH_2PR'_2)_2$ and *m*-$Ph_3Si(C_6H_4)P^iPr_2$ analogues.[164,196]

2.6 – Cationic [Rh(CO)(TXPB)][PF_6]

A halide-free rhodium-TXPB cation was targeted to gain additional insight into the electronic environment in zwitterionic **4**. Cationic [Rh(CO)(TXPB)][PF_6] (**5**) was prepared by Prof. David J. H. Emslie by treatment of **1** with Tl[PF_6] in CH_2Cl_2, and was isolated as bright orange crystals in an isolated yield of 92 % (Scheme 2.3). Complex **5** is the fluoride-free and formally cationic cousin of zwitterionic **4**, so sonication of **5** with CsF and 18-Crown-6 in CH_2Cl_2 provided an alternative route to **4**. The $^{31}P\{^1H\}$ NMR spectrum of **5** shows a doublet at 64.9 ppm ($^1J_{31P,103Rh}$ = 166.8 Hz), which is shifted 12.7 ppm to higher frequency of complex **4** (Table 2.1). In solution, exchange of the C*Me*$_2$ groups in **5** is slow, as was observed for complex **4**; the coalescence temperature for C*Me*$_2$ exchange in **5** is 312(2) K, leading to a $\Delta G^{\ddagger}$ of 61.2(8) KJ mol^{-1} at this temperature.

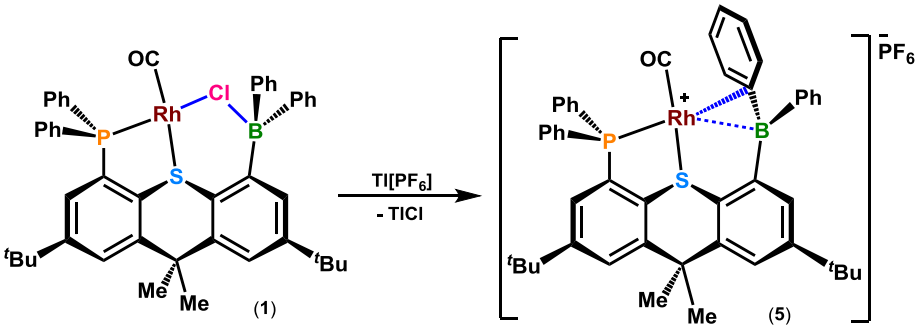

Scheme 2.3. Synthesis of [Rh(CO)(TXPB)][PF_6] (**5**).

X-ray quality crystals of **5** (Figure 2.8, Table 2.1) were obtained by Prof. David J. H. Emslie from CH_2Cl_2/hexane at –30 °C, and revealed a T-shaped arrangement of the phosphine, thioether, and carbonyl groups [S–Rh–CO = 172.48(9)°, P–Rh–CO = 88.35(9)°, P–Rh–S = 84.84(2)°]. In addition, close approach of boron and the *ipso*-carbon of one *B*-phenyl ring to rhodium is observed [Rh–B = 2.557(3) Å and Rh–C(42) = 2.362(2) Å]. A weak interaction between rhodium and the *ortho*-carbon of the coordinated *B*-phenyl ring is also plausible based on the Rh–C(43) distance of 2.797(3) Å. However, pair-wise equivalence of the *ortho*- and *meta*-positions of each *B*-phenyl

ring in the solution ^{1}H and ^{13}C NMR spectra, even at –80 °C, argues against a significant Rh–C_{ortho} interaction. For comparison, two CH_{ortho} and two CH_{meta} environments were observed for the coordinated *B*-phenyl ring in the low temperature ^{1}H and ^{13}C NMR spectra of the η^3-arylborane complexes [Pd(TXPB)], [Ni(TXPB)],[122] and [(TXPB)Rh(μ-CO)$_2$Fe(CO)Cp].[1] The metal–arylborane interaction in **5** is therefore best considered to involve η^2*BC*-coordination. This assignment is supported by the observation of a broad singlet at 57ppm ($\omega_{1/2}$ ~ 1800 Hz) in the ^{11}B NMR spectrum of **5**, which is shifted 12 ppm to lower frequency of free TXPB, consistent with the presence of a significant, albeit weak, Rh–B interaction (*vide infra*).

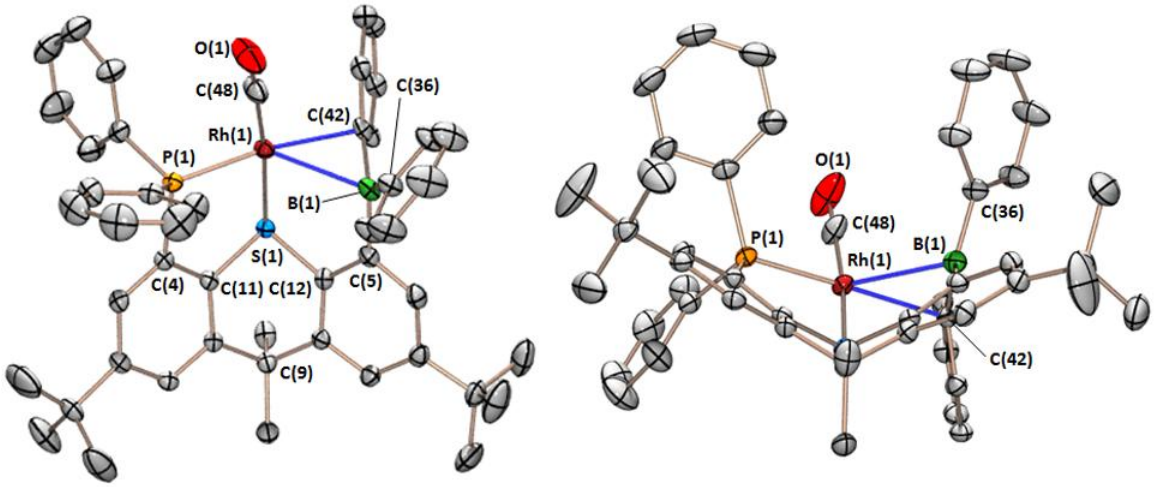

Figure 2.8. Two different views of the solid-state structure for [Rh(CO)(TXPB)][PF_6]·CH_2Cl_2 (**5**·CH_2Cl_2) with ellipsoids drawn at 50 % probability. Hydrogen atoms and lattice solvent have been omitted for clarity. This X-ray crystal structure was obtained by Prof. David J. H. Emslie.

Both η^1*B*- and η^3*BCC*-coordination modes have previously been reported in metal arylborane complexes (*vide supra*), and the relationship between these arylborane coordination modes parallels that between η^1-benzyl and η^3-benzyl coordination; examples of η^n-coordinated triarylmethyl complexes are [(η^3-CPh_3)M(acac)] (M = Pd, Pt),[197] [(η^5-CPh_3)(η^n-CPh_3)Yb(THF)$_2$] (n = 1–2),[198] and [{κ^4*COO'O''*-C($C_6H_2{}^tBu_2$O-*o*)$_3$}Zr(THF)$_3$].[199] The η^2*BC*-coordination mode in **5** provides a link between the η^1*B*- and

η^3*BCC*-bonding extremes, much as η^2-benzyl coordination lies intermediate between the η^1- and η^3-benzyl coordination modes. For comparison, M–B bond distances of 2.320, 2.297, and 2.63 Å, and M–C_{ipso} distances of 2.198, 2.019, and 2.33 Å were observed in the η^3-arylborane complexes [Pd(TXPB)], [Ni(TXPB)],[122] and [(TXPB)Rh(μ-CO)$_2$Fe(CO)Cp],[1] respectively. However, the M–C_{ortho} distances of 2.325, 2.081, and 2.46 Å in these complexes are much shorter than the Rh–C_{ortho} distance in **5**.

At the time of publication, an η^2*BC*-coordination mode had previously been reported for the boratalkene complexes [$Cp_2Ta(CO)\{\eta^2$-$CH_2B(C_6F_5)_2\}$][200] and [$Cp_2Ta(CN^tBu)\{\eta^2$-$CH_2B(C_6F_5)_2\}$],[201] with Ta–C bond distances of 2.337 and 2.348 Å, Ta–B bond distances of 2.728 and 2.738 Å, and B–C distances of 1.508 and 1.525 Å, respectively. However, the B–C distance of 1.576(4) Å in **5** is in the usual range for a B–C_{sp2} single bond (e.g., 1.571–1.589 Å in BPh_3),[202] and C–C distances in the coordinated *B*-phenyl ring are not obviously perturbed from typical values. The η^2*BC*-interaction in complex **5** is therefore not significantly boratalkene-like, and presumably involves η^1-arene coordination and a dative η^1-borane interaction.

On the basis of this bonding description, the approximate planarity of the borane, and the long Rh–B distance of 2.557(3) Å in **5** is not unusual; boron remains planar in the weakly coordinated η^1-borane complexes [AuCl(^{iPr}MPB^{Flu})] (^{iPr}MPB^{Flu} = (*o*-^{i}Pr$_2$P)C_6H_4BFlu, BFlu = 9-borafluorenyl; Σ(C–B–C) = 356°) and [AuCl(^{iPr}MPB^{Cy})] [Σ(C–B–C) = 359°],[47] which exhibit long Au–B distances of 2.66 Å and 2.90 Å, respectively. The borane is also approximately planar in the η^3-coordinated arylborane complexes [Pd(TXPB)], [Ni(TXPB)], and [(TXPB)Rh(μ-CO)$_2$Fe(CO)Cp]. However, cationic ambiphilic ligand complexes with short metal–borane distances are not without precedent; a somewhat shorter M–B distance was observed in cationic [Au(^{iPr}TPB)][$GaCl_4$] (^{iPr}TPB = {(*o*-^{i}Pr$_2$P)C_6H_4}$_3$B; Au–B = 2.448 Å),[133] and substantially shorter M–B bonds were observed in the structurally rigid B(mt^R)$_3$ (mt^R = 2-sulfanyl-1-R-imidazolyl; R = methyl, *tert*-butyl) and B(taz)$_3$ complexes [Rh(CO)(PPh_3){B(taz)$_3$}][PF_6] (taz = 5-sulfanyl-4-ethyl-3-methyl-1,2,4-triazolyl) (Rh–B = 2.155 Å),[99] [Co(PPh_3){B(mt^{tBu})$_3$}][X] (X = BPh_4, PF_6, or SbF_6) (Co–B = 2.132 Å),[82]

[Rh(CN^{t}Bu)(PPh$_3$){B(mt^{Me})$_3$}]Cl (Rh–B = 2.155 Å), [Rh(CNXyl)(PPh$_3$){B(mt^{Me})$_3$}]Cl (Rh–B = 2.146 Å), and [Rh(PMe$_3$)$_2${B(mt^{Me})$_3$}]Cl (Rh–B = 2.148 and 2.153 Å).[74]

The CO stretching frequency for **5** is 2028 cm^{-1} in Nujol and 2038 cm^{-1} in CH_2Cl_2. These values are much higher than those for complexes **1**–**4**, indicating significantly reduced electron density at the rhodium centre. The difference in ν(CO) between zwitterionic **4** and cationic **5** can be attributed in large part to more effective electron donation from the TXPB-F ligand in **4**, relative to the TXPB ligand in **5**. This may be explained in terms of the formal negative charge on the TXPB-F ligand, combined with different arylborate/arylborane binding modes; η^2-arene binding in **4** versus η^2*BC*-arylborane coordination in **5**. However, increasing positive charge at a carbonyl ligated metal centre has been shown to reduce the extent to which the bonding orbitals of CO are polarized toward oxygen, resulting in enhanced covalency and an increase in the CO stretching force constant.[203] A portion of the increase in ν(CO) from **4** to **5** may therefore arise from polarization effects due to the overall positive charge on complex **5**, rather than a decrease in the extent of π-backdonation.

2.7 – A Rhodium(I) Hydride Complex of the TXPB Ligand

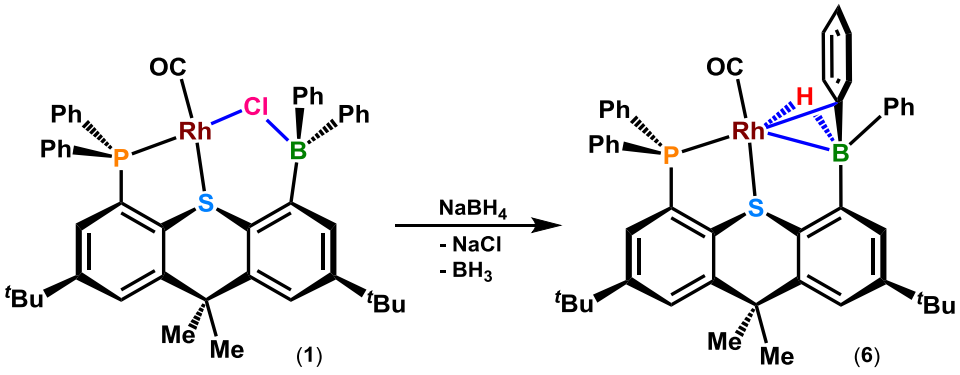

Scheme 2.4. Synthesis of [Rh(μ-H)(CO)(TXPB)] (**6**).

Reaction of [Rh(μ-Cl)(CO)(TXPB)] (**1**) with one equivalent of $NaBH_4$ afforded dark brown/orange [Rh(μ-H)(CO)(TXPB)] (**6**) in 65 % yield (Scheme 2.4). The $^{31}P\{^1H\}$

NMR spectrum contains a doublet located at 57.9 ppm with $^{1}J_{31P,103Rh}$ coupling of 144 Hz. The ^{11}B NMR shift for **6** is 3 ppm, indicative of 4-coordinate boron, and a hydride signal was observed at –4.05 ppm in the ^{1}H NMR spectrum featuring ^{103}Rh and ^{31}P coupling (57 and 25 Hz, respectively) as well as quadrupolar broadening ($\omega_{1/2}$ ~ 103 Hz) due to coordination to boron; the ^{1}H NMR spectrum of **4**, in addition to an expanded view of the aromatic region are displayed in Figures 2.9 and 2.10. These data are consistent with a rhodium(I) complex bearing a hydride ligand in a bridging position between the metal and a pendant borane, and similar NMR features (^{11}B NMR chemical shifts between 13.5 and –4.2 ppm, and hydride signals between –2.76 and –30.4 ppm in the ^{1}H NMR spectra) have been reported for the crystallographically characterized ambiphilic ligand complexes in Table 2.3, all of which feature a hydride ligand bridging to a pendant borane. Low frequency ^{11}B NMR chemical shifts (–0.7 to –5.5 ppm) have also been observed for rhodium(I) complexes of pre-formed hydroborate ligands (Table 2.3), however the ^{1}H NMR chemical shifts for the bridging hydrogen atom in these complexes are less shielded, ranging from 4.21 to –0.7 ppm. Overall, rhodium complexes of the latter description possess stronger B–H and weaker Rh–H coordination than is observed in complex **6** and other complexes exhibiting bridging M–H–BR_3 interactions involving the borane of an ambiphilic ligand.

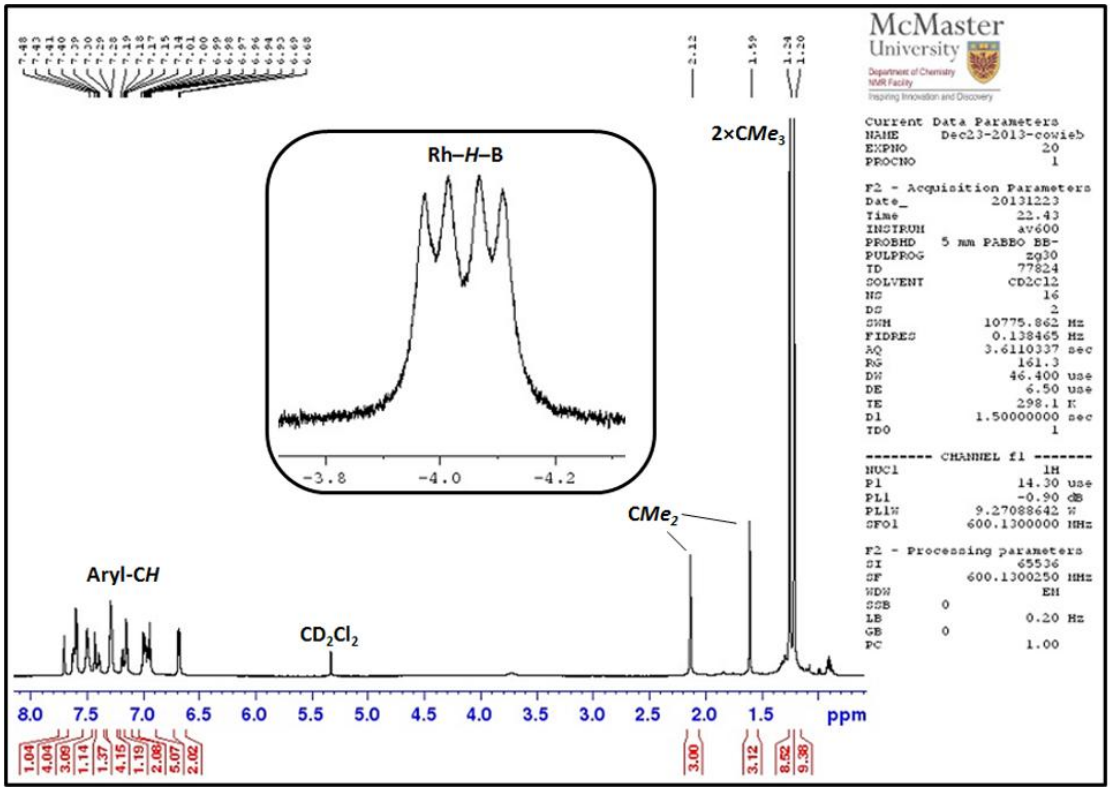

Figure 2.9. ^{1}H NMR spectrum of [Rh(μ-H)(CO)(TXPB)] (**6**; 600 MHz, 298 K, CD_2Cl_2).

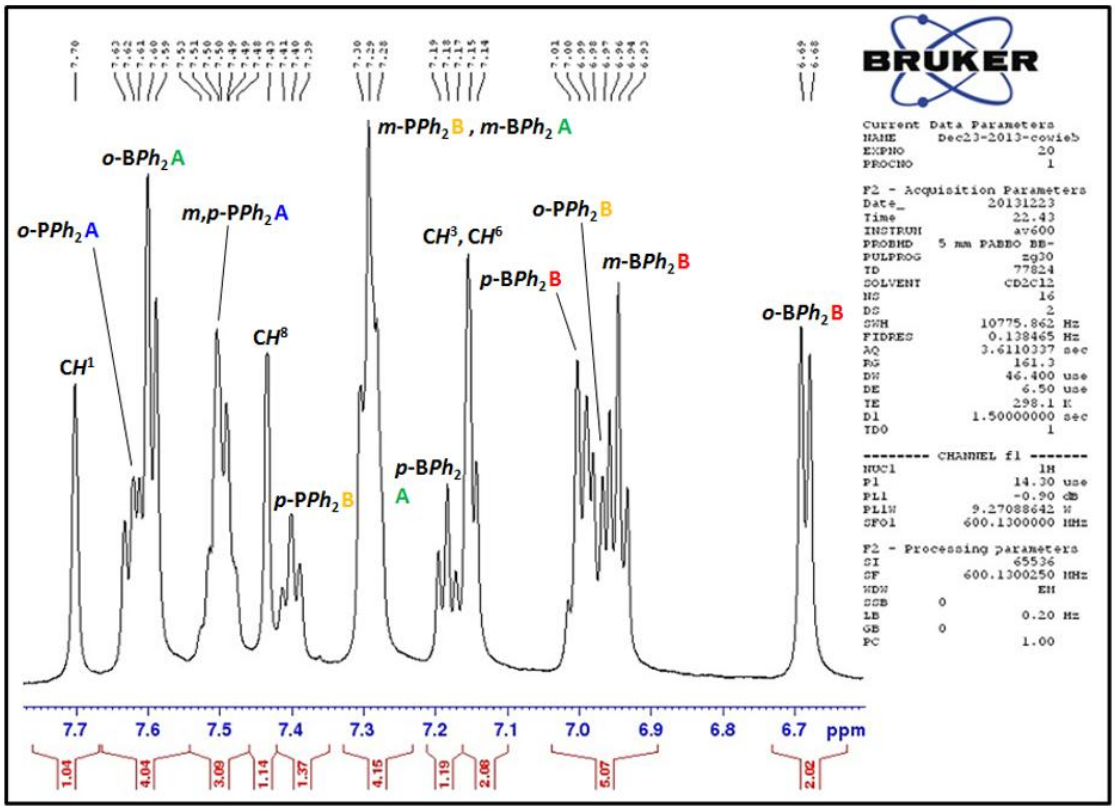

Figure 2.10. Expanded aromatic region of the ^{1}H NMR spectrum of [Rh(μ-H)(CO)(TXPB)] (**6**; 600 MHz, 298 K, CD_2Cl_2).

Table 2.3. Spectroscopic and structural data for crystallographically characterized borane-containing ambiphilic ligand and hydroborate ligand complexes featuring a M–H–BR_3 bridging interaction.

A. Complexes Bearing a Metal–Hydride–Borane Interaction through Coordination of a Borane-Containing Ambiphilic Ligand								
Complex	**M–H (Å)**	**B–H (Å)**	**M···B (Å)**	**M–H–B (°)**	**Σ(CBC) (°)**	**^{1}H NMR δ (ppm)**	**^{11}B NMR δ (ppm)**	**Ref.**
[(η^5-C_5H_5)Ru(μ-H)(PB)]	1.60(6)	1.43(6)	2.895(6)	146.24[a]	338.6(7)	–15.4	–4.2	[111]
[(η^5-C_5Me_5)Ru(μ-H)(PB)]	1.68(2)	1.41(3)	2.922(3)	141.53[a]	341.6(3)	–13.9	–4.2	[111]
[Rh(CO)(PPh_3)(μ-H)(^{Ph}DPB^{Ph})]	1.76(6)	1.24(5)	2.849	143.07[a]	341.2(6)	–11.61	11.5	[124]
[Rh(CO)(PMe_3)(μ-H)(^{Ph}DPB^{Ph})]	–	–	–	–	–	–11.55	13.5	[124]
[Rh(PPh_3)(μ-H)(^{Ph}DPB^{Ph})]	1.65(4)	1.34(4)	2.734	132.01[a]	337.2(6)	–7.6	1.9	[124]
[NiH(μ-H)(^{iPr}DPB^{Ph})]	–	–	–	–	–	–6.65	–2.3	[128]
[Fe(N_2)(H)(μ-H)(^{iPr}TPB)]	1.49(2)	1.17(2)	2.604(3)	152.66[a]	343.4(4)	–30.4	8.2	[60]
[Fe(H_2)(H)(μ-H)(^{iPr}TPB)]	1.56(2)	1.21(2)	2.63(2)	142.86[a]	343.7(2)	–25[b,c]	7.5	[60]
[Fe(CN^tBu)(H)(μ-H)(^{iPr}TPB)]	1.52(2)	1.20(2)	2.673(2)	158.59[a]	344.7(2)	–23.9	~8[b]	[60]

B. Complexes Bearing a Metal–Hydride–Borane Interaction through Coordination of a Pre-Formed Hydroborate Ligand								
Complex	**M–H (Å)**	**B–H (Å)**	**M···B (Å)**	**M–H–B (°)**	**Σ(CBC) (°)**	**^{1}H NMR δ (ppm)**	**^{11}B NMR δ (ppm)**	**Ref.**
[Rh(cod){$H_2B(mt^{Me})_2$}]	2.13(3)	1.139[a]	3.033(6)	134(2)	324.9[a]	Not Given	–5.5	[204]
[Rh(cod)(Tai)]	1.99(2)	1.17(3)	2,971[a]	139(2)	337.9(4)	0.88	–2.2	[205]
[Rh(nbd)(Tai)]	1.98(5)	1.15(2)	2.922[a]	137.7[a]	337.8(5)	Not Given	–1.5	[90]
[$Rh(H)_2(P^tBu_3)$(Tai)]	1.86(2)	1.24(2)	2.789[a]	131.8[a]	332.7(1)	–0.7	–0.7	[89]
[Rh(cod)(^{Ph}Bai)]	2.00(4)	1.15(4)	2.937(4)	143(5)	337.4(5)	4.21	–4.6	[90]
[$Rh(CO)(PPh_3)${$HB(taz)_3$}]	2.41	1.00	3.239	139	328.8(5)	Not Given	–5.0	[99]
[Rh{$P(C_7H_7)_3$}(Tp')]	1.789(7) 1.899(7)	1.288(7) 1.200(7)	2.809[a] 2.829[a]	131.1[a] 130.0[a]	337.7[a] 337.0[a]	0.90	–1.9	[206]

Boron and hydrogen atoms in the table refer specifically to those engaged in an Rh–H–BR_3 bridging interaction. [a] values obtained from the CSD (Cambridge Structural Database); [b] values estimated from NMR spectra provided in the referenced publications or the ESI associated with this work. [c] ^{1}H NMR signal observed at –90 °C; PB = $Ph_2P(CH_2)_2B(C_6F_5)_2$; ^{R}DPB^{Ph} = {(*o*-$R_2P)C_6H_4\}_2$BPh; $^{i\text{Pr}}$TPB = {(*o*-$^{i}Pr_2P)C_6H_4\}_3$B; mt^{Me} = 2-sulfanyl-1-methylimidazolyl; Tai = HB(7-azaindolyl)$_3$; ^{Ph}Bai = HBPh(7-azaindolyl)$_2$; taz = 4-ethyl-3-methyl-5-thioxo-1,2,4-triazolyl; hpp = 1,3,4,6,7,8-hexahydro-2H-pyrimido-[1,2-a]pyrimidinate; Tp' = HB(3,5-dimethylpyrazolyl)$_3$; C_7H_7 = cycloheptatrienyl. [Rh{$P(C_7H_7)_3$}(Tp')] gave rise to a $^{1}J_{1H,103Rh}$ constant of 19.6 Hz.

X-ray quality crystals of **6**·2(C_6H_{14}) (Figure 2.11; Table 2.1) were obtained by slow diffusion of hexanes into a solution of **6** in CH_2Cl_2 at –30 °C. The solid-state structure confirmed that the hydride ligand in **6** bridges between rhodium and the pendant borane of TXPB, with short Rh–H, Rh–B and Rh–C_{ipso} [C_{ipso} = C(42)] distances of 1.84(5), 2.456(6) and 2.568(5) Å, respectively. The geometry at rhodium is distorted square planar with P–Rh–H and S–Rh–C(48) angles of 162(2)° and 157.7(2)°, respectively, and the Rh–H–B angle is 92(2)°. Boron is significantly pyramidalized, with the sum of the C–B–C angles equal to 337.1(8)°, and the B–H distance is 1.59(6) Å. The H(48)–B–C angles for complex **6** are 121(2), 102(2) and 96(2)° with the most acute angle to the phenyl *ipso*-carbon uninvolved in η^2*BC*-coordination to rhodium, C(36), which is approximately *trans* to rhodium across the B–H bond [Rh-H(48)-B-C(42) torsion angle = 145.02°].

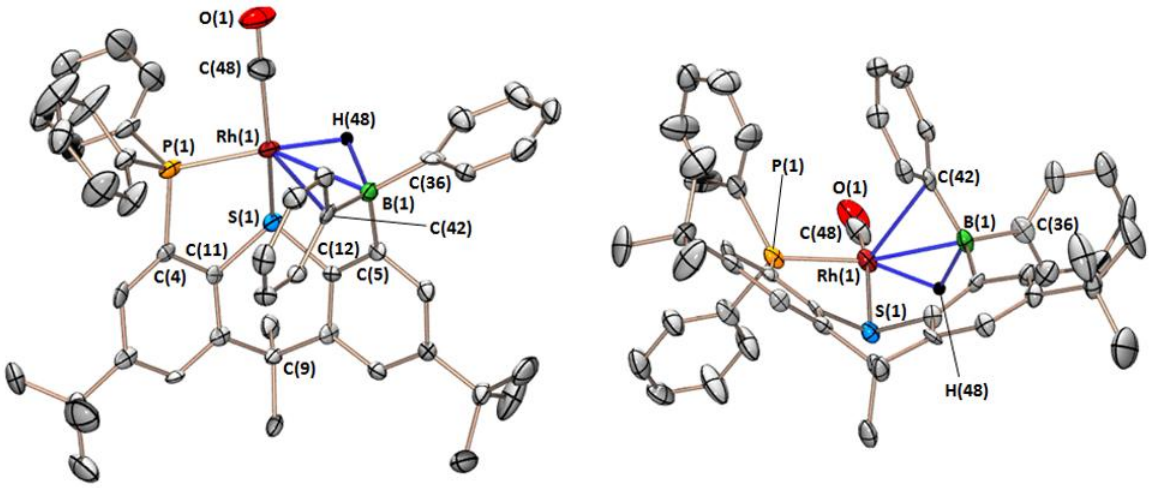

Figure 2.11. Two different views of the solid-state structure for [Rh(μ-H)(CO)(TXPB)]·2(C_6H_{14}) [**4**·2(C_6H_{14})] with ellipsoids drawn at 50 % probability. Hydrogen atoms and lattice solvent have been omitted for clarity.

The Rh–B distance in **6** is remarkably short, even compared with related [Rh(CO)(TXPB)][PF_6], which features η^2*BC*-coordination of a *B*-phenyl group to rhodium (*vide supra*); the Rh–B and Rh–C_{ipso} distances in [Rh(CO)(TXPB)][PF_6] are 2.557(3) and 2.362(2) Å, respectively [cf. 2.456(6) and 2.568(5) Å in **6**]. However, a similar bonding situation was found in [PtH(μ-H)(FcPPB)], with the following calculated bond distances, angles and bond orders: a Pt–H–B angle of 110.1°, an acute H–B–C angle of 92.4° to the phenyl ring oriented approximately *trans* to the transition metal across the B–H bond, Pt–B, Pt–H and B–H bond distances of 2.524, 1.686 and 1.386 Å (Chapter 6; the covalent radii of Rh and Pt are 1.42 and 1.36 Å, respectively).[68] A shared feature of the TXPB and FcPPB ligands is the positioning of the borane moiety on the periphery of the ligand framework, rather than in a central position, which may allow for a more acute M–H–B angle, and by extension, shorter M–B distances.

At 20 °C, each of the two *B*-phenyl rings in **6** gave rise to just three signals in the ^{1}H NMR spectrum. However, the *ortho*-protons of one *B*-phenyl ring decoalesced at –67 °C, indicating that the interaction between rhodium and the *ipso*-carbon atom of one of the *B*-phenyl rings is maintained on the NMR timescale at low temperature. The CO stretching frequency for **6** is 1984 cm^{-1} in Nujol versus 2006 cm^{-1} in CH_2Cl_2, suggesting

the accessibility of solution structures which differ significantly from the solid-state structure; decreased electron density at rhodium is consistent with the accessibility of solution structures in which the Rh–C_{ipso} interaction is not maintained or the hydride ligand is more completely abstracted from rhodium. The CO stretching frequency for **6** in Nujol is substantially lower than those of [RhX(CO)(TXPB)] (X = Cl (**1**), Br (**2**), I (**3**), F (**4**); ν(CO)(Nujol) = 2004-2013 cm^{-1}, *vide supra*), indicating that the hydride ligand in **6** remains a strong donor relative to a halide ligand, despite partial abstraction by the borane. Additionally, the low CO stretching frequency may reflect the presence of a Rh–C_{ipso} interaction in **6** that is absent in **1**–**4**.

In keeping with the low CO stretching frequency, complex **6** possesses the longest Rh–P bond length in the series (2.261(2) Å in **6** vs. 2.196(2)–2.224(1) Å in **1**–**4**) and the smallest $^{1}J_{31P,103Rh}$ coupling constant (144 Hz in **6** vs. 161–167 Hz in **1**–**4**). However, the Rh–S bond length of 2.289(1) Å in **6** is shorter than the Rh–S distances in **1**–**4** (2.300(1)–2.405(1) Å), suggesting that the Rh–S and Rh–P distances may be strongly influenced by the structural requirements of the ambiphilic framework, especially those stemming from the much shorter Rh–B distance in **6** than in **1**–**4** [2.456(6) Å vs. 3.231(5)–3.647(9) Å].

2.8 – Summary

A series of ambiphilic ligand rhodium(I) halide complexes, [RhX(CO)(TXPB)] [X = Cl (**1**), Br (**2**), I (**3**), and F (**4**); TXPB = a phosphine-thioether-borane ligand], have been prepared, as well as the halide-free cation [Rh(CO)(TXPB)][PF_6] (**5**), and a rhodium(I) hydride complex, [Rh(μ-H)(CO)(TXPB)] (**6**). Complex **1** was accessed via reaction of TXPB with [{Rh(μ-Cl)$(CO)_2$}$_2$] and was used as the starting material for the preparation of complexes **2**–**6**, either by halide substitution or halide abstraction. In all complexes, the TXPB ligand binds to rhodium via the phosphine and thioether groups, as well as an additional Rh–X–B, Rh-(η^2*CC*-Ar_3BF), or Rh-(η^2*BC*-BAr_3) interaction. In complex **3**, the iodide proved to form a strong bonding interaction with rhodium, but only a weak interaction with the borane in TXPB because of the incompatibility of a hard borane

Lewis acid with a soft iodide ligand. By contrast, the bromide and chloride ligands in **1** and **2** adopt bridging positions between rhodium and boron, with a stronger halide-boron interaction in the chloro-complex. Bridging chloride interactions between a metal and a Lewis acidic borane are rare, and to the best of our knowledge, complex **2** is the first example of a bridging metal–bromide–borane interaction. In the case of complex **4**, fluoride binds to the borane to form an anionic TXPB-F ligand, and the complex exhibits a weak 6.2 Hz $J_{31P,19F}$ coupling in the room temperature $^{31}P\{^{1}H\}$ NMR spectrum. In contrast to zwitterionic **4**, the metal centre in cationic **5** engages in η^2*BC*-coordination of the borane in TXPB. The metal-boron interaction in this complex is weak, based on an ^{11}B NMR chemical shift of 57 ppm, which combined with an overall positive charge on the complex, and less effective electron donation from neutral TXPB (relative to the anionic TXPB-F ligand in **4**), leads to a carbonyl stretching frequency shifted 20–25 cm^{-1} to higher frequency of that in **4**. Finally, the strongly σ-donating hydride ligand participates in a bridging Rh–H–BR_3 interaction in **6**, as evidenced by a slightly broadened ^{1}H NMR signal at –4.05 ppm with $^{1}J_{1H,103Rh}$ and $^{2}J_{1H,31P}$ coupling constants of 57 and 25 Hz, respectively. Furthermore, the ^{11}B chemical shift of 3 ppm is very similar to that of complex **4**, indicating that boron is 4-coordinate, and the existence of a bridging Rh–H–BR_3 interaction in **6** results in close approach of a *B*-phenyl ring to rhodium, enabling participation of both boron and the *ipso*-carbon atom in coordination to the metal centre.

On the basis of these crystallographic and spectroscopic data, it may be concluded that Rh–X coordination becomes increasingly favorable, relative to B–X bond formation, as group 17 is descended, consistent with the predictions of hard-soft acid-base theory.[98] However, in this system a significant M–X–B bridging interaction is maintained for bromide, and a weak interaction persists even in the case of iodide. Nonetheless, iodide is by a wide margin the most suitable choice for the preparation of halide-containing ambiphilic ligand complexes in which a free pendant borane is required for cooperative reactivity. These results also confirm that in principle, it should be possible to use ambiphilic borane-containing ligands to provide an additional thermodynamic driving

force for oxidative addition of less reactive aryl-chloride and aryl-fluoride substrates, either by the formation of a bridging M–Cl–BR_3 interaction or by fluoride abstraction to yield an anionic fluoroborate and a cationic metal centre. However, [Pd(TXPB)], [Ni(TXPB)] and [Pd(η^2:η^2-dvds)(TXPB)][122] proved to be unreactive towards various aryl-chloride and aryl-fluoride substrates (e.g. octafluoronaphthalene, decafluorobiphenyl, 4-fluorobiphenyl, chlorobenzene in C_6D_6 between 25 and 75 °C), both in stoichiometric reactions, and under catalytic conditions in the presence of phenylboronic acid pinacol ester as a coupling reagent.

Ph.D. Thesis
Bradley E. Cowie
Department of Chemistry and Chemical Biology
McMaster University

Chapter 3

Bridging Rhodium−Iron Borataaminocarbyne Complexes Formed by Intramolecular Isonitrile−Borane Coordination

Adapted with permission from: Cowie, B. E.; Emslie, D. J. H. *Organometallics* **2013**, *32*, 7297-7305.

3.1 – Introduction

In 2006 and 2008, the first examples of transition metal complexes in which a triarylborane is η^3*BCC*-coordinated to a metal centre were prepared by the Emslie research group: [(TXPB)Rh(μ-CO)$_2$Fe(CO)Cp] (**7**),[1] [Pd(TXPB)], and [Ni(TXPB)][122] (Figure 3.1; TXPB = 2,7-di-*tert*-butyl-5-diphenylboryl-4-diphenylphosphino-9,9-dimethylthioxanthene).[59] While a variety of reactions have been carried out to probe the potential for these borane complexes to engage in cooperative substrate binding and reactivity, most resulted in displacement of both the thioether donor and the borane from the metal or displacement of the entire TXPB ligand from the metal. For example, reaction of [Pd(TXPB)] with CO yielded free TXPB, and reaction of [Pd(TXPB)] with 1,3-divinyltetramethydisiloxane (dvds) yielded [Pd(η^2:η^2-dvds)(κ^1*P*-TXPB)], in which TXPB acts as a monodentate phosphine ligand (Figure 3.1).[122] One of the few more productive reactions was the reaction of [Pd(TXPB)] with *trans,trans*-dibenzylideneacetone (dba) to form [Pd(μ-dba)(TXPB)] (Figure 3.1), which can be described as a zwitterionic palladium(II) boratoxyallyl complex.[59] Described herein are the reactions of **7** with isonitriles to yield products in which both *P*- and *S*-coordination is maintained and boron is bound to the nitrogen atom of the CNR unit in the product. Spectroscopic and structural studies to ascertain the most appropriate bonding description for the resulting CNRBR'$_3$ ligand are described, along with attempts to prepare a borane-free analogue of these complexes using the TXPH (2,7-di-*tert*-butyl-4-diphenylphosphino-9,9-dimethylthioxanthene) ligand.[123]

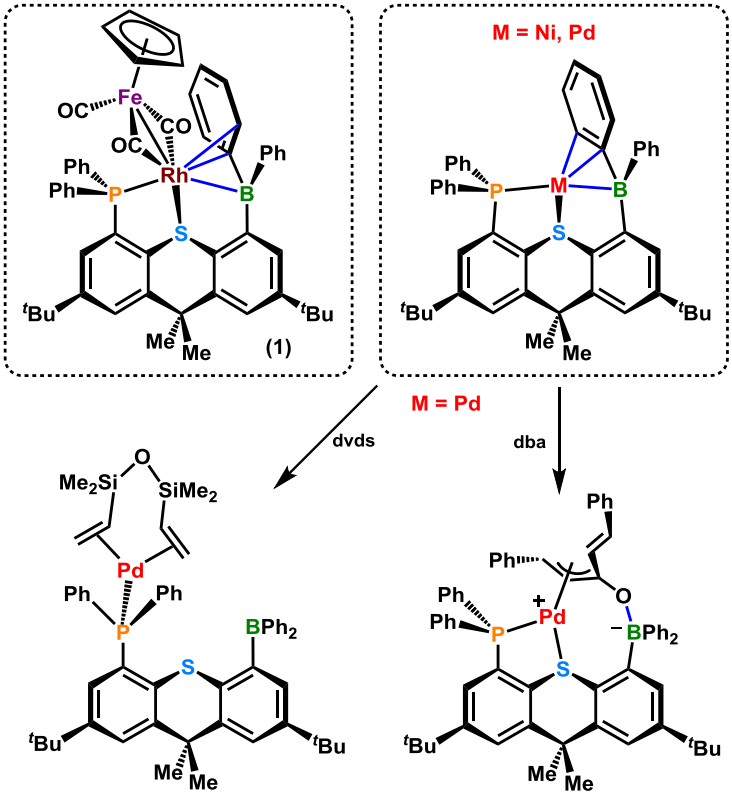

Figure 3.1. TXPB complexes in which the borane is η^3*BCC*-coordinated to the metal (enclosed in dashed boxes), and reactions of [Pd(TXPB)] with dvds and dba.

In light of the fact that this work deals with isonitrile ligand−borane coordination, a brief discussion of the canonical forms relevant to CNR, CNR(LA) (LA = Lewis acid), and related CNR_2 ligands is provided below.

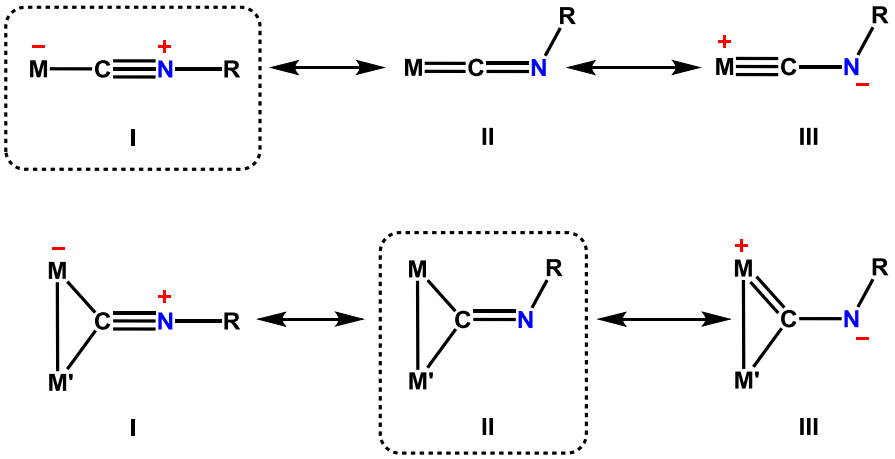

Figure 3.2. Three canonical forms for terminal and bridging isonitrile ligands. In each case, dashed lines enclose the canonical form that typically plays a dominant role.

Three canonical forms can be used to describe CNR ligands (Figure 3.2): form **I** is most prevalent in terminal CNR complexes, form **II** tends to dominate for bridging CNR complexes, and form **III** is generally not considered to play an important role.[207-209] However, coordination of a Lewis acid at the nitrogen atom of a bridging isonitrile ligand has in a few cases resulted in complexes with long C−N bonds and/or particularly low C−N stretching frequencies; see **A**,[210,§] **B**,[211] and **C**[212,¶] in Figure 3.3. These complexes are essentially Lewis acid adducts of canonical form **III**, and **B** is to the best of our knowledge the only example of a borataaminocarbyne complex; it is certainly the only crystallographically characterized example.

[§] Complex A was not identified as a Lewis acid substituted aminocarbyne complex in the paper and was not drawn as shown in Figure 3.3. However, the data, especially ν(CN), support this bonding description.

[¶] Related niobium amidocarbyne complexes have also been reported, see: Caselli, A.; Solari, E.; Scopelliti, R.; Floriani, C. *J. Am. Chem. Soc.* **1999**, *121*, 8296.

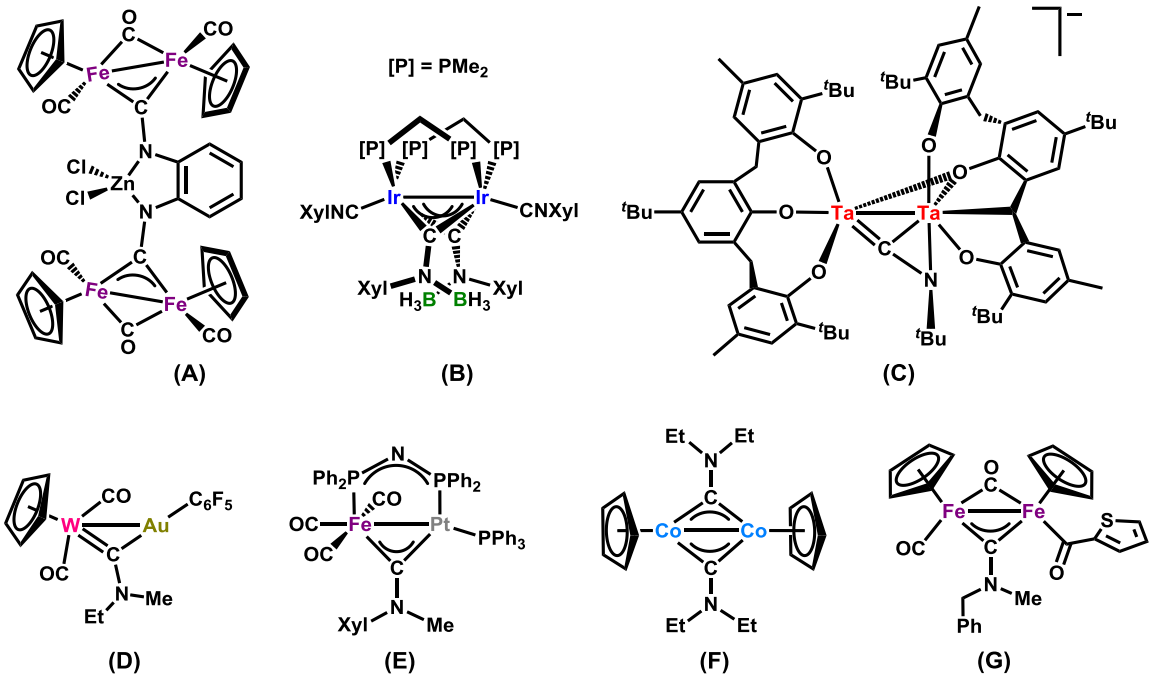

Figure 3.3. Literature examples of μ-C–NR(LA) complexes where LA is a Lewis acid (LA = $ZnCl_2$ in **A**, BH_3 in **B**, and TaR_x in **C**), and literature examples of late transition metal μ-aminocarbyne complexes (**D**–**G**).

The Lewis acid substituted aminocarbyne [CNR(LA)] complexes described above are related to aminocarbyne (CNR_2) complexes, in which an alkyl cation or a proton can be considered, conceptually, to play the role of the Lewis acid (see Figure 3.3 for examples).[213-216] Naturally, aminocarbyne ligands represent just one of two possible canonical forms for a CNR_2 ligand. The other canonical form is that of an azavinylidene ligand,[217] which is related to a borane-coordinated bent isonitrile ligand (a borataazavinylidene) in the same way that an aminocarbyne ligand is related to a borataaminocarbyne ligand (Figure 3.4).

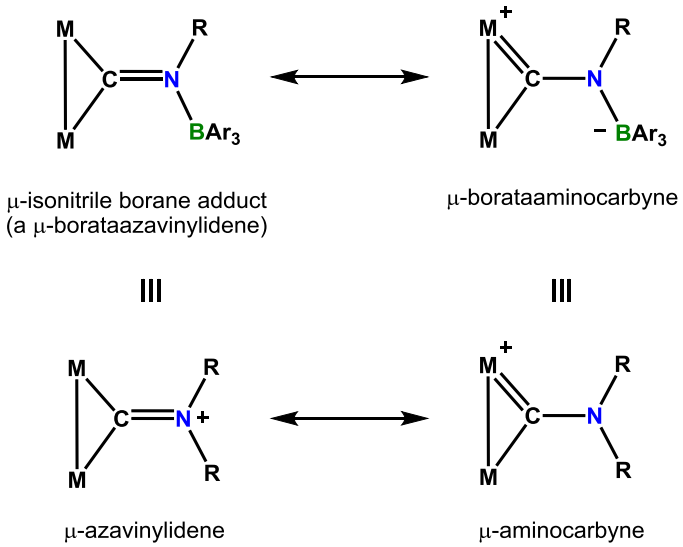

Figure 3.4. Canonical forms for a bridging CNR(BR'$_3$) ligand, and the analogous canonical forms for a CNR_2 ligand. For directly analogous CNR(BR'$_3$) and CNR_2 complexes, the overall charge on the CNR_2 complex would be more positive by one unit.

3.2 – Reactivity of [(TXPB)Rh(μ-CO)$_2$Fe(CO)Cp] with Isonitriles

The reaction of olive green [(TXPB)Rh(μ-CO)$_2$Fe(CO)Cp][1] (**7**) with one equivalent of CNC_6H_4Cl-*p*, CNXyl, and CN^{n}Bu (Xyl = 2,6-Me$_2$-C$_6$H$_3$) yielded dark purple or dark red [(TXPB)Rh(μ-CO)(μ-CNR)Fe(CO)Cp] [R = C_6H_4Cl-*p* (**8**), Xyl (**9**), ^{n}Bu (**10**)]. In contrast, reaction of **7** with one equivalent of the more electron donating and sterically encumbered ^{t}BuNC afforded the ^{t}BuNC adduct of TXPB, accompanied by unidentified metal complexes (Scheme 3.1; the ^{1}H NMR spectrum of independently synthesized TXPB–CN^{t}Bu is displayed in Figure 3.5). Boron in starting complex **7** is involved in η^3*BCC*-coordination to rhodium, whereas boron in **8**–**10** is bound solely to the nitrogen atom of the bridging CNR ligand.

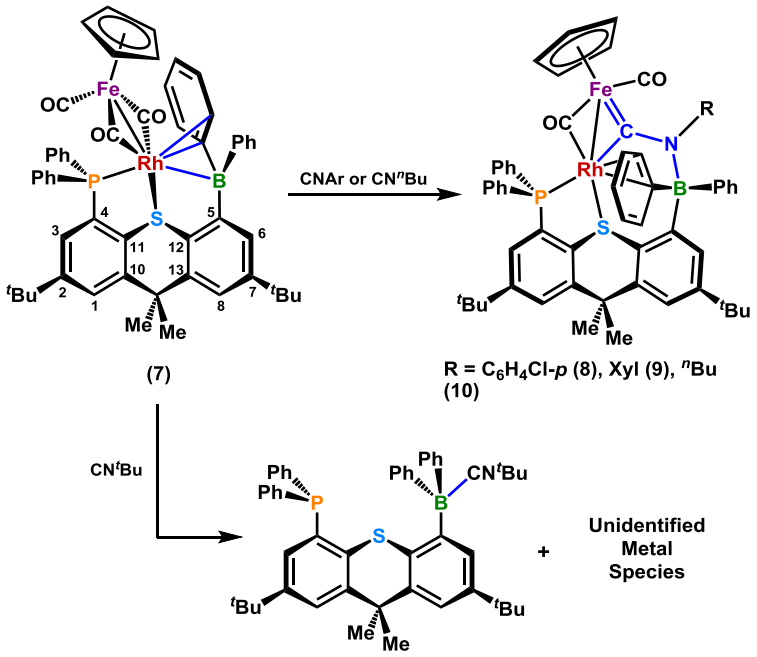

Scheme 3.1. Reaction of TXPB complex [(TXPB)Rh(μ-CO)$_2$Fe(CO)Cp] (**7**) with isonitriles.

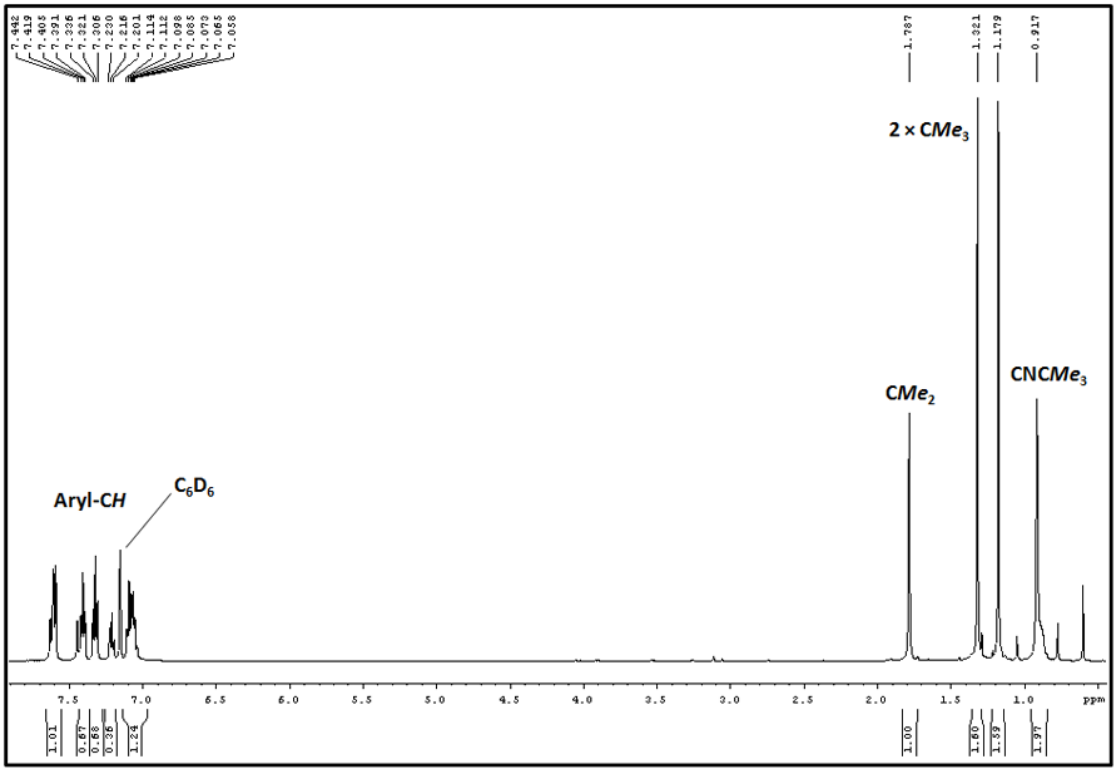

Figure 3.5. ^{1}H NMR spectrum of the TXPB–CN^{t}Bu adduct (500 MHz, 298 K, C$_6$D$_6$).

Complexes **8**−**10** gave rise to a doublet at 44−47 ppm in their ^{31}P NMR spectra ($^{1}J_{31P,103Rh}$ = 148−151 Hz) and a broad ^{11}B NMR signal between 2 and 4 ppm, indicative of four-coordinate boron. Consistent with the structure depicted in Scheme 3.1, both *B*-phenyl rings are inequivalent in the ^{1}H and ^{13}C NMR spectra, and all positions on one of the *B*-phenyl rings became inequivalent below 0 °C (the ^{1}H NMR spectrum of **8**, in addition to an expanded view of the aromatic region are displayed in Figures 3.6 and 3.7; numbered protons refer to the positions of the thioxanthene backbone in the TXPB ligand, as shown in Scheme 3.1). However, ^{13}C-^{103}Rh or ^{1}H-^{103}Rh coupling was not observed for any of the *B*-phenyl signals down to −90 °C on a 500 MHz NMR spectrometer, indicating that the η^2-arene interaction observed in the solid-state structures of **8**−**10** (*vide infra*) is labile in solution.

In the ^{13}C NMR spectra of **8**−**10**, the CO ligand on iron is located at 215−216 ppm and the bridging CO ligand appears as a doublet of doublets at 241−243 ppm ($^{1}J_{13C,103Rh}$ = 60 Hz, $^{2}J_{13C,31P}$ = 10−11 Hz). The CNR signal appears as a doublet of doublets at 312 ppm (complexes **8** and **9**) or 304 ppm (complex **10**) with a $^{1}J_{13C,103Rh}$ coupling of 51−53 Hz and a $^{2}J_{13C,31P}$ coupling of 23−24 Hz. This CNR signal is at unusually high frequency for a bridging isonitrile ligand (typically < 250 ppm)[207,208] but is in the range for an aminocarbyne complex (~200−350 ppm). In addition, the C−N stretching frequencies for complexes **8**−**10** lie between 1571 and 1521 cm^{-1}, which is significantly lower than is typically observed for a μ-isonitrile complex (>1600 cm^{-1})[207,209] but is in line with an aminocarbyne complex (most often 1500−1600 cm^{-1}),[217] indicating that a borataaminocarbyne bonding description is appropriate for **8**−**10**. For comparison, the C−N stretching frequencies for the CNR(LA) ligands in complexes **A** and **B** in Figure 3.3 are 1534 and 1514 cm^{-1} (**A**; LA = $ZnCl_2$),[210] and 1520 and 1502 cm^{-1} (**B**; LA = BH_3).[211]

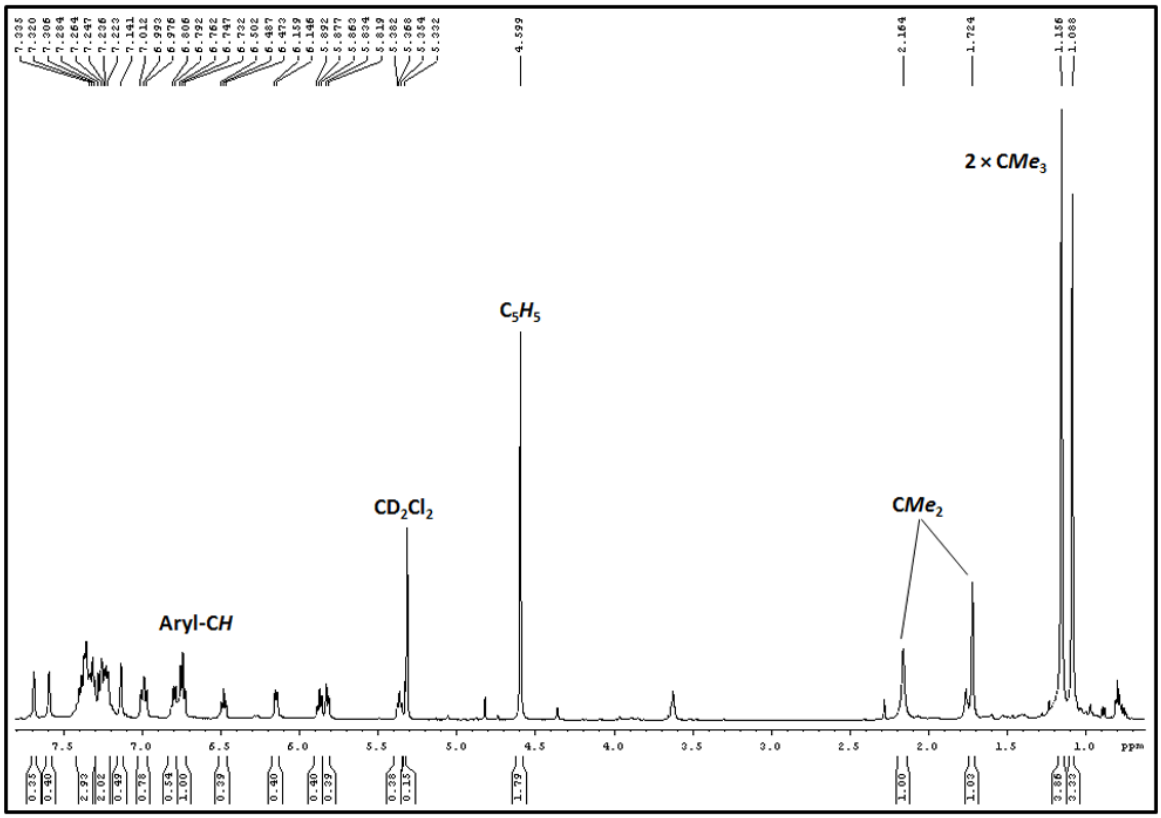

Figure 3.6. ^{1}H NMR spectrum of [(TXPB)Rh(μ-CO)(μ-CNC$_6$H$_4$Cl-*p*)Fe(CO)Cp] (**8**; 500 MHz, 194 K, CD_2Cl_2).

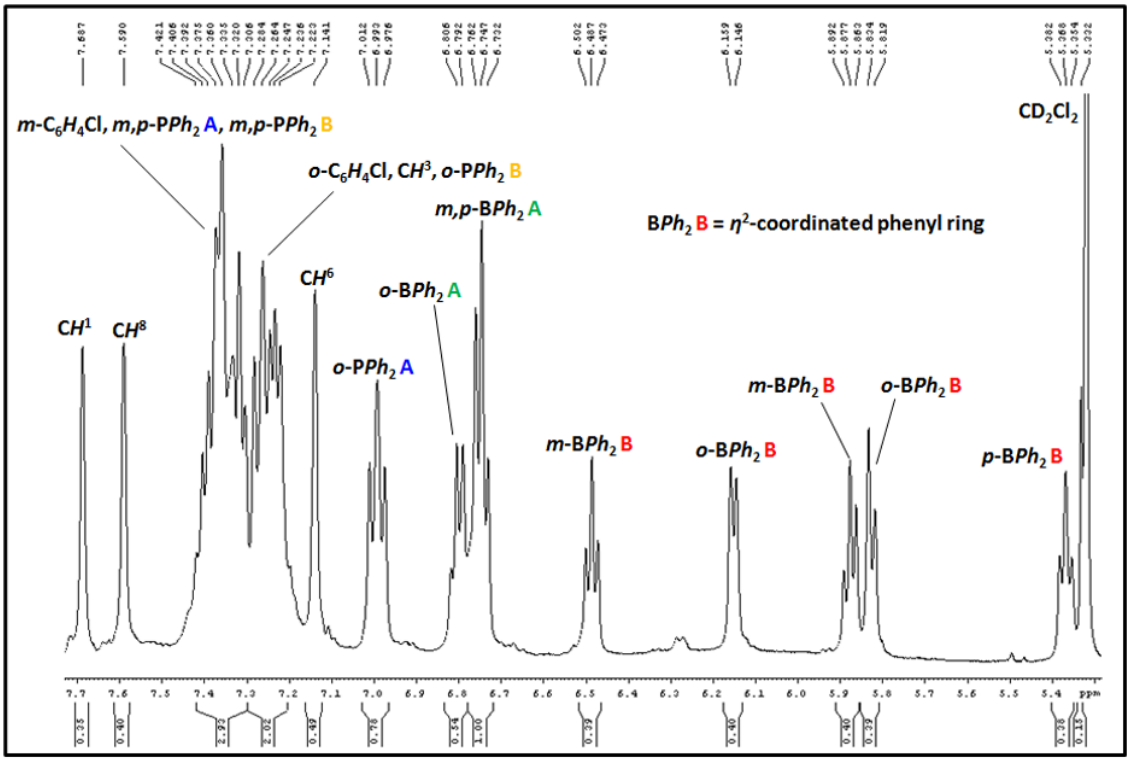

Figure 3.7. Expanded aromatic region of the ^{1}H NMR spectrum of [(TXPB)Rh(μ-CO)(μ-CNC$_6$H$_4$Cl-*p*)Fe(CO)Cp] (**8**; 500 MHz, 194 K, CD_2Cl_2).

X-ray quality crystals of **8**·2hexane, **9**·5toluene, and **10**·2hexane were grown from hydrocarbon solvents at −30 °C; the structures of **8**, **9** and **10** are provided in Figures 3.8 and 3.9. Key bond lengths and angles are summarized in Table 3.2. All three structures share the same general features: the TXPB ligand is κ^2*PS*-coordinated to rhodium, the Rh−Fe distance is 2.594−2.606 Å, one CO and one CNR group bridge between rhodium and the Fe(CO)(η^5-Cp) group, boron is coordinated to the nitrogen atom of the bridging CNR unit, and one *B*-phenyl ring is η^2-coordinated to rhodium.

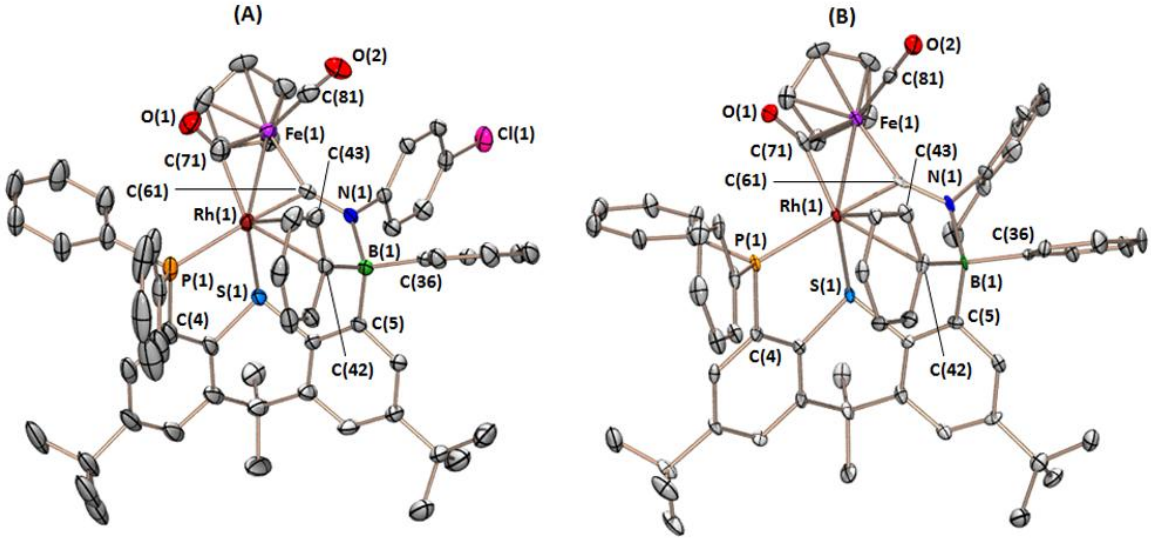

Figure 3.8. A. X-ray crystal structure for [(TXPB)Rh(μ-CO)(μ-CNC_6H_4Cl-*p*)Fe(CO)Cp]·2(hexane) [**8**·2(hexane)], and **B.** X-ray crystal structure for [(TXPB)Rh(μ-CO)(μ-CNXyl)Fe(CO)Cp]·5(toluene) [**9**·5(toluene)]; hydrogen atoms and solvent are omitted for clarity, and ellipsoids are set to 50 %. One of the *tert*-butyl substituents in **8**·2(hexane) was rotationally disordered over two positions; only the orientation with the highest occupancy is displayed above.

The Fe−C(61) bonds in **8−10** are 1.833(3), 1.864(6), and 1.851(5) Å, respectively, falling well within the range for complexes with an Fe−C double bond. For example, the Fe−C_{CR2} distances in the terminal carbene complexes [Cp{CO_2Zr-(NR_2)$_3$}(CO)Fe=CR_2] (CR_2 = 1,2-diphenylcyclopropenylidene)[218] and [Cp($SSiPh_3$)(CO)Fe=CH(NMe_2)][219] are 1.860(5) and 1.889(2) Å, whereas the Fe−C_{CNR} and Fe−C_{CCR2} bonds in [{CpFe(CO)}$_2$(μ-CO)(μ-CNPh)][220] (a bent isonitrile complex) and [{CpFe(CO)}$_2$(μ-CO)(μ-C=CH^{i}Pr)][221] are 1.915(3)−1.969(8) Å. The Rh−C(61) bonds in **8−10** are 1.968(3), 1.981(5), and 1.975(5) Å, respectively, indicative of a Rh−C single bond; the Rh−C_{CR2} double bonds in [Cp(CO)Rh=CPh_2][222] and *trans*-[Cl(Sb^{i}Pr$_3$)$_2$Rh=CPh_2][223] are 1.906(3) and 1.863(4) Å, while the Rh−C_{CNR} and Rh−C_{CCR2} single bonds in [(Cp*Rh)$_2$(μ-CNXyl)$_2$],[224] [{Cp*Rh(CO)}$_2$(μ-C=CMe_2)],[225] and [{Rh(CO)(PCy_3)}$_2$(μ-O_2CMe)(μ-C=CPh_2)][226] range from 1.967(6) to 2.043(1) Å.

Consistent with the low C−N stretching frequencies for **8−10** (*vide supra*), the C−N bonds in **8−10** are notably long at 1.284(3), 1.298(7), and 1.294(6) Å, respectively. For comparison, the C−N distances in the μ-isonitrile complexes described above are 1.229(4) and 1.234(8) Å, whereas the C−N bonds in μ-aminocarbyne complexes **D**−**G** (Figure 3.3) are 1.29(2),[213] 1.296(6),[215] 1.312(4),[216] and 1.303(5) Å,[214] respectively, and the C−N bond in borataaminocarbyne complex **B** (Figure 3.3) is 1.34(2) Å.[211] Taken together, these structural data point to a μ-borataaminocarbyne bonding description for the CNRBR'$_3$ unit in **8−10**; one in which the carbyne carbon atom is doubly bound to iron and singly bound to rhodium.

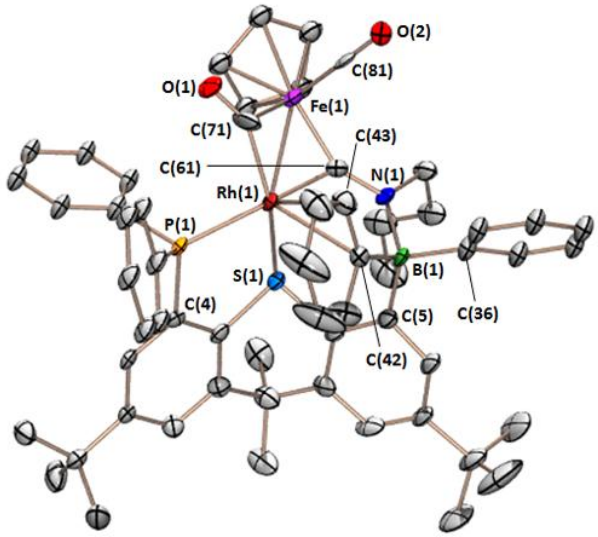

Figure 3.9. X-ray crystal structure for [(TXPB)Rh(μ-CO)(μ-CN^{n}Bu)Fe(CO)Cp]·2(hexane) [**10**·2(hexane)]; hydrogen atoms and solvent are omitted for clarity, and ellipsoids are set to 50 %. The Cp-ring bound to iron, the carbonyl ligand bridging between rhodium and iron, and one of the phenyl groups bound to boron were positionally disordered over two positions. In addition, both of the phenyl groups bound to phosphorus were rotationally disordered over two positions; in all cases, only the orientation with the highest occupancy is displayed above.

The only features of **8−10** that are at first glance incommensurate with a μ-borataaminocarbyne bonding description are the long B−N bond lengths of 1.641(4), 1.660(8), and 1.654(7) Å, respectively. These distances are more in keeping with the B−N

distances in neutral Lewis base−borane adducts such as MePhC=N(CH_2Ph)−B(C_6F_5)$_3$ [1.630(6) and 1.658(6) Å][227] and 1-phenylimidazole−BPh_3 [1.630(3) Å].[227] The elongated B−N bonds in **8−10** can likely be explained on the basis of steric arguments. The B−N distance in **B** (Figure 3.3) is 1.59(3) Å,[211] but meaningful comparison is impossible given the large standard deviation on this measurement.

Table 3.1. Crystallographic Data Collection and Refinement Parameters for Complexes **8–12.**

Structure	**8 · 2hexane**	**9 · 5toluene**	**10 · 2hexane**	**11 · $2C_2H_4Cl_2$**	**12 · CH_2Cl_2**
Formula	$C_{73}H_{85}BClFeNO_2PRhS$	$C_{98}H_{102}BFeNO_2PRhS$	$C_{71}H_{90}BFeNO_2PRhS$	$C_{47}H_{52}Cl_4FeO_3PRhS$	$C_{57}H_{54}Cl_4FeN_2O_2PRhS$
Formula wt	1266.36	1654.40	1222.04	1028.48	1162.61
T (K)	100(2)	100(2)	100(2)	100(2)	100(2)
Cryst. Syst.	Monoclinic	Triclinic	Monoclinic	Triclinic	Triclinic
Space Group	*P*2(1)/*c*	*P*–1	*C*2/*c*	*P*–1	*P*–1
a (Å)	17.776(2)	11.544(1)	27.207(7)	14.548(2)	12.513(2)
b (Å)	17.235(2)	14.717(2)	22.061(5)	14.940(2)	13.682(2)
c (Å)	21.196(3)	23.728(3)	20.075(5)	15.159(2)	15.469(2)
α [deg]	90	92.065(2)	90	112.777(5)	92.902(2)
β [deg]	99.332(3)	98.126(2)	98.150(5)	103.455(5)	92.532(3)
γ [deg]	90	104.399(2)	90	118.734(4)	96.036(3)
Volume [$Å^3$]	6408(1)	3854.8(7)	11927(5)	2278.5(6)	2627.0(7)
Z	4	2	8	2	2
μ (mm^{-1})	0.629	0.499	0.627	1.036	0.908
F(000)	2624	1540	4912	1056	1192
Crystal Size (mm^3)	0.46×0.30×0.15	0.44×0.18×0.04	0.21×0.08×0.04	0.12×0.06×0.05	0.16×0.12×0.08
θ Range for Collection [deg]	1.82–28.65	1.74–26.60	1.19–25.49	1.76–25.43	1.32–25.46
No. of Reflns Collected	83485	35237	63899	18767	27677
No. of Indep Reflns	16335	15693	10990	8229	9662
Completeness to θ Max (%)	99.1	97.1	98.9	97.9	99.1
Absorption Correction	Numerical	Numerical	Numerical	Numerical	Numerical
Max and Min Transmission	0.9116, 0.7607	0.9803, 0.8103	0.9754, 0.8797	0.9500, 0.8857	0.9309, 0.8683

GOF on F^2	1.075	1.039	1.028	0.974	1.020
Final R_1 [$I > 2\sigma(I)$] (%)	4.92	8.08	7.09	6.37	5.07

3.3 – Synthesis of [(TXPH)Rh(μ-CO)$_2$Fe(CO)Cp] and Reactivity with CNC$_6$H$_4$Cl-*p*

As an alternative means to probe the effects of boron−nitrogen coordination in TXPB complexes **8**−**10**, a borane-free analogue of **8** was targeted. Reaction of [RhCl(CO)(TXPH)] (TXPH = 2,7-di-*tert*-butyl-4-diphenylphosphino-9,9-dimethylthioxanthene)[123] with K[CpFe(CO)$_2$] provided the borane-free analogue of **7**, orange-brown [(TXPH)Rh(μ-CO)$_2$Fe(CO)Cp] (**11**) (Scheme 3.2); the ^{1}H NMR spectrum of **11** is displayed below in Figure 3.10; numbered protons refer to the positions of the thioxanthene backbone in the TXPB ligand, as shown in Scheme 3.2. Subsequent reaction of **11** with one equivalent of CNC$_6$H$_4$Cl-*p* afforded [(TXPH)Rh(CO)(μ-CNC$_6$H$_4$Cl-*p*)$_2$Fe(CO)Cp] (**12**) and remaining **11**, and addition of a second equivalent of CNC$_6$H$_4$Cl-*p* pushed the reaction to completion. Unlike TXPB complex **8**, TXPH complex **12** contains two bridging isonitrile ligands. Furthermore, while **8** features an η^2-interaction between rhodium and one of the phenyl rings on boron, a terminal CO ligand resides on the rhodium centre in **12**. The divergent reactivity of **7** and **11** with CNC$_6$H$_4$Cl-*p* can be ascribed either to the increased steric bulk of TXPB relative to TXPH or to differences between the electronic structures of **8** and the undetected TXPH analogue of **8** as a result of boron−nitrogen coordination in the former (leading to a μ-borataaminocarbyne complex). The ^{1}H NMR spectrum of **12**, in addition to an expanded view of the aromatic region are displayed below in Figures 3.11 and 3.12.

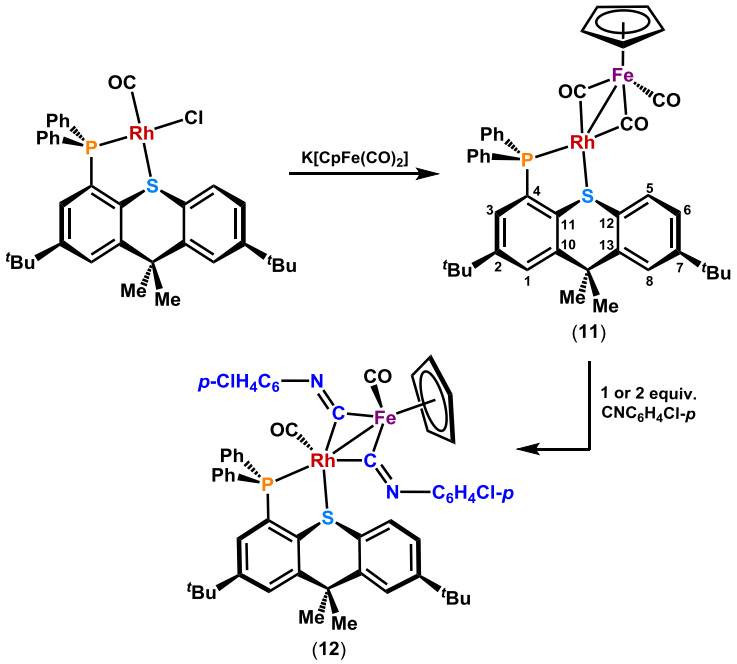

Scheme 3.2. Synthesis of TXPH complexes [(TXPH)Rh(μ-CO)$_2$Fe(CO)Cp] (**11**) and [(TXPH)Rh(CO)(μ-CNC$_6$H$_4$Cl-*p*)$_2$Fe(CO)Cp] (**12**).

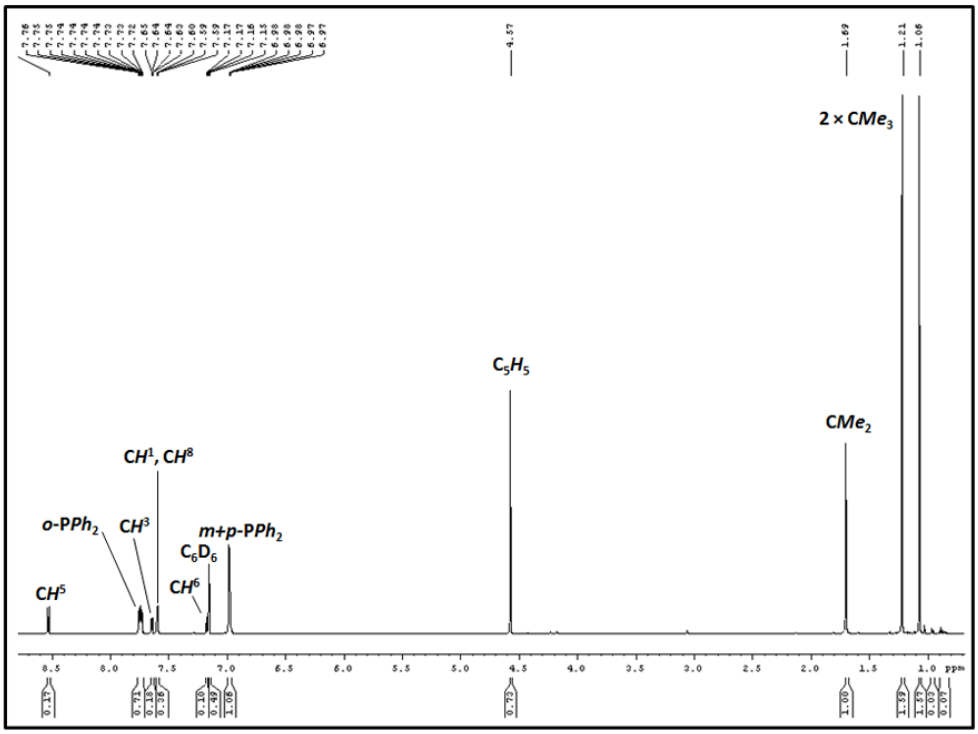

Figure 3.10. ^{1}H NMR spectrum of [(TXPH)Rh(μ-CO)$_2$Fe(CO)Cp] (**11**; 600 MHz, 298 K, C$_6$D$_6$).

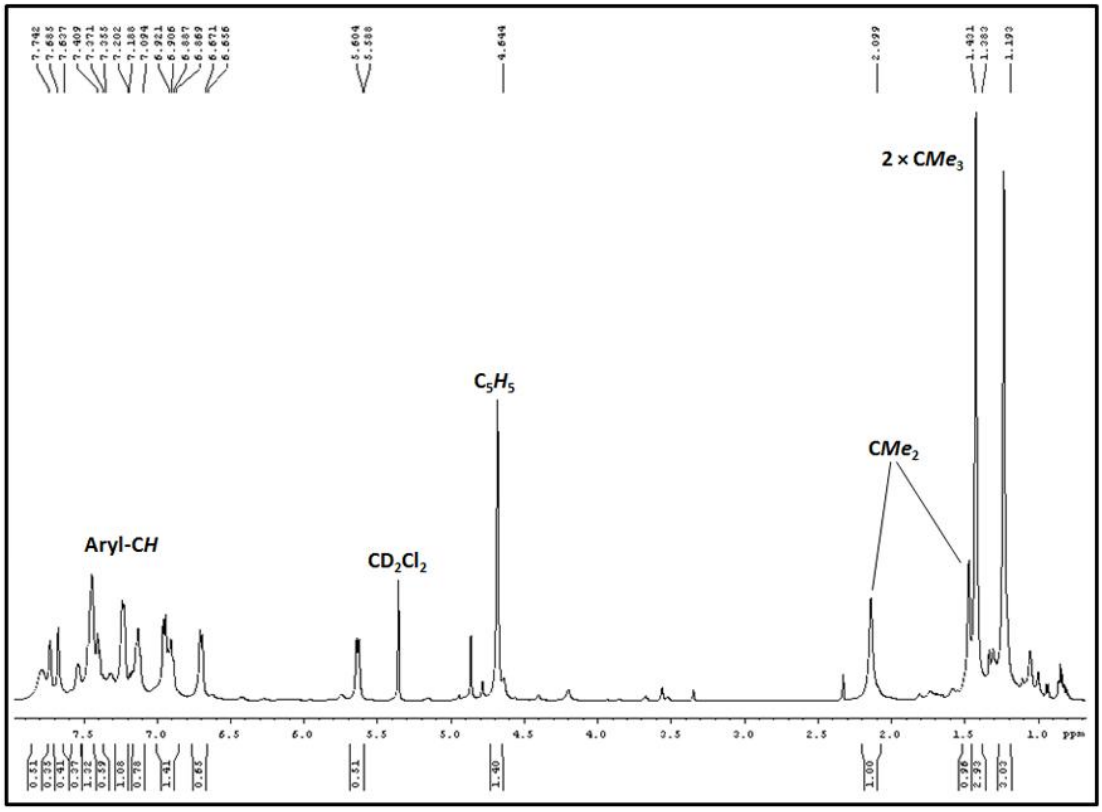

Figure 3.11. ^{1}H NMR spectrum of [(TXPH)Rh(CO)(μ-CNC$_6$H$_4$Cl-*p*)$_2$Fe(CO)Cp] (**12**; 500 MHz, 194 K, CD_2Cl_2).

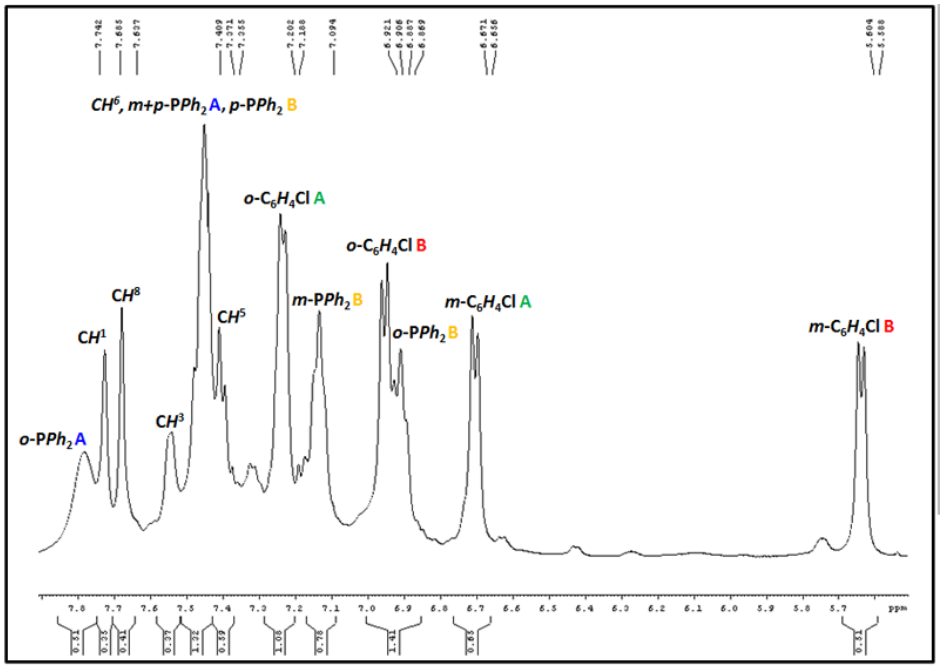

Figure 3.12. Expanded aromatic region of the ^{1}H NMR spectrum of [(TXPH)Rh(CO)(μ-CNC$_6$H$_4$Cl-*p*)Fe(CO)Cp] (**12**; 500 MHz, 194 K, CD_2Cl_2).

Complexes **11** and **12** gave rise to doublets at 45 and 44 ppm in their ^{31}P{^{1}H} NMR spectra ($^{1}J_{31P,103Rh}$ = 183 and 178 Hz, respectively). In the ^{13}C{^{1}H} NMR spectrum of **11**, the CO ligand on iron and the bridging CO ligands appear as a broad singlet at 245.7 ppm, indicative of rapid exchange.[§] For compound **12**, the CO ligand on iron appears at 215 ppm, a peak at 202 ppm is tentatively assigned to the terminal CO ligand on rhodium, and the inequivalent bridging isonitrile ligands are assigned to signals at 248 and 242 ppm. For these quaternary signals, coupling was not observed due to low solubility (which resulted in low signal to noise even after 10000 scans in a ^{13}C_uDEFT NMR experiment) and perhaps some residual fluxionality at −80 °C. However, the CNR signals for **6** are clearly at much lower frequency than the CNR signals for **8**−**10** and fall within the range observed for related μ-isonitrile complexes (*vide supra*). Furthermore,

[§] In order for the bridging CO ligands to appear equivalent in the room-temperature ^{13}C NMR spectrum of **11**, a low-energy pathway must exist for their exchange, perhaps via an intermediate with a tetrahedral arrangement of the phosphine, thioether, and carbonyl ligands or a pathway involving thioether dissociation.

the C−N stretching frequency for **12** is 1661 cm^{-1} (broad), which is 124 cm^{-1} higher than the C−N stretching frequency for **8**, highlighting the extent to which the C−N bond order is reduced in TXPB complex **8** relative to borane-free **12**.

X-ray quality crystals of [(TXPH)Rh(μ-CO)$_2$Fe(CO)Cp]·2(1,2-$C_2H_4Cl_2$) [**11**·2(1,2-$C_2H_4Cl_2$)] were grown from 1,2-dichloroethane/hexanes at −30 °C. The structure of **11** is compositionally analogous to that of **7**, except that **7** features an η^3*BCC*-interaction between rhodium and the pendant borane, and this interaction is absent in borane-free **11** (Figure 3.13). The effects of the borane unit in **7** are reflected in very different geometries at rhodium. The phosphine, thioether, and carbonyl ligands in **11** form a square plane. In contrast, in compound **7**, rhodium, one bridging carbonyl ligand [C(61)], the phosphine, and the centroid of the η^3*BCC*-coordinated arylborane ($Cent^{BCC}$) occupy a plane [P(1)−Rh(1)−C(61) = 111.4°; C(61)−Rh(1)−$Cent^{BCC}$ = 120.4°; P(1)−Rh(1)−$Cent^{BCC}$ = 126.5°], with the thioether and the other bridging carbonyl ligand [C(71)] in axial positions relative to this plane [S(1)−Rh(1)−C(71) = 169.7°]. The Rh−Fe and Rh−P distances in TXPH complex **11** are also significantly shorter than those in **7**, likely as a consequence of greater steric hindrance and the geometric constraints of the TXPB ligand in compound **7**.

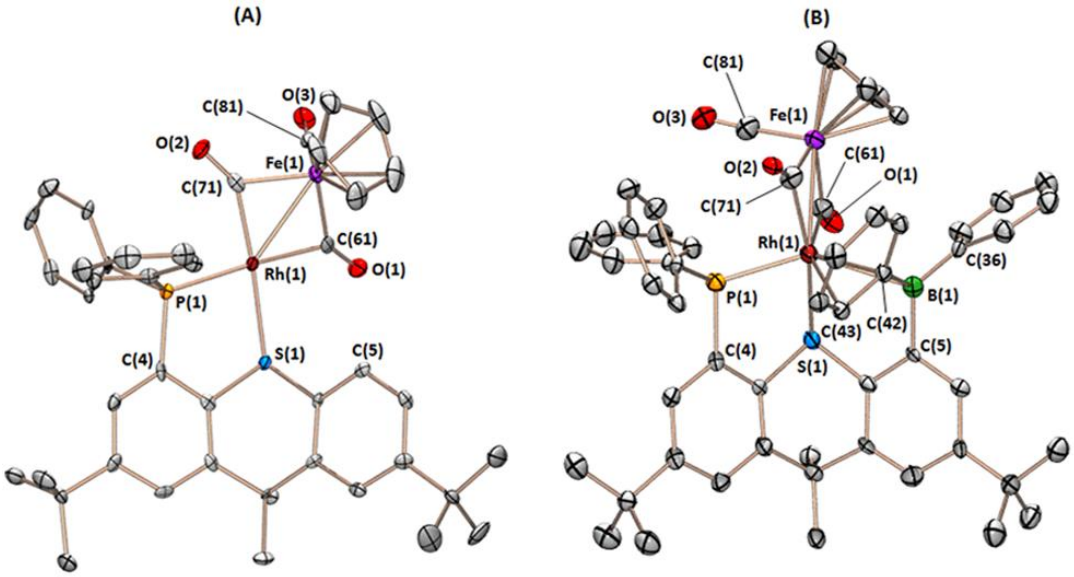

Figure 3.13. A. X-ray crystal structure for [(TXPH)Rh(μ-CO)$_2$Fe(CO)Cp]·2(1,2-$C_2H_4Cl_2$) [**11**·2(1,2-$C_2H_4Cl_2$)], and **B.** previously reported X-ray crystal structure for [(TXPB)Rh(μ-CO)$_2$Fe(CO)Cp]·solvent (**7**·solvent; the disordered solvent contains ~6.5 carbon atoms).[1] Hydrogen atoms and solvent are omitted for clarity, and ellipsoids for **11**·2(1,2-$C_2H_4Cl_2$) and **7**·solvent are set to 50 % and 30 %, respectively.

X-ray quality crystals of the bis-isonitrile complex, **12**·CH_2Cl_2, were grown from dichloromethane/hexanes at −30 °C, and the structure features a κ^2-coordinated TXPH ligand on rhodium, a cyclopentadienyl ring on iron, a Rh−Fe distance of 2.631(1) Å, two bridging isonitrile ligands, and two terminal carbonyl ligands: one on iron and one on rhodium (Figure 3.14). Excluding the Rh−Fe bond, the geometry at rhodium is distorted square pyramidal with the phosphine in the axial position; the S(1)−Rh(1)−C(71) angle is 171.7(1)°, while the C(61)−Rh(1)−C(82) angle is 154.5(2)°. In comparison with TXPB complex **8**, the most distinct metrical features of **12** are: (a) Elongated Fe−CNR bonds [1.908(5) and 1.943(5) Å in **12** versus 1.833(3) Å in **8**], (b) elongated Rh−CNR bonds [2.021(5) and 2.051(5) Å in **12** versus 1.968(3) Å in **8**], (c) shorter C−N distances [1.239(6) and 1.246(7) Å in **12** versus 1.284(3) Å in **8**], and (d) significantly more obtuse C−N−C angles [126.8(4) and 132.7(4)° in **12** versus 117.5(2)° in **8**]. All features of **12** are unremarkable for a μ-isonitrile complex, and the structural and spectroscopic differences

between **8** and **12** support the arguments for classification of the CNR(BR'$_3$) unit in **8**–**10** as a μ-borataaminocarbyne ligand, rather than a μ-borataazavinylidene ligand (a simple adduct between a borane and a μ-isonitrile ligand; see Figure 3.4).

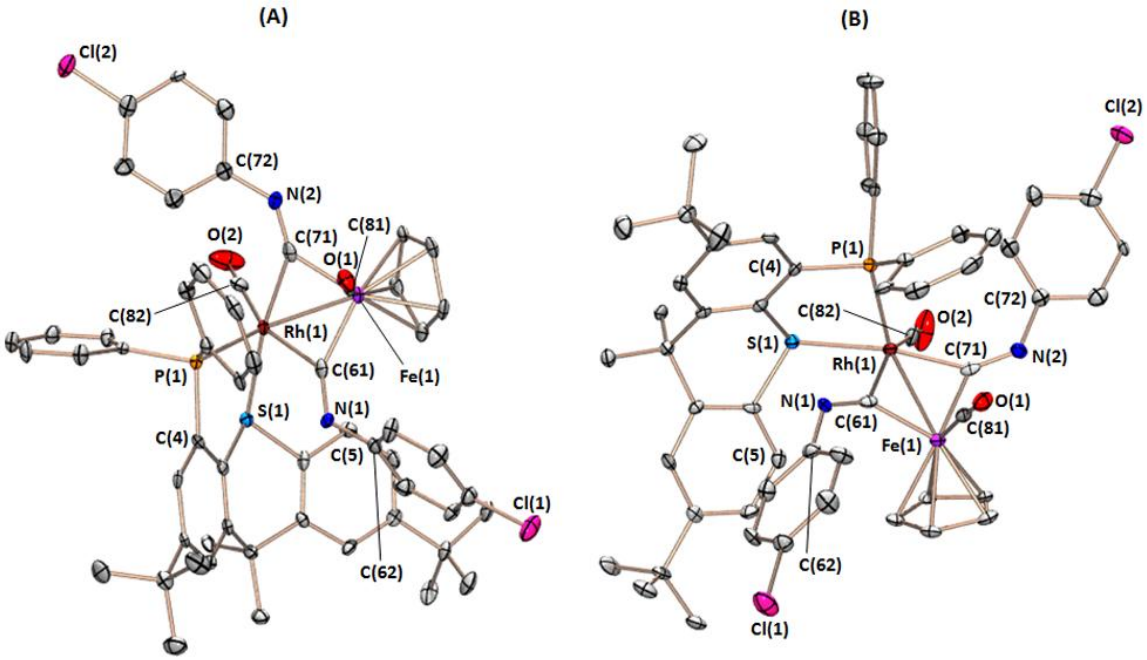

Figure 3.14. Two different views of the X-ray crystal structure for [(TXPH)Rh(CO)(μ-CNC_6H_4Cl-*p*)$_2$Fe(CO)Cp]·CH_2Cl_2 (**12**·CH_2Cl_2); hydrogen atoms and solvent are omitted for clarity, and ellipsoids are set to 50 %.

Table 3.2. Selected bond lengths (Å) and angles (°) for TXPB and TXPH complexes **8**–**12**.

Complex number	**8**	**9**	**10**	**11**	**12**
Multidentate Ligand	TXPB	TXPB	TXPB	TXPH	TXPH
Bridging Ligands	(CO)(CNC_6H_4Cl-*p*)	(CO)(CNXyl)	(CO)(CN^nBu)	$(CO)_2$	$(CNC_6H_4Cl$-*p*$)_2$
Lattice Solvent	2 hexane	5 toluene	2 hexane	2 $C_2H_4Cl_2$-1,2	CH_2Cl_2
Rh(1)–P(1)	2.333(1)	2.321(1)	2.339(1)	2.290(2)	2.330(1)
Rh(1)–S(1)	2.426(1)	2.403(2)	2.386(1)	2.355(2)	2.441(1)
Rh(1)–C(61)	1.968(3)	1.981(5)	1.975(5)	2.055(8)	2.051(5)
Rh(1)–C(71)	1.912(3)	1.906(7)	1.908(6)	1.947(7)	2.021(5)

Rh(1)–C(82)	n/a	n/a	n/a	n/a	1.926(6)
Rh(1)–Fe(1)	2.606(1)	2.597(1)	2.601(1)	2.594(1)	2.631(1)
Fe(1)–C(61)	1.833(3)	1.864(6)	1.851(5)	1.909(8)	1.908(5)
Fe(1)–C(71)	2.116(3)	2.088(5)	2.090(7)	1.981(7)	1.943(5)
Fe(1)–C(81)	1.760(4)	1.756(6)	1.748(6)	1.768(9)	1.755(6)
C(61)–N(1)	1.284(3)	1.298(7)	1.294(6)	n/a	1.239(6)
C(71)–N(2)	n/a	n/a	n/a	n/a	1.246(7)
N(1)–B(1)	1.641(4)	1.660(8)	1.654(7)	n/a	n/a
C(61)–N(1)–B(1)	119.1(2)	119.1(4)	119.1(4)	n/a	n/a
C(61)–N(1)–C(62)	117.5(2)	114.0(5)	118.4(4)	n/a	126.8(4)
C(62)–N(1)–B(1)	123.4(2)	126.8(4)	122.4(4)	n/a	n/a
C(71)–N(2)–C(72)	n/a	n/a	n/a	n/a	132.7(4)
C(36)–B(1)–C(5)	111.9(2)	111.2(5)	111.0(8), 118.1(8)[a]	n/a	n/a
C(36)–B(1)–C(42)	108.7(2)	111.8(5)	114.7(7), 103.9(7)[a]	n/a	n/a
C(42)–B(1)–C(5)	110.5(2)	108.4(4)	109.7(4)	n/a	n/a

(a) One of the *B*-phenyl rings in **10**·2hexane [C(36)–C(41)] was disordered over two positions, therefore values have been tabulated for both orientations.

3.4 – Summary

Heterobimetallic **8**−**10**, [(TXPB)Rh(μ-CO)(μ-CNR)Fe(CO)Cp] (R = C_6H_4Cl-*p*, Xyl, ^{n}Bu), were prepared in order to probe the nature of any interaction between a CNR ligand and a pendant borane. Isolated examples of transition metal complexes in which a group 13 Lewis acid is bound to the oxygen atom of carbon monoxide or the β-position of an isoelectronic neutral ligand are rare,[4,211,228] despite the potential for interactions of this type to greatly increase the thermodynamic favorability of 1,1-insertion reactions.[64,229] On the basis of their ^{13}C NMR data, C−N stretching frequencies, C−N and M−C bond distances, C−N−C angles, and comparison with a borane-free rhodium−iron isonitrile complex, [(TXPH)Rh(CO)(μ-CNC_6H_4Cl-*p*)$_2$Fe(CO)Cp] (**12**), complexes **8**−**10** are assigned as borataaminocarbyne {C−NR(BR'$_3$)} complexes with a double bond between

iron and the carbyne carbon atom, rather than borataazavinylidene {C=NR(BR'_3)} complexes. To the best of our knowledge, [{Ir(CNXyl)}$_2${μ-C−NXyl(BH_3)}$_2$(μ-dmpm)$_2$] is the only other example of a borataaminocarbyne complex.

Ph.D. Thesis
Bradley E. Cowie
Department of Chemistry and Chemical Biology
McMaster University

Chapter 4

Bis-hydrocarbyl Platinum(II) Ambiphilic Ligand Complexes: Alkyl−Aryl Exchange between Platinum and Boron

Adapted with permission from: Cowie, B. E.; Emslie, D. J. H. *Organometallics* **2015**, *34*, 2737-2746.

4.1 – Introduction

Studies of the behaviour of borane-containing ambiphilic ligands in combination with alkyl or aryl co-ligands[27,28,32,53-58] have received little attention (*vide infra*), despite the integral role of alkyl- and aryl-ligands in a large percentage of late transition metal catalysis. In 2004, Tilley and Turculet described the reaction of [{PhB($CH_2P^iPr_2$)$_3$}Li(THF)] with 0.5 equivalents of [{Rh(μ-Cl)(C_2H_4)$_2$}$_2$] to form [Rh(η^2-CH_2PPh_2){κ^2-PhB($CH_2P^iPr_2$)$_2$}] (**A** in Figure 4.1). Addition of 2 equivalents of PMe_3 to this compound resulted in an equilibrium between the starting material and zwitterionic [Rh(PMe_3)$_2${κ^2-PhB($CH_2P^iPr_2$)$_3$}] (**B** in Figure 4.1), providing an example of reversible alkyl transfer between rhodium and a pendant borane. Reaction of this equilibrium mixture with H_2 yielded zwitterionic *cis*-[RhH_2(PMe_3){κ^3-PhB($CH_2P^iPr_2$)$_3$}] (**C** in Figure 4.1), whereas reaction with H_2SiPh_2 generated neutral [RhH_2($SiHPh_2$)(PMe_3){κ^2-PhB($CH_2P^iPr_2$)$_2$}].[53]

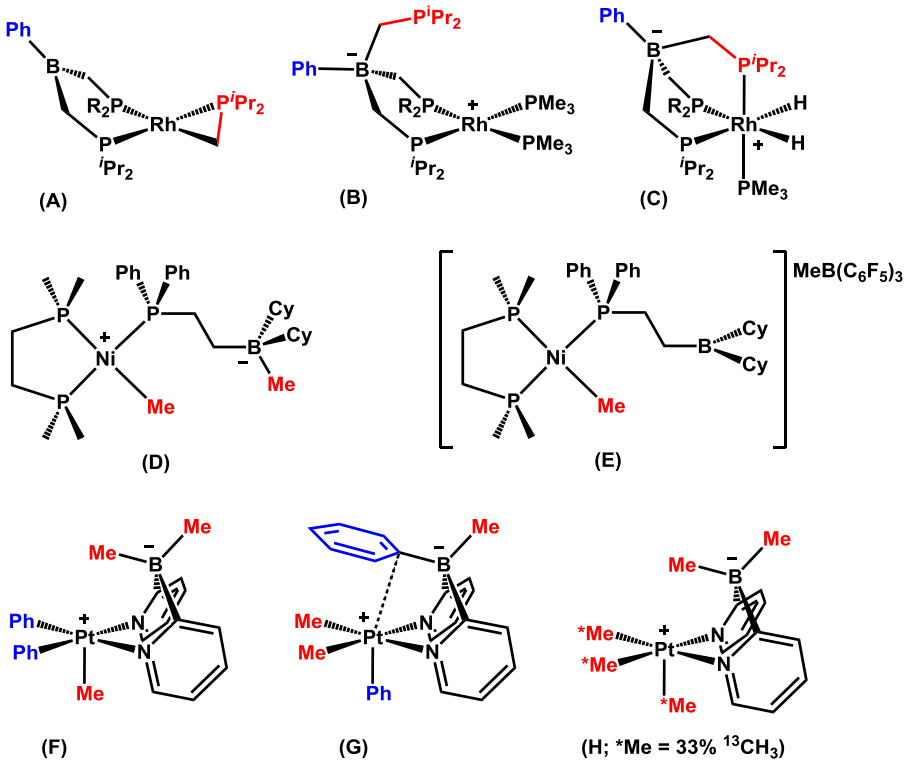

Figure 4.1. Late transition metal hydrocarbyl complexes bearing borane-containing ambiphilic ligands or anionic tetra(hydrocarbyl)borate ligands.

In 2008, Tilley and Waterman reported the reaction of $Ph_2P(CH_2)_2BR'_2$ (BR'_2 = BCy_2 or 9-BBN) with [$NiMe_2(\kappa^2$-dmpe)] to afford [$NiMe\{Ph_2P(CH_2)_2BR'_2Me\}(\kappa^2$-dmpe)] (**D** in Figure 4.1), the product of alkyl ligand abstraction by the borane. Zwitterionic [$NiMe\{Ph_2P(CH_2)_2BR'_2Me\}(\kappa^2$-dmpe)] did not react with a second equivalent of the ambiphilic ligand, and treatment with $B(C_6F_5)_3$ generated [$NiMe\{Ph_2P(CH_2)_2BR'_2\}(\kappa^2$-dmpe)][$MeB(C_6F_5)_3$], with the remaining methyl group residing on the cationic platinum centre (**E** in Figure 4.1).[54] Erker also outlined the reactions of $Mes_2P(CH_2)_2B(C_6F_5)_2$ with [Cp_2ZrMe_2] and [$Cp^*_2ZrMe_2$], yielding zwitterionic [$Cp_2ZrMe\{\kappa^1P$-$Mes_2P(CH_2)_2B(C_6F_5)_2Me)$] in the former case and [Cp^*_2ZrMe][$MeB(C_6F_5)_2(CH_2)_2PMes_2$] (a contact ion pair in which the methyl group of the borate anion interacts with zirconium) in the latter.[56]

In 2008, Vedernikov reported that [$PtMePh_2\{\kappa^2$-$Me_2B(py)_2\}$] (**F** in Figure 4.1) is stable in benzene but isomerizes slowly in THF or DMSO to form [$PtMe_2Ph\{\kappa^2$-$MePhB(py)_2\}$] (**G** in Figure 4.1), in which the *B*-phenyl ring occupies the endo position with the *ipso*-carbon atom η^1-bound to platinum. Similarly, [$Pt(^{13}CH_3)Me_2\{\kappa^2$-$Me_2B(py)_2\}$] (**H** in Figure 4.1) reacted slowly in DMSO to produce isomers in which the $^{13}CH_3$ group occupies either the endo or the exo position of the borate.[55] These reactivities achieve: (a) Alkyl/aryl exchange between boron and platinum(IV), with the aryl group migrating from platinum to boron, and (b) bidirectional alkyl exchange between boron and platinum(IV). Aryl group migration from boron to platinum was also observed in the reaction of $Na[PtMe_2\{\kappa^2$-$Ph_2B(py)_2\}]$ with $^{i}PrOH$ (2 equivalents) and O_2 (0.5 equivalents) to form [$PtMe_2Ph\{\kappa^3$-$PhB(py)_2(O^{i}Pr)\}$], $NaO^{i}Pr$, and H_2O. Analogous alkyl group migration was observed in the reactions of $Na[PtR_2\{\kappa^2$-$Me_2B(py)_2\}]$ (R = Me or Ph) with EtOH and O_2, and [$PtR_2Me\{\kappa^2$-$Me_2B(py)_2\}$] (R = Me or Ph) was shown to react with MeOH to form [$PtRMe_2\{\kappa^3$-$MeB(py)_2(OMe)\}$] and HR.[55,57]

Described herein is the synthesis and reactivity of bis-hydrocarbyl platinum(II) complexes bearing phosphine-thioether-borane ambiphilic ligands. These ligands are derived from 2,7-di-*tert*-butyl-5-diphenylboryl-4-diphenylphosphino-9,9-dimethylthioxanthene (TXPB)[59] through alkyl-aryl exchange between platinum and the borane in TXPB.

4.2 – Synthesis and Dynamic Behaviour of [PtMePh(TXPB')]

The reaction of TXPB with [$PtMe_2$(cod)] (cod = 1,5-cyclooctadiene) was initially surveyed by Natalie Huk, a former M.Sc. student in the Emslie group, and yielded [PtMePh(TXPB′)] (**13**; TXPB′ = 2,7-di-*tert*-butyl-5-methylphenylboryl-4-diphenylphosphino-9,9-dimethylthioxanthene), in which a methyl group on platinum has been exchanged for a phenyl group on boron (Scheme 4.1). The ^{1}H NMR spectrum of **13** is displayed below in Figure 4.2; numbered protons refer to the positions of the thioxanthene backbone in the TXPB ligand, as shown in Scheme 4.1. The reaction

proceeds over the course of 16 hours at room temperature, with no intermediates detectable by NMR spectroscopy. Single crystals of **13**·1.5(C_6H_{14}) were grown from hexanes at −30 °C (Figure 4.3), highlighting a square planar geometry at platinum with the phenyl group *trans* to the phosphorus and the methyl group *trans* to sulfur. The Pt−P, Pt−S, Pt−C, and B−C distances fall within the typical ranges,[166,230,231] and the trigonal plane of the borane is oriented approximately parallel to the square plane at platinum, with the *B*-phenyl group directed back toward platinum.

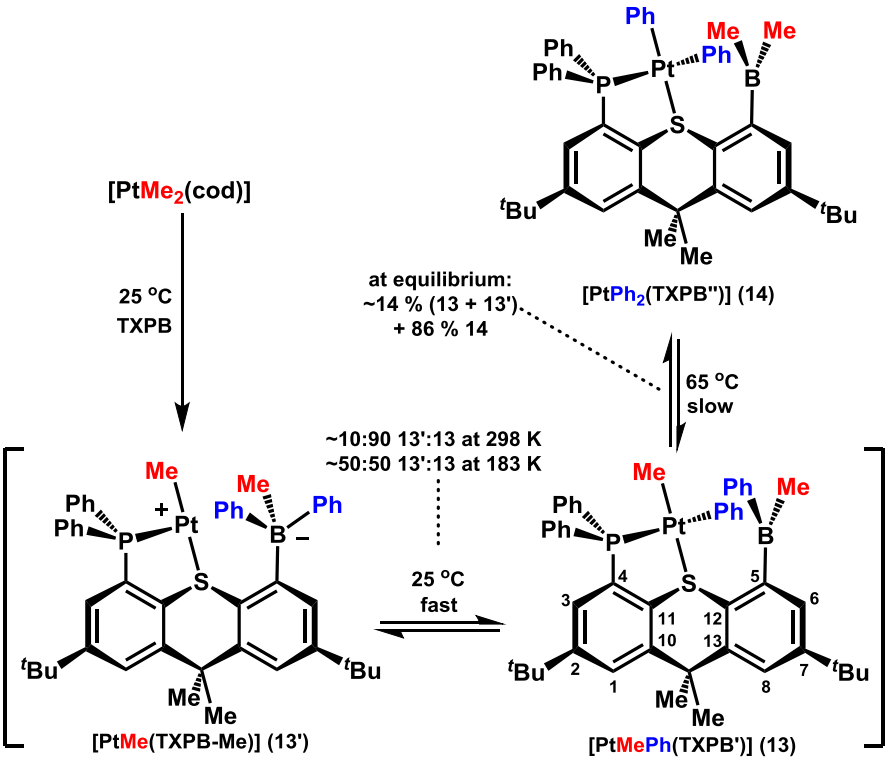

Scheme 4.1. Reaction scheme for the synthesis of [PtMePh(TXPB')] (**13**), [PtMe(TXPB-Me)] (**13'**) and [$PtPh_2$(TXPB'')] (**14**).

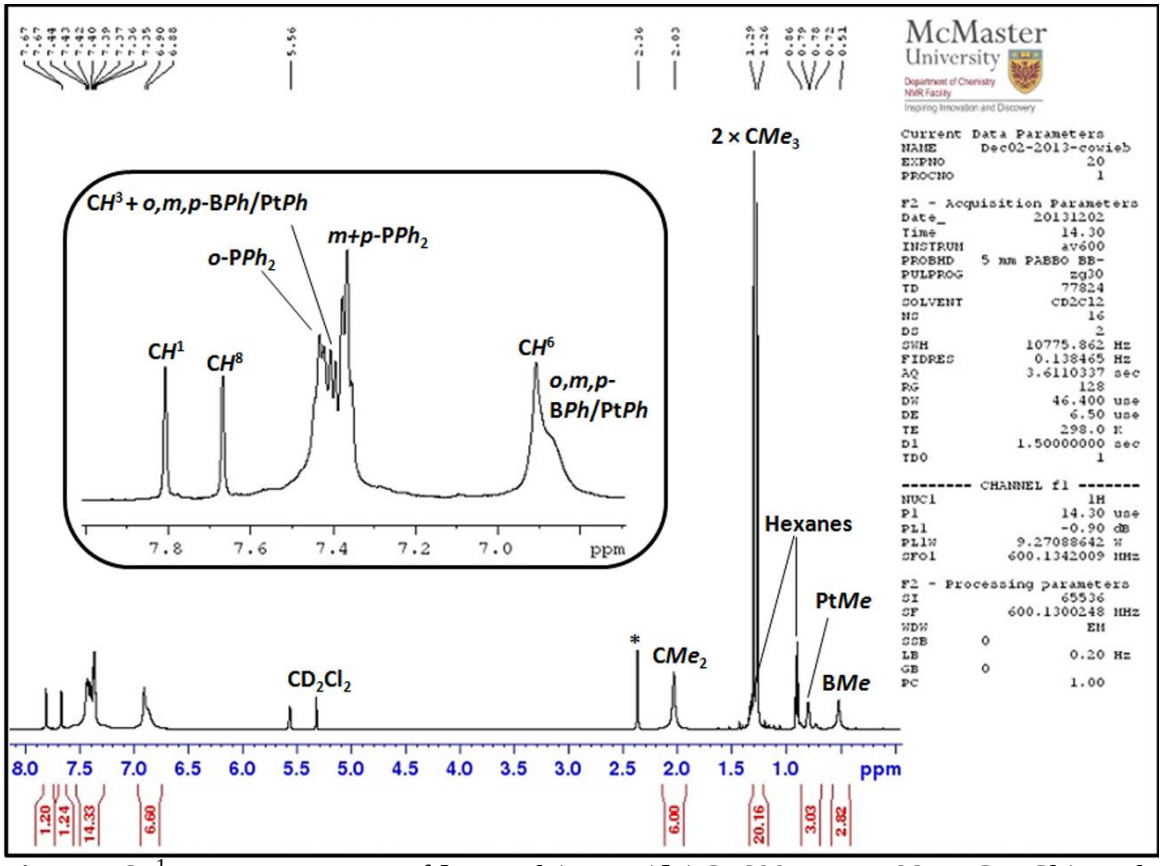

Figure 4.2. ^{1}H NMR spectrum of [PtMePh(TXPB')] (**13**; 600 MHz, 298 K, CD_2Cl_2), with a labelled, expanded view of the aromatic region. * Represents an unknown impurity.

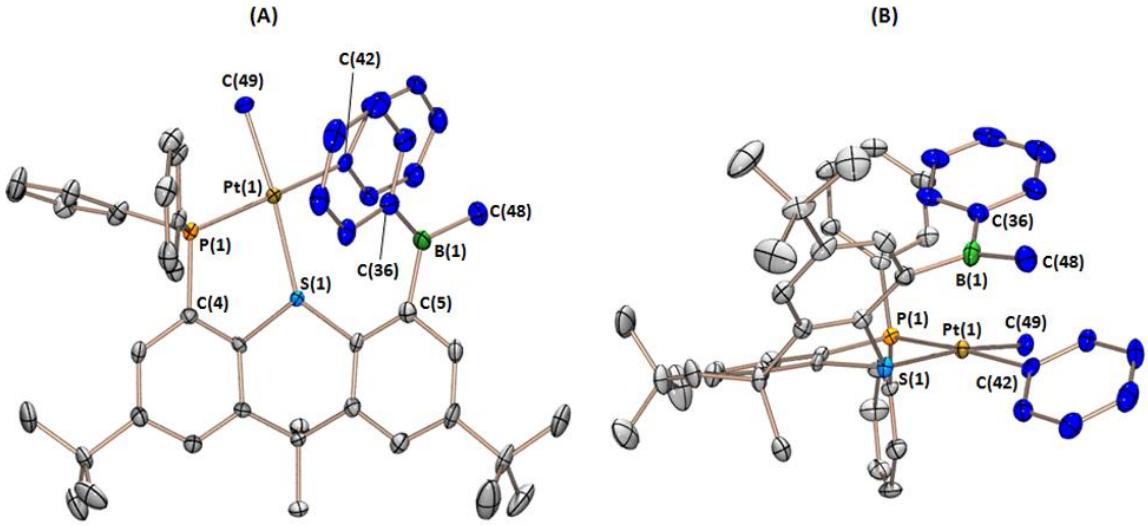

Figure 4.3. Two different views of the X-ray crystal structure for [PtMePh(TXPB')]·1.5(C_6H_{14}) [**13**·1.5(C_6H_{14})]; hydrogen atoms and solvent are omitted for clarity, ellipsoids are set to 50 % and the platinum- and boron-bound methyl and phenyl groups are coloured in blue.

Solid samples of **13** are pure by powder X-ray diffraction (PXRD; Figure 4.4) and elemental analysis. Additionally, room temperature ^{1}H, ^{13}C{^{1}H}, and ^{31}P{^{1}H} NMR spectra of **13** in CD_2Cl_2 show single TXPB ligand and platinum environments, and two distinct methyl groups were observed in the ^{1}H NMR spectrum at 0.79 and 0.51 ppm; the former is sharp with platinum satellites ($^{2}J_{1H,195Pt}$ = 85 Hz), while the latter is a broad singlet, consistent with attachment to quadrupolar boron. However, the ^{31}P NMR signal (Figure 4.5) and the ^{13}C and ^{1}H NMR signals representing the *Pt*-phenyl and *B*-phenyl groups are broadened at room temperature, suggesting an equilibrium between multiple species in solution.

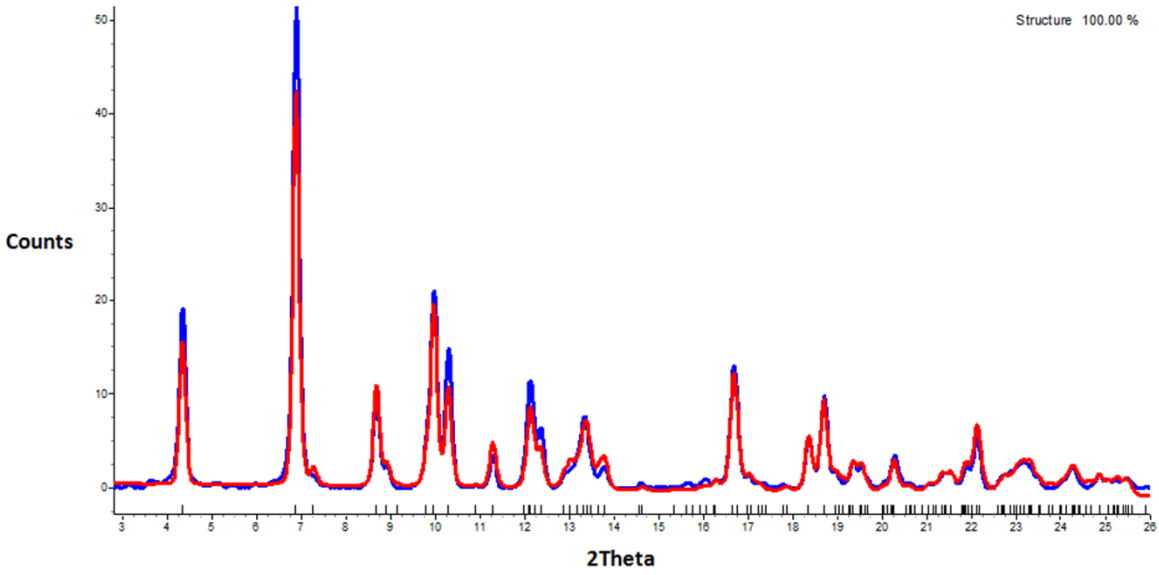

Figure 4.4. PXRD pattern of [PtMePh(TXPB')] (**13**) (blue) matched with the PXRD pattern generated from the single crystal data. The red line represents the calculated spectrum from the cif data. PXRD data was collected by Jeffrey S. Price, and Topas 4.2 was utilized to relate unit cell measurements obtained at room temperature to those obtained at 100 K.

Below −90 °C, two major isomers with vastly different $^{1}J_{195Pt,31P}$ coupling constants of 1963 and 5042 Hz were observed in an approximate 1:1 ratio, with ^{31}P chemical shifts of 38.7 and 36.4 ppm and ^{195}Pt chemical shifts of −4322 and −4700 ppm, respectively (Figure 4.5). The smaller $^{1}J_{195Pt,31P}$ coupling constant is consistent with neutral [PtMePh(TXPB′)] (**13**; Scheme 4.1), where the phosphine is *trans* to a strongly donating hydrocarbyl ligand[232] (a similar ^{195}Pt NMR chemical shift and $^{1}J_{195Pt,31P}$ coupling was observed for neutral [PtPh$_2$(TXPB″)] (**14**); *vide infra*). By contrast, the uncommonly large $^{1}J_{195Pt,31P}$ coupling constant is indicative of a phosphine *trans* to a very low *trans*-influence ligand or a vacant coordination site, accordant with zwitterionic [PtMe(TXPB-Me)] (**13'**; Scheme 4.1). For comparison, zwitterionic [Pt{CH$_2$CH$_2$B(C$_6$F$_5$)$_3$}(κ^2-dcpp)] {dcpp = 1,3-bis-(dicyclohexylphosphino)propane}, which features a β-agostic C−H−Pt interaction, has $^{1}J_{195Pt,31P}$ couplings of 4755 and 2738 Hz, with the larger coupling constant assigned to the phosphine *trans* to the agostic

interaction.[233] The $^{1}J_{195Pt,31P}$ coupling constant for **13'** is not consistent with a platinum(IV) tris-hydrocarbyl boryl complex (the product of B−C bond-breaking oxidative addition; **B** in Scheme 4.2; *vide infra*), since platinum(IV) complexes exhibit smaller $^{1}J_{195Pt,31P}$ coupling constants than closely related platinum(II) complexes.[234]

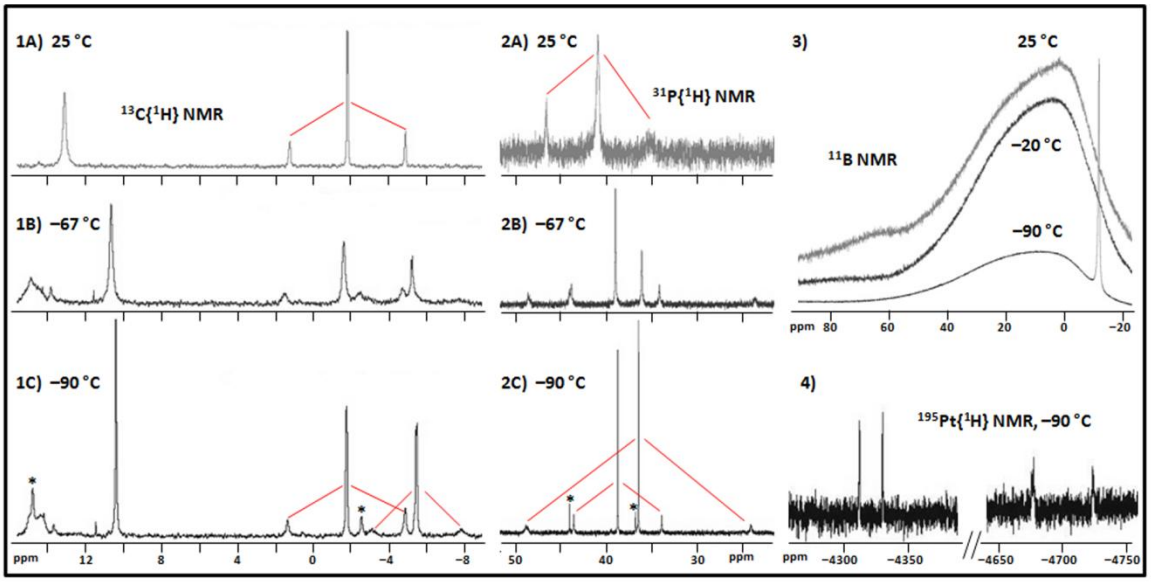

Figure 4.5. Variable temperature $^{13}C\{^{1}H\}$ NMR spectra of **13-^{13}C** (1A–1C), $^{31}P\{^{1}H\}$ NMR spectra of **13** (2A–2C), ^{11}B NMR spectra of **13** (3) and $^{195}Pt\{^{1}H\}$ NMR spectra of **13** (4) in CD_2Cl_2. Signals labeled with * represent an unidentified species.

At 25 °C, the $^{13}C\{^{1}H\}$ NMR spectrum of **13-^{13}C** (**13** in which the methyl ligands are ^{13}C-labeled) revealed only two methyl environments, representing B*Me* (13.1 ppm) and Pt*Me* (−1.9 ppm, $^{1}J_{13C,195Pt}$ = 767 Hz) groups. By contrast, at −90 °C, four methyl environments were observed in the $^{13}C\{^{1}H\}$ NMR spectrum of **13-^{13}C**, only two of which exhibit platinum satellites, consistent with isomers **13** and **13'** (Figure 4.5). The B*Me* signal for **13-^{13}C** is a broad singlet at 14.2 ppm ($\omega_{1/2}$ ~ 65 Hz), whereas the B*Me* signal for **13'-^{13}C** is a sharp singlet at 10.4 ppm, consistent with suppression of the quadrupolar broadening brought about by boron upon pyramidalization. In addition, while the Pt*Me* signal for **13-^{13}C** is observed at −5.5 ppm with a $^{1}J_{13C,195Pt}$ coupling of 586 Hz, the Pt*Me*

signal for **13'-^{13}C** is located at −1.8 ppm with a $^{1}J_{13C,195Pt}$ coupling of 779 Hz, consistent with a stronger Pt−Me bond to the cationic platinum centre in **13'**.

The ^{11}B NMR spectrum of **13** at −90 °C features a sharp singlet at −12 ppm, consistent with four-coordinate boron (isomer **13'**), rather than a three-coordinate borane or boryl ligand[235] (Figure 4.5; presumably the low-temperature ^{11}B NMR signal for neutral **13** is too broad to be observed). By contrast, only a broad singlet at 63 ppm ($\omega_{1/2}$ ~ 3000 Hz) was observed in the ^{11}B NMR spectrum of **13** at 25 °C, suggesting that neutral **13** is the dominant isomer at room temperature. The magnitude of the $^{1}J_{31P,195Pt}$ coupling constant for the equilibrium mixture of **13** and **13'** at 25 °C, relative to the $^{1}J_{31P,195Pt}$ coupling constants for isomers **13** and **13'** at −90 °C (*vide supra*), also suggests that **13** is the dominant isomer at room temperature, with an approximate 9:1 ratio of **13** to **13'**.

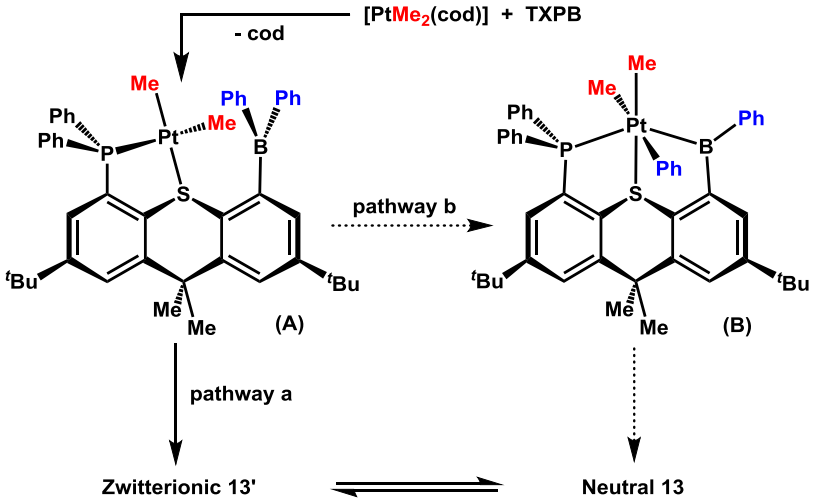

Scheme 4.2. Two possible reaction pathways to compound **13** proceeding (a) directly via intermediate **A**, or (b) via intermediates **A** and **B**.

Taken together, the ^{195}Pt{^{1}H}, ^{31}P{^{1}H}, ^{13}C{^{1}H}, and ^{11}B NMR data identify the two solution isomers as neutral **13** and zwitterionic **13'**. While isomer **13** was crystallographically characterized (*vide infra*), the structure and geometry of **13'** are unknown. However, it may bear resemblance to that of the [Rh(CO)(TXPB-F)] zwitterion (TXPB-F = {5-(2,7-di-*tert*-butyl-4-diphenylphosphino-9,9-dimethyl-

thioxanthenyl)}diphenylfluoroborate; Chapter 2), in which a *B*-phenyl ring is η^2*CC*-coordinated (via the *ipso*- and one *ortho*-carbon atoms) to the cationic metal centre (Chapter 2).

Table 4.1. Crystallographic Data Collection and Refinement Parameters for Complexes **13, 14, 16** and **17**.

Structure	**13 · 1.5(C_6H_{14})**	**14 · (CH_2Cl_2)(C_6H_{14})$_{0.5}$**	**16 · 1.5($C_2H_4Cl_2$)**	**17 · 2.6(CH_2Cl_2)**
Formula	$C_{56}H_{75}BPPtS$	$C_{53}H_{63}BCl_2PPtS$	$C_{70}H_{75}BCl_3O_3P_2PtS$	$C_{69.6}H_{77.2}BCl_{5.2}N_2PPtS$
Formula wt	1041.11	1039.86	1370.55	1393.80
T (K)	100(2)	100(2)	100(2)	100(2)
Cryst. Syst.	Triclinic	Triclinic	Triclinic	Triclinic
Space Group	*P*–1	*P*–1	*P*–1	*P*–1
a (Å)	9.553(3)	13.306(3)	9.5920(7)	13.498(1)
b (Å)	13.221(4)	14.095(3)	12.7606(9)	13.667(1)
c (Å)	20.742(6)	14.176(3)	26.770(2)	19.036(2)
α [deg]	101.583(5)	97.362(4)	97.074(1)	93.409(2)
β [deg]	90.792(6)	105.671(4)	93.659(1)	105.034(2)
γ [deg]	97.863(5)	107.033(3)	102.019(1)	95.788(2)
Volume [Å^3]	2540(1)	2384.7(9)	3166.8(4)	3360.6(6)
Z	2	2	2	2
μ (mm^{-1})	2.871 mm	3.166	2.472	2.382
F(000)	1074	1058	1398	1414
Crystal Size (mm^3)	0.23×0.17 ×0.05	0.42×0.05×0.05	0.29×0.27×0.14	0.49×0.07×0.03
θ Range for Collection [deg]	1.00–27.93	1.53–26.36	1.54–31.87	1.57–32.44
No. of Reflns Collected	11912	26200	52103	49314
No. of Indep Reflns	11912	9570	20793	23292
Completeness to θ Max (%)	97.4	98.0	95.6	96.1
Absorption Correction	Numerical	Numerical	Numerical	Numerical
Max and Min Transmission	0.8698, 0.5581	0.8577, 0.3498	0.7235, 0.5342	0.9320, 0.3882
GOF on F^2	1.069	1.038	1.086	0.988
Final R_1 [$I > 2\sigma(I)$] (%)	3.81	5.21	2.99	5.56

In the reaction of TXPB with [$PtMe_2$(cod)], the initial product is presumably [$PtMe_2$(TXPB)] (**A**), which isomerizes rapidly to afford compound **13**. This reaction

could proceed via (a) a zwitterionic platinum(II) intermediate (**13'**) formed by abstraction of a methyl group from platinum by the pendant borane or (b) a neutral platinum(IV) boryl intermediate (**B**) resulting from B−C bond oxidative addition (Scheme 4.2). The former pathway is likely given the presence of an equilibrium between **13** and **13'** in solution, as evidenced by low-temperature NMR spectroscopy (*vide supra*). The higher bond strength of Pt−aryl versus Pt−alkyl bonds likely provides the thermodynamic driving force for conversion of [$PtMe_2$(TXPB)] (**A**) to [PtMePh(TXPB')] (**13**). This reactivity contrasts that observed for [$PtMePh_2\{\kappa^2$-$Me_2B(py)_2\}$], in which phenyl/methyl exchange occurs to transfer a phenyl group from platinum to boron (*vide supra*); the driving force in this literature example is likely the formation of an η^1-arene interaction between platinum and the newly installed *B*-phenyl ring.

4.3 – Thermal Isomerization of [PtMePh(TXPB')] to [$PtPh_2$(TXPB'')]

Heating a solution of compound **13** in CH_2Cl_2 at 65 °C or in C_6D_6 between 65 and 125 °C provided [$PtPh_2$(TXPB")] (**14**; TXPB" = 2,7-di-*tert*-butyl-5-dimethylboryl-4-diphenylphosphino-9,9-dimethylthioxanthene) as an approximate 86:14 mixture with remaining **13** (Scheme 4.1). Compound **13** could be completely removed from **14** by recrystallization from hexanes. However, **14** always contained 15% of an unidentified neutral platinum(II) or platinum(IV) compound with a methyl group coordinated *cis* to the phosphine donor of TXPB [selected NMR spectroscopic data for the unidentified impurity in samples of **14**: ^{1}H NMR δ 0.32; $^3J_{1H,31P}$ = 6 Hz (cf. 6 Hz for **13**), $^2J_{1H,195Pt}$ = 72 Hz (cf. 85 Hz for **13**); ^{31}P NMR δ 46.9; $^1J_{31P,195Pt}$ = 1889 Hz (cf. 1963 Hz for **13**); this impurity was not identified, and we were not able to determine whether or not it is an isomer in slow equilibrium with **14**; the ^{1}H NMR spectrum of **14**, along with expanded views of the aromatic and aliphatic regions are displayed in Figures 4.6–4.8]. X-ray quality crystals of **14**·$(CH_2Cl_2)(C_6H_{14})_{0.5}$ (Figure 4.9) were obtained from CH_2Cl_2/hexanes at −30 °C; the structure of **14** is very similar to that of **13**, but with two phenyl groups on platinum and two methyl substituents on boron. The ^{11}B and ^{195}Pt NMR

chemical shifts for **14** are 80 and −4268 ppm, respectively, and the $^{1}J_{195Pt,31P}$ coupling is 1811 Hz. Unlike **13**, complex **14** does not participate in an NMR-detectable (25 to −80 °C) equilibrium with a zwitterionic isomer; this can be rationalized based on the reduced Lewis acidity of the pendant borane in **14** ($ArBMe_2$) relative to the borane in **13** (ArBMePh).

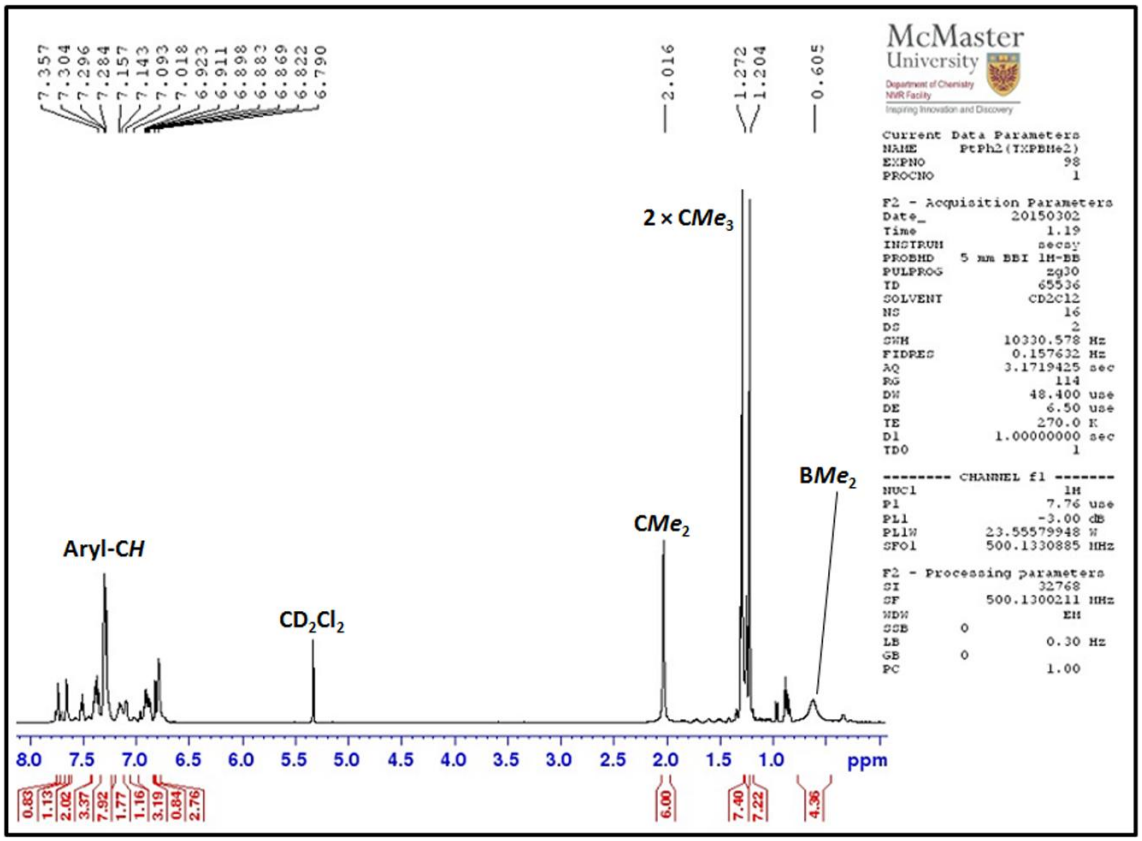

Figure 4.6. ^{1}H NMR spectrum of [$PtPh_2$(TXPB")] (**14**; 500 MHz, 265 K, CD_2Cl_2).

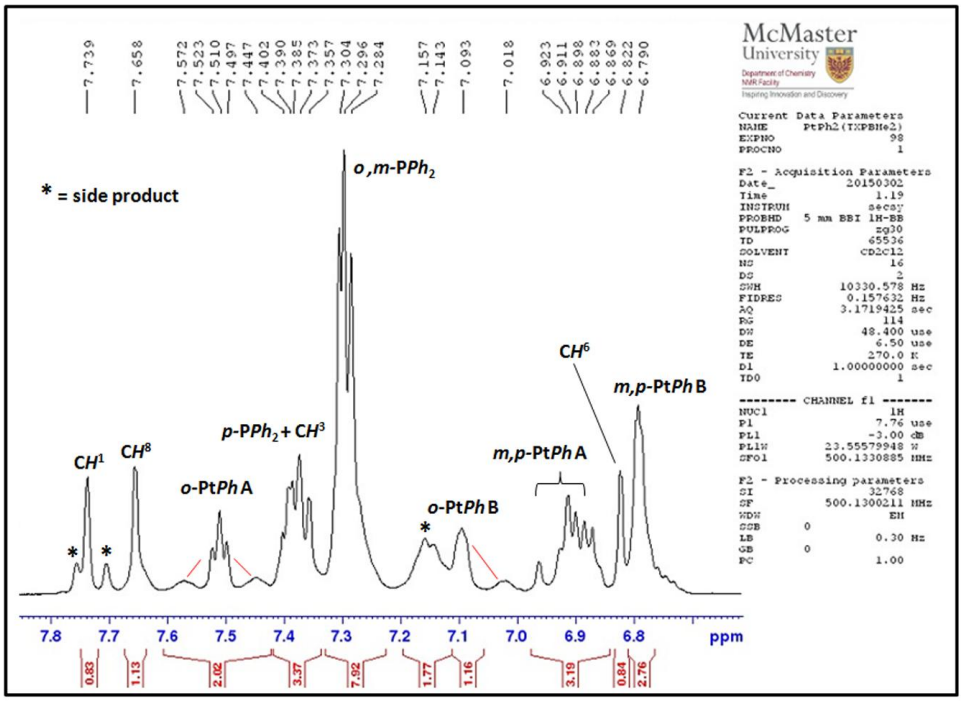

Figure 4.7. Expanded aromatic region of the ^{1}H NMR spectrum of [$PtPh_2$(TXPB")] (**14**; 500 MHz, 265 K, CD_2Cl_2).

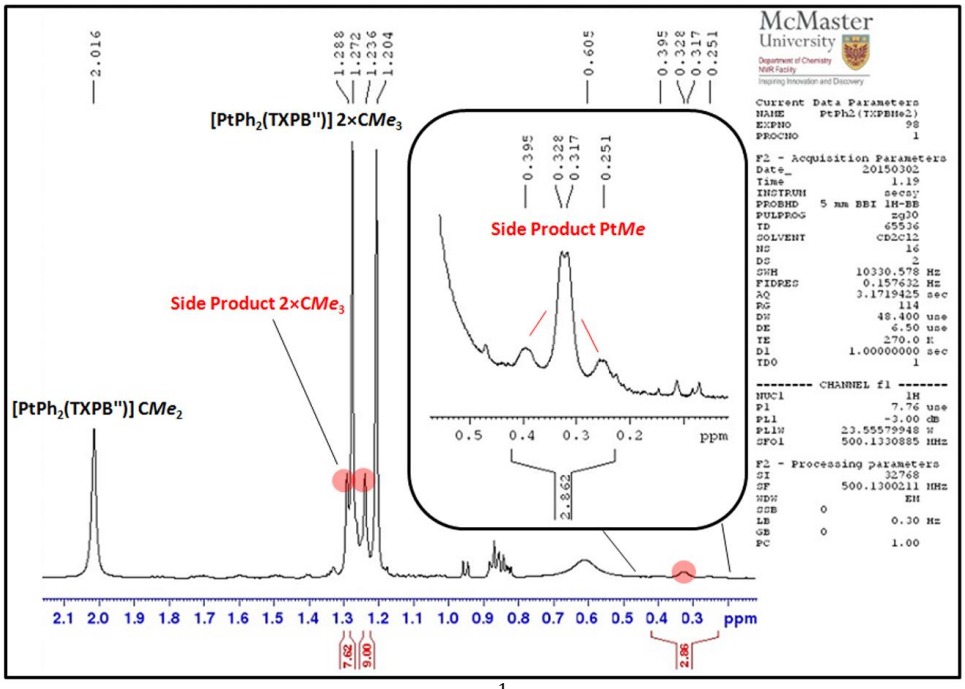

Figure 4.8. Expanded aliphatic region of the ^{1}H NMR spectrum of [$PtPh_2$(TXPB")] (**14**; 500 MHz, 265 K, CD_2Cl_2), highlighting the presence of an unknown side product.

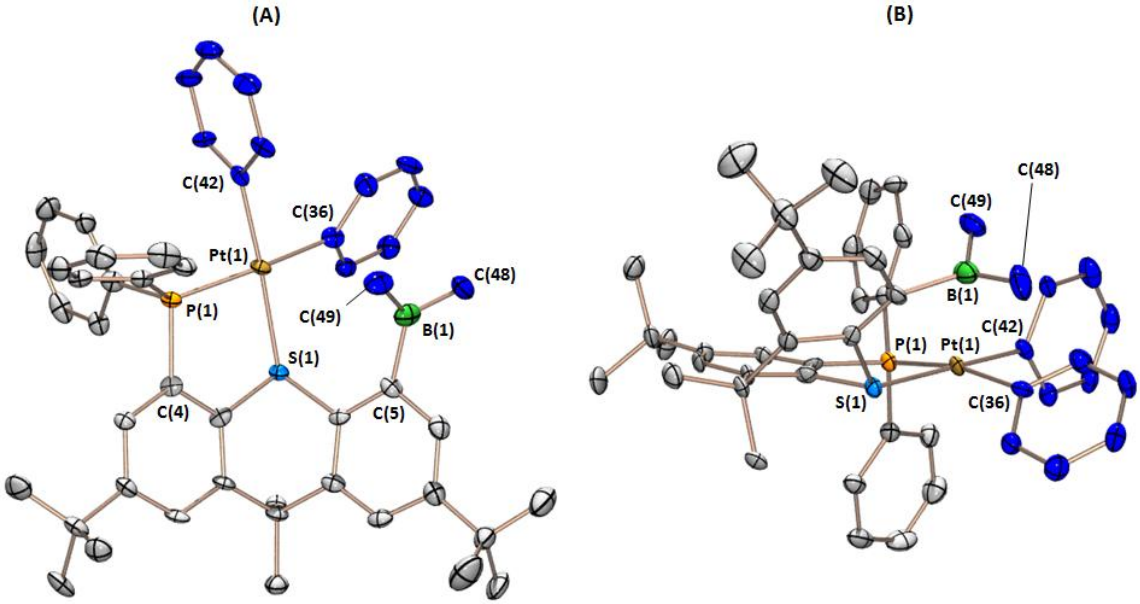

Figure 4.9. Two different views of the X-ray crystal structure for $[PtPh_2(TXPB'')]\cdot(CH_2Cl_2)(C_6H_{14})_{0.5}$ [**14**$\cdot(CH_2Cl_2)(C_6H_{14})_{0.5}$]; hydrogen atoms and solvent are omitted for clarity, ellipsoids are set to 50 % and the Pt*Ph*$_2$ and B*Me*$_2$ groups are coloured in blue.

Complex **14** is the result of a second methyl-phenyl exchange between platinum and boron (Schemes 4.1 and 4.3), and the ratio of **13** to **14** did not change by more than 2% over the temperature range investigated. Heating samples of **14** that did not contain **13** re-established the 86:14 ratio of compounds **14** and **13**, respectively, confirming an equilibrium between **13** and **14** involving bidirectional transfer of alkyl and aryl groups between platinum and boron. Conversion of **13** to an equilibrium mixture of **13** and **14** was monitored in C_6D_6 by NMR spectroscopy between 65 and 125 °C in 10 degree increments. At these elevated temperatures, [**13**] ≫ [**13'**] (*vide supra*), and reversible first-order kinetic treatment [$([\mathbf{14}]_{eq}/[\mathbf{13}]_0)\ \ln\{[\mathbf{14}]_{eq}/([\mathbf{14}]_{eq}-[\mathbf{14}]_t)\} = kt$][236] followed by Eyring analysis (Figure 4.10) provided values of 94(4) kJ mol^{-1} for $\Delta H^{\ddagger}$ and −45(12) J mol^{-1} K^{-1} for $\Delta S^{\ddagger}$ for the forward reaction.

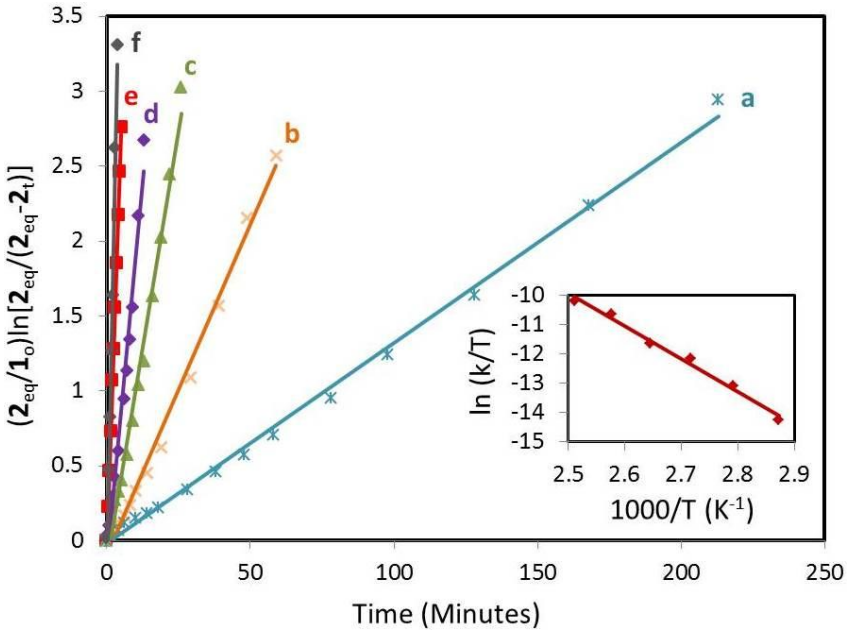

Figure 4.10. Reversible first order analyses for the thermal conversion of **13** to **14** in C_6D_6 at: (a) 75 °C (k = 2.12(2) × 10^{-4} s^{-1}), (b) 85 °C (k = 7.0(2) × 10^{-4} s^{-1}), (c) 95 °C (k = 1.83(5) × 10^{-3} s^{-1}), (d) 105 °C (k = 3.3(1) × 10^{-3} s^{-1}), (e) 115 °C (k = 8.93(9) × 10^{-3} s^{-1}), and (f) 125 °C (k = 1.49(9) × 10^{-2} s^{-1}). The inset shows an Eyring plot for the resulting rate data.

Possible reaction pathways from **13** to **14** are shown in Scheme 4.3. Pathway 'a' proceeds via a zwitterionic intermediate (**D** in Scheme 4.3), which is analogous to the zwitterionic intermediate (**13'**) between [$PtMe_2$(TXPB)] (**A**) and **13** (pathway 'a' in Scheme 4.2). However, prior to the formation of **D**, compound **13** must isomerize to form **C**, in which the remaining Pt*Me* group is *trans* to phosphorus and is therefore positioned in close proximity to the pendant borane (intermediate **C** in Scheme 4.3). If isomerization to form **C** does not take place, pathway 'b' involving B−C_{phenyl} bond-cleaving oxidative addition followed by B−C_{methyl} bond-forming reductive elimination may be operative. The large negative $\Delta S^{\ddagger}$ is inconsistent with the formation of intermediate **C** in Scheme 4.3 via thioether dissociation. However, it is consistent with either: (a) Rate-limiting isomerization to form **C** via a five-coordinate intermediate, perhaps due to intramolecular

coordination of platinum to the *B*-phenyl ring, or (b) concerted B−C_{phenyl} bond oxidative addition to form platinum(IV) intermediate **E** (pathway 'b' in Scheme 4.3).[237]

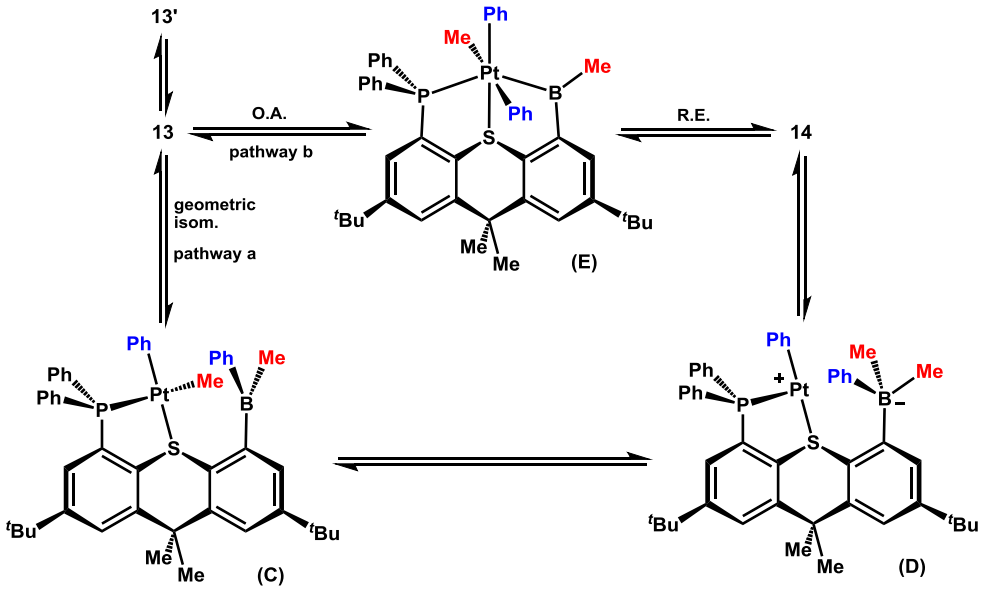

Scheme 4.3. Possible reaction pathways for conversion of **13** to **14**: (a) Via an isomer of **13** in which the platinum methyl group is *trans* to phosphorus (intermediate **C**), followed by abstraction of the platinum methyl group to form zwitterionic intermediate **D**, or (b) via platinum(IV) intermediate **E**.

4.4 – Reaction of [PtMePh(TXPB')] with Neutral Donors

Compound **13** reacted rapidly with one equivalent of PPh_3 or $P(OPh)_3$ to afford neutral [PtMePh(L)(TXPB')] {L = PPh_3 (**15**) or $P(OPh)_3$ (**16**)}, in which the TXPB' ligand is κ^1*P*-coordinated and positioned *trans* to the phenyl group on platinum (Scheme 4.4). By contrast, **13** reacted with two equivalents of CNXyl to produce zwitterionic *trans*-[PtMe(CNXyl)$_2$(TXPB-Me)] (**17**; Scheme 4.4) in which TXPB-Me is a κ^1*P*-coordinated anionic phosphine and the isonitrile ligands are *trans* to one another on platinum (addition of one equivalent of CNXyl afforded a 1:1 mixture of **13** and **17**). These divergent reactivities are consistent with the accessibility of both neutral (**13**) and zwitterionic (**13'**)

in solution.[§] Complexes **15** and **16** gave rise to ^{11}B NMR signals at 76 and ~82 ppm, respectively, consistent with a three-coordinate borane. Conversely, the ^{11}B chemical shift for **17** is found at −10 ppm, indicative of a four-coordinate anionic borate. The ^{195}Pt chemical shifts for **15**−**17** are similar at −4569, −4495, and −4575, ppm, respectively.

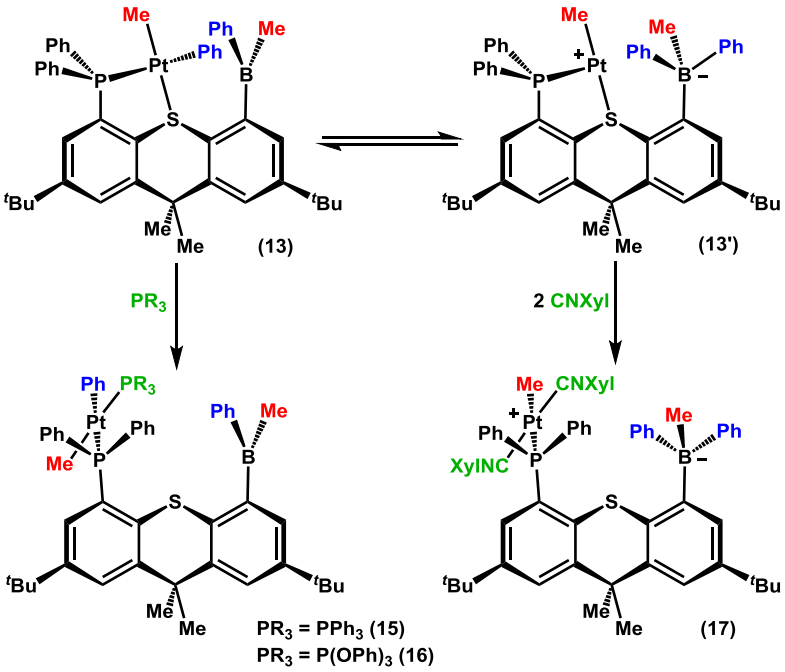

Scheme 4.4. Reaction of **13**, which exists in equilibrium with **13'** in solution, with PPh_3, $P(OPh)_3$ and CNXyl. The reaction products are neutral **15** and **16**, and zwitterionic **17**.

[§] By ^{1}H NMR spectroscopy, compound **13** did not react with ethylene (1 atm, 20 °C).

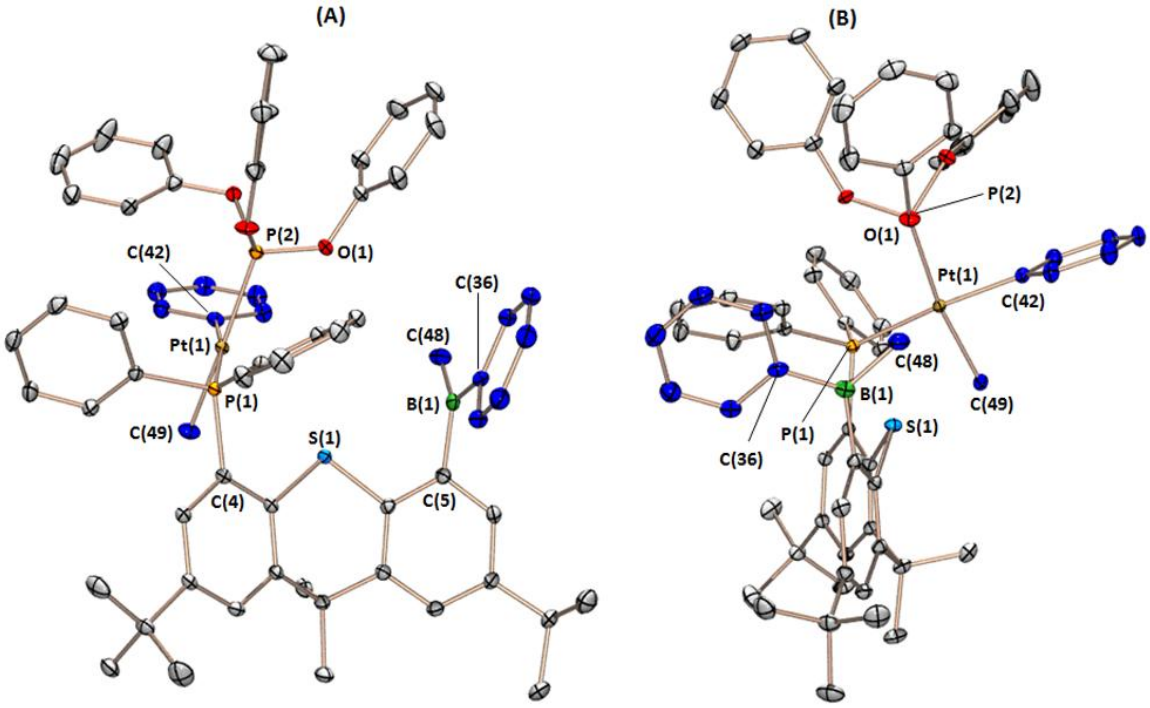

Figure 4.11. Two different views of the X-ray crystal structure for [PtMePh{P(OPh)$_3$}(TXPB')]·(1,2-$C_2H_4Cl_2$)$_{1.5}$ [**16**·(1,2-$C_2H_4Cl_2$)$_{1.5}$]; hydrogen atoms and solvent are omitted for clarity, ellipsoids are set to 50 % and the platinum- and boron-bound methyl and phenyl groups are coloured in blue.

Although all attempts to acquire X-ray quality crystals of **15** resulted in preferential crystallization of *trans*-[$PtMe_2(PPh_3)_2$], X-ray quality crystals of **16**·1.5(1,2-$C_2H_4Cl_2$) and **17**·2.6(CH_2Cl_2) were grown at −30 °C from 1,2-dichloroethane/hexanes and dichloromethane/hexanes, respectively (Figures 4.11 and 4.12, respectively). Platinum is square planar in both complexes, but while boron is trigonal planar in **16**, it is tetrahedral in **17** with correspondingly elongated B−C bonds[§] [1.631(7)−1.673(7) Å in **17** versus 1.564(3)–1.573(3) Å in **16**]. The neutral TXPB' and anionic TXPB-Me ligands in **16** and **17**, respectively, are κ^1*P*-coordinated to platinum, highlighting the lability of the

[§] All attempts to crystallize **15** yielded *trans*-[$PtMe_2(PPh_3)_2$] as clear and colourless needle-shaped crystals, with **15** and small amounts of *trans*-[$PtMePh(PPh_3)_2$], *trans*-[$PtMe_2(PPh_3)_2$], and free TXPB/TXPB' remaining in solution.

central thioether donor. All Pt−C_{Ph}, Pt−C_{Me}, and Pt−C_{CNR} distances in **16** and **17** are within expected ranges.[166,230,238] The Pt−PAr_3 and Pt−$P(OPh)_3$ distances in **16** are 2.2958(5) and 2.2204(5) Å, respectively, indicating stronger binding to the phosphite than the phosphine ligand. The Pt−PAr_3 bond in **13** [2.350(1) Å] is appreciably elongated relative to the Pt−PAr_3 bonds in **13**, **14**, and **16** [2.261(2)−2.2958(5) Å], consistent with less effective PAr_3 binding and more effective coordination of the *trans*-disposed methyl group, due to the positive charge at platinum.[239] Weaker phosphine coordination in **17** is also evidenced by a shift of the ^{31}P NMR signal to lower frequency for the TXPB ligand (14.4 ppm vs 25−43 ppm in **13**−**16**) with a decreased ^{31}P–^{195}Pt coupling constant ($^1J_{31P,195Pt}$ = 1603 Hz vs 1698−1963 Hz in **13**−**16**).

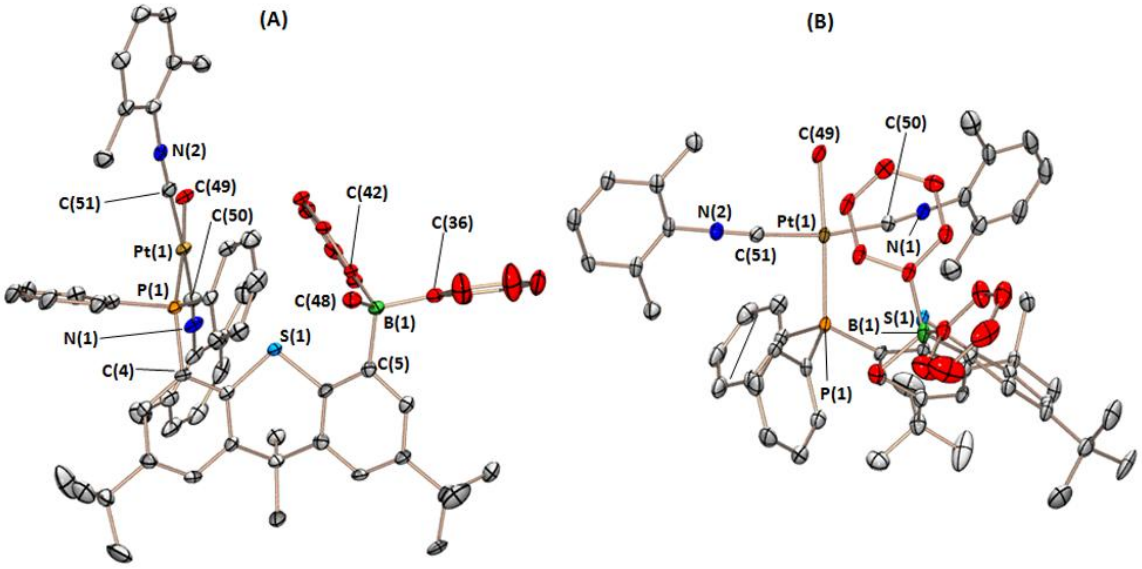

Figure 4.12. Two different views of the X-ray crystal structure for [PtMe(CNXyl)$_2$(TXPB-Me)]·$(CH_2Cl_2)_{2.6}$ (**17**·$(CH_2Cl_2)_{2.6}$); hydrogen atoms and solvent are omitted for clarity, ellipsoids are set to 50 % and the Pt*Me*, B*Me* and B*Ph*$_2$ groups are coloured in red.

4.5 – Summary

Reaction of TXPB with [$PtMe_2$(cod)] yielded [PtMePh(TXPB')] (**13**), which is converted to an approximate 14:86 mixture of **13** and [$PtPh_2$(TXPB")] (**14**) upon heating;

13 and **14** are in equilibrium at elevated temperatures. The *in situ* generated TXPB' and TXPB'' ambiphilic ligands are related to the original TXPB ligand through stepwise exchange of the phenyl groups on boron for methyl groups. In solution, compound **13** exists in equilibrium with a zwitterionic isomer, [PtMe(TXPB-Me)] (**13'**), and both solution species can be trapped by the addition of phosphines or isonitriles. Given the accessibility of both **13** and **13'** in solution, the reaction to form **13** from [$PtMe_2$(TXPB)] is likely to proceed via zwitterionic **13'**, rather than a platinum(IV) boryl intermediate. An analogous mechanism could potentially convert **13** to **14**, except that initial geometric isomerization would be required in order to position the remaining platinum methyl group in close proximity to the pendant borane. Application of reversible first-order kinetics and Eyring analysis to the conversion of **13** to **14** gave a large negative $\Delta S^{\ddagger}$ of −45(12) J mol^{-1} K^{-1}, which is consistent with either: (a) Rate-limiting formation of a five-coordinate intermediate en route to isomer **C** in Scheme 4.3, followed by methyl group abstraction by the borane and subsequent transfer of the phenyl group on boron to platinum, or (b) concerted oxidative addition of a B−Ph bond, followed by B−Me bond-forming reductive elimination.

The reactivity described in this chapter provides examples of intramolecular alkyl abstraction by a pendant borane, reversible aryl abstraction by a pendant borane with spectroscopic identification and trapping of neutral and zwitterionic isomers, and *in situ* generation of new ambiphilic ligands by stepwise alkyl/aryl exchange between platinum and boron. These alkyl/aryl exchange reactions differ fundamentally from those reported by Vedernikov *et al.* in that: (a) They do not require strongly basic solvent to promote the exchange and (b) the reactions en route to **13** and **13'** likely maintain the platinum(II) oxidation state.

Chapter 5

Design and Synthesis of 2nd Generation Ambiphilic Ligands

Adapted with permission from: Cowie, B. E.; Emslie, D. J. H. *Organometallics* **2015**, *34*, 4093-4101. Copyright 2015 American Chemical Society.

Adapted with permission from: Cowie, B. E.; Emslie, D. J. H. *Chem. –Eur. J.* **2014**, *20*, 16899-16912. Copyright 2014 John Wiley & Sons.

Adapted with permission from: Cowie, B. E.; Tsao, F. A.; Emslie, D. J. H. *Angew. Chem. Int. Ed.* **2015**, *54*, 2165-2169. Copyright 2015 John Wiley & Sons.

5.1 – Introduction to Ambiphilic Ligand Design

In order to explore the late transition metal chemistry of Group 13 Lewis acid-containing ambiphilic ligands, the Emslie group envisioned a ligand platform that possesses a Lewis acidic entity in the periphery of the ligand framework (Figure 5.1). This design contrasts the design of most other tri- or tetradentate ambiphilic ligands prepared to-date, in which the Lewis acid entity occupies a central position. The strategic positioning of the Lewis acid in a terminal position may render the Lewis acid more accessible to interact with either co-ligands or external substrates, which is an important feature if the ligand is to be applied to cooperative catalysis.

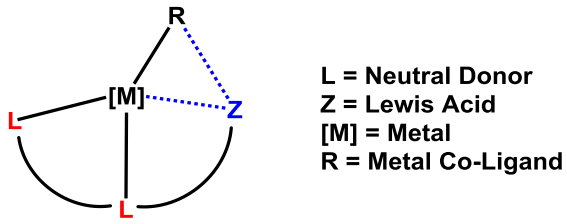

Figure 5.1. General depiction of the donor–donor–acceptor motif of ambiphilic ligands prepared in the Emslie group, with dotted lines illustrating possible metal–Lewis acid and metal–co-ligand–Lewis acid interactions.

A bidentate donor system in combination with a structurally rigid ligand backbone was chosen to ensure close approach of the pendant Lewis acid to either the metal centre or metal co-ligands. “Soft” donor groups were chosen for compatibility with “soft” electron-rich late transition metals, which are typically targeted in ambiphilic ligand research due to their willingness to donate to Z-type ligands. Given the aforementioned ambiphilic ligand design criteria, initial research conducted in the Emslie lab probed the coordination and organometallic chemistry of a thioxanthene-backbone ligand, 2,7-di-*tert*-butyl-5-diphenylboryl-4-diphenylphosphino-9,9-dimethylthioxanthene; TXPB.

Despite a range of interesting results obtained through deployment of the TXPB ligand, as outlined in Chapter 1, and expanded upon in Chapters 2–4, the anchoring thioether donor of TXPB is susceptible to displacement in the presence of other neutral donors, such as carbon monoxide, phosphines, phosphites (Chapter 4) isonitriles (Chapter 3) and dienes.[122] In addition, although the first three steps of the synthetic protocol for TXPB can be performed on multi-gram scales (~60 grams for step 1, ~15 grams for step 2 and ~10 grams for step 3), the final two steps do not scale well, so cannot be used to prepare more than 1-2 grams each, with the most challenging procedure being the recrystallization of the TXPB ligand from acetonitrile, which inexplicably provides product (in 60 % yield) on the first attempt 50 % of the time, after multiple attempts/trouble shooting strategies 30 % of the time, and in 0 % yield the remaining 20 % of the time. In order to overcome these disadvantages in the design and synthesis of the TXPB ligand, a new ambiphilic ligand with a more coordinating central donor and a more scalable synthesis was designed.

5.2 – The FcPPB Ligand

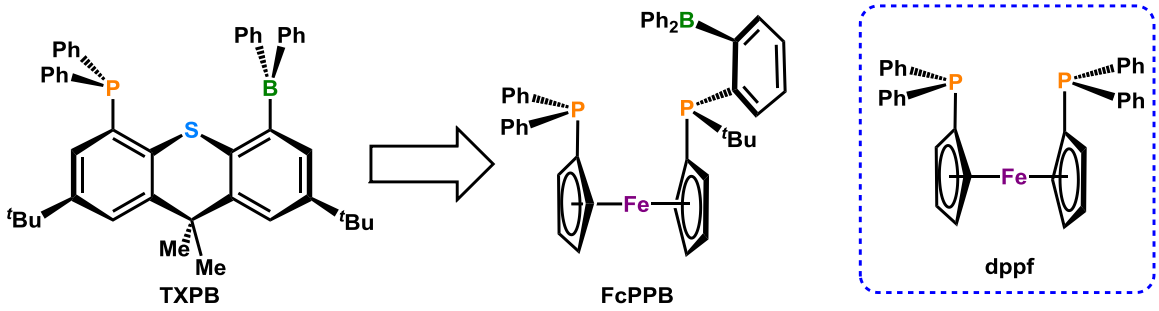

Figure 5.2. Evolution of the previously utilized borane-containing ambiphilic ligand in the Emslie lab, TXPB (displayed on the left), towards the newly designed ligand, FcPPB (displayed in the middle); the design of the FcPPB ligand is based on dppf, depicted on the right.

The FcPPB ligand, 1'-{(*ortho*-diphenylborylphenyl)-*tert*-butylphosphino}-1-diphenylphosphinoferrocene (Figure 5.2), exhibits the same donor–donor–acceptor motif as the TXPB ligand, rendering it suitable to encourage either metal–Lewis acid coordination or metal–co-ligand–borane coordination. However, the FcPPB ligand is built upon ferrocene as the ligand backbone, which provides the ligand frame with greater flexibility relative to the thioxanthene backbone employed for the TXPB ligand. For example, the coordination chemistry of 1,1'-bis(diphenylphosphino)ferrocene (dppf, Figures 5.2 and 5.3) has been extensively studied, and while mononuclear metal-dppf complexes typically involve κ^2*PP*-coordination of the ligand, a wide variety of coordination modes have been observed for multimetallic dppf complexes, as shown in Figure 5.3. The aforementioned flexibility of dppf and related ligands stems from the torsional twist of the cyclopentadienyl rings along the Cp–Fe–Cp axis, or tilting of the cyclopentadienyl rings to move the phosphorus donors towards or away from iron, depending on the steric requirements of the complexed metal centre.[240] A similar level of conformational flexibility can be expected for the 1,1'-bis(phosphino)ferrocene portion of the FcPPB ligand.

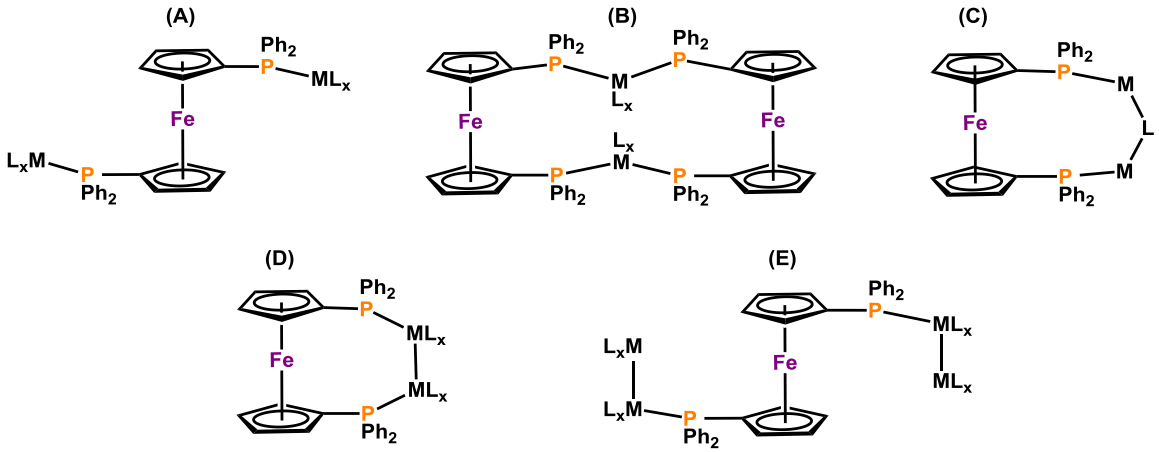

Figure 5.3 – Varying coordination modes of dppf in multimetallic complexes.

The bisphosphine donor set of FcPPB provides significantly improved donor ability relative to TXPB; the diphenylphosphino moiety at the 1-position of the ferrocene backbone electronically similar to the phosphine donor in TXPB, while the central *tert*-butyl substituted phosphine in the 1'-position of the ferrocene backbone is a much stronger donor than the phosphine or thioether groups in TXPB, and also provides a useful ^{1}H NMR handle to assist in evaluating the reactivity of the FcPPB ligand.

The FcPPB ligand was prepared in seven steps in a convergent synthesis starting from commercially available ferrocene and 1,2-dibromobenzene (Scheme 5.1). The addition of two equivalents of ^{n}BuLi in the presence of *N*,*N*,*N*',*N*'-tetramethylethane-1,2-diamine (TMEDA) resulted in the precipitation of TMEDA-coordinated 1,1'-dilithioferrocene ([Fe(η^5-$C_5H_4Li)_2$]·TMEDA),[241] which was isolated rather than used *in situ* because it is more straightforward to remove unreacted ferrocene at this point of the synthesis. The subsequent addition of 1,1,2,2-tetrabromoethane to [Fe(η^5-$C_5H_4Li)_2$]·TMEDA provided 1,1'-dibromoferrocene in >95 % yield,[242] which afforded access to 1-bromo-1'-diphenylphosphinoferrocene (>95 % yield) via monolithiation using ^{n}BuLi at –78 °C for 10 minutes, followed with the addition of Cl–PPh_2.[243] In parallel, (*ortho*-bromophenyl)chloro-*tert*-butylphosphine, (*o*-BrC_6H_4)P(^{t}Bu)Cl, was prepared in three steps from 1,2-dibromobenzene, first by monolithiation of 1,2-dibromobenzene with ^{n}BuLi and quenching with Cl–$P(NEt_2)_2$ to provide (*o*-BrC_6H_4)$P(NEt_2)_2$ (**18**), followed by

reaction with HCl to form (*o*-BrC_6H_4)PCl_2 (**19**), then finally through substitution of a chloride substituent for a *tert*-butyl substituent via reaction of (*o*-BrC_6H_4)PCl_2 with ^{t}BuMgCl; (*o*-BrC_6H_4)P(^{t}Bu)Cl (**20**) was obtained in an overall yield of 60 %. Lithiation of the remaining bromide in [Fe(η^5-C_5H_4Br)(η^5-$C_5H_4PPh_2$)] and quenching with (*o*-BrC_6H_4)P(^{t}Bu)Cl installed the second phosphine, which incorporates the phenylene linker onto which the Lewis acid will be installed; [Fe(η^5-$C_5H_4PPh_2$){η^5-$C_5H_4P^tBu(C_6H_4Br$-*o*)}] (FcPPBr; **21**) was obtained in ~75 % yield, and gives rise to ^{31}P NMR signals at 4.9 and –17.0 ppm, representing the C_5H_4P(^{t}Bu)Ar (Ar = phenylene linker) and $C_5H_4PPh_2$ phosphines, respectively (Scheme 5.1, **A** in Figure 5.11).

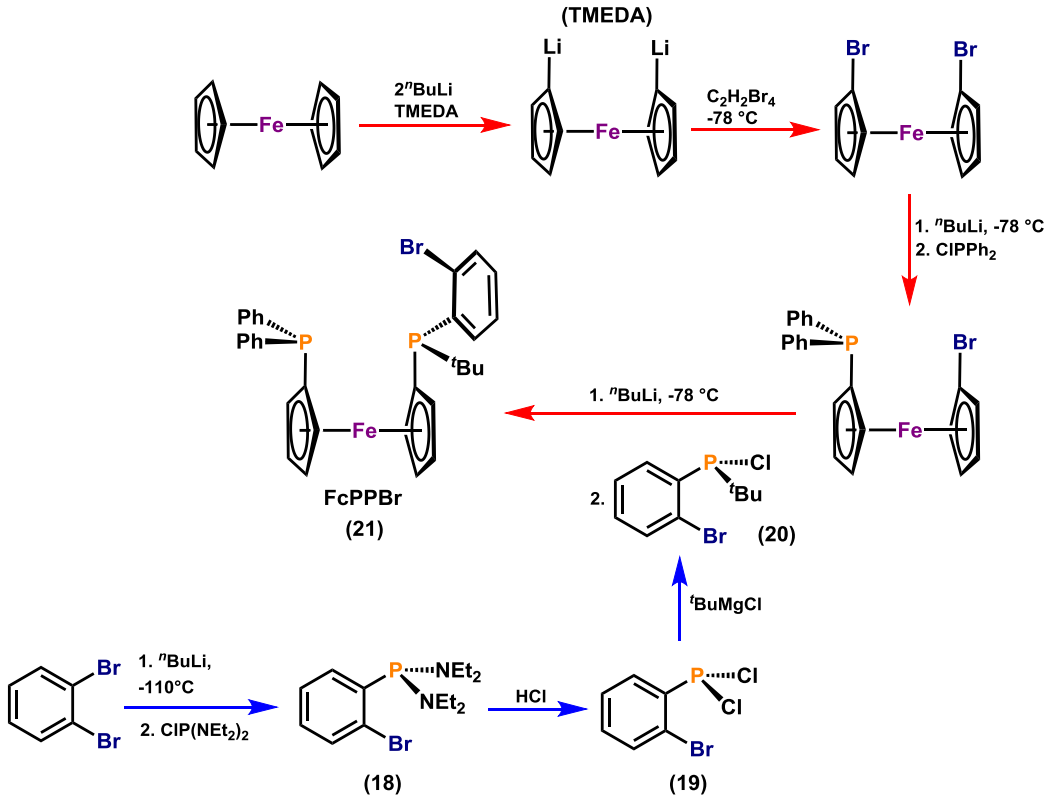

Scheme 5.1. Synthetic scheme used to prepare FcPPBr; the precursor to the FcPPP, FcPPB and FcPPAl ligands.

While attachment of the second phosphine, –P^{t}Bu(C_6H_4Br-*o*), was accomplished via lithiation of [Fe(η^5-C_5H_4Br)(η^5-$C_5H_4PPh_2$)] followed by the addition of (*o*-C_6H_4Br)P(^{t}Bu)Cl (**20**), this was not the route initially chosen for the synthesis of [Fe(η^5-$C_5H_4PPh_2$){η^5-$C_5H_4P^tBu(C_6H_4X$-*o*)}] [FcPPX; X = Br (**21**) or I (**21-I**)]. Initial attempts focused on reactivity stemming from [Fe(η^5-$C_5H_4PPh_2$){η^5-$C_5H_4P(^tBu)Cl$}] (**22**), which was obtained by slow, dropwise addition of [Fe(η^5-$C_5H_4PPh_2$)(η^5-C_5H_4Li)] to Cl_2P^tBu (Scheme 5.2). Next, in order to prepare **21** or **21-I**, three different synthetic routes were pursued: (A) Addition of monolithiated 1,2-dibromobenzene, C_6H_4LiBr-*o*, to compound **22** (**A** in Scheme 5.2), (B) reaction of **22** with lithium metal, providing [Fe(η^5-$C_5H_4PPh_2$){η^5-$C_5H_4P(^tBu)$Li}] (**23**) with concomitant formation of LiCl, followed by reaction with C_6H_4FI-*o* (**B** in Scheme 5.2), and (C) reaction of **22** with $LiAlH_4$, providing [Fe(η^5-$C_5H_4PPh_2$){η^5-$C_5H_4P(^tBu)$H}] (**24**), followed by lithiation using ^{n}BuLi and quenching with C_6H_4FI-*o* (**C** in Scheme 5.2). While the synthesis of compound **22** was successful, routes **A**–**C** were not. Route **A** was unsuccessful because C_6H_4BrLi-*o* did not react with **22** at or below –110 °C, and warming the reaction to temperatures exceeding –110 °C resulted in decomposition of the aryl lithium reactant. In route **B**, the reaction of **22** with lithium metal appeared to be successful, providing a new compound with ^{31}P NMR signals located at 1.0 and –17.3 ppm. However, no reaction occurred between this compound, tentatively assigned as [Fe(η^5-$C_5H_4PPh_2$){η^5-$C_5H_4P(^tBu)$Li}] (**23**), and C_6H_4FI-*o*, even when heated to 70 °C. Finally, with respect to route **C**, reduction of **22** to [Fe(η^5-$C_5H_4PPh_2$){η^5-$C_5H_4P(^tBu)$H}] (**24**) appeared to be successful, providing ^{31}P NMR signals in C_6D_6 located at –17.3, –28.2 ppm with a $^1J_{1H,31P}$ coupling constant of 208 Hz. However, the reaction of **24** with ^{n}BuLi unexpectedly required 2 equivalents of the alkyl lithium to proceed to completion, the reaction product [^{31}P{^{1}H} NMR: –15.1, –20.9 ppm (THF-d_8)] was different from that obtained in the reaction of [Fe(η^5-$C_5H_4PPh_2$){η^5-$C_5H_4P(^tBu)$Cl}] with lithium metal, and subsequent reaction with C_6H_4FI-*o* failed to yield [Fe(η^5-$C_5H_4PPh_2$){η^5-$C_5H_4P^tBu(C_6H_4I$-*o*)}] (**21-I**).

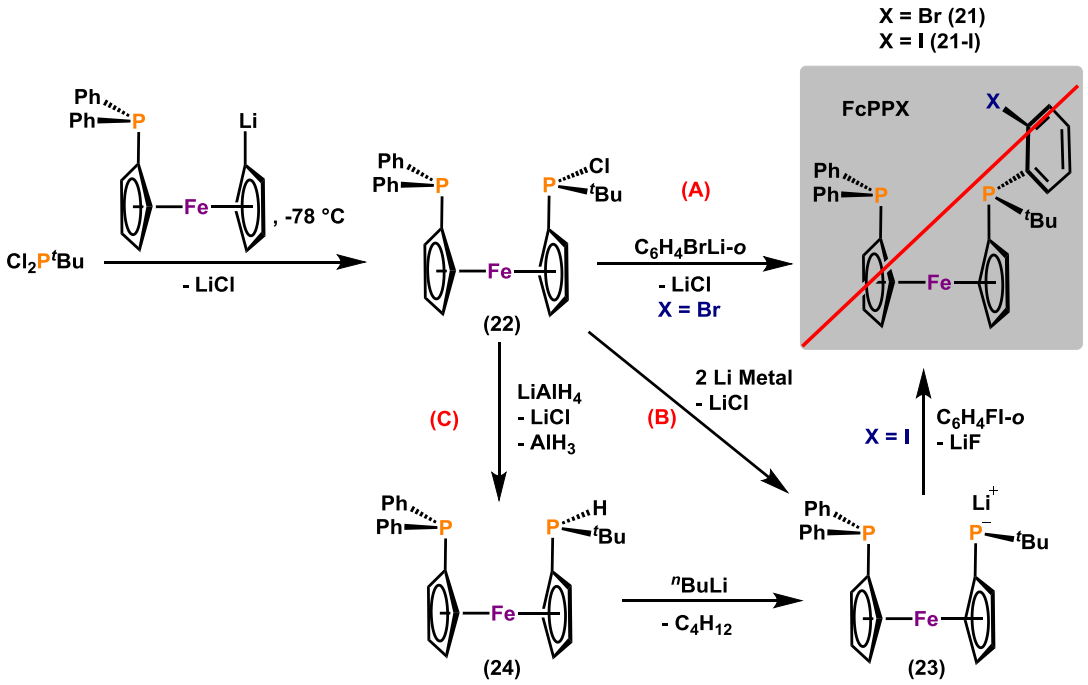

Scheme 5.2. Alternative reaction pathways surveyed for the synthesis of [Fe(η^5-$C_5H_4PPh_2$){η^5-$C_5H_4P^tBu(C_6H_4X$-*o*)}] [FcPPX; X = Br (**21**) or I (**21-I**)].

With FcPPBr in hand, it was necessary to determine appropriate conditions for lithiation and installation of a Lewis acid onto the phenylene linker. Therefore, the synthesis of the trisphosphine analogue of FcPPB, 1'-{(*ortho*-diphenylphosphinophenyl)-*tert*-butylphosphino}-1-diphenylphosphinoferrocene (FcPPP, Scheme 5.3), was initially targeted. The FcPPP ligand was selected as the initial synthetic target due to: (1) The reliability of reactions between RLi reagents and R_2PCl electrophiles, and (2) the viability of $^{31}P\{^1H\}$ NMR spectroscopy as a straightforward method to determine whether successful installation of the phosphine moiety had been achieved. Attempted lithiations of FcPPBr using ^{t}BuLi below –20 °C were unsuccessful due to a lack of reactivity, and at room temperature, undesired side reactions occurred. In addition, lithiation reactions performed in coordinating solvents such as diethyl ether or THF were unsuccessful due to the occurrence of undesired side reactions. Thus, the optimal method for lithium-bromide exchange involved using toluene as the solvent, and the slow addition of ^{t}BuLi at –45 °C followed by warming the reaction mixture to 0 °C; the reaction was maintained at this

temperature for 3 hours before quenching with Cl–PPh_2 at –45 °C. The FcPPP ligand was isolated in nearly 80 % yield, and successful installation of the –PPh_2 moiety was evidenced by ^{31}P signals located at –7.5, –11.2 and –16.5 ppm (**B** in Figure 5.11). The signals located at –7.5 and –11.2 ppm represent the $C_5H_4P(^tBu)Ar$ and $ArPPh_2$ moieties (Ar = phenylene linker), respectively, and exhibit $^3J_{31P,31P}$ coupling constants of 176 Hz, whereas the singlet located at –16.5 ppm represents the $C_5H_4PPh_2$ group. The ^{1}H NMR spectrum of FcPPP, as well as labeled expanded views of the aromatic and C_5H_4-regions are displayed below in Figures 5.4–5.6; numbered protons refer to positions on the ferrocene backbone and the phenylene linker in the FcPPP ligand, as shown in Scheme 5.3. The FcPPP ligand contains one chiral phosphorus centre and was isolated as a racemic mixture.

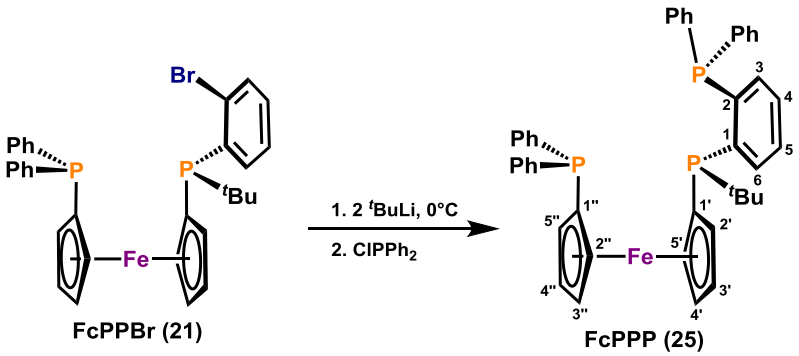

Scheme 5.3. Synthesis of the FcPPP ligand from FcPPBr.

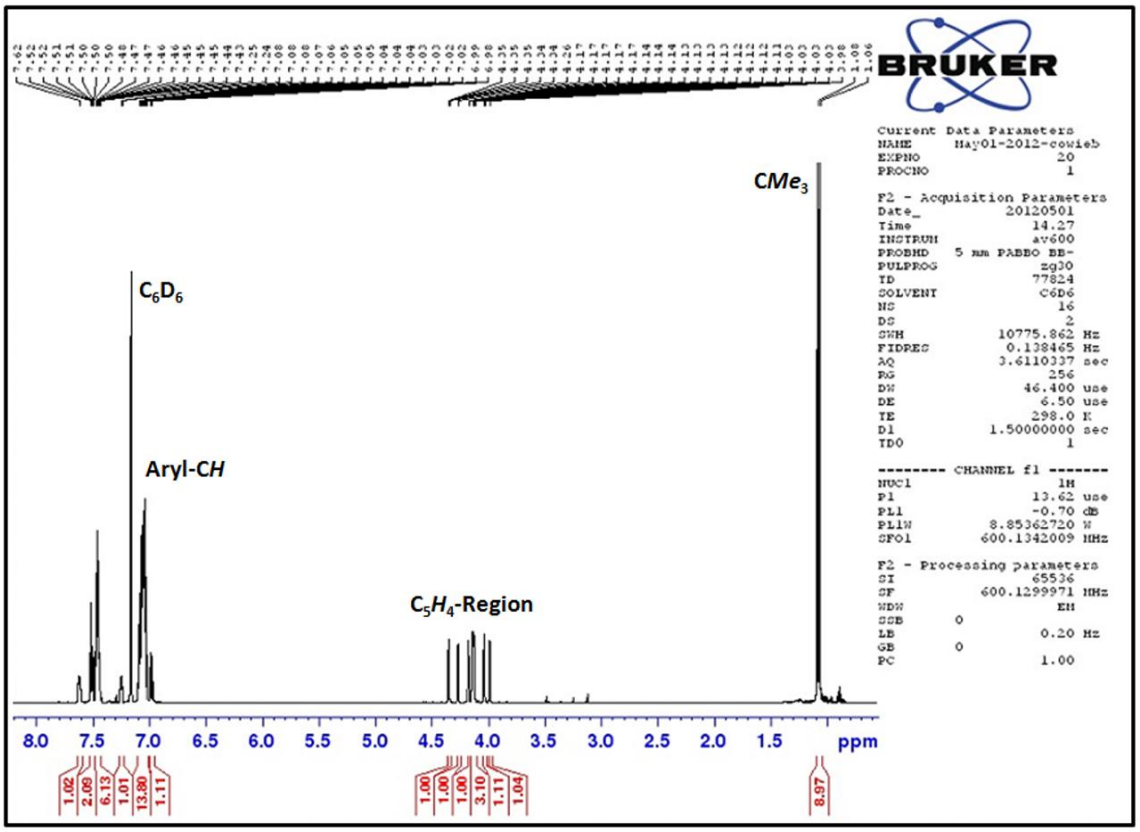

Figure 5.4. ^{1}H NMR spectrum of the FcPPP ligand (600 MHz, 298 K, C_6D_6).

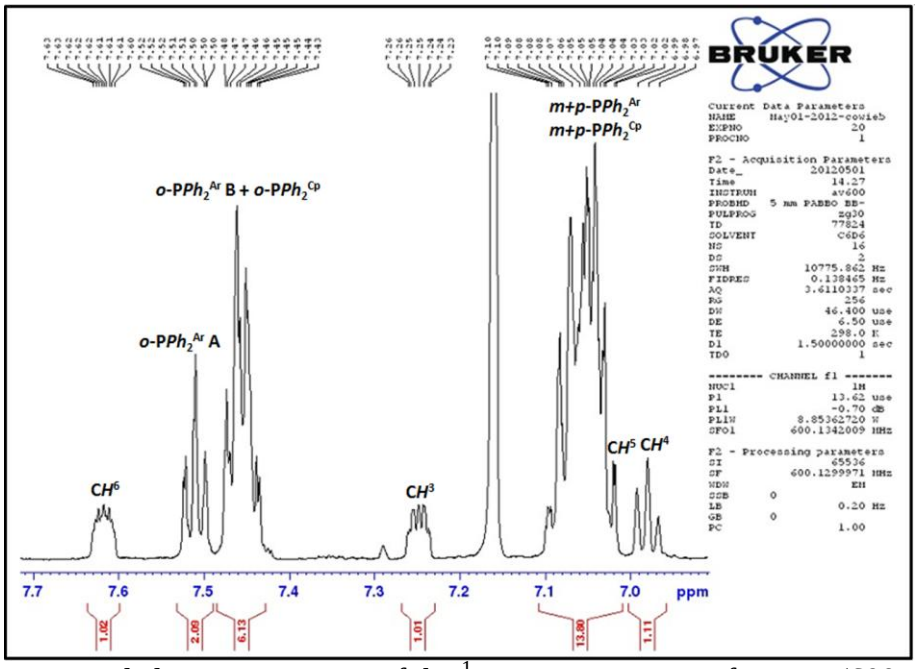

Figure 5.5. Expanded aromatic region of the ^{1}H NMR spectrum of FcPPP (600 MHz, 298 K, C_6D_6).

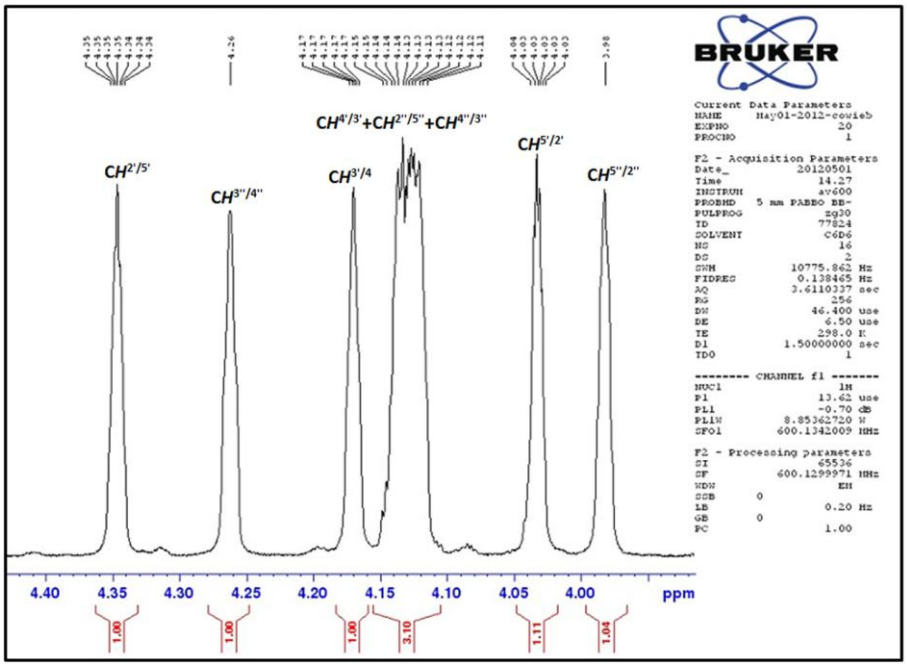

Figure 5.6. Expanded C_5H_4-region of the ^{1}H NMR spectrum of FcPPP (600 MHz, 298 K, C_6D_6).

The use of FcPPP to prepare nickel and palladium complexes is discussed in Chapter 6. These complexes allowed comparison of the coordinative properties of FcPPB with those of a tridentate borane-free analogue.

The FcPPB ligand was prepared using the same synthetic protocol deployed to synthesize FcPPP, but employing $Br–BPh_2$ as the electrophile in place of $Cl–PPh_2$ (Scheme 5.4). The FcPPB ligand contains one chiral phosphorus centre and was isolated as a mixture of enantiomers in nearly 80 % yield.

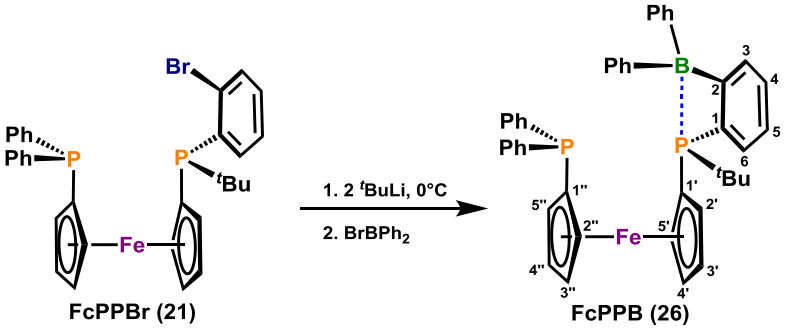

Scheme 5.4. Synthesis of the FcPPB ligand from FcPPBr.

The ^{11}B NMR signal for FcPPB in C_6D_6 is 17 ppm, which is at much lower frequency than expected for a free triarylborane, indicating that intramolecular phosphine–borane adduct formation may occur in solution.[244] A high frequency shift in the ^{31}P NMR signal for the $C_5H_4P(^tBu)Ar$ moiety from 4.9 ppm in FcPPBr to 19.7 ppm in FcPPB further supports this interpretation (**C** in Figure 5.11). Similar ^{31}P NMR shifts to higher frequency were reported by Bourissou and co-workers for the $(o\text{-}^iPr_2P)C_6H_4BPh_2$ and $\{(o\text{-}^iPr_2P)C_6H_4\}_3B$ ligands; the former gave rise to a ^{31}P NMR signal at 24.8 ppm, which is shifted to higher frequency relative to the calculated structure that does not possess intramolecular P→B adduction formation (16.5 ppm),[105] and the latter gave rise to one ^{31}P NMR signal located at 4.9 ppm at room temperature, but two signals located at 26.1 and –2.9 ppm in a 1:2 ratio at 173 K, the former signal representing the phosphine involved in P→B adduct formation.[104] The ^{31}P NMR signal for the $C_5H_4PPh_2$ group of

FcPPB is located at –17.2 ppm (**C** in Figure 5.11). Displayed below is the ^{1}H NMR spectrum of FcPPB, along with labelled expanded views of the aromatic and C_5H_4-regions (Figures 5.7–5.9); numbered protons refer to the positions on the ferrocene backbone and the phenylene linker of the FcPPB ligand, as shown in Scheme 5.4.

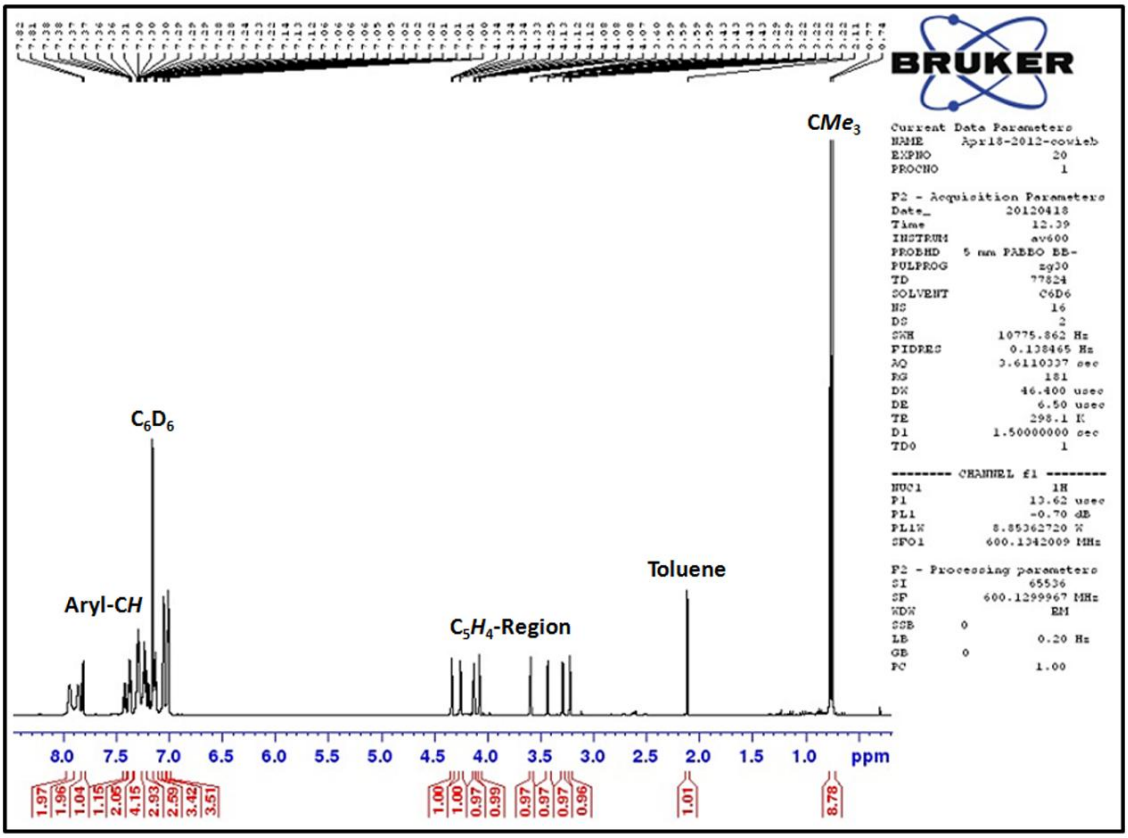

Figure 5.7. ^{1}H NMR spectrum of the FcPPB ligand (600 MHz, 298 K, C_6D_6).

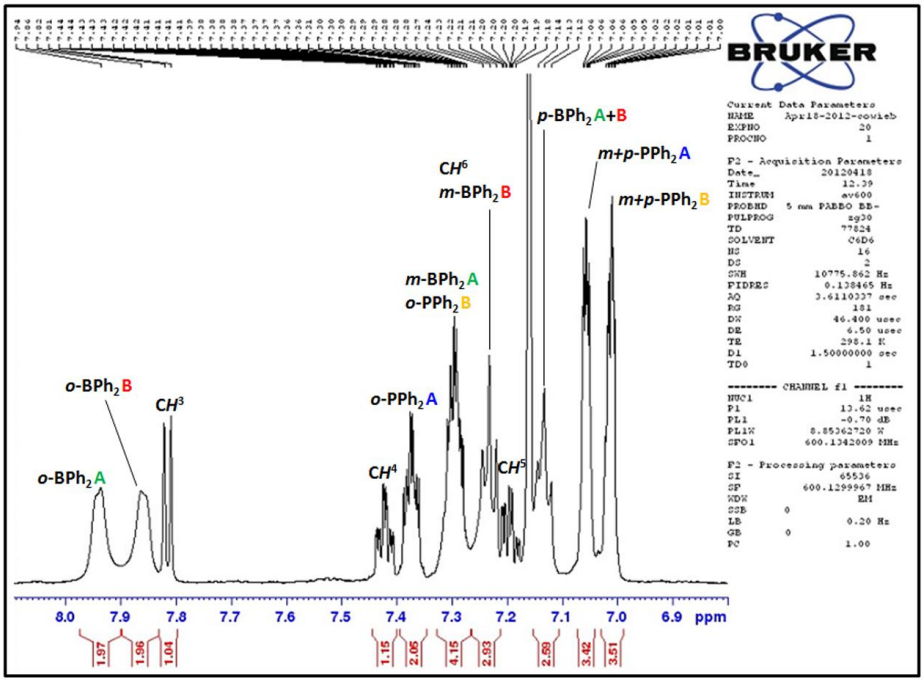

Figure 5.8. Expanded aromatic region of the ^{1}H NMR spectrum of FcPPB (600 MHz, 298 K, C_6D_6).

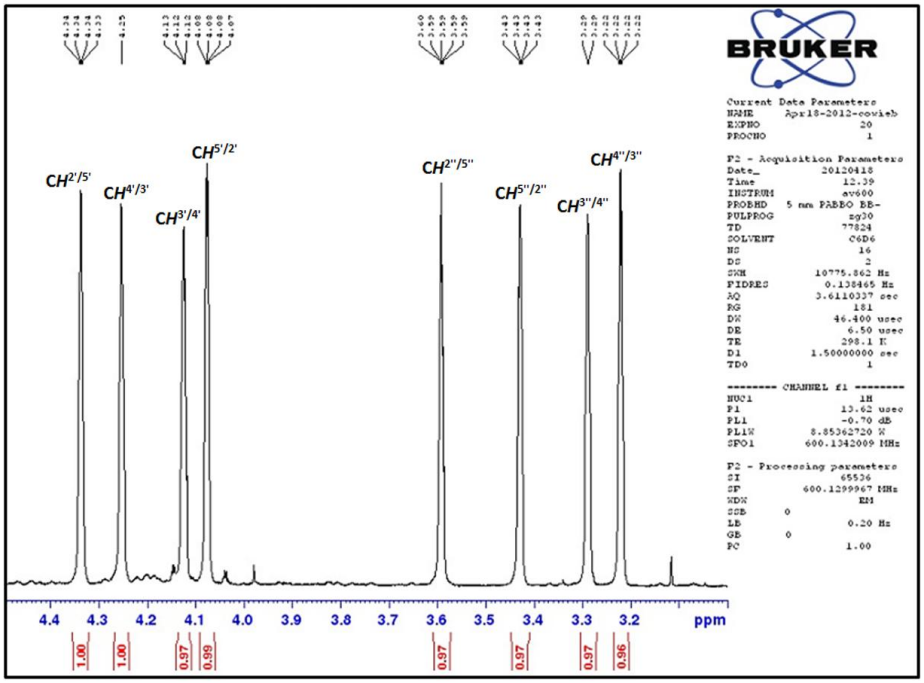

Figure 5.9. Expanded C_5H_4-region of the ^{1}H NMR spectrum of FcPPB (600 MHz, 298 K, C_6D_6).

X-ray quality crystals of FcPPB were obtained by slow evaporation of a solution in CH_2Cl_2/hexanes at 298 K, and the solid-state structure of FcPPB (Figure 5.10) indeed revealed adduct formation between the *tert*-butyl substituted phosphorus donor, P(2), and the borane; the B–P(2) bond distance in FcPPB is 2.146(2) Å, the P(2)–C(27)–C(28) and B–C(28)–C(27) angles are 98.4(1)° and 106.6(1)°, respectively (rather than 120°) and the sum of the C–B–C angles is 347.5(2)° (rather than 360°). The B–P(2) bond distance in FcPPB is very similar to the B–P distance in {*o*-(^{i}Pr$_2$P)C$_6$H$_4$}$_3$B [B–P = 2.150(3) Å].[104]

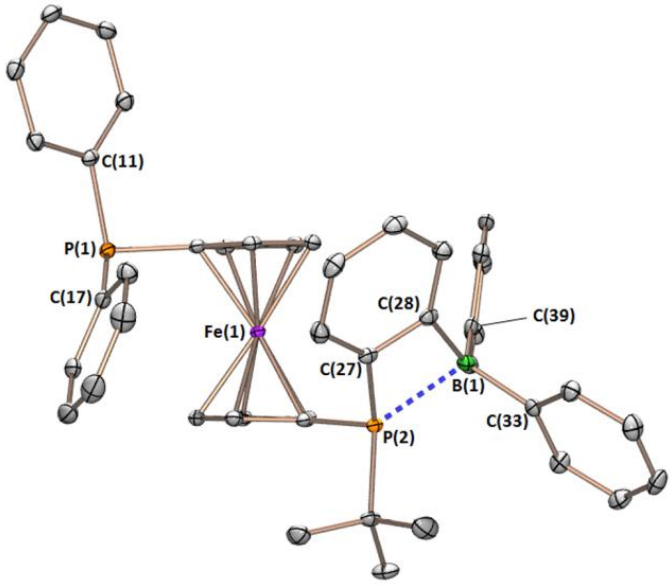

Figure 5.10. Solid-state structure of FcPPB with ellipsoids drawn at 50% probability. Hydrogen atoms have been omitted for clarity.

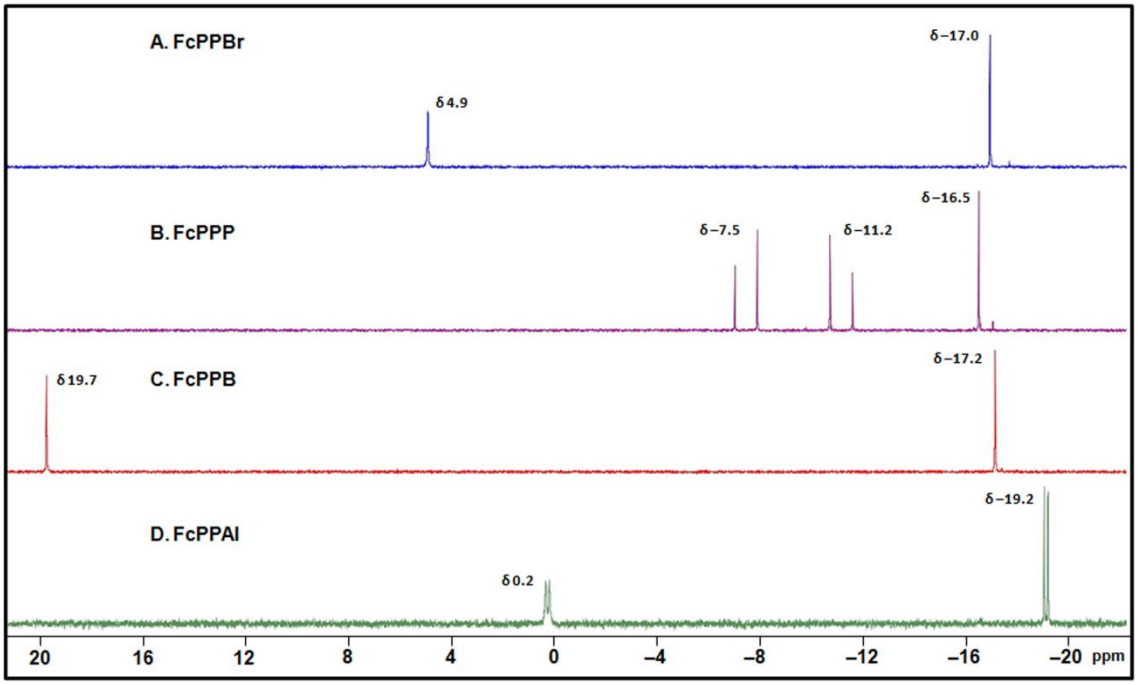

Figure 5.11. $^{31}P\{^{1}H\}$ NMR spectra for **A.** FcPPBr, **B.** FcPPP, **C.** FcPPB and **D.** FcPPAl; the $^{31}P\{^{1}H\}$ NMR spectra were collected in C_6D_6 at 298 K (203 MHz).

Similarly to the synthesis of TXPB, the initial steps in the preparation of FcPPP and FcPPB (synthesis of $[Fe(\eta^5\text{-}C_5H_4Br)(\eta^5\text{-}C_5H_4PPh_2)]$ and $(o\text{-}BrC_6H_4)P(^tBu)Cl$, Scheme 5.1) can be performed on multi-gram scales (5-10 grams). However, conversely to the synthesis of TXPB, the final two steps can be performed on 2-4 gram scales with high reproducibility and a significantly improved yield in the final step (~80 % for FcPPP/FcPPB vs. ~60 % for TXPB). The final step in the synthesis of the FcPPP and FcPPB ligands provides an avenue to install a wide variety of appended Lewis acidic or Lewis basic moieties onto the ligand backbone, depending on the properties desired for a particular ligand framework. Consequently, an alane appended analogue of FcPPB, 1'-{(*ortho*-dimethylalanylphenyl)-*tert*-butylphosphino}-1-diphenylphosphinoferrocene (FcPPAl, Section 5.3), was prepared. The transition metal (nickel, palladium, platinum, tungsten, ruthenium and gold) chemistry of FcPPB is discussed in Chapters 6 and 7, and the platinum chemistry of FcPPAl is discussed in Chapter 8.

Table 5.1. Crystallographic Data Collection and Refinement Parameters for FcPPB (**26**) and FcPPAl (**27**).

Structure	**FcPPB**	**FcPPAl**
Formula	$C_{44}H_{41}BFeP_2$	$C_{34}H_{37}AlFeP_2$
Formula wt	698.37	590.41
T (K)	100(2)	100(2)
Cryst. Syst.	Triclinic	Monoclinic
Space Group	*P*–1	*P*2(1)/*c*
a (Å)	9.0532(8)	13.887(3)
b (Å)	10.3272(9)	12.128(3)
c (Å)	19.361(2)	19.196(4)
α [deg]	101.061(2)	90
β [deg]	91.972(2)	110.851(4)
γ [deg]	102.617(2)	90
Volume [$Å^3$]	1728.1(3)	3021(1)
Z	2	4
μ (mm^{-1})	0.561	0.656
F(000)	732	1240
Crystal Size (mm^3)	0.22×0.10×0.08	0.21×0.09×0.08
θ Range for Collection [deg]	1.08–28.33	2.03–26.45
No. of Reflns Collected	33862	17437
No. of Indep Reflns	8547	6078
Completeness to θ Max (%)	99.3	97.5
Absorption Correction	Numerical	Numerical
Max and Min Transmission	0.9565, 0.8865	0.9494, 0.8746
GOF on F^2	1.086	0.983
Final R_1 [$I > 2\sigma(I)$] (%)	3.52	5.35

5.3 – The FcPPAl Ligand

In order to explore the coordination chemistry of an alane-containing ambiphilic ligand, an alane-appended analogue of FcPPB, [Fe(η^5-$C_5H_4PPh_2$){η^5-$C_5H_4P^tBu(C_6H_4AlMe_2$-*o*)}] (FcPPAl), was targeted. The FcPPAl ligand possesses a dimethylalane group, as opposed to a diphenylalane group, due to the advantageous ^{1}H NMR handle provided by methyl substituents relative to phenyl substituents, and the commercial availability of Cl–$AlMe_2$ solutions; neither X–$AlPh_2$ (X = halide) reagents, nor base-free $AlPh_3$ (the synthetic pre-cursor to X–$AlPh_2$ reagents) are commercially available.[245] Furthermore, smaller substituents on the appended Lewis acid will provide insight into the effects of reduced sterics on metal–Lewis acid and/or metal–co-ligand–Lewis acid coordination.

The FcPPAl ligand was initially prepared by Judy Tsao, a 4th year undergraduate thesis student, under the supervision and direction of B. E. Cowie, and was achieved by lithiation of FcPPBr and quenching with Cl–$AlMe_2$ (Scheme 5.5); FcPPAl was isolated in 64 % yield. Similarly to the FcPPB ligand, FcPPAl is chiral at phosphorus and was used as a racemic mixture. The ^{1}H NMR spectrum of FcPPAl, along with expanded views of the aromatic and C_5H_4-regions are displayed below in Figures 5.12–5.14; numbered protons refer to the positions on the ferrocene backbone and the phenylene linker of the FcPPAl ligand, as shown in Scheme 5.5.

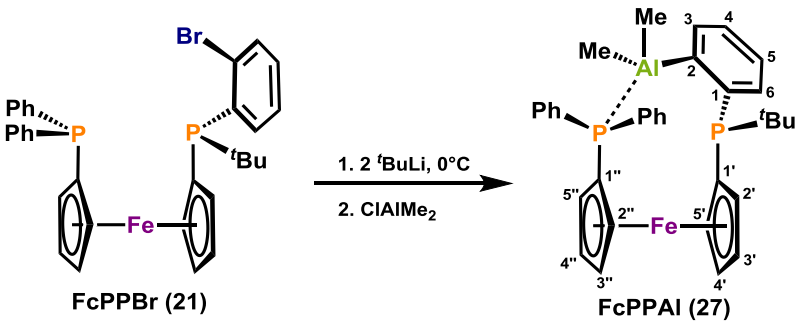

Scheme 5.5. Synthesis of the FcPPAl ligand from FcPPBr.

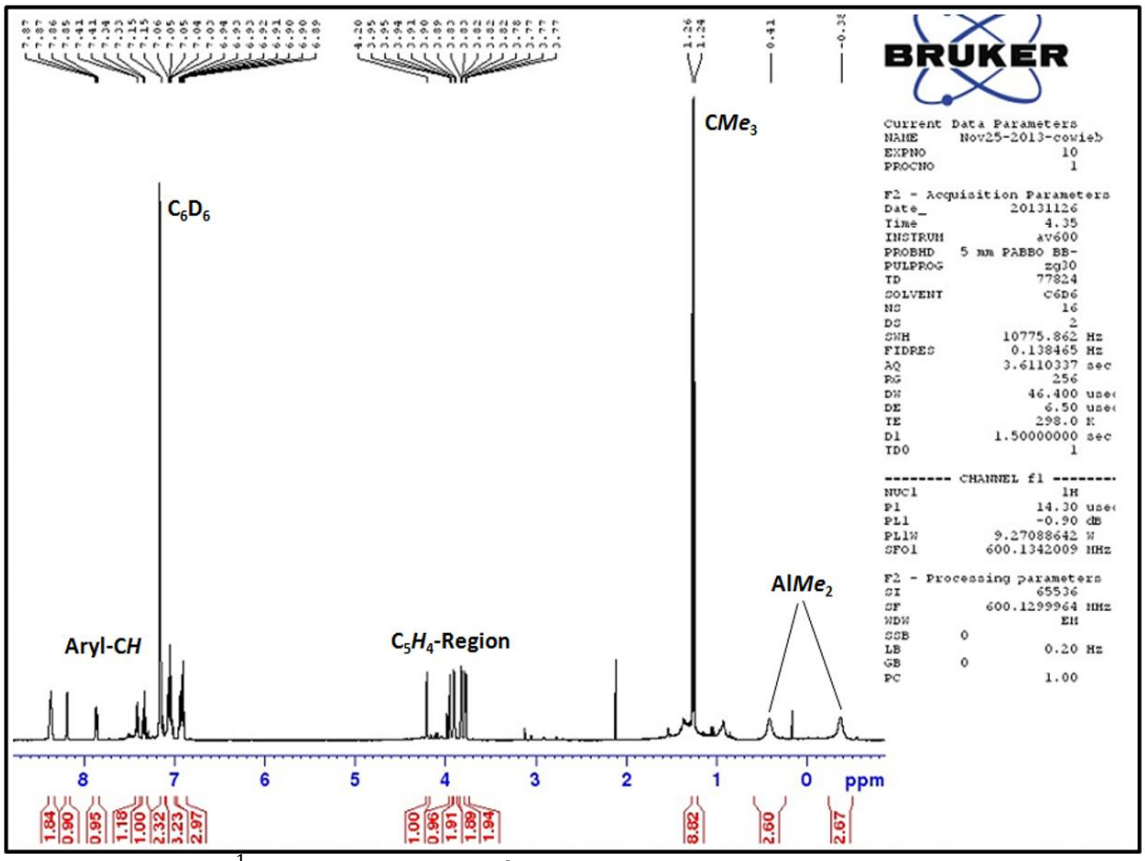

Figure 5.12. ^{1}H NMR spectrum of the FcPPAl ligand (600 MHz, 298 K, C_6D_6).

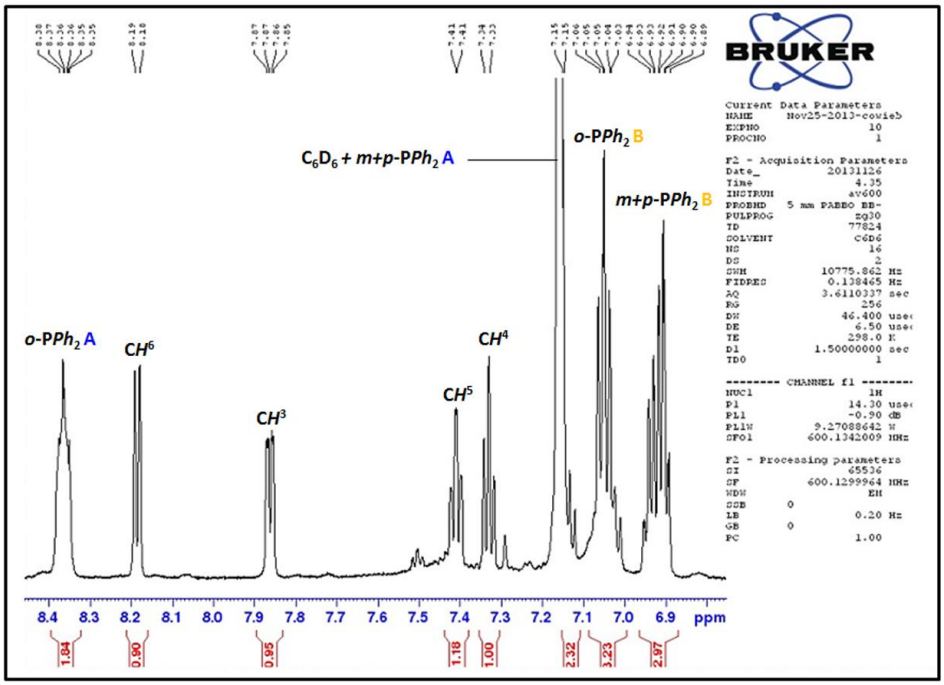

Figure 5.13. Expanded aromatic region of the ^{1}H NMR spectrum of FcPPAl (600 MHz, 298 K, C_6D_6).

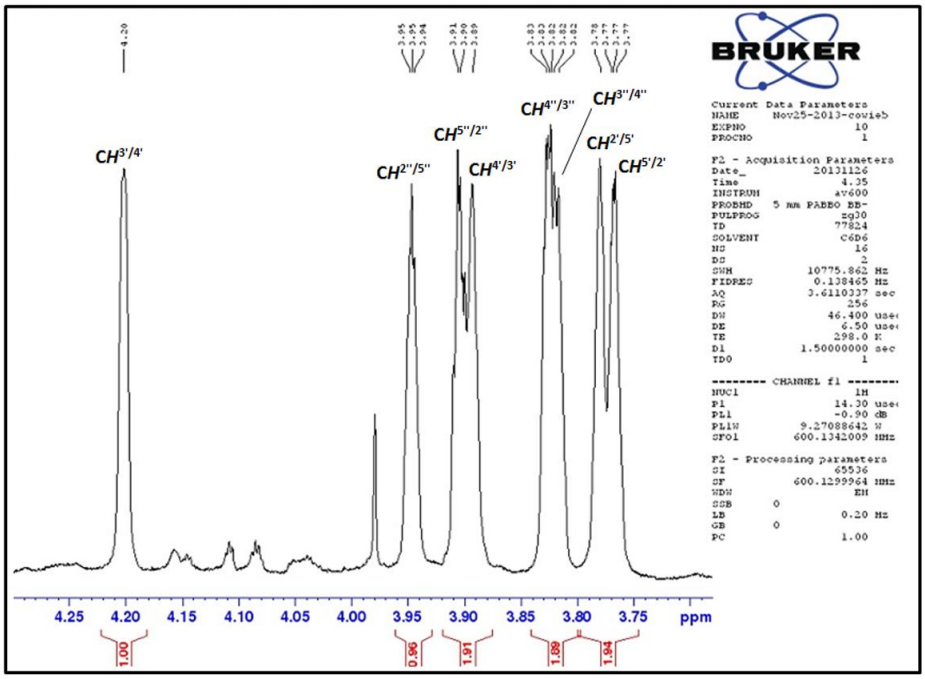

Figure 5.14. Expanded C_5H_4-region of the ^{1}H NMR spectrum of FcPPAl (600 MHz, 298 K, C_6D_6).

X-ray quality crystals of the FcPPAl ligand were obtained by slow diffusion of pentane into a toluene solution of FcPPAl at –30 °C, and in the solid-state P(1) is engaged in adduct formation with the alane, resulting in a P(1)–Al distance of 2.554(2) Å, and significant pyramidalization of aluminum [Σ(C–Al–C) = 339.9(3)°; Figure 5.15]. Shorter P–Al bond lengths were reported for $\{Ph_2PCH_2AlMe_2\}_2$ [P(1)–Al(2) = 2.5183(9) Å, P(2)–Al(1) = 2.4502(9) Å][246] and $Ph_3P–AlMe_3$ [P–Al = 2.535(1) Å],[247] and while similar pyramidalization of aluminum is observed in the former compound [Σ(C–Al–C) = 339.0(2)°],[246] aluminum is significantly less pyramidalized in the latter [Σ(C–Al–C) = 349.9(4)°].[247]

In the ^{31}P NMR spectrum of FcPPAl, the signals for the $C_5H_4P(^tBu)Ar$ and $C_5H_4PPh_2$ phosphines were observed at 0.4 and –19.0 ppm, respectively, with a ^{31}P-^{31}P coupling of 31 Hz (**D** in Figure 5.11). The magnitude of this coupling constant is indicative of through-space coupling arising from a non-bonding interaction between the lone pair on the $C_5H_4P(^tBu)Ar$ phosphine [P(2)] and the bonding pair between the $C_5H_4PPh_2$ phosphine [P(1)] and Al. Such couplings have rarely been observed, but can arise when NMR active nuclei are constrained to reside in close proximity with an appropriate orientation of the lone pair and bonding pair. For example, in $[MX_2\{\kappa^2PP\text{-}(1,2\text{-}PPh_2\text{-}4\text{-}^tBu\text{-}C_5H_2)_2Fe\}]$ (M = Ni, X = Br; M = Pd, X = Br, Cl) complexes, ^{31}P-^{31}P couplings of 24 to 31 Hz were observed for phosphorus atoms separated by between 3.64 and 3.84 Å;[187,248] the P(1)–P(2) distance in FcPPAl is 3.601(2) Å. Observation of through-space ^{31}P-^{31}P coupling for FcPPAl indicates that the P–Al interaction is maintained in solution at room temperature, and this interpretation is supported by inequivalence of the Al*Me*$_2$ groups in the ^1H and $^{13}C\{^1H\}$ NMR spectra. Increasing the temperature from 25 to 75 °C did not lead to loss of ^{31}P-^{31}P coupling despite coalescence of the Al*Me*$_2$ signals in the ^1H NMR spectrum, indicative of persistant adduct formation even at elevated temperatures.

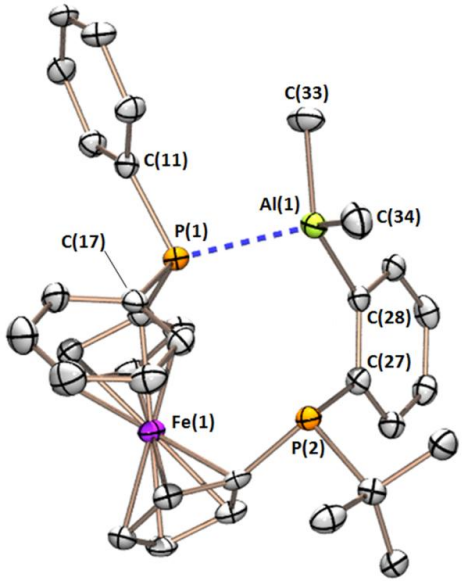

Figure 5.15. Solid-state structure of FcPPAl, obtained by Judy Tsao (supervised by B. E. Cowie) with ellipsoids drawn at 50% probability. Hydrogen atoms have been omitted for clarity.

A noteworthy feature of the FcPPAl ligand is preferential intramolecular adduct formation between aluminum and the C_5H_4*P*Ph_2 phosphine [P(1)], whereas in the FcPPB ligand intramolecular adduct formation occurs between boron and the C_5H_4*P*(^{t}Bu)Ar phosphine [P(2)]. The preference for the borane in FcPPB to coordinate to P(2) is likely a consequence of the unfavourable steric interactions between neighbouring phenyl substituents that would occur upon coordination of boron to P(1), resulting in adduct formation with P(2) despite the considerable strain associated with 4-membered ring formation.

Chapter 6

Group 10 Metal Complexes of a Borane-Appended Analogue of 1,1'-Bis(diphenylphosphino)ferrocene, FcPPB, and Comparison of Coordinative Properties with a Trisphosphine Derivative, FcPPP

Adapted with permission from: Cowie, B. E.; Emslie, D. J. H. *Organometallics* **2015**, *34*, 4093-4101. Copyright 2015 American Chemical Society.

Adapted with permission from: Cowie, B. E.; Emslie, D. J. H. *Chem. –Eur. J.* **2014**, *20*, 16899-16912. Copyright 2014 John Wiley & Sons.

6.1 – Introduction

Despite successful application of the TXPB ligand for the synthesis of late transition metal complexes featuring a variety of metal–borane and metal–co-ligand–borane bonding interactions, a new borane-containing ambiphilic ligand, 1'-{(*ortho*-diphenylborylphenyl)-*tert*-butylphosphino}-1-diphenylphosphinoferrocene (FcPPB), was synthesized, as outlined in Chapter 5.1. The principal impedus for transitioning from the TXPB ligand to the FcPPB ligand was the central thioether donor in TXPB, which is undesirably susceptible to displacement from the metal centre, especially in low valent complexes. For example, addition of dvds (dvds = 1,3-divinyltetramethydisiloxane) to [Pd(TXPB)] formed [Pd(η^2:η^2-dvds)(κ^1*P*-TXPB)], in which palladium is removed from the central binding pocket of the ligand and TXPB acts as a monodentate phosphine.[122] Furthermore, addition of CO to [Pd(TXPB)] resulted in complete displacement of the TXPB ligand from the metal – the FcPPB ligand was designed to provide a solution to the problems encountered with the TXPB ligand.

The reactivity of FcPPB with zero-valent nickel, palladium and platinum pre-cursors is discussed here-in. Additionally, the reactivity of [Pt(FcPPB)] with H_2, CO and CNXyl to afford platinum-FcPPB complexes featuring a range of different FcPPB coordination modes will be discussed. Furthermore, the unexpected reaction of phenylacetylene with [Pt(FcPPB)] to form a vinylborane complex is described. The

coordination behaviour of FcPPB is also compared with that of a trisphosphine analogue, [Fe(η^5-$C_5H_4PPh_2$){η^5-$C_5H_4P^tBu(C_6H_4PPh_2$-*o*)}] (FcPPP) (Scheme 5.3, *vide supra*), highlighting trends in the propensity of the resultant palladium and nickel complexes to bind dba and N_2.

Direct comparisons between the coordination behaviour of borane-containing ambiphilic ligands and conventional ligand analogues (ligands in which the borane is replaced by a σ-donor) are scarce,[§] especially for tridentate or tetradentate ligands. However, several prominent examples are discussed below. In some cases, the structures of ambiphilic ligand complexes and their conventional donor counterparts are analogous; for example, [FeF(TPP)] (TPP = {(*o*-$Ph_2P)C_6H_4$}$_3$P)[249] and [Na(12-C-4)$_2$][Fe(SiP^{iPr}_3)(N_2)] (12-C-4 = 12-crown-4; SiP^{iPr}_3 = {(*o*-^{i}$Pr_2P)C_6H_4$}$_3$Si)[250] adopt the same distorted trigonal bipyramidal coordination geometry as [FeX(^{iPr}TPB)] (^{iPr}TPB = {(*o*-^{i}$Pr_2P)C_6H_4$}$_3$B; X = Br, NH_2 or OH) and [Fe(N_2)(^{iPr}TBP)].[46,136] By contrast, [AuCl($PP^{Ph}P$)] (**A** in Figure 6.1; $PP^{Ph}P$ = {(*o*-$Ph_2P)C_6H_4$}$_2$PPh)[251] is pseudo-tetrahedral, whereas [AuCl(^{iPr}DPB^{Ph})] (**B**; ^{iPr}DPB^{Ph} = {(*o*-^{i}$Pr_2P)C_6H_4$}$_2$BPh)[44] approaches square planarity at gold. Additionally, while [Fe(SiP^{iPr}_3)(CO)Na($THF)_3$] (**C**)[252] is almost a perfect trigonal bipyramid at iron, [Fe(CO)(^{iPr}TPB)] (**D**)[46] features η^4*BCCP*-coordination, leading to a more complex geometry. Furthermore, while [{Ni($PP^{Me}P$)}$_2$(μ-N_2)] (**E**; $PP^{Me}P$ = {(*o*-$Ph_2P)C_6H_4$}$_2$PMe),[253] [{Ni(^{iPr}DPB^{Ph})}$_2$(μ-N_2)][40] (**F**) and [Ni(THF)(^{Ph}DPB^{Ph})][128] (^{Ph}DPB^{Ph} = {(*o*-$Ph_2P)C_6H_4$}$_2$BPh) are pseudo-tetrahedral, albeit with an η^2*BC*-arylborane interaction and more acute P–M–P angles in the ^{R}DPB^{Ph} complexes, related [Ni(^{Ph}DPB^{Mes})] (**G**; ^{Ph}DPB^{Mes} = {(*o*-$Ph_2P)C_6H_4$}$_2$BMes; Mes = 2,4,6-Me_3-C_6H_2) features an η^3*BCC*-arylborane interaction, and does not coordinate N_2 or THF (Figure 6.1).[128]

[§] Direct comparisons have been made between complexes of neutral {(*o*-$R_2P)C_6H_4$}$_3$B and monoanionic {(*o*-$R_2P)C_6H_4$}$_3$Si ligands with the same overall charge, but different electronic configurations. See for example refs 60 and 139.

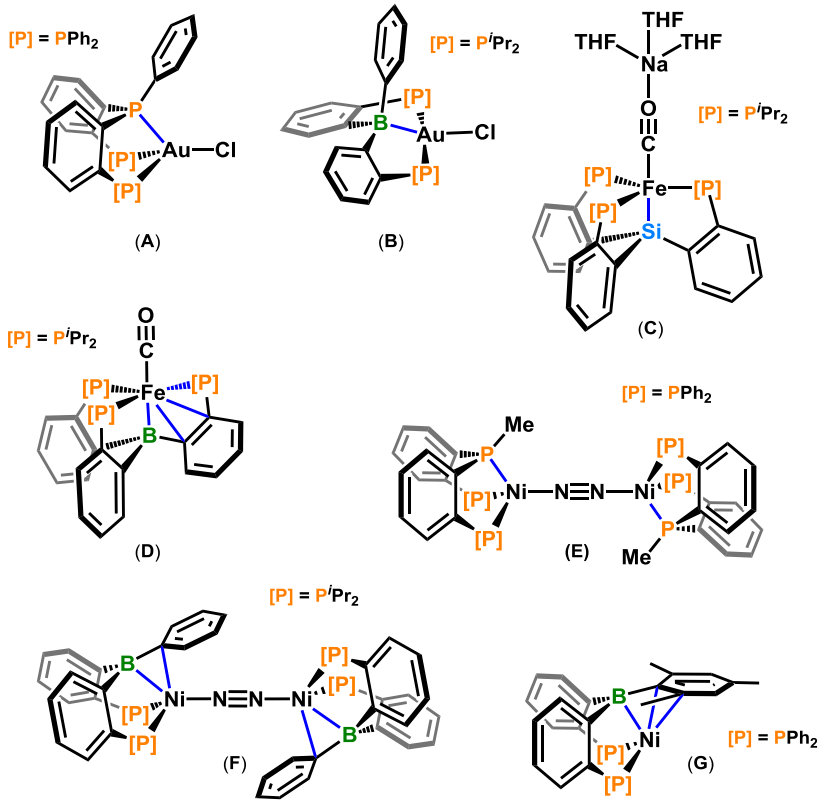

Figure 6.1. Trisphosphine and trisphosphine-silyl ligand complexes compared with analogues in which one neutral phosphine or anionic silyl donor is replaced with a borane Lewis acid.

6.2 – Isolation of [M(FcPPB)] (M = Ni, Pd, Pt) Complexes

The FcPPB ligand was prepared in a seven step convergent synthesis from commercially available ferrocene and 1,2-dibromobenzene, as outlined in Chapter 5.2. Reaction of FcPPB with either $[Ni(cod)_2]$ (cod = 1,5-cyclooctadiene), $[Pd_2(dba)_3]$ (dba = *trans*,*trans*-dibenzylideneacetone) or $[Pt(nb)_3]$ (nb = norbornene) in toluene afforded [Ni(FcPPB)] (**28**), [Pd(FcPPB)] (**29**) and [Pt(FcPPB)] (**30**) (Scheme 6.1). Complex **28** was isolated as a brick red solid in 78 % yield, complex **29** was obtained as a bright yellow solid in 63 % yield, and complex **30** was obtained as a pale yellow solid in 76 % yield. All three complexes feature low frequency solution ^{11}B NMR chemical shifts (28 ppm for **28**, 23 ppm for **29** and 21 ppm for **30**), indicative of metal–borane coordination.[244] Furthermore, all three complexes feature *cis*-κ^2*PP*-coordination, as

evidenced by $^{31}P\{^{1}H\}$ NMR chemical shifts of 47.3 and 12.2 ppm ($^{2}J_{31P,31P}$ = 29 Hz in C_6D_6) for **28**, 43.9 and 11.9 ppm ($^{2}J_{31P,31P}$ = 19 Hz in CD_2Cl_2) for **29**, and 51.3 ($^{1}J_{31P,195Pt}$ = 5657 Hz; $^{2}J_{31P,31P}$ = 55 Hz) and 28.4 ppm ($^{1}J_{31P,195Pt}$ = 4157 Hz; $^{2}J_{31P,31P}$ = 55 Hz) for **30** in CD_2Cl_2. In all cases, ^{1}H-^{31}P HMBC NMR spectroscopy allowed assignment of the higher frequency ^{31}P signal to the $C_5H_4P(^{t}Bu)Ar$ moiety. Displayed below in Figures 6.2–6.4 is the ^{1}H NMR spectrum of **29**, in addition to expanded views of the aromatic and C_5H_4-regions, which provides a representative example of a ^{1}H NMR spectrum for the [M(FcPPB)] complexes [M = Ni (**28**), Pd (**29**), Pt (**30**)]. Numbered protons refer to the positions on the ferrocene backbone and the phenylene linker, as shown in Scheme 6.1 below.

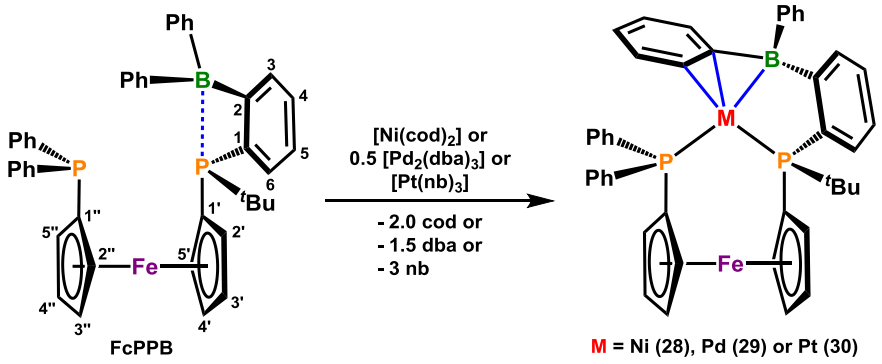

Scheme 6.1. Synthesis of [M(FcPPB)] [M = Ni (**28**), Pd (**29**), Pt (**30**)] complexes.

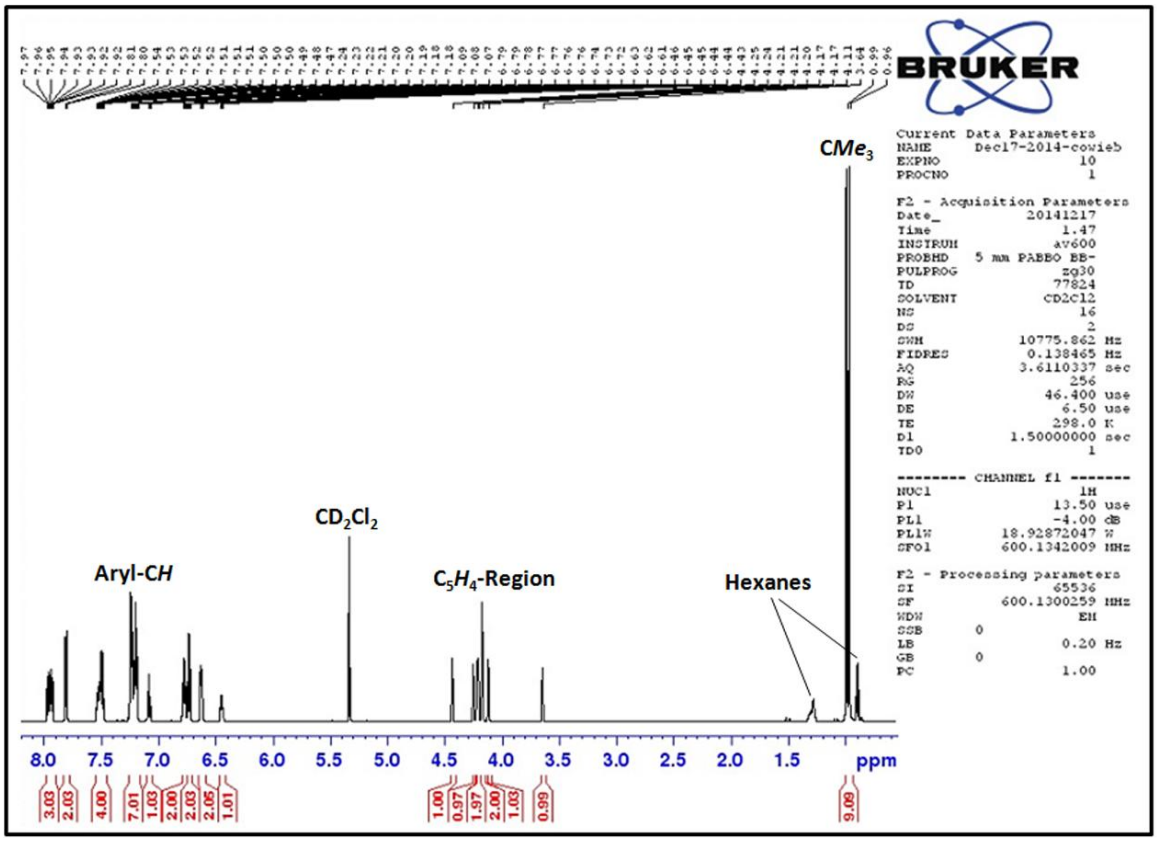

Figure 6.2. ^{1}H NMR spectrum of [Pd(FcPPB)] (**29**; 600 MHz, 298 K, CD_2Cl_2).

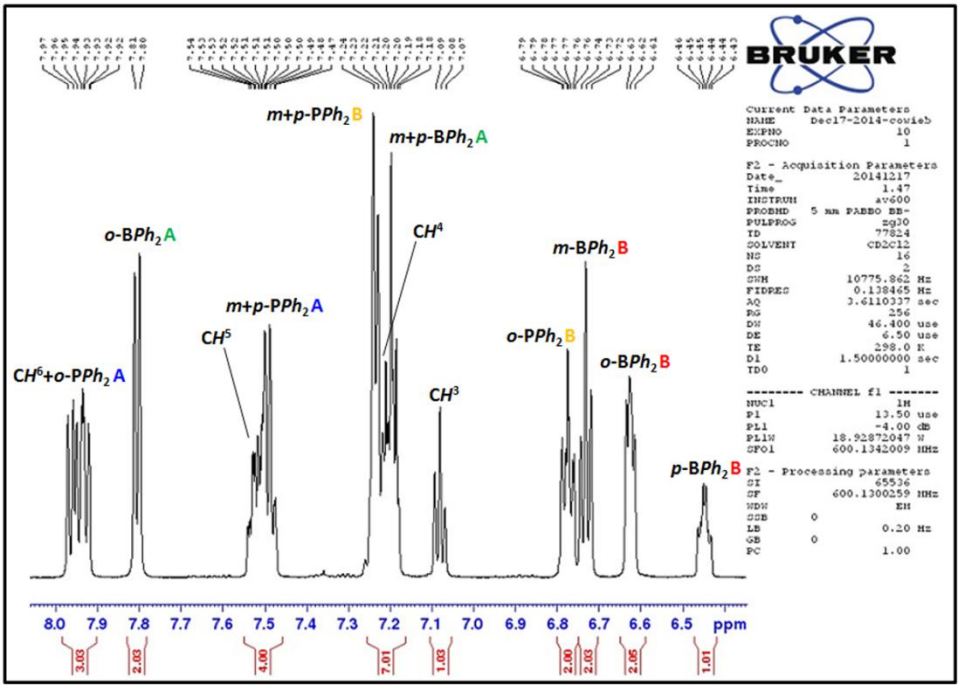

Figure 6.3. Expanded aromatic region of the ^{1}H NMR spectrum of [Pd(FcPPB)] (**29**; 600 MHz, 298 K, CD_2Cl_2).

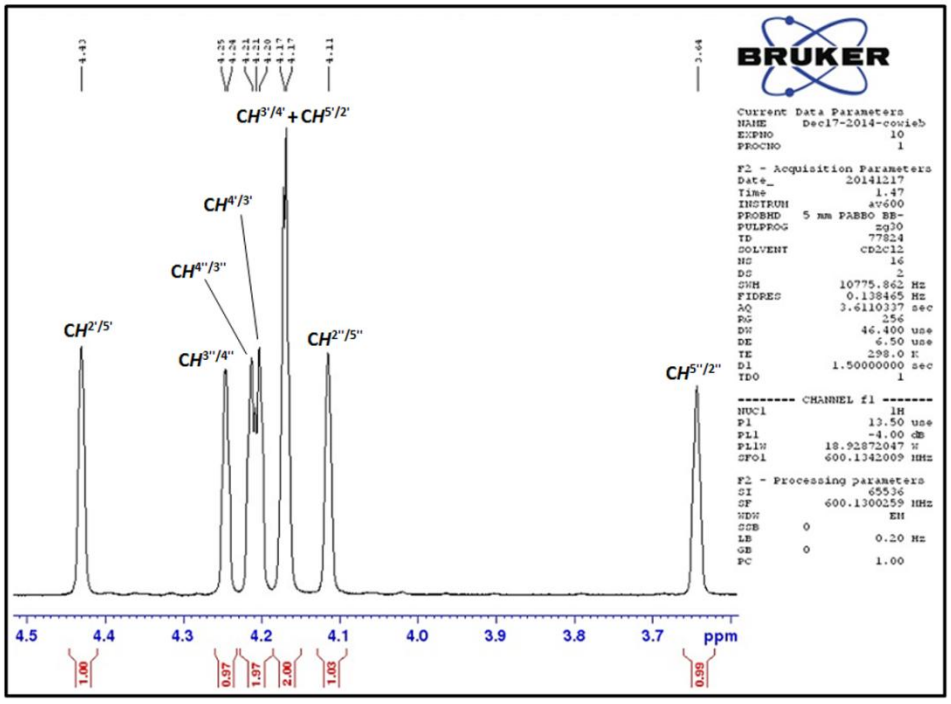

Figure 6.4. Expanded C_5H_4-region of the ^{1}H NMR spectrum of [Pd(FcPPB)] (**29**; 600 MHz, 298 K, CD_2Cl_2).

X-ray quality crystals of **28**·0.7(C_7H_8), **29**·$C_2H_4Cl_2$ and **30**·CH_2Cl_2 were obtained by slow diffusion of hexanes into a –30 °C solution of **28** in toluene, **29** in 1,2-dichloroethane and **30** in dichloromethane, respectively. The solid-state structures of **28**·0.7(C_7H_8), **29**·$C_2H_4Cl_2$ and **30**·CH_2Cl_2 are shown in Figures 6.5–6.7, and in all cases the FcPPB ligand is coordinated to the metal centre via both phosphine donors as well as an η^3*BCC*-interaction with boron and the *ipso*- and *ortho*-carbon atoms of a *B*-phenyl group; the M–B, M–C_{ipso} and M–C_{ortho} (M = Ni, Pd, Pt) bond lengths are 2.220(4), 2.058(4) and 2.101(4) Å in **28**, 2.279(4), 2.254(3) and 2.456(3) Å in **29**, and 2.292(3), 2.225(3) and 2.329(3) Å in **30**, and the P(1)–M–P(2) bite angles in **28**, **29** and **30** are 107.71(4)°, 112.07(3)° and 108.53(3)°, respectively. The metal centre in complexes **28**–**30** assumes a highly distorted square planar geometry, with '*trans*' P(1)–M–B and P(2)–M–C_{ipso}/C_{ortho} angles of 151.3(1) and 132.7(1)° in **28**, 163.8(1) and 128.1(1)° in **29** and 171.1(1) and 131.2(1)° in **30** (M = Ni, Pd, Pt; C_{ipso}/C_{ortho} = centroid between C_{ipso} and C_{ortho}), analogous to that in [Pt(η^3-allyl)(PPh_3)$_2$]$^+$.[254] In complex **28**, P(1), P(2), Ni, C_{ipso} and C_{ortho} form a plane, with B(1) located 1.072 Å out of the plane. By contrast, in complexes **29** and **30**, P(1), P(2), M, B(1) and C_{ortho} (M = Pd, Pt) lie approximately in the same plane, with C_{ipso} located 0.763 and 0.727 Å from the plane in **29** and **30**, respectively. In compound **28**, the non-coordinated *B*-phenyl ring is oriented away from the *tert*-butyl group on the central phosphine, whereas in **29** and **30**, it is positioned above the *tert*-butyl group.

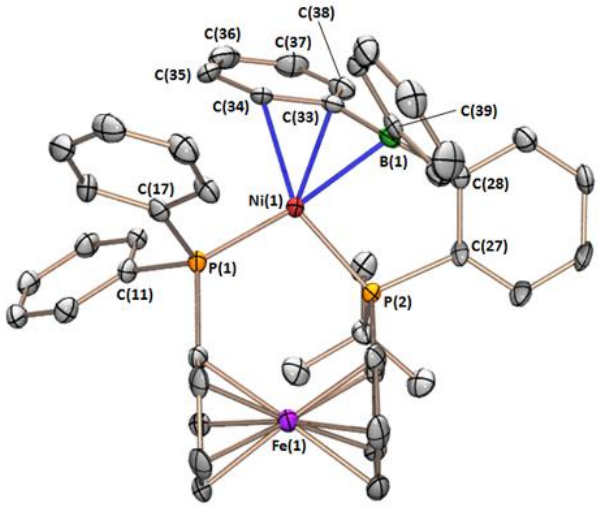

Figure 6.5. Solid-state structure for [Ni(FcPPB)]·0.7(C_7H_8) [**28**·0.7(C_7H_8)] with ellipsoids drawn at 50 % probability. Hydrogen atoms and lattice solvent have been omitted for clarity.

Boron is planar in **28** and only slightly pyramidalized in **29** and **30**, with the sum of the C–B–C angles equal to 359.1(6)° in **28**, 354.8(5)° in **29** and 354.3(5)° in **30**. An increase in pyramidalization of boron in **30** relative to **28** and **29**, in addition to a low frequency shift of the ^{11}B NMR signal for **30** (21 ppm, *vide supra*) is suggestive of a slightly stronger metal–boron bonding interaction in the platinum complex, likely due to the increased basicity of Pt relative to Pd and Ni.[133] However, despite observation of η^3*BCC*-coordination in the solid-state structures of **28–30**, the *ortho*- and *meta*-protons on the *B*-phenyl rings remain equivalent in the ^{1}H NMR spectra of these complexes from 25 to –90 °C, indicating that the η^3*BCC*-interaction is not maintained in solution.

The B–C_{ipso} bond length in **28** is 1.526(6) Å, which is significantly contracted relative to the other two B–C_{aryl} bonds [B–C(28) = 1.607(6) Å, B–C(39) = 1.614(6) Å]. The B–C_{ipso} bonds in **29** and **30** are also somewhat contracted, with B–C_{ipso} distances of 1.563(6) and 1.551(5) Å, respectively (the remaining B–C_{aryl} distances lie between 1.596(6) and 1.611(4) Å). For comparison, the B–C_α bond distances in the vinylborane and borataalkene complexes [Ni(PPh_3)$_2$(VB^{Ph})] (VB^{Ph} = (*E*)-PhHC=CH–B(C_6F_5)$_2$), [Pt(P^tBu_3)(VB^{Ph})],[255] [Cp_2Ta(CO){η^2*BC*-H_2CB(C_6F_5)$_2$}][200] and [Cp_2Ta(CN^tBu){η^2*BC*-

$H_2CB(C_6F_5)_2\}]$[256] are 1.483(4), 1.517(6)/1.519(7), 1.508(8) and 1.525(7) Å, respectively. The coordinated *B*-phenyl ring in **28** also shows considerable bond alternation with C(33)–C(34), C(34)–C(35), C(35)–C(36), C(36)–C(37), C(37)–C(38) and C(33)–C(38) distances of 1.443(5), 1.423(6), 1.365(7), 1.412(7), 1.354(6) and 1.449(6) Å, respectively. Similar bond alternation is also observed in **29** and **30**, with the equivalent bond lengths equal to 1.424(5), 1.404(6), 1.371(7), 1.397(6), 1.376(5) and 1.427(5) Å in **29**, and 1.443(4), 1.423(5), 1.360(5), 1.418(4), 1.368(5) and 1.437(4) Å in **30**. Furthermore, comparable bond length alternations have been observed by Peters and co-workers in $\eta^n BC_{n-1}$- (n = 3 or 4) coordinated arylborane complexes.[46,128,130]

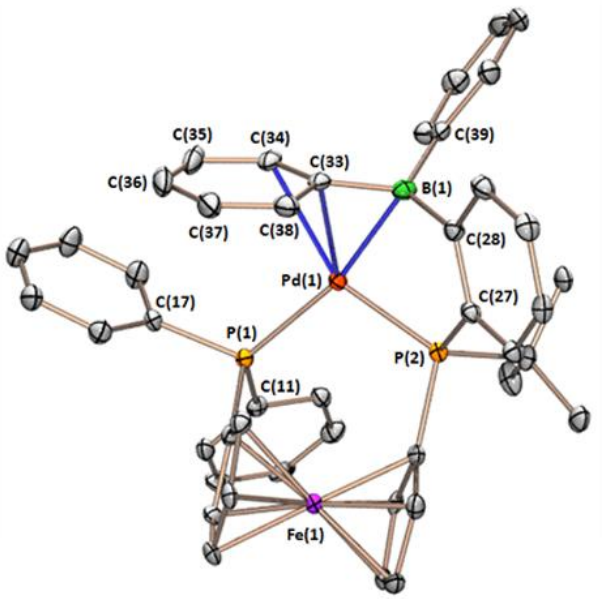

Figure 6.6. Solid-state structure for [Pd(FcPPB)]·$C_2H_4Cl_2$ (**29**·$C_2H_4Cl_2$) with ellipsoids drawn at 50 % probability. Hydrogen atoms and lattice solvent have been omitted for clarity.

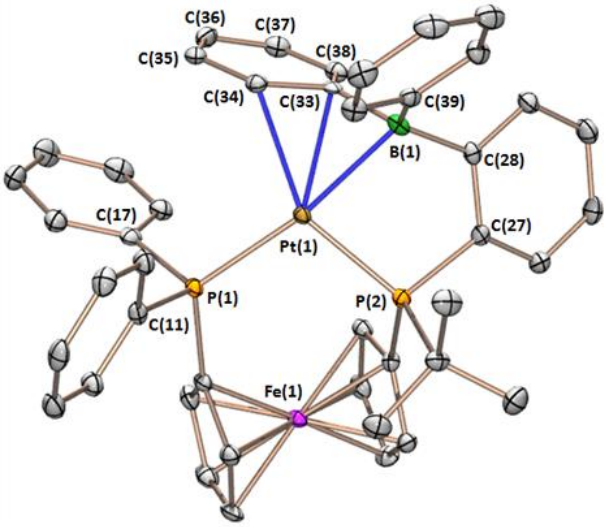

Figure 6.7. Solid-state structure for [Pt(FcPPB)]·CH_2Cl_2 (**30**·CH_2Cl_2) with ellipsoids drawn at 50 % probability. Hydrogen atoms and lattice solvent have been omitted for clarity.

The Ni–B bond length in **28** is significantly contracted relative to the Ni–B bond length in previously reported [Ni(TXPB)] [2.297(4) Å], while the Ni–C_{ipso} and Ni–C_{ortho} bond lengths in **28** are significantly elongated relative to those found in [Ni(TXPB)] [Ni–C_{ipso} = 2.019(3) Å; Ni–C_{ortho} = 2.081(3) Å].[122] The same trend is observed in the comparison of **29** with previously reported [Pd(TXPB)] [Pd–B = 2.320(5) Å; Pd–C_{ipso} = 2.198(4) Å; Pd–C_{ortho} = 2.325(4) Å].[122] This trend may reflect: (a) Differences in the backbone of the ligands, which alter the distance and orientation of the BCC unit relative to the metal coordination pocket defined by the phosphine donors, and/or (b) an intrinsically stronger metal–borane interaction in the FcPPB complexes due to the improved donor ability of the central phosphine in FcPPB, relative to the diarylthioether moiety in TXPB. For comparison, the [Ni(^{Ph}DPB^{Mes})] [^{Ph}DPB^{Mes} = {*o*-(Ph_2P)C_6H_4}$_2$BMes] complex reported by Peters also features η^3*BCC*-coordination of the arylborane, and in this case the Ni–B distance [2.1543(9) Å] is shorter than that in **28**, while the Ni–C_{ipso} and Ni–C_{ortho} bond lengths are longer than those in **28** [2.0751(8) and 2.1616(8) Å, respectively].[128]

Surprisingly, the reaction of FcPPB with $[Pd_2(dba)_3]$ differs from the reaction of TXPB with $[Pd_2(dba)_3]$; the latter reaction affords [Pd(μ-dba)(TXPB)], in which dba is η^3*CCC*-coordinated to palladium and κ^1*O*-coordinated to boron, yielding a zwitterionic palladium(II) boratoxyallyl ($CHPhCHCR–O–BAr_3$) complex (Scheme 6.2).[59] Moreover, dba does not react with **28**, whereas addition of one equivalent of dba to [Ni(TXPB)] yields [Ni(μ-dba)(TXPB)] (**31**), as evidenced by the consumption of free dba while maintaining coordination of TXPB ($^{31}P\{^1H\}$ NMR (C_6D_6) = 34.1 ppm versus 33.9 ppm for [Ni(TXPB)]), in addition to a low frequency shift of the ^{11}B NMR signal from 30 ppm in [Ni(TXPB)] to 5 ppm (C_6D_6; ^{11}B NMR = 5 ppm for [Pd(μ-dba)(TXPB)]).[59] The divergent reactivity of FcPPB and TXPB can most straightforwardly be rationalized on the basis of steric differences in the ambiphilic ligand backbones, given that greater electron donation from the central donor of FcPPB versus TXPB would be expected to promote zwitterion formation.

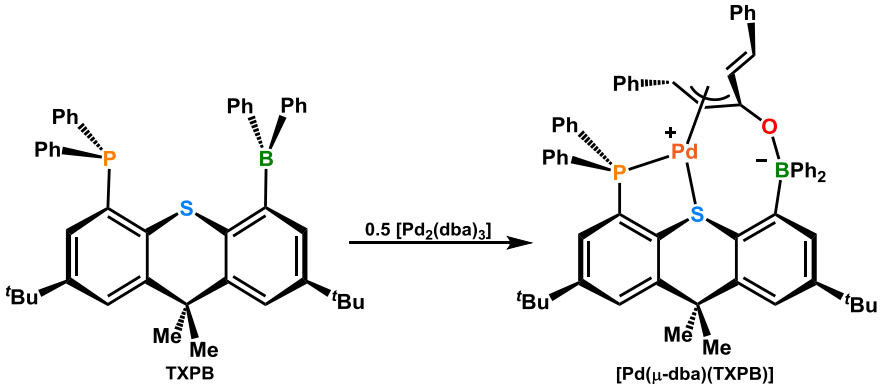

Scheme 6.2. Reaction of TXPB with 0.5 equivalents of $[Pd_2(dba)_3]$, yielding [Pd(μ-dba)(TXPB)].

6.3 – Comparison of the Coordinative Properties of FcPPB Relative to a Trisphosphine Analogue, FcPPP, with Nickel and Palladium

In order to probe the extent to which the coordination chemistry of the FcPPB ligand differs from that of a conventional tridentate ligand, a trisphosphine analogue of FcPPB, $[Fe(\eta^5\text{-}C_5H_4PPh_2)(\eta^5\text{-}C_5H_4P^tBu\{C_6H_4(PPh_2)\text{-}o\})]$ (FcPPP) was developed. This

FcPPP ligand was synthesized following a route analogous to that used to prepare FcPPB, but with the addition of Ph_2PCl, rather than Ph_2BBr, to [Fe(η^5-$C_5H_4PPh_2$)(η^5-$C_5H_4P^tBu\{C_6H_4Li\text{-}o\}$] (Chapter 5.2, Scheme 5.3).

Reaction of FcPPP with [Ni(cod)$_2$] yielded a red/orange solid in 87 % yield (Scheme 6.3). While elemental analysis (C and H) indicates the stoichiometry of the product is "Ni(FcPPP)" (**32**), ^{1}H and ^{31}P{^{1}H} NMR spectra between 195 and 348 K feature numerous broadened signals (15 signals in the ^{31}P NMR spectrum at 195 K), consistent with a mixture of isomers in rapid equilibrium. Importantly though, all signals in the ^{31}P{^{1}H} NMR spectra are located between 60 and 15 ppm, indicative of κ^3*PPP*-coordination, which suggests the involvement of multinuclear complexes, rather than complexes featuring different FcPPP ligand denticities.

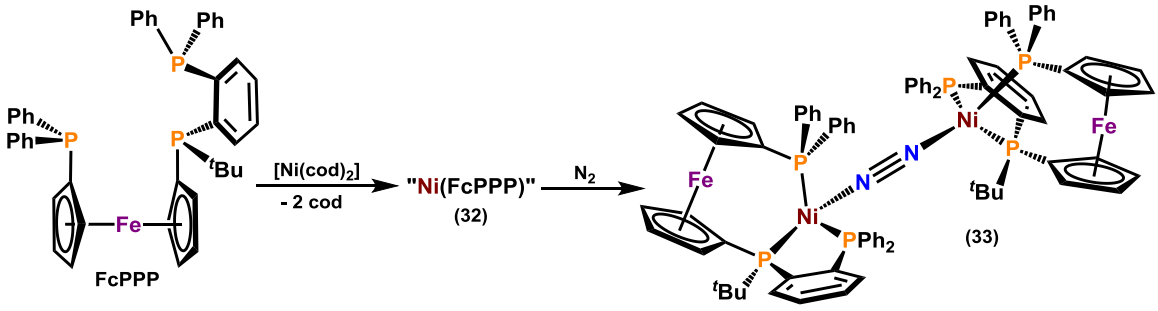

Scheme 6.3. Reaction of FcPPP with [Ni(cod)$_2$], which ultimately provides [{Ni(FcPPP)}$_2$(μ-N_2)] (**33**) in the presence of trace N_2.

Attempts were made to obtain X-ray quality crystals of **32** by slow diffusion of hexanes into a solution of **32** in benzene at room temperature in an argon-filled glove box. However, ruby red crystals of *rac*-[{Ni(FcPPP)}$_2$(μ-N_2)]·(C_6H_6)(C_6H_{14}) [*rac*-**33**·(C_6H_6)(C_6H_{14})] (Figure 6.8) were invariably isolated due to the reaction of **32** with trace nitrogen in the glovebox atmosphere. Dimetallic **33** was also isolated on a preparative scale in 64 % yield by placing a solution of **32** in benzene/hexanes under 1 atm of N_2 at room temperature (Scheme 6.3). Complex **33** is stable *in vacuo* in the solid-state, and is only slightly soluble in THF; N_2 is not displaced by THF after days in solution. In THF-d_8, compound **32** gave rise to signals at 51.6, 35.6 and 19.2 ppm in the

$^{31}P\{^{1}H\}$ NMR spectrum ($^{2}J_{P,P}$ = 59-87 Hz), which are in the same range as the signals observed for **32**. Clean conversion of **32** to **33** further supports the identification of **32** as "Ni(FcPPP)"; the ^{1}H NMR spectrum of **33**, in addition to expanded views of the aromatic and C_5H_4-regions are given below in Figures 6.9–6.11.

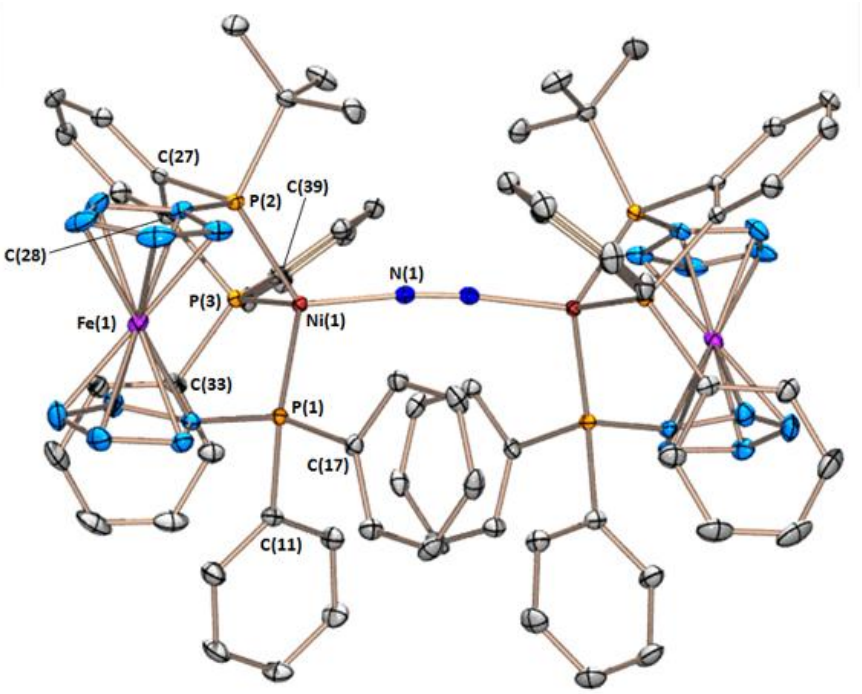

Figure 6.8. Solid-state structure of *rac*-[{Ni(FcPPP)}$_2$(μ-N_2)]·(C_6H_6)(C_6H_{14}) [**33**·(C_6H_6)(C_6H_{14})] with ellipsoids drawn at 50 % probability. Hydrogen atoms and lattice solvent have been omitted, and the carbon atoms of the ferrocene backbone of each FcPPP unit are coloured slate blue for clarity.

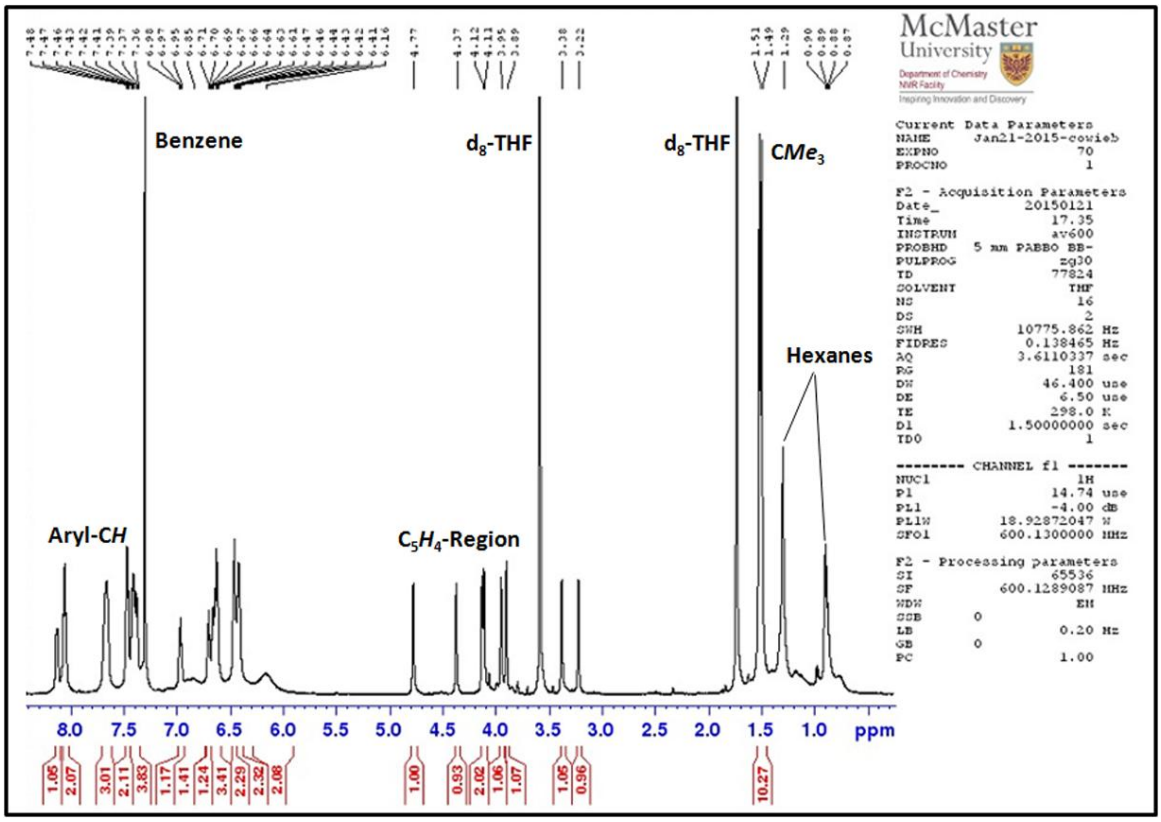

Figure 6.9. ^{1}H NMR spectrum of [{Ni(FcPPP)}$_2$(μ-N$_2$)] (**33**; 600 MHz, 298 K, THF-d$_8$).

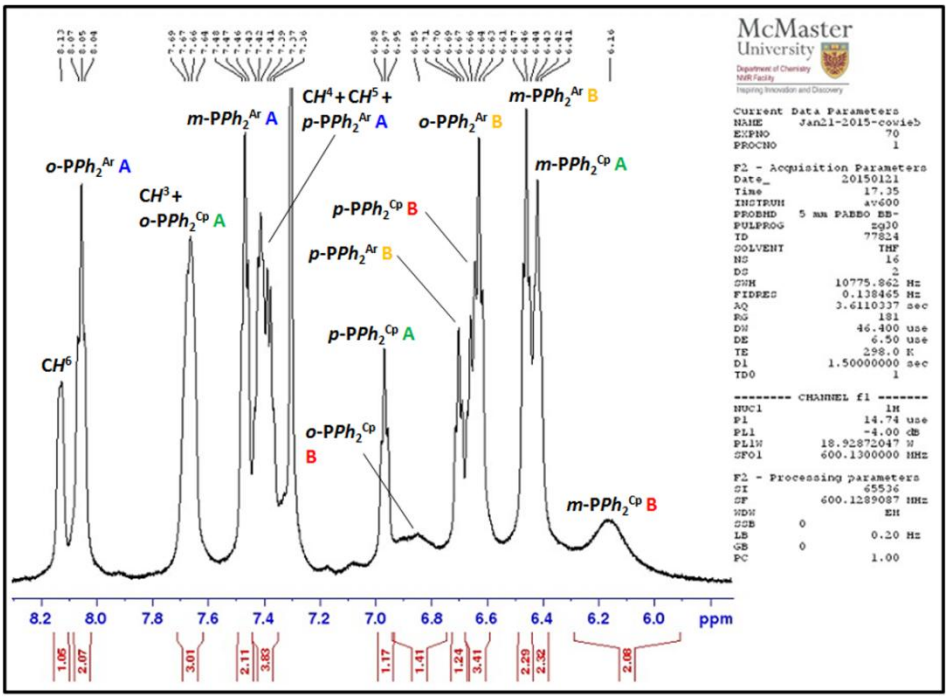

Figure 6.10. Expanded aromatic region of the ^{1}H NMR spectrum of [{Ni(FcPPP)}$_2$(μ-N$_2$)] (**33**; 600 MHz, 298 K, THF-d$_8$).

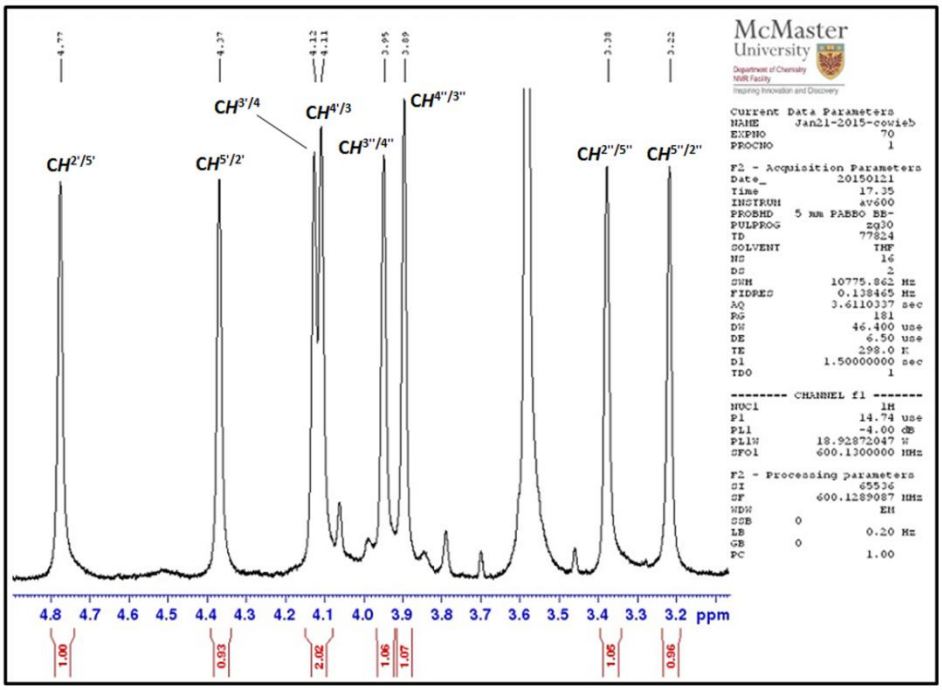

Figure 6.11. Expanded C$_5$*H*$_4$-region of the ^{1}H NMR spectrum of [{Ni(FcPPP)}$_2$(μ-N$_2$)] (**33**; 600 MHz, 298 K, THF-d$_8$).

In the solid-state structure of **33**, a molecule of N_2 bridges between two Ni(FcPPP) units. The Ni–P(1), Ni–P(2) and Ni–P(3) bond lengths are 2.1699(5), 2.1643(5) and 2.1474(5) Å, respectively, and the geometry of each nickel centre is pseudo-tetrahedral, with the P–Ni–P and P–Ni–N angles ranging from 91.50(2) to 118.32(5)°. The bridging N_2 unit is coordinated end-on [Ni–N(1)–N(1') = 174.12(7)°] to both Ni centers with a Ni–N bond distance of 1.840(2) Å, and a N≡N distance of 1.122(3) Å, which is only very slightly elongated relative to that in free N_2.

Very similar structural features were observed in [{Ni(PP^RP)}$_2$(μ-N_2)] (PP^RP = {(*o*-^{i}Pr$_2$P)C$_6$H$_4$}$_2$PR; R = Me, OMe) reported by Lee and co-workers, in which each Ni centre is also pseudo-tetrahedral with Ni–N bond lengths of 1.830(2) and 1.837(4) Å, N–N bond lengths of 1.124(3) and 1.112(5) Å, and Ni–N–N bond angles of 178.6(2) and 176.3(4)°, respectively (in solution under N_2, both dimetallic complexes exist in equilibrium with a monometallic N_2-species).[253,257] Peters *et al.* have also reported the synthesis of [Ni(N_2)($^{i\text{Pr}}$DPB$^{\text{Ph}}$)] ($^{i\text{Pr}}$DPB$^{\text{Ph}}$ = {(*o*-^{i}Pr$_2$P)C$_6$H$_4$}$_2$BPh), which crystallized with three independent molecules within the unit cell, two of which are [Ni(N_2)($^{i\text{Pr}}$DPB$^{\text{Ph}}$)] and one of which is [{Ni($^{i\text{Pr}}$DPB$^{\text{Ph}}$)}$_2$(μ-N_2)]. Similarly to **33**, the nickel centre in the dimetallic compound is pseudo-tetrahedral with Ni–N and N–N bond lengths of 1.920(1) and 1.123(3) Å, respectively.[40] The N≡N stretching frequency in **33** is 2006 cm^{-1}, which is shifted to lower frequency relative to the aforementioned [{Ni(PP^RP)}$_2$(μ-N_2)] complexes [ν(N≡N) = 2045 cm^{-1} (R = Me) and 2038 cm^{-1} (R = OMe)]. However, it is consistent with the crystallographically determined N–N bond length, according to the plot of N–N bond distance versus N–N stretching frequency in a 2010 review by Holland.[258]

The reaction of FcPPP with 0.5 equivalents of [Pd$_2$(dba)$_3$] produced a bright orange solid in 76 % yield, identified as [Pd(η^2-dba)(FcPPP)] (**34**) (Scheme 6.4). Elemental analysis is consistent with this formulation, but similarly to **32**, complete characterization of **34** by ^{1}H and ^{13}C NMR spectroscopy was hampered by fluxional behaviour involving multiple solution isomers. Nevertheless, the room temperature

$^{31}P\{^{1}H\}$ NMR spectrum of **34** gave rise to broad singlets at 57.3, 38.9 and –16.7 ppm ($\omega_{1/2}$ ~ 150 Hz, C_6D_6), indicative of an equilibrium between κ^2*PP*- rather than κ^3*PPP*-coordinated isomers. These signals decoalesce at low temperature, and at 230 K, the non-coordinated C_5H_4*P*Ph_2 phosphine signal split into four sharp singlets at –17.90, –18.16, –18.22 and –18.25 ppm in an approximate 6:2:3:3 ratio, consistent with four κ^2*PP*-coordinated solution isomers. Furthermore, four *tert*-butyl resonances were observed in the ^{1}H NMR spectrum of **34** at 230 K, with $^{3}J_{1H,31P}$ couplings of 12-15 Hz.

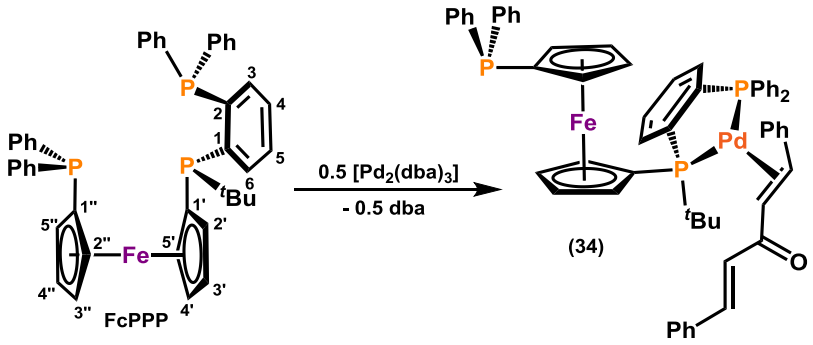

Scheme 6.4. Synthesis of [Pd(η^2-dba)(FcPPP)] (**34**) via reaction of FcPPP with 0.5 equivalents of [$Pd_2(dba)_3$].

X-ray quality crystals of **34**·CH_2Cl_2 were obtained by slow diffusion of hexanes into a solution of **34** in CH_2Cl_2 at –30 °C (Figure 6.12). The solid-state structure of **34**, representing one of the accessible solution isomers, confirms κ^2*PP*-coordination via the C_5H_4*P*(^{t}Bu)Ar and Ar*P*Ph_2 phosphines (Ar = phenylene linker), with a P(2)–Pd–P(3) bite angle of 87.11(6)°, and Pd–P(2) and Pd–P(3) bond lengths of 2.308(2) and 2.253(2) Å; the C_5H_4*P*Ph_2 phosphine remains uncoordinated and is positioned 7.500(2) Å from the metal centre. One molecule of dba is η^2*CC*-coordinated to palladium, with Pd–C(51) and Pd–C(52) bond lengths of 2.113(6) and 2.160(6) Å, respectively. The C–C bond length of the η^2*CC*-coordinated unit [C(51)–C(52)] is 1.416(9) Å, which is significantly elongated relative to the C=C bond of free dba [1.315(9) Å]. Similar deviations in C–C bond lengths are observed in [Pd(η^2-dba)(PPh_3)$_2$], [Pd(η^2-dba)(PCy_3)$_2$][259] and [Pd(η^2-dba){κ^2*PP*-{(*o*-^{i}Pr_2P)C_6H_4}$_2$$CH_2$}],[260] consistent with metallacyclopropane bonding of the coordinated

alkene. The geometry at palladium in **34** is pseudo-square planar, with P(2)–Pd–C(51) and P(3)–Pd–C(52) bond angles equal to 164.8(2) and 146.7(2)°, respectively.

The inability of the FcPPP ligand to completely displace dba from palladium contrasts the reactivity of FcPPB with $[Pd_2(dba)_3]$. Similarly, [Ni(FcPPB)] (**28**) did not react with dba, whereas nickel-FcPPP complexes **32** and **33** reacted with dba to form a new product, presumably [Ni(η^2-dba)(FcPPP)]; this compound exists as two major isomers in solution at room temperature, as evidenced by two distinct *tert*-butyl resonances in the ^{1}H NMR spectrum at 0.95 and 0.71 ppm ($^3J_{1H,31P}$ = 14 Hz), and two singlets in the $^{31}P\{^1H\}$ NMR spectrum at –16.7 and –16.9 ppm, assigned as the uncoordinated $C_5H_4PPh_2$ phosphine of the two different species (the remaining two ^{31}P NMR signals were located at 65.4 and 50.2 ppm, each appearing as a doublet: $^2J_{31P,31P}$ = 54 Hz).

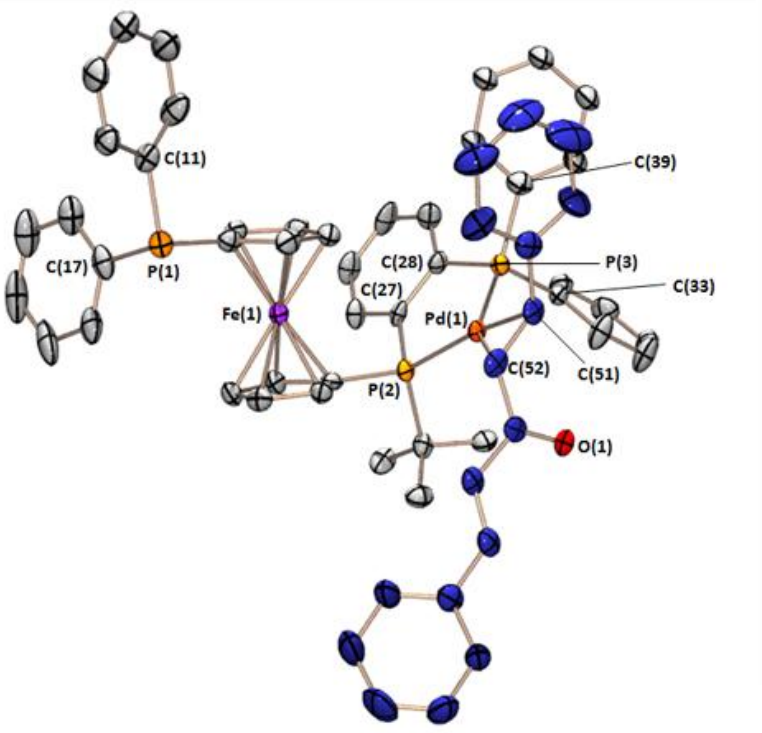

Figure 6.12. Solid-state structure of [Pd(η^2-dba)(FcPPP)]·CH_2Cl_2 (**34**·CH_2Cl_2) with ellipsoids drawn at 50 % probability. Hydrogen atoms and lattice solvent have been omitted, and the carbon atoms of the η^2*CC*-coordinated dba co-ligand are coloured navy blue for clarity. The *P*-phenyl ring containing atoms C(39)–C(44) is disordered over two positions; position B is omitted for clarity.

6.4 – Reactivity of [Pt(FcPPB)] with CO, CNXyl and H_2

Reaction of [Pt(FcPPB)] (**30**) with CO or CNXyl (Xyl = 2,6-Me_2-C_6H_3) afforded [Pt(CO)(FcPPB)] (**35**) and [Pt(CNXyl)(FcPPB)] (**36**) (Scheme 6.5) with ν(CO) and ν(CN) of 1982 and 2128 cm^{-1} in CH_2Cl_2, respectively, consistent with terminally bound carbonyl and isonitrile ligands.[204,261] Compound **35** did not react with $B(C_6F_5)_3$, whereas compound **36** reacted with $B(C_6F_5)_3$ over several days at 90 °C to re-form complex **30** and XylNC–$B(C_6F_5)_3$ [^{11}B NMR (C_6D_6): δ –21]. For **35** and **36**, as in complex **30**, each of the *B*-phenyl groups gave rise to just three signals in the ^{1}H NMR spectrum between 25 and –90 °C. The ^{11}B chemical shifts for **35** and **36** are 19 and 10 ppm, consistent with four-coordinate boron. The ^{1}H NMR spectra of **35** and **36**, along with expanded views of the aromatic and C_5H_4-regions are displayed below in Figures 6.13–6.15 and Figures 6.17–6.19, respectively.

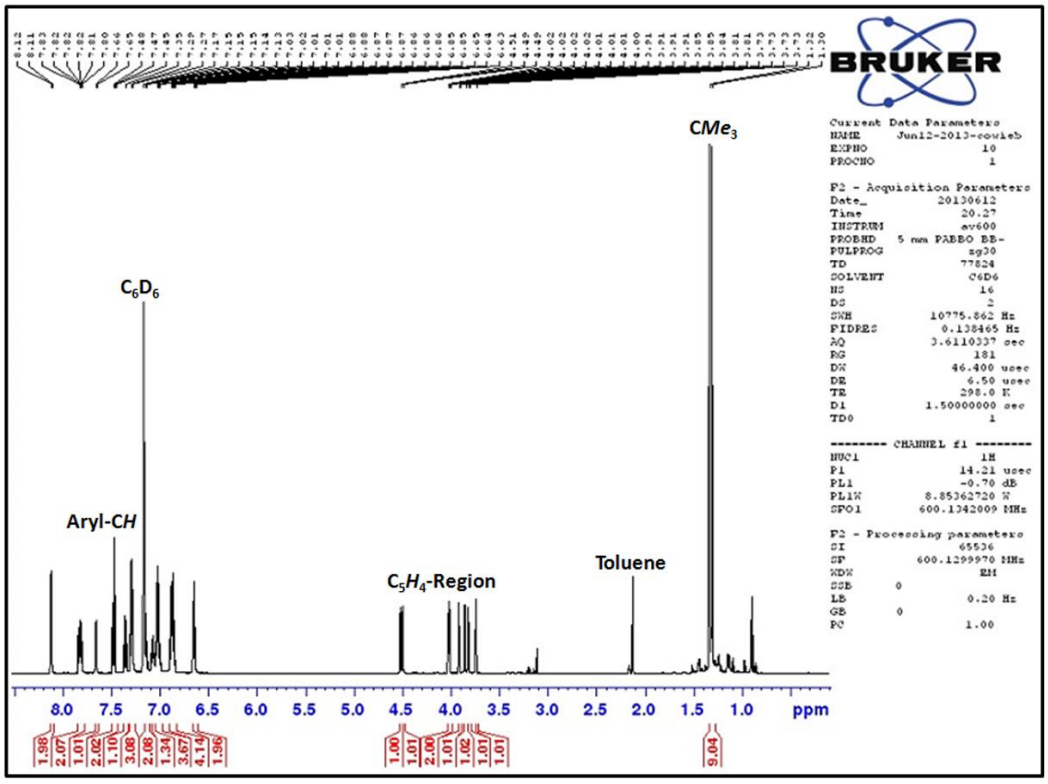

Figure 6.13. ^{1}H NMR spectrum of [Pt(CO)(FcPPB)] (**35**; 600 MHz, 298 K, C_6D_6).

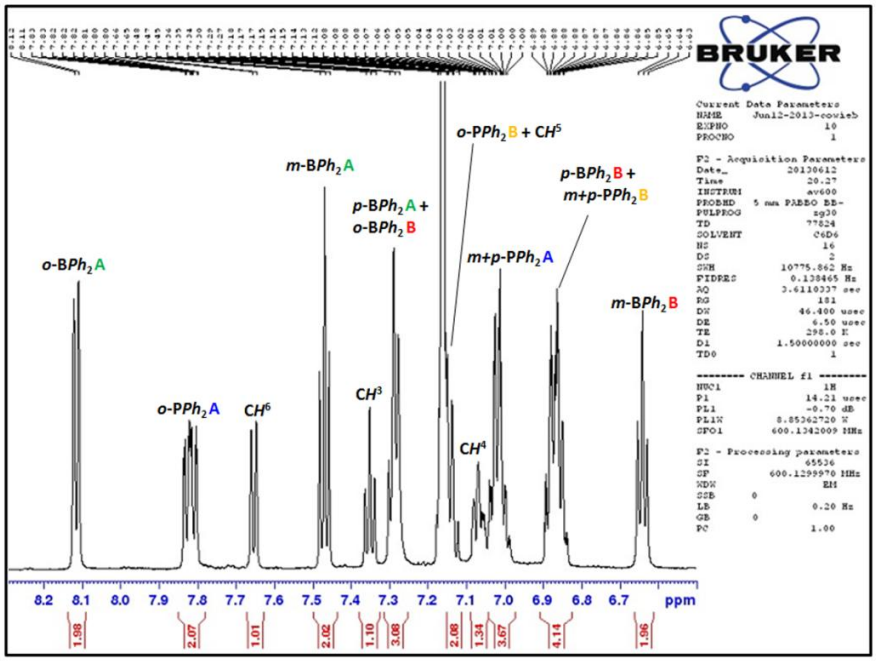

Figure 6.14. Expanded aromatic region of the ^{1}H NMR spectrum of [Pt(CO)(FcPPB)] (**35**; 600 MHz, 298 K, C_6D_6).

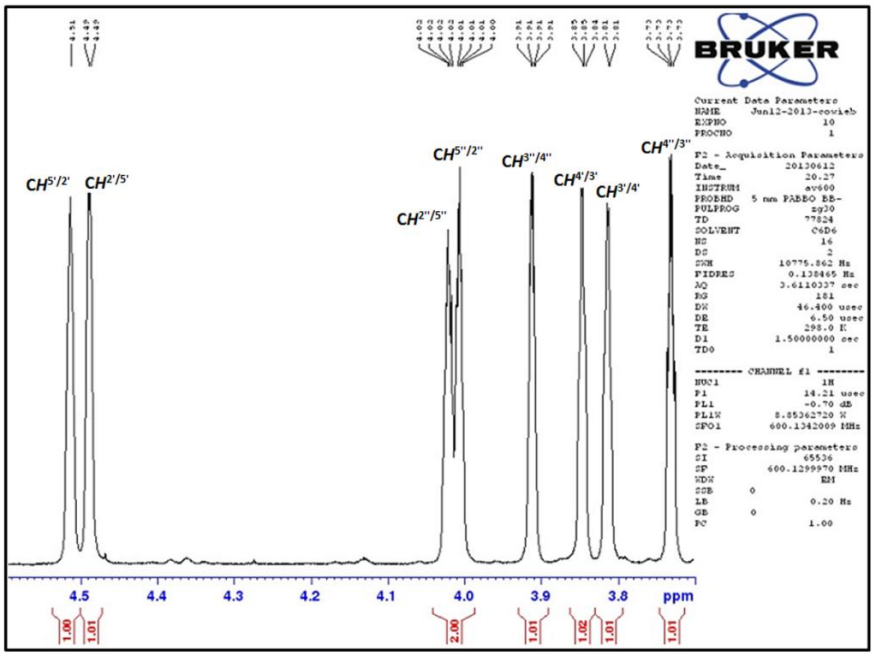

Figure 6.15. Expanded C_5H_4-region of the ^{1}H NMR spectrum of [Pt(CO)(FcPPB)] (**35**; 600 MHz, 298 K, C_6D_6).

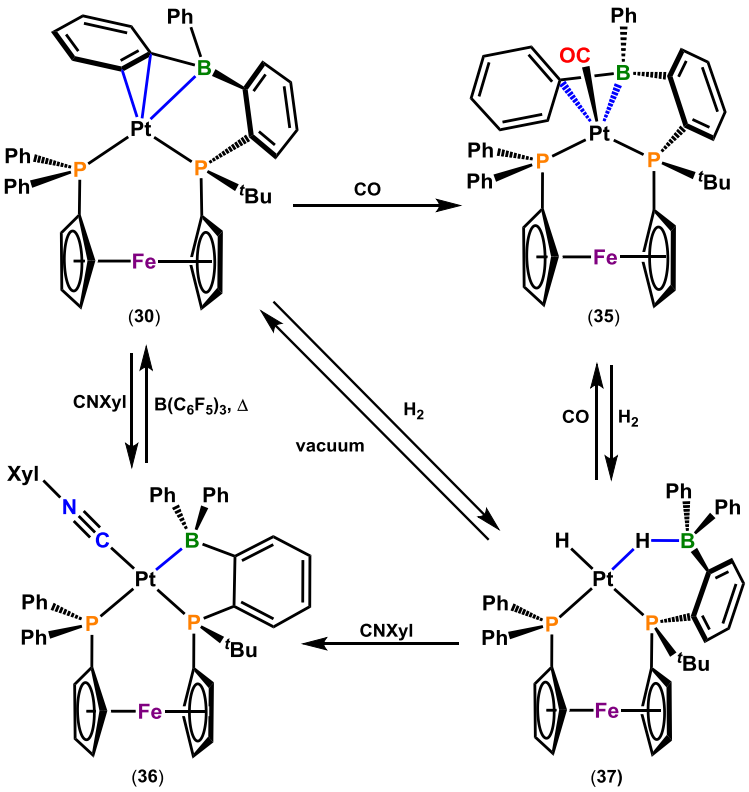

Scheme 6.5. Reactivity of [Pt(FcPPB)] (**30**) with CO, CNXyl and H_2, providing [Pt(CO)(FcPPB)] (**35**), [Pt(CNXyl)(FcPPB)] (**36**) and [PtH(μ-H)(FcPPB)] (**37**), respectively.

Single crystals of [Pt(CO)(FcPPB)]·2CH_2Cl_2 (**35**·2CH_2Cl_2) were obtained from CH_2Cl_2/hexane at –30 °C, and X-ray diffraction revealed that the η^3*BCC*-arylborane coordination mode in **30** has been converted to an η^2*BC*-coordination mode in **35** (**A** in Figure 6.16). The two phosphorus donors, CO and C_{ipso} [C_{CO} = C(45) ; C_{ipso} = C(33)] adopt a distorted tetrahedral arrangement around platinum with a 73.2° angle between the P(1)–Pt–P(2) plane and the C(33)–Pt–C(45) plane (the angle between the the P(1)–Pt–P(2) plane and the B–Pt–C(45) plane is 50.4°). The P(1)–Pt–P(2), P(X)–Pt–C(45) (X = 1 or 2), P(2)–Pt–C(33) and C(33)–Pt–C(45) angles are all between 100 and 107°, whereas P(2)–Pt–C(45) is 134.0(2)°. The Pt–B and Pt–C_{ipso} distances are 2.319(5) and 2.490(5) Å, respectively, and boron is significantly pyramidalized with the sum of the C–B–C angles equal to 345.0(7)°. Related Group 10 complexes featuring bisphosphine and η^2*BC*-

arylborane coordination include [Ni(THF)(^{Ph}DPB^{Ph})] [^{R}DPB^{Ph} = {(*o*-R_2P)C_6H_4}$_2$BPh; Ni–B: 2.124(2) Å; Ni–C_{ipso}: 2.176(2) Å; Σ(C–B–C): 352.1(3)°],[128] and [Ni(N_2)(^{iPr}DPB^{Ph})] [Ni–B: 2.201(2)/2.181(2) Å; Ni–C_{ipso} : 2.170(2)/2.149(2) Å; Σ(C–B–C): 353°; ^{11}B NMR 20 ppm].[40] Similarly to **35**, the two phosphorus donors, C_{ipso} and the remaining co-ligand (THF and N_2, respectively), in the above nickel complexes exhibit distorted tetrahedral geometry. While the M–B bond lengths in the above two literature complexes are in good agreement with **35**, taking into account the smaller covalent radius of Ni (1.24 Å) versus Pt (1.36 Å),[68] the M–C_{ipso} bond length in **35** is significantly longer than those in the nickel complexes and boron is more pyramidal, indicating that the arylborane–platinum coordination in **35** consists of a strong Pt–B and a weak Pt–C_{ipso} bonding interaction. The Pt–C_{ipso} distance in **35** is also significantly longer than either the Pt–C_{ipso} or the Pt–C_{ortho} distance in [Pt(FcPPB)] (**30**), despite comparable Pt–B bond lengths.

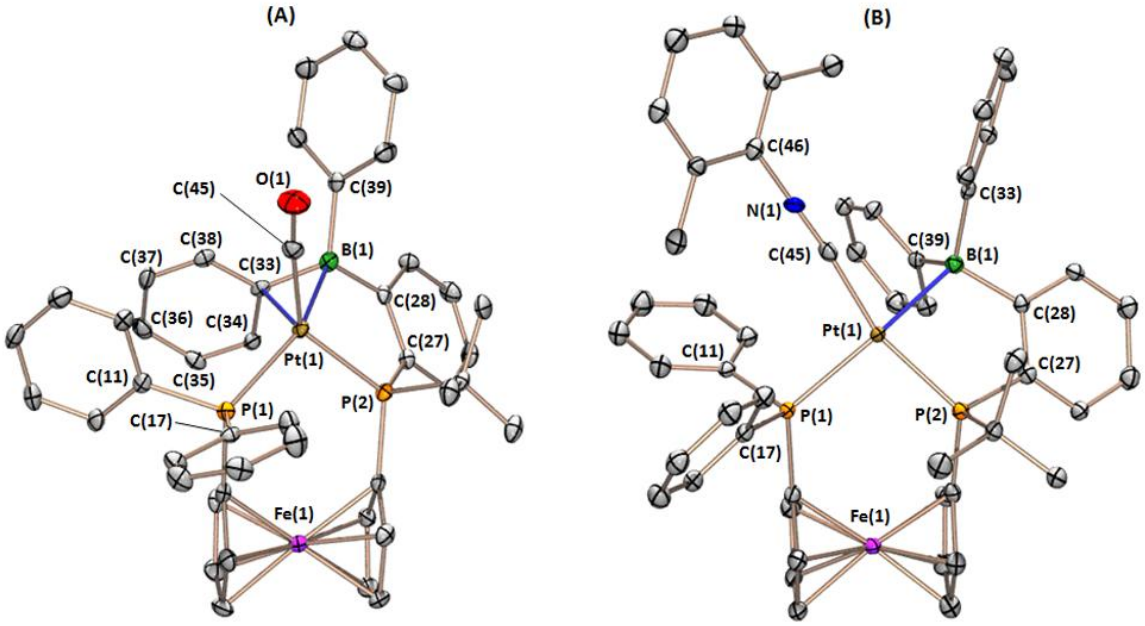

Figure 6.16. Solid-state structures for **A.** [Pt(CO)(FcPPB)]·$2CH_2Cl_2$ (**35**·$2CH_2Cl_2$) and **B.** [Pt(CNXyl)(FcPPB)]·CH_2Cl_2 (**36**·CH_2Cl_2) with ellipsoids drawn at 50 % probability. Hydrogen atoms and lattice solvent have been omitted for clarity.

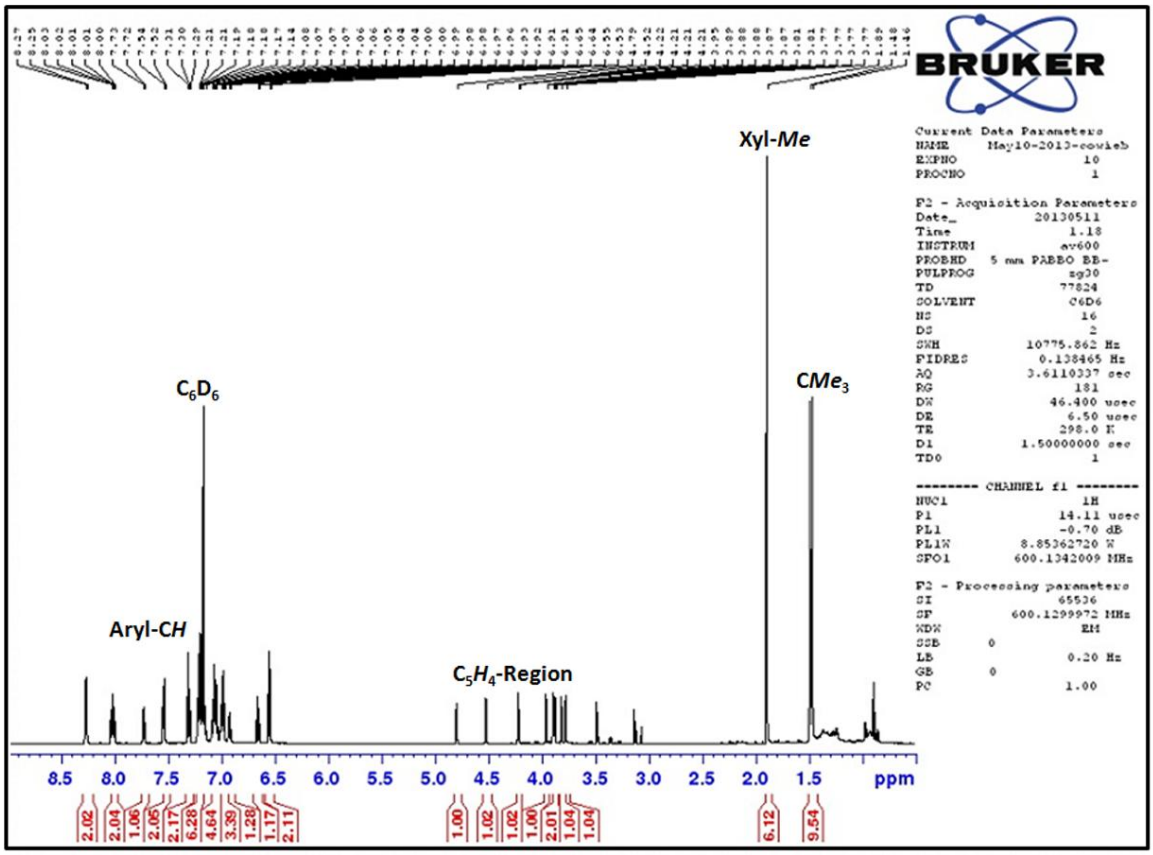

Figure 6.17. ^{1}H NMR spectrum of [Pt(CNXyl)(FcPPB)] (**36**; 600 MHz, 298 K, C_6D_6).

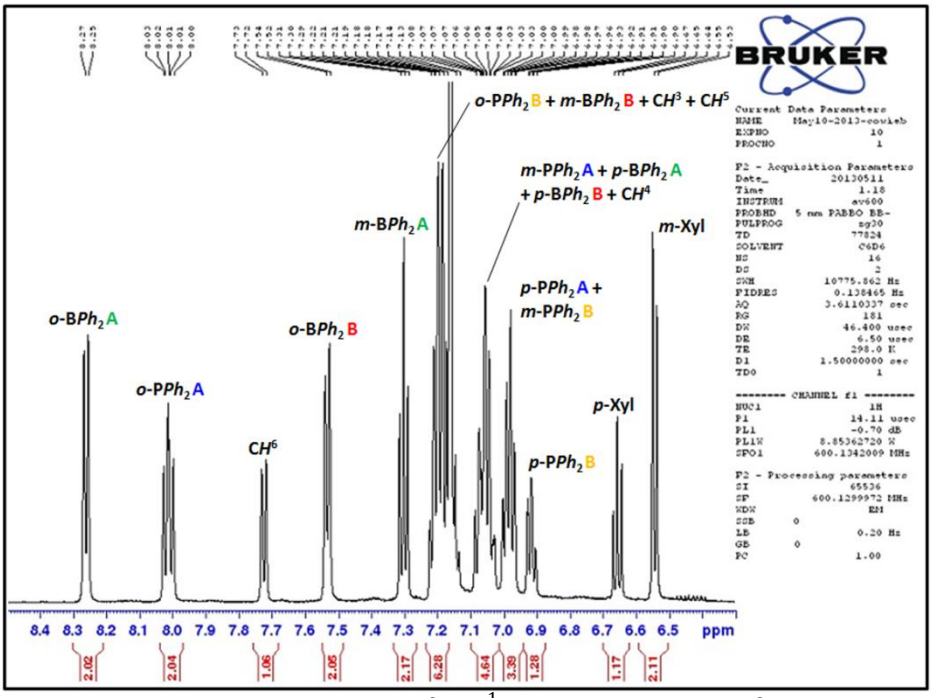

Figure 6.18. Expanded aromatic region of the ^{1}H NMR spectrum of [Pt(CNXyl)(FcPPB)] (**36**; 600 MHz, 298 K, C_6D_6).

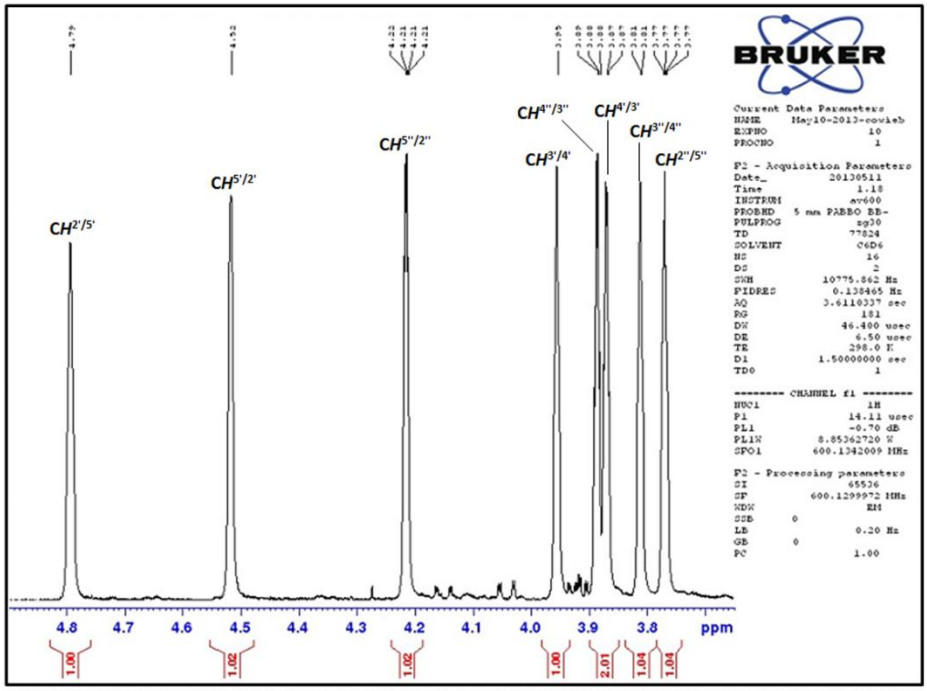

Figure 6.19. Expanded C_5H_4-region of the ^{1}H NMR spectrum of [Pt(CNXyl)(FcPPB)] (**36**; 600 MHz, 298 K, C_6D_6).

X-ray quality crystals of [Pt(CNXyl)(FcPPB)]·CH_2Cl_2 (**36**·CH_2Cl_2) were grown by slow diffusion of hexanes into a solution of **36** in CH_2Cl_2 at –30 °C; **36** crystallizes with two independent molecules within the unit cell. In contrast to [Pt(FcPPB)] (**30**) and [Pt(CO)(FcPPB)] (**35**), the borane in compound **36** is η^1*B*-coordinated, and the geometry at platinum is distorted square planar with P(1)–Pt–B and P(2)–Pt–C(45) angles of 157.9(3) and 159.9(3)°, respectively (**B** in Figure 6.16). The Pt–B distance is 2.27(1)/ 2.28(1) Å and boron is almost tetrahedral with the sum of the C–B–C angles equal to 333(1)°. The P(1)–Pt–P(2) bite angle decreases from 108.53(3)° in **30**, to 104.56(4)° in **35**, and 100.7(1)/101.0(1)° in **36**, and the conformational flexibility of the bis(phosphino)ferrocene backbone is highlighted by the very different P(1)–$Cent_{1–5}$–$Cent_{6–10}$–P(2) [$Cent_{x–y}$ = centroid of the cyclopentadienyl ring containing atoms C(x) to C(y)] dihedral angles: –30.4, –20.9 and 4.4/–0.9° in **30**, **35** and **36**, respectively.

Table 6.1. Crystallographic Data Collection and Refinement Parameters for Complexes **28–30** and **33**.

Structure	**28 · 0.7toluene**	**29 · $C_2H_4Cl_2$**	**30 · CH_2Cl_2**	**33 · (C_6H_{14})(C_6H_6)**
Formula	$C_{48.9}H_{46.6}BFeNiP_2$	$C_{46}H_{45}BCl_2FeP_2Pd$	$C_{45}H_{43}BCl_2FeP_2Pt$	$C_{100}H_{102}Fe_2N_2Ni_2P_6$
Formula wt	817.13	903.72	978.38	1746.78
T (K)	100(2)	100(2)	100(2)	100(2)
Cryst. Syst.	Monoclinic	Monoclinic	Triclinic	Monoclinic
Space Group	*P*2$_1$/*n*	*P*2$_1$/*n*	*P*–1	*C*2/*c*
a (Å)	10.051(3)	10.478(1)	10.787(2)	14.700(2)
b (Å)	19.984(5)	20.181(2)	13.260(2)	21.599(2)
c (Å)	19.267(5)	18.560(2)	14.740(3)	26.750(3)
α [deg]	90	90	71.759(4)	90
β [deg]	99.260(5)	99.191(2)	77.594(3)	91.956(2)
γ [deg]	90	90	83.677(3)	90
Volume [Å^3]	3820(2)	3874.2(7)	1953.5(6)	8489(2)
Z	4	4	2	4
μ (mm^{-1})	0.992	1.093	4.199	0.935
F(000)	1696	1848	972	3656
Crystal Size (mm^3)	0.19×0.04×0.04	0.27×0.15×0.12	0.26×0.12×0.04	0.22×0.18×0.03
θ Range for Collection [deg]	1.48–26.49	1.50–30.60	1.48–31.62	1.68–28.39
No. of Reflns Collected	35960	59335	27043	82671

No. of Indep Reflns	7868	11858	12749	10615
Completeness to θ Max (%)	99.4	99.4	97.1	99.6
Absorption Correction	Numerical	Numerical	Numerical	Numerical
Max and Min Transmission	0.9614, 0.8339	0.8800, 0.7567	0.8500, 0.4081	0.9725, 0.8208
GOF on F^2	1.080	1.038	1.004	1.035
Final R_1 [$I > 2\sigma(I)$] (%)	6.07	5.12	3.45	3.43

Table 6.2. Crystallographic Data Collection and Refinement Parameters for Complexes **34–36** and **39A**.

Structure	**34 · CH_2Cl_2**	**35 · $2CH_2Cl_2$**	**36 · CH_2Cl_2**	**39A · $4C_6H_6$**
Formula	$C_{62}H_{57}Cl_2FeOP_3Pd$	$C_{47}H_{45}BCl_4FeOP_2Pt$	$C_{108}H_{104}B_2Cl_4Fe_2N_2P_4Pt_2$	$C_{76}H_{71}BFeP_2Pt$
Formula wt	1144.14	1091.32	2219.11	1308.02
T (K)	100(2)	100(2)	100(2)	100(2)
Cryst. Syst.	Monoclinic	Triclinic	Monoclinic	Monoclinic
Space Group	$P2_1$	$P\bar{1}$	Cc	$P2_1/n$
a (Å)	9.8528(9)	9.897(1)	21.645(3)	17.313(3)
b (Å)	18.641(2)	11.960(2)	12.008(2)	19.108(3)
c (Å)	15.581(1)	19.840(3)	35.074(5)	19.095(3)
α [deg]	90	101.204(3)	90	90
β [deg]	106.827(2)	92.005(2)	94.283(3)	104.823(2)
γ [deg]	90	109.936(2)	90	90
Volume [$Å^3$]	2739.3(4)	2152.5(5)	9090(2)	6107(2)
Z	2	2	4	4
μ (mm^{-1})	0.819	3.942	3.621	2.622
F(000)	1176	1084	4448	2664
Crystal Size (mm^3)	0.23×0.13×0.11	0.21×0.14×0.08	0.19×0.16×0.09	0.17×0.08×0.04
θ Range for Collection [deg]	1.75–26.41	1.05–26.29	1.89–26.45	1.62–26.66
No. of Reflns Collected	27598	23370	51591	82018
No. of Indep Reflns	7570	8557	11518	12677
Completeness to θ Max (%)	99.7	98.1	99.8	98.6
Absorption Correction	Numerical	Numerical	Numerical	Numerical
Max and Min Transmission	0.9153, 0.8340	0.7433, 0.4915	0.7364, 0.5462	0.9024, 0.6641
GOF on F^2	1.084	1.034	1.043	1.063

Final R_1 [$I > 2\sigma(I)$] (%)	4.30	3.47	4.00	4.60

The ^{195}Pt resonances for [Pt(FcPPB)] (**30**), [Pt(CO)(FcPPB)] (**35**) and [Pt(CNXyl)(FcPPB)] (**36**) are located at –4934, –4422 and –4486 ppm, respectively. In the $^{31}P\{^1H\}$ NMR spectra of complexes **30**, **35** and **36**, the $C_5H_4PPh_2$ signal is observed at 28.5, 22.8 and 21.8 ppm, respectively ($^1J_{31P,195Pt}$ = 4183, 2343 and 1381 Hz), and the $C_5H_4P(^t$Bu)Ar group is observed at 50.8, 59.4 and 62.7 ppm, respectively ($^1J_{31P,195Pt}$ = 5651, 4884 and 4549 Hz). The marked decrease in ^{31}P-^{195}Pt coupling constants for the $C_5H_4PPh_2$ groups in **30**, **35** and **36** is likely due to the changes in arylborane coordination mode, with a greater *trans*-influence exerted by the η^1-borane, even though the P(1)–Pt–B bond angle more closely approaches 180° in compound **30** [P(1)–Pt–B = 171.0(1)° in **30**, 146.2(1)° in **35**, and 157.9(3)–159.9(3)° in **36**]. A marked increase in peak broadness is also observed in the $^{195}Pt\{^1H\}$ NMR spectra for **30**, **35** and **36**, with $\omega_{1/2}$ increasing from 95 to 125 to 300 Hz, respectively, arguably due to stronger bonding of platinum to quadrupolar boron in the order **30** < **35** < **36**.

Reaction of [Pt(FcPPB)] (**30**) with H_2 (1 atm) afforded [PtH(μ-H)(FcPPB)] (**37**), which is also generated by exposing [Pt(CO)(FcPPB)] (**35**) to H_2 (1 atm). Compound **37** is stable under an atmosphere of H_2, but in solution under argon (slowly) or under vacuum (rapidly) it loses H_2 to re-form **30** (Scheme 6.5). Additionally, under an atmosphere of CO, **37** readily re-forms carbonyl complex **35**. The hydride signals for **37** are located at –2.76 and –5.19 ppm in the ^{1}H NMR spectrum. The lower frequency hydride signal is a sharp doublet-of-doublets and is *trans* to the $C_5H_4P(^t$Bu)Ar group, whereas the hydride ligand *trans* to the $C_5H_4PPh_2$ group is a slightly broadened doublet-of-doublets, suggestive of a Pt–H–B bridging interaction; the ^{11}B NMR chemical shift of 5 ppm is consistent with this assignment. The ^{1}H NMR spectrum of **37**, in addition to expanded views of the aromatic and C_5H_4-regions are displayed below in Figures 6.20–6.22.

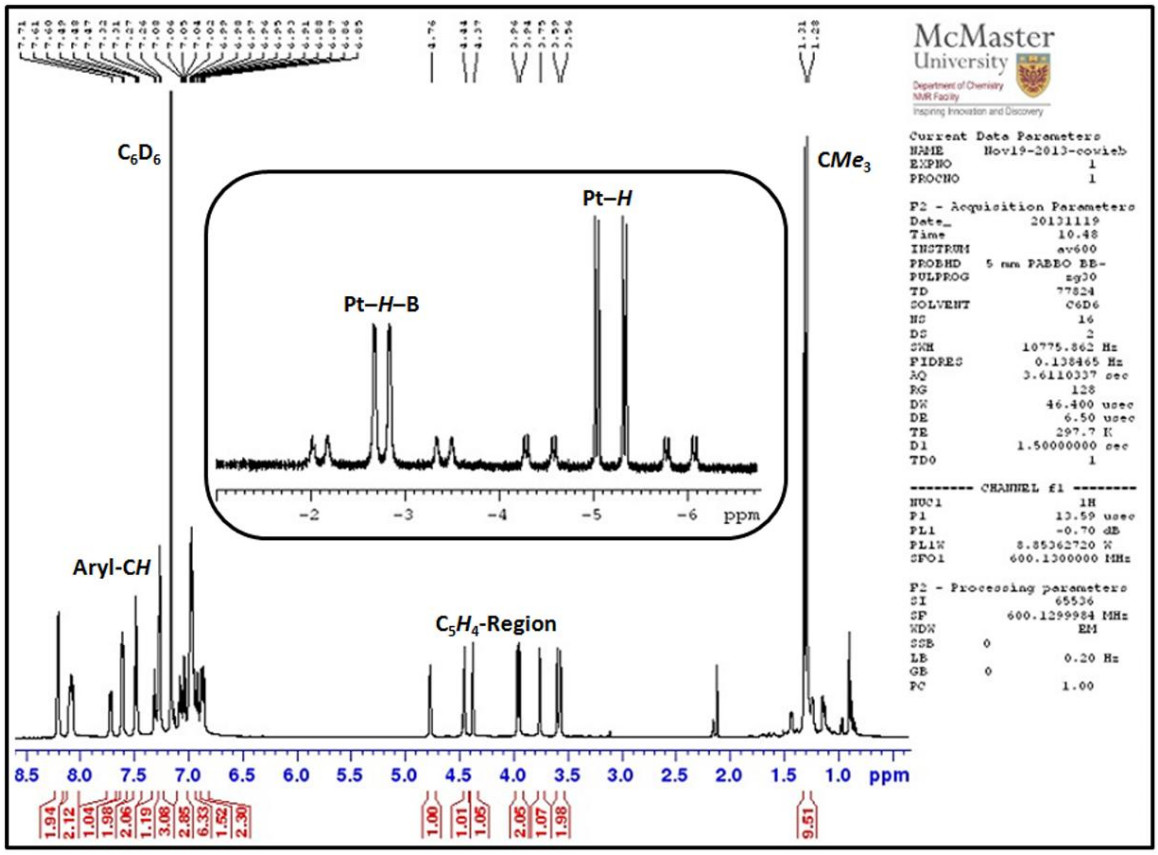

Figure 6.20. ^{1}H NMR spectrum of [PtH(μ-H)(FcPPB)] (**37**; 600 MHz, 298 K, C_6D_6).

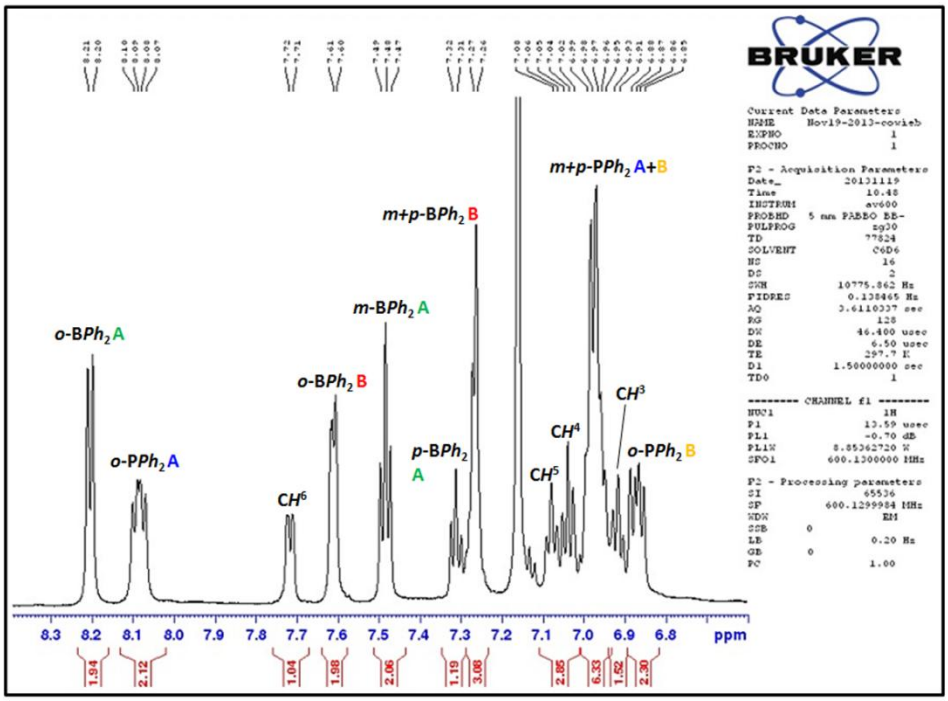

Figure 6.21. Expanded aromatic region of the ^{1}H NMR spectrum of [PtH(μ-H)(FcPPB)] (**37**; 600 MHz, 298 K, C_6D_6).

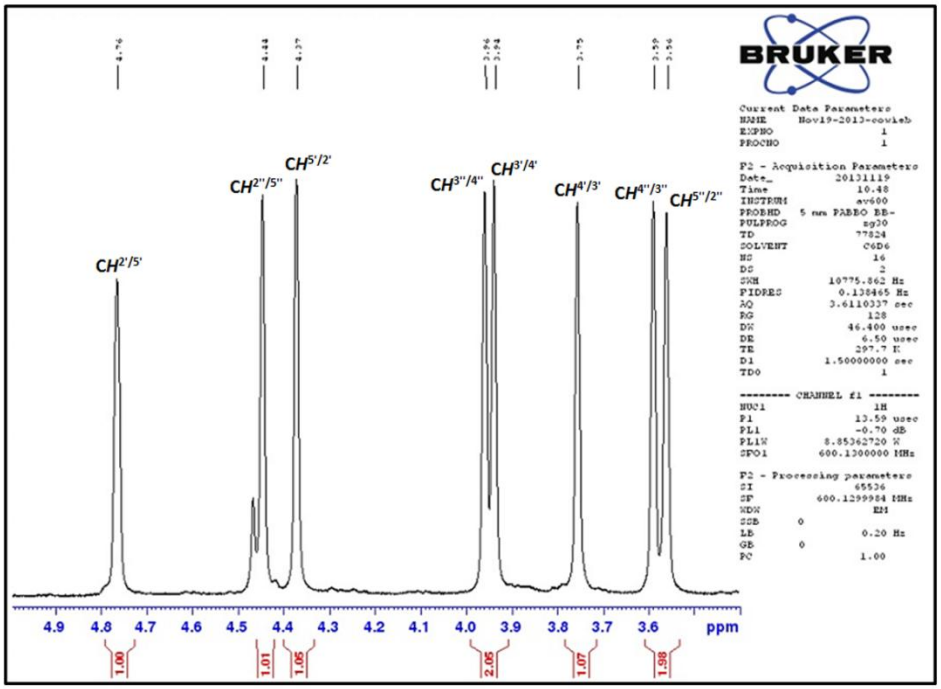

Figure 6.22. Expanded C_5H_4-region of the ^{1}H NMR spectrum of [PtH(μ-H)(FcPPB)] (**37**; 600 MHz, 298 K, C_6D_6).

Solid-state IR spectroscopy of **37** was not possible due to the propensity of **37** to eliminate H_2 in the absence of a hydrogen atmosphere. However, in CH_2Cl_2, broad Pt–H and very broad Pt–H–B stretches were located at 2020 and 1822 cm^{-1}, respectively, in fair agreement with calculated values (2065 and 1868 cm^{-1}; see the Experimental Section for details of the calculations). The Pt–H stretch for the terminally bound hydride is also in good agreement with platinum complexes *cis*-[PtH(Se^{t}Bu)(PPh_3)$_2$] [ν(Pt–H) = 2088 cm^{-1}][262] and [Pt_2H_2(μ-PR_2)$_2$(PEt_3)$_2$] [ν(Pt–H) = 2004 cm^{-1} (R = Ph) ; 2022 cm^{-1} (R = ^{t}Bu)].[263] Furthermore, [PtD(μ-D)(FcPPB)] (**[D]-37**) was prepared from the reaction of [Pt(FcPPB)] with D_2, and the Pt–D stretching frequency (1478 cm^{-1}) was located by subtraction of the IR spectrum of **37** from that of **[D]-37** due to overlap of these stretches with the C=C and C–C stretches (the Pt–D–B stretch was not located).

Complete abstraction of the hydride ligand from platinum by boron does not occur in **37**, given that both hydride signals show coupling to ^{31}P and ^{195}Pt. However, a smaller ^{1}H-^{195}Pt coupling is observed for the bridging hydride (792 vs. 905 Hz), consistent with a weakened Pt–H bond, despite its position *trans* to the lower *trans*-influence phosphine. The greater *trans*-influence of the terminal hydride is also evident from the ^{31}P{^{1}H} NMR spectrum of **37**, which shows a larger $^1J_{31P,195Pt}$ coupling of 3721 Hz for the $C_5H_4PPh_2$ group (*trans* to the bridging hydride), relative to 2123 Hz for the C_5H_4P(^{t}Bu)Ar group, even though the latter is the better donor and has the higher $^1J_{31P,195Pt}$ coupling in complexes **30**, **35** and **36**. The ^{195}Pt signal for **37** is a sharp doublet-of-doublets located at –4980 ppm.

Due to the propensity for **37** to revert back to **30** and H_2 in the absence of an H_2 atmosphere, we were unsuccessful in obtaining single crystals of **37**. However, DFT calculations on **37** (see the Experimental Section for details of the calculations) converged to a minimum with one bridging and one terminal hydride (Figure 6.23), consistent with the NMR data. The geometry at platinum is square planar, with Pt–P distances of 2.246 and 2.322 Å to the $C_5H_4PPh_2$ and C_5H_4P(^{t}Bu)Ar groups, respectively (the corresponding Mayer bond orders are 1.21 and 1.05), and Pt–H distances of 1.613 and 1.686 Å to the terminal and bridging hydride ligands, respectively. Boron is significantly pyramidalized

[Σ(C–B–C) = 338°], the Pt–B distance remains fairly short at 2.524 Å, and the B–H distance is 1.386 Å, which is longer than that observed for a free hydroborate anion (e.g. 1.10(2) Å in $[HC(SiMe_2OCH_2CH_2OCH_3)_3Na][Ph_3BH]$).[264] The Pt–H(terminal), Pt–H(bridging), H–B and Pt–B Mayer bond orders are 0.81, 0.58, 0.39 and 0.23, respectively, suggesting that the borane in **37** interacts with both the bridging hydride and the metal centre. The H–B–C angles are 115.4, 109.3 and 92.4°, with the acute angle to the phenyl *ipso*-carbon, C(33), which is closest to *trans* to platinum across the H–B bond [Pt–H–B–C(33) torsion angle = 153°]; an acute (< 100°) H–B–C angle was previously observed in the experimental and calculated structures of $[Rh(\mu\text{-}H)(PPh_3)(CO)_n\{(o\text{-}Ph_2P)C_6H_4\}BPh)_2\}]$ (n = 0 and 1).[124]

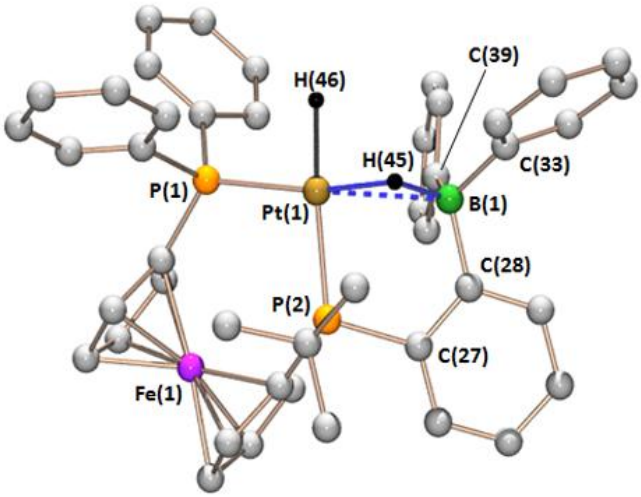

Figure 6.23. DFT optimized structure for [PtH(μ-H)(FcPPB)] (**37**); hydrogen atoms have been omitted for clarity. DFT calculations were performed by Prof. D. J. H. Emslie.

6.5 – Conversion of [Pt(FcPPB)] to [Pt(FcPPB')] via Reaction with Phenylacetylene

The potential of **30** to hydrogenate alkenes and internal alkynes (C_2H_4, styrene, norbornene, cyclooctene, 1-octene, C_2Ph_2; 20 or 60 °C) was investigated, but significant catalytic activity was only observed for certain batches, and only in the absence of metallic mercury, indicative of heterogeneous catalysis by a small amount of elemental platinum. This contrasts the hydrogenation activity of the first row ambiphilic ligand

complexes [Fe(N_2)($^{i\text{Pr}}$TPB)] and [Ni($^{i\text{Pr}}$DPB$^{\text{Mes}}$)] ($^{i\text{Pr}}$TPB = {(*o*-^{i}Pr$_2$P)C_6H_4}$_3$B; $^{i\text{Pr}}$DPB$^{\text{Mes}}$ = {(*o*-^{i}Pr$_2$P)C_6H_4}$_2$BMes) reported recently by Peters *et al.*[60,128] Compound **30** does not react with any of the aforementioned alkenes or alkynes to an extent detectable by ^{1}H NMR spectroscopy. By contrast, reaction of **30** with PhC_2H resulted in rapid oxidative addition to provide [Pt(C_2Ph)(μ-H)(FcPPB)] (**38**), which immediately began to isomerise to afford an η^3*BCC*-coordinated vinylborane complex, [Pt(FcPPB')] (**39A**; FcPPB' = [Fe(η^5-$C_5H_4PPh_2$)(η^5-$C_5H_4P^t$Bu{C_6H_4(BPh-CPh=CHPh-*Z*)-*o*}]); after 5 minutes at room temperature, the reaction of **30** with PhC_2H contained a 1:1 mixture of **38** and **39A** (Scheme 6.6). Complete isomerisation from **38** to vinylborane **39A** required either ~36 hours at room temperature, or overnight heating to 95 °C.

The hydride signal in **38** is located at –3.69 ppm in the ^{1}H NMR spectrum, with a $^1J_{1H,195Pt}$ coupling of 760 Hz and $^2J_{1H,31P}$ couplings of 115 and 12 Hz. An ^{11}B NMR chemical shift of 11 ppm indicates that the hydride ligand in **38** resides in a bridging position between platinum and boron, as was observed in **37**. The C≡C stretch for **38** was located at 2126 cm^{-1} in the IR spectrum,[§] which is very similar to that observed for *trans*-[PtH($C_2C_6H_4$Me-*p*)(PPh_3)$_2$] [ν(C≡C) = 2111 cm^{-1}].[265] Similar oxidative addition reactivity with HC_2Ph was reported recently for [Fe(N_2)($^{i\text{Pr}}$TPB)], but in this case the resulting hydride is completely abstracted by the borane to afford zwitterionic [Fe(C_2Ph)($^{i\text{Pr}}$TPB-H)] [ν(C≡C) = 2040 cm^{-1}; ν(B–H) = 2490 cm^{-1}].[60]

Complex **39A** is a vinylborane analogue of arylborane complex **30**, and both complexes feature an η^3*BCC*-coordination mode, almost identical ^{31}P NMR chemical shifts (50.3 and 27.6 for **39A**, 50.8 and 28.5 ppm for **30**) and similar ^{11}B NMR chemical shifts (24 and 21 ppm for **39A** and **30**, respectively). The platinum resonance is a sharp doublet-of-doublets located at –5117 ppm in the ^{195}Pt{^{1}H} NMR spectrum. In the ^{1}H NMR spectrum of **39A**, the BCPh=C***H***Ph signal is observed at 5.86 ppm as a doublet-of-doublets with platinum satellites; the ^{1}H NMR spectrum of **39A**, along with expanded views of the aromatic and C_5H_4-regions are displayed below in Figures 6.24–6.26. The

[§] The Pt–H–B stretch was not located for compound **38**, presumably due to extreme broadness of the peak; the Pt–H–B stretch for compound **37** was extremely broad.

vinyl carbon atoms in **39A** are located at 114.0 (C_α, broad singlet) and 77.7 ppm (C_β, dd, $^2J_{13C,31P}$ = 34, 4 Hz) in the ^{13}C NMR spectrum, demonstrating that η^3*BCC*-vinylborane coordination is maintained in solution, in contrast to η^3*BCC*-arylborane coordination in **30**. The $^1J_{31P,195Pt}$ couplings for the $C_5H_4PPh_2$ groups in **39A** and **30** are similar (3937 Hz in **39A** vs. 4183 Hz in **30**), whereas the $^1J_{31P,195Pt}$ coupling for the $C_5H_4P(^tBu)Ar$ group is much smaller in **39A** than that in **30** (3695 Hz in **39A** vs. 5651 Hz in **30**), suggesting that the vinyl group in **39A** exerts a substantially greater *trans*-influence than the phenyl group in **30**. The improved coordination ability of the *B*-vinyl group in **39A** relative to the *B*-phenyl group in **30** is also reflected in the reactivity of **39A**, which does not react at room temperature with CO, CNXyl, H_2 or HC_2Ph.

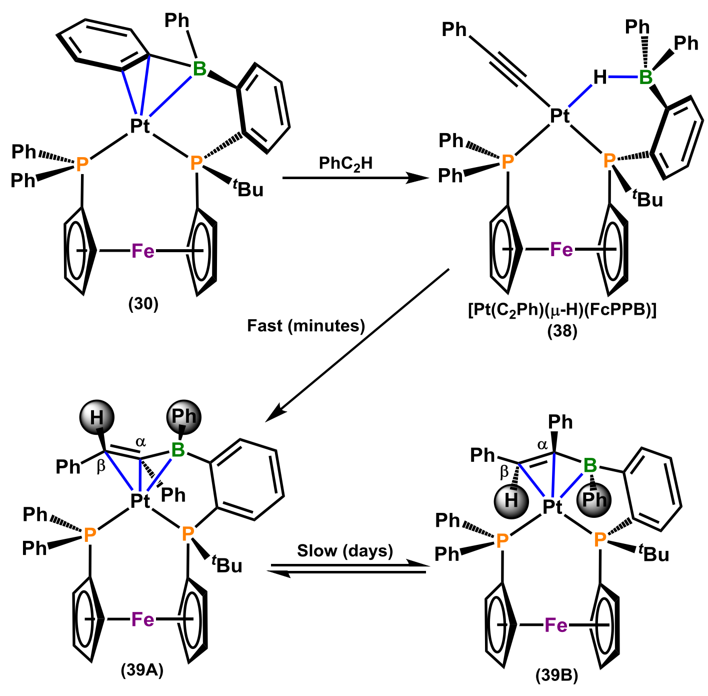

Scheme 6.6. Reaction of [Pt(FcPPB)] (**30**) with PhC_2H, providing [Pt(C_2Ph)(μ-H)(FcPPB)] (**38**), followed by isomerization to yield [Pt(FcPPB')] (**39**).

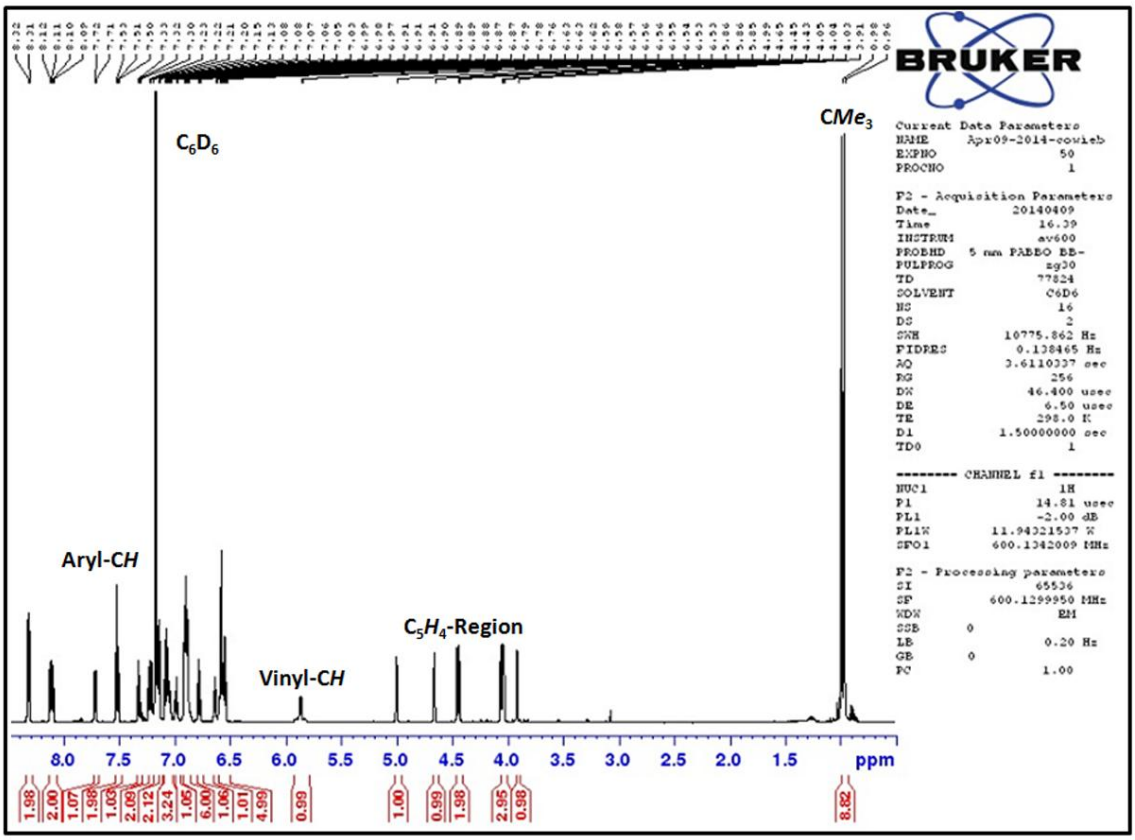

Figure 6.24. ^{1}H NMR spectrum of [Pt(FcPPB')] (Isomer A) (**39A**; 600 MHz, 298 K, C_6D_6).

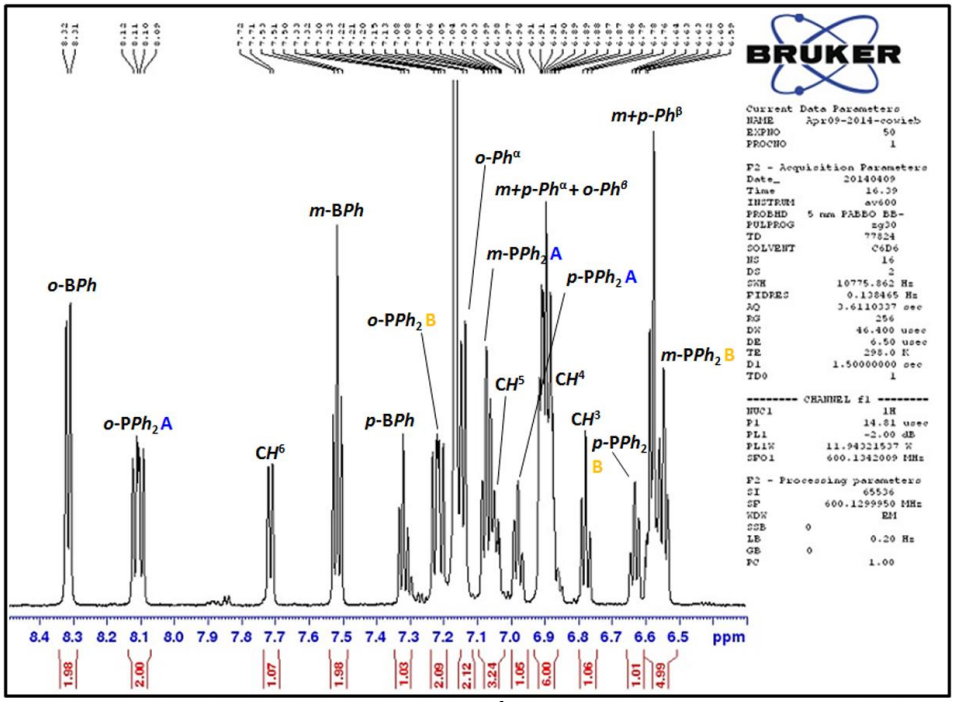

Figure 6.25. Expanded aromatic region of the ^{1}H NMR spectrum of [Pt(FcPPB')] (Isomer A) (**39A**; 600 MHz, 298 K, C_6D_6).

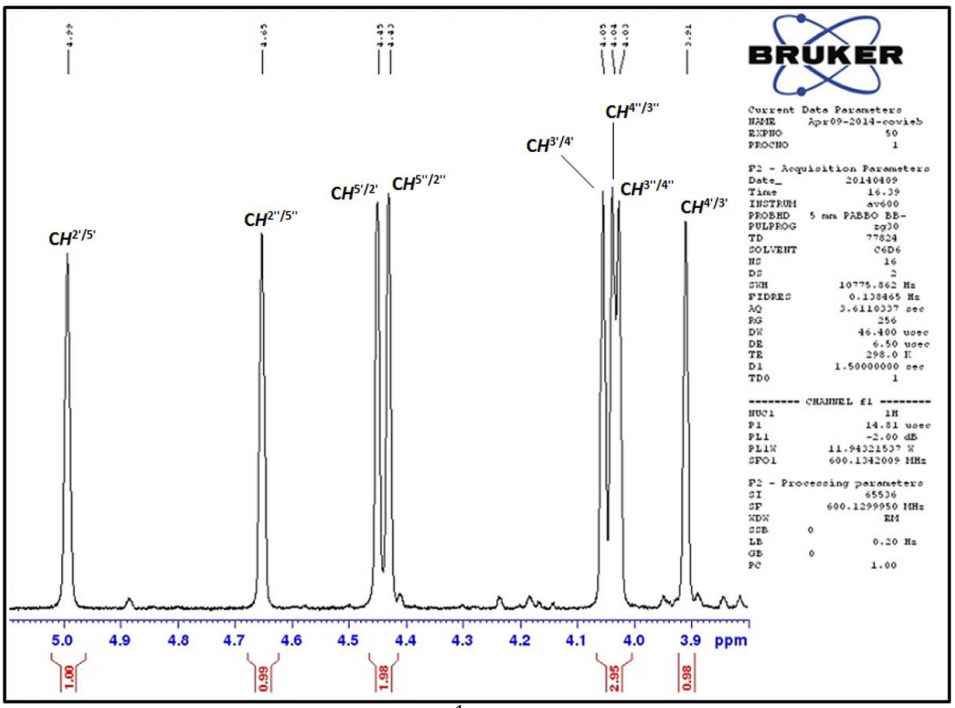

Figure 6.26. Expanded C_5H_4-region of the ^{1}H NMR spectrum of [Pt(FcPPB')] (Isomer A) (**39A**; 600 MHz, 298 K, C_6D_6).

Single crystals of [Pt(FcPPB')] (Isomer A)·4C_6H_6 (**39A**·4C_6H_6) were obtained from a benzene/hexane solution cooled to –30 °C. In the solid-state, complex **39A** adopts a distorted square planar geometry, with P(2)–Pt–C(46) and P(1)–Pt–B angles equal to 149.0(2) and 165.8(2)°, respectively (Figure 6.27). The Pt–B distance is 2.303(6) Å and the sum of the C–B–C angles is 356.5(9)°; these data are identical within error to those in **30**. By contrast, the Pt–C_α and Pt–C_β distances in **39A** [2.184(5) and 2.194(5) Å, respectively] are shorter than those in **30** by 0.041 and 0.135 Å. Even shorter Pt–C distances have previously been described for [Pt(P^tBu_3)(VB^{Ph})] [VB^{Ph} = (*E*)-PhHC=C(H)-$B(C_6F_5)_2$; two independent molecules in the unit cell; Pt–C_α = 2.126(4)/2.130(4) Å; Pt–C_β = 2.137(4)/2.155(4) Å; Pt–B = 2.273(5)/2.319(5) Å],[255] likely due to decreased steric hindrance and the greater Lewis acidity of the borane in VB^{Ph} (VB^{Ph} was shown to be an overall acceptor ligand in [Pt(P^tBu_3)(VB^{Ph})]). The B–C_α distance in **39A** is 1.546(8) Å, compared with 1.551(5) Å in **30** and 1.517(6)/1.519(7) Å in [Pt(P^tBu_3)(VB^{Ph})], but unfortunately, the standard deviation associated with the B–C_α bond in **39A** is too large to draw any conclusions regarding the extent of multiple bond character. The vinylic proton and the *B*-Ph ring [H(46) and C(39)] reside in the exo positions of the coordinated vinyl group and are located 0.419 and 0.922 Å above the B–C_α–C_β plane, respectively, whereas C_β–Ph and the phenylene linker of the backbone [C(47) and C(28)] reside in endo positions and bend towards the metal, placing them 0.565 and 0.086 Å below the B–C_α–C_β plane, respectively. Such distortions are typical of late transition metal-allyl complexes,[266] suggesting that the vinylborane in **39A** is more borataallyl-like than alkyl/borataalkene-like.[255]

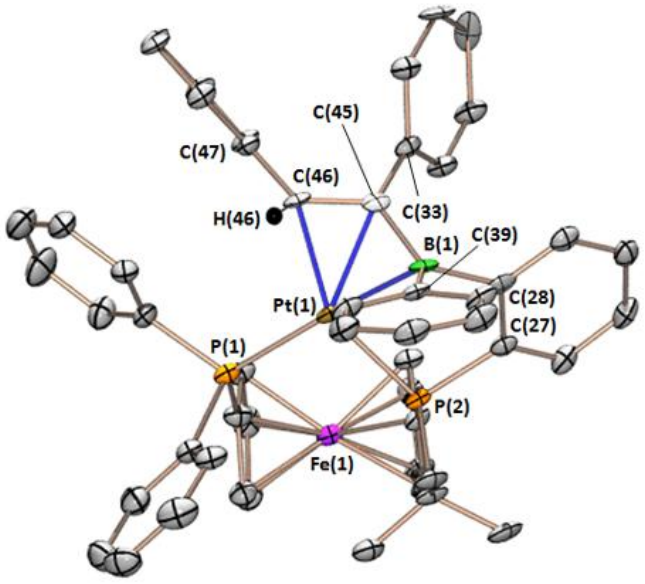

Figure 6.27. Solid-state structure for [Pt(FcPPB')]·4C_6H_6 (**39A**·4C_6H_6) with ellipsoids drawn at 50 % probability. H(46) was located in the difference map, whereas all other hydrogen atoms were placed in calculated positions; hydrogen atoms [excluding H(46)] and solvent have been omitted for clarity.

Complex **39A** isomerized over a period of six days at room temperature to an approximate 45:55 mixture of the original isomer and a new isomer, **39B**, giving rise to a new set of ^{31}P (55.7 and 23.3 ppm), ^{11}B (30 ppm) and ^{195}Pt (–4840 ppm) signals; the ratio of **39A**:**39B** is displayed below in Figure 6.28, which is an expanded view of the vinyl-C*H* ^{1}H NMR signals for **39A** and **39B**, and Figure 6.29, which is the resulting ^{195}Pt{^{1}H} NMR spectrum of the **39A**/**39B** equilibrium mixture. As with **39A**, isomer **39B** features an η^3*BCC*-coordinated (*Z*)-(B–C$^{\alpha}$Ph=C$^{\beta}$HPh) group based on the following evidence: (1) ^{1}H-^{13}C HSQC NMR confirmed that the vinyl proton is located in the β-position, (2) coupling between the BCPh=C***H***Ph signal and the *o*-B***Ph*** signal in a selective 1D ^{1}H-^{1}H ROESY NMR experiment demonstrated that the ligand has a *Z*-arrangement of the phenyl substituents on the vinyl group (the vinyl-C*H* proton in **39A** shows an analogous ROESY coupling), (3) the ^{11}B NMR chemical shift (30 ppm) confirmed coordination of boron to platinum, and (4) vinyl group ^{1}H-^{195}Pt, ^{13}C-^{195}Pt and ^{13}C-^{31}P coupling confirmed coordination of both the α- and β-carbon atoms of the vinyl ligand. The selective 1D ^{1}H-^{1}H ROESY NMR experiments also revealed that the vinyl proton and the *B*-phenyl

groups in both **39A** and **39B** are positioned in the exo positions of the η^3*BCC*-coordinated vinylborane. Isomer **39B** is therefore related to **39A** by coordination of platinum to the opposite face of the vinylborane, with all of the regiochemistry of the *BCC*-unit preserved (Scheme 6.6; isomer **39B** shows through-space coupling between the B–C***Ph***=CHPh group and the PC***Me***$_3$ group).

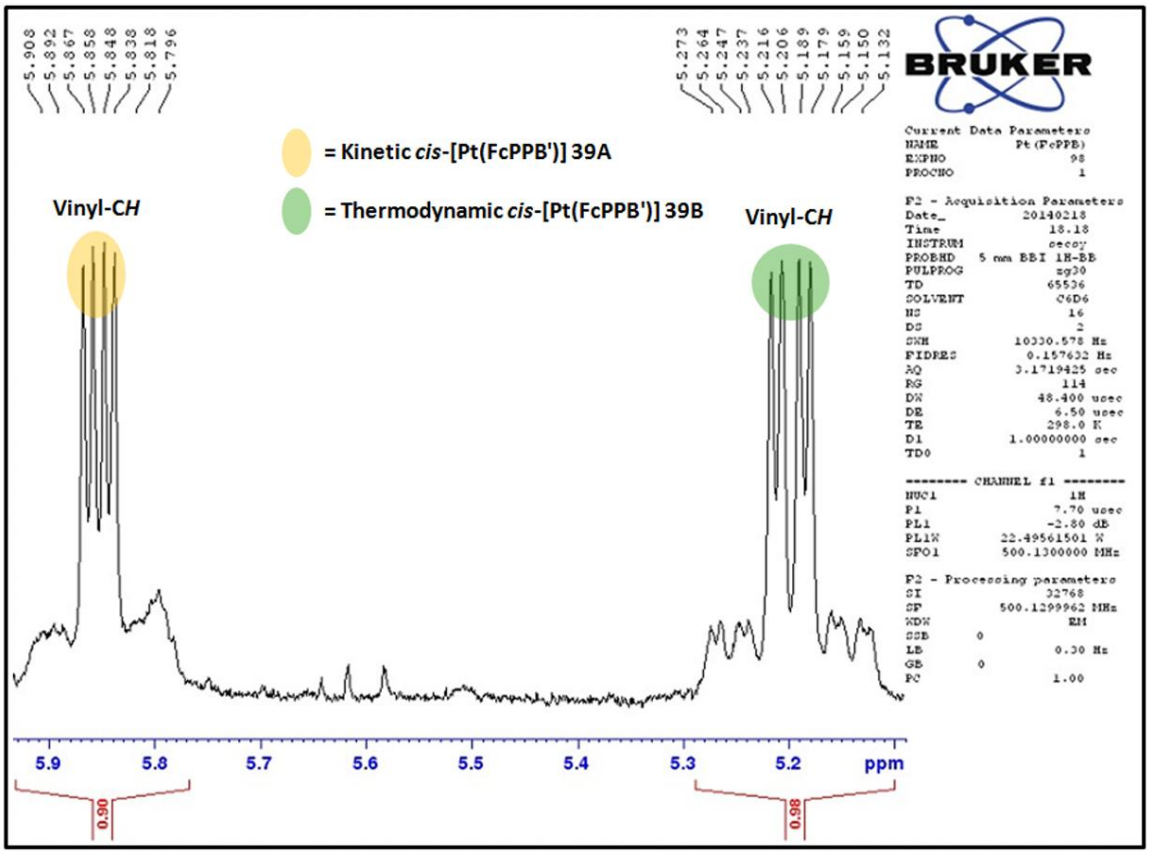

Figure 6.28. Expanded vinyl-C*H* region of the ^{1}H NMR spectrum of an equilibrium mixture of the thermodynamic and kinetic products of [Pt(FcPPB')] (**39A/B**; 600 MHz, 298 K, C_6D_6).

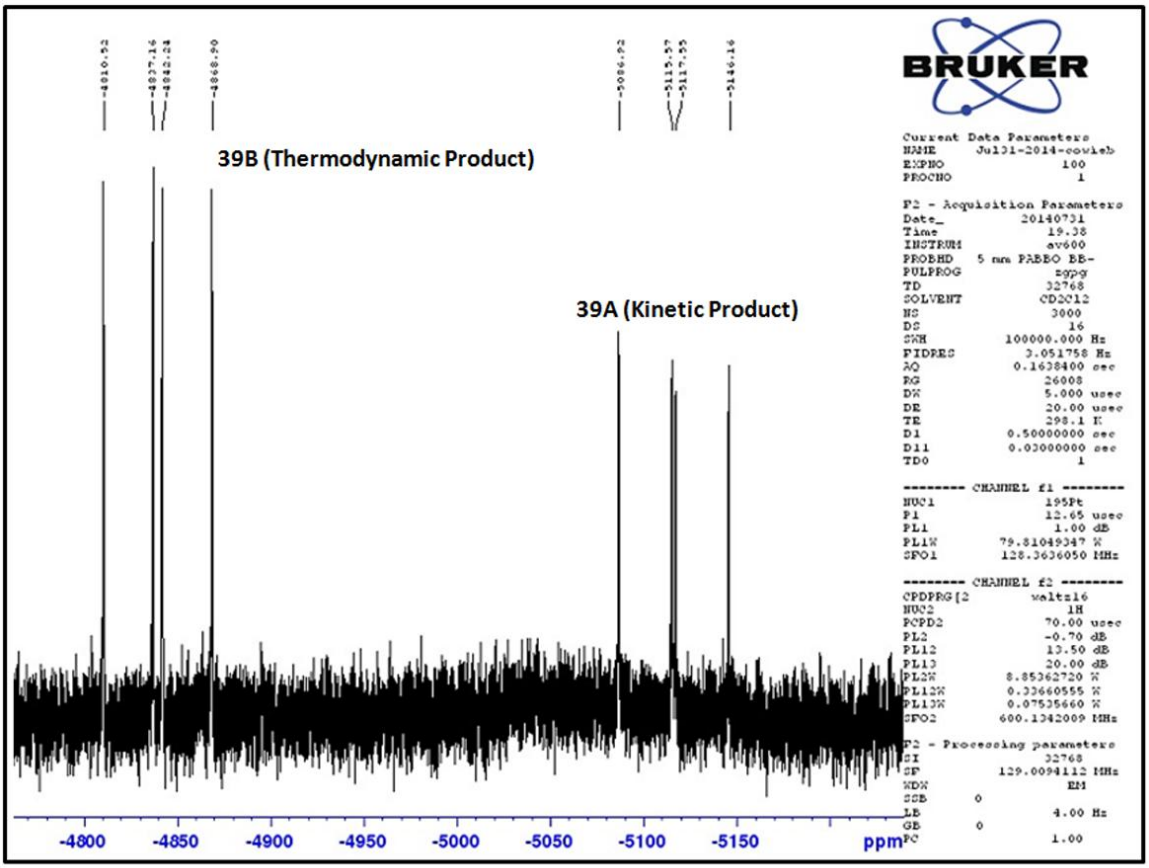

Figure 6.29. $^{195}Pt\{^{1}H\}$ NMR spectrum of an equilibrium mixture of the thermodynamic and kinetic products of [Pt(FcPPB')] (**39A/B**; 128 MHz, 298 K, C_6D_6).

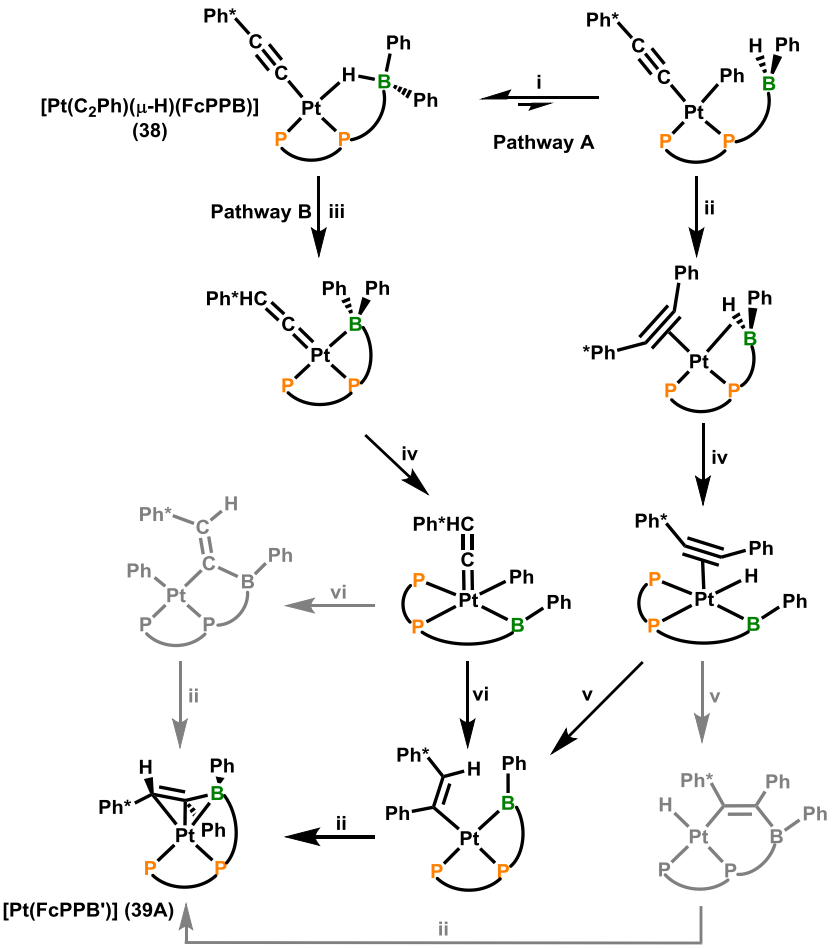

Scheme 6.7. Two possible reaction pathways for the formation of **39A.** Ph* indicates the phenyl group originating from phenylacetylene. Only one possible geometry and/or borane coordination mode is shown for proposed intermediates. Pathways relying on B–C bond-forming insertion reactions are shown in gray. Reactions: (**i**) hydride abstraction by the borane, followed by phenyl group transfer from boron to platinum, (**ii**) reductive elimination, (**iii**) alkynyl hydride-alkyne-vinylidene isomerisation, (**iv**) oxidative addition, (**v**) 1,2-insertion, and (**vi**) 1,1-insertion.

Two plausible reaction pathways for the formation of **39A** from **38** are shown in Scheme 6.7. Pathway **A** involves initial phenylacetylene C–H bond oxidative addition, exchange of a hydride on platinum with a phenyl group on boron, and C–C bond-forming reductive elimination to generate a platinum(0) diphenylacetylene intermediate. Subsequent B–H bond oxidative addition, 1,2-insertion involving the C_2Ph_2 ligand and the newly formed hydride ligand (or less likely the boryl ligand), and reductive

elimination yields **39A**. By contrast, pathway **B** involves initial vinylidene formation, followed by sequential B–C bond oxidative addition, 1,1-insertion involving the vinylidene and a platinum phenyl or boryl group, and reductive elimination to form **39A**. A pathway involving migration of the vinylidene in [Pt(=C=CHPh)(FcPPB)] to a bridging position between boron and platinum was not considered viable given the electrophilic nature of the α-carbon atom of a vinylidene ligand.

Pathway **A** seems less likely given that [PtH(μ-H)(FcPPB)] (**37**) does not eliminate benzene, which might be anticipated if the pendant borane is able to abstract a hydride and return a phenyl group to the metal centre. Additionally: (1) In the presence of a large excess of HC_2Ph, products consistent with C_2Ph_2 substitution by HC_2Ph and subsequent 1,2-insertion and reductive elimination are not observed, and (2) if free rotation or dissociation of C_2Ph_2 can occur, the phenyl group originating from boron could occupy either the α- or the β-position, and only the former is observed when the reaction is conducted with $HC_2(C_6D_5)$. However, with respect to the 1,1-insertion step in pathway **B**, it is of note that equivalent reactivity is not observed for [Pt(CO)(FcPPB)] (**35**) or [Pt(CNXyl)(FcPPB)] (**36**), which are analogues of proposed [Pt(=C=CHPh)(FcPPB)].

6.6 – Summary

A wide bite-angle phosphine–phosphine–borane ambiphilic ligand, FcPPB {[Fe(η^5-$C_5H_4PPh_2$){η^5-$C_5H_4P^tBu(C_6H_4BPh_2$-*o*)}]; Scheme 6.1}, has been utilized in the synthesis of a range of Group 10 metal complexes. Reaction of FcPPB with $[Ni(cod)_2]$, $[Pd_2(dba)_3]$ or $[Pt(nb)_3]$ provided [M(FcPPB)] complexes [M = Ni (**28**), Pd (**29**), Pt (**30**)] in which the FcPPB ligand is κ^2*PP*- and η^3*BCC*-coordinated to the metal centre. FcPPB is a superior ligand framework relative to our formerly employed phosphine–thioether–borane ambiphilic ligand, TXPB, given its overall improved donor ability and increased ligand backbone flexibility. The reactivity of [Pt(FcPPB)] (**30**) with CO, CNXyl, H_2 and HC_2Ph highlights the coordinative flexibility of the triarylborane unit in FcPPB,

providing reversible access to η^3*BCC*-, η^2*BC*- and η^1*B*-borane coordination modes, as well as Pt–H–BR_3 bridging interactions. This reactivity also demonstrates the ability of the FcPPB ligand to promote oxidative addition, to maintain coordination of both donor groups in a range of oxidation states and to stabilize varied coordination geometries at platinum, ranging from pseudo-square planar to pseudo-tetrahedral. Furthermore, the reaction of [Pt(FcPPB)] (**30**) with HC_2Ph afforded [Pt(FcPPB')] (**39**; FcPPB' = [Fe(η^5-$C_5H_4PPh_2$){η^5-$C_5H_4P^tBu${C_6H_4(BPh-CPh=CHPh-*Z*)-*o*}}]) featuring the first vinylborane-containing ambiphilic ligand. This complex provides a unique opportunity for direct comparison of η^3*BCC*-arylborane and η^3*BCC*-vinylborane bonding and reactivity, and in the solid-state [Pt(FcPPB)] (**30**) and [Pt(FcPPB')] (**39**) are structurally similar. However, the latter features shorter Pt–C bonds, and whereas [Pt(FcPPB)] (**30**) reacts with CO, CNXyl, H_2 and HC_2Ph at room temperature, [Pt(FcPPB')] (**39**) does not, consistent with much tighter η^3*BCC*-coordination in the vinylborane complex. This suggests that arylborane-appended complexes are likely to be of more utility than vinylborane-appended complexes in the future development of cooperative catalysis.

Moreover, the observation that FcPPB reacts with [Pd_2(dba)$_3$] to generate dba-free [Pd(FcPPB)] (**29**) while FcPPP (a trisphosphine analogue of FcPPB) forms [Pd(η^2-dba)(FcPPP)] (**34**) leads to the unanticipated conclusion that in the present work, FcPPB is a superior ligand relative to FcPPP; effectively, after coordination of two phosphine donors in FcPPB or FcPPP to palladium, the binding preference follows the order BAr_3 > dba > PR_3 (where BAr_3 and PR_3 are pendant borane and phosphine groups of the FcPPB and FcPPP ligands, respectively). The same binding preference was observed for nickel, since [Ni(FcPPB)] (**28**) did not react with dba, whereas "Ni(FcPPP)" (**32**) and *rac*-[{Ni(FcPPP)}$_2$(μ-N_2)] (**33**) reacted with dba to form a new product tentatively assigned as [Ni(η^2-dba)(FcPPP)]. Additionally, while "Ni(FcPPP)" (**32**) reacted readily with even traces of N_2, FcPPB compounds [Ni(FcPPB)] (**28**) and [Pd(FcPPB)] (**29**) did not react with N_2. [Pd(η^2-dba)(FcPPP)] (**34**) also did not react with N_2 due to preferential dba coordination. The much greater tendency of arylboranes versus arylphosphines to engage in polyhapto-coordination can be attributed to the potential for delocalization within the

η^n-coordinated BC_{n-1} fragment ($n \geq 2$),[122] and the approximate trigonal planarity of boron in $\eta^n BC_{n-1}$-coordinated complexes, which allows for close approach of the aryl substituents on boron to the metal.

Chapter 7

Tungsten, Ruthenium and Gold Complexes of a Borane Appended Analogue of 1,1'-Bisphosphinoferrocene: Examples of Intramolecular C–H Bond Activation and Boronium Cation Generation

7.1 – Introduction

The vast majority of the Emslie group's ambiphilic ligand research has centred around Group 9 and 10 complexes. However, to further explore the coordination behaviour of pendant borane Lewis acids, we sought to extend the chemistry of FcPPB to both earlier and later transition metals. Originally, we envisioned that FcPPB may provide access to $[Au^{I}(FcPPB)]X$ (X = counter-anion) complexes with unusual (i.e. non-linear) coordination geometries, and that these complexes would be susceptible to small molecule coordination and perhaps oxidative addition.[§] Furthermore, we were optimistic that *cis*-κ^2*PP*-coordination of the 1,1'-bisphosphinoferrocene backbone to metal-carbonyl pre-cursors would provide an opportunity for the pendant borane of the FcPPB ligand to interact with metal-coordinated CO ligands, with the potential to assist in functionalization of carbon monoxide. Described here-in is the reactivity of the FcPPB ligand in combination with gold, tungsten and ruthenium, including unanticipated intramolecular C–H bond activation observed during the formation of the tungsten and ruthenium complexes. Moreover, the reactivity of the free FcPPB ligand with the boron Lewis acids $B(C_6F_5)_3$ and $BF_3{\cdot}OEt_2$ was explored in an attempt to encourage electrophilic borylation reactivity in the free ligand. These reactions lead to a phosphine–borane adduct and a bisphosphine-stabilized boronium cation, respectively.

[§] For recent examples of oxidative addition reactivity featuring gold(I) complexes, see: (a) Joost, M.; Estévez, L.; Miqueu, K.; Amgoune, A.; Bourissou, D. *Angew. Chem. Int. Ed.* **2015**, *54*, 5236. (b) Winston, M. S.; Wolf, W. J.; Toste, F. D. *J. Am. Chem. Soc.* **2014**, *136*, 7777. (c) Rekhroukh, F.; Brousses, R.; Amgoune, A.; Bourissou, D. *Angew. Chem. Int. Ed.* **2015**, *54*, 1266. (d) Joost, M.; Zeineddine, A.; Estévez, L.; Mallet-Ladeira, S.; Miqueu, K.; Amgoune, A.; Bourissou, D. *J. Am. Chem. Soc.* **2014**, *136*, 14654.

7.2 – Synthesis of a Gold(I) Complex Featuring the FcPPB Ligand

The reactions of [AuCl(SMe_2)], [AuCl(PPh_3)] or [AuCl(CO)] with FcPPB resulted in precipitation of white, insoluble solids that were not investigated further. By contrast, initial treatment of [AuCl(PPh_3)] with $GaCl_3$, followed by the addition of FcPPB provided [{Au(FcPPB)}$_2$][$GaCl_4$]$_2$ (**40**) as a tangerine-coloured solid in 90 % yield (Scheme 7.1). Complex **40** was obtained as a mixture of diastereomers in an approximate 3:2 ratio, giving rise to one set of signals in the $^{31}P\{^1H\}$ NMR spectrum at 63.3 and 40.7 ppm ($^2J_{31P,31P}$ = 310 Hz), and a second set of signals located at 63.1 and 39.1 ppm ($^2J_{31P,31P}$ = 302 Hz); in both cases, the signal located at the highest frequency represents the $C_5H_4P(^tBu)Ar$ phosphine, whereas the signal located at the lowest frequency represents the $C_5H_4PPh_2$ phosphine, based on ^1H-^{31}P-HMBC NMR experiments. The ^{31}P-^{31}P coupling constants for each diastereomer are characteristic of *trans*-disposed phosphine ligands bound to gold, and are in good agreement with $^2J_{31P,31P}$ values reported for [Au(PPh_3){(Ph_2P)CH(PPh_2)$_2$M(cod)}] (M = Rh, Ir; cod = 1,5-cyclooctadiene)[267] and [Au(PPh_3){κ^1*P*-7-PPh_2-8-Ph-7,8-nido-$C_2B_9H_{10}$}],[268] which are 329, 328 and 320 Hz, respectively.

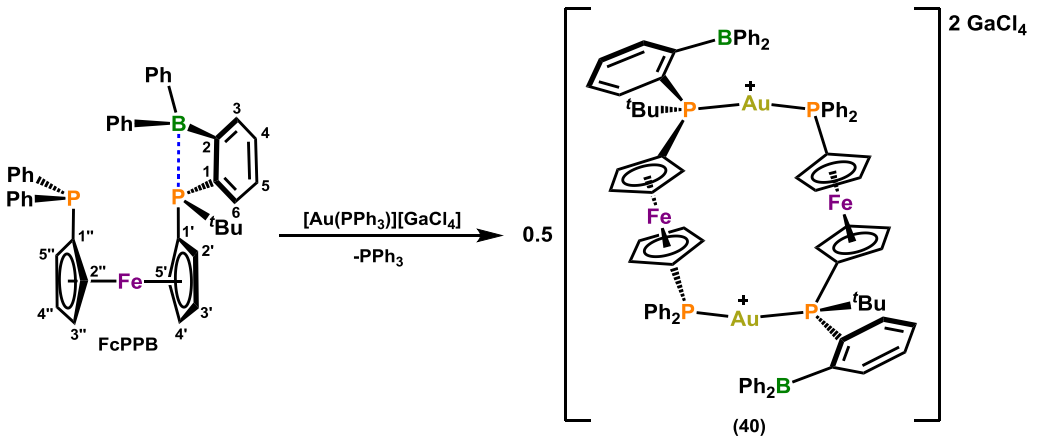

Scheme 7.1. Synthesis of [{Au(FcPPB)}$_2$][$GaCl_4$]$_2$ (**40**).

We were not able to separate the *rac*- and *meso*-diastereomers of complex **40**, but an X-ray crystal structure of *meso*-**40**·$2C_6H_{14}$ was obtained from a batch of X-ray quality crystals containing both the *rac*- and *meso*-diatereomers (Figure 7.1); PXRD was used to ascertain that crystallization of **40** yielded a mixture of diastereomers. The X-ray crystal structure for *meso*-**40** verified dimerization of two {Au(FcPPB)} units, allowing for *trans*-κ^2*PP*-coordination at gold, similarly to [{Pt(FcPPAl)}$_2$] (FcPPAl = [Fe(η^5-$C_5H_4PPh_2$)(η^5-$C_5H_4P^tBu${(*o*-$AlMe_2$)C_6H_4})]; Chapter 8). The Au–P(1) and Au–P(2) bond lengths are 2.3149(6) and 2.3178(7) Å, respectively, and are in good agreement with the reported Au–P bond lengths in $[Au(PR_3)_2]^+$ complexes in the literature.[268,269] The coordination geometry at gold is approximately linear with a P(1)–Au–P(2) bond angle of 158.84(2)°, and the two Au(I) centres are separated by a distance of ~6.8 Å, negating the possibility of aurophilic interactions.[270] The ^{11}B NMR chemical shift for **40** is 68 ppm, and the geometry of boron is nearly planar [Σ(C–B–C) = 359.4(4)°] which suggests that the borane in FcPPB is free of any interaction with the gold centre. Furthermore, the Au–B bond distance in *meso*-**40** is 3.121(3) Å, which is significantly longer than the sum of the covalent radii (2.20 Å)[68] as well as the Au–B bond lengths reported for [AuCl($^{i\text{Pr}}$MPB$^{\text{R}'}$)] [$^{i\text{Pr}}$MPB$^{\text{R}'}$ = (*o*-^{i}Pr$_2$P)C_6H_4BR'$_2$; BR'$_2$ = BCy_2, Au–B = 2.90 Å; BR'$_2$ = BFlu, BFlu = 9-boraflourenyl, Au–B = 2.66 Å),[47] [AuCl($^{\text{R}}$DPB$^{\text{Ph}}$)] [$^{\text{R}}$DPB$^{\text{Ph}}$ = {(*o*-R_2P)C_6H_4}$_2$BPh; R = ^{i}Pr, Au–B = 2.309(8) Å; R = Ph, Au–B = 2.335(5) Å],[44] [AuCl($^{i\text{Pr}}$TPB)] ($^{i\text{Pr}}$TPB = {(*o*-^{i}Pr$_2$P)C_6H_4}$_3$B; Au–B = 2.318(8) Å),[132] [Au($^{i\text{Pr}}$TPB)][$GaCl_4$] (Au–B = 2.448 Å)[133] and [Au($^{\text{Ph}}$DPB$^{\text{Ph}}$)][SbF_6] (Au–B = 2.521 Å),[271] which feature direct κ^1*B*-coordination of a pendant borane to gold. However, the Au–B bond distance in *meso*-**40** is within the sum of the Van der Waals radii (~3.75 Å)[182] and the gold centre is puckered towards the borane of FcPPB, lying 0.425 Å above the centroid of the P(1)···P(2) intercept, and bent at an angle of 21.16(2)° towards the borane, which suggests that a weak interaction may exist between boron and gold, despite the cationic charge on the metal centre.

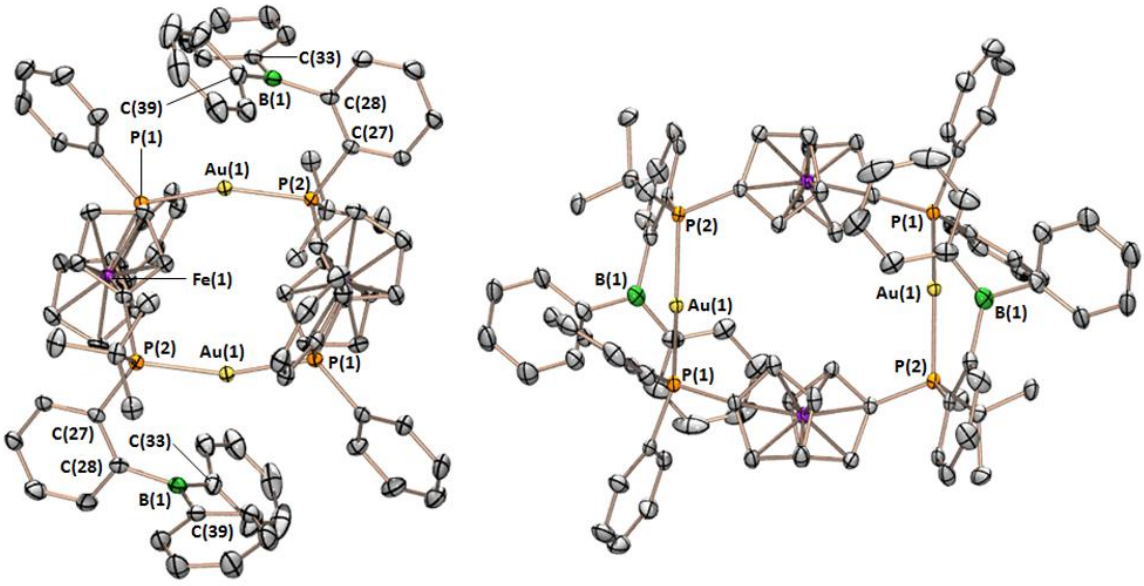

Figure 7.1. Two different views of the solid-state structure for *meso*-[{Au(FcPPB)}$_2$][GaCl$_4$]$_2$·2C$_6$H$_{14}$ (*meso*-**40**·2C$_6$H$_{14}$) with ellipsoids drawn at 50% probability. Hydrogen atoms, lattice solvent, and the GaCl$_4$ counter anion have been omitted for clarity.

7.3 – Synthesis of [W(CO)$_4$(FcPPB*)]

As mentioned in Section 7.1, we sought to explore the coordination chemistry of FcPPB with metal-carbonyl pre-cursors in an attempt to encourage functionalization of the carbonyl co-ligands through CO–borane coordination. Bercaw and Labinger were able to accomplish this task by utilizing the phosphine-borane ligand Ph$_2$P(CH$_2$)$_2$(9-BBN) (9-BBN = 9-borabicyclo[3.3.1]nonanyl) to promote hydride and alkyl group insertion into a carbonyl co-ligand bound to rhenium in *trans*-[Re(CO)$_4${κ^1*P*-Ph$_2$P(CH$_2$)$_2$(9-BBN)$_2$}][BF$_4$] (see Section 1.3.1.4 for discussion).[63,64,110] The reaction of FcPPB with [W(CO)$_6$] under photochemical conditions provided an orange solid in 82 % yield (Scheme 7.2). Coordination of the 1,1'-bisphosphinoferrocene backbone of the FcPPB ligand was evidenced by signals located at 19.7 and 14.2 ppm in the ^{31}P{^{1}H} NMR spectrum, which exhibited $^1J_{31P,183W}$ coupling equal to 233 and 236 Hz, respectively, and a *cis*-$^2J_{31P,31P}$ coupling of 24 Hz. However, the C$_5$*H*$_4$-region of the ^{1}H NMR spectrum of **41** only integrated to seven protons as opposed to eight, and the ^{11}B NMR signal was

located at 57 ppm, which is uncharacteristic of metal-FcPPB complexes that exhibit either metal–borane or metal–co-ligand–borane coordination; displayed below in Figures 7.3–7.5 is the ^{1}H NMR spectrum of **41** with expanded views of the aromatic and C_5H_4-regions, and Figure 7.6 displays the $^{31}P\{^{1}H\}$ NMR spectrum. Numbered protons refer to the postions of the ferrocene backbone and the phenylene linker in the FcPPB* ligand, as shown in Scheme 7.2.

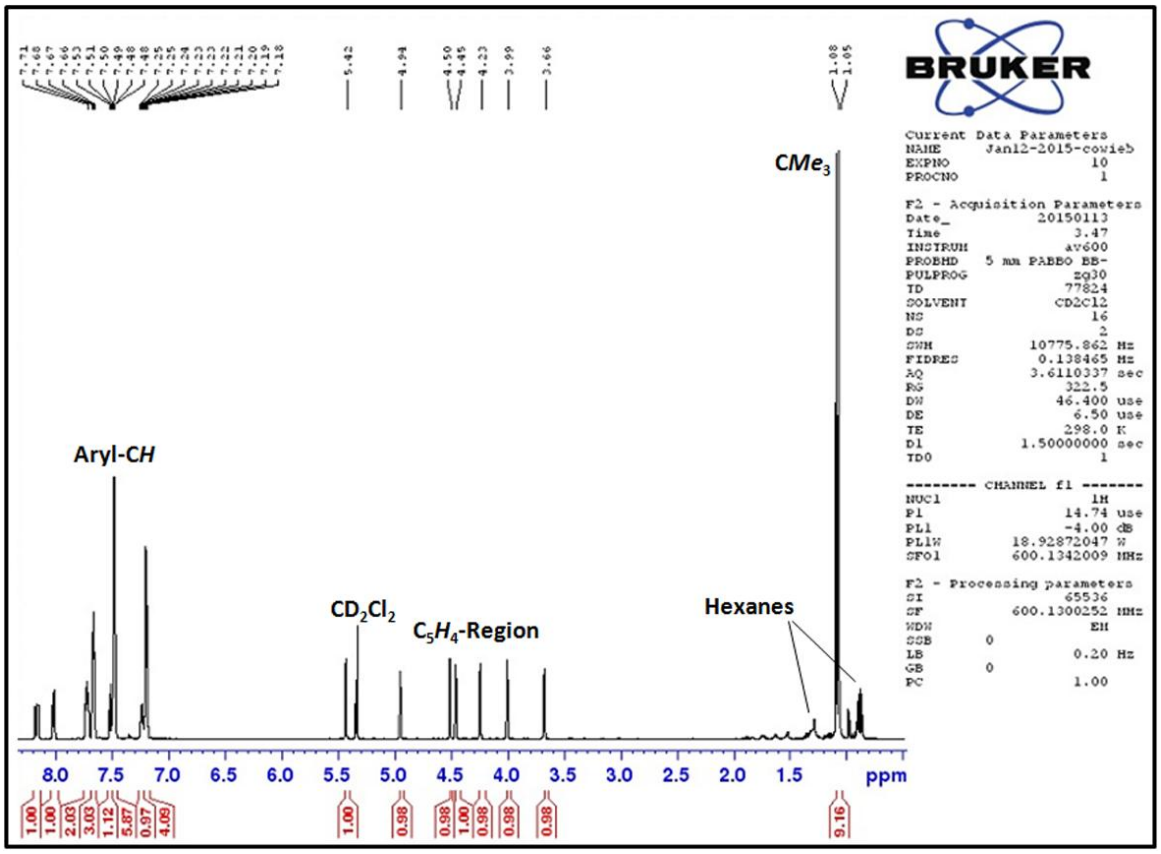

Figure 7.2. ^{1}H NMR spectrum of $[W(CO)_4(FcPPB^*)]$ (**41**; 600 MHz, 298 K, CD_2Cl_2).

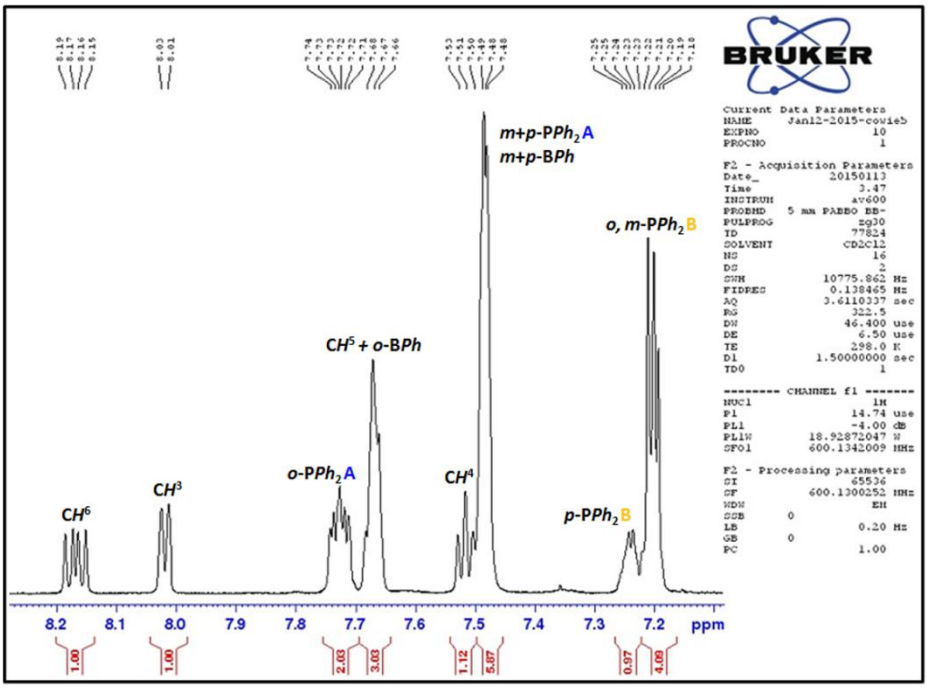

Figure 7.3. Expanded aromatic region of the ^{1}H NMR spectrum of [W(CO)$_4$(FcPPB*)] (**41**; 600 MHz, 298 K, CD_2Cl_2).

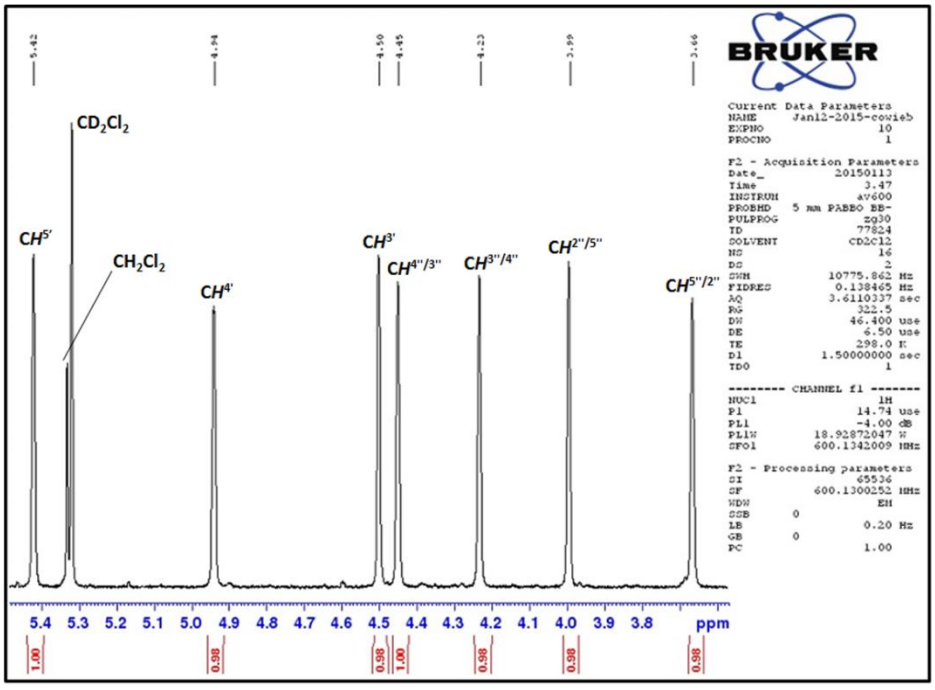

Figure 7.4. Expanded C_5H_4-region of the ^{1}H NMR spectrum of [W(CO)$_4$(FcPPB*)] (**41**; 600 MHz, 298 K, CD_2Cl_2).

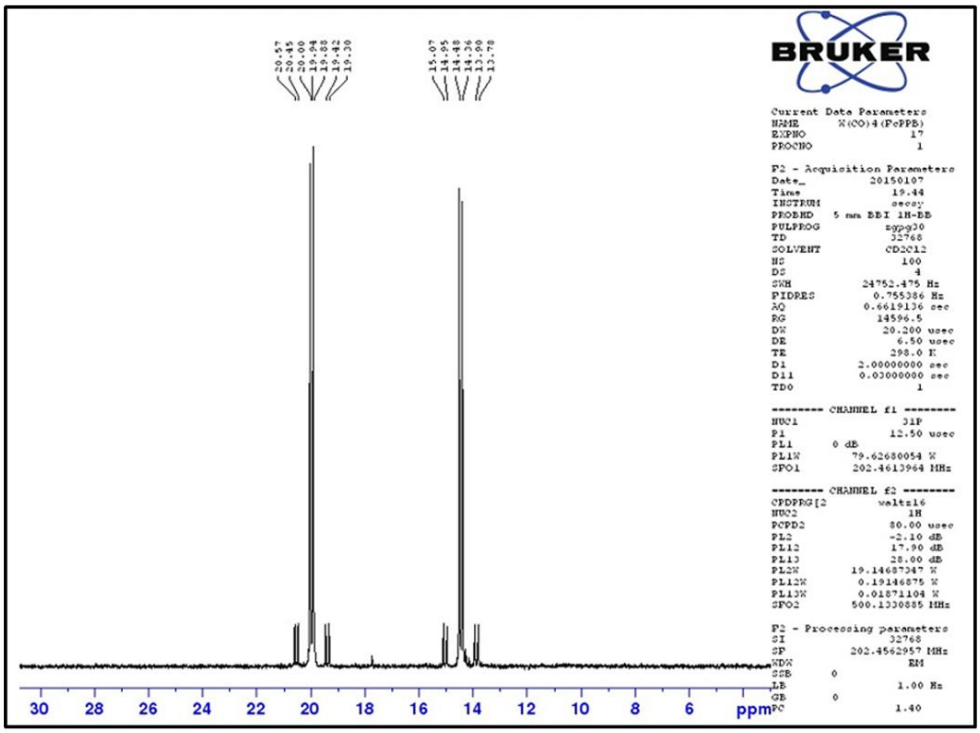

Figure 7.5. $^{31}P\{^{1}H\}$ NMR spectrum of $[W(CO)_4(FcPPB^*)]$ (**41**; 203 MHz, 298 K, CD_2Cl_2).

X-ray diffraction performed on orange crystals obtained by slow diffusion of hexanes into a benzene solution of **41** at room temperature verified bisphosphine-coordination, and revealed that the triarylborane in FcPPB had been converted into a diarylferrocenylborane, as boron was bound to the adjacent cyclopentadienyl ring of the ferrocene backbone and only retained one phenyl-substituent, ultimately providing $[W(CO)_4(FcPPB^*)]$ (**41**; FcPPB* = $[Fe(\eta^5\text{-}C_5H_4PPh_2)\{\eta^5\text{-}C_5H_3P(^t\!Bu)C_6H_4BPh\text{-}o\}]$, Figure 7.6). The W–P(1) and W–P(2) bond lengths in **41** are 2.569(1) and 2.572(1) Å, respectively, and tungsten adopts distorted octahedral geometry with *cis* and *trans* P–W–CO and OC–W–CO angles ranging from 82.03(9) to 97.73(3)° and 169.1(1) to 178.5(1)°, respectively; the P(1)–W–P(2) bite angle is 97.73(3)°.

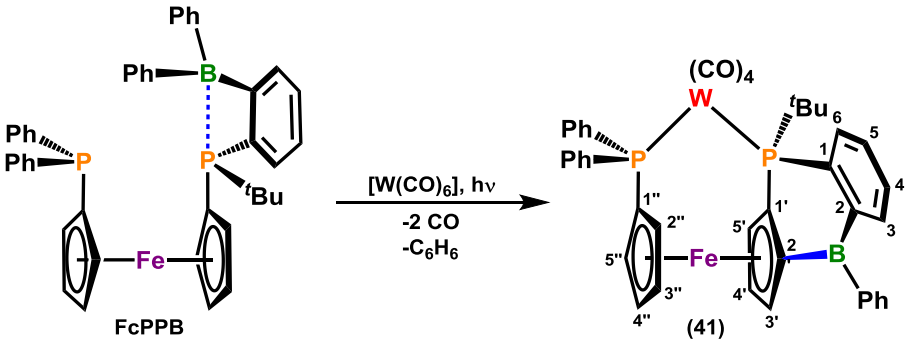

Scheme 7.2. Synthesis of $[W(CO)_4(FcPPB^*)]$ (**41**).

The ^{11}B NMR chemical shift for **41** is 57 ppm (*vide supra*) and the sum of the C–B–C angles is 360.0(5)°, characteristic of three-coordinate boron adopting trigonal planar coordination geometry. In addition, the B–C_{Cp} bond length [C_{Cp} = C(7)] is 1.533(5) Å. Similar values were reported for the borane-substituted ferrocenes [Fe(η^5-$C_5H_4BPh_2$)(η^5-C_5H_5)][272] and [Fe{η^5-C_5H_4B(*o*-tol)$_2$}(η^5-C_5H_5)],[273] as well as the 1,1'-phosphine/borane-disubstituted ferrocene [Fe(η^5-$C_5H_4PPh_2$)(η^5-$C_5H_4BMes_2$)][117] (Mes = 2,4,6-Me_3-C_6H_2), which possess ^{11}B NMR chemical shifts of 63, 70 and 85 ppm, B–C_{Cp} bond lengths of 1.542(5), 1.522(8) and 1.565(9) Å, and Σ(C–B–C) values of 360.2(5), 359.5(9) and 359.7(9)°, respectively. The B–C_{Cp} bond length in **41** is shorter than the B–C_{ipso} bond distances between boron and its phenyl substituents [B–C(28) = 1.572(5) Å; B–C(33) = 1.567(5) Å], indicating superior π-donation from the C_5H_3-ring relative to the phenyl groups. As a result, a borafulvene-type distortion is observed within the fused C_5H_3-ring, in which the C(6)–C(7) and C(7)–C(8) bond lengths are 1.443(5) and 1.446(5) Å, and the remaining C–C bond lengths range from 1.406(5)–1.426(5) Å [the C(9)–C(10) bond length is 1.426(5) Å]; the C–C bond lengths range from 1.415(5)–1.434(5) Å in the $C_5H_4PPh_2$-ring. Similar distortions have been reported for the aforementioned borane- and 1,1'-borane/phosphine-disubstituted ferrocenes, in which the longest cyclopentadienyl C–C bond lengths are the C_{ortho}–C_{ipso} bonds of the borane-substituted C_5H_4-ring.

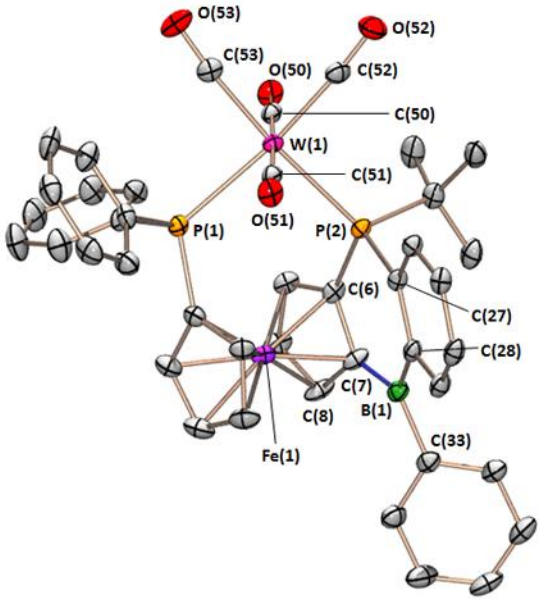

Figure 7.6. Solid-state structure for $[W(CO)_4(FcPPB^*)]\cdot C_6H_6$ (**41**$\cdot C_6H_6$) with ellipsoids drawn at 50 % probability. Hydrogen atoms and lattice solvent have been omitted for clarity.

A remarkable feature of **41** is the degree of bending of the borane towards iron in the ligand backbone. Wagner and co-workers have explored this feature within a series of borane-substituted ferrocenes, and concluded that bending of the borane towards iron is due primarily to: (1) A localized bonding interaction between the iron d_{x2-y2} orbital and the B–C_{ipso} π-system, (2) a delocalized through-space interaction involving the B–C_{ipso} π-system and the other Cp-ring, and (3) an electrostatic interaction involving the borane and the other Cp-ring. The degree of bending of the ferrocenyl-borane towards iron is referred to as the dip angle, α*, which is obtained by subtracting α from 180° (α = Cp_{cent}–C_{ipso}–B; Cp_{cent} = centroid of the borane-substituted Cp-ring), and decreases as the Lewis acidity of the borane unit decreases.[272,274,275] Complex **41** possesses a dip angle of 12°, which is in good agreement with the aforementioned borane-substituted ferrocenes [Fe(η^5-$C_5H_4BPh_2$)(η^5-C_5H_5)] and [Fe{η^5-C_5H_4B(*o*-tol)$_2$}(η^5-C_5H_5)] (α* = 13 and 8°, respectively). However, it is smaller than α* for [Fe(η^5-$C_5H_4BBr_2$)(η^5-C_5H_5)] (α* = 17.7, 18.9°)[274] and [Fe{η^5-$C_5H_4B(C_6F_5)_2$}(η^5-C_5H_5)] (α* = 16°),[276] in accordance with the reduced Lewis acidity of the borane in **41**.

7.4 – Synthesis of [Ru_3(μ-H)(CO)$_{10}$(FcPPB**)]

Heating a benzene solution of FcPPB and [$Ru_3(CO)_{12}$] to 85 °C resulted in a rapid colour change from orange to deep blood red, along with CO evolution (Scheme 7.3). After one hour, the reaction mixture gave rise to three singlets in the $^{31}P\{^1H\}$ NMR spectrum at 27.9, 17.6 and 17.2 ppm, and continued heating for an additional 4 hours resulted in disappearance of the singlet at 17.6 ppm (while the other two remained), and emergence of a pair of doublets at 42.6 and 41.3 ppm, which became the major product after 5 days of heating (a small amount of impurities were also present). Repeated recrystallization from hexanes at –30 °C resulted in precipitation of the impurities and isolation of the major product (**42**) in moderate purity. Similarly to complex **41**, the ^1H NMR spectrum of **42** contained only seven C_5H_4-signals as opposed to eight, indicating that reactivity similar to that observed en route to tungsten complex **41** may be operative.

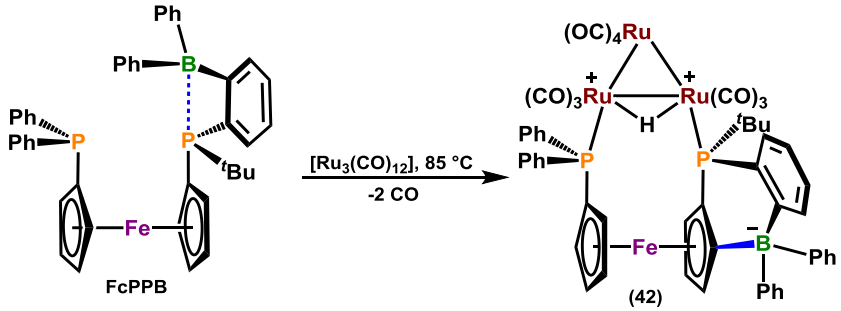

Scheme 7.3. Synthesis of [Ru_3(μ-H)(CO)$_{10}$(FcPPB**)] (**42**).

X-ray quality crystals were obtained by cooling a hexanes solution of the major product to –30 °C, and X-ray diffraction revealed the structure of [Ru_3(μ-H)(CO)$_{10}$(FcPPB**)]·1.3(C_6H_{14}) (Figure 7.7). Similarly to complex **41**, [Ru_3(μ-H)(CO)$_{10}$(FcPPB**)] (**42**) possesses a new B–C bond between boron and the adjacent C_5H_4-ring. However, as opposed to concomitant elimination of benzene, as is observed in the formation of **41**, the fused ligand backbone in **42** contains an anionic borate that retains both phenyl rings, and a newly created hydride ligand is observed to bridge

between two Ru(I) centres. The neutral FcPPB ligand has therefore been transformed into anionic FcPPB** (FcPPB** = $[Fe(\eta^5\text{-}C_5H_4PPh_2)\{\eta^5\text{-}C_5H_3P(^t\text{Bu})C_6H_4BPh_2\text{-}o\}]^-$). Examples of electrophilic borylation of a cyclopentadienyl ring, resulting in formation of a cyclopentadienylborate and electrophilic addition of a Cp–H proton to a metal centre have also been reported by Braunschweig and co-workers; reaction of $^t\text{BuBCl}_2$ with $[Cp_2WH_2]$ yielded $[WH_3(\eta^5\text{-}C_5H_5)(\eta^5\text{-}C_5H_4B^t\text{BuCl}_2)]$,[23] and reaction of $B(C_6F_5)_3$ and $Me_2NB(CF_3)_2$ with $[Cp_2WH_2]$ lead to the formation of zwitterionic $[WH_3(\eta^5\text{-}C_5H_5)\{\eta^5\text{-}C_5H_4B(C_6F_5)_3\}]$ and $[WH_3(\eta^5\text{-}C_5H_5)\{\eta^5\text{-}C_5H_4B(NMe_2)(CF_3)_2\}]$, respectively.[25]

The Ru(1)–Ru(2), Ru(1)–Ru(3) and Ru(2)–Ru(3) distances in **42** are 3.0312(5), 2.8961(6) and 2.8797(5) Å, respectively, which are longer than those observed in $[Ru_3(\mu\text{-}H)(CO)_{10}(\kappa^2\textit{CN}\text{-L})]$ (L = quinoxaline) (Ru–Ru = 2.9014(5), 2.8664(4), 2.8407(5) Å),[277] but are in good agreement with $[\{Ru_3(\mu\text{-}H)\{\mu\text{-}P(CF_3)_2\}(CO)_{10}\}_2]$ (Ru–Ru = 3.047(1), 2.884(1), 2.878(1) Å).[278] The $B–C_{Cp}$ [C_{Cp} = C(7)] bond length in **42** is 1.624(6) Å, which is longer than the $B–C_{Cp}$ distance in **41** [1.533(5) Å], but is in good agreement with the ferrocenylborates $Li[\{Fe(\eta^5\text{-}C_5H_5)(\eta^5\text{-}C_5H_4)\}_2(\mu\text{-}BMe_2)]$ [$B–C_{Cp}$ = 1.641(1), 1.638(3) Å][275] and $[Fe(\eta^5\text{-}C_5H_5)\{\eta^5\text{-}C_5H_3\text{-}1\text{-}(CH_2NH^i\text{Pr}_2)\text{-}2\text{-}BF_3\}]$ [$B–C_{Cp}$ = 1.604(2) Å].[279] Additionally, boron is significantly pyramidalized, as is expected for an anionic borate, with the sum of the $C_{aryl}–B–C_{aryl}$ angles equal to 327.4(5)°.

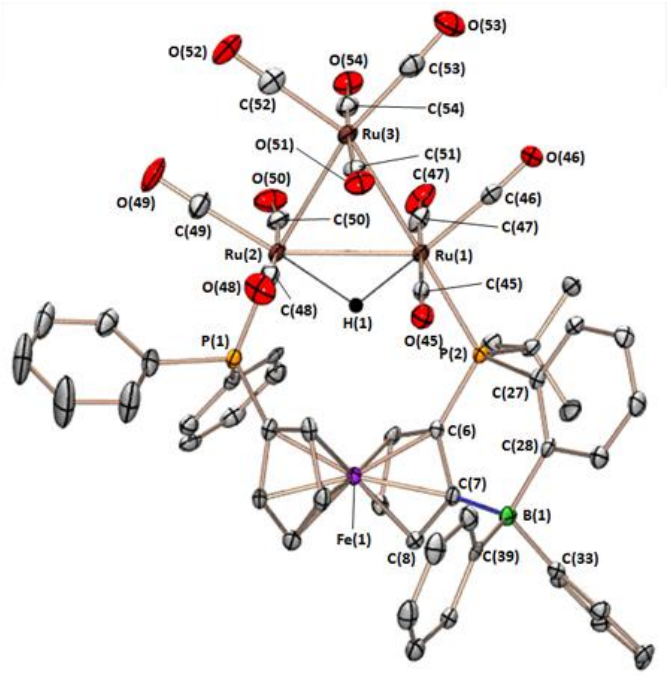

Figure 7.7. Solid-state structure for $[Ru_3(\mu\text{-}H)(CO)_{10}(FcPPB^{**})]\cdot 1.3(C_6H_{14})$ [**42**$\cdot 1.3(C_6H_{14})$] with ellipsoids drawn at 50 % probability. With exception of H(1), which was located in the difference map, all hydrogen atoms and lattice solvent have been omitted for clarity.

The ^{11}B NMR spectrum of complex **42** contains a signal at –11.4 ppm exhibiting a $^{3}J_{11B,31P}$ coupling of 29 Hz. Additionally, the ^{31}P NMR signals located at 42.6 and 41.3 ppm exhibit a $^{2}J_{31P,31P}$ coupling of 22 Hz. The Ru(1)–P(2) and Ru(2)–P(1) bond lengths are 2.425(1) and 2.370(1) Å, respectively, and the Ru(1)–H(1) and Ru(2)–H(1) bond distances are 1.72(5) and 1.97(6) Å, respectively. However, the bridging hydride ligand was not located by NMR (206 to 298 K) or IR spectroscopy. Noteworthy of complex **42** is the conformational flexibility of the ferrocene backbone, accommodating κ^1*P*-coordination of the phosphines to two different Ru(I) centres. The P(1)–Cent$^{1–5}$–Cent$^{6–10}$–P(2) dihedral angle [Cent$^{x–y}$ = centroid of the cyclopentadienyl ring containing atoms C(x)–C(y)] is 66.9°, which is greater than the corresponding dihedral angle in **41** (50.4°), but smaller than that in **40** (–146.9°). The ability for the 1,1'-bis(phosphino)ferrocene ligand backbone to support κ^1*P*-coordination to different metal centres with drastically different P(1)–Cent$^{1–5}$–Cent$^{6–10}$–P(2) torsion angles highlights the enhanced

conformational flexibility of this particular ligand backbone over the thioxanthene backbone of the TXPB ligand utilized in Chapters 2–4.

Table 7.1. Crystallographic Data Collection and Refinement Parameters for Complexes **40**, **41**, **42** and **44**.

Structure	**40 · 2C_6H_{14}**	**41 · C_6H_6**	**42 · 1.3(C_6H_{14})**	**44**
Formula	$C_{100}H_{110}Au_2B_2Cl_8Fe_2Ga_2P_4$	$C_{48}H_{41}BFeO_4P_2W$	$C_{62}H_{41}BFeO_{10}P_2Ru_3$	$C_{38}H_{36}B_2F_4FeP_2$
Formula wt	2386.08	994.26	1377.76	708.08
T (K)	100(2)	100(2)	100(2)	100(2)
Cryst. Syst.	Monoclinic	Monoclinic	Triclinic	Orthorhombic
Space Group	$P2_1/n$	$P2_1/n$	$P\bar{1}$	$P2_12_12_1$
a (Å)	16.674(3)	11.819(3)	14.288(2)	10.475(1)
b (Å)	17.471(3)	11.940(3)	15.083(2)	17.090(2)
c (Å)	18.579(3)	29.045(7)	15.410(2)	18.218(3)
α [deg]	90	90	83.334(2)	90
β [deg]	116.221(3)	96.912(4)	62.353(2)	90
γ [deg]	90	90	70.878(2)	90
Volume [$Å^3$]	4855(2)	4069(2)	2776.8(6)	3261.3(8)
Z	2	4	2	4
μ (mm^{-1})	4.185	3.305	1.174	0.612
F(000)	2464	1984	1372	1464
Crystal Size (mm^3)	0.30×0.22×0.12	0.31×0.23×0.08	0.26×0.13×0.08	0.24×0.10×0.03
θ Range for Collection [deg]	1.37–31.25	1.95–31.59	1.43–29.66	1.63–26.38
No. of Reflns Collected	102971	65062	34087	17563
No. of Indep Reflns	15754	13587	13594	6652
Completeness to θ Max (%)	99.6	99.5	86.5	99.9
Absorption Correction	Numerical	Numerical	Numerical	Numerical
Max and Min Transmission	0.6336, 0.3666	0.7779, 0.4272	0.9119/0.7500	0.9819, 0.8671
GOF on F^2	0.989	1.028	0.930	1.019
Final R_1 [$I > 2\sigma(I)$] (%)	2.79	3.66	4.36	5.89

7.5 – Discussion of the Reaction Pathways En Route to Complexes 41 and 42

Examples of direct electrophilic borylation of cyclopendadienyl rings of ferrocene and other metals, resulting in the formation of a metal-coordinated $C_5H_4BR_3$ ligand, are prevalent in the literature, however it has only been achieved through the use of highly Lewis acidic boranes, such as BX_3 (X = Cl, Br, I), B_2Cl_4, $HBCl_2$, $RBBr_2$ (R = Me, Ph), $B(C_6F_5)_3$, and $HB(C_6F_5)_2$, and typically requires refluxing solvent (e.g. hexanes, toluene, CS_2).[280] Therefore, to the best of our knowledge, formation of **41** is the first example of direct, room temperature electrophilic borylation of ferrocene involving an aryldiphenylborane. The formation of $[Ru_3(\mu\text{-}H)(CO)_{10}$(FcPPB**)] (**42**) only occurred under thermal conditions, and the synthesis of $[W(CO)_4$(FcPPB*)] (**41**) only proceeded under photochemical conditions; no reaction took place when a benzene solution of FcPPB and $[W(CO)_6]$ was heated to 80 °C. Additionally, free FcPPB does not react with itself in a similar manner, even after heating a benzene solution to ~90 °C for days, or subjecting a benzene solution to photochemical reaction conditions for 24 hours.

Photochemical reaction conditions will undoubtedly promote dissociation of carbonyl ligands from $[W(CO)_6]$, which would allow for initial κ^2*PP*-coordination of the 1,1'-bisphosphinoferrocene backbone of FcPPB. At this point, the pendant borane will no longer be phosphine-coordinated, allowing for attack of the borane on the cyclopentadienyl ring. However, $[\{Au(FcPPB)\}_2][GaCl_4]$ (**40**) also contains a free (or only very weakly coordinated) pendant borane, and no reaction was observed when a CD_2Cl_2 solution of this complex was subjected to photochemical reaction conditions, or heated to 75 °C for 16 hours. The reluctance of compound **40** to engage in thermally- or photochemically-induced cyclopentadienyl ring borylation may be a consequence of the linear κ^2*PP*-coordination geometry enforced through dimerization of two {Au(FcPPB)} units. By contrast, in $[W(CO)_4$(FcPPB)], which is proposed as the initial product in the reaction of FcPPB with $[W(CO)_6]$, the absence of W–B or W–CO–B coordination, combined with the possibility for close approach of the pendant borane to the adjacent cyclopentadienyl ring of ferrocene (via rotation of the $P–C_{ipso}$ bond to the phenylene linker; Scheme 7.4) may allow for electrophilic addition of the borane to the

cyclopentadienyl ring, transforming the FcPPB ligand into FcPPB* via subsequent loss of benzene. Formation of triruthenium complex **42** likely follows the same initial reaction pathway (bisphosphine coordination followed by electrophilic addition of the borane to the adjacent cyclopentadienyl ring), and whereas no intermediate species were detected during the formation of **41**, the $^{31}P\{^{1}H\}$ NMR spectrum in the early stages of formation of **42** contained two singlets at 27.9 and 17.2 ppm (*vide supra*), which are shifted to slightly higher frequency relative to the ^{31}P chemical shifts for **41** (19.7 and 14.2 ppm). Additionally, at this point in the reaction, all eight cyclopentadienyl protons are present, suggesting the initially formed intermediate is $[Ru_3(CO)_{10}(FcPPB)]$. The lower frequency shift of the ^{31}P NMR signals for $[Ru_3(CO)_{10}(FcPPB)]$ relative to **42** (42.6 and 41.3 ppm, *vide supra*) can be attributed to coordination to Ru(0) in the former, as opposed to Ru(I) in the latter. The formation of a ferrocenylborane **41** via loss of benzene, rather than formation of a ferrocenylborate anion via electrophilic addition of the Cp–H proton to the metal, as is observed for **42**, is likely due to differences in oxidation potential; a 2-electron process would be required for Cp–H electrophilic addition at W(0), whereas two 1-electron oxidations can achieve this transformation in the Ru_3-fragment.[§]

[§] In an attempt to compare intramolecular and intermolecular borane addition to a cyclopentadienyl ring of a transition metal-coordinated 1,1'-bis(phosphino)ferrocene ligand, borane-free $[W(CO)_4(dppf)]$ (dppf = 1,1'-bis(diphenylphosphino)ferrocene) was subject to reactions with various unsupported boranes. Heating benzene solutions of $[W(CO)_4(dppf)]$ with either BEt_3, BPh_3 or $B(C_6F_5)_3$ to 80 °C for days did not produce a reaction in the case of BEt_3 and BPh_3, and yielded an insoluble orange precipitate in the case of $B(C_6F_5)_3$, which was not further characterized.

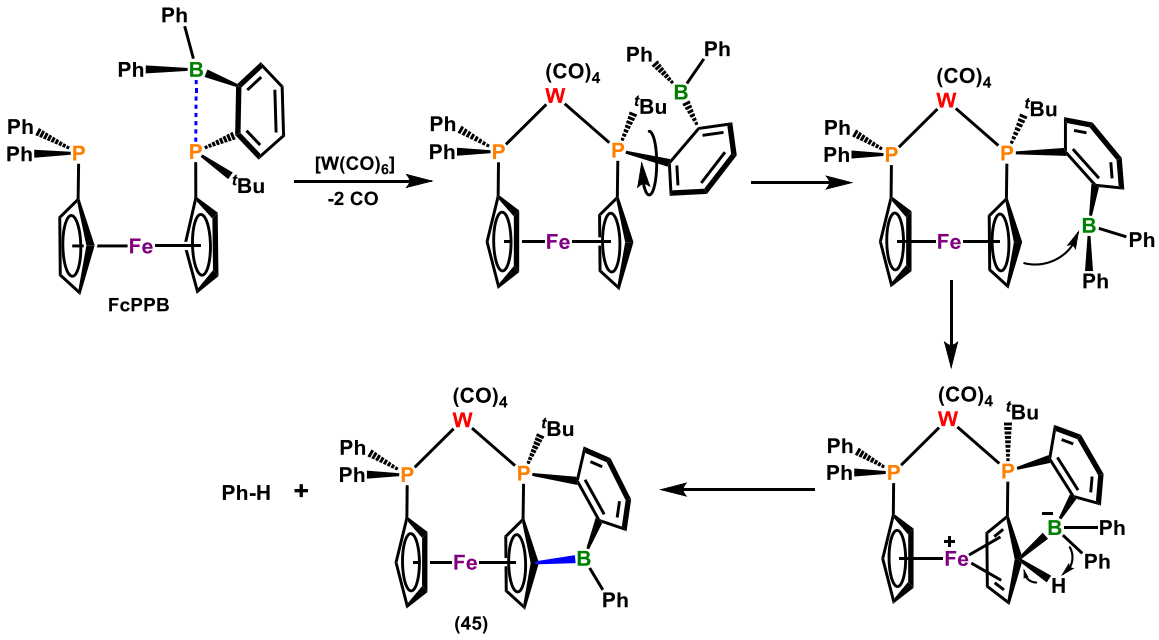

Scheme 7.4. Proposed reaction pathway for the formation of [W(CO)$_4$(FcPPB*)] (**41**).

7.6 – Attempts to Promote Intramolecular Electrophilic Borylation of the Ferrocene Backbone in Free FcPPB

The lack of borylation reactivity observed for free FcPPB under both thermal and photochemical conditions is noteworthy, and is perhaps due to the presence of intramolecular P→B adduct formation involving the $C_5H_4P(^tBu)Ar$ phosphine, which prevents the borane from interacting with the adjacent cyclopentadienyl ring. In order to probe whether intramolecular electrophilic borylation is possible within the free ligand, various Lewis acids were introduced to FcPPB in an attempt to displace the intramolecular P→B adduct; Lewis acids of appropriate size and acidity should preferentially bind to the ferrocenyl-phosphines, rendering the pendant borane free and potentially capable of interacting with the adjacent Cp-ring. While the addition of either BEt_3 or BPh_3 did not result in a reaction, and $AlMe_3$ yielded a complex mixture of products, FcPPB reacted cleanly with both $B(C_6F_5)_3$ and $BF_3{\cdot}OEt_2$ (Schemes 7.5 and 7.6, respectively).

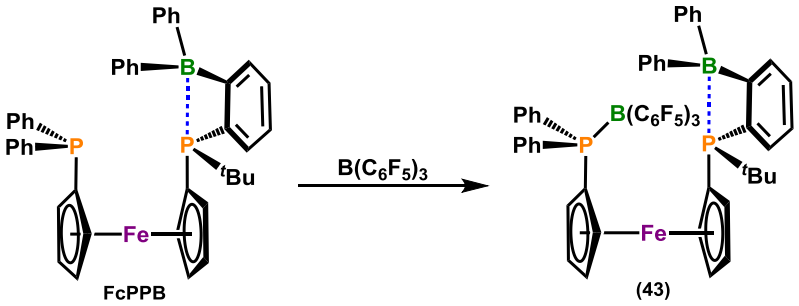

Scheme 7.5. Synthesis of FcPPB{$B(C_6F_5)_3$} (**43**).

The addition of one equivalent of $B(C_6F_5)_3$ to FcPPB provided [Fe(η^5-$C_5H_4PPh_2${$B(C_6F_5)_3$})(η^5-$C_5H_4P^tBu(C_6H_4BPh_2$-*o*)}], FcPPB{$B(C_6F_5)_3$} (**43**); the product of intermolecular adduct formation between $B(C_6F_5)_3$ and the $C_5H_4PPh_2$ phosphine. However, the intramolecular adduct between the non-fluorinated borane and the $C_5H_4P(^t$Bu)Ar phosphine is maintained in **43** (Scheme 7.5). Although X-ray quality crystals of **43** proved elusive, key spectroscopic evidence for the formation of **43** consists of: (1) A shift in the ^{31}P NMR signals from 19.7 and –17.2 ppm for FcPPB to 15.1 and 20.0 ppm for **43**, in which the signal located at 20.0 ppm is a broad singlet ($\omega_{1/2}$ ~ 93 Hz; Figure 7.11) indicating strong coordination to quadrupolar boron, (2) ^{1}H-^{31}P-HMBC NMR experiments verified that the ^{31}P NMR signal located at 20.0 ppm corresponds to the $C_5H_4PPh_2$ moiety (versus –17.2 ppm in FcPPB), indicating that this phosphine is significantly depleted of electron density in **43** relative to FcPPB, (3) a shift in the ^{11}B NMR signal from 17 ppm in FcPPB to 25 ppm, in conjunction with the emergence of a signal at –4 ppm, representing the adducted $B(C_6F_5)_3$ molecule, (4) ^{19}F NMR signals located at –125.1, –156.7 and –164.3 ppm with a ^{19}F $\Delta_{p\text{-}m}$ value of 7.6 ppm; these signals are significantly shifted relative to free $B(C_6F_5)_3$ and are in good agreement with those for $(C_6F_5)_3B$–PPh_3,[281] and (5) the ^{1}H NMR signals in the C_5H_4-region maintaining an integration of eight protons as opposed to seven, indicating that electrophilic addition of a borane to one of the cyclopentadienyl rings did not occur. The relatively small shifts in the $C_5H_4P(^t$Bu)Ar ^{31}P NMR signal (from 19.7 ppm in FcPPB to 15.1 ppm in **43**) and the Ar*B*Ph_2 ^{11}B NMR signal (from 17 ppm in FcPPB to 25 ppm in **43**) indicate that although the bonding interaction involving the pendant borane and the $C_5H_4P(^t$Bu)Ar phosphine

has been weakened, likely as a consequence of steric congestion imparted by the $B(C_6F_5)_3$ unit in **43**, the intramolecular adduct remains intact. Thus, a second equivalent of $B(C_6F_5)_3$ was added to **43** to again attempt to promote displacement of the intramolecular P–B interaction. However, this only resulted in sharpening of the singlet in the $^{31}P\{^1H\}$ NMR spectrum representing the $C_5H_4PPh_2$ moiety likely due to an equilibrium between **43** and a small amount of free FcPPB and $B(C_6F_5)_3$ in solution. The ^1H NMR spectrum of **43**, in addition to expanded views of the aromatic and C_5H_4-regions are displayed below in Figures 7.8–7.10, and the $^{31}P\{^1H\}$ NMR spectrum of **43** is displayed in Figure 7.11. Numbered protons refer to the positions on the ferrocene backbone and the phenylene linker of the FcPPB ligand, as shown in Scheme 7.1.

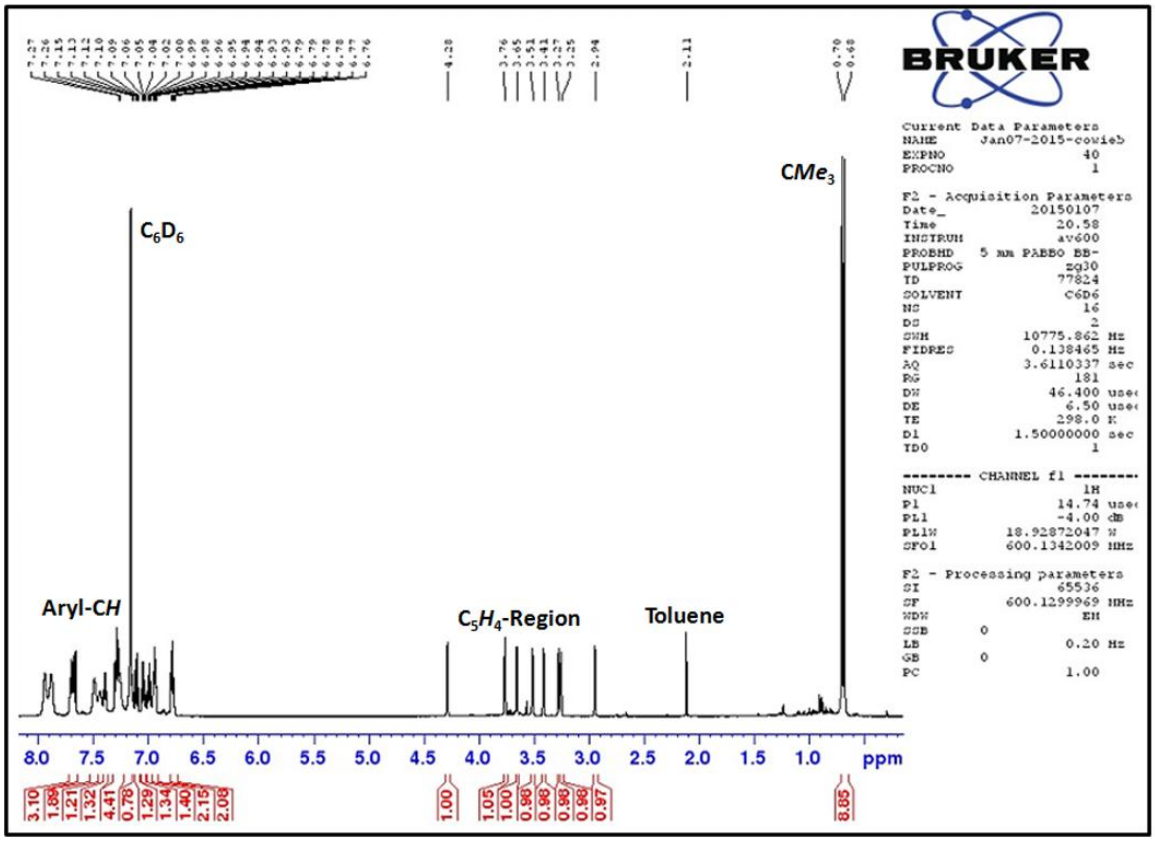

Figure 7.8. ^1H NMR spectrum of FcPPB{$B(C_6F_5)_3$} (**43**; 600 MHz, 298 K, C_6D_6).

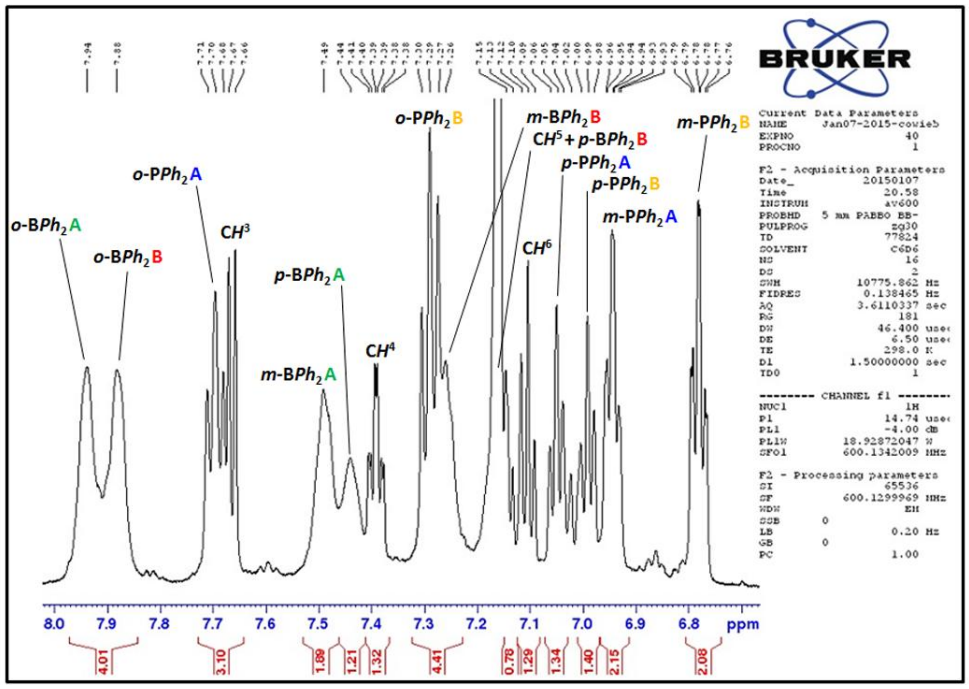

Figure 7.9. Expanded aromatic region of the ^{1}H NMR spectrum of FcPPB{B(C_6F_5)$_3$} (**43**; 600 MHz, 298 K, C_6D_6).

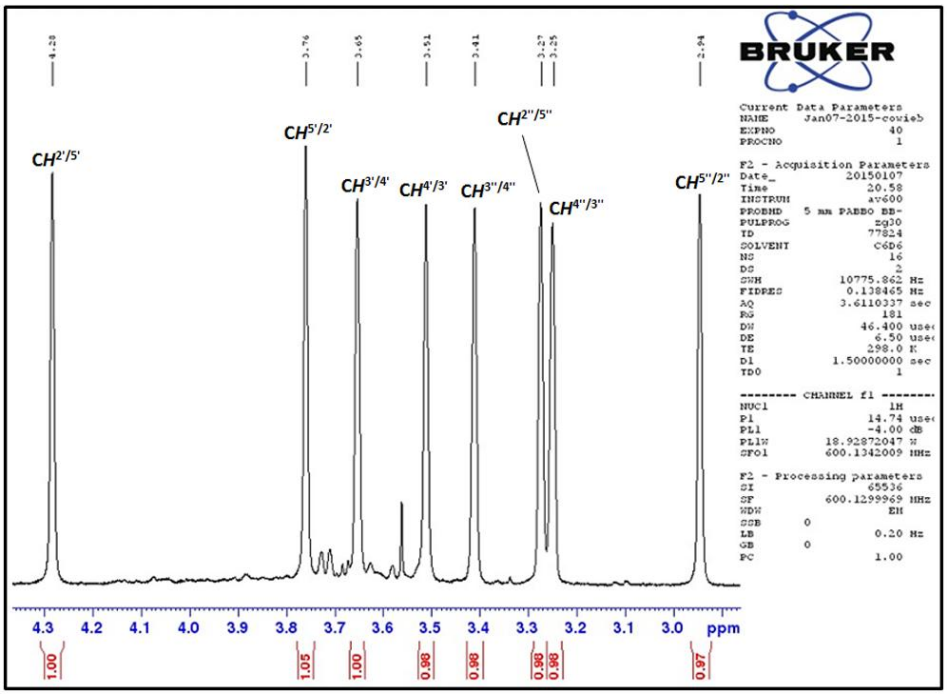

Figure 7.10. Expanded C_5H_4-region of the ^{1}H NMR spectrum of FcPPB{B(C_6F_5)$_3$} (**43**; 600 MHz, 298 K, C_6D_6).

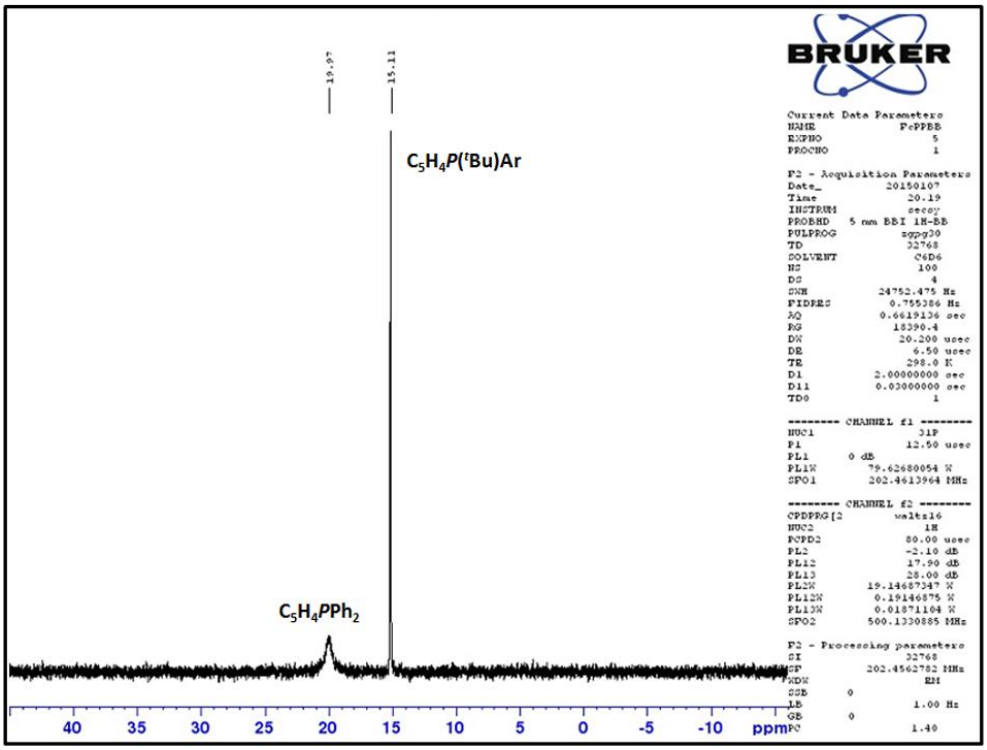

Figure 7.11. $^{31}P\{^{1}H\}$ NMR spectrum of FcPPB{$B(C_6F_5)_3$} (**43**; 203 MHz, 298 K, C_6D_6).

We hypothesized that the failure of $B(C_6F_5)_3$ to coordinate to the more electron donating $C_5H_4P(^tBu)Ar$ phosphine, rather than the $C_5H_4PPh_2$ phosphine, may be due to steric congestion resulting from the large size of the borane. Therefore, we sought to explore the reactivity of $BF_3{\cdot}OEt_2$ with FcPPB. However, rather than forming the $C_5H_4(^tBu)ArP\rightarrow BF_3$ adduct, an intramolecular bisphosphine-stabilized boronium cation was generated; $[Fe(\eta^5\text{-}C_5H_4PPh_2)\{\eta^5\text{-}C_5H_4P^tBu(C_6H_4BPh\text{-}o)\}][BF_4]$, $[FcPPB^{\text{-Ph}}][BF_4]$ (**44**) (Scheme 7.6). Formation of **44** likely proceeds via initial abstraction of a phenyl substituent from the pendant borane in FcPPB by BF_3, yielding the boronium cation **44** and BF_3Ph^-, followed by abstraction of F^- from BF_3Ph^- by a second equivalent of BF_3, yielding BF_4^- and BF_2Ph. The ^1H NMR spectrum of **44**, along with expanded views of the aromatic and C_5H_4-regions are displayed below in Figure 7.12–7.14.

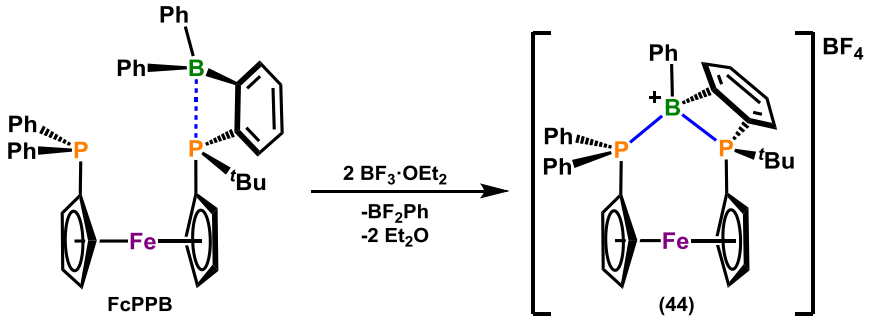

Scheme 7.6. Synthesis of [FcPPB^{-Ph}][BF_4] (**44**).

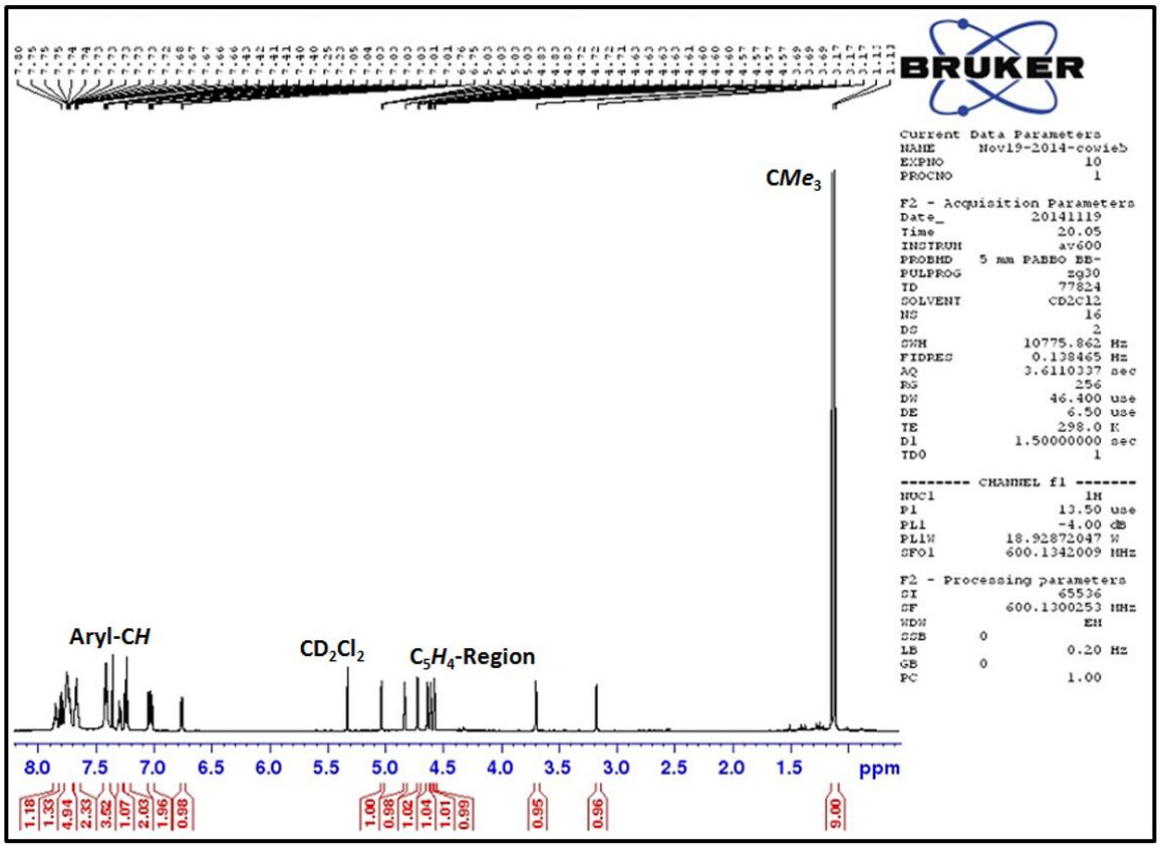

Figure 7.12. ^{1}H NMR spectrum of [FcPPB^{-Ph}][BF_4] (**44**; 600 MHz, 298 K, CD_2Cl_2).

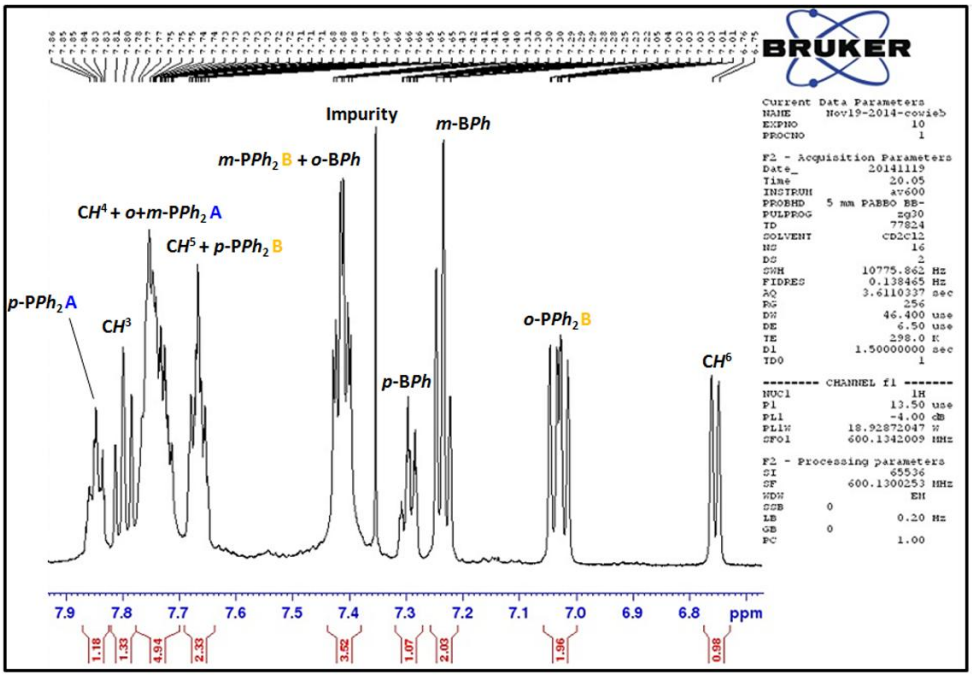

Figure 7.13. Expanded aromatic region of the ^{1}H NMR spectrum of [FcPPB^{-Ph}][BF_4] (**44**; 600 MHz, 298 K, CD_2Cl_2).

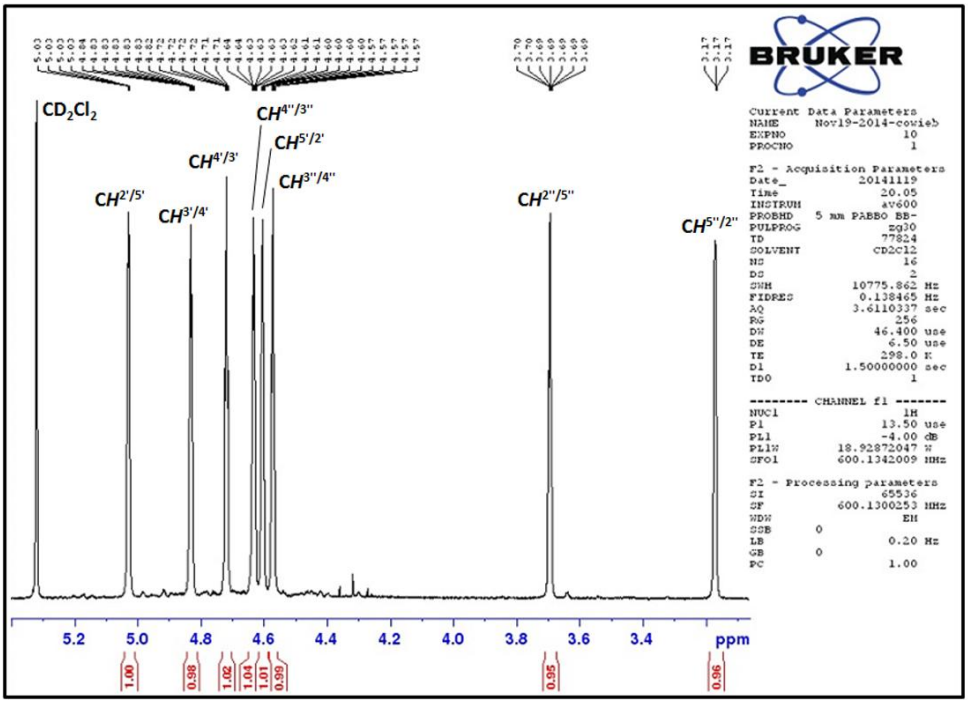

Figure 7.14. Expanded C_5H_4-region of the ^{1}H NMR spectrum of [FcPPB^{-Ph}][BF_4] (**44**; 600 MHz, 298 K, CD_2Cl_2).

Complex **44** crystallized as the *meso*-diastereomer over several days from a room temperature benzene solution of FcPPB and two equivalents of $BF_3{\cdot}OEt_2$. Moreover, the reaction rate and product yield was significantly increased by heating a benzene solution of the two reactants for several days at 70 °C, resulting in precipitation of **44** as a pale orange solid in 64 % yield; PXRD confirmed that **44** was isolated as the *meso*-diastereomer and not as a diastereomeric mixture. The solid-state structure of *meso*-**44** (Figure 7.15) features B–P(1) and B–P(2) bond lengths of 1.981(6) and 2.059(6) Å, respectively; the P(1)–B bonding interaction was non-existent in FcPPB, and the B–P(2) bond length in **44** is significantly shorter than that in FcPPB [2.146(2) Å], as expected for coordination to a cationic rather than a neutral boron centre. The P–B bond lengths in **44** are longer than those reported for the bisphosphineboronium salts $[(^tBu_2HP)_2BH_2]X$ (X = Br, P–B = 1.934(5), 1.948(5) Å; X = OTf, P–B = 1.938(2), 1.941(2) Å; X = BAr^F_4, P–B = 1.933(3), 1.936(3) Å; BAr^F_4 = $B\{C_6H_3\text{-}3,5\text{-}(CF_3)_2\}_4$)[282] and $[(Et_3P)_2BH_2][B(cat)_2]$ (cat = $C_6H_4\text{-}1,2\text{-}O_2$; P–B = 1.896(6)–1.913(6) Å),[283] which may be attributed to steric restraints imparted by the $FcPPB^{\text{-Ph}}$ ligand framework. To the best of our knowledge, **44** is the first intramolecular bisphosphine-stabilized boronium cation, although intramolecular phosphine-coordinated borenium cations $[C_{10}H_6\text{-}1\text{-}(PPh_2)\text{-}8\text{-}(BMes)]X$ (X = $GaBr_4$, NTf_2) were recently reported by Bourissou *et al.*[284]

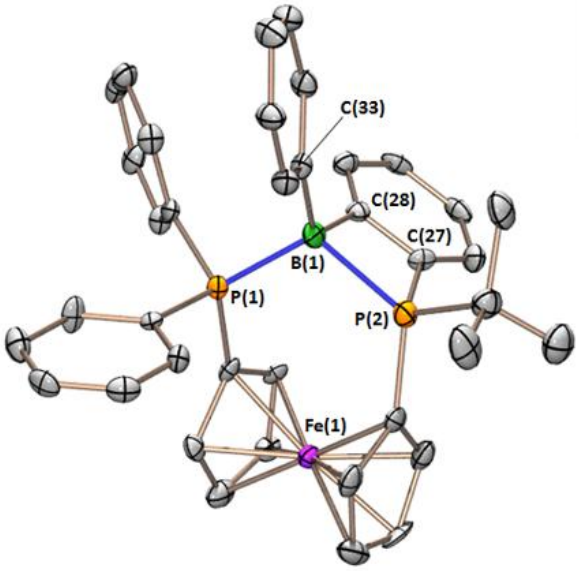

Figure 7.15. Solid-state structure for [FcPPB^{-Ph}][BF_4] (**44**) with ellipsoids drawn at 50 % probability. Hydrogen atoms, lattice solvent and the BF_4^- anion have been omitted for clarity.

Despite its insolubility in arene solvents, compound **44** is readily soluble in CH_2Cl_2, and gave rise to ^{31}P NMR signals at 27.8 and 1.0 ppm, representing the $C_5H_4P(^tBu)Ar$ and $C_5H_4PPh_2$ phosphines, respectively, and a ^{19}F NMR signal at –152.9 ppm (CD_2Cl_2). The ^{31}P NMR signals are broadened singlets with $\omega_{1/2}$ values of 65 and 150 Hz, respectively, indicative of coordination to quadrupolar boron, and are shifted to high frequency relative to FcPPB (*vide supra*) as a consequence of stronger coordination to cationic boron. The ^{11}B NMR signals are located at –1.4 and –2.0 ppm; the former is a sharp singlet representing the BF_4^- anion, and the latter is a broadened singlet ($\omega_{1/2}$ ~ 250 Hz) that corresponds to the FcPPB^{-Ph} boronium cation. The low frequency shift of the ^{11}B NMR signal from 17 ppm in FcPPB to –2.0 ppm in **44**, in conjunction with an increase in pyramidalization of boron in **4** relative to FcPPB [Σ(P–B–C) = 338.7(8)° in **44**; Σ(C–B–C) = 347.5(2)° in FcPPB) is also noteworthy. Similar features have been observed in the boronium cations [$Ph_2B(\mu$-py)$_2BMe_2$] [py = 2-pyridyl; ^{11}B NMR = 4.0 ppm; Σ(N–B–C) = 331.1(4)°],[285] and [Fe{η^5-$C_5H_4BMe(\kappa^2$*NN*-2,2'-bipy)}$_2$][PF_6]$_2$ [^{11}B NMR = 8.5 ppm; Σ(N–B–C) = 336.6(4)°],[286] the former being a zwitterion incorporating both a boronium cation and a borate anion within the same molecule. The bonding situation in **44** can be

best described as a superposition of two possible canonical structures, namely a bisphosphine-coordinated boronium cation, and a bisphosphonium-borate cation; a similar bonding description was used to describe the phosphine-borenium cation, [(cat)BP^{t}Bu$_3$][HB(C$_6$F$_5$)$_3$] (B(cat) = catecholboranyl, C$_6$H$_4$BO$_2$), prepared by Stephan and co-workers.[287]

7.7 – Summary

The coordination chemistry of the FcPPB ligand, [Fe(η^5-C$_5$H$_4$PPh$_2$){η^5-C$_5$H$_4$P^{t}Bu(C$_6$H$_4$BPh$_2$-*o*)}], has been expanded beyond the Group 10 metals. We were successful in isolating a molecular gold(I) complex of the FcPPB ligand, [{Au(FcPPB)}$_2$][GaCl$_4$]$_2$ (**40**), through the reaction of FcPPB with *in situ* generated [Au(PPh$_3$)][GaCl$_4$]. However, complex **40** features *trans*-κ^2*PP*-bisphosphine coordination of two different FcPPB units to each gold centre, resulting in a near linear geometry, and the pendant borane is not coordinated to gold. Nonetheless, future work involving complex **40** will survey the accessibility of the Au(I)–Au(III) oxidative addition pathway, with particular focus on the involvement/influence of the pendant Lewis acid. Moreover, the FcPPB ligand has proven suitable for coordination to a zero-valent Group 6 metal centre, tungsten, via reaction with [W(CO)$_6$] under photochemical conditions to provide [W(CO)$_4$(FcPPB*)] (**41**) and benzene. Compound **41** features a new borane-containing 6-membered *BCCPCC*-ring, and the new ligand is *cis*-κ^2*PP*-coordinated to tungsten. Additionally, FcPPB reacted with [Ru$_3$(CO)$_{12}$] to yield [Ru$_3$(μ-H)(FcPPB**)] (**42**), which features a new borate-containing *BCCPCC*-ring, with κ^1*P*-coordination of the phosphine donors to two different Ru(I) centres that are bridged by a hydride ligand. Initially, we had hoped that the pendant borane of FcPPB would be capable of interacting with a carbonyl co-ligand on tungsten or ruthenium, providing a means to promote insertion chemistry with the C≡O bond.[34-37,63,64,110] However, we instead achieved intramolecular electrophilic borylation of the adjacent cyclopentadienyl ring of the ferrocene backbone, resulting in the formation of a new phosphine–phosphine–borane ligand in the case of **41**,

and a phosphine–phosphine–borate ligand in the case of **42**. These results highlight a potential limitation of the FcPPB ligand, and will enable future structural modifications designed to prevent intramolecular borylation, thereby increasing the potential for intramolecular metal–CO–borane coordination.

Finally, the FcPPB ligand readily reacted with the Lewis acids $B(C_6F_5)_3$ and $BF_3{\cdot}OEt_2$. In the former case, $[Fe(\eta^5\text{-}C_5H_4PPh_2\{B(C_6F_5)_3\})\{\eta^5\text{-}C_5H_4P^tBu(C_6H_4BPh_2\text{-}o)\}]$ [FcPPB{$B(C_6F_5)_3$}, **43**], was isolated, featuring intermolecular $C_5H_4(Ph_2)P\rightarrow B(C_6F_5)_3$ and intramolecular $C_5H_4(^t\text{Bu})(\text{Ar})P\rightarrow BPh_2\text{Ar}$ adducts. In the latter case, phenyl group abstraction by BF_3 afforded the bisphosphine-stabilized boronium cation, $[Fe(\eta^5\text{-}C_5H_4PPh_2)\{\eta^5\text{-}C_5H_4P^tBu(C_6H_4BPh\text{-}o)\}][BF_4]$ ($[FcPPB^{\text{-Ph}}][BF_4]$, **44**). Overall, compounds **40**, **41**, **42** and **44**, in combination with the previously discussed Group 10-FcPPB complexes (Chapter 6) highlight the versatility in the coordinative properties of the FcPPB ligand, given its ability to accommodate metals and non-metals with widley varying sizes, and electropositivities.

Ph.D. Thesis
Bradley E. Cowie
Department of Chemistry and Chemical Biology
McMaster University

Chapter 8

Synthesis and Platinum Complexes of an Alane-Appended 1,1'-Bis(phosphino)ferrocene Ligand

Adapted with permission from: Cowie, B. E.; Tsao, F. A.; Emslie, D. J. H. *Angew. Chem. Int. Ed.* **2015**, *54*, 2165-2169.

8.1 – Introduction

The vast majority of the research on Group 13 Lewis acid-containing ambiphilic ligand coordination chemistry has focused on borane Lewis acids,[288] and has relied upon ambiphilic ligands to stabilize metal–borane interactions, since unsupported metal–borane compounds have thus far evaded isolation (Sections 1.2–1.4). The situation changes upon moving down Group 13, where $[Cp(CO)_2Fe(AlPh_3)]^-$, featuring an unsupported iron–alane bond, was described by Burlitch in 1979,[4] $[Cp^*IrH_2(PMe_3)(AlPh_3)]$ was reported in 1998 by Bergman and Andersen,[289] and a series of rhodium and platinum AlX_3 (X = Cl, Br, and I) complexes was recently prepared by Braunschweig *et al.*[6-9]

Only a handful of alane-containing ambiphilic ligands have been reported (Figure 8.1), and in contrast to the chemistry of borane-containing ambiphilic ligands, most of these ligands have not yielded complexes featuring metal–alane coordination. This is the case for ligands **L1**–**L5** in Figure 8.1, which engage in halide or alkyl coordination and abstraction reactions,[27-32] neutral ligand (NEt_3 and DMSO) abstraction reactions,[27,28,33] and acyl or formyl ligand (formed through 1,1-insertion) coordination to form η^2*CO*-coordinated five-membered CR-O-AlR_2-N^{t}Bu-PR_2 rings in preference to metal–alane bonding.[34-37] However, Lu and co-workers recently developed the alumatrane-containing ligand, AltraPhos [AltraPhos = Al{N(*o*-$C_6H_4NCH_2P$*i*$Pr_2)_3$}; **L6** in Figure 8.1], and reported the synthesis of Ni, Fe, and Co complexes featuring κ^4*PPPAl*-coordination; these are the first examples of κ^1*Al*-coordination to a metal by an alane within an ambiphilic ligand framework.[38,39] Ligand **L7** in Figure 8.1, which was generated *in situ* through the reaction of $[(Ph_2PCH_2SiMe_2)_2N]Ir{=}C{=}CH_2$ with $AlMe_3$ to form [(**L7**)Ir(CMe=CH_2)],

was also shown to engage in iridium–aluminum bonding, but in this case, the metal is η^2-bound to nitrogen and aluminum, in addition to both phosphines.[142]

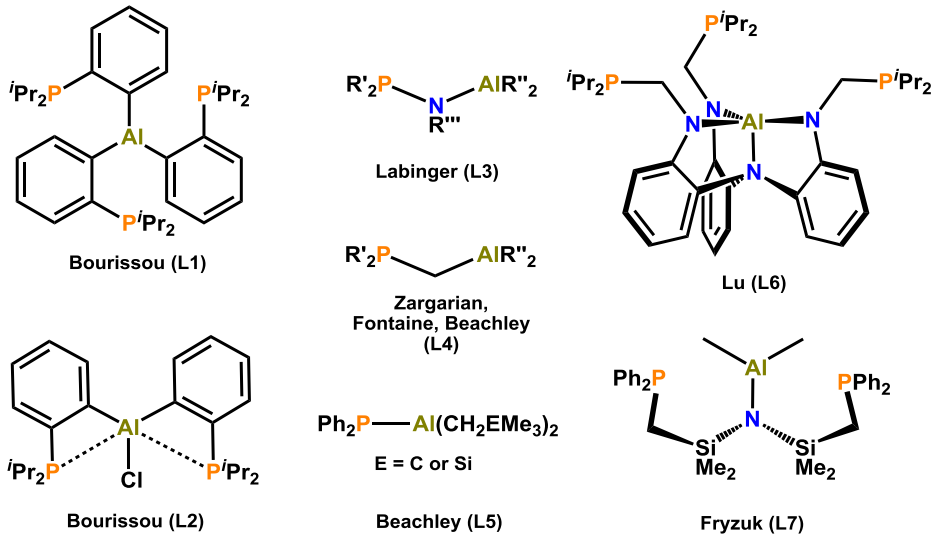

Figure 8.1. Previously reported alane-containing ambiphilic ligands.

Previously, a rigid phosphine–thioether–borane ligand, TXPB, and a much more electron-donating borane-containing ambiphilic ligand, [Fe(η^5-$C_5H_4PPh_2$){η^5-$C_5H_4P^tBu(C_6H_4BPh_2$-*o*)}] (FcPPB), were utilized to investigate the behaviour of a pendant borane in the coordination sphere of late transition metals bearing a variety of co-ligands (Chapters 2–7). Given the small number of known κ^1*Al*-coordinated alane complexes, we sought to explore the coordination chemistry of an alane-containing analogue of FcPPB. This ligand, [Fe(η^5-$C_5H_4PPh_2$){η^5-$C_5H_4P^tBu(C_6H_4AlMe_2$-*o*)}] (FcPPAl; Scheme 8.1), features an –$AlMe_2$ group in place of a –BPh_2 group, and presented herein are the first unambiguous examples of κ^1*Al*-coordinated alkylalane complexes.[§]

[§] Several [$CpML_2(AlMe_3)$] (M = Rh or Co; L = PR_3 or C_2H_4) complexes have been reported, however none of these complexes were structurally authenticated (see ref 5).

8.2 – Synthesis and Reactivity of [Pt(η^2-nb)(FcPPAl)]

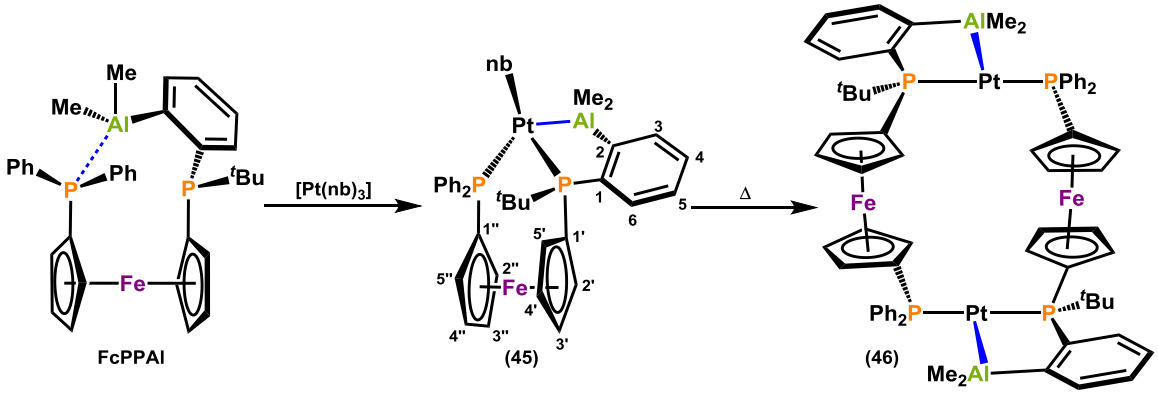

Scheme 8.1. Synthesis of [Pt(η^2-nb)(FcPPAl)] (**45**), and subsequent dimerization under thermal conditions to provide [{Pt(FcPPAl)}$_2$] (**46**).

The FcPPAl ligand was prepared in seven steps from commercially available ferrocene, as discussed in Section 5.3, and reaction of FcPPAl with [Pt(nb)$_3$] (nb = norbornene) afforded [Pt(η^2-nb)(FcPPAl)] (**45**; Scheme 8.1) in which platinum is coordinated to both phosphines and one equivalent of norbornene, based on ^{1}H, ^{13}C, ^{31}P, and ^{195}Pt NMR data; the ^{1}H NMR spectrum of **45**, as well as expanded views of the aromatic and C$_5$*H*$_4$-regions are displayed in Figures 8.2–8.4. Numbered protons refer to the positions on the ferrocene backbone and the phenylene linker in the FcPPAl ligand, as shown in Scheme 8.1. Two sharp Al*Me*$_2$ signals were observed in the ^{1}H NMR spectrum of at –0.06 and –0.54 ppm, suggestive of η^1*Al*-coordination to platinum, resulting in relaxation of the quadrupolar broadening brought about by aluminum; the Al*Me*$_2$ signals for free FcPPAl are broadened singlets located at 0.41 and –0.38 ppm ($\omega_{1/2}$ ~ 30 Hz). The presence of ^{195}Pt-satellites associated with the vinylic norbornene protons ($^2J_{1H,195Pt}$ = 53–58 Hz) in the ^{1}H NMR spectrum, in combination with observed ^{13}C-^{31}P coupling for the alkenyl carbon atoms (*trans*-$^2J_{13C,31P}$ = 36–37 Hz; *cis*-$^2J_{13C,31P}$ = 6–7 Hz) in the ^{13}C NMR spectrum indicates that one norbornene ligand remains η^2*CC*-coordinated to platinum.

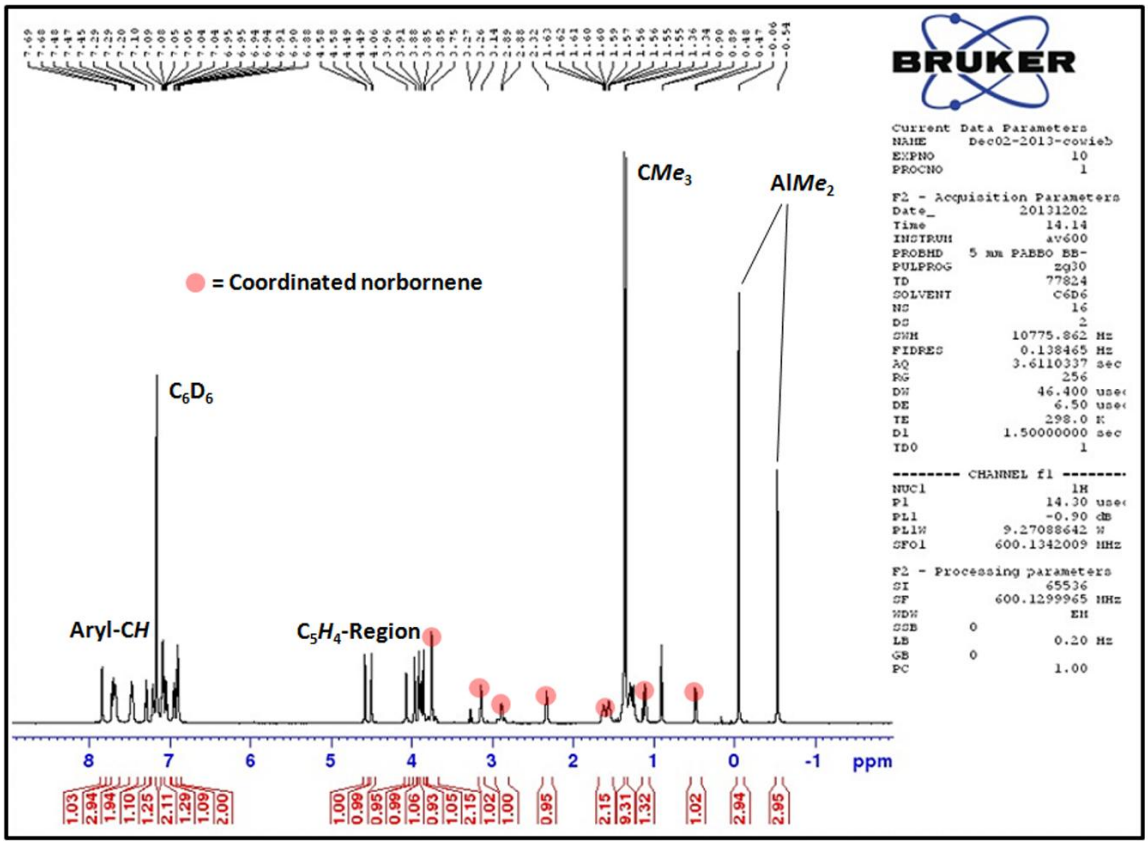

Figure 8.2. ^{1}H NMR spectrum of [Pt(η^2-nb)(FcPPAl)] (**45**; 600 MHz, 298 K, C_6D_6).

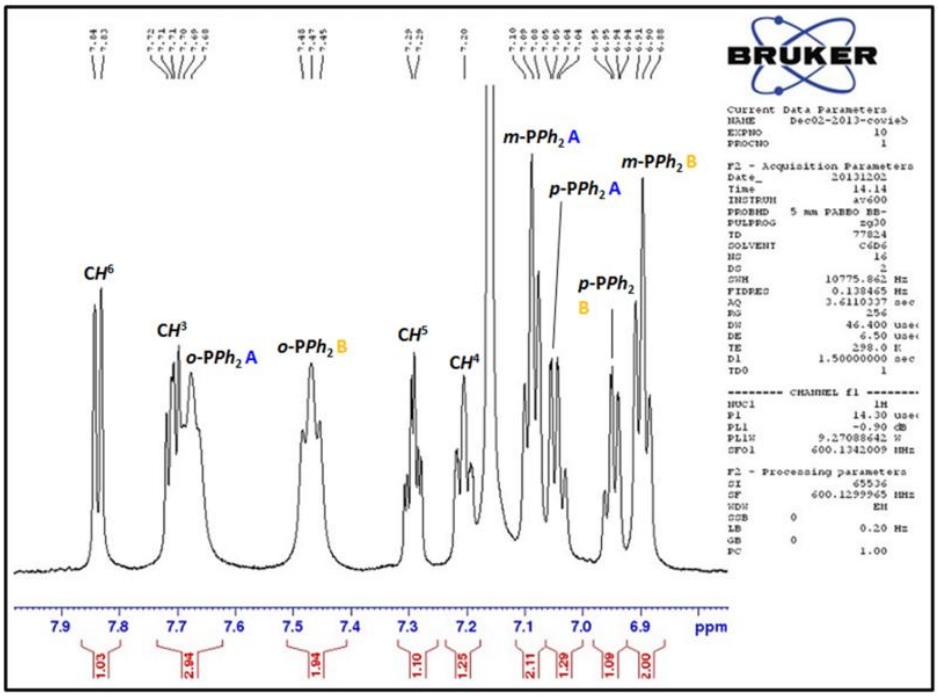

Figure 8.3. Expanded aromatic region of the ^{1}H NMR spectrum of [Pt(η^2-nb)(FcPPAl)] (**45**; 600 MHz, 298 K, C_6D_6).

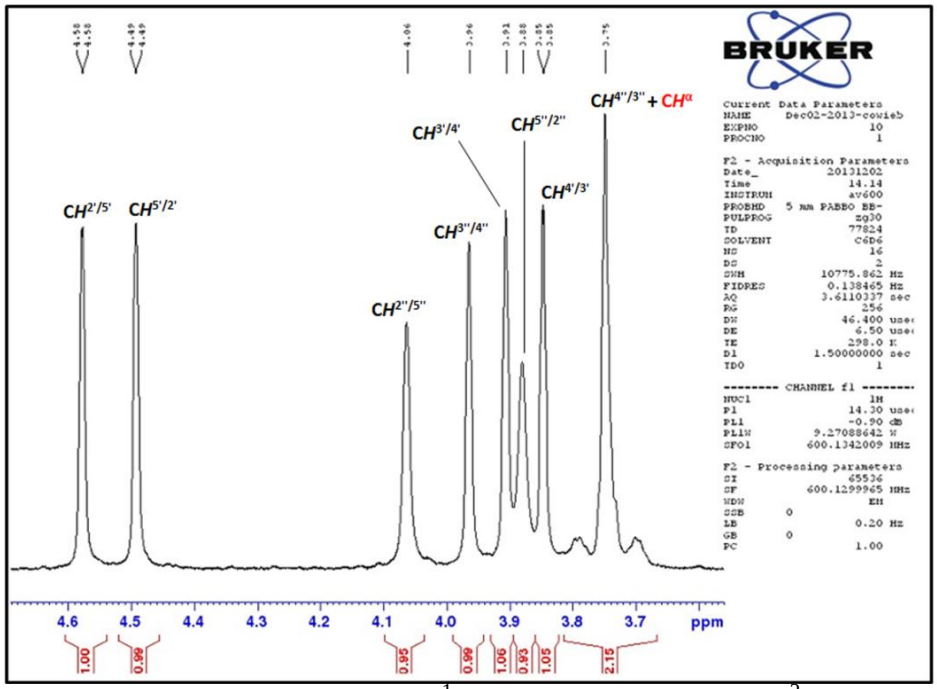

Figure 8.4. Expanded C_5H_4-region of the ^{1}H NMR spectrum of [Pt(η^2-nb)(FcPPAl)] (**45**; 600 MHz, 298 K, C_6D_6).

The ^{195}Pt NMR signal was located at –4615 ppm, displaying coupling to both phosphorus atoms, and the ^{31}P NMR signals for the $C_5H_4P(^t$Bu)Ar and $C_5H_4PPh_2$ groups were located at 66.5 ($^1J_{31P,195Pt}$ = 3050 Hz) and 26.2 ppm ($^1J_{31P,195Pt}$ = 2654 Hz), respectively, with the lowest frequency signal showing significant broadening ($\omega_{1/2}$ ~ 25 Hz). Variable temperature $^{31}P\{^1H\}$ NMR spectroscopy performed down to –171 K in toluene-d_8 revealed that complex **45** is present in solution as a mixture of two isomers in an approximate 1:1 ratio, which are tentatively assigned as rotational isomers involving the η^2-bound norbornene ligand (Figure 8.5).[§]

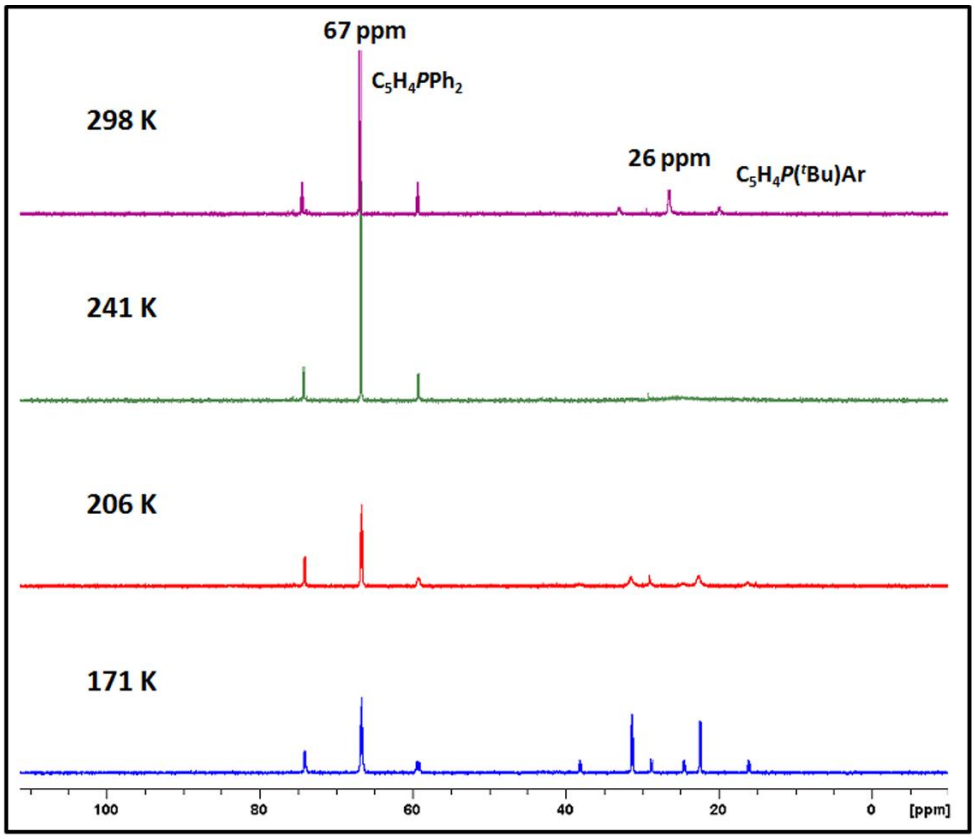

Figure 8.5. Variable temperature $^{31}P\{^1H\}$ NMR spectra for [Pt(η^2-nb)(FcPPAl)] (**45**; 203 MHz, 298–171 K, toluene-d_8).

[§] For other examples of metal-norbornene complexes existing as a mixture of rotamers, see: (a) Edwards, P. G.; Knight, J. C.; Newman, P. D. *Dalton Trans.* **2010**, 3851. (b) Adams, J. J.; Arulsamy, N.; Roddick, D. M. *Organometallics* **2011**, *30*, 697.

Table 8.1. Crystallographic Data Collection and Refinement Parameters for Complexes **46**–**50**.

Structure	**46**	**47**	**48**	**49**	**50**
Formula	$C_{68}H_{74}Al_2Fe_2P_4Pt_2$	$C_{36}H_{41}AlFeP_2Pt$	$C_{48}H_{47}AlFeP_2Pt$	$C_{34}H_{39}AlFeP_2Pt$	$C_{35}H_{37}AlFeOP_2Pt$
Formula wt	1570.99	813.55	963.72	787.51	813.51
T (K)	100(2)	100(2)	100(2)	100(2)	100(2)
Cryst. Syst.	Monoclinic	Monoclinic	Monoclinic	Monoclinic	Monoclinic
Space Group	*C*2/*c*	*P*2(1)/*c*	*P*2(1)/*n*	*P*2(1)/*c*	*P*2(1)/*c*
a (Å)	15.373(1)	13.631(3)	11.896(1)	14.0178(3)	11.192(1)
b (Å)	16.685(1)	11.929(3)	22.989(3)	11.2946(3)	18.750(2)
c (Å)	24.760(2)	20.416(5)	14.714(2)	20.5018(5)	15.908(2)
α [deg]	90	90	90	90	90
β [deg]	106.243(1)	102.546(7)	90.988(3)	101.563(1)	105.063(2)
γ [deg]	90	90	90	90	90
Volume [$Å^3$]	6097.6(7)	3240(1)	4023.6(8)	3180.1(1)	3223.4(6)
Z	4	4	4	4	4
μ (mm^{-1})	5.216	4.911	3.969	5.000	4.938 mm
F(000)	3104	1616	1928	1560	1608
Crystal Size (mm^3)	0.27×0.09×0.02	0.16×0.03×0.02	0.19×0.09×0.03	0.32×0.22×0.20	0.33×0.27×0.03
θ Range for Collection [deg]	1.71–26.37	1.53–25.43	1.64–26.53	2.03–36.35	1.71–26.44
No. of Reflns Collected	51285	24587	41145	150249	34788
No. of Indep Reflns	6237	5975	8266	15439	6593
Completeness to θ Max (%)	100.0	99.5	98.8	100.0	99.5
Absorption Correction	Numerical	Numerical	Numerical	Numerical	Numerical
Max and Min Transmission	0.9029, 0.3333	0.9082, 0.5071	0.8902, 0.5193	0.4346, 0.2975	0.8660, 0.2926
GOF on F^2	1.043	1.045	1.033	1.098	1.043
Final R_1 [$I > 2\sigma(I)$] (%)	2.16	7.14	4.36	3.00	3.65

In toluene at 80 °C, **45** dissociates norbornene and dimerizes to afford [{Pt(FcPPAl)}$_2$] (**46**), which precipitates as an orange, crystalline material from solution (Scheme 8.1). Despite the insolubility of complex **46**, during the course of the reaction, unreacted **45** and trace amounts of **46** may be observed by $^{31}P\{^1H\}$ NMR spectroscopy,

giving rise to signals located at 74.9 and 40.7 ppm with large $^{31}P–^{31}P$ coupling (356 Hz) indicative of *trans*-disposed phosphines. An X-ray crystal structure of **46** is displayed in Figure 8.6, revealing that each FcPPAl ligand is κ^2*PAl*-coordinated to one platinum centre and κ^1*P*-coordinated to the other. Both platinum centres are equivalent with a distorted T-shaped geometry and *trans* phosphine ligands; the P(1)–Pt–Al, P(2)–Pt–Al and P(1)–Pt–P(2) angles are 100.86(3), 85.40(3) and 172.17(3)°, respectively. The Pt–Al distance in **46** is 2.482(1) Å, and the alane is substantially pyramidalized, with the sum of the C–Al–C angles equal to 336.7(3)°. The geometry of **46** stands in stark contrast to that of [Pt(FcPPB)], which is pseudo square planar with η^3*BCC*-coordination of the arylborane (Chapter 6). Only the *rac*-diastereomer is observed in the single crystal X-ray structure, and powder X-ray diffraction (PXRD) confirmed that the bulk sample of **46** consists only of the *rac*-diastereomer (Figure 8.7).

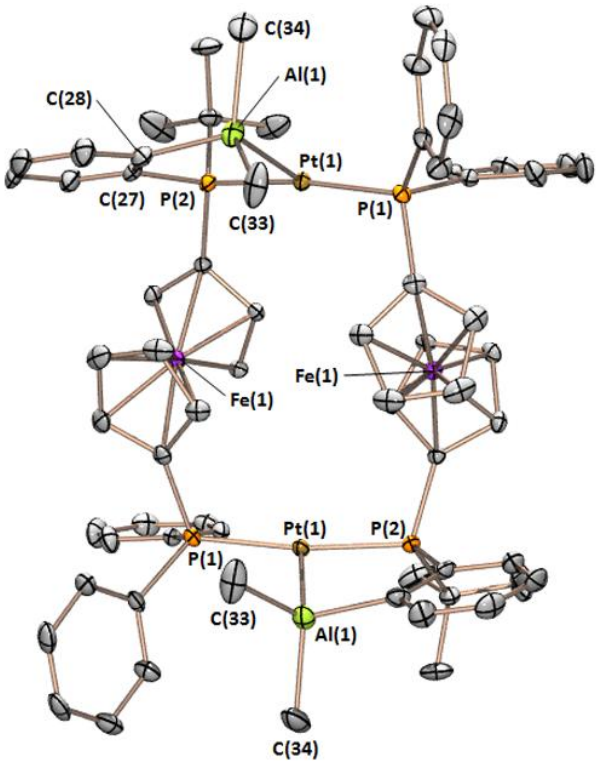

Figure 8.6. X-ray crystal structure for [{Pt(FcPPAl)}$_2$] (**46**); hydrogen atoms are omitted for clarity, and ellipsoids are set to 50 %.

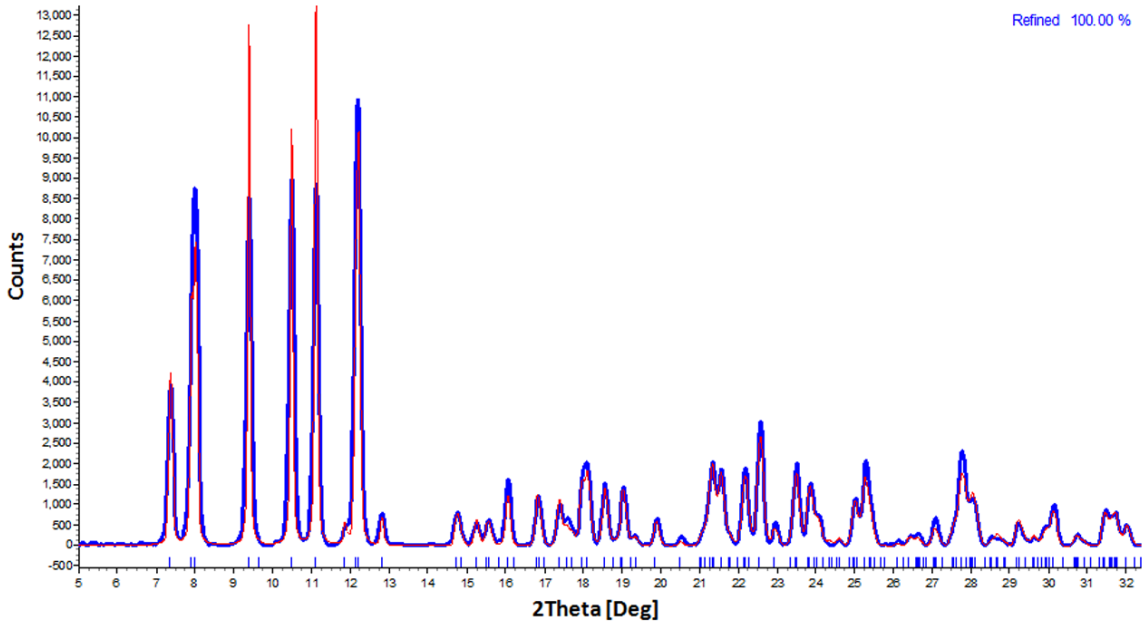

Figure 8.7. PXRD pattern of [{Pt(FcPPAl)}$_2$] (**46**; blue) matched with PXRD pattern generated from the single crystal data; the red line is the calculated spectrum from the cif data. PXRD data was collected by Jeffrey S. Price, and Topas 4.2 was utilized to relate unit cell measurements obtained at room temperature to those obtained at 100 K.

Reaction of **45** with ethylene or diphenylacetylene afforded [Pt(η^2-C_2H_4)(FcPPAl)] (**47**) and [Pt(η^2-C_2Ph_2)(FcPPAl)] (**48**) (Scheme 8.2); the ^{1}H NMR spectrum of **47**, in addition to expanded views of the aromatic, C_5H_4- and C_2H_4-regions are given below in Figures 8.8–8.10). In both cases, the alane ligand remains η^1-*Al*-coordinated to the metal centre in solution and in the solid-state, as evidenced by sharp Al*Me*$_2$ signals located at –0.16, –0.71 and 0.18, –0.54 ppm in the ^{1}H NMR spectra for **47** and **48**, respectively, and Pt–Al distances of 2.533(4) and 2.570(2) Å [Σ(C–Al–C) = 333(1) and 334.0(5)°, respectively; Figure 8.11]. Complex **47** gave rise to ^{31}P NMR signals at 67.2 [$C_5H_4P(^t$Bu)Ar] and 27.9 ppm [C_5H_4PPh$_2$; $^1J_{31P,195Pt}$ = 3270, 2979 Hz], whereas **48** gave rise to signals at 59.1 ppm [$C_5H_4P(^t$Bu)Ar] and 20.6 ppm [C_5H_4PPh$_2$; $^1J_{31P,195Pt}$ = 2961, 2933 Hz]; ^{31}P-^{31}P coupling constants of 43 and 24 Hz were also observed for **47** and **48**, respectively, consistent with *cis*-bisphosphine coordination. In addition, the ^{195}Pt NMR signals for **47** and **48** were located at –4734 and –4443 ppm.

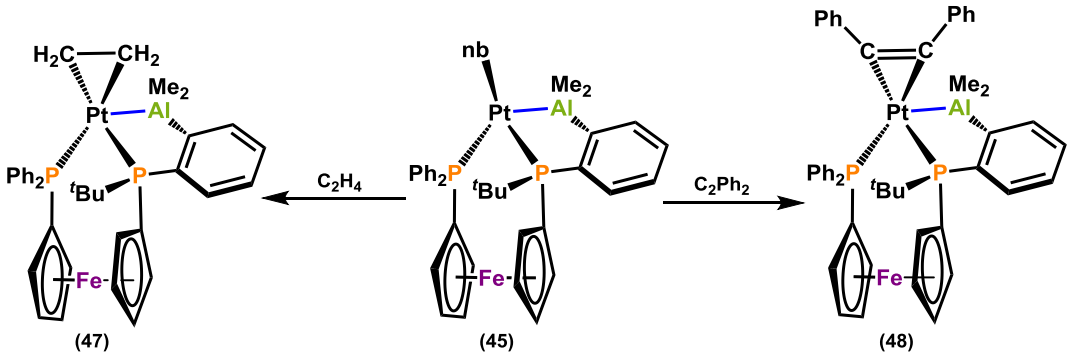

Scheme 8.2. Reactions of **45** with C_2H_4 and C_2Ph_2, forming [Pt(η^2-C_2H_4)(FcPPAl)] (**47**) and [Pt(η^2-C_2Ph_2)(FcPPAl)] (**48**), respectively.

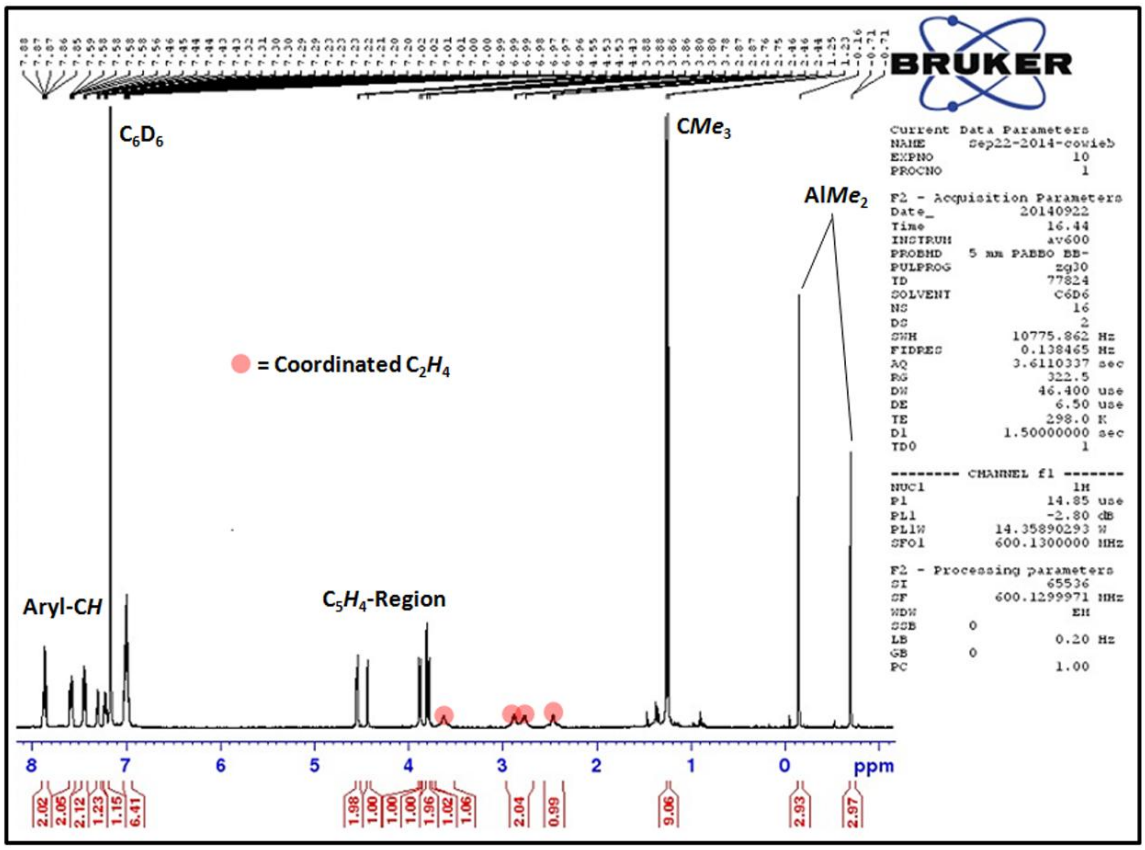

Figure 8.8. ^{1}H NMR spectrum of [Pt(η^2-C_2H_4)(FcPPAl)] (**47**; 600 MHz, 298 K, C_6D_6).

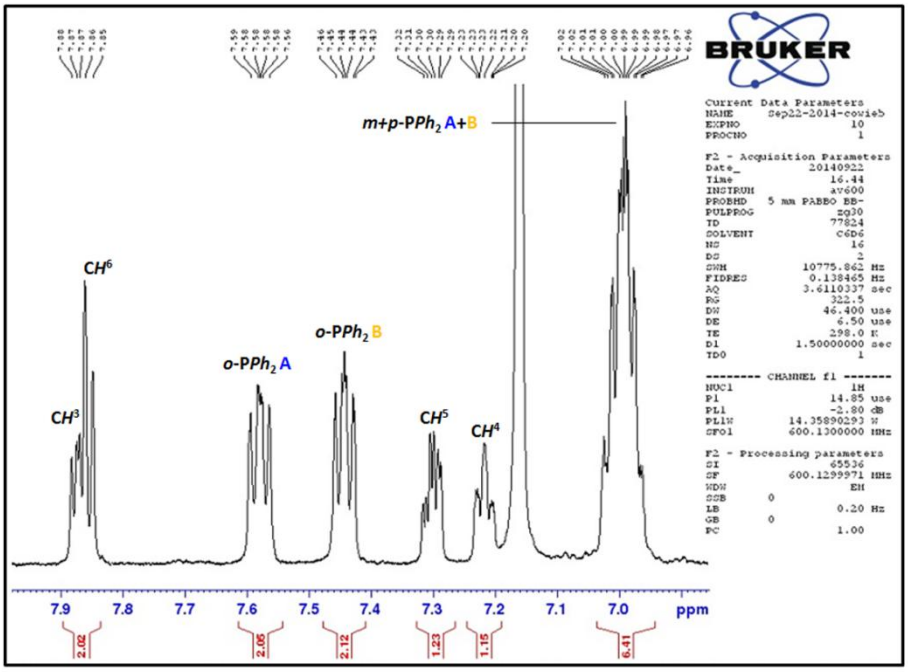

Figure 8.9. Expanded aromatic region of the ^{1}H NMR spectrum of [Pt(η^2-C_2H_4)(FcPPAl)] (**47**; 600 MHz, 298 K, C_6D_6).

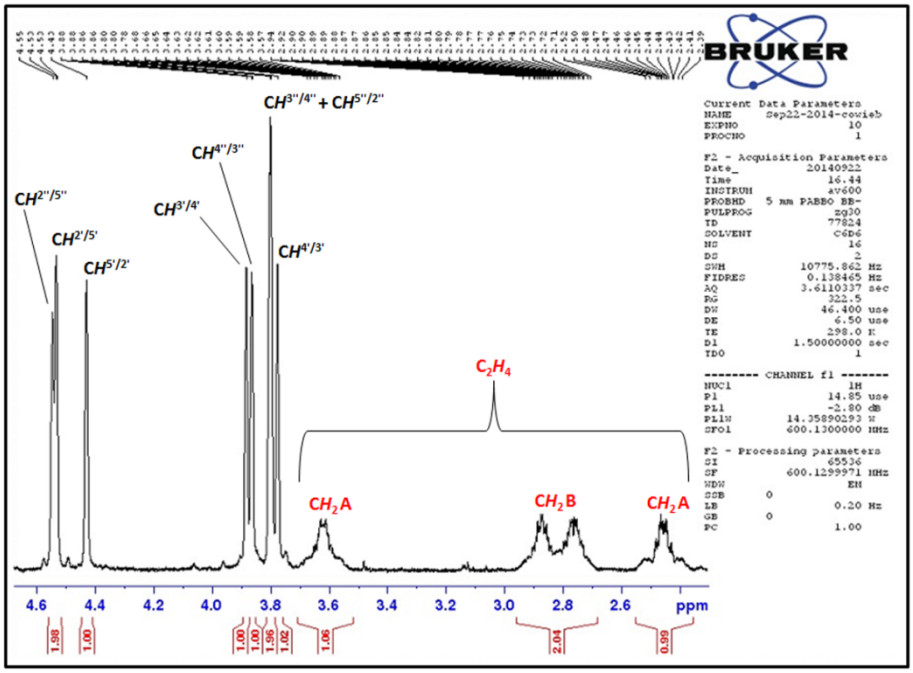

Figure 8.10. Expanded C_5H_4- and C_2H_4-regions of the ^{1}H NMR spectrum of [Pt(η^2-C_2H_4)(FcPPAl)] (**47**; 600 MHz, 298 K, C_6D_6).

Coordination of a C_2H_4 ligand in **47** and a C_2Ph_2 ligand in **48** in the solution-state is evidenced by: (1) $C_2\boldsymbol{H}_4$ signals found between 3.68–2.42 ppm in the ^{1}H NMR spectrum of **47** with ^{1}H-^{195}Pt coupling constants ranging from 63–69 Hz, (2) $\boldsymbol{C}_2H_4$ signals located at 42.0 and 37.7 ppm in the ^{13}C NMR spectrum of **47** with *cis*- and *trans*-^{13}C-^{31}P coupling constants of ~7 and ~30 Hz, respectively, (3) $C_2\boldsymbol{Ph}_2$ signals found at 132.3 and 131.8 ppm in the ^{13}C{^{1}H} NMR spectrum of **48** with *cis*- and *trans*-^{13}C–^{31}P coupling constants of ~8 and ~75 Hz, respectively, and (4) ^{13}C-^{195}Pt coupling observed for the *o*-Ph carbon atoms of the $C_2\boldsymbol{Ph}_2$ group in **48**, equal to ~24 Hz. The C(35)–C(36) bond distances in **47** and **48** are 1.40(2) and 1.291(8) Å, respectively, which are significantly elongated relative to C=C or C≡C bonds, consistent with metallacyclopropane and metallacyclopropene coordination modes, respectively. This bonding description is further corroborated by C–C stretching frequencies of 1156 and 1735 cm^{-1} for complexes **47** and **48**, and C(37)–C(35)–C(36) and C(43)–C(36)–C(35) bond angles of 140.0(6) and 139.2(6)° in **48**.[290] The coordination geometry in complexes **47** and **48** is best described as distorted square-pyramidal, with P(1), P(2), C(35) and C(36) lying in the square-basal plane, and Al(1) occupying the apical position. The reactivity of "Pt(FcPPAl)" with alkenes and alkynes is distinct from that of [Pt(FcPPB)], which does not react with norbornene, C_2H_4, or C_2Ph_2 (Chapter 6).

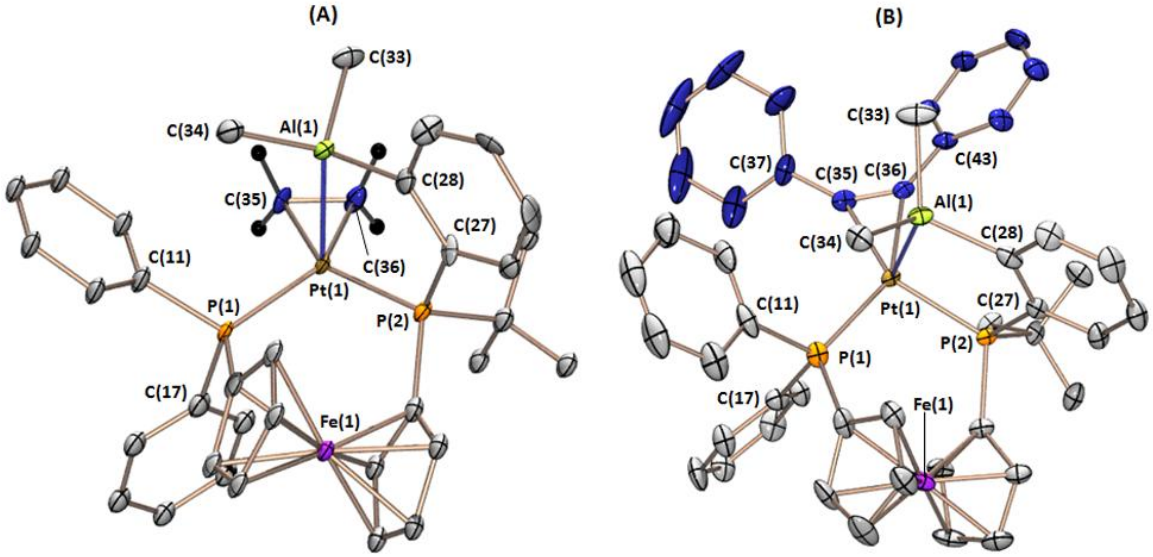

Figure 8.11. A. X-ray crystal structure for [Pt(η^2-C_2H_4)(FcPPAl)] (**47**), and **B.** X-ray crystal structure for [Pt(η^2-C_2Ph_2)(FcPPAl)] (**48**); hydrogen atoms are omitted and the coordinated C_2H_4 and C_2Ph_2 ligands are coloured navy blue for clarity, and ellipsoids are set to 50 %.

The dihydride complex, [PtH_2(FcPPAl)] (**49**), was prepared through reaction of **45** with H_2 (Scheme 8.3), and whereas [PtH_2(FcPPB)] reverts back to [Pt(FcPPB)] and H_2 at room temperature *in vacuo* in the solid-state, or in solution under argon (Chapter 6, *vide supra*), **49** is stable *in vacuo*, and at 75 °C in solution. The thermal stability of **49** is also notable in light of the reactivity of [Cp*$IrH_2(PMe_3)$] with $AlPh_3$ and $AlEt_3$; the former reaction provided stable [Cp*$IrH_2(PMe_3)(AlPh_3)$], whereas in the latter reaction, the weaker Al–C bonds in $AlEt_3$ resulted in ethane elimination to form [{Cp*$Ir(PMe_3)$(μ-AlEt)}$_2$].[289] The ^{1}H NMR spectrum of **49**, along with expanded views of the aromatic, C_5H_4- and metal-hydride regions are given below in Figures 8.12–8.14; the hydride ligands of **49** gave rise to signals at –2.44 and –3.31 ppm in the ^{1}H NMR spectrum, with ^{1}H-^{195}Pt, *trans*-^{1}H-^{31}P and *cis*-^{1}H-^{31}P coupling constants of 1002/993, 177/159 and 18 Hz, respectively. No ^{1}H–^{1}H coupling was observed between the hydride signals. Additionally, the Pt–H stretches were observed at 2101 and 2049 cm^{-1} in the IR spectrum (Nujol). The FcPPAl ligand in **49** is κ^3*PPAl*-coordinated, resulting in a distorted square pyramidal geometry at platinum with the alane in the apical position [Figure 8.15; Pt–Al = 2.5105(7)

Å; Σ(C–Al–C) = 337.0(2)°]; the ^{195}Pt NMR signal for **49** was observed at –5001 ppm. Notably, the Al–H(36) and Al–H(35) distances are 2.46(4) and 2.86(3) Å, respectively, and the Al–Pt–H(36) bond angle is 69(1)°, versus 86(1)° for Al–Pt–H(35), suggestive of a bonding interaction between the alane and H(36). Furthermore, a smaller ^{31}P-^{195}Pt coupling constant was observed for the $C_5H_4P(^tBu)Ar$ phosphine (64.3 ppm, $^1J_{31P,195Pt}$ = 1892 Hz) relative to the $C_5H_4PPh_2$ phosphine (34.3 ppm, $^1J_{31P,195Pt}$ = 2373 Hz) despite the greater donor ability of the former, which is suggestive of a bridging interaction between aluminum and the hydride bound *trans* to the $C_5H_4PPh_2$ group. For comparison, the DFT-calculated structure for [PtH(μ-H)(FcPPB)] is square-planar with a short bond distance between the borane and one of the hydride ligands (B–H = 1.386 Å; Pt–B = 2.524 Å; Chapter 6, *vide supra*).

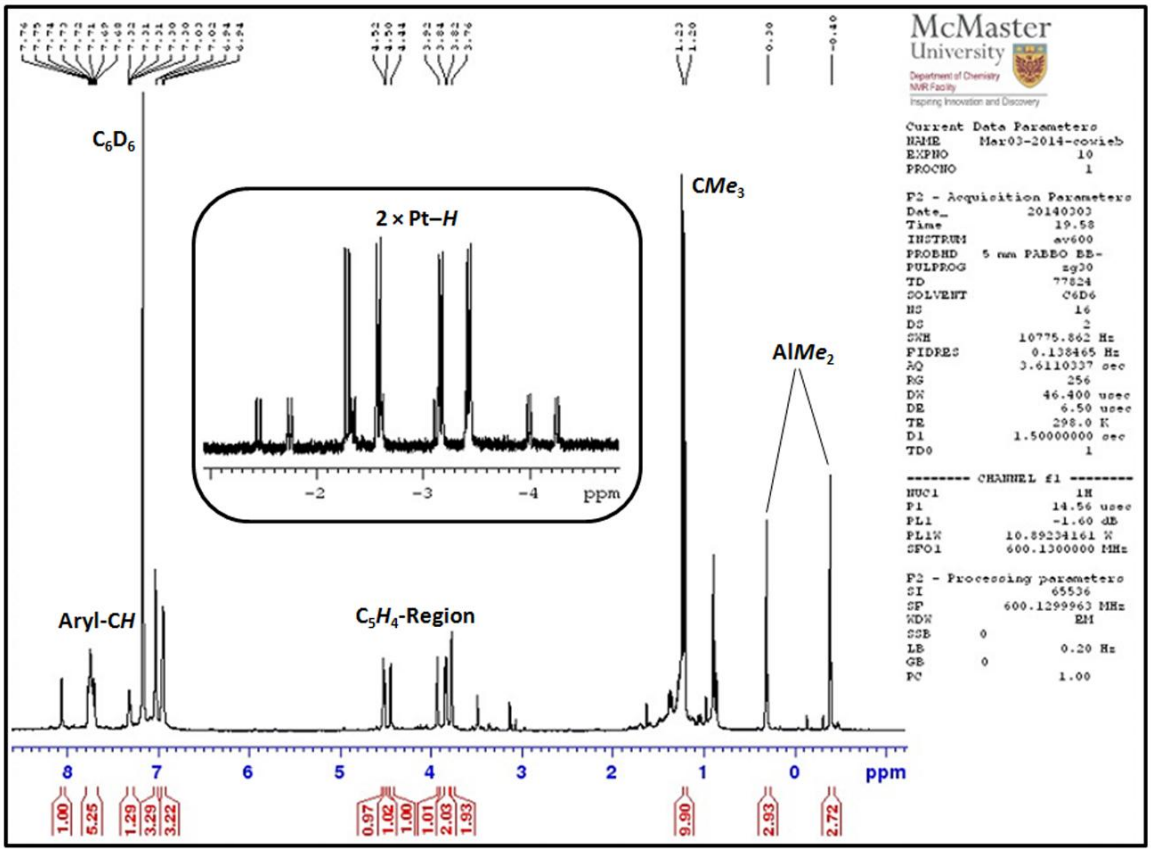

Figure 8.12. ^{1}H NMR spectrum of [PtH$_2$(FcPPAl)] (**49**; 600 MHz, 298 K, C_6D_6).

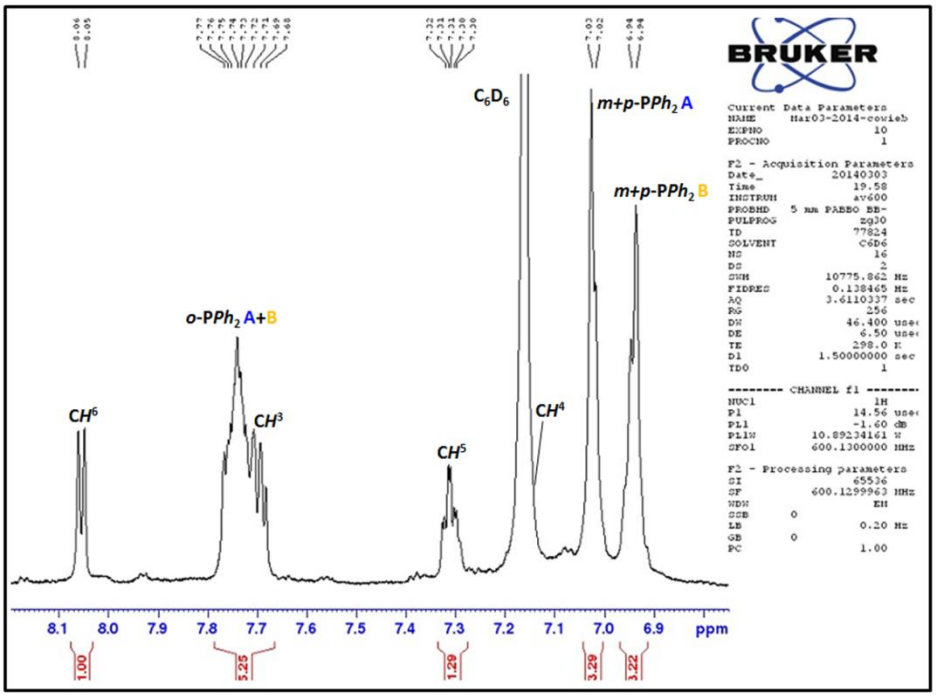

Figure 8.13. Expanded aromatic region of the ^{1}H NMR spectrum of [PtH_2(FcPPAl)] (**49**; 600 MHz, 298 K, C_6D_6).

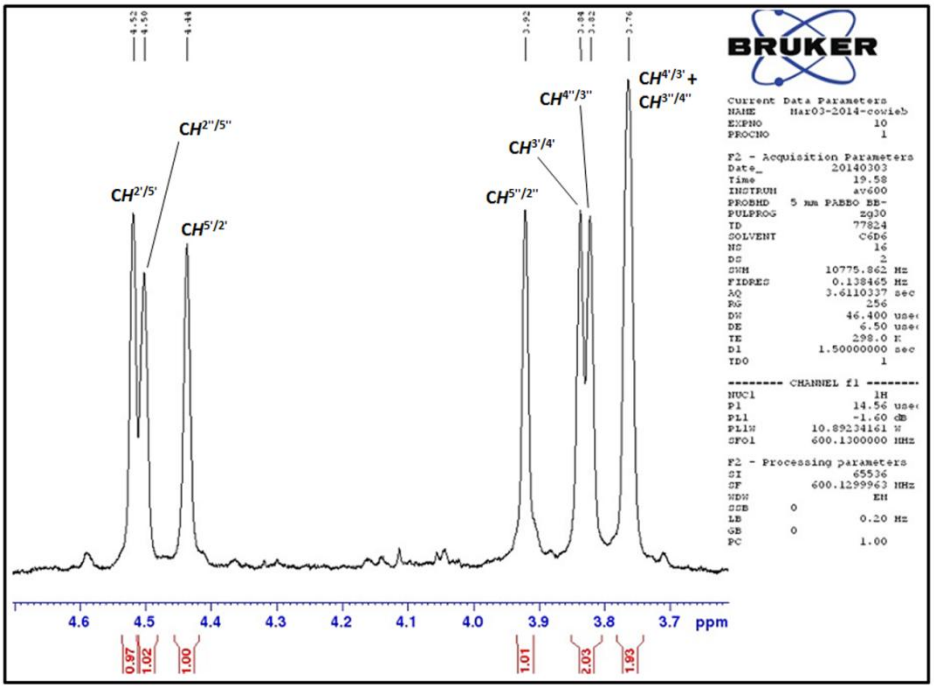

Figure 8.14. Expanded C_5H_4-region of the ^{1}H NMR spectrum of [PtH_2(FcPPAl)] (**49**; 600 MHz, 298 K, C_6D_6).

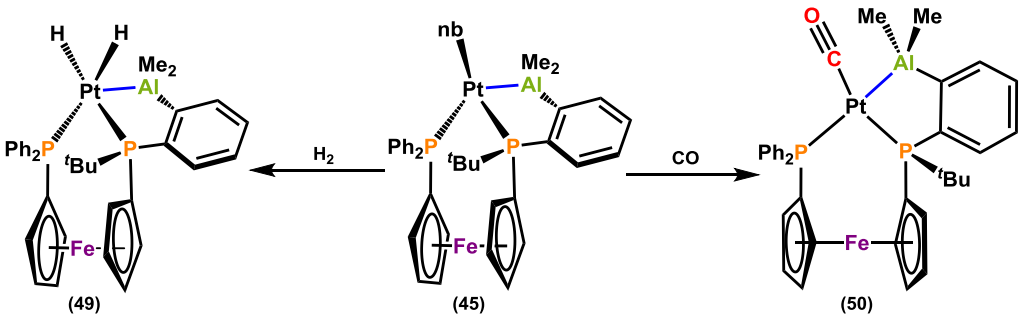

Scheme 8.3. Reactions of **45** with H_2 and CO, providing [PtH_2(FcPPAl)] (**49**) and [Pt(CO)(FcPPAl)] (**50**), respectively.

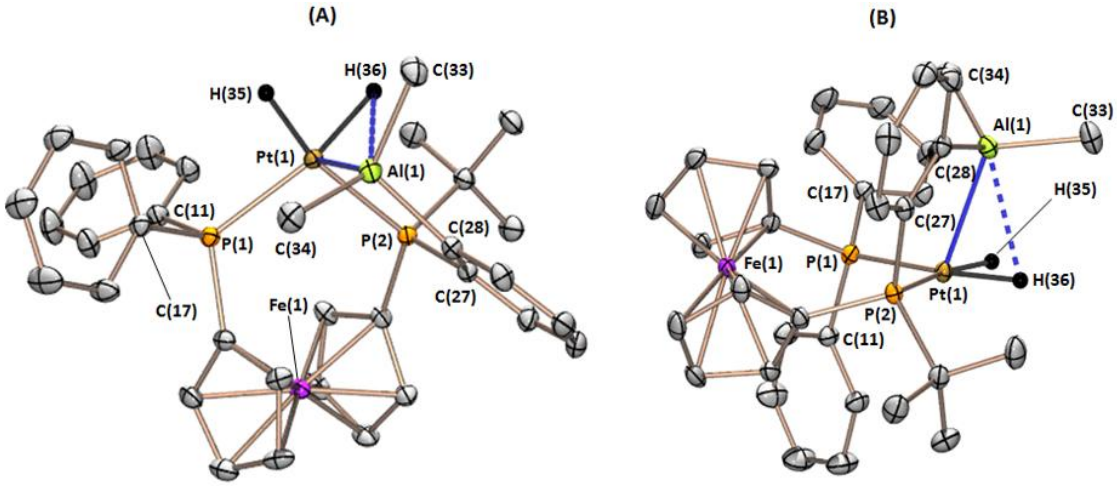

Figure 8.15. Two different views of the X-ray crystal structure for [PtH_2(FcPPAl)] (**49**); aside from H(35) and H(36), which were located in the difference map, hydrogen atoms are omitted for clarity, and ellipsoids are set to 50 %.

Reaction of **45** with CO afforded [Pt(CO)(FcPPAl)] (**50**; Scheme 8.3) with a Pt–Al distance of 2.624(2) Å [Σ(C–Al–C) = 337.9(5)°; Figure 8.16], and a CO stretch at 1982 cm^{-1} (Nujol). Platinum is distorted square-planar with CO located approximately in the P(1)–Pt–P(2) plane, and Al is located 1.05 Å out of the plane, leading to a P(1)–Pt–Al angle of 155.38(5)°. The Al–Pt–CO angle in **50** is extremely acute [73.0(2)°], placing CO just 2.736(8) Å from Al, hinting at a bonding interaction between the alane and the CO co-ligand. The ^{195}Pt NMR signal is observed at –4413 ppm, and the ^{31}P NMR signals

were observed at 73.8 and 41.1 ppm, with ^{31}P-^{195}Pt coupling constants of 4089 and 2191 Hz, and 18 Hz *cis*-^{31}P-^{31}P coupling. A notably larger $^{1}J_{31P,195Pt}$ coupling constant for the $C_5H_4P(^t$Bu)Ar phosphine in **50** relative to complexes **46**–**49** may be attributed to coordination to a formally Pt(0) centre versus Pt(II), despite being bound *trans* to the high *trans* influence alane ligand.[40-43] The bonding situation in **50** differs from that in [Pt(CO)(FcPPB)], which is distorted tetrahedral with η^2*BC*-coordination of the arylborane to platinum (Chapter 6).

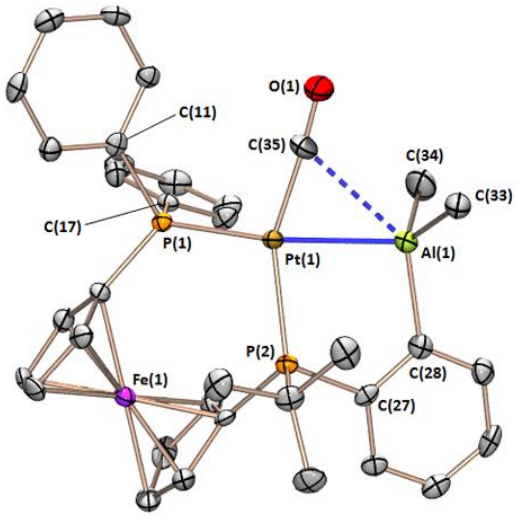

Figure 8.16. X-ray crystal structure for [Pt(CO)(FcPPAl)] (**50**); hydrogen atoms are omitted for clarity, and ellipsoids are set to 50 %.

The Pt–Al distances in **46**–**50** range from 2.482(1) to 2.624(2) Å, increasing in the order **46** < **49** < **47** < **48** < **50**. The Pt–Al distances in [PtL(PR_3)(AlX_3)] (L = PR_3, NHC; X = Cl, Br)[9] are considerably shorter than those in **46**–**50**, ranging from 2.37 to 2.39 Å, likely due to the greater Lewis acidity of AlX_3 relative to a dialkylarylalane. However, after adjusting for differences in covalent radius (Pt = 1.36 Å; Ni = 1.24 Å; Fe (high spin) = 1.52 Å),[68] the M–Al distances in Lu's diamagnetic [Ni(AltraPhos)] [Ni–Al = 2.450(1) Å] and paramagnetic [Fe(N_2)(AltraPhos)] [Fe–Al = 2.809(2) Å] complexes are comparable with those in **46**–**50**.[38,39]

8.3 – DFT Calculations

DFT calculations (ADF, gas phase, PBE, D3-BJ, all-electron, TZ2P, ZORA) on **47**–**50** were performed by Prof. David J. H. Emslie, and afforded geometries (**47$_{calc}$**–**50$_{calc}$**) in good agreement with the X-ray crystal structures. The Pt–Al Nalewajski–Mrozek (NM; Set 3)[291] bond orders in **47$_{calc}$**–**50$_{calc}$** are 0.39, 0.37, 0.37, and 0.34, respectively (cf. 0.40–0.46 for the Pt–P bonds), indicative of significant Pt–Al bonding. The Al–H(36) and Al–C(35) NM bond orders [H(36) = hydride ligand in [PtH$_2$(FcPPAl)] (**49**); C(35) = carbonyl carbon atom in [Pt(CO)(FcPPAl)] (**50**)] in **49$_{calc}$** and **50$_{calc}$** are 0.12 and 0.18, respectively, suggesting an interaction between the alane and an adjacent H or CO ligand, consistent with the acute Al–Pt–H(36) and Al–Pt–C(35) angles (calcd. 72° and 73°, respectively).

For each structure, several MOs exhibit Pt–Al bonding character, but the bonding picture is complicated by the highly delocalized nature of the MOs. Consequently, the structures of model [PtH$_2$(PMe$_3$)$_2$(AlMe$_2$Ph)] (**49$_{calc}$'**) and [Pt(CO)(PMe$_3$)$_2$(AlMe$_2$Ph)] (**50$_{calc}$'**) were geometry optimized, constraining the Pt, P, Al, C_{CO} and hydride positions to be identical to those in **49$_{calc}$** and **50$_{calc}$**. The Pt–Al NM bond orders for **49$_{calc}$'** and **50$_{calc}$'** are 0.38 and 0.34, respectively, the Al–H(36) NM bond order in **49$_{calc}$'** is 0.12, and the Al–C(35) bond order in **50$_{calc}$'** is 0.18. The bonding situation in **49$_{calc}$'** and **50$_{calc}$'** was further examined using natural bond order (NBO) and natural localized molecular orbital (NLMO) analysis.

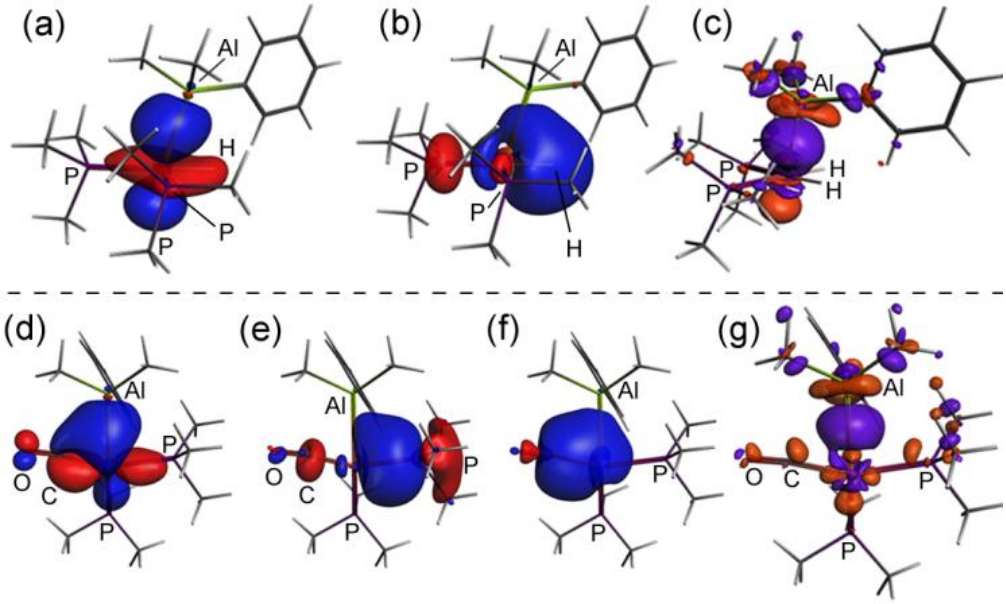

Figure 8.17. (**a**–**b**) NLMOs for **49**$_{calc}$', (**d**–**f**) NLMOs for **50**$_{calc}$', and (**c** and **g**) SCF deformation density (SCFDD) isosurfaces from fragment analysis of **49**$_{calc}$' and **50**$_{calc}$', respectively; purple and orange indicate regions of increased and depleted electron density, respectively. In all cases, platinum is the central atom. Isosurfaces are set to 0.03 for NLMOs, and 0.003 in the SCFDD plots.

For **49$_{calc}$'**, two NLMOs participate significantly in Pt–Al and Al–H bonding; (**a**) in Figure 8.17 contributes 0.10 to the total Pt–Al NLMO bond order of 0.33, and (**b**) contributes 0.12 to both the Pt–Al and Al–H bond orders (the total Al–H NLMO bond order in **49$_{calc}$'** is 0.12). In compound **50$_{calc}$'**, NLMOs (**d**)–(**f**) in Figure 8.17 contribute 0.18, 0.06, and 0.13, respectively to the total Pt–Al NLMO bond order of 0.31, and NLMOs **d** and **f** contribute 0.12 and 0.13 to the total Al–C(35) bond order of 0.25. These NLMOs highlight the presence of an unusual multicentre bonding situation involving Pt, Al, and the carbonyl carbon atom; effectively, the electrons involved in σ-donation and π-backdonation between C(35) and Pt are also involved in bonding to Al. SCF deformation density isosurfaces for **49$_{calc}$'** and **50$_{calc}$'** in Figure 8.17 illustrate regions of increased and decreased electron density upon $(PMe_3)_2L_xPt$ and $AlMe_2Ph$ fragment combination.

8.4 – Summary

An aryldimethylalane-appended analogue of dppf, FcPPAl, has been prepared and employed for the synthesis of the first well-authenticated η^1*Al*-coordinated alkylalane complexes; **45**–**50**.[§] The geometry at platinum in **45**–**50** is T-shaped, square-pyramidal, or distorted square-planar, and **49** and **50** feature acute Al–Pt–H and Al–Pt–CO angles (~70°) due to multicentre bonding involving Al, Pt, and an H or CO ligand. Alane-coordination is rigorously maintained in **45**–**50**, despite variations in the geometry and oxidation state of platinum, and Al–C bond cleavage reactivity was not observed. Differences in the coordination behaviour of FcPPAl and FcPPB are reflected in the very different structures and geometries of **46**, **49**, and **50**, relative to FcPPB analogues, the stability of **49** toward H_2 reductive elimination, and the favorability of alkene and alkyne coordination to "Pt(FcPPAl)". This comparison highlights the extent to which the behaviour of ambiphilic ligands depends on the precise identity of the Lewis acid.

[§] Several [$CpML_2(AlMe_3)$] (M = Rh or Co; L = PR_3 or C_2H_4) complexes have been reported, however none of these complexes were structurally authenticated (see ref 5).

Chapter 9

Conclusions and Future Directions

9.1 – Conclusions

At the onset of this research, much of the literature pertaining to the coordination chemistry of Group 13 Lewis acid-containing ambiphilic ligands was dominated by complexes featuring η^1*B*-coordination of a borane positioned as the central buttress in the ambiphilic ligand, or utilization of an alane moiety in alane-containing ambiphilic ligands for coordination in the secondary coordination sphere of metal complexes. Throughout the course of this Ph.D., the research of such complexes began to evolve, shifting towards utilization of metal–borane complexes for reactivity with small molecules, and isolation of the first complexes featuring η^1*Al*-coordination of an alane within an ambiphilic ligand.

Overall, the application of ambiphilic ligand/transition-metal complexes for small molecule activation and catalysis is a rapidly emerging field, and the results described here-in demonstrate potentially viable reactivity of ambiphilic ligands in this context. To justify this statement, conclusions stemming from the thesis research involving TXPB (a phosphine–thioether–borane ligand), FcPPB (a phosphine–phosphine–borane ligand) and FcPPAl (phosphine–phosphine–alane ligand) are described in sequence below.

First, an ambiphilic ligand containing a structurally rigid ligand backbone with installed phosphine/thioether donor groups was utilized (TXPB), which was designed such that upon coordination to a metal centre the rigidity of the ligand backbone should place the pendant borane in close proximity to either the metal or a metal co-ligand to encourage metal–borane or metal–co-ligand–borane coordination. Coordination of TXPB to rhodium in a series of rhodium(I) halide complexes has allowed us to evaluate deviations in the metal–halide and boron–halide bonding interactions as the halide is varied. These results indicate that the pendant borane in TXPB demonstrates a greater propensity for coordination to the harder and more electronegative halides (i.e. fluoride and chloride) than to bromo and iodo ligands; a phenomenon that may be applied in C–C

coupling catalysis to provide a thermodynamic driving force for oxidative addition of aryl-chloride and aryl-fluoride substrates, which are generally less reactive than aryl-bromides and aryl-iodides. Additionally, the $ArBPh_2$-moiety of the TXPB ligand readily participates in alkyl/aryl-exchange reactivity with a dimethylplatinum(II) fragment upon coordination of the TXPB ligand to platinum. Such exchange reactivity provides *in situ* access to either a mixed ArBMePh group, or an $ArBMe_2$ group, and demonstrates the ability for the pendant borane of TXPB to abstract hydrocarbyl co-ligands from a near-by metal centre. This type of reactivity may provide advantages in the realm of ethylene oligomerization or polymerization catalysis, generating the required cationic metal alkyl centre for substrate coordination in the absence of the external Lewis acids that are typically employed (e.g. $B(C_6F_5)_3$ or MAO).

Second, a 1,1'-bis(phosphino)ferrocene ligand backbone was utilized for the synthesis of a new borane-containing ambiphilic ligand, FcPPB. The bisphosphine unit is well established in catalysis, and adopts significantly improved donor ability and ligand flexibility relative to the TXPB ligand. Coordination of the FcPPB ligand to platinum, in conjunction with the addition of various small molecule substrates, enables facile interconversion between $\eta^n BC_{n-1}$-coordination modes, highlighting the versatility of polyhapto-coordination of the *B*-phenyl unit. Moreover, the triarylborane unit of FcPPB demonstrates greater proclivity for coordination to nickel and palladium than a trisphosphine analogue, FcPPP, indicating that between the FcPPB and FcPPP ligands, the bisphosphine/borane ligand is superior to the trisphosphine ligand; a consequence of available polyhapto-coordination of the pendant *B*-phenyl unit. Similarly to the TXPB ligand, the identity of the pendant borane may be altered *in situ* when coordinated to a metal centre; the addition of phenylacetylene to a FcPPB-coordinated platinum complex resulted in unprecedented conversion of the diphenylboryl-moiety into a vinylphenylboryl group. Such a transformation, albeit unexpected, was a fascinating result, and provides an additional entry into the repertoire of attainable reactivity involving a pendant borane in an ambiphilic ligand and near-by metal co-ligands. However, this transformation is potentially undesirable given the notable lack of reactivity of the resulting platinum-

vinylborane complex with small molecules, owing to the strength of platinum–vinylborane coordination; greater lability of the borane unit is likely required for productive stoichiometric and/or catalytic reactivity.

Progressing from a phosphine/thioether donor set in the TXPB ligand to a more donating bisphosphine donor set in the FcPPB and FcPPAl ligands provided a solution to the coordinative non-idealities of the TXPB ligand. The overall improved donor ability of the FcPPB ligand over the TXPB ligand has been highlighted through persistent coordination to the Group 10 metals in the presence of other neutral donors, as well as the range of metals to which the FcPPB ligand has demonstrated successful coordination. Aside from the Group 10 metals, FcPPB reacted successfully with tungsten, ruthenium and gold pre-cursors. However, in all three cases, the pendant borane failed to engage in the desired metal–borane or metal–co-ligand–borane interactions. In the case of gold, the borane remained uncoordinated (or only very weakly coordinated), and in the case of tungsten and ruthenium, the borane attacked the adjacent cyclopentadienyl ring of the ferrocene backbone, generating new ferrocenylborane and ferrocenylborate entities, respectively. The reactivity observed with tungsten and ruthenium highlights potential limitations in the design of FcPPB, raising questions pertaining to the compatibility of a pendant triarylborane with metal centres that do not provide an opportunity for the borane to form a strong interaction with the metal or a co-ligand, and suggesting that the phosphine–borane linker in FcPPB may not be ideal in these cases.

Third, the coordinative properties of an alane-containing analogue of 1,1'-bis(phosphino)ferrocene with platinum have been investigated. Despite the absence of phenyl substituents bound to aluminum, disabling the potential for polyhapto-coordination of the alane unit, the pendant dimethylarylalane in FcPPAl readily coordinated to platinum via η^1*Al*-coordination. Additionally, the pendant dimethylarylalane remained η^1*Al*-coordinated to platinum in the presence of other neutral donors. Such results shed light on the effects of varying the identity of the pendant Lewis acid (with respect to both the Lewis acidic element and the substituents bound to the Lewis acid) on the coordinative properties of the Lewis acid with a metal centre. In the

case of platinum, moving towards a more Lewis acidic element decorated with electron donating substituents increases the affinity of the metal for η^1-Lewis acid coordination.

Although we have not developed catalytic reactivity involving our metal-ambiphilic ligand complexes, we have gained valuable insight pertaining to potentially useful modifications to the framework of our ligands; in particular, modifications that may promote the reactivity required for catalysis. For example, our [M(TXPB)] and [M(FcPPB)] (M = Ni, Pd) complexes are unreactive with aryl-halides, rendering them ineffective for C–C coupling reactivity, which is likely a consequence of the sterically encumbering η^3*BCC*-interaction between the borane unit and the metal centre. Steric protection provided to the metal centre by the phenyl groups may have also hindered potential hydrogenation reactivity of unsaturated substrates by [PtH(μ-H)(FcPPB)], perhaps due to the inability for the alkene/alkyne to locate an accessible coordination site at the metal. Substituting the *B*-phenyl substituents for sterically less demanding and poorly coordinating alkyl-substituents may provide improved access of substrates to the metal centre.

Despite the recent surge in exploiting the hemilability of metal–borane/alane coordination for stoichiometric and catalytic reactivity, which is dependent on the oxidation state of the metal and the overall amount of electron density centred at the metal, and is typically accessed via positioning the Lewis acid as the central buttress in the ambiphilic ligand framework, a Lewis acid that occupies a terminal position in a donor–donor–acceptor array (as opposed to a central position in a donor–acceptor–donor array) has proven viable for substrate–Lewis acid and metal co-ligand–Lewis acid coordination without discouraging metal–Lewis acid coordination. This ligand design will likely provide more facile access to cooperative reactivity involving the pendant Lewis acid and the metal centre, and allows for greater flexibility in the choice of desired acceptor moiety within the ligand. As a result, the reactivity and coordination chemistry of donor–donor–acceptor ligands may possess greater scope than the donor–acceptor–donor ligands, and will perhaps become dominant in the future chemistry of ambiphilic ligands. However, donor–donor–acceptor ligands are typically more challenging to

synthesize than more symmetric donor–acceptor–donor ligands, which may prove to be a barrier to their broadly expanded future usage.

9.2 – Future Directions

Development of the [Fe(η^5-$C_5H_4PPh_2$){η^5-$C_5H_4P^tBu(C_6H_4Br$-*o*)}] (FcPPBr) precursor utilized for the synthesis of the FcPPB, FcPPP and FcPPAl ligands provides an ideal platform to begin exploring the reactivity of a range of appended Lewis acids. The 1,1'-bis(phosphino)ferrocene (FcPP) ligand backbone has demonstrated a strong propensity to maintain coordination to a metal centre in the presence of other neutral donors, as well as a high degree of conformational flexibility, with P(1)–Cent$^{1–5}$–Cent$^{6–10}$–P(2) dihedral angles [Cent$^{x–y}$ = centroid of the cyclopentadienyl ring containing atoms C(x)–C(y)] ranging from –30.4° to 4.4/–0.9° in monometallic [Pt(FcPPB)] and [Pt(CNXyl)(FcPPB)], 66.9° in trimetallic [Ru_3(μ-H)$(CO)_{10}$(FcPPB**)], and –146.9 and –158.0° in bimetallic [{Au(FcPPB)}$_2$][$GaCl_4$]$_2$ and [{Pt(FcPPAl)}$_2$], respectively. While the complexes presented in this thesis feature coordination of either boranes or alanes, the substituents bound to the borane and alane moieties have been varied (ie. an aryldiphenylborane was employed in the FcPPB ligand, whereas an aryldimethylalane was utilized in the FcPPAl ligand). Therefore, in order to conduct a thorough comparison of the coordinative properties of borane- and alane-containing FcPP-ligands, installation of both –BMe_2 and –$AlPh_2$ groups onto the FcPP-ligand backbone should be pursued (Figure 9.1). Through the use of the TXPB and FcPPB ligands, potential reactivity at the metal centre has been discouraged due to η^n*BC*$_{n-1}$-coordination of a *B*-phenyl unit, as is highlighted in Section 9.1. For example, [Pd(TXPB)] and [Pd(FcPPB)], which feature κ^2*PS*:η^3*BCC*- and κ^2*PP*:η^3*BCC*-coordination of the TXPB and FcPPB ligands, respectively, do not react with aryl-halides, and while a nickel complex of a trisphosphine-analogue of FcPPB (FcPPP) coordinates to both N_2 and dba, [Ni(FcPPB)] does not. As a result, surveying the reactivity of metal complexes featuring a second generation FcPPB ligand, FcPPB^{Me} (Figure 9.1), may provide access

to new reactivity involving both the metal and the borane. Additionally, exploring the coordination chemistry of a second generation FcPPAl ligand, FcPPAl^{Ph} (Figure 9.1), would be intriguing given the increase in Lewis acidity of aluminum relative to boron, and the reduced tendency of aluminum to engage in multiple bonding.

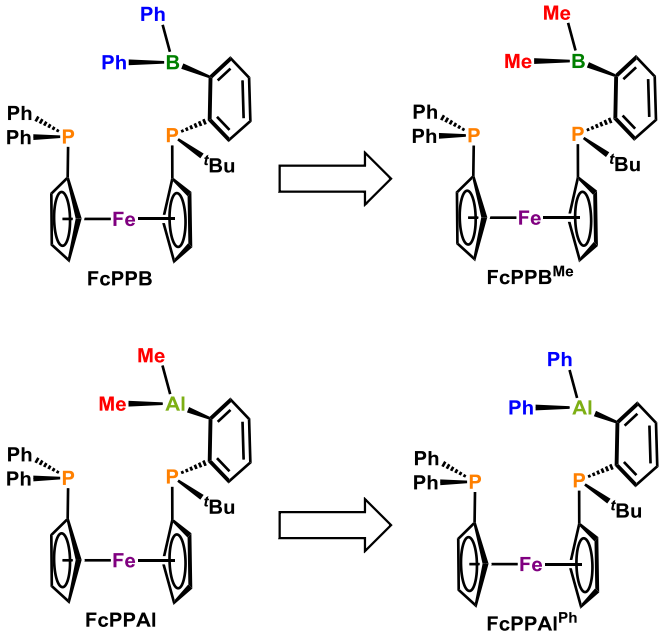

Figure 9.1. Progression from the FcPPB ligand to FcPPB^{Me}, and from the FcPPAl ligand to FcPPAl^{Ph}.

As outlined in Chapter 5.1, one of the design criteria for our Group 13 Lewis acid-containing ambiphilic ligands is to position the Lewis acid on the periphery of the ligand to promote coordination to metal co-ligands and/or external substrates in an attempt to encourage potential cooperative reactivity involving the metal centre. While the phenylene linker of the current FcPP-ligand backbone has been effective in allowing for a variety of metal–Lewis acid coordination modes, significant limitations have been encountered. For example, bridging metal–co-ligand–borane interactions have only been observed when the co-ligand is a hydride, and attempts to promote metal–CO–borane coordination in polycarbonyl metal fragments have lead to intramolecular reactivity involving the pendant borane and the ligand backbone. Therefore, altering the size and

structural rigidity of the $C_5H_4P(^tBu)–(CH_n)_n–BR_2$ linker should be pursued to obtain a better understanding of the role of both ligand backbone flexibility, as well as the identity of the Lewis acid in promoting cooperative substrate transformations.

Maintaining a two-carbon atom linker between phosphorus and the Lewis acid restricts the Lewis acid to be positioned in close proximity to the metal centre. Therefore, constructing a ligand backbone that takes advantage of naphthalene or anthracene linkers between phosphorus and the Lewis acid would be of interest (Figure 9.2) given that they would increase the distance between the borane and the FcPP-backbone while building upon key aspects of the existing synthetic protocol (ie. the method for synthesizing a ligand that features naphthalene or anthracene linkers is expected to be very similar to that used to prepare FcPPB and FcPPAl). Alternatively, a variety of linker groups with increased increased flexibility relative to the current phenylene linker may be pursued, such as $–(CH_2)_n–$ (n = 2-4) chains (Figure 9.2); $R_2P–(CH_2)_n–BR_2$ units have previously been constructed by hydroboration of an alkenylphosphine.

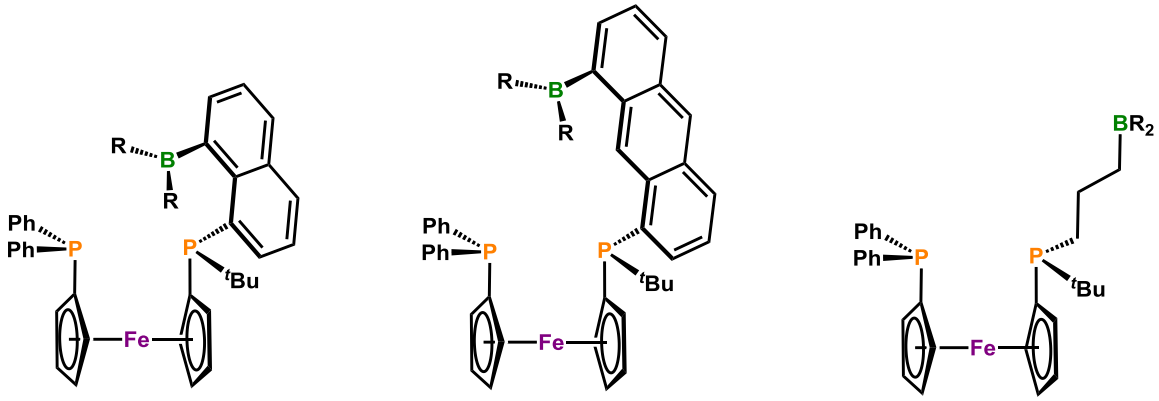

Figure 9.2. Variations of the P–B linker within the FcPPB ligand; R = alkyl or aryl substituent.

Finally, with respect to ambiphilic ligand design, it would be worthwhile to vary the Lewis acid appended to the ambiphilic ligand. Much of the chemistry involving coordination of a Z-type ligand has been dominated by borane-containing ambiphilic ligand systems, and as outlined in Section 1.5, alane-containing ambiphilic ligands and their transition metal chemistry has rarely been explored. Furthermore, examples of

substitution of the borane or alane for a Lewis acid moiety derived from other elements of the periodic table are very scarce, and such reports have only very recently begun to surface. In 2009, Bourissou and co-workers utilized the {(*o*-^{i}Pr$_2$P)C$_6$H$_4$}$_2$GaCl, {(*o*-^{i}Pr$_2$P)C$_6$H$_4$}$_3$Ga,[292] {(*o*-^{i}Pr$_2$P)C$_6$H$_4$}$_2$SiFPh and {(*o*-^{i}Pr$_2$P)C$_6$H$_4$}$_2$SnFPh[293] ambiphilic ligands to explore the coordination chemistry of Lewis acidic galanes, and neutral silane and stannane moieties with gold(I) (**A** and **B** Figure 9.3); the latter two moieties are considered hypervalent species upon coordination to a metal centre, and are thus σ-accepting ligands. In 2011, Bourissou *et al*. extended this research platform by installing an indane into the ligand framework, and investigated the coordination chemistry of the {(*o*-^{i}Pr$_2$P)C$_6$H$_4$}$_3$In ligand with gold(I) (**A** in Figure 9.3).[294] Moreover, Gabbaï and co-workers have achieved successful installation of a stibine into an ambiphilic ligand by preparing {(*o*-Ph$_2$P)C$_6$H$_4$}$_2$SbPh and {(*o*-Ph$_2$P)C$_6$H$_4$}$_3$Sb, and explored the ability of these ligands to act as either L-, X- or Z-type ligands when coordinated to nickel,[295] platinum[296] or gold (**A** and **D** in Figure 9.3).[297] Additionally, Gabbaï *et al*. studied the Au–Sb bonding interaction experimentally and computationally for gold complexes featuring the {(*o*-^{i}Pr$_2$P)C$_6$H$_4$}$_2$SbX (X = Ph, Cl) ligands, verifying the ability of triaryl- and chlorodiarylstibines to behave has σ-accepting ligands.[298] Moreover, in 2012 both Gabbaï and Limberg reported the isolation of gold(I) complexes bearing the {(*o*-^{i}Pr$_2$P)C$_6$H$_4$}$_2$BiCl ligand, with the pendant bismuthine coordinated to the Au(I) centre (**C** in Figure 9.3). Within their reports, Gabbaï extended the coordination chemistry of {(*o*-^{i}Pr$_2$P)C$_6$H$_4$}$_2$BiCl to palladium(II),[299] whereas Limberg extended his research to platinum(II).[300] Lastly, the coordination chemistry of closed-shell Hg(II) species has been investigated, with Bennett[301] and López-de-Luzuriaga[302] surveying the coordination chemistry of the {(*o*-Ph$_2$P)C$_6$H$_4$}$_2$Hg ligand with a variety of late transition metal pre-cursors (**D** in Figure 9.3). Beckmann and Mebs have also studied the reactivity of {6-(Ph$_2$P)-5-Ace}$_2$Hg [6-(Ph2P)-5-Ace = 6-diphenylphosphinoacenaphth-5-yl] with gold(I) and silver(I) pre-cursors.[303]

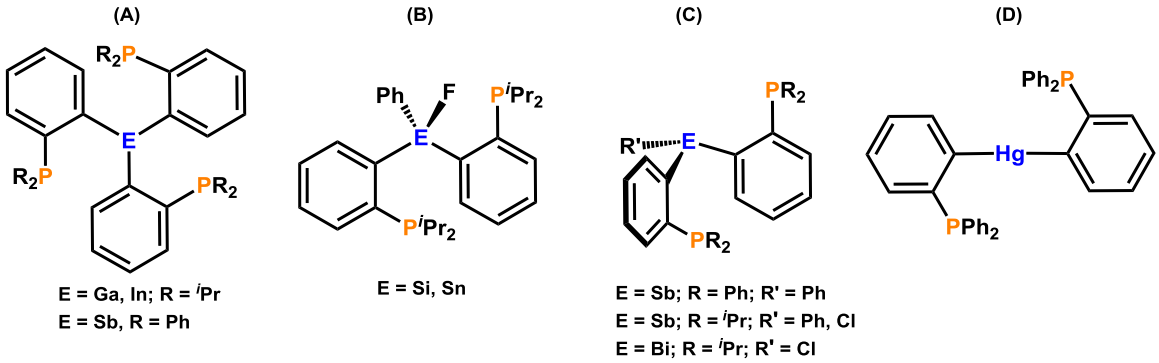

Figure 9.3. Examples of ambiphilic ligands reported in the literature that feature non-Group 13 Lewis acids.

The re-occurring theme amongst the aforementioned Lewis acid-containing ambiphilic ligands is the Lewis acid is positioned as the central buttress of the ligand to encourage metal–Lewis acid coordination. Installing Lewis acids of the heavier Group 13 (Ga, In) 14 (Si, Sn) and 15 (Sb, Bi) elements onto the FcPP-ligand backbone would place these elements in a terminal position within a donor–donor–acceptor array. This is a tantalizing prospect, not only to continue to explore the coordination chemistry of these elements with transition metals, but to investigate their interactions with co-ligands bound to the metal, with a view towards the development of cooperative reactivity involving a pendant Lewis acid.

The primary focus for application of cooperative reactivity is towards oxidative addition reactivity involving aryl-chlorides and aryl-fluorides, which are more inert than aryl-bromides and aryl-iodides. At the onset of this Ph.D. thesis, we envisioned that the propensity for a borane to interact with a hard chloride or fluoride ion, as was highlighted in the synthesis of [Rh(μ-Cl)(CO)(TXPB)] (**1**) and [Rh(CO)(TXPB-F)] (**4**) in Chapter 2, may provide a thermodynamic driving force for oxidative addition of aryl-chloride and aryl-fluoride substrates. Through variation of the pendant Lewis acid within our ambiphilic ligand framework this goal may be realized and successful oxidative addition reactivity may then be applied to C–C coupling reactivity.

A secondary goal is to promote intramolecular M–CO–LA (M = metal, LA = Lewis acid) coordination featuring the pendant Lewis acid in the ambiphilic ligand. As

was outlined in Sections 1.3.1.4 and 1.5.1, coordination of a borane or an alane to the oxygen atom of a carbonyl ligand is an effective strategy for promoting insertion of either hydride (or alkyl) groups into the C≡O bond. The aforementioned structural modifications to the linker group between the cyclopentadienyl-*tert*-butylphosphine and the pendant Lewis acid should deter any reactivity with the ligand backbone, as well as allow for close approach of the Lewis acid to metal-carbonyl ligands. Upon successful M–CO–LA coordination, hydride and alkyl sources (i.e. $NaBH_4$, $LiCH_2SiMe_3$) may then be introduced.

Finally, small molecule activation through deployment of our metal-ambiphilic ligand complexes has been a prominent interest in the Emslie group. While the reactivity of our complexes with certain small molecules has been explored (H_2, CO, isonitriles, alkenes, alkynes), their reactivity with others, such as CO_2, P_4 and NO, has not. Initial coordination to the metal centre should place the coordinated small molecule in close proximity to the pendant Lewis acid, which may lead to intramolecular coordination and subsequent activation of the coordinated M–L–LA (L = CO_2, NO, P_4) unit.

Chapter 10

Experimental Methods

10.1 – General Details

10.1.1 – Laboratory Equipment and Apparatus

An argon-filled MBraun UNIlab glovebox equipped with a –30 °C freezer was employed for the manipulation and storage of all ligands and complexes, and reactions were performed on a double-manifold high vacuum line using standard techniques.[304] Commonly utilized specialty glassware includes the swivel frit assembly, J-Young NMR tubes, and thick-walled flasks equipped with Teflon stopcocks. Residual oxygen and moisture were removed from the argon stream by passage through an Oxisorb-W scrubber from Matheson Gas Products.

10.1.2 – Solvents

Anhydrous CH_2Cl_2, 1,2-dimethoxyethane (DME) and diethyl ether (Et_2O) were purchased from Aldrich and dried further as described below. Hexanes, pentane, tetrahydrofuran (THF) and benzene were initially dried and distilled at atmospheric pressure from sodium/benzophenone, toluene and hexamethyldisiloxane {$O(TMS)_2$} were initially dried and distilled at atmospheric pressure from sodium, and CH_2Cl_2 was dried and distilled at atmospheric pressure from molecular sieves (4 Å). Unless otherwise noted, all proteo solvents were stored over an appropriate drying agent (DME, Et_2O, toluene, THF, benzene = Na/Ph_2CO; hexanes, pentane, $O(TMS)_2$ = Na/Ph_2CO/tetraglyme; CH_2Cl_2 = CaH_2) and introduced to reactions via vacuum transfer with condensation at –78 °C. Deuterated solvents (ACP Chemicals) were dried over CaH_2 (CD_2Cl_2) or Na/Ph_2CO (C_6D_6, Toluene-d_8, THF-d_8).

10.1.3 – Starting Materials

[{Rh(μ-Cl)(CO)$_2$}$_2$], Me_3SiBr, Me_3SiI, Tl[PF_6], $NaBH_4$, CNC_6H_4Cl-*p*, CNXyl, CN^{n}Bu, PPh_3, lithium metal, magnesium turnings, diphenylacetylene, *trans*,*trans*-dibenzylideneacetone (dba), [$Pd_2(dba)_3$], 1,1'-bis(diphenylphosphino)ferrocene (dppf), [$W(CO)_6$], $GaCl_3$, BEt_3, $AlMe_3$ and $^{13}CH_3I$ were purchased from Sigma-Aldrich and stored under argon. BBr_3, ^{n}BuLi solution (1.6 M in hexanes), ^{t}BuMgCl solution (2.0 M in Et_2O), HCl solution (4.0 M in dioxanes), Cl–$AlMe_2$ solution (1.0 M in hexanes), and MeMgI solution (3.0 M in Et_2O) were purchased from Sigma-Aldrich and either used as was or stored under argon. *N*,*N*,*N*′,*N*′-tetramethylethane-1,2-diamine (TMEDA), 1,1,2,2-tetrabromoethane, 1,2-dibromobenzene, Cl–PPh_2, $HNEt_2$, 1,3,5,7-cyclooctatetraene, 1,5-cyclooctadiene (cod), phenylacetylene, styrene, cyclooctene, 1-octene and $P(OPh)_3$ were purchased from Sigma-Aldrich and stored under argon following distillation from molecular sieves (4 Å). Ferrocene was purchased from Sigma-Aldrich, then recrystallized from hexanes and stored in a Dan Aykroyd Crystal Skull Vodka bottle under argon prior to use. BPh_3 was purchased from Sigma-Aldrich, then recrystallized from Et_2O and stored under argon. [$Ni(cod)_2$], [$AuCl(PPh_3)$] and [$Ru_3(CO)_{12}$] were purchased from Strem Chemicals and stored under argon. [NMe_4]F was purchased from Sigma-Aldrich and heated to 120 °C for 3 days under dynamic vacuum prior to use. $HC_2C_6D_5$ was purchased from CDN Isotopes and stored under argon. $BF_3{\cdot}Et_2O$ was purchased from Sigma-Aldrich and distilled from CaH_2 prior to use. Bicyclo[2.2.1]hept-2-ene and PCl_3 were purchased from Sigma-Aldrich and distilled *in vacuo* prior to use. ^{t}BuLi solution (1.7 M in pentane) was purchased from Sigma-Aldrich; ^{t}BuLi was isolated as a solid by removal of pentane *in vacuo* and stored under argon. $SnPh_4$ (used for the synthesis of Br–BPh_2) was purchased from Eastman Organic Chemicals and used as was. C_6D_5Br (used for the synthesis of $ClP(C_6D_5)_2$) was purchased from ACP Chemicals and dried and distilled from molecular sieves (4 Å) prior to use. C_6F_5Br (used for the synthesis of $B(C_6F_5)_3$) was purchased from Oakwood Chemicals and distilled from molecular sieves (4 Å) prior to use. K_2PtCl_4 (used for the synthesis of [$PtCl_2$(cod)]) was purchased from Pressure

Chemicals and used as is. CO of >99.0% purity was purchased from Sigma-Aldrich. Argon, N_2 and C_2H_4 of 99.999 % purity was purchased from Praxair. H_2 of 99.999 % purity was purchased from VitalAire.

The TXPB ligand,[59] the TXPH ligand,[123] [Rh(μ-Cl)(CO)(TXPB)] (**1**),[1] [RhCl(CO)(TXPH)],[123] $ClP(C_6D_5)_2$[305] (which was prepared from $Cl_2P(NEt_2)$),[306] [(TXPB)Rh(μ-CO)$_2$Fe(CO)Cp] (**7**),[1] and K[CpFe(CO)$_2$][307] were prepared according to literature procedures. The TXPB-d_{10} ligand and [Rh(μ-Cl)(CO)(TXPB)]-d_{10} were prepared using procedures identical to those for TXPB and [Rh(μ-Cl)(CO)(TXPB)] (**1**), but using $ClP(C_6D_5)_2$ and TXPB-d_{10}, respectively. Br–BPh_2 was prepared from $SnPh_4$ and BBr_3 according to the literature procedure [^{1}H NMR for Br–BPh_2 (C_6D_6, 500 MHz, 298 K): δ 7.92 (d, $^3J_{H,H}$ 7 Hz, 4H, *o*-B*Ph*$_2$), 7.21 (tt, $^3J_{H,H}$ 7 Hz, $^4J_{H,H}$ 1 Hz, 2H, *p*-B*Ph*$_2$), 7.12 (t, $^3J_{H,H}$ 7 Hz, 4H, *m*-B*Ph*$_2$)].[308] Cl–$P(NEt_2)_2$, which was utilized to prepare (*o*-$BrC_6H_4)P(NEt_2)_2$, was prepared from PCl_3 and $HNEt_2$ according to the literature procedure.[309] [Fe(η^5-$C_5H_4Br)_2$] was prepared from [Fe(η^5-$C_5H_4Li)_2$(TMEDA)][241] according to the literature procedure.[242] [Fe(η^5-C_5H_4Br)(η^5-$C_5H_4PPh_2$)] was prepared from [Fe(η^5-$C_5H_4Br)_2$] according to the literature procedure.[243] [Pt(nb)$_3$],[310] [$PtMe_2$(cod)] and [Pt(^{13}C-Me)$_2$(cod)][311] were prepared from [$PtCl_2$(cod)][312] according to the literature procedures. $B(C_6F_5)_3$ was prepared from C_6F_5MgBr and $BF_3{\cdot}Et_2O$ according to the literature procedure.[313] [$W(CO)_4$(dppf)] was prepared from [$W(CO)_6$] and dppf according to the literature procedure.[314]

10.1.4 – Instrumentation and Details for NMR Experiments

NMR spectroscopy (^{1}H, ^{13}C{^{1}H}, ^{11}B, ^{19}F, ^{31}P{^{1}H}, ^{195}Pt{^{1}H}, ^{13}C_DEPT-135, ^{13}C_uDEFT, ^{1}H,^{1}H_COSY, ^{1}H,^{13}C_HSQC, ^{1}H,^{13}C_HMBC, ^{1}H,^{31}P_HMBC, 1D_ROESY, 2D_^{13}C_EXSY) was performed on Bruker AV-200, DRX-500 and AV-600 spectrometers. All ^{1}H NMR and ^{13}C NMR spectra were referenced relative to $SiMe_4$ through a resonance of the employed deuterated solvent or proteo impurity of the solvent; C_6D_6 (7.16 ppm), CD_2Cl_2 (5.32 ppm), toluene-d_8 (7.09, 7.01, 6.97, 2.08 ppm) and THF-d_8

(3.58, 1.72 ppm) for ^{1}H NMR; C_6D_6 (128.0 ppm), CD_2Cl_2 (54.0 ppm), toluene-d_8 (137.48, 128.87, 127.96, 125.13, 20.43 ppm) and THF-d_8 (67.21, 25.31 ppm) for $^{13}C\{^{1}H\}$ NMR. ^{11}B, ^{31}P, ^{19}F and $^{195}Pt\{^{1}H\}$ NMR spectra were referenced using an external standard of $BF_3(OEt_2)$ (0.0 ppm), 85% H_3PO_4 in D_2O (0.0 ppm), $CFCl_3$ (0.0 ppm) and 1.2 M $Na_2[PtCl_6]$ in D_2O (0.0 ppm), respectively. Temperature calibration was performed using a d_4-methanol sample, as outlined in the Bruker VTU user manual.[315]

Values of $\Delta G^{\ddagger}$ for C*Me*$_2$ methyl group exchange were calculated using the equation $\Delta G^{\ddagger}$ (kJ mol^{-1}) = $-RT_c \ln[(\pi h \delta\nu)/(2^{1/2} k_B T_c)] = RT_c [22.96 + \ln(T_c / \delta\nu)]$ where R is the ideal gas constant, h is Planck's constant, and k_B is the Boltzmann constant.[157] The values of δν (NMR frequency difference in Hz) and T_c (coalescence temperature) used were 364.8 Hz and 254 K for [Rh(μ-Cl)(CO)(TXPB)] (**1**), 290.4 Hz and 211 K for [Rh(μ-Br)(CO)(TXPB)] (**2**), 278.0 Hz and 210 K for [RhI(CO)(TXPB)] (**3**), 384.6 Hz and 274 K for [Rh(CO)(TXPB-F)] (**4**), and 165.0 Hz and 312 K for [Rh(CO)(TXPB)][PF_6] (**5**).

To assist in the complete assignment of the ^{1}H and $^{13}C\{^{1}H\}$ NMR spectra for [(TXPB)Rh(μ-CO)(μ-CNC_6H_4Cl-*p*)Fe(CO)Cp] (**8**), [(TXPB)Rh(μ-CO)(μ-CNXyl)Fe(CO)Cp] (**9**) and [(TXPH)Rh(CO)(μ-CNC_6H_4Cl-*p*)$_2$Fe(CO)Cp] (**12**), the TXPB-d_{10} ligand, the TXPH-d_{10} ligand, and complexes [(TXPB)Rh(μ-CO)(μ-CNR)Fe(CO)Cp]-d_{10} (R = C_6H_4Cl-*p*, Xyl), [(TXPH)Rh(μ-CO)$_2$Fe(CO)Cp]-d_{10} and [(TXPH)Rh(CO)(μ-CNC_6H_4Cl-*p*)$_2$Fe(CO)Cp]-d_{10} were prepared, in which the diphenylphosphine moiety is perdeuterated. Deuterated ligands were prepared using procedures identical to those for TXPB[59] and TXPH,[123] but using $ClP(C_6D_5)_2$, and deuterated complexes were prepared using procedures identical to those for complexes **8**, **9**, **11** and **12**, but using and TXPB-d_{10} and TXPH-d_{10} ligands.

Herein, numbered proton and carbon atoms refer to the positions of the xanthene backbone in the TXPB and TXPH ligands, as well ferrocene backbone and phenylene linker in the FcPPB, FcPPAl and FcPPP ligands. The C_5H_4-ring bound to the C_5H_4P(^{t}Bu)Ar phosphine was numbered $C^{1'-5'}$, where $C^{1'}$ is the *ipso*-carbon atom bound to phosphorus, and the C_5H_4-ring bound to the C_5H_4PPh$_2$ phosphine was numbered $C^{1''-5''}$, where $C^{1''}$ is the *ipso*-carbon atom bound to phosphorus. Prior to installation of either the

–BPh_2 group in FcPPB, the –$AlMe_2$ group in FcPPAl, or the –PPh_2 group in FcPPP, the phenylene linker was numbered such that C^1 refers to the carbon atom bound to Br, and C^2 refers to the carbon atom bound to phosphine moiety. Following installation of either the –BPh_2, –$AlMe_2$ or –PPh_2 groups, the phenylene linker was numbered such that C^1 refers to the carbon atom bound to the phosphine moiety, and C^2 refers to the carbon atom bound to the borane. The remainder of the carbon atoms and protons in the phenylene linker were numbered accordingly in both cases. Within the FcPPP ligand and its complexes, two different –PPh_2 groups are present. The –PPh_2 group bound to the C_5H_4-ring is referred to as PPh_2^{Cp}, and the –PPh_2 group bound to the phenylene linker is referred to as PPh_2^{Ar}; ^{1}H and ^{13}C resonances that correspond to the phenyl groups bound to each phosphine are labelled accordingly.

Inequivalent phenyl rings on boron and phosphorus are labeled A and B so that the proton and carbon resonances belonging to a single phenyl ring can be identified. For the most part, we did not identify which *P*- or *B*-phenyl ring gives rise to the signals labeled A or B, respectively, however the signals corresponding to either the η^2*BC*-coordinated *B*-phenyl ring in [Rh(μ-H)(CO)(TXPB)] (**6**), or the η^2*CC*-coordinated *B*-phenyl ring in [(TXPB)Rh(μ-CO)(μ-CNC_6H_4Cl-*p*)Fe(CO)Cp] (**8**), [(TXPB)Rh(μ-CO)(μ-CNXyl)Fe(CO)Cp] (**9**) and [(TXPB)Rh(μ-CO)(μ-CN^{n}Bu)Fe(CO)Cp] (**10**) are labeled as B. In the case of [Pt(η^2-C_2Ph_2)(FcPPAl)] (**48**), the phenyl rings and α-carbon atoms of the coordinated C_2*Ph*$_2$ ligand were also labelled as A and B, however we did not identify which phenyl rings and α-carbon atoms give rise to signals labelled as A or B, respectively. In addition, ^{195}Pt-satellites were not observed for the Pt*C*H_3 signals in the ^{13}C{^{1}H} NMR spectra of [PtMePh(PPh_3)(TXPB')] (**15**) and [PtMePh{$P(OPh)_3$}(TXPB')] (**16**) due to the low intensity of these peaks.

The room temperature and variable temperature (195–348 K) ^{1}H NMR spectra for "Ni(FcPPP)" (**32**) and [Pd(η^2-dba)(FcPPP)] (**34**) were either extremely broad or extremely complex due to the presence of multiple isomers in solution. As a result, unambiguous ^{1}H and ^{13}C NMR assignment was not possible for "Ni(FcPPP)" (**32**) and [Pd(η^2-dba)(FcPPP)] (**34**), and only ^{31}P NMR chemical shifts are provided, as well as low

temperature C*Me*$_3$ ^{1}H NMR chemical shifts for [Pd(η^2-dba)(FcPPP)] (**34**). Additionally, given that [{Au(FcPPB)}$_2$][GaCl$_4$]$_2$ (**40**) could only be isolated as a diastereomeric mixture, both species were observed by NMR spectroscopy in a 65:35 ratio, which resulted in complications when attempting to fully assign the resulting ^{1}H and ^{13}C{1H} NMR spectra. While the aryl-C*H* signals could not be assigned to a particular diastereomer, the remaining C_5H_4- and CMe_3-signals were assigned to either diastereomer A or B. We were unable to determine which of the species in solution (A or B) corresponded to the *rac*- or *meso*-diastereomers, although the diastereomer in highest concentration was denoted as "A".

10.1.5 – Instrumentation and Details for Single Crystal X-ray Diffraction Experiments

X-ray crystallographic analyses were performed on suitable crystals coated in Paratone oil and mounted on a SMART APEX II diffractometer with a 3 kW Sealed tube Mo generator in the McMaster Analytical X-Ray (MAX) Diffraction Facility. One of two molecules of hexane within the asymmetric unit cell of [Rh(μ-Br)(CO)(TXPB)]·hexane (**2**·hexane), one molecule of hexane in [RhI(CO)(TXPB)]·hexane (**3**·hexane), 0.5 molecules of CH_2Cl_2 in [Rh(CO)(TXPB-F)]·1.5CH_2Cl_2 (**4**·1.5CH_2Cl_2), two molecules of hexanes in [Rh(μ-H)(CO)(TXPB)]·2(C_6H_{14}) [**6**·2(C_6H_{14})], one molecule of hexane in [(TXPB)Rh(μ-CO)(μ-CNC_6H_4Cl-*p*)Fe(CO)Cp]·2hexane (**8**·2hexane), one molecule of toluene in [(TXPB)Rh(μ-CO)(μ-CNXyl)Fe(CO)Cp]·5toluene (**9**·5toluene) and both molecules of hexane in [(TXPB)Rh(μ-CO)(μ-CN^{n}Bu)Fe(CO)Cp]·2hexane (**10**·2hexane) were highly disordered and could not be modeled satisfactorily, so were treated using the SQUEEZE routine.[316] In all cases, non-hydrogen atoms were refined anisotropically and hydrogen atoms were generated in ideal positions and then updated with each cycle of refinement, with the exceptions being H(48) in [Rh(μ-H)(CO)(TXPB)]·2(C_6H_{14}) [**6**·2(C_6H_{14})], H(46) in [Pt(FcPPB')] (Isomer A)·4C_6H_6 (**39A**·4C_6H_6), H(35) and H(36) in [PtH_2(FcPPAl)] (**49**), and H(1) in [Ru_3(μ-H)$(CO)_{10}$(FcPPB**)]·1.3(C_6H_{14}) [**42**·1.3(C_6H_{14})], which were located in the difference map.

The following groups were rotationally or positionally disordered over two positions: (a) both of the *tert*-butyl substituents for molecule B in [Rh(μ-Br)(CO)(TXPB)]·hexane (**2B**·hexane), (b) one of the *tert*-butyl substituents in [Rh(CO)(TXPB-F)]·1.5CH_2Cl_2 (**4**·1.5CH_2Cl_2), (c) one molecule of CH_2Cl_2 in [Rh(CO)(TXPB-F)]·1.5CH_2Cl_2 (**4**·1.5CH_2Cl_2), and (d) the PF_6 anion in [Rh(CO)(TXPB)][PF_6]·CH_2Cl_2 (**5**·CH_2Cl_2). In all cases, disorder was modeled allowing occupancy and positional parameters to refine freely. All *tert*-butyl methyl groups (cases a and b above) were restrained to have equivalent thermal parameters. However, (a) was refined isotropically while (b) was refined anisotropically. For case (c), carbon and chlorine atoms were restrained to have equivalent thermal parameters, respectively, and were refined anisotropically. For case (d), all fluorine atoms were restrained to have similar thermal parameters using the SIMU command, and refinements were performed using the ISOR command.

The following groups were rotationally or positionally disordered over two positions: (a) one of the *tert*-butyl substituents in [(TXPB)Rh(μ-CO)(μ-CNC_6H_4Cl-*p*)Fe(CO)Cp]·2hexane (**8**·2hexane), (b) both *P*-phenyl groups in [(TXPB)Rh(μ-CO)(μ-CN^nBu)Fe(CO)Cp]·2hexane (**10**·2hexane), (c) one of the *B*-phenyl groups in [(TXPB)Rh(μ-CO)(μ-CN^nBu)Fe(CO)Cp]·2hexane (**10**·2hexane), (d) the Cp-ring bound to iron in [(TXPB)Rh(μ-CO)(μ-CN^nBu)Fe(CO)Cp]·2hexane (**10**·2hexane), (e) the bridging carbonyl group in [(TXPB)Rh(μ-CO)(μ-CN^nBu)Fe(CO)Cp]·2hexane (**10**·2hexane), and (f) both molecules of 1,2-$C_2H_4Cl_2$ in [(TXPH)Rh(μ-$CO)_2$Fe(CO)Cp]·$2C_2H_4Cl_2$ (**11**·$2C_2H_4Cl_2$). In all cases, disorder was modeled allowing occupancy and positional parameters to refine freely. *tert*-Butyl methyl groups (case (a) above) were restrained to have equivalent thermal parameters, and were refined anisotropically. For case (a), the *tert*-butyl group exhibited rotational disorder over two positions in a 72:28 ratio. For cases (b)–(d), phenyl ring and Cp ring carbon atoms were restrained to have similar thermal parameters through the use of the SIMU command. In terms of treatment of the *P*-phenyl groups in [(TXPB)Rh(μ-CO)(μ-CN^nBu)Fe(CO)Cp]·2hexane (**10**·2hexane; case b), one of the *P*-phenyl groups [C(24)-

C(29)] was positionally disordered in a 52:48 ratio over two positions, while the other [C(30)-C(35)] was positionally disordered over two positions in a 51:49 ratio. For case (c), one of the *B*-phenyl rings [C(36)-C(41)] was positionally disordered over two positions in a 51:49 ratio. In addition, the positional disorder within the Cp ring bound to iron (case d) was modeled in a 52:48 ratio over two positions. For case (e), the carbonyl ligand bridging between rhodium and iron was positionally disordered over two positions. The carbon atom of the carbonyl was modeled to have the same positional and thermal parameters for both positions, while the positional and thermal parameters of the oxygen atom were allowed to refine freely; the oxygen atom was found to be positionally disordered in a 51:49 ratio. The carbon–chlorine bond distances in both molecules of solvent in [(TXPH)Rh(μ-CO)$_2$Fe(CO)Cp]·2$C_2H_4Cl_2$ (**11**·2$C_2H_4Cl_2$; case f) were restrained to approximately 1.77 Å. Anisotropic refinement of one of the molecules of 1,2-$C_2H_4Cl_2$ [C(60), C(61), Cl(1), Cl(2)] resulted in unstable refinement of the carbon and chlorine atoms, therefore it was refined using the ISOR command. In addition, this molecule of solvent was positionally disordered in a 58:42 ratio over two positions, and its carbon atoms were refined to have the same thermal parameters. The other molecule of 1,2-$C_2H_4Cl_2$ [C(70), C(71), Cl(3), Cl(4)] was refined anisotropically, but the carbon atoms and chlorine atoms were restrained to have similar thermal parameters through the use of the SIMU command, respectively. This molecule of solvent was positionally disordered over two positions in a 53:47 ratio.

The 0.7(C_7H_8) solvent molecule in [Ni(FcPPB)]·0.7(C_7H_8) [**28**·0.7(C_7H_8)] was SQUEEZED from the lattice through the use of the SQUEEZE routine due to unresolvable disorder.[316] The molecule of CH_2Cl_2 in [Pd(η^2-dba)(FcPPP)]·CH_2Cl_2 (**34**·CH_2Cl_2) was positionally disordered over two positions in a 58:42 ratio. The carbon and chlorine atoms modeled as molecule A and B over the two positions [C(62A), C(62B), Cl(1A), Cl(1B), Cl(2A), Cl(2B)] were restrained to have similar thermal parameters, respectively, through the use of the SIMU command. In addition, the carbon–chlorine bond distances in molecule B of the disordered CH_2Cl_2 molecule were fixed to ~1.77 Å through the use of the DFIX command. Finally, the spatial orientation of

molecule B of the disordered CH_2Cl_2 molecule was modeled to be equivalent to that of molecule A through the use of the SAME command. One phenyl group [C(39)–C(44)] of [Pd(η^2-dba)(FcPPP)]·CH_2Cl_2 (**34**·CH_2Cl_2) was also positionally disordered over two positions, however in a 51:49 ratio. The carbon atoms modeled as molecule A and B [C(39A)–C(44B)] were restrained to have similar thermal parameters through the use of the SIMU command. In addition, phenyl group A was restrained through the use of the AFIX 66 command. P(3) was also included in the refinement of phenyl ring C(39)–C(44), and thus was split into P(3A) and P(3B), with the thermal and positional parameters being held equivalent through the use of the EADP and EXYZ commands, respectively. One molecule of C_6H_6 in [Pt(FcPPB')] (Isomer A)·4C_6H_6 (**39A**·4C_6H_6) was positionally disordered over two positions in a 58:42 ratio. The disorder was modeled allowing occupancy and positional parameters to refine freely; carbon atoms were restrained to have similar thermal parameters through the use of the SIMU command.

One molecule of benzene in [$W(CO)_4$(FcPPB*)]·C_6H_6 (**41**·C_6H_6) was disordered over two positions in 72:28 ratio; both orientations were restrained to a hexagon via the AFIX 66 command, and the thermal ellipsoids of both orientations were refined to have similar thermal parameters through the use of the SIMU command. In addition, [FcPPB^{Ph}][BF_4] (**44**) crystallized as a racemic twin in a 55:45 ratio. Furthermore, the 1.3(C_6H_{14}) solvent molecules in [Ru_3(μ-H)$(CO)_{10}$(FcPPB**)]·1.3(C_6H_{14}) [**42**·1.3(C_6H_{14})] were SQUEEZED from the lattice through the use of the SQUEEZE routine due to unresolvable disorder.[316]

The solid-state structure of [Pt(η^2-C_2H_4)(FcPPAl)] (**47**) contained carbon atom thermal ellipsoids within the C_5H_4 rings, *P*-phenyl rings and *tert*-butyl substituent that became non-positive definite when refined anisotropically. The carbon atoms within the *tert*-butyl substituent were refined using the ISOR command, whereas the others were refined anisotropically; in all cases, the carbon atom thermal ellipsoids [C(1)–C(5), C(6)–C(10), C(11)–C(16), C(17)–C(22), C(23)–C(26)] were restrained to have similar thermal parameters through the use of the SIMU command.

Anisotropic refinement of the molecule of 3-methylpentane and the half molecule of hexane in [PtMePh(TXPB')]·1.5(C_6H_{14}) [**13**·1.5(C_6H_{14})], and the half molecule of hexane in [$PtPh_2$(TXPB'')]·(CH_2Cl_2)(C_6H_{14})$_{0.5}$ [**14**·(CH_2Cl_2)(C_6H_{14})$_{0.5}$] resulted in unstable refinement of the carbon atoms, therefore they were refined using the ISOR command. In addition, the carbon atoms of each respective solvent molecule were restrained to have similar thermal parameters through the use of the SIMU command. One molecule of CH_2Cl_2 [C(120), H(120), H(121), Cl(5), Cl(6)] in [PtMe(CNXyl)$_2$(TXPB-Me)]·2.6(CH_2Cl_2) (**17**·2.6CH_2Cl_2) was refined with partial occupancy (60%).

10.1.6 – Instrumentation and Details for Powder X-ray Diffraction Experiments

Powder X-ray diffraction (PXRD) experiments were performed by Jeffrey S. Price of the Emslie Lab on a Bruker D8 Advance powder diffractometer with Cu Kα radiation (λ = 0.154 nm) operated at 40 kV and 40 mA. Powders were packed in 0.5 mm o.d. special glass (SG; wall thickness 0.01 mm) capillary tubes for X-ray diffraction (purchased from Charles Supper Co.) and sealed by inverting to submerge the open end in a pool of Apiezon H-grease within a glovebox. The calculated powder pattern for [PtMePh(TXPB')] (**13**), [{Au(FcPPB)}$_2$] (**40**), [$FcPPB^{-Ph}$][BF_4] (**44**) and [{Pt(FcPPAl)}$_2$] (**46**) were generated from the low-temperature single-crystal data and then refined using Topas 4.2 (Bruker software).

10.1.7 – Other Instrumentation and Analysis

A Fisher Scientific Ultrasonic FS-30 bath and a Branson 2510 Ultrasonic bath was used to sonicate reaction mixtures where indicated. In some cases, either a Fischer Scientific Model 228 centrific centrifuge in combination with airtight Kimble-Kontes 15 mL conical centrifuge tubes, or a VWR Clinical 200 Large Capacity Centrifuge (with 28° fixed-angle rotors that hold 12 × 15 mL or 6 × 50 mL tubes) in combination with VWR

high-performance polypropylene conical centrifuge tubes was used when required to remove insoluble byproduct or to collect precipitated products; the former centrifuge was located on the benchtop, whereas the latter was located inside the glovebox. IR Spectra were recorded on a Thermo Scientific Nicolet 6700 FTIR spectrometer. Raman spectra were collected by Dr. Steve Kornic on a Renishaw Invia Laser Raman microscope equipped with 785 nm excitation. For [{Ni(FcPPP)}$_2$(μ-N$_2$)], [Pt(η^2-C$_2$H$_4$)(FcPPAl)] and [Pt(η^2-C$_2$Ph$_2$)(FcPPAl)], the 1200 lines per mm grating and 5× objective was employed, with the laser set to 50% power and the spectrum collected from 100 to 3200 cm^{-1}. Combustion elemental analyses were performed on a Thermo EA1112 CHNS/O analyzer by Dr. Steve Kornic and Megan Fair. High-resolution (HR) electron ionization (EI) mass spectrometry measurements were carried out by Dr. Kirk Green on the Waters Micromass GCT instrument (quadrupole time-of-flight). A 0.75 × 1.5 × 0.5 metre UV cabinet equipped with a 4 × 25 watt (18"), Sylvania Ecologic 350 blacklight bulb (model: F25T8/350BL/ECO), in conjunction with quartz J-Young NMR tubes and 125 mL single-necked round bottom flasks were utilized for the synthesis of [W(CO)$_4$(FcPPB*)].

10.1.8 – Kinetics

All rate constants for the conversion of [PtMePh(TXPB')] (**13**) to [PtPh$_2$(TXPB")] (**14**) were determined by monitoring the ^{1}H NMR resonances of the TXPB-(C*Me*$_3$)$_2$ groups of complex [PtMePh(TXPB')] (**13**) over the course of the reaction at a given temperature. In a typical experiment, [PtMePh(TXPB')] (**13**; 7.6 mg, 8.3×10^{-3} mmol) and a small amount of ferrocene was dissolved in C$_6$D$_6$ (0.6 mL) in a sealed J-Young NMR tube. The NMR tube was fully submerged into an oil bath of the appropriate temperature (75, 85, 95, 105, 115 or 125 °C) and removed at the indicated time intervals for analysis of the reaction progression; to avoid extended periods of time at which NMR samples were still hot and the reaction could still proceed, albeit at reduced temperatures, NMR samples were immediately submerged under cold water once removed from the oil bath. The extent of reaction at each time interval was determined by integration of the peak

intensity of the TXPB-(C*Me*$_3$)$_2$ resonances of [PtPh$_2$(TXPB')] (**13**) relative to ferrocene, which was present as an internal standard.

Due to the equilibrium between [PtMePh(TXPB')] (**13**) and [PtPh$_2$(TXPB")] (**14**), the rate constants for the conversion of [PtMePh(TXPB')] (**13**) to [PtPh$_2$(TXPB")] (**14**) were determined by plotting ([**14**]$_{eq}$/[**13**]$_o$)[ln([**14**]$_{eq}$/[**14**]$_{eq}$-[**14**]$_t$)] versus time for a given temperature,[236] where [**14**]$_{eq}$ is the equilibrium concentration of [PtPh$_2$(TXPB")] (**14**), [**13**]$_o$ is the initial concentration of [PtMePh(TXPB')] (**13**), and [**14**]$_t$ is the concentration of [PtPh$_2$(TXPB")] (**14**) at time t (although ([**14**]$_{eq}$/[**13**]$_o$)[ln([**14**]$_{eq}$/[**14**]$_{eq}$-[**14**]$_t$)] vs. time plots are shown with minutes as the units on the x-axis, rate constant values were obtained from plots with seconds as the x-axis units, or by dividing the slope of the lines on the former plots by 60). An Eyring plot was then constructed to determine the $\Delta H^{\ddagger}$ and $\Delta S^{\ddagger}$ values for the conversion of [PtMePh(TXPB')] (**13**) to [PtPh$_2$(TXPB")] (**14**; 94(4) kJ mol^{-1} and –45(12) J mol^{-1} K^{-1}, respectively). Similarly, for the reverse reaction, [([**13**]$_{eq}$/[**13**]$_0$)ln{[**14**]$_{eq}$/([**14**]$_{eq}$-[**14**]$_t$)} = $k_{-1}t$, which gave a $\Delta H^{\ddagger}$ value of 97(4) kJ mol^{-1} and a $\Delta S^{\ddagger}$ value of –52(11) J mol^{-1} K^{-1}. The errors (σk) associated with the rates (k) for conversion of [PtMePh(TXPB')] (**13**) to [PtPh$_2$(TXPB")] (**14**) were calculated in Excel using the 'linest' function: k = 1.49(9)×10^{-2} (125 °C), 8.93(9)×10^{-3} (115 °C), 3.25(12)×10^{-3} (105 °C), 1.83(5)×10^{-3} (95 °C), 7.04(16)×10^{-4} (85 °C) and 2.12(2)×10^{-4} s^{-1} (75 °C). The errors in the activation parameters were computed from the following error propagation formulae: $(\sigma\Delta S)^2 = (R^2/\Delta T^2)\cdot\{(\sigma T/T)^2[T_{max}^2\{1 + T_{min}(\Delta L/\Delta T)\}^2 + T_{min}^2\{1 + T_{max}(\Delta L/\Delta T)\}^2] + (\sigma k/k)^2(T_{max}^2 + T_{min}^2)\}$ and $(\sigma\Delta H)^2 = \{(R^2T_{max}^2T_{min}^2)/(\Delta T^2)\}\cdot\{(\sigma T/T)^2[\{1 + T_{min}(\Delta L/\Delta T)\}^2 + \{1 + T_{max}(\Delta L/\Delta T)\}^2] + 2(\sigma k/k)^2\}$ where $\Delta T = (T_{max} - T_{min})$ and $\Delta L = [\{\ln(k_{max}/T_{max})\}-\{\ln(k_{min}/T_{min})\}]$.[317] A Fischerbrand thermometer (–20 to 150 °C, 305 mm length, 76 mm immersion) with an intrinsic accuracy of 1 °C was utilized, so the error associated with temperature (σT) was equal to 1.5 degrees.

10.1.9 – DFT Calculations (Performed by Prof. D. J. H. Emslie)

All structures were fully optimized with the ADF DFT package (SCM, version

2013.01).[318] Calculations were conducted in the gas phase using the zero-order regular approximation (ZORA)[319] for relativistic effects, and 1996 Perdew-Burke-Ernzerhof exchange and correlation for the GGA part of the density functional (PBE),[320] combined with Grimme's DFT-D3-BJ dispersion correction.[321] All calculations for [PtH(μ-H)(FcPPB)] (**37**) were restricted gas-phase calculations. Structures $[PtH_2(FcPPAl)]_{calc}$' (**49$_{calc}$'**) and $[Pt(CO)(FcPPAl)]_{calc}$' (**50$_{calc}$'**) were geometry optimized with the core atoms (Pt and all attached atoms) fixed in position using the GEOVAR keyword.[§] All other structures ($[Pt(\eta^2\text{-}C_2H_4)(FcPPAl)]_{calc}$ (**47$_{calc}$**), $[Pt(\eta^2\text{-}C_2Ph_2)(FcPPAl)]_{calc}$ (**48$_{calc}$**), $[PtH_2(FcPPAl)]_{calc}$ (**49$_{calc}$**), $[Pt(CO)(FcPPAl)]_{calc}$ (**50$_{calc}$**), $[PtH_2(FcPPAl)]_{calc}$* (**49$_{calc}$***) and $[Pt(CO)(FcPPAl)]_{calc}$* (**50$_{calc}$***)) were geometry optimized without constraints.[¶] Preliminary geometry optimizations were conducted with frozen cores corresponding to the configuration of the preceding noble gas (core = medium) using a double-ζ basis set with one polarization function (DZP), an integration value of 5, and default convergence criteria. These structures were further refined using an all-electron TZ2P basis set (the size and quality of ADF basis sets increases in the order SZ < DZ < DZP < TZP < TZ2P < QZ4P) with an integration value of 7. Analytical frequency calculations for [PtH(μ-H)(FcPPB)] (**37**) showed no imaginary frequencies.

Mayer,[322] Gopinathan-Jug[323] and Nalewajski-Mrozek[291,324] bond orders were obtained using the BONDORDER keyword [bond orders discussed in Chapter 8 are Set 3 Nalewajski-Mrozek (abbreviated NM) bond orders]. NBO analysis[325] was carried out

[§] Unconstrained geometry optimization of **49$_{calc}$'** and **50$_{calc}$'** afforded calculated structures in poor agreement with experimental structures.

[¶] The geometries of **49$_{calc}$*** and **50$_{calc}$*** are in excellent agreement with **49$_{calc}$** and **50$_{calc}$**. This indicates that bidentate $Fe(C_5H_4PPh_2)(C_5H_4P^tBuAr)$ is electronically comparable with one PMe_3 and one PMe_2Ar ligand, as would be predicted on the basis of Tolman's electronic parameters, taking into account that a ferrocenyl group is electronically more similar to an alkyl than an aryl substituent; see: (a) Salas, G.; Casares, J. A.; Espinet, P. *Dalton Trans.* **2009**, 8413. (b) Tolman, C. A. *Chem. Rev.* **1977**, *77*, 313. Attempts to further simplify the structures of **49$_{calc}$*** and **50$_{calc}$*** by replacement of the methyl groups on phosphorus and aluminum with hydrogen atoms afforded calculated structures in poor agreement with experimental structures.

using nbo 6.0 within ADF 2013.1. Visualization of the computational results was performed using the ADF-GUI (SCM) or Discovery Studio Visualizer (Accelrys).

Bonding in $[PtH_2(FcPPAl)]_{calc}$' (**49$_{calc}$'**) and $[Pt(CO)(FcPPAl)]_{calc}$' (**50$_{calc}$'**) was analyzed in more detail using a fragment approach (with the Energy Decomposition Analysis)[326] that considered the interaction of an uncharged *cis*-$PtH_2(PMe_3)_2$ or $Pt(CO)(PMe_3)_2$ fragment with a neutral $AlMe_2Ph$ Lewis acid (fragments were generated from the TZ2P geometry optimized structures of each structure, and geometries were frozen). Preparation energies were obtained by allowing the fragments to adopt equilibrium geometries; these relaxed (i.e. geometry optimized) fragments were used only to obtain the difference in energy between the prepared and relaxed fragments.

10.2 – Synthetic Procedures and Characterization Pertaining to Chapter 2

[Rh(μ-Br)(CO)(TXPB)]·hexane (2·hexane): Me_3SiBr (25.0 μL, 0.190 mmol) was added dropwise at room temperature to [Rh(μ-Cl)(CO)(TXPB)] (**1**) (160 mg, 0.188 mmol) in CH_2Cl_2 (10 mL). The reaction mixture was stirred vigorously for 2 hours at room temperature before evaporation to dryness *in vacuo*. The resulting tangerine-coloured powder was left under dynamic vacuum for 3 hours to ensure removal of all solvent and Me_3SiCl. Further purification entailed washing with hexanes (× 2) with cooling to –30 °C for 1 hour before decanting the mother liquors during each washing, and subsequent drying *in vacuo.* Yield = 125 mg (74 %). X-ray quality crystals of [Rh(μ-Br)(CO)(TXPB)·hexane were grown by cooling a saturated solution of [Rh(μ-Br)(CO)(TXPB)] in hexanes to –30 °C for several days. **^{1}H NMR (CD_2Cl_2, 600 MHz, 298 K):** δ 7.78 (d, $^4J_{H,H}$ 2 Hz, 1H, C*H*^{1}), 7.63 (d, $^4J_{H,H}$ 2 Hz, 1H, C*H*^{8}), 7.47 (tt, $^3J_{H,H}$ 7 Hz, $^4J_{H,H}$ 2 Hz, 2H, *p*-P*Ph*$_2$), 7.41–7.33 (m, 8H, *o*, *m*-P*Ph*$_2$), 7.32 (dd, $^3J_{H,H}$ 8 Hz, $^4J_{H,H}$ 1 Hz, 4H, *o*-B*Ph*$_2$), 7.28 (dd, $^3J_{H,P}$ 9 Hz, $^4J_{H,H}$ 2 Hz, 1H, C*H*^{3}), 7.07 (app t, $^3J_{H,H}$ 7 Hz, 4H, *m*-B*Ph*$_2$), 7.02 (d, $^4J_{H,H}$ 2 Hz, 1H, C*H*^{6}), 7.00 (t, $^3J_{H,H}$ 7 Hz, 2H, *p*-B*Ph*$_2$), 1.86 (s, 6H, C*Me*$_2$), 1.25, 1.15 (2×s, 18H, C*Me*$_3$). **^{13}C{^{1}H} NMR (CD_2Cl_2, 151 MHz, 298 K):** δ 187.6 (dd, $^1J_{C,Rh}$ 77 Hz, $^2J_{C,P}$ 15 Hz, Rh*C*O), 153.1 (d, $^3J_{C,P}$ 6 Hz, *C*^{2}CMe$_3$), 150.0 (s,

C^{7}CMe$_3$), 148.5 (broad s, *ipso*-B*Ph*$_2$), 148.0 (broad s, *C*^{5}), 146.0 (d, $^{3}J_{C,P}$ 14 Hz, *C*^{10}), 142.2 (s, *C*^{13}), 137.3 (d, $^{2}J_{C,P}$ 27 Hz, *C*^{11}), 136.5 (s, *o*-B*Ph*$_2$), 133.8 (d, $^{1}J_{C,P}$ 50 Hz, *C*^{4}), 133.7 (d, $^{2}J_{C,P}$ 12 Hz, *o*-P*Ph*$_2$), 133.5 (s, *C*^{6}), 133.0 (d, $^{1}J_{C,P}$ 55 Hz, *ipso*-P*Ph*$_2$), 131.6 (s, *p*-P*Ph*$_2$), 130.2 (s, *C*^{12}), 129.1 (d, $^{3}J_{C,P}$ 11 Hz, *m*-P*Ph*$_2$), 128.4 (s, *C*^{3}), 127.4 (s, *p*-B*Ph*$_2$), 127.0 (*m*-B*Ph*$_2$), 125.8 (s, *C*^{1}), 122.2 (s, *C*^{8}), 42.9 (s, *C*Me$_2$), 35.6, 35.2 (s, 2×*C*Me$_3$), 31.5 (s, 2×C*Me*$_3$), 26.7 (s, C*Me*$_2$). **^{31}P {^{1}H} (CD$_2$Cl$_2$, 243 MHz, 298 K):** δ 64.5 (d, $^{1}J_{P,Rh}$ 164 Hz). **^{11}B (CD$_2$Cl$_2$, 161 MHz, 298 K):** δ 27 (v.broad s, $\omega_{1/2}$ ~ 900 Hz). **IR:** ν(CO) = 2013 cm^{-1} (nujol), 2008 cm^{-1} (CH_2Cl_2). **Elemental Analysis Calcd (%)** for $C_{54}H_{62}OBrPSBRh$: C, 65.93; H, 6.35. Found: C, 66.17; H, 5.91%.

[RhI(CO)(TXPB)]·0.5hexane (3·0.5hexane): A solution of Me_3SiI (48.1 mg, 0.240 mmol) in CH_2Cl_2 (2 mL) was added dropwise at room temperature to [Rh(μ-Cl)(CO)(TXPB)] (**1**) (205 mg, 0.240 mmol) in CH_2Cl_2 (10 mL). The reaction mixture was stirred vigorously for 1 hour before evaporation to dryness *in vacuo*. The resulting rust-red powder was left under dynamic vacuum for 3 hours to ensure all solvent and Me_3SiCl had been removed. Further purification entailed washing with hexanes (× 2) with cooling to –30 °C for 1 hour before decanting the mother liquors during each washing, and subsequent drying *in vacuo*. Yield = 187 mg (83 %). X-ray quality crystals of [RhI(CO)(TXPB)]·hexane were grown by cooling a saturated solution of [RhI(CO)(TXPB)] in hexanes to –30 °C for several days. **^{1}H NMR (C$_6$D$_6$, 600 MHz, 298 K):** δ 7.83 (d, $^{3}J_{H,H}$ 7 Hz, 4H, *o*-B*Ph*$_2$), 7.80 (s, 1H, C*H*^{8}), 7.69 (s, 1H, C*H*^{1}), 7.56 (d, $^{3}J_{H,P}$ 8 Hz, 1H, C*H*^{3}), 7.48–7.41 (m, 5H, C*H*^{6}, *o*-P*Ph*$_2$), 6.95 (t, $^{3}J_{H,H}$ 7 Hz, 2H, *p*-P*Ph*$_2$), 6.92-6.83 (m, 8H, *m*-P*Ph*$_2$, *m*-B*Ph*$_2$), 6.76 (t, $^{3}J_{H,H}$ 6 Hz, 2H, *p*-B*Ph*$_2$), 1.73 (s, 6H, C*Me*$_2$), 1.18, 1.10 (2×s, 18H, 2×C*Me*$_3$). **^{13}C{^{1}H} NMR (C$_6$D$_6$, 151 MHz, 298 K):** δ 189.7 (dd, $^{1}J_{C,Rh}$ 74 Hz, $^{3}J_{C,P}$ 14 Hz, Rh*C*O), 152.5 (d, $^{3}J_{C,P}$ 5 Hz, *C*^{2}CMe$_3$), 149.7 (s, *C*^{7}CMe$_3$), 147.6 (broad s, *C*^{5}), 146.9 (d, $^{3}J_{C,P}$ 14 Hz, *C*^{10}), 143.8 (broad s, *ipso*-B*Ph*$_2$), 143.7 (s, *C*^{13}), 140.4 (d, $^{2}J_{C,P}$ 32 Hz, *C*^{11}), 139.1 (s, *o*-B*Ph*$_2$), 134.2 (s, *C*^{6}), 134.1 (d, $^{1}J_{C,P}$ 51 Hz, *ipso*-P*Ph*$_2$), 133.4 (d, $^{2}J_{C,P}$ 12 Hz, *o*-P*Ph*$_2$), 133.1 (s, *C*^{4}), 132.4 (s, *C*^{12}), 130.5 (s, *p*-P*Ph*$_2$), 129.0 (s, *p*-B*Ph*$_2$), 128.5 (d, $^{3}J_{C,P}$ 11 Hz, *m*-P*Ph*$_2$), 128.3 (s, *C*^{3}), 126.8 (s, *m*-B*Ph*$_2$), 125.1

(s, C^1), 123.1 (s, C^8), 43.3 (s, CMe$_2$), 35.1, 35.0 (s, 2×CMe$_3$), 31.4, 31.3 (s, 2×CMe_3), 26.1 (s, CMe_2). **^{31}P {^{1}H} (CD_2Cl_2, 243 MHz, 298 K):** δ 67.2 (d, $^1J_{P,Rh}$ 167 Hz). **^{11}B (CD_2Cl_2, 161 MHz, 298 K):** δ 56 (v.broad s, $\omega_{1/2}$ ~ 1800 Hz). **IR:** ν(CO) = 2004 cm^{-1} (Nujol), 2002 cm^{-1} (CH_2Cl_2). **Elemental Analysis Calcd (%)** for $C_{51}H_{55}OBrPSBRh$: C, 62.02; H, 5.61. Found: C, 61.95; H, 5.79%.

[Rh(CO)(TXPB-F)] (4): A mixture of [Rh(μ-Cl)(CO)(TXPB)] (**1**) (50 mg, 5.9×10^{-2} mmol) and [NMe$_4$]F (5.5 mg, 5.9×10^{-2} mmol) in CH_2Cl_2 (5 mL) was stirred vigorously for 1 hour at room temperature. The resulting orange, opaque mixture was filtered through a column of celite, and the red/orange mother liquors were evaporated to dryness *in vacuo* to yield a rust-red powder. Yield = 35 mg (72 %). X-ray quality crystals of [Rh(CO)(TXPB-F)]·1.5CH_2Cl_2 were grown by slow diffusion of hexanes into a solution of [Rh(CO)(TXPB-F)] in CH_2Cl_2 at –30 °C. **^{1}H NMR (CD_2Cl_2, 500 MHz, 223 K):** δ 7.68 (s, 2H, CH^1), 7.66 (m, 2H, *o*-PPh_2 A), 7.59 (broad s, 3H, *p*-PPh_2 A, *o*-BPh_2 A), 7.55 (t, 2H, *o*-PPh_2 A), 7.48–7.41 (m, 3H, *p*-PPh_2 B, *m*-BPh_2 A), 7.39 (s, 1H, CH^8), 7.34 (broad s, 2H, *m*-PPh_2 B), 7.25 (m, 2H, *o*-PPh_2 B), 7.21 (t, $^3J_{H,H}$ 7 Hz, 1H, *p*-BPh_2 A), 7.13 (app t, $^3J_{H,H}$ 7 Hz, 2H, *m*-BPh_2 B), 7.03 (s, 1H, CH^6), 7.01 (t, 1H, *p*-BPh_2 B), 6.96 (broad s, 2H, *o*-BPh_2 B), 6.91 (d, $^3J_{H,P}$ 11 Hz, 1H, CH^3), 2.03, 1.26 (2×s, 6H, CMe_2), 1.16, 1.13 (2×s, 18H, 2×CMe_3). **^{13}C{^{1}H} NMR (CD_2Cl_2, 126 MHz, 223 K):** δ 186.8 (dd, $^1J_{C,Rh}$ 75 Hz, $^3J_{C,P}$ 19 Hz, RhCO), 151.9 (d, $^3J_{C,P}$ 7 Hz, C^2CMe$_3$), 149.5 (s, C^7CMe$_3$), 141.1 (d, $^3J_{C,P}$ 14 Hz, C^{10}), 138.1 (s, C^{13}), 135.7 (d, $^2J_{C,P}$ 23 Hz, C^{11}), 134.3 (d, $^1J_{C,P}$ 53 Hz, C^4), 133.6 (d, $^3J_{C,P}$ 12 Hz, *m*-PPh_2 A), 133.1 (broad s, *ipso*-BPh_2 A), 132.6 (d, $^2J_{C,P}$ 12 Hz, *o*-PPh_2 B), 131.9 (s, *p*-PPh_2 A), 131.7 (s, *o*-BPh_2 A, *o*-BPh_2 B, *p*-PPh_2 B), 131.5 (app s, *ipso*-PPh_2 A, *ipso*-BPh_2 B), 131.2 (d, $^1J_{C,P}$ 37 Hz, *ipso*-PPh_2 B), 129.9 (broad s, C^6), 129.4 (d, $^2J_{C,P}$ 12 Hz, *m*-PPh_2 A), 129.2 (s, *m*-BPh_2 A), 128.8 (d, $^3J_{C,P}$ 12 Hz, *m*-PPh_2 B), 128.6 (s, *p*-BPh_2 A), 128.1 (broad s, C^5), 127.6 (s, C^3), 127.2 (s, *m*-BPh_2 B), 126.2 (s, C^{12}), 125.4 (s, C^1), 125.1 (s, *p*-BPh_2 B), 119.7 (s, C^8), 40.7 (s, CMe$_2$), 35.1, 34.8 (s, 2×CMe$_3$), 31.2, 30.8 (s, 2×CMe_3), 27.8, 24.9 (s, 2×CMe_2). **^{31}P {^{1}H} (CD_2Cl_2, 203 MHz, 298 K):** δ 51.5 (dd, $^1J_{P,Rh}$ 167 Hz, $J_{P,F}$ 6.2 Hz). **^{19}F (CD_2Cl_2, 471 MHz, 298 K):** δ –186 (broad s, $\omega_{1/2}$ ~ 180

Hz). **^{11}B (CD_2Cl_2, 161 MHz, 298 K):** δ 4 (broad s, $\omega_{1/2}$ ~ 350 Hz). **IR:** ν(CO) = 2008 cm^{-1} (Nujol), 2011 cm^{-1} (CH_2Cl_2). **Elemental Analysis Calcd (%)** for $C_{48}H_{48}OFPSBRh$: C, 68.91; H, 5.78. Found: C, 69.27; H, 5.60%.

[Rh(CO)(TXPB)][PF_6]·0.5CH_2Cl_2 (5·0.5CH_2Cl_2): A mixture of [Rh(μ-Cl)(CO)(TXPB)] (**1**) (350 mg, 0.410 mmol) and Tl[PF_6] (350 mg, 1.00 mmol) in CH_2Cl_2 (10 ml) was stirred vigorously for 4.5 hours at room temperature. After allowing any solid to settle over 24 hours at –30 °C, the mother liquors were carefully decanted, layered with hexanes, and cooled to –30 °C for several days. The resulting orange needles were washed with hexanes (×1) and dried *in vacuo*. Yield = 363 mg (92 %). X-ray quality crystals of [Rh(CO)(TXPB)][PF_6]·CH_2Cl_2 were grown by slow diffusion of hexanes into a solution of [Rh(CO)(TXPB)][PF_6] in CH_2Cl_2 at –30°C. **^{1}H NMR (CD_2Cl_2, 500 MHz, 203 K):** δ 8.27 (d, $^3J_{H,H}$ 7 Hz, 2H, *o*-B*Ph*$_2$ A), 8.08 (t, $^3J_{H,H}$ 7 Hz, 1H, *p*-B*Ph*$_2$ A), 7.81 (app t, $^3J_{H,H}$ 7 Hz, 2H, *m*-B*Ph*$_2$ A), 7.75 (s, 1H, C*H*^{1}), 7.71 (s, 1H, C*H*^{8}), 7.66 (t, $^3J_{H,H}$ 8 Hz, 1H, *p*-B*Ph*$_2$ B), 7.60 (d, $^3J_{H,H}$ 7 Hz, 2H, *o*-B*Ph*$_2$ B), 7.56 (t, $^3J_{H,H}$ 8 Hz, 2H, *p*-P*Ph*$_2$), 7.54 (app t, $^3J_{H,H}$ 8 Hz, 2H, *m*-B*Ph*$_2$ B), 7.54–7.45 (m, 4H, *o*/*m*-P*Ph*$_2$), 7.38-7.30 (m, 4H, *o*/*m*-P*Ph*$_2$), 7.21 (s, 1H, C*H*^{6}), 7.13 (d, $^3J_{H,P}$ 10 Hz, 1H, C*H*^{3}), 2.13, 1.80 (2×s, 6H, C*Me*$_2$), 1.21, 1.14 (2×s, 18H, 2×C*Me*$_3$). **^{13}C{^{1}H} NMR (CD_2Cl_2, 151 MHz, 203 K):** δ 183.3 (dd, $^1J_{C,Rh}$ 72 Hz, $^3J_{C,P}$ 13 Hz, Rh*C*O), 155.3 (s, *C*^{2}CMe$_3$), 152.0 (s, *C*^{7}CMe$_3$), 145.7 (d, $^3J_{C,P}$ 13 Hz, *C*^{10}), 144.5 (s, *C*^{12}), 142.3 (s, *C*^{13}), 139.8 (s, *p*-B*Ph*$_2$ A), 139.3 (broad s, *ipso*-B*Ph*$_2$ B), 137.4 (s, *o*-B*Ph*$_2$ B), 136.2 (s, *o*-B*Ph*$_2$ A), 135.9 (d, $^2J_{C,P}$ 24 Hz, *C*^{11}), 133.3 (d, *J* 12 Hz, *o*/*m*-P*Ph*$_2$), 133.0 (s, *C*^{6}), 132.8 (s, *p*-B*Ph*$_2$ B), 132.4 (s, *p*-P*Ph*$_2$), 132.3 (d, *J* 12 Hz, *o*/*m*-P*Ph*$_2$), 132.2 (s, *C*^{5}), 130.0 (d, $^1J_{C,P}$ ~ 60 Hz, *C*^{4} or *ipso*-P*Ph*$_2$), 129.7 (d, *J* 12 Hz, *o*/*m*-P*Ph*$_2$), 129.4 (s, *m*-B*Ph*$_2$ A), 129.0 (d, *J* 12 Hz, *o*/*m*-P*Ph*$_2$), 128.9 (d, $^1J_{C,P}$ 59 Hz, C^4 or *ipso*-P*Ph*$_2$), 128.3 (s, *m*-B*Ph*$_2$ B), 127.4 (s, *C*^{1}), 127.1 (s, *C*^{3}), 125.60 (s, *C*^{8}), 110.8 (broad s, *ipso*-B*Ph*$_2$ A), 43.3 (s, *C*Me$_2$), 35.2, 35.0 (s, 2×*C*Me$_3$), 30.8, 30.6 (s, 2×C*Me*$_3$), 26.4, 25.0 (s, 2×C*Me*$_2$). **^{31}P{^{1}H} (CD_2Cl_2, 243 MHz, 298 K):** δ 64.9 (d, $^1J_{P,Rh}$ 166.8 Hz). **^{11}B (CD_2Cl_2, 161 MHz, 298 K):** δ57 (broad s, $\omega_{1/2}$ ≈ 1800 Hz). **IR:** ν(CO) = 2028 cm^{-1}

(Nujol), 2038 cm^{-1} (CH_2Cl_2). **Elemental Analysis Calcd (%)** for $C_{48}H_{48}P_2SBF_6Rh$: C, 57.96; H, 4.91. Found: C, 57.73; H, 5.09 %.

[Rh(μ-H)(CO)(TXPB)] (6): THF (10 mL) was condensed into a 100 mL round bottom flask containing [Rh(μ-Cl)(CO)(TXPB)] (**1**) (165 mg, 0.193 mmol) and $NaBH_4$ (7.30 mg, 0.193 mmol) through the use of a dry ice/acetone bath. The reaction was left to stir overnight at room temperature, over which time the initially yellow solution progressively became dark brown/orange. The reaction mixture was then evaporated to dryness *in vacuo* to yield a red/brown oily residue. Toluene (20 mL) was added to the crude residue and the resulting mixture was sonicated for 15 minutes and filtered to remove any NaCl (which was washed with 10 mL of toluene). The dark brown/orange filtrate was evaporated to dryness *in vacuo*, again yielding a red/orange oily residue, to which hexanes (20 mL) were added; the crude hexanes solution was sonicated for 15 minutes, allowing for [Rh(μ-H)(CO)(TXPB)] to precipitate from solution as a light brown powder. The hexanes solution was filtered and the collected product was washed with hexanes (2 × 10 mL) then dried *in vacuo*. Yield = 102 mg (65 %). X-ray quality crystals of [Rh(μ-H)(CO)(TXPB)]·2(C_6H_{14}) were obtained by slow diffusion of hexanes (~10 mL) into a solution of [Rh(μ-H)(CO)(TXPB)] (~30 mg) in CH_2Cl_2 (~3 mL) at –30 °C. **^{1}H NMR (CD_2Cl_2, 600 MHz, 298 K):** δ 7.70 (s, 1H, C*H*^{1}), 7.63–7.59 (m, 4H, *o*-P*Ph*$_2$ A, *o*-B*Ph*$_2$ A), 7.53–7.48 (m, 3H, *m*,*p*-P*Ph*$_2$ A), 7.43 (s, 1H, C*H*^{8}), 7.40 (t, $^3J_{H,H}$ 7 Hz, 1H, *p*-P*Ph*$_2$ B), 7.30–7.28 (m, 4H, *m*-P*Ph*$_2$ B, *m*-B*Ph*$_2$ A), 7.18 (t, $^3J_{H,H}$ 7 Hz, 1H, *p*-B*Ph*$_2$ A), 7.15–7.14 (m, 2H, C*H*^{3}, C*H*^{6}), 7.01–6.93 (m, 5H, *o*-P*Ph*$_2$ B, *m*+*p*-B*Ph*$_2$ B), 6.69 (t, $^3J_{H,H}$ 7 Hz, 2H, *o*-B*Ph*$_2$ B), 2.12, 1.59 (2×s, 6H, C*Me*$_2$), 1.24, 1.20 (2×s, 18H, 2×C*Me*$_3$), –4.05 (dd, $^1J_{H,Rh}$ 57 Hz, $^2J_{H,P}$ 25 Hz, 1H, Rh–*H*–B). **^{13}C{^{1}H} NMR (CD_2Cl_2, 151 MHz, 298 K):** δ 188.7 (dd, $^1J_{C,Rh}$ 77 Hz, $^2J_{C,P}$ 16 Hz, Rh–*C*O), 155.7 (broad s, *C*^{5}), 153.9 (broad s, *ipso*-B*Ph*$_2$ A), 153.5 (d, $^3J_{C,P}$ 6 Hz, *C*^{2}), 151.2 (s, *C*^{7}), 145.7 (d, $^3J_{C,P}$ 13 Hz, *C*^{10}), 143.9 (broad s, *ipso*-B*Ph*$_2$ B), 141.0 (s, *C*^{13}), 138.6 (d, $^2J_{C,P}$ 26 Hz, *C*^{11}), 137.1 (s, *o*-B*Ph*$_2$ B), 136.6 (d, $^1J_{C,P}$ 49 Hz, *C*^{4}), 135.7 (s, *o*-B*Ph*$_2$ A), 133.7 (d, $^2J_{C,P}$ 13 Hz, *o*-P*Ph*$_2$ B), 133.2 (d, $^1J_{C,P}$ 50 Hz, *ipso*-P*Ph*$_2$ A), 133.2 (d, $^2J_{C,P}$ 13 Hz, *o*-P*Ph*$_2$ A), 132.0 (d, $^1J_{C,P}$ 51 Hz, *ipso*-P*Ph*$_2$ B), 131.9 (d,

$^{4}J_{C,P}$ 4 Hz, *C*^{12}), 131.4 (s, *p*-P*Ph*$_2$ B), 131.3 (s, *p*-P*Ph*$_2$ A), 130.5 (s, *C*^{6}), 129.5 (d, $^{3}J_{C,P}$ 11 Hz, *m*-P*Ph*$_2$ A), 128.7 (d, $^{3}J_{C,P}$ 11 Hz, *m*-P*Ph*$_2$ B), 128.2 (s, *C*^{3}), 127.4 (s, *m*-B*Ph*$_2$ A), 126.6 (s, *m*-B*Ph*$_2$ B), 125.7 (s, *p*-B*Ph*$_2$ B), 125.5 (s, *p*-B*Ph*$_2$ A), 125.4 (s, *C*^{1}), 119.8 (s, *C*^{8}), 43.2 (s, *C*Me$_2$), 35.6, 35.2 (2×s, 2×*C*Me$_3$), 31.7, 31.4 (2×s, 2×C*Me*$_3$), 26.6, 25.4 (2×s, C*Me*$_2$). **^{31}P{^{1}H} NMR (CD_2Cl_2, 203 MHz, 298 K):** δ 57.9 (d, $^{2}J_{P,Rh}$ 144 Hz). **^{11}B NMR (CD_2Cl_2, 161 MHz, 298 K):** δ 3 (broad s, $\omega_{1/2}$ ~ 1000 Hz). **IR:** ν(CO) = 1984 cm^{-1} (nujol), 2006 cm^{-1} (CH_2Cl_2).

10.3 – Synthetic Procedures and Characterization Pertaining to Chapter 3

[(TXPB)Rh(μ-CO)(μ-CNC$_6$H$_4$Cl-*p*)Fe(CO)Cp] (8): CNC$_6$H$_4$Cl-*p* (18.0 mg, 0.130 mmol) dissolved in CH_2Cl_2 (3 mL) was added dropwise at room temperature to [(TXPB)Rh(μ-CO)$_2$Fe(CO)Cp]· 0.6(hexanes) [**7**·0.6(hexanes] (146 mg, 0.140 mmol) in CH_2Cl_2 (8 mL). The reaction mixture was stirred vigorously for 30 minutes at room temperature before evaporating to dryness *in vacuo*. The resulting black-purple powder was dissolved in hexanes and cooled to −30 °C overnight, after which time the hexane mother liquors were decanted and the dark purple crystals were dried *in vacuo*. Yield: 145 mg (94 %). X-ray quality crystals of [(TXPB)Rh(μ-CO)(μ-CNC$_6$H$_4$Cl-*p*)Fe(CO)Cp]·2hexane were grown by cooling a saturated solution of [(TXPB)Rh(μ-CO)(μ-CNC$_6$H$_4$Cl-*p*)Fe(CO)Cp] in hexanes to −30 °C for several days. **^{1}H NMR (CD_2Cl_2, 500 MHz, 194 K):** δ 7.69 (s, 1H, C*H*^{1}), 7.59 (s, 1H, C*H*^{8}), 7.43−7.30 (m, 8H, *m*-*Ph*Cl, *m*,*p*-PPh$_2$ A, *m*,*p*-P*Ph*$_2$ B), 7.30−7.20 (m, 5H, C*H*^{3}, *o*-*Ph*Cl, *o*-P*Ph*$_2$ B), 7.14 (s, 1H, C*H*^{6}), 6.99 (t, $^{3}J_{H,P}$ 9 Hz, 2H, *o*-P*Ph*$_2$ A), 6.82−6.73 (m, 5H, *o*,*m*,*p*-B*Ph*$_2$ A), 6.49 (t, $^{3}J_{H,H}$ 7 Hz, 1H, *m*-B*Ph*$_2$ B), 6.16 (d, $^{3}J_{H,H}$ 7 Hz, 1H, *o*-B*Ph*$_2$ B), 5.88 (t, $^{3}J_{H,H}$ 7 Hz, 1H, *m*-B*Ph*$_2$ B), 5.83 (d, $^{3}J_{H,H}$ 7 Hz, 1H, *o*-B*Ph*$_2$ B), 5.37 (t, $^{3}J_{H,H}$ 7 Hz, 1H, *p*-B*Ph*$_2$ B), 4.60 (s, 5H, C$_5$*H*$_5$), 2.16, 1.72 (2×broad s, 6H, C*Me*$_2$), 1.16, 1.09 (2×s, 28H, C*Me*$_3$). **^{13}C{^{1}H} NMR (CD_2Cl_2, 126 MHz, 298 K, selected data only):** δ 312.4 (dd, $^{1}J_{C,Rh}$ 53 Hz, $^{2}J_{C,P}$ 24 Hz, μ-*C*N(C$_6$H$_4$Cl-*p*)), 239.6 (dd, $^{1}J_{C,Rh}$ 56 Hz, $^{2}J_{C,P}$ 8 Hz, μ-*C*O), 216.3 (s, Fe-*C*O). **^{13}C{^{1}H} NMR (CD_2Cl_2, 126 MHz, 194 K):** δ 312.4 (dd, $^{1}J_{C,Rh}$ 53 Hz, $^{2}J_{C,P}$ 24 Hz, μ-

*C*N(C_6H_4Cl-*p*)), 241.9 (dd, $^1J_{C,Rh}$ 60 Hz, $^2J_{C,P}$ 10 Hz, μ-*C*O), 215.1 (s, Fe-*C*O), 150.6 (s, C^2), 149.2 (s, *p*-*Ph*Cl), 148.9 (broad s, C^5), 147.9 (s, C^7), 146.4 (d, $^3J_{C,P}$ 11 Hz, C^{10}), 142.9 (s, C^{13}), 137.7 (d, $^2J_{C,P}$ 34 Hz, C^{11}), 136.8 (d, $^1J_{C,P}$ 39 Hz, *ipso*-P*Ph*$_2$ B), 135.5 (broad s, *ipso*-B*Ph*$_2$ A), 133.6 (s, C^6), 133.0 (broad s, *ipso*-B*Ph*$_2$ B), 132.9 (d, $^2J_{C,P}$ 11 Hz, *o*-P*Ph*$_2$ A), 132.6 (d, $^1J_{C,P}$ 38 Hz, C^4), 132.6 (d, $^2J_{C,P}$ 14 Hz, *o*-P*Ph*$_2$ B), 132.4 (s, C^{12}), 130.8 (s, *ipso*-*Ph*Cl), 129.9 (s, *p*-P*Ph*$_2$ A), 129.6 (s, *o*-B*Ph*$_2$ B), 129.1 (s, *p*-P*Ph*$_2$ B), 128.8 (appt. s, C^3), 128.8 (s, *m*-*Ph*Cl), 128.1 (d, $^3J_{C,P}$ 10 Hz, *m*-P*Ph*$_2$ B), 127.6 (s, *p*-B*Ph*$_2$ A), 127.5 (d, $^3J_{C,P}$ 9 Hz, *m*-P*Ph*$_2$ A), 127 (d, *ipso*-P*Ph*$_2$ A), 126.5 (s, *m*-B*Ph*$_2$ B), 126.0 (broad s, *o*-*Ph*Cl), 125.8 (s, *m*-B*Ph*$_2$ B), 125.2 (broad s, *m*-B*Ph*$_2$ A), 124.5 (s, *p*-B*Ph*$_2$ B), 124.4 (s, C^1), 124.0 (s, *o*-B*Ph*$_2$ A), 121.0 (s, C^8), 115.7 (s, *o*-B*Ph*$_2$ B), 83.7 (s, C_5H_5), 42.7 (s, *C*Me$_2$), 34.7, 34.6 (2×s, 2×*C*Me$_3$), 30.8, 30.6 (2×s, 2×C*Me*$_3$), 25.4, 24.3 (2×s, 2×C*Me*$_2$). **^{31}P{^{1}H} NMR (CD_2Cl_2, 203 MHz, 298 K):** δ 45.3 (d, $^1J_{P,Rh}$ 149 Hz). **^{11}B NMR (CD_2Cl_2, 161 MHz, 298 K):** δ 4 (broad s, $\omega_{1/2}$ 880 Hz). **IR:** ν(CO) = 1961, 1815 cm^{-1} (nujol); 1962, 1805 cm^{-1} (CH_2Cl_2); ν(CN) = 1536 cm^{-1} (nujol); 1537 cm^{-1} (CH_2Cl_2). **Elemental Analysis Calcd (%)** for $C_{61}H_{57}O_2NClBPSRhFe$: C, 66.35; H, 5.20; N, 1.27. Found: C, 66.90; H, 5.55; N, 1.03.

[(TXPB)Rh(μ-CO)(μ-CNXyl)Fe(CO)Cp] (9): CNXyl (12.2 mg, 9.30×10^{-2} mmol) dissolved in CH_2Cl_2 (3 mL) was added dropwise at room temperature to [(TXPB)Rh(μ-CO)$_2$Fe(CO)Cp]·0.6(hexanes) [**7**·0.6(hexanes] (115 mg, 0.110 mmol) in CH_2Cl_2 (10 mL). The reaction mixture was stirred vigorously for 30 min at room temperature before evaporating to dryness *in vacuo*. Yield: 92 mg (76 %). For further purification, the resulting black-red powder was dissolved in hexanes and cooled to −30 °C overnight, after which time the hexane mother liquors were decanted and the resulting black needles were dried *in vacuo*. Yield: 59 mg (49 %). X-ray-quality crystals of [(TXPB)Rh(μ-CO)(μ-CNXyl)Fe(CO)Cp]·5toluene were grown by cooling a saturated solution of [(TXPB)Rh(μ-CO)(μ-CNXyl)Fe(CO)Cp] in toluene to −30 °C for several days. **^{1}H NMR (CD_2Cl_2, 500 MHz, 194 K):** δ 7.68 (s, 1H, C*H*^{1}), 7.51 (s, 1H, C*H*^{8}), 7.42 (d, $^3J_{H,H}$ 7 Hz, 1H, *p*-P*Ph*$_2$ A), 7.38 (t, $^3J_{H,H}$ 7 Hz, 3H, *m*,*p*-P*Ph*$_2$ B), 7.32 (t, $^3J_{H,H}$ 7 Hz, 2H, *m*-P*Ph*$_2$ A),

7.28−7.25 (m, 2H, *o*-P*Ph*$_2$ A), 7.19 (d, $^3J_{H,P}$ 7 Hz, 1H, C*H*^{3}), 7.08 (d, $^3J_{H,H}$ 5 Hz, 2H, *m*-Xyl), 7.06 (s, 1H, *o*-B*Ph*$_2$ B), 7.03 (s, 1H, C*H*^{6}), 6.85 (t, $^3J_{H,H}$ 7 Hz, 1H, *o*-B*Ph*$_2$ A), 6.78 (broad s, 1H, *p*-Xyl), 6.71 (t, $^3J_{H,H}$ 7 Hz, 1H, *m*-B*Ph*$_2$ A), 6.69 (t, $^3J_{H,H}$ 7 Hz, 1H, *m*-B*Ph*$_2$ A), 6.52−6.49 (m, 2H, *o*-B*Ph*$_2$ A, *m*-B*Ph*$_2$ B), 6.38 (d, $^3J_{H,H}$ 6 Hz, 1H, *o*-B*Ph*$_2$ B), 5.93 (t, $^3J_{H,H}$ 7 Hz, 1H, *m*-B*Ph*$_2$ B), 5.87 (d, $^3J_{H,H}$ 7 Hz, 1H, *o*-B*Ph*$_2$ B), 5.52 (d, $^3J_{H,H}$ 7 Hz, 1H, *p*-B*Ph*$_2$ A), 5.37 (t, $^3J_{H,H}$ 7 Hz, 1H, *p*-B*Ph*$_2$ B), 4.57 (s, 5H, C_5H_5), 2.34 (s, 3H, Xyl-C*H*$_3$), 2.14, 1.67 (2×s, 2×3H, C*Me*$_2$), 1.23 (s, 3H, Xyl-C*H*$_3$), 1.15, 1.04 (2×s, 18H, C*Me*$_3$). **^{13}C{^{1}H} NMR (CD_2Cl_2, 126 MHz, 194 K):** δ 312.0 (dd, $^1J_{C,Rh}$ 52 Hz, $^2J_{C,P}$ 23 Hz, μ-*C*NXyl), 243.1 (dd, $^1J_{C,Rh}$ 60 Hz, $^2J_{C,P}$ 10 Hz, μ-*C*O), 215.5 (s, Fe-*C*O), 151.0 (broad s, *ipso*-B*Ph*$_2$ A), 150.5 (s, *C*^{2}), 150.0 (broad s, *C*^{5}), 148.6 (s, *ipso*-Xyl), 147.9 (s, *C*^{7}), 146.4 (d, $^3J_{C,P}$ 9 Hz, *C*^{10}), 142.4 (s, *C*^{13}), 138.0 (d, $^2J_{C,P}$ 34 Hz, *C*^{11}), 137.2 (d, $^1J_{C,P}$ 40 Hz, *ipso*-P*Ph*$_2$ A), 136.6 (s, *o*-B*Ph*$_2$ A), 135.0 (s, *p*-B*Ph*$_2$ A), 134.6 (s, *o*-Xyl), 134.0 (s, *C*^{12}), 133.5 (broad s, *ipso*-B*Ph*$_2$ B), 133.0 (s, *C*^{6}), 132.9 (d, $^2J_{C,P}$ 12 Hz, *o*-PPh$_2$ B), 132.8 (s, *o*-Xyl), 132.3 (d, $^2J_{C,P}$ 13 Hz, *o*-P*Ph*$_2$ A), 130.6 (d, $^1J_{C,P}$ 41 Hz, *C*^{4}), 130.0 (s, *o*-B*Ph*$_2$ B), 129.8 (s, *p*-P*Ph*$_2$ B), 129.1 (s, *p*-P*Ph*$_2$ A), 128.7 (s, *p*-Xyl), 128.7 (s, *C*^{3}), 128.1 (d, $^3J_{C,P}$ 9 Hz, *m*-P*Ph*$_2$ A), 127.8 (s, *m*-Xyl), 127.5 (d, $^3J_{C,P}$ 9 Hz, *m*-P*Ph*$_2$ B), 127 (d, *ipso*-P*Ph*$_2$ B), 126.7 (s, *m*-B*Ph*$_2$ B), 126.1 (s, *m*-Xyl), 125.9 (s, *m*-B*Ph*$_2$ B), 125.9 (s, *m*-B*Ph*$_2$ A), 124.7 (s, *p*-B*Ph*$_2$ B), 124.4 (s, *C*^{1}), 124.1 (s, *o*-B*Ph*$_2$ A), 123.9 (s, *m*-B*Ph*$_2$ A), 120.4 (s, *C*^{8}), 114.7 (s, *o*-B*Ph*$_2$ B), 83.5 (s, C_5H_5), 42.5 (s, *C*Me$_2$), 34.8, 34.6 (2×s, 2×*C*Me$_3$), 30.9, 30.7 (2×s, 2×C*Me*$_3$), 26.2, 23.6 (2×s, C*Me*$_2$), 19.6, 17.6 (2×s, 2×Xyl-C*H*$_3$). **^{31}P{^{1}H} NMR (CD_2Cl_2, 203 MHz, 298 K):** δ 47.3 (d, $^1J_{P,Rh}$ 148 Hz). **^{11}B NMR (CD_2Cl_2, 161 MHz, 298 K):** δ 4 (broad s, $\omega_{1/2}$ 840 Hz). **IR:** ν(CO) = 1965, 1953, 1795 cm^{-1} (nujol); 1961, 1798 cm^{-1} (CH_2Cl_2); ν(CN) = 1523 cm^{-1} (nujol); 1521 cm^{-1} (CH_2Cl_2). **Elemental Analysis Calcd (%)** for $C_{63}H_{62}O_2NBPSRhFe$: C, 68.93; H, 5.69; N, 1.28. Found: C, 69.13; H, 6.01; N, 1.17.

[(TXPB)Rh(μ-CO)(μ-CN^{n}Bu)Fe(CO)Cp] (10): CN^{n}Bu (9.7 mg, 0.12 mmol) dissolved in CH_2Cl_2 (2 mL) was added dropwise at room temperature to [(TXPB)Rh(μ-CO)$_2$Fe(CO)Cp]·0.6(hexane) [**7**·0.6(hexanes)] (120 mg, 0.12 mmol) in CH_2Cl_2 (10 mL).

The reaction mixture was stirred vigorously for 30 minutes at room temperature before evaporating to dryness *in vacuo*, yielding a dark purple powder. Yield: 99 mg (86 %). X-ray quality crystals of [(TXPB)Rh(μ-CO)(μ-CN^{n}Bu)Fe(CO)Cp]·2hexane were grown by cooling a saturated solution of [(TXPB)Rh(μ-CO)(μ-CN^{n}Bu)Fe(CO)Cp] in hexane/pentane to −30 °C for several days. **^{1}H NMR (CD_2Cl_2, 500 MHz, 253 K):** δ 7.69 (s, 1H, C*H*^{1}), 7.62 (s, 1H, C*H*^{6}), 7.59 (s, 1H, C*H*^{8}), 7.39−7.34 (m, 4H, *m,p*-P*Ph*$_2$ B, *p*-P*Ph*$_2$ A), 7.30 (t, $^3J_{H,H}$ 8 Hz, 2H, *m*-P*Ph*$_2$ A), 7.25−7.21 (m, 3H, C*H*^{3}, *o*-P*Ph*$_2$ A), 7.08−7.02 (m, 4H, *m*-B*Ph*$_2$ A, *o*-P*Ph*$_2$ B), 6.97 (t, $^3J_{H,H}$ 8 Hz, 1H, *p*-B*Ph*$_2$ A), 6.91 (d, $^3J_{H,H}$ 8 Hz, 2H, *o*-B*Ph*$_2$ A), 6.46 (t, $^3J_{H,H}$ 7 Hz, 1H, *m*-B*Ph*$_2$ B), 5.99 (t, $^3J_{H,H}$ 5 Hz, 2H, *o*-B*Ph*$_2$ B), 5.85 (t, $^3J_{H,H}$ 7 Hz, 1H, *m*-B*Ph*$_2$ B), 5.57 (t, $^3J_{H,H}$ 7 Hz, 1H, *p*-B*Ph*$_2$ B), 4.85 (s, 5H, C_5H_5), 4.38 (dt, $^2J_{H,H}$ 11 Hz, $^3J_{H,H}$ 4 Hz, 1H, ^{n}Bu-CH_2^{α}), 4.11 (dt, $^2J_{H,H}$ 12 Hz, $^3J_{H,H}$ 6 Hz, 1H, ^{n}Bu-CH_2^{α}) 2.14 (s, 3H, C*Me*$_2$), 1.87 (do, $^3J_{H,H}$ 5 Hz, 1H, ^{n}Bu-CH_2^{β}), 1.71 (s, 3H, C*Me*$_2$), 1.45 (do, $^3J_{H,H}$ 5 Hz, 1H, ^{n}Bu-CH_2^{β}), 1.34 (septet, $^3J_{H,H}$ 7 Hz, 2H, ^{n}Bu-CH_2^{γ}), 1.24, 1.18 (2×s, 18H, 2×C*Me*$_3$), 0.78 (t, $^3J_{H,H}$ 7 Hz, 3H, ^{n}Bu-C*H*$_3$). **^{13}C{^{1}H} NMR (CD_2Cl_2, 126 MHz, 253 K):** δ 304.3 (dd, $^1J_{C,Rh}$ 51 Hz, $^2J_{C,P}$ 24 Hz, μ-*C*N^{n}Bu), 241.6 (dd, $^1J_{C,Rh}$ 60 Hz, $^2J_{C,P}$ 11 Hz, μ-*C*O), 215.9 (s, Fe-*C*O), 153.1 (broad s, *ipso*-B*Ph*$_2$ A), 151.0 (d, $^3J_{C,P}$ 4 Hz, *C*^{2}), 149.7 (broad s, *C*^{5}), 148.4 (s, *C*^{7}), 146.8 (d, $^3J_{C,P}$ 11 Hz, *C*^{10}), 143.3 (s, *C*^{13}), 138.5 (d, $^2J_{C,P}$ 33 Hz, *C*^{11}), 138.0 (d, $^1J_{C,P}$ 39 Hz, *ipso*-P*Ph*$_2$ A), 135.3 (s, *o*-B*Ph*$_2$ A), 133.7 (d, $^2J_{C,P}$ 12 Hz, *o*-P*Ph*$_2$ B), 133.5 (s, *C*^{6}), 132.9 (s, *C*^{12}, *ipso*-B*Ph*$_2$ B), 132.4 (d, $^2J_{C,P}$ 14 Hz, *o*-P*Ph*$_2$ A), 131.7 (d, $^1J_{C,P}$ 40 Hz, *C*^{4}), 130.5 (s, *o*-B*Ph*$_2$ B), 129.8 (s, *p*-P*Ph*$_2$ A), 129.5 (s, *p*-P*Ph*$_2$ B), 129.3 (s, *C*^{3}), 129.2 (d, $^1J_{C,P}$ 32 Hz, *ipso*-P*Ph*$_2$ B), 128.4 (d, $^2J_{C,P}$ 10 Hz, *m*-P*Ph*$_2$ A), 127.9 (d, $^2J_{C,P}$ 9 Hz, *m*-P*Ph*$_2$ B), 126.7 (s, *m*-B*Ph*$_2$ A), 126.3, 126.0 (2×s, *m*-B*Ph*$_2$ B), 124.9 (s, *p*-B*Ph*$_2$ B), 124.7 (s, *p*-B*Ph*$_2$ A), 124.6 (s, *C*^{1}), 120.6 (s, *C*^{8}), 117.7 (broad s, *o*-B*Ph*$_2$ B), 83.4 (s, *C*$_5$H$_5$), 62.5 (d, $^3J_{C,Rh}$ 3 Hz, ^{n}Bu-*C*H$_2^{\alpha}$), 43.0 (s, *C*Me$_2$), 35.2 (s, 2 × *C*Me$_3$), 32.7 (s, ^{n}Bu-*C*H$_2^{\beta}$), 31.5, 31.2 (2×s, 2×C*Me*$_3$), 26.7, 25.1 (2×s, C*Me*$_2$), 20.9 (s, ^{n}Bu-C*H*$_2^{\gamma}$), 14.0 (s, ^{n}Bu-C*H*$_3$). **^{31}P{^{1}H} NMR (CD_2Cl_2, 203 MHz, 298 K):** δ 44.1 (d, $^1J_{P,Rh}$ 151 Hz). **^{11}B NMR (CD_2Cl_2, 161 MHz, 298 K):** δ 2 (broad s, $\omega_{1/2}$ ~615 Hz). **IR:** ν(CO) = 1963, 1809 cm^{-1} (nujol); 1958, 1802 cm^{-1} (CH_2Cl_2); ν(CN) = 1571, 1560 cm^{-1}

(nujol); 1572, 1561 cm^{-1} (CH_2Cl_2). **Elemental Analysis Calcd (%)** for $C_{59}H_{62}O_2NBPSRhFe$: C, 67.51; H, 5.95; N, 1.33. Found: C, 68.12; H, 6.10; N, 1.46.

TXPB–CN^{t}Bu: TXPB (19 mg, 2.8×10^{-2} mmol) and CN^{t}Bu (2.3 mg, 2.8×10^{-2} mmol) were dissolved in C_6D_6 (0.6 mL) in an NMR tube at room temperature. The NMR scale reaction was left at room temperature for 30 minutes. **^{1}H NMR (C_6D_6, 298 K):** δ 7.63–7.59 (m, 6H, Aryl-C*H*), 7.44 (d, *J* 1.5 Hz, 4H, Aryl-C*H*), 7.41 (t, *J* 8 Hz, 4H, Aryl-C*H*), 7.32 (t, *J* 8 Hz, 4H, Aryl-C*H*), 7.22 (t, *J* 8 Hz, 2H, Aryl-C*H*), 7.11–7.06 (m, 8H, Aryl-C*H*), 1.79 (s, 6H, C*Me*$_2$), 1.32, 1.18 (s, 2 x 9H, C*Me*$_3$), 0.92 (s, 6H, CNC*Me*$_3$). **^{31}P{^{1}H} (C_6D_6, 298 K):** δ –13.0 (s). **^{11}B NMR (C_6D_6, 298 K):** δ –11 (broad s, $\omega_{1/2}$ ~ 560 Hz). **IR:** ν(CN) = 2261 cm^{-1} (CH_2Cl_2)

[(TXPH)Rh(μ-CO)$_2$Fe(CO)Cp] (11): Toluene (25 mL) was added to a mixture of K[CpFe(CO)$_2$] (178 mg, 0.822 mmol) and [RhCl(CO)(TXPH)] (283 mg, 0.411 mmol) and was stirred vigorously for 1.5 hours at room temperature. The cherry red reaction mixture was then filtered; the brown solid that was collected on the surface of the frit was washed with toluene (2 × 5 mL). The filtrate was evaporated to dryness *in vacuo* to yield a red-brown oily solid, to which hexanes (30 mL) was added. The mixture was sonicated and filtered to collect an orange-brown powder. The collected product was washed with hexanes (2 × 5 mL) and dried *in vacuo*. Yield: 266 mg (78 %). X-ray quality crystals of [(TXPH)Rh(μ-CO)$_2$Fe(CO)Cp]·2$C_2H_4Cl_2$ were grown by slow diffusion of hexanes into a saturated solution of [(TXPH)Rh(μ-CO)$_2$Fe(CO)Cp] in 1,2-dichloroethane at −30 °C. **^{1}H NMR (C_6D_6, 600 MHz, 298 K):** δ 8.53 (d, $^3J_{H,H}$ 8 Hz, 1H, C*H*^{5}), 7.76−7.72 (m, 4H, *o*-P*Ph*$_2$), 7.64 (dd, $^3J_{H,H}$ 7 Hz, $^4J_{H,H}$ 2 Hz, 1H, C*H*^{3}), 7.60 (t, $^4J_{H,H}$ 2 Hz, 1H, C*H*^{1}), 7.59 (d, $^4J_{H,H}$ 2 Hz, 1H, C*H*^{8}), 7.17 (dd, $^3J_{H,P}$ 8 Hz, $^4J_{H,H}$ 2 Hz, 1H, C*H*^{6}), 6.98−6.97 (m, 6H, *m*,*p*-P*Ph*$_2$), 4.57 (s, 5H, C_5H_5), 1.69 (s, 6H, C*Me*$_2$), 1.21, 1.06 (2×s, 18H, 2×C*Me*$_3$). **^{13}C{^{1}H} NMR (C_6D_6, 151 MHz, 298 K):** δ 245.7 (broad s, 3 × *C*O), 151.8 (d, $^3J_{C,P}$ 3 Hz, *C*^{2}), 151.5 (s, *C*^{7}), 145.9 (d, $^3J_{C,P}$ 10 Hz, *C*^{10}), 144.0 (s, *C*^{13}), 141.1 (d, $^2J_{C,P}$ 37 Hz, *C*^{11}), 135.6 (d, $^1J_{C,P}$ 40 Hz, *C*^{4}), 135.2 (d, $^1J_{C,P}$ 38 Hz, *ipso*-P*Ph*$_2$), 134.1 (d, $^2J_{C,P}$ 14 Hz, *o*-P*Ph*$_2$),

131.2 (s, *C*^{5}), 130.3 (s, *p*-P*Ph*$_2$), 130.1 (s, *C*^{3}), 129.6 (d, $^{4}J_{C,P}$ 4 Hz, *C*^{12}), 129.0 (d, $^{3}J_{C,P}$ 10 Hz, *m*-P*Ph*$_2$), 124.8 (s, *C*^{6}), 124.5 (s, *C*^{1}), 122.5 (s, *C*^{8}), 87.0 (s, C_5H_5), 42.8 (s, *C*Me$_2$), 35.3, (s, 2×*C*Me$_3$), 31.8, 31.6 (2×s, 2×C*Me*$_3$), 25.8 (s, C*Me*$_2$). **Note:** in the $^{13}C\{^{1}H\}$ NMR of **X** in toluene-d_8 at 230 K, the CO signal was broadened into the baseline, consistent with rapid exchange between the three CO environments. **$^{31}P\{^{1}H\}$ NMR (C_6D_6, 203 MHz, 298 K):** δ 45.3 (d, $^{1}J_{P,Rh}$ 183 Hz). **IR:** ν(CO) = 1956, 1946, 1938, 1756, 1750, 1740 cm^{-1} (nujol); 1960, 1741 cm^{-1} (CH_2Cl_2). **Elemental Analysis Calcd (%)** for $C_{43}H_{44}O_3PSRhFe$: C, 62.18; H, 5.34. Found: C, 62.26; H, 5.62.

[(TXPH)Rh(CO)(μ-CNC$_6$H$_4$Cl-*p*)$_2$Fe(CO)Cp]·CH$_2$Cl$_2$ (12·CH$_2$Cl$_2$): CNC$_6$H$_4$Cl-*p* (25 mg, 0.18 mmol) dissolved in CH_2Cl_2 (1 mL) was added dropwise at room temperature to [(TXPH)Rh(μ-CO)$_2$Fe(CO)Cp] (**11**) (75 mg, 9.0×10^{-2} mmol) in CH_2Cl_2 (3 mL). The reaction mixture was stirred vigorously for 15 min at room temperature. The black-yellow solution was then layered with hexanes (10 mL) and cooled to −30 °C for several days, after which point the mother liquors were decanted and the resulting black crystals were dried *in vacuo*. Yield: 49 mg (51 %). X-ray quality crystals of [(TXPH)Rh(CO)(μ-CNC$_6$H$_4$Cl-*p*)$_2$Fe(CO)Cp]·CH$_2$Cl$_2$ were grown by slow diffusion of hexanes into a saturated solution of [(TXPH)Rh(CO)(μ-CNC$_6$H$_4$Cl-*p*)$_2$Fe(CO)Cp] in CH_2Cl_2 at −30 °C. **^{1}H NMR (CD_2Cl_2, 500 MHz, 194 K):** δ 7.74 (broad s, 2H, *o*-P*Ph*$_2$ A), 7.69 (s, 1H, C*H*^{1}), 7.74 (s, 1H, C*H*^{8}), 7.51 (s, 1H, C*H*^{3}), 7.46−7.38 (m, 5H, C*H*^{6}, *m,p*-P*Ph*$_2$ A, *p*-P*Ph*$_2$ B), 7.36 (d, $^{3}J_{H,H}$ 7 Hz, 1H, C*H*^{5}), 7.20 (d, $^{3}J_{H,H}$ 7 Hz, 2H, *o*-*Ph*Cl A), 7.09 (t, $^{3}J_{H,H}$ 7 Hz, 2H, *m*-P*Ph*$_2$ B), 6.91 (d, $^{3}J_{H,H}$ 7 Hz, 2H, *o*-*Ph*Cl B), 6.87 (t, $^{3}J_{H,H}$ 8 Hz, 2H, *o*-P*Ph*$_2$ B), 6.66 (d, $^{3}J_{H,H}$ 7 Hz, 2H, *m*-*Ph*Cl A), 5.60 (d, $^{3}J_{H,H}$ 7 Hz, 2H, *m*-*Ph*Cl B), 4.64 (s, 5H, C_5H_5), 2.10, 1.43 (2×s, 6H, C*Me*$_2$), 1.38, 1.19 (2×s, 18H, 2×C*Me*$_3$). **$^{13}C\{^{1}H\}$ NMR (CD_2Cl_2, 126 MHz, 194 K):** δ 247.5, 242.3 (2 × broad s, μ-*C*N(C$_6$H$_4$Cl-*p*)), 214.9 (s, Fe-*C*O), 202.1 (broad d, $^{1}J_{C,Rh}$ 60 Hz, Rh-*C*O), 150.9 (s, *C*^{7}), 149.7 (s, *C*^{2}), 149.2 (s, *p*-*Ph*Cl A), 148.4 (s, *p*-*Ph*Cl B), 144.3 (d, $^{3}J_{C,P}$ 9 Hz, *C*^{10}), 144.0 (s, *C*^{13}), 138.3 (appt. s, *C*^{11}), 135.9 (d, $^{1}J_{C,P}$ 32 Hz, *ipso*-P*Ph*$_2$ B), 133.9 (d, $^{1}J_{C,P}$ 32 Hz, *ipso*-P*Ph*$_2$ A), 132.9 (d, $^{2}J_{C,P}$ 14 Hz, *o*-P*Ph*$_2$ A), 131.8 (d, $^{1}J_{C,P}$ 39 Hz, *C*^{4}), 130.5 (s, *C*^{3}), 130.2 (d, $^{2}J_{C,P}$ 10 Hz, *o*-P*Ph*$_2$ B), 129.9 (s, *p*-P*Ph*$_2$

A and B), 128.6 (s, *C*^{5}), 128.5 (s, *o*-*Ph*Cl A), 128.4 (d, $^{3}J_{C,P}$ 10 Hz, *m*-P*Ph*$_2$ A), 128.2 (s, *o*-*Ph*Cl B), 128.1 (s, *C*^{12}), 127.4 (d, $^{3}J_{C,P}$ 8 Hz, *m*-P*Ph*$_2$ B), 126.9 (s, *ipso*-*Ph*Cl A), 126.5 (s, *ipso*-*Ph*Cl B), 123.6 (s, *C*^{1}), 123.2 (s, *C*^{6}), 121.6 (s, *C*^{8}, *m*-*Ph*Cl A), 120.0 (s, *m*-*Ph*Cl B), 82.3 (s, *C*$_5$H$_5$), 41.5 (s, *C*Me$_2$), 34.9, 34.8 (2×s, 2×*C*Me$_3$), 31.2, 30.7 (2×s, 2×C*Me*$_3$), 25.8, 24.8 (2×s, 2×C*Me*$_2$). **^{31}P{^{1}H} NMR (CD$_2$Cl$_2$, 203 MHz, 298 K):** δ 43.7 (d, $^{1}J_{P,Rh}$ 178 Hz). **IR:** ν(CO) = 1950 (broad, nujol), 1954 cm^{-1} (broad, CH_2Cl_2); ν(CN) = 1659 (broad, nujol), 1661 cm^{-1} (broad, CH_2Cl_2). **Elemental Analysis Calcd (%)** for $C_{57}H_{54}O_2N_2Cl_4PSRhFe$: C, 58.88; H, 4.68; N, 2.41. Found: C, 59.02; H, 4.64; N, 2.14.

10.4 – Synthetic Procedures and Characterization Pertaining to Chapter 4

[PtMePh(TXPB')] (13): CH_2Cl_2 (20 mL) was condensed into a round bottom flask containing [PtMe$_2$(cod)] (173 mg, 0.518 mmol) and TXPB (356 mg, 0.518 mmol) through the use of a dry ice/acetone bath. The lemon yellow reaction solution was left to stir for 16 hours at room temperature (during which time the solution lost most of its colour, taking on only a slightly yellow tinge) before being evaporated to dryness *in vacuo*. Hexanes (15 mL) were condensed into the reaction flask and the oily suspension was sonicated for 15 minutes, after which point the hexanes solution was cooled to –78 °C for ~15 minutes then filtered while cold. The product was collected as a white solid and washed with hexanes (10 mL). Yield = 318 mg (67 %). X-ray quality crystals of [PtMePh(TXPB')]·1.5(C_6H_{14}) were obtained by cooling a solution of [PtMePh(TXPB')] in hexanes to –30 °C for several days. **^{1}H NMR (CD$_2$Cl$_2$, 600 MHz, 298 K):** δ 7.81 (s, 1H, C*H*^{1}), 7.67 (s, 1H, C*H*^{8}), 7.44–7.35 (m, 16H, C*H*^{3}, *o*,*m*,*p*-B*Ph*/Pt*Ph*, *o*,*m*,*p*-P*Ph*$_2$), 6.90 (s, 1H, C*H*^{6}), 6.88 (broad s, 5H, *o*,*m*,*p*-B*Ph*/Pt*Ph*), 2.03 (s, 6H, C*Me*$_2$), 1.29, 1.26 (2×s, 18H, 2×C*Me*$_3$), 0.79 (d, $^{2}J_{H,Pt}$ 85, $^{3}J_{H,P}$ 6 Hz, 3H, Pt*Me*), 0.51 (broad s, 3H, B*Me*). **^{13}C{^{1}H} NMR (CD$_2$Cl$_2$, 151 MHz, 298 K):** δ 152.9 (d, $^{3}J_{C,P}$ 5 Hz, *C*^{2}), 150.0 (s, *C*^{7}), 146.7 (d, $^{2}J_{C,P}$ 11 Hz, *C*^{11}), 144.2 (s, *C*^{12}), 140.8 (d, $^{1}J_{C,P}$ 30 Hz, *C*^{4}), 136.8 (broad s, *o*,*m*,*p*-B*Ph*/Pt*Ph*), 133.7 (d, $^{3}J_{C,P}$ 10 Hz, *m*-P*Ph*$_2$), 132.0 (d, $^{1}J_{C,P}$ 50 Hz, *ipso*-P*Ph*$_2$), 130.7 (s, *p*-P*Ph*$_2$), 130.5 (appt s, *C*^{10}), 129.5 (s, *C*^{3}), 129.0 (s, *C*^{13}), 128.7 (d, $^{2}J_{C,P}$ 10 Hz, *o*-

P*Ph*$_2$), 127.8 (broad s, *o*,*m*,*p*-B*Ph*$_2$/Pt*Ph*), 126.4 (s, *C*^{6}), 125.8 (s, *C*^{1}), 122.1 (s, *C*^{8}), 43.5 (s, *C*Me$_2$), 35.3, 35.1 (2×s, 2×*C*Me$_3$), 31.5, 31.4 (2×s, 2×C*Me*$_3$), 26.0 (s, C*Me*$_2$), 12.9 (broad s, B*Me*), –2.0 (d, $^1J_{C,Pt}$ 767, $^2J_{C,P}$ 5 Hz, Pt*Me*); *ipso*-Pt*Ph*, *ipso*-B*Ph* and *C*^{5} could not be located. **^{31}P{^{1}H} NMR (CD$_2$Cl$_2$, 203 MHz, 298 K):** δ 40.9 (broad s, $^1J_{P,Pt}$ 2280 Hz). **^{31}P{^{1}H} NMR (CD$_2$Cl$_2$, 203 MHz, 183 K):** δ 38.7 (s, $^1J_{P,Pt}$ 1963 Hz). **^{11}B NMR (CD$_2$Cl$_2$, 161 MHz, 298 K):** δ 63 (broad s, $\omega_{1/2}$ 3000 Hz). **^{195}Pt{^{1}H} NMR (CD$_2$Cl$_2$, 107 MHz, 183 K):** δ –4322 (d, $^1J_{Pt,P}$ 1958 Hz). **Elemental Analysis Calcd (%)** for $C_{49}H_{54}BPPtS$ (%): C, 64.54; H, 5.97. Found: C, 64.37; H, 5.92.

Spectroscopic Data for [PtMe(TXPB-Me)] (13'): ^{31}P{^{1}H} NMR (CD$_2$Cl$_2$, 203 MHz, 183 K): δ 36.4 (s, $^1J_{P,Pt}$ 5024 Hz). **^{11}B NMR (CD$_2$Cl$_2$, 161 MHz, 183 K):** δ –12 (s). **^{195}Pt{^{1}H} NMR (CD$_2$Cl$_2$, 107 MHz, 183 K):** δ –4700 (broad d, $^1J_{Pt,P}$ 5042 Hz, $\omega_{1/2}$ ~150 Hz).

[Pt(C-Me)Ph(TXPB'-^{13}C) (13-^{13}C): This product was prepared from [Pt(C-Me)$_2$(cod)] and TXPB following the procedure for the synthesis of **13**, but on a smaller scale (Yield = 70.4 mg; 45 %). **Key ^{13}C{^{1}H} NMR data for 13-^{13}C (CD$_2$Cl$_2$, 126 MHz, 298 K):** δ 13.1 (s, B*Me*), –1.9 (d, $^1J_{C,Pt}$ 767 Hz, $^2J_{C,P}$ 5 Hz, Pt*Me*); **^{13}C{^{1}H} NMR (CD$_2$Cl$_2$, 126 MHz, 183 K):** δ 14.2 (broad s, $\omega_{1/2}$ 65 Hz, B*Me*), –5.5 (d, $^1J_{C,Pt}$ 586 Hz, $^2J_{C,P}$ 5 Hz, Pt*Me*). **Key ^{13}C{^{1}H} NMR data for 13'-^{13}C (CD$_2$Cl$_2$, 126 MHz, 183 K):** δ 10.4 (s, B*Me*), –1.8 (d, $^1J_{C,Pt}$ 779 Hz, $^2J_{C,P}$ 5 Hz, Pt*Me*). All other ^{1}H, ^{13}C{^{1}H} and ^{31}P{^{1}H} NMR data for **13-^{13}C** is consistent with that of **13** at 298 K and 183 K.

[PtPh$_2$(TXPB'')] (14): CH_2Cl_2 (10 mL) was condensed into a 50 mL Schlenk flask containing [PtMePh(TXPB')] (**13**) (79.0 mg, 8.66×10^{-2} mmol) through the use of a dry ice/acetone bath. The reaction mixture was heated to 65 °C for 48 hours, after which the solvent was removed *in vacuo*. Hexanes (10 mL) were then condensed into the reaction flask and the oily residue was sonicated until fully dissolved; the hexanes solution was then brought into the dry box and stored at –30 °C for recrystallization. After 3 days a

white powder had precipitated out of solution; the mother liquors were decanted and the resulting white solid was dried *in vacuo*. Crude yield = 48.9 mg [62 %; this product did not contain [PtMePh(TXPB')] (**13**), but always contained ~15 % of an unidentified impurity which contains a Pt*Me* group *cis* to the phosphine donor of the TXPB ligand. The Pt-*Me* signal for the impurity is located at 0.32 ppm in the ^{1}H NMR spectrum in CD_2Cl_2 ($^{2}J_{H,Pt}$ 72 Hz, $^{3}J_{H,P}$ 6 Hz), and the ^{t}Bu signals for this compound were singlets located at 1.29 and 1.24 ppm; the relative integration of these signals is 3H and 18H]. X-ray quality crystals of $[PtPh_2(TXPB'')]\cdot(CH_2Cl_2)(C_6H_{14})_{0.5}$ were obtained by slow diffusion of hexanes into a solution of $[PtPh_2(TXPB'')]$ in CH_2Cl_2 at –30 °C. **^{1}H NMR (CD_2Cl_2, 500 MHz, 265 K):** δ 7.74 (s, 1H, C*H*^{1}), 7.66 (d, $^{3}J_{H,H}$ 2 Hz, 1H, C*H*^{8}), 7.51 (t, $^{3}J_{H,Pt}$ 61 Hz, $^{3}J_{H,H}$ 6 Hz, 2H, *o*-Pt*Ph* A), 7.40–7.35 (m, 3H, C*H*^{3}, *p*-P*Ph*$_2$), 7.30–7.28 (m, 8H, *o,m*-P*Ph*$_2$), 7.09 (t, $^{3}J_{H,Pt}$ 74 Hz, $^{3}J_{H,H}$ 3 Hz, 2H, *o*-Pt*Ph* B), 6.92–6.86 (m, 3H, *m,p*-Pt*Ph* A), 6.82 (d, $^{3}J_{H,H}$ 2 Hz, 1H, C*H*^{6}), 6.79–6.77 (m, 3H, *m,p*-Pt*Ph* B), 2.02 (s, 6H, C*Me*$_2$), 1.27, 1.20 (2×s, 18H, 2×C*Me*$_3$), 0.61 (broad s, 6H, B*Me*$_2$). **^{13}C{^{1}H} NMR (CD_2Cl_2, 126 MHz, 265 K):** δ 155.5 (d, $^{1}J_{C,Pt}$ 112 Hz, *ipso*-Pt*Ph* A), 153.2 (d, $^{3}J_{C,P}$ 5 Hz, *C*^{2}), 151.4 (d, $^{2}J_{C,P}$ 9 Hz, *C*^{11}), 150.7 (s, *C*^{7}), 149.5 (s, *C*^{12}), 146.2 (d, $^{3}J_{C,P}$ 10 Hz, *C*^{10}), 145.1 (s, *C*^{13}), 140.7 (s, $^{2}J_{C,Pt}$ 33 Hz, *o*-Pt*Ph* A), 137.0 (s, $^{2}J_{C,Pt}$ 32 Hz, *o*-Pt*Ph* B), 133.8 (d, $^{2}J_{C,P}$ 12 Hz, *o*-P*Ph*$_2$), 131.4 (d, $^{1}J_{C,P}$ 49 Hz, *ipso*-P*Ph*$_2$), 130.7 (s, *p*-P*Ph*$_2$), 129.5 (s, *C*^{3}), 128.5 (d, $^{3}J_{C,P}$ 10 Hz, *m*-P*Ph*$_2$), 127.5 (appt. d, *J* 7 Hz, *m*-Pt*Ph* A), 127.5 (s, *m*-Pt*Ph* B), 126.0 (s, *C*^{1}), 124.1 (s, *p*-Pt*Ph* A), 123.9 (s, *C*^{6}), 123.0 (s, *C*^{8}), 122.0 (s, *p*-Pt*Ph* B), 43.6 (s, *C*Me$_2$), 35.1, 35.0 (2×s, 2×*C*Me$_3$), 31.4, 31.3 (2×s, 2×C*Me*$_3$), 25.8 (s, C*Me*$_2$), 16.6 (broad s, B*Me*$_2$); *ipso*-Pt*Ph* B, *C*^{4} and *C*^{5} could not be located. **^{31}P{^{1}H} NMR (CD_2Cl_2, 203 MHz, 298 K):** δ 42.7 (s, $^{1}J_{P,Pt}$ 1811 Hz). **^{11}B NMR (CD_2Cl_2, 161 MHz, 298 K):** δ 80 (broad s, $\omega_{1/2}$ ~2200 Hz). **^{195}Pt{^{1}H} NMR (CD_2Cl_2, 128 MHz, 298 K):** δ –4268 (d, $^{1}J_{Pt,P}$ 1824 Hz). **Elemental Analysis Calcd (%)** for $C_{49}H_{54}BPPtS$ (%): C, 64.54; H, 5.97. Found: C, 64.82; H, 6.36.

[PtMePh(PPh_3)(TXPB')] (15): CH_2Cl_2 (10 mL) was condensed into a round bottom flask containing [PtMePh(TXPB')] (**13**) (92.6 mg, 0.102 mmol) through the use of a dry

ice/acetone bath. A solution of PPh_3 (26.6 mg, 0.102 mmol) in CH_2Cl_2 (5 mL) was added dropwise at room temperature, and the resulting clear and colourless reaction solution was left to stir for 1 hour at room temperature before being evaporated to dryness *in vacuo* to yield an off-white oily residue. Hexanes (~20 mL) were added to the crude product, and the mixture was sonicated for 20 minutes before removal of the solvent *in vacuo*. Yield = 89.2 mg (75 %). All attempts to acquire X-ray quality crystals of [PtMePh(PPh_3)(TXPB')] resulted in preferential crystallization of *trans*-[$PtMe_2(PPh_3)_2$] (over the course of several days, the reaction of 2 equivalents of PPh_3 with [PtMePh(PPh_3)(TXPB')] also formed a mixture of poorly soluble *trans*-[$PtMe_2(PPh_3)_2$] and *trans*-[$PtMePh(PPh_3)_2$] in a 2:1 ratio, as well as free TXPB and TXPB'). **^{1}H NMR (CD_2Cl_2, 500 MHz, 298 K):** δ 8.43 (d, $^{3}J_{H,P}$ 13 Hz, 1H, C*H*^{3}), 7.72 (s, 1H, C*H*^{1}), 7.56–7.50 (m, 4H, C*H*^{8}, *m*,*p*-B*Ph*), 7.33 (t, $^{3}J_{H,H}$ 7 Hz, 2H, *o*-B*Ph*), 7.18 (t, $^{3}J_{H,H}$ 9 Hz, 6H, *o*-P*Ph*$_3$), 7.10 (t, $^{3}J_{H,H}$ 7 Hz, 3H, *p*-P*Ph*$_3$), 7.03–6.92 (m, 15H, C*H*^{6}, *o*,*p*-P*Ph*$_2$, *o*-Pt*Ph*, *m*-P*Ph*$_3$), 6.79 (t, $^{3}J_{H,H}$ 6 Hz, 4H, *m*-P*Ph*$_2$), 6.50 (t, $^{3}J_{H,H}$ 7 Hz, 2H, *m*-Pt*Ph*), 6.41 (t, $^{3}J_{H,H}$ 7 Hz, 1H, *p*-Pt*Ph*), 1.71 (s, 6H, C*Me*$_2$), 1.37, 1.30 (2×s, 18H, 2×C*Me*$_3$), 1.11 (s, 3H, B*Me*), 0.22 (dd, $^{2}J_{H,Pt}$ 70 Hz, $^{3}J_{H,P}$ 9 Hz, $^{3}J_{H,P}$ 7 Hz, 3H, Pt*Me*). **^{13}C{^{1}H} NMR (CD_2Cl_2, 151 MHz, 298 K):** δ 166.2 (dd, $^{2}J_{C,P}$ 114, 13 Hz, *ipso*-Pt*Ph*), 148.5 (s, *C*^{7}), 148.3 (d, $^{3}J_{C,P}$ 12 Hz, *C*^{2}), 144.8 (s, *C*^{5}), 143.3 (d, $^{3}J_{C,P}$ 5 Hz, *C*^{10}), 141.7 (s, *C*^{13}, *ipso*-B*Ph*), 137.5 (s, *m*-B*Ph*), 137.1 (s, $^{2}J_{C,Pt}$ 35 Hz, *o*-Pt*Ph*), 135.4 (broad s, *C*^{3}), 134.5 (d, $^{2}J_{C,P}$ 11 Hz, *o*-P*Ph*$_3$), 133.8 (broad s, *o*-P*Ph*$_2$), 133.0 (s, *p*-B*Ph*), 132.7 (s, *C*^{12}), 129.2 (s, *p*-P*Ph*$_3$), 129.0 (s, *p*-P*Ph*$_2$), 128.0 (s, *o*-B*Ph*), 127.6 (d, $^{3}J_{C,P}$ 9 Hz, *m*-P*Ph*$_2$, *m*-P*Ph*$_3$), 127.1 (s, *C*^{6}), 127.0 (d, $^{4}J_{C,P}$ 6 Hz, *m*-Pt*Ph*), 123.9 (s, *C*^{1}), 121.8 (s, *C*^{8}), 120.4 (s, *p*-Pt*Ph*), 41.2 (s, *C*Me$_2$), 35.3, 35.1 (2×s, 2×*C*Me$_3$), 31.6 (2×s, 2×C*Me*$_3$), 25.2 (s, C*Me*$_2$), 12.7 (s, B*Me*), 8.5 (dd, $^{2}J_{C,P}$ 94 Hz, $^{2}J_{C,P}$ 6 Hz, Pt*Me*); *ipso*-P*Ph*$_3$, *ipso*-P*Ph*$_2$, *C*^{4} and *C*^{11} could not be located. **^{31}P{^{1}H} NMR (CD_2Cl_2, 203 MHz, 298 K):** δ 24.6 (d, $^{1}J_{P,Pt}$ 1736 Hz, $^{2}J_{P,P}$ 11 Hz, Ar*P*Ph$_2$), 24.2 (d, $^{1}J_{P,Pt}$ 1916, $^{2}J_{P,P}$ 11 Hz, *P*Ph$_3$). **^{11}B NMR (CD_2Cl_2, 161 MHz, 298 K):** δ 76 (broad s, $\omega_{1/2}$ ~1900 Hz). **^{195}Pt{^{1}H} NMR (CD_2Cl_2, 128 MHz, 298 K):** δ –4569 (broad dd, $^{1}J_{Pt,P}$ 1957 Hz, $^{1}J_{Pt,P}$ 1767 Hz, $\omega_{1/2}$ ~120 Hz). **Elemental Analysis Calcd (%)** for $C_{67}H_{69}BP_2PtS$ (%): C, 68.53; H, 5.92. Found: C, 68.62; H, 6.39.

[PtMePh{P(OPh)$_3$}(TXPB')] (16): CH_2Cl_2 (10 mL) was condensed into a round bottom flask containing [PtMePh(TXPB')] (**13**) (110 mg, 0.121 mmol) through the use of a dry ice/acetone bath. A solution of $P(OPh)_3$ (37.5 mg, 0.121 mmol) in CH_2Cl_2 (5 mL) was added dropwise at room temperature, and the resulting clear and colourless reaction solution was left to stir for 3 hours at room temperature before being evaporated to dryness *in vacuo* to yield an off-white oily residue. Hexamethyldisiloxane (~ 20 mL) was added to the crude product, and the mixture was sonicated for 20 minutes; the resulting slurry was brought into the dry box and stored at –30 °C to enable precipitation of the product. After several days a white solid had precipitated out of solution; the mother liquors were decanted and the white powder was dried *in vacuo*. Yield = 86.2 mg (58 %). X-ray quality crystals of [PtMePh{P(OPh)$_3$}(TXPB')]·1.5$C_2H_4Cl_2$ were obtained by slow diffusion of hexanes into a solution of [PtMePh{P(OPh)$_3$}(TXPB')] in $C_2H_4Cl_2$ at –30 °C (over the course of 3 days at room temperature, compound [PtMePh{P(OPh)$_3$}(TXPB')] reacted with 1.5 equivalents of $P(OPh)_3$ to form an approximate 2:1:1 mixture of [PtMePh{P(OPh)$_3$}(TXPB')], *cis*-[PtMe$_2${P(OPh)$_3$}$_2$] and free TXPB, as well as unreacted $P(OPh)_3$; this reaction was monitored by $^{31}P\{^1H\}$ NMR spectroscopy). **^{1}H NMR (CD_2Cl_2, 600 MHz, 298 K):** δ 7.69 (d, $^3J_{H,H}$ 7 Hz, 2H, *o*-B*Ph*), 7.60 (s, 1H, C*H*^{1}), 7.58–7.52 (m, 7H, C*H*^{3}, C*H*^{8}, *o*-P*Ph*$_2$, *p*-B*Ph*), 7.39 (t, $^3J_{H,H}$ 8 Hz, 2H, *m*-B*Ph*), 7.23 (dt, $^3J_{H,H}$ 8 Hz, $^4J_{H,H}$ 1 Hz, 2H, *p*-P*Ph*$_2$), 7.14 (dt, $^3J_{H,H}$ 8 Hz, $^4J_{H,P}$ 2 Hz, 4H, *m*-P*Ph*$_2$), 7.05–6.96 (m, 10H, C*H*^{6}, *m*,*p*-P(O*Ph*)$_3$), 6.91 (t, $^3J_{H,Pt}$ 61 Hz, $^3J_{H,H}$ 6 Hz, 2H, *o*-Pt*Ph*), 6.75–6.70 (m, 3H, *m*,*p*-Pt*Ph*), 6.50 (d, $^3J_{H,H}$ 8 Hz, 6H, *o*-P(O*Ph*)$_3$), 1.72 (s, 6H, C*Me*$_2$), 1.38 (s, 3H, B*Me*), 1.30, 1.14 (2×s, 18H, 2×C*Me*$_3$), 0.23 (t, $^2J_{H,Pt}$ 69 Hz, $^3J_{H,P}$ 10 Hz, 3H, Pt*Me*). **$^{13}C\{^1H\}$ NMR (CD_2Cl_2, 151 MHz, 298 K):** δ 158.9 (dd, $^2J_{C,P}$ 111 Hz, $^2J_{C,P}$ 15 Hz, *ipso*-Pt*Ph*), 152.1 (d, $^3J_{C,P}$ 11 Hz, *C*^{2}), 148.7 (s, *C*^{7}), 145.2 (s, *C*^{5}), 143.5 (d, $^3J_{C,P}$ 7 Hz, *C*^{10}), 141.8 (broad s, *ipso*-B*Ph*), 141.7 (s, *C*^{13}), 138.0 (s, *o*-Pt*Ph*), 137.8 (s, *o*-B*Ph*), 136.4 (d, $^2J_{C,P}$ 10 Hz, *C*^{11}), 135.5 (d, $^2J_{C,P}$ 11 Hz, *o*-P*Ph*$_2$), 133.3 (s, *p*-B*Ph*), 132.5 (s, *C*^{12}), 132.3 (d, $^1J_{C,P}$ 46 Hz, *ipso*-P*Ph*$_2$), 130.6 (d, $^2J_{C,P}$ 9 Hz, *C*^{3}), 130.1 (s, *p*-P*Ph*$_2$), 129.5 (s, *ipso*,*m*-P(O*Ph*)$_3$), 128.3 (s, *m*-B*Ph*), 128.2 (d, $^3J_{C,P}$ 10 Hz, *m*-P*Ph*$_2$), 127.3 (d, $^3J_{C,Pt}$ 66 Hz, $^4J_{C,P}$ 7 Hz, *m*-Pt*Ph*), 127.1 (s, *C*^{6}), 124.5 (s, *p*-P(O*Ph*)$_3$), 124.0 (s, *C*^{1}), 122.0 (s, *C*^{8}, *p*-Pt*Ph*),

121.1 (d, $^{3}J_{C,P}$ 5 Hz, *o*-P(O*Ph*)$_3$), 41.4 (s, *C*Me$_2$), 35.3, 35.2 (2×s, 2×*C*Me$_3$), 31.7, 31.5 (2×s, 2×C*Me*$_3$), 25.4 (s, C*Me*$_2$), 13.0 (s, B*Me*), 9.5 (dd, $^{2}J_{C,P}$ 149 Hz, $^{2}J_{C,P}$ 7 Hz, Pt*Me*); *C*^{4} could not be located. **^{31}P{^{1}H} NMR (CD_2Cl_2, 203 MHz, 298 K):** δ 108.1 (d, $^{1}J_{P,Pt}$ 3292 Hz, $^{2}J_{P,P}$ 18 Hz, *P*(OPh)$_3$), 25.4 (d, $^{1}J_{P,Pt}$ 1698 Hz, $^{2}J_{P,P}$ 18 Hz, Ar*P*Ph$_2$). **^{11}B NMR (CD_2Cl_2, 161 MHz, 298 K):** δ ~82 (broad s, $\omega_{1/2}$ ~ 4000 Hz). **^{195}Pt{^{1}H} NMR (CD_2Cl_2, 128 MHz, 298 K):** δ –4495 (dd, $^{1}J_{Pt,P}$ 3285 Hz, $^{1}J_{Pt,P}$ 1694 Hz). **Elemental Analysis Calcd (%)** for $C_{67}H_{69}BO_3P_2PtS$ (%): C, 65.84; H, 5.69. Found: C, 66.40; H, 6.48.

[PtMe(CNXyl)$_2$(TXPB-Me)] (17): CH_2Cl_2 (10 mL) was condensed into a round bottom flask containing [PtMePh(TXPB')] (**13**) (83.8 mg, 9.19×10^{-2} mmol) through the use of a dry ice/acetone bath. A solution of CNXyl (24.1 mg, 0.184 mmol) in CH_2Cl_2 (5 mL) was added dropwise at room temperature, and the resulting bright green/yellow reaction solution was left to stir for 5 hours at room temperature before being evaporated to dryness *in vacuo* to yield a bright green/yellow powder. Yield = 81.7 mg (76 %). X-ray quality crystals of [PtMe(CNXyl)$_2$(TXPB-Me)]·$(CH_2Cl_2)_{2.6}$ were obtained by slow diffusion of hexanes into a solution of [PtMe(CNXyl)$_2$(TXPB-Me)] in CH_2Cl_2 at –30 °C. **^{1}H NMR (CD_2Cl_2, 600 MHz, 298 K):** δ 7.56–7.49 (m, 7H, C*H*^{1}, *o*,*p*-P*Ph*$_2$), 7.44 (dt, $^{3}J_{H,H}$ 8 Hz, $^{4}J_{H,P}$ 2 Hz, 4H, *m*-P*Ph*$_2$), 7.25 (d, $^{3}J_{H,H}$ 8 Hz, 4H, *o*-B*Ph*$_2$), 7.23 (s, 2H, *p*-Xyl), 7.07 (d, $^{3}J_{H,H}$ 8 Hz, 4H, *m*-Xyl), 7.00–6.97 (m, 6H, C*H*^{6}, C*H*^{8}, *m*-BPh$_2$), 6.83 (t, $^{3}J_{H,H}$ 7 Hz, 2H, *p*-B*Ph*$_2$), 6.70 (dd, $^{3}J_{H,P}$ 12 Hz, $^{4}J_{H,H}$ 2 Hz, 1H, C*H*^{3}), 2.06 (s, 12H, Xyl-*Me*), 1.24 (t, $^{2}J_{H,Pt}$ 48 Hz, $^{3}J_{H,P}$ 6 Hz, 3H, Pt*Me*), 1.22 (s, 6H, C*Me*$_2$), 1.08, 1.07 (2×s, 18H, 2×C*Me*$_3$), –0.13 (s, 3H, B*Me*). **^{13}C{^{1}H} NMR (CD_2Cl_2, 151 MHz, 298 K):** δ 167.1 (broad s, *ipso*-B*Ph*$_2$), 147.3 (d, $^{3}J_{C,P}$ 8 Hz, *C*^{2}), 146.2 (s, *C*^{7}), 144.5 (d, $^{3}J_{C,P}$ 7 Hz, *C*^{10}), 140.8 (broad s, *C*NXyl), 139.8 (d, $^{2}J_{C,P}$ 14 Hz, *C*^{11}), 137.2 (s, *C*^{13}), 136.1 (s, *o*-Xyl), 135.6 (broad s, *C*^{5}), 134.8 (d, $^{2}J_{C,P}$ 12 Hz, *o*-P*Ph*$_2$), 134.4 (s, *o*-B*Ph*$_2$), 133.6 (s, *C*^{12}), 132.7 (s, *C*^{6}), 131.8 (s, *p*-P*Ph*$_2$), 130.7 (d, $^{1}J_{C,P}$ 50 Hz, *ipso*-P*Ph*$_2$), 130.6 (s, *p*-Xyl), 129.4 (d, $^{3}J_{C,P}$ 11 Hz, *m*-P*Ph*$_2$), 128.5 (s, *m*-Xyl), 128.1 (d, $^{2}J_{C,P}$ 5 Hz, *C*^{3}), 126.2 (s, *m*-B*Ph*$_2$), 124.6 (s, *C*^{1}), 122.3 (s, *ipso*-Xyl, *p*-B*Ph*$_2$), 115.8 (s, *C*^{8}), 40.5 (s, *C*Me$_2$), 35.0, 34.7 (2×s, 2×*C*Me$_3$), 31.7, 31.2 (2×s, 2×C*Me*$_3$), 25.4 (s, C*Me*$_2$), 18.7 (s, Xyl-*Me*), 11.3 (broad s, B*Me*), –9.6 (d, $^{1}J_{C,Pt}$ 393

Hz, $^{2}J_{C,P}$ 70 Hz, Pt*Me*); C^{4} could not be located. **^{31}P{^{1}H} NMR (CD_2Cl_2, 203 MHz, 298 K):** δ 14.4 (s, $^{1}J_{P,Pt}$ 1603 Hz). **^{11}B NMR (CD_2Cl_2, 161 MHz, 298 K):** δ –10 (s). **^{195}Pt{^{1}H} NMR (CD_2Cl_2, 128 MHz, 298 K):** δ –4575 (broad d, $^{1}J_{P,Pt}$ 1645 Hz, $\omega_{1/2}$ ~300 Hz). **IR:** ν(C≡N) = 2170 (nujol), 2181 cm^{-1} (CH_2Cl_2). **Elemental Analysis Calcd (%)** for $C_{67}H_{72}BN_2PPtS$ (%): C, 68.53; H, 6.18; N, 2.39. Found: C, 68.31; H, 6.11; N, 2.88.

10.5 – Synthetic Procedures and Characterization Pertaining to Chapter 5

(*o*-BrC_6H_4)$P(NEt_2)_2$ (18): THF (50 mL) and diethylether (50 mL) were condensed into a 250 mL two-necked round bottom flask using a dry ice/acetone bath, to which 1,2-dibromobenzene (6.86 g, 29.1 mmol) in THF (10 mL) was added via syringe. The solution was cooled to –110 °C through the use of a diethyl ether/liquid nitrogen bath, and a solution of ^{n}BuLi in hexanes (18 mL, 1.6 M) was added dropwise over 20 minutes. The reaction mixture was maintained at –110 °C for 2 hours, after which point a solution of Cl–$P(NEt_2)_2$ (6.13 g, 29.1 mmol) in THF (20 mL) was added dropwise over 10 minutes. The reaction mixture was maintained at –110 °C for an additional hour before warming to room temperature overnight. The resulting light orange, opaque solution was evaporated to dryness *in vacuo* to yield an opaque orange oil. Hexanes (100 mL) were added to the crude oil and the resulting slurry was sonicated and filtered to remove any unwanted LiCl, which was washed with hexanes (2 × 20 mL). The clear and light yellow filtrate was evaporated to dryness *in vacuo* to yield a translucent fawn yellow oil. Yield = 9.26 g (96 %). **^{1}H NMR (C_6D_6, 500 MHz, 298 K):** δ 7.49 (dt, $^{3}J_{H,H}$ 8 Hz, $^{3}J_{H,P}$ 2 Hz, 1H, CH^{3}), 7.44 (ddd, $^{3}J_{H,H}$ 8 Hz, $^{4}J_{H,P}$ 5 Hz, $^{4}J_{H,H}$ 1 Hz, 1H, CH^{6}), 7.08 (t, $^{3}J_{H,H}$ 8 Hz, 1H, CH^{4}), 6.78 (tt, $^{3}J_{H,H}$ 8 Hz, $^{4}J_{H,H}$ 2 Hz, 1H, CH^{5}), 3.09–2.94 (m, 8H, $N(CH_2CH_3)_2$), 1.02 (t, $^{3}J_{H,H}$ 7 Hz, 12H, $N(CH_2CH_3)_2$). **^{13}C{^{1}H} NMR (C_6D_6, 126 MHz, 298 K):** δ 143.9 (d, $^{2}J_{C,P}$ 15 Hz, C^{2}), 134.5 (s, C^{6}), 133.3 (d, $^{2}J_{C,P}$ 6 Hz, C^{3}), 129.9 (s, C^{5}), 128.2 (d, $^{1}J_{C,P}$ 30 Hz, C^{1}), 127.6 (s, C^{4}), 44.7 (d, $^{2}J_{C,P}$ 19 Hz, $N(CH_2CH_3)_2$), 15.8 (d, $^{3}J_{C,P}$ 3 Hz, $N(CH_2CH_3)_2$). **^{31}P{^{1}H} NMR (C_6D_6, 203 MHz, 298 K):** δ 96.4 (s) **MS:** calcd for $C_{14}H_{24}BrN_2P$: 331.2217 [M^{+}]; found: 332.0854.

(*o*-BrC$_6$H$_4$)PCl$_2$ (19): THF (200 mL) was condensed into a 500 mL two-necked round bottom flask using a dry ice/acetone bath, to which a solution of (*o*-BrC$_6$H$_4$)P(NEt$_2$)$_2$ (**18**) (9.01 g, 27.2 mmol) in THF (20 mL) was added via syringe. A solution of HCl in dioxanes (54 mL, 4.0 M) was then added dropwise at room temperature, which resulted in the immediate formation of a white precipitate; the reaction mixture was left to stir for 1 hour at room temperature. Next, the reaction mixture was evaporated to dryness *in vacuo* to yield an opaque white oil. Diethyl ether (80 mL) was added to the crude oil and the resulting slurry was sonicated and filtered to remove any unwanted HCl·HNEt$_2$, which was washed with diethyl ether (1 × 20 mL). The clear and colourless filtrate was evaporated to dryness *in vacuo* to yield a translucent fawn yellow oil. Yield = 6.35 g (91 %). **^{1}H NMR (C$_6$D$_6$, 500 MHz, 298 K):** δ 7.80 (appt. d, $^3J_{H,H}$ 8 Hz, 1H, C*H*^{3}), 7.00 (ddd, $^3J_{H,H}$ 8 Hz, $^4J_{H,P}$ 5 Hz, $^4J_{H,H}$ 1 Hz, 1H, C*H*^{6}), 6.81 (t, $^3J_{H,H}$ 8 Hz, 1H, C*H*^{4}), 6.60 (dt, $^3J_{H,H}$ 8 Hz, $^4J_{H,H}$ 2 Hz, 1H, C*H*^{5}). **^{13}C{^{1}H} NMR (C$_6$D$_6$, 126 MHz, 298 K):** δ 140.2 (d, $^1J_{C,P}$ 57 Hz, *C*^{2}), 134.2 (s, *C*^{5}), 133.5 (s, *C*^{6}), 132.4 (d, $^2J_{C,P}$ 5 Hz, *C*^{3}), 128.9 (s, *C*^{4}), 127.2 (d, $^2J_{C,P}$ 45 Hz, *C*^{1}). **^{31}P{^{1}H} NMR (C$_6$D$_6$, 203 MHz, 298 K):** δ 153.7 (s). **MS:** calcd for C$_6$H$_4$BrCl$_2$P: 257.8749 [M$^+$]; found: 257.8601.

(*o*-BrC$_6$H$_4$)P(^{t}Bu)Cl (20): Diethyl ether (100 mL) was condensed into a 250 mL two-necked round bottom flask equipped with a reflux condenser using a dry ice/acetone bath, to which (*o*-BrC$_6$H$_4$)PCl$_2$ (**19**) (6.31 g, 24.5 mmol) in diethyl ether (20 mL) was added via syringe. The solution was cooled to –20 °C through the use of a brine/liquid nitrogen bath, and a solution of ^{t}BuMgCl in diethyl ether (12 mL, 2.0 M) was added dropwise over 10 minutes (the addition of ^{t}BuMgCl resulted in the formation of a white precipitate). The reaction mixture was maintained at –20 °C for 30 minutes and then refluxed for 6 hours. The resulting light orange, opaque solution was evaporated to dryness *in vacuo* to yield a white/yellow oil. At this point, the reflux condenser was replaced with a swivel frit and diethyl ether (80 mL) was added to the crude oil; the resulting slurry was sonicated and filtered to remove any unwanted MgCl$_2$, which was washed with diethyl ether (2 × 10 mL). The clear light yellow filtrate was evaporated to dryness *in vacuo* to yield a

translucent fawn yellow oil, which was then distilled *in vacuo* at 130 °C to yield a clear colourless oil. Yield = 4.71 g (69 %). **^{1}H NMR (C_6D_6, 500 MHz, 298 K):** δ 7.72 (dt, $^{3}J_{H,H}$ 8 Hz, $^{4}J_{H,P}$ 2 Hz, 1H, C*H*^{6}), 7.22 (ddd, $^{3}J_{H,H}$ 8 Hz, $^{3}J_{H,P}$ 4 Hz, $^{4}J_{H,H}$ 1 Hz, 1H, C*H*^{3}), 6.90 (dt, $^{3}J_{H,H}$ 8 Hz, $^{4}J_{H,H}$ 1 Hz, 1H, C*H*^{5}), 6.66 (t, $^{3}J_{H,H}$ 7 Hz, 1H, C*H*^{4}), 1.02 (d, $^{3}J_{H,P}$ 13 Hz, 9H, C*Me*$_3$). **^{13}C{^{1}H} NMR (C_6D_6, 126 MHz, 298 K):** δ 137.3 (d, $^{1}J_{C,P}$ 46 Hz, *C*^{2}), 134.5 (s, *C*^{6}), 133.0 (d, $^{2}J_{C,P}$ 1 Hz, *C*^{3}), 131.7 (s, *C*^{4}), 129.6 (d, $^{2}J_{C,P}$ 42 Hz, *C*^{1}), 127.2 (s, *C*^{5}), 36.4 (d, $^{1}J_{C,P}$ 33 Hz, *C*Me$_3$), 25.8 (d, $^{2}J_{C,P}$ 17 Hz, C*Me*$_3$). **^{31}P{^{1}H} NMR (C_6D_6, 203 MHz, 298 K):** δ 105.5 (s). **MS:** calcd for $C_{10}H_{13}BrClP$: 279.5337 [M^+]; found: 279.9598.

[Fe(η^5-$C_5H_4PPh_2$){η^5-$C_5H_4P(^tBu)(C_6H_4Br$-*o*)}] · 0.4pentane (21·0.4pentane): THF (125 mL) was condensed into a 250 ml two-necked round bottom flask containing [Fe(η^5-C_5H_4Br)(η^5-$C_5H_4PPh_2$)] (3.62 g, 8.07 mmol) through the use of a dry ice/acetone bath. The THF solution was cooled to –78 °C and a solution of ^{n}BuLi in hexanes (5.0 mL, 1.6 M) was added dropwise, causing the transparent orange solution to turn crimson red. The reaction mixture was left to stir at –78 °C for 2 hours, after which a solution of (*o*-BrC_6H_4)P(^{t}Bu)Cl (**20**) (2.26 g, 8.07 mmol) in THF (10 mL) was added dropwise. The reaction mixture was then left to stir overnight at room temperature. After stirring overnight the transparent crimson red solution was evaporated to dryness *in vacuo* to yield a bright red oil. Hexanes (100 mL) were added to the oil and the resulting slurry was sonicated, which resulted in the precipitation of LiCl. The hexanes solution was filtered to remove LiCl and the filtrate was evaporated to dryness *in vacuo* to again yield an orange/red oil. The crude oil was brought into the dry box and recrystallized from pentane, which yielded [Fe(η^5-$C_5H_4PPh_2$){η^5-$C_5H_4P^tBu(C_6H_4Br$-*o*)}] · 0.4pentane as an orange/yellow solid. Yield = 3.83 g (74 %). **^{1}H NMR (C_6D_6, 600 MHz, 298 K):** δ 7.47 (dd, $^{3}J_{P,H}$ 4 Hz, $^{3}J_{H,H}$ 1 Hz, 1H, C*H*^{3}), 7.46–7.43 (m, 4H, *o*-P*Ph*$_2$), 7.42 (d, $^{3}J_{H,H}$ 2 Hz, 1H, C*H*^{6}), 7.07–7.03 (m, 6H, *m*,*p*-P*Ph*$_2$), 6.87 (dt, $^{3}J_{H,H}$ 8 Hz, $^{4}J_{H,H}$ 1 Hz, 1H, C*H*^{5}), 6.71 (ddt, $^{3}J_{H,H}$ 8 Hz, $^{4}J_{H,P}$ 2 Hz, $^{4}J_{H,H}$ 1 Hz, 1H, C*H*^{4}), 4.35 (septet, $^{3}J_{H,H}$ 1 Hz, 1H, C*H*$^{5'/2'}$), 4.23 (sextet, $^{3}J_{H,H}$ 1 Hz, 1H, C*H*$^{3''/4''}$), 4.20 (septet, $^{3}J_{H,H}$ 1 Hz, 1H, C*H*$^{4'/3'}$), 4.15 (sextet, $^{3}J_{H,H}$ 1 Hz, 1 H, C*H*$^{3'/4'}$), 4.15–4.13 (m, 2H, C*H*$^{2''/5''}$, C*H*$^{4''/3''}$), 4.04 (sextet, $^{3}J_{H,H}$ 1 Hz, 1H, C*H*$^{2'/5'}$),

3.87 (octet, $^{3}J_{H,H}$ 1 Hz, 1H, C*H*$^{5''/2''}$), 1.10 (d, $^{3}J_{H,P}$ 12 Hz, 9H, C*Me*$_3$). **^{13}C{^{1}H} NMR (C_6D_6, 151 MHz, 298 K):** δ 140.0 (appt. t, $^{1}J_{C,P}$ 12 Hz, *ipso*-P*Ph*$_2$), 139.7 (d, $^{2}J_{C,P}$ 22 Hz, *C*^{1}), 137.1 (s, *C*^{6}), 134.0 (appt. t, $^{2}J_{C,P}$ 20 Hz, *o*-P*Ph*$_2$), 133.4 (d, $^{2}J_{C,P}$ 3 Hz, *C*^{3}), 133.2 (d, $^{1}J_{C,P}$ 40 Hz, *C*^{2}), 130.5 (s, *C*^{4}), 128.7 (d, $^{3}J_{C,P}$ 4 Hz, *p*-P*Ph*$_2$), 128.5 (appt. t, $^{3}J_{C,P}$ 6 Hz, *m*-P*Ph*$_2$), 126.4 (s, *C*^{5}), 77.4 (d, $^{1}J_{C,P}$ 9 Hz, *C*$^{1''}$), 76.3 (d, $^{1}J_{C,P}$ 22 Hz, *C*$^{1'}$), 76.2 (d, $^{3}J_{C,P}$ 28 Hz, *C*$^{5'/2'}$), 74.5 (d, $^{2}J_{C,P}$ 16 Hz, *C*$^{2''/5''}$), 74.1 (d, $^{2}J_{C,P}$ 14 Hz, *C*$^{5''/2''}$), 73.5 (s, *C*$^{3''/4''}$), 73.3 (s, *C*$^{4''/3''}$), 73.2 (d, $^{2}J_{C,P}$ 4 Hz, *C*$^{2'/5'}$), 72.8 (s, *C*$^{3'/4'}$), 72.0 (d, $^{2}J_{C,P}$ 6 Hz, *C*$^{4'/3'}$), 32.6 (d, $^{1}J_{C,P}$ 16 Hz, *C*Me$_3$), 28.5 (d, $^{2}J_{C,P}$ 16 Hz, C*Me*$_3$). **^{31}P{^{1}H} NMR (C_6D_6, 203 MHz, 298 K):** δ 4.9 (s, $C_5H_4P(^{t}Bu)Ar$), –17.0 (s, $C_5H_4PPh_2$). **Elemental Analysis Calcd (%)** for $C_{34}H_{35.8}BrFeP_2$: C, 63.59, H, 5.62. Found: C, 63.50, H, 5.75.

FcPPP (25): Toluene (50 mL) was condensed into a 100 mL Schlenk flask containing [Fe(η^5-$C_5H_4PPh_2$){η^5-$C_5H_4P^tBu(C_6H_4Br$-*o*)}]·0.4pentane (**21**·0.4pentane) (529 mg, 0.824 mmol) through the use of a dry ice/acetone bath. The toluene solution was cooled to –45 °C and a solution of ^{t}BuLi (111 mg, 1.73 mmol) in toluene (5 mL) was added dropwise. The reaction mixture was then warmed to 0 °C and left to stir at that temperature for 3.5 hours, during which time a fine, white precipitate had precipitated out of solution turning the previously transparent orange solution opaque. The reaction mixture was then cooled to –45 °C and a solution of Cl–PPh_2 (190 mg, 0.863 mmol) in toluene (5 mL) was added dropwise; the reaction mixture was then left to stir overnight while warming to room temperature. After stirring overnight, the opaque tangerine coloured solution was evaporated to dryness *in vacuo* to yield an orange oil. Hexanes (15 mL) were added to the crude oil and the mixture was sonicated for 15 minutes to dissolve the crude product; the hexanes solution was brought into the dry box and stored at –30 °C for several days. The hexanes mother liquors were decanted, and the remaining sunset orange solid was dried *in vacuo*. Yield = 480 mg (77 %). **^{1}H NMR (C_6D_6, 600 MHz, 298 K):** δ 7.63–7.60 (m, 1H, C*H*^{6}), 7.52–7.50 (m, 2H, *o*-P*Ph*$_2^{Ar}$ A), 7.48–7.43 (m, 6H, *o*-P*Ph*$_2^{Ar}$ B, *o*-P*Ph*$_2^{Cp}$), 7.26–7.23 (m, 1H, C*H*^{3}), 7.10–7.02 (m, 13H, C*H*^{5}, *m*,*p*-P*Ph*$_2^{Ar}$, *m*,*p*-P*Ph*$_2^{Cp}$), 6.98 (t, $^{3}J_{H,H}$ 8 Hz, 1H, C*H*^{4}), 4.35 (app. septet, $^{3}J_{H,H}$ 1 Hz, 1H, C*H*$^{2'/5'}$), 4.26 (s, 1H, C*H*$^{3''/4''}$), 4.17 (app.

quintet, $^{3}J_{H,H}$ 1 Hz, 1H, C*H*$^{3'/4'}$), 4.15–4.11 (m, 3H, C*H*$^{4'/3'}$, C*H*$^{2''/5''}$, C*H*$^{4''/3''}$), 4.04–4.03 (m, 1H, C*H*$^{5'/2'}$), 3.98 (s, 1H, C*H*$^{5''/2''}$), 1.07 (d, $^{3}J_{H,P}$ 12 Hz, 9H, C*Me*$_3$). **^{13}C NMR (C_6D_6, 151 MHz, 298 K):** δ 147.4 (dd, $^{1}J_{C,P}$ 37 Hz, $^{2}J_{C,P}$ 12 Hz, *C*^{2}), 143.7 (dd, $^{1}J_{C,P}$ 29 Hz, $^{2}J_{C,P}$ 18 Hz, *C*^{1}), 140.2 (dd, $^{1}J_{C,P}$ 17 Hz, $^{4}J_{C,P}$ 12 Hz, *ipso*-P*Ph*$_2^{Ar/Cp}$), 139.0–138.7 (app. m, *ipso*-P*Ph*$_2^{Ar/Cp}$), 136.1 (s, *C*^{6}), 135.1 (d, $^{2}J_{C,P}$ 20 Hz, *o*-P*Ph*$_2^{Ar}$ B), 134.7 (d, $^{2}J_{C,P}$ 20 Hz, *o*-P*Ph*$_2^{Ar}$ A), 134.1 (d, $^{2}J_{C,P}$ 9 Hz, *o*-P*Ph*$_2^{Cp}$), 134.0 (d, $^{2}J_{C,P}$ 8 Hz, *o*-P*Ph*$_2^{Cp}$), 133.9 (s, *C*^{3}), 129.6 (s, *C*^{4}), 128.9 (d, $^{3}J_{C,P}$ 7 Hz, *m*-P*Ph*$_2^{Ar/Cp}$), 128.8 (d, $^{3}J_{C,P}$ 6 Hz, *m*-P*Ph*$_2^{Ar/Cp}$), 128.7 (d, $^{3}J_{C,P}$ 6 Hz, *m*-P*Ph*$_2^{Ar/Cp}$), 128.6 (d, $^{3}J_{C,P}$ 8 Hz, *m*-P*Ph*$_2^{Ar/Cp}$), 128.5, 128.4, 128.4, 128.4 (4×s, *p*-P*Ph*$_2^{Ar/Cp}$), 128.0 (s, *C*^{5}), 77.6 (dd, $^{1}J_{C,P}$ 23 Hz, $^{4}J_{C,P}$ 7 Hz, *C*$^{1'}$), 77.0 (d, $^{1}J_{C,P}$ 8 Hz, *C*$^{1''}$), 75.8 (d, $^{2}J_{C,P}$ 26 Hz, *C*$^{2'/5'}$), 74.5 (d, $^{2}J_{C,P}$ 15 Hz, *C*$^{2''/5''}$), 74.1 (d, $^{2}J_{C,P}$ 15 Hz, *C*$^{5''/2''}$), 73.8 (s, *C*$^{3''/4''}$), 73.5 (s, *C*$^{4''/3''}$), 73.0 (s, *C*$^{5'/2'}$), 72.1 (s, *C*$^{4'/3'}$), 71.8 (d, $^{3}J_{C,P}$ 5 Hz, *C*$^{3'/4'}$), 32.7 (d, $^{1}J_{C,P}$ 16 Hz, *C*Me$_3$), 28.7 (d, $^{2}J_{C,P}$ 14 Hz, C*Me*$_3$). **^{31}P{^{1}H} NMR (C_6D_6, 203 MHz, 298 K):** δ –7.5 (d, $^{2}J_{P,P}$ 176 Hz, $C_5H_4P(^{t}Bu)Ar$), –11.2 (d, $^{2}J_{P,P}$ 176 Hz, Ar*P*Ph$_2$), –16.5 (s, C_5H_4*P*Ph$_2$). **Elemental Analysis Calcd (%)** for $C_{44}H_{41}FeP_3$: C, 73.54; H, 5.75%. Found: C, 73.89; H, 6.00%.

FcPPB (26): Toluene (120 mL) was condensed into a 250 ml round bottom flask containing [Fe(η^5-$C_5H_4PPh_2$){η^5-$C_5H_4P^tBu(C_6H_4Br$-*o*)}]·0.4pentane (**21**·0.4pentane) (1.54 g, 2.40 mmol) through the use of a dry ice/acetone bath. The toluene solution was cooled to –45 °C and a solution of ^{t}BuLi (0.321 g, 5.01 mmol) in toluene (5 mL) was added dropwise. The reaction mixture was then warmed to 0 °C and left to stir at that temperature for 3.5 hours, during which time a fine, white solid precipitated from solution, turning the previously transparent orange solution translucent. The reaction mixture was then cooled to –45 °C and a solution of Br–BPh$_2$ (0.61 g, 2.5 mmol) in toluene (5 mL) was added dropwise; the reaction mixture was then left to stir overnight at room temperature. After stirring overnight, the opaque tangerine coloured solution was evaporated to dryness *in vacuo* to yield a red/orange oil. The crude oil was brought into the dry box, at which point toluene (30 mL) was added to precipitate out LiBr. The crude mixture was centrifuged to separate LiBr from the desired FcPPB ligand, and the clear

orange mother liquors were evaporated to dryness *in vacuo* to again yield a red/orange oil. Hexanes (50 mL) were added to the oil and the resulting slurry was sonicated, which resulted in the precipitation of FcPPB as a light yellow solid. The hexanes solution was filtered, and the collected FcPPB ligand was washed with hexanes (2 × 10 mL). Yield = 1.36 g (78 %). X-ray quality crystals of FcPPB were obtained by slow evaporation of a solution of FcPPB in CH_2Cl_2/hexanes at room temperature under an argon atmosphere. **^{1}H NMR (C_6D_6, 600 MHz, 298 K):** δ 7.95 (broad d, $^3J_{H,H}$ 5 Hz, 2H, *o*-B*Ph*$_2$ A), 7.86 (broad d, $^3J_{H,H}$ 5 Hz, 2H, *o*-B*Ph*$_2$ B), 7.82 (d, $^3J_{H,H}$ 7 Hz, 1H, C*H*^{3}), 7.42 (ddt, $^3J_{H,H}$ 7 Hz, $^4J_{H,H}$ 3 Hz, $^5J_{H,P}$ 1 Hz, 1H, C*H*^{4}), 7.39–7.36 (m, 2H, *o*-P*Ph*$_2$ A), 7.31–7.28 (m, 4H, *o*-B*Ph*$_2$ B, *m*-B*Ph*$_2$ A), 7.23 (appt. tt, $^3J_{H,H}$ 8 Hz, $^2J_{H,P}$ 1 Hz, 3H, *m*-B*Ph*$_2$ B, C*H*^{6}), 7.19 (ddt, $^3J_{H,H}$ 7 Hz, $^4J_{H,P}$ 3 Hz, $^4J_{H,H}$ 1 Hz, 1H, C*H*^{5}), 7.15–7.12 (m, 2H, *p*-B*Ph*$_2$ A and B), 7.06 (dt, $^3J_{H,H}$ 3 Hz, $^4J_{H,H}$ 1 Hz, 3H, *m,p*-P*Ph*$_2$ A), 7.02–7.01 (m, 3H, *m,p*-P*Ph*$_2$ B), 4.34 (sextet, $^3J_{H,H}$ 1 Hz, 1H, C*H*$^{2'/5'}$), 4.25 (sextet, $^3J_{H,H}$ 1 Hz, 1H, C*H*$^{4'/3'}$), 4.12 (septet, $^3J_{H,H}$ 1 Hz, 1H, C*H*$^{3'/4'}$), 4.08 (sextet, $^3J_{H,H}$ 1 Hz, 1H, C*H*$^{5'/2'}$), 3.59 (septet, $^3J_{H,H}$ 1 Hz, 1H, C*H*$^{2''/5''}$), 3.43 (sextet, $^3J_{H,H}$ 1 Hz, 1H, C*H*$^{5''/2''}$), 3.29 (sextet, $^3J_{H,H}$ 1 Hz, 1H, C*H*$^{3''/4''}$), 3.22 (sextet, $^3J_{H,H}$ 1Hz, 1H, C*H*$^{4''/3''}$), 0.76 (d, $^3J_{H,P}$ 14 Hz, 9H, C*Me*$_3$). **^{13}C{^{1}H} NMR (C_6D_6, 151 MHz, 298 K):** δ 164.9 (broad d, $^2J_{C,P}$ 43 Hz, *C*^{2}), 149.5 (broad s, *ipso*-B*Ph*$_2$ A or B), 148.2 (broad s, *ipso*-B*Ph*$_2$ A or B), 140.0 (d, $^1J_{C,P}$ 12 Hz, *ipso*-P*Ph*$_2$ B), 139.2 (d, $^1J_{C,P}$ 12 Hz, *ipso*-P*Ph*$_2$ A), 135.7 (d, $^1J_{C,P}$ 45 Hz, *C*^{1}), 134.8 (broad s, *o*-B*Ph*$_2$ B), 134.2 (d, $^2J_{C,P}$ 20 Hz, *o*-P*Ph*$_2$ A), 133.7 (d, $^2J_{C,P}$ 20 Hz, *o*-P*Ph*$_2$ B), 133.4 (broad s, *o*-B*Ph*$_2$ A), 132.0 (s, *C*^{4}), 131.9 (s, *C*^{3}), 129.3 (s, *m*-B*Ph*$_2$ B), 128.4 (s, *p*-P*Ph*$_2$ A), 128.4 (d, $^3J_{C,P}$ 7 Hz, *m*-P*Ph*$_2$ A), 128.3 (d, $^3J_{C,P}$ 7 Hz, *m*-P*Ph*$_2$ B), 128.2 (s, *p*-P*Ph*$_2$ B), 127.6 (s, *C*^{6}, *m*-B*Ph*$_2$ A), 127.5 (d, $^3J_{C,P}$ 6 Hz, *C*^{5}), 126.9 (broad s, *p*-B*Ph*$_2$ A or B), 126.1 (broad s, *p*-B*Ph*$_2$ A or B), 77.7 (d, $^1J_{C,P}$ 8 Hz, *C*$^{1''}$), 75.9 (d, $^2J_{C,P}$ 20 Hz, *C*$^{2'/5'}$), 74.5 (s, *C*$^{3''/4''}$), 74.4 (d, $^2J_{C,P}$ 14 Hz, *C*$^{2''/5''}$), 73.8 (s, *C*$^{4''/3''}$), 73.6 (d, $^2J_{C,P}$ 3 Hz, *C*$^{5''/2''}$), 73.5 (d, $^2J_{C,P}$ 10 Hz, *C*$^{5'/2'}$), 72.8 (s, *C*$^{4'/3'}$), 72.4 (d, $^3J_{C,P}$ 9 Hz, *C*$^{3'/4'}$), 70.6 (d, $^1J_{C,P}$ 16 Hz, *C*$^{1'}$), 34.2 (d, $^1J_{C,P}$ 7 Hz, *C*Me$_3$), 27.4 (d, $^2J_{C,P}$ 4 Hz, C*Me*$_3$). **^{31}P{^{1}H} NMR (C_6D_6, 203 MHz, 298 K):** δ 19.7 (s, $C_5H_4P(^t$Bu)Ar), –17.2 (s, C_5H_4PPh$_2$). **^{11}B NMR (C_6D_6, 161 MHz, 298 K):** δ 17 (broad s, $\omega_{1/2}$ = 1300 Hz). **Elemental Analysis Calcd (%)** for $C_{44}H_{41}BFeP_2$: C, 75.67, H, 5.92. Found: C, 75.70, H, 6.12.

FcPPAl (27): Toluene (50 mL) was condensed into a 100 mL Schlenk flask containing [Fe(η^5-$C_5H_4PPh_2$){η^5-$C_5H_4P^tBu(C_6H_4Br$-*o*)}] (**21**·0.4pentane) (906 mg, 1.41 mmol) through the use of a dry ice/acetone bath. The toluene solution was cooled to –45 °C and a solution of ^{t}BuLi (190 mg, 2.96 mmol) in toluene (5 mL) was added dropwise. The reaction mixture was then warmed to 0 °C and left to stir for 3 hours, during which time a fine, white solid precipitated from solution, turning the previously transparent orange solution translucent. The reaction mixture was then cooled to –45 °C and a solution of Cl–$AlMe_2$ in hexanes (1.5 mL, 1.0 M) was added dropwise; the reaction mixture was then left to stir overnight while it warmed to room temperature. After stirring overnight the opaque tangerine coloured solution was brought into the dry box, at which point centrifugation was utilized to removed LiBr and LiCl from the reaction mixture. The separated salt byproducts were washed with toluene (2 × 60 mL), and the combined toluene mother liquors were evaporated to dryness *in vacuo* to yield an orange, oily residue. Hexanes (80 mL) were added to the crude residue and the resulting slurry was sonicated, which resulted in the precipitation of FcPPAl as an orange solid. The hexanes solution was filtered, and the collected FcPPAl ligand was washed with hexanes (2 × 15 mL). Yield = 559 mg (64 %). X-ray quality crystals of FcPPAl were obtained by slow diffusion of pentane into a solution of FcPPAl in toluene at –30 °C. **^{1}H NMR (C_6D_6, 600 MHz, 298 K):** δ 8.37 (broad s, 2H, *o*-P*Ph*$_2$ A), 8.19 (d, $^3J_{H,H}$ 7 Hz, 1H, C*H*^{6}), 7.86 (dd, $^3J_{H,H}$ 8 Hz, $^4J_{H,P}$ 3 Hz, 1H, C*H*^{3}), 7.41 (tt, $^3J_{H,H}$ 7 Hz, $^4J_{H,P}$ 1 Hz, 1H, C*H*^{5}), 7.33 (t, $^3J_{H,H}$ 8 Hz, 1H, C*H*^{4}), 7.15–7.14 (m, 3H, *m*,*p*-P*Ph*$_2$ A), 7.05 (dt, $^3J_{H,H}$ 8 Hz, $^3J_{H,P}$ 2 Hz, 2H, *o*-P*Ph*$_2$ B), 6.95–6.89 (m, 3H, *m*,*p*-P*Ph*$_2$ B), 4.20 (s, 1H, C*H*$^{3'/4'}$), 3.95 (septet, $^3J_{H,P}$ 1 Hz, 1H, C*H*$^{2''/5''}$), 3.91–3.89 (m, 2H, C*H*$^{5''/2''}$, C*H*$^{4'/3'}$), 3.83–3.81 (m, 2H, C*H*$^{3''/4''}$, C*H*$^{4''/3''}$), 3.78 (s, 1H, C*H*$^{2'/5'}$), 3.77 (septet, $^3J_{H,P}$ 1 Hz, 1H, C*H*$^{5'/2'}$), 1.25 (d, $^3J_{H,P}$ 12 Hz, 9H, C*Me*$_3$), 0.41, –0.38 (2×broad s, 6H, Al*Me*$_2$). **^{13}C{^{1}H} NMR (C_6D_6, 151 MHz, 298 K):** δ 166.2 (broad s, *C*^{2}), 143.3 (appt. s, *C*^{1}), 139.0 (d, $^2J_{C,P}$ 28 Hz, *C*^{6}), 136.7 (appt. t, $^2J_{C,P}$ 11 Hz, *o*-P*Ph*$_2$ A), 135.7 (d, $^1J_{C,P}$ 28 Hz, *ipso*-P*Ph*$_2$ B), 132.3 (s, *C*^{3}), 132.3 (d, $^2J_{C,P}$ 11 Hz, *o*-P*Ph*$_2$ B), 131.7 (d, $^1J_{C,P}$ 30 Hz, *ipso*-P*Ph*$_2$ A), 131.2 (s, *p*-P*Ph*$_2$ A), 129.4 (s, *C*^{5}), 129.3 (s, *p*-P*Ph*$_2$ B), 128.3 (d, $^3J_{C,P}$ 8 Hz, *m*-P*Ph*$_2$ B), 128.1 (d, $^3J_{C,P}$ 9 Hz, *m*-P*Ph*$_2$ A), 127.4 (s, *C*^{4}), 78.4

(d, $^{1}J_{C,P}$ 16 Hz, $C^{1'}$), 77.3 (s, $C^{2'/5'}$), 77.1 (d, $^{2}J_{C,P}$ 9 Hz, $C^{2''/5''}$), 73.9 (d, $^{3}J_{C,P}$ 5 Hz, $C^{3'/4'}$), 72.9 (d, $^{2}J_{C,P}$ 7 Hz, $C^{5'/2'}$), 72.8 (d, $^{3}J_{C,P}$ 8 Hz, $C^{3''/4''}$), 72.0 (s, $C^{5''/2''}$), 71.2 (s, $C^{4''/3''}$), 71.0 (s, $C^{4'/3'}$), 70.6 (d, $^{1}J_{C,P}$ 33 Hz, $C^{1''}$), 32.5 (d, $^{1}J_{C,P}$ 14 Hz, CMe$_3$), 29.1 (d, $^{2}J_{C,P}$ 14 Hz, CMe_3), –5.7, –6.7 (2×broad s, AlMe_2). **^{31}P{^{1}H} NMR (C_6D_6, 203 MHz, 298 K):** δ 0.2 (d, $J_{P,P}$ 31 Hz, C_5H_4P(^{t}Bu)Ar), –19.2 (d, $J_{P,P}$ 31 Hz, C_5H_4PPh$_2$). **Elemental Analysis Calcd (%)** for $C_{34}H_{37}AlFeP_2$: C, 69.16; H, 6.32. Found: C, 68.83; H, 6.56.

10.6 – Synthetic Procedures and Characterization Pertaining to Chapter 6

[Ni(FcPPB)] (28): Toluene (25 mL) was condensed into a 50 mL round bottom flask containing [Ni(cod)$_2$] (114 mg, 0.413 mmol) and FcPPB (288 mg, 0.413 mmol) through the use of a dry ice/acetone bath. The reaction was left to stir for 4 hours at room temperature, over which time the initially orange solution progressively became blood red. The reaction mixture was then evaporated to dryness *in vacuo* yielding a dark red, oily residue. Hexanes (25 mL) were added to the crude residue and the resulting mixture was sonicated for 15 minutes, allowing for [Ni(FcPPB)] to precipitate from solution as a brick red powder. The hexanes solution was filtered and the collected product was washed with hexanes (2 × 10 mL) then dried *in vacuo*. Yield = 245 mg (78 %). X-ray quality crystals of [Ni(FcPPB)]·0.7(C_7H_8) were obtained by slow diffusion of hexanes (~10 mL) into a solution of [Ni(FcPPB)] (~25 mg) in toluene (~5 mL) at –30 °C. **^{1}H NMR (C_6D_6, 600 MHz, 298 K):** δ 7.83 (app. q, $^{3}J_{H,H}$ 9 Hz, 3H, CH^{6}, *o*-PPh_2 A), 7.33 (t, $^{3}J_{H,H}$ 7 Hz, 1H, CH^{5}), 7.26–7.25 (m, 2H, *o*-BPh_2 A), 7.21 (t, $^{3}J_{H,H}$ 8 Hz, 2H, *o*-PPh_2 B), 7.17–7.13 (m, 3H, CH^{3}, *m*-BPh_2 A), 7.10–7.05 (m, 5H, CH^{4}, *p*-BPh_2 A, *m*,*p*-PPh_2 A), 6.94–6.90 (m, 6H, *m*,*p*-BPh_2 B, *m*,*p*-PPh_2 B), 6.81 (t, $^{3}J_{H,H}$ 7 Hz, 2H, *o*-BPh_2 B), 4.67 (s, 1H, C$H^{2'/5'}$), 4.27 (s, 1H, C$H^{5'/2'}$), 4.24 (s, 1H, C$H^{2''/5''}$), 4.13 (s, 1H, C$H^{5''/2''}$), 3.96 (s, 1H, C$H^{3'/4'}$), 3.93 (s, 1H, C$H^{4''/3''}$), 3.85 (s, 2H, C$H^{4'/3'}$, C$H^{3''/4''}$), 1.09 (d, $^{3}J_{H,P}$ 13 Hz, 9H, CMe_3). **^{13}C{^{1}H} NMR (C_6D_6, 151 MHz, 298 K):** δ 162.8 (broad s, C^{2}), 143.5 (dd, $^{1}J_{C,P}$ 39, $^{3}J_{C,P}$ 11 Hz, C^{1}), 138.4 (dd, $^{1}J_{C,P}$ 28 Hz, $^{3}J_{C,P}$ 3 Hz, *ipso*-PPh_2 B), 136.6 (d, $^{2}J_{C,P}$ 17 Hz, *o*-PPh_2 A), 135.1 (d, $^{1}J_{C,P}$ 31 Hz, *ipso*-PPh_2 A), 133.1 (s, C^{3}), 132.6 (d, $^{2}J_{C,P}$ 26 Hz,

C^{6}), 131.4 (d, $^{2}J_{C,P}$ 12 Hz, *o*-P*Ph*$_2$ B), 130.5 (s, *p*-P*Ph*$_2$ A), 129.8 (s, *C*^{5}), 129.2 (s, *o*-B*Ph*$_2$ B), 128.5 (d, $^{3}J_{C,P}$ 9 Hz, *m*-P*Ph*$_2$ A), 128.4 (d, $^{3}J_{C,P}$ 9 Hz, *m*-P*Ph*$_2$ B), 128.4 (s, *m*-B*Ph*$_2$ A), 128.3 (s, *p*-P*Ph*$_2$ B), 125.8 (d, $^{4}J_{C,P}$ 6 Hz, *C*^{4}), 125.4 (s, *p*-B*Ph*$_2$ B), 124.4 (s, *p*-B*Ph*$_2$ A), 123.3 (s, *m*-B*Ph*$_2$ B), 121.8 (s, *o*-B*Ph*$_2$ A), 83.5 (d, $^{1}J_{C,P}$ 40 Hz, *C*$^{1''}$), 82.6 (d, $^{1}J_{C,P}$ 30 Hz, *C*$^{1'}$), 75.2 (d, $^{2}J_{C,P}$ 14 Hz, *C*$^{2'/5'}$), 74.2 (d, $^{2}J_{C,P}$ 12 Hz, *C*$^{2''/5''}$), 73.1 (d, $^{3}J_{C,P}$ 5 Hz, *C*$^{5''/2''}$), 72.6 (s, *C*$^{5'/2'}$), 71.1 (d, $^{2}J_{C,P}$ 7 Hz, *C*$^{3'/4'}$), 69.6 (d, $^{3}J_{C,P}$ 6 Hz, *C*$^{4''/3''}$), 69.4 (d, $^{2}J_{C,P}$ 3Hz, *C*$^{4'/3'}$), 69.1 (s, *C*$^{3''/4''}$), 35.1 (d, $^{2}J_{C,P}$ 21 Hz, *C*Me$_3$), 30.2 (d, $^{2}J_{C,P}$ 6 Hz, C*Me*$_3$); *ipso*-B*Ph*$_2$ A could not be located. **^{31}P{^{1}H} (C_6D_6, 203 MHz, 298 K):** δ 43.7 (d, $^{2}J_{P,P}$ 29 Hz, $C_5H_4P(^{t}Bu)Ar$), 12.2 (d, $^{2}J_{P,P}$ 29 Hz, $C_5H_4PPh_2$). **^{11}B NMR (C_6D_6, 161 MHz, 298 K):** δ 28 (broad s, $\omega_{1/2}$ = 2400 Hz). **Elemental Analysis Calcd (%)** for $C_{44}H_{41}BFeNiP_2$: C, 69.80 H, 5.46%. Found: C, 69.64; H, 5.75%.

[Pd(FcPPB)]·0.5CH_2Cl_2 (29·0.5CH_2Cl_2): Toluene (30 mL) was condensed into a 50 mL round bottom flask containing [$Pd_2(dba)_3$] (215 mg, 0.235 mmol) and FcPPB (327 mg, 0.469 mmol) through the use of a dry ice/acetone bath, and the reaction was left to stir overnight at room temperature. The black/yellow reaction solution was filtered to remove any unreacted [$Pd_2(dba)_3$], and the residual solid was washed with toluene (2 × 10 mL). The resulting clear, bright orange filtrate was evaporated to dryness *in vacuo*, yielding an orange, oily residue. Hexanes (25 mL) were added to the crude residue and the resulting mixture was sonicated for 15 minutes, allowing for [Pd(FcPPB)] to precipitate from solution as a yellow powder. The hexanes solution was filtered and the collected product was washed with hexanes (3 × 10 mL) then dried *in vacuo*. Yield = 237 mg (63 %). X-ray quality crystals of [Pd(FcPPB)]·$C_2H_4Cl_2$ were obtained by slow diffusion of hexanes (~10 mL) into a solution of [Pd(FcPPB)] (~40 mg) in $C_2H_4Cl_2$ (~3 mL) at –30 °C. For the purposes of elemental analysis, a portion of [Pd(FcPPB)] (~40 mg) was recrystallized by slow diffusion of hexanes (~10 mL) into a solution of [Pd(FcPPB)] in CH_2Cl_2 (~3 mL) at –30 °C. **^{1}H NMR (CD_2Cl_2, 600 MHz, 298 K):** δ 7.97 (d, $^{3}J_{H,H}$ 8 Hz, 1H, C*H*^{6}), 7.96–7.92 (m, 2H, *o*-P*Ph*$_2$ A), 7.81 (d, $^{3}J_{H,H}$ 7 Hz, 2H, *o*-B*Ph*$_2$ A), 7.55–7.47 (m, 4H, C*H*^{5}, *m*,*p*-P*Ph*$_2$ A), 7.24–7.18 (m, 7H, C*H*^{4}, *m*,*p*-P*Ph*$_2$ B, *m*,*p*-B*Ph*$_2$ A), 7.08 (t, $^{3}J_{H,H}$ 7 Hz, 1H, C*H*^{3}),

6.80–6.76 (m, 2H, *o*-P*Ph*$_2$ B), 6.73 (t, $^3J_{H,H}$ 7 Hz, 2H, *m*-B*Ph*$_2$ B), 6.64–6.62 (m, 2H, *o*-B*Ph*$_2$ B), 6.45 (td, $^3J_{H,H}$ 7 Hz, $^4J_{H,H}$ 4 Hz, 1H, *p*-B*Ph*$_2$ B), 4.43 (d, $^3J_{H,H}$ 1 Hz, 1H, C*H*$^{2'/5'}$), 4.25 (q, $^3J_{H,H}$ 2 Hz, 1H, C*H*$^{3''/4''}$), 4.22–4.21 (m, 2H, C*H*$^{4'/3'}$, C*H*$^{4''/3''}$), 4.17 (q, $^3J_{H,H}$ 3 Hz, 1H, C*H*$^{3'/4'}$, C*H*$^{5'/2'}$), 4.12 (s, C*H*$^{2''/5''}$), 3.65 (app. septet, $^3J_{H,H}$ 1 Hz, 1H, C*H*$^{5''/2''}$), 0.98 (d, $^3J_{H,P}$ 14 Hz, 9H, C*Me*$_3$). **^{13}C{^{1}H} NMR (CD$_2$Cl$_2$, 151 MHz, 298 K):** δ 161.3 (broad s, *C*^{2}), 152.0 (broad s, *ipso*-B*Ph*$_2$ A), 145.1 (dd, $^1J_{C,P}$ 36, $^3J_{C,P}$ 12 Hz, *C*^{1}), 136.8 (d, $^1J_{C,P}$ 26 Hz, *ipso*-P*Ph*$_2$ A), 136.3 (d, $^1J_{C,P}$ 23 Hz, *ipso*-P*Ph*$_2$ B), 136.1 (d, $^2J_{C,P}$ 19 Hz, *o*-P*Ph*$_2$ A), 133.2 (app. d, *J* 6 Hz, *o*-B*Ph*$_2$ A), 133.0 (s, *p*-B*Ph*$_2$ A), 132.8 (dd, $^2J_{C,P}$ 33, $^4J_{C,P}$ 3 Hz, *C*^{6}), 132.3 (d, $^2J_{C,P}$ 14 Hz, *o*-P*Ph*$_2$ B), 130.6 (s, *p*-P*Ph*$_2$ A), 129.5 (s, *C*^{5}), 128.9 (app. d, *J* 4 Hz, *m*-B*Ph*$_2$ B), 128.7 (d, $^3J_{C,P}$ 10 Hz, *m*-P*Ph*$_2$ A), 128.4 (s, *p*-P*Ph*$_2$ B), 127.9 (d, $^3J_{C,P}$ 8 Hz, *m*-P*Ph*$_2$ B), 127.0 (app. d, *J* 5 Hz, *p*-B*Ph*$_2$ B), 126.9 (s, *m*-B*Ph*$_2$ A), 125.3 (d, $^4J_{C,P}$ 5 Hz, *C*^{4}), 125.1 (s, *C*^{3}), 121.3 (app. d, *J* 5 Hz, *o*-B*Ph*$_2$ B), 84.7 (dd, $^1J_{C,P}$ 27, $^3J_{C,P}$ 3 Hz, *C*$^{1'}$), 79.1 (d, $^1J_{C,P}$ 36 Hz, *C*$^{1''}$), 75.9 (d, $^2J_{C,P}$ 20 Hz, *C*$^{5''/2''}$), 75.7 (d, $^3J_{C,P}$ 9 Hz, *C*$^{5'/2'}$), 73.4 (d, $^3J_{C,P}$ 5 Hz, *C*$^{2''/5''}$), 72.0 (d, $^2J_{C,P}$ 7 Hz, *C*$^{2'/5'}$), 71.3 (d, $^2J_{C,P}$ 7 Hz, *C*$^{4''/3''}$), 71.0 (d, $^3J_{C,P}$ 3 Hz, *C*$^{3''/4''}$), 70.3 (d, $^3J_{C,P}$ 4 Hz, *C*$^{3'/4'}$), 70.0 (d, $^2J_{C,P}$ 5 Hz, *C*$^{4'/3'}$), 36.9 (d, $^1J_{C,P}$ 12 Hz, *C*Me$_3$), 29.5 (d, $^2J_{C,P}$ 7 Hz, C*Me*$_3$); *ipso*-B*Ph*$_2$ B could not be located. **^{31}P{^{1}H} (CD$_2$Cl$_2$, 203 MHz, 298 K):** δ 43.9 (d, $^2J_{P,P}$ 19 Hz, C$_5$H$_4$*P*(^{t}Bu)Ar), 11.9 (d, $^2J_{P,P}$ 19 Hz, C$_5$H$_4$*P*Ph$_2$). **^{11}B NMR (CD$_2$Cl$_2$, 161 MHz, 298 K):** δ 23 (broad s, $\omega_{1/2}$ = 1100 Hz). **Elemental Analysis Calcd (%)** for C$_{44.5}$H$_{42}$BClFeP$_2$Pd: C, 63.08; H, 5.00%. Found: C, 62.80; H, 5.25%.

[Pt(FcPPB)]·0.3hexanes (30·0.3hexanes): Toluene (50 mL) was condensed into a round bottom flask containing [Pt(nb)$_3$] (351 mg, 0.734 mmol) and FcPPB (513 mg, 0.734 mmol) through the use of a dry ice/acetone bath. The fawn yellow reaction solution was left to stir for 5 hours at room temperature before being evaporated to dryness *in vacuo*. Hexanes (50 mL) were condensed into the reaction flask and the oily suspension was sonicated for 15 minutes, after which point the hexanes solution was filtered and the product was collected as a fawn yellow solid. The collected product was washed with hexanes (2 × 10 mL) Yield = 515 mg (76 %). X-ray quality crystals of

[Pt(FcPPB)]·CH_2Cl_2 were obtained by slow diffusion of hexanes (~10 mL) into a solution of [Pt(FcPPB)] (~30 mg) in CH_2Cl_2 (~3 mL) at –30 °C. **^{1}H NMR (CD_2Cl_2, 600 MHz, 298 K):** δ 8.01 (d, $^3J_{H,H}$ 7 Hz, 1H, C*H*^{6}), 7.94 (broad s, 2H, *o*-P*Ph*$_2$ A), 7.62 (d, $^3J_{H,H}$ 7 Hz, 2H, *o*-B*Ph*$_2$ A), 7.53 (s, 3H, *m,p*-P*Ph*$_2$ A), 7.49 (t, $^3J_{H,H}$ 7 Hz, 1H, C*H*^{5}), 7.28–7.22 (m, 3H, *m,p*-P*Ph*$_2$ B), 7.16–7.12 (m, 3H, C*H*^{4}, *m*-B*Ph*$_2$ A), 7.00 (t, $^3J_{H,H}$ 7 Hz, 1H, *p*-B*Ph*$_2$ A), 6.90 (t, $^3J_{H,H}$ 8 Hz, 1H, C*H*^{3}), 6.79 (t, $^3J_{H,H}$ 9 Hz, 2H, *o*-P*Ph*$_2$ B), 6.65 (t, $^3J_{H,H}$ 7 Hz, 2H, *m*-B*Ph*$_2$ B), 6.19 (t, $^3J_{H,H}$ 7 Hz, 1H, *p*-B*Ph*$_2$ B), 6.10 (t, $^3J_{H,H}$ 5 Hz, 2H, *o*-B*Ph*$_2$ B), 4.60 (s, 1H, C*H*$^{5'/2'}$), 4.36 (s, 1H, C*H*$^{5''/2''}$), 4.33 (s, 1H, C*H*$^{4''/3''}$), 4.27 (s, 1H, C*H*$^{3'/4'}$), 4.23 (s, 1H, C*H*$^{4'/3'}$), 4.16 (s, 1H, C*H*$^{3''/4''}$), 3.93 (s, 1H, C*H*$^{2'/5'}$), 3.79 (s, 1H, C*H*$^{2''/5''}$), 1.07 (d, $^3J_{H,P}$ 12 Hz, 9H, C*Me*$_3$). **^{13}C{^{1}H} NMR (CD_2Cl_2, 151 MHz, 298 K):** δ 161.9 (broad d, $^2J_{C,P}$ 38 Hz, *C*^{2}), 149.6 (appt. broad d, *J* 15 Hz, *ipso*-B*Ph*$_2$ A), 148.0 (dd, $^1J_{C,P}$ 50 Hz, $^3J_{C,P}$ 13 Hz, *C*^{1}), 137.3 (d, $^1J_{C,P}$ 41 Hz, *ipso*-PPh$_2$ A), 136.1 (d, $^2J_{C,P}$ 16 Hz, *o*-P*Ph*$_2$ A), 134.9 (dd, $^1J_{C,P}$ 35 Hz, $^3J_{C,P}$ 4 Hz, *ipso*-P*Ph*$_2$ B), 134.3 (s, *C*^{3}), 133.9 (dd, $^2J_{C,P}$ 28 Hz, $^4J_{C,P}$ 3 Hz, *C*^{6}), 132.3 (d, $^2J_{C,P}$ 13 Hz, *o*-P*Ph*$_2$ B), 132.2 (s, *o*-B*Ph*$_2$ A), 131.1 (s, *p*-P*Ph*$_2$ A), 129.9 (s, *C*^{5}), 129.7 (s, *m*-B*Ph*$_2$ B), 129.0 (s, *p*-P*Ph*$_2$ B), 129.0 (appt. s, *m*-P*Ph*$_2$ A), 128.0 (d, $^3J_{C,P}$ 10 Hz, *m*-P*Ph*$_2$ B), 126.9 (s, *m*-B*Ph*$_2$ A), 125.9 (appt. d, *J* 5 Hz, *p*-B*Ph*$_2$ B), 125.3 (d, $^4J_{C,P}$ 7 Hz, *C*^{4}), 124.7 (s, *p*-B*Ph*$_2$ A), 114.2 (broad s, *ipso*-B*Ph*$_2$ B), 113.5 (broad s, *o*-B*Ph*$_2$ B), 83.7 (d, $^1J_{C,P}$ 45 Hz, *C*$^{1'}$), 82.7 (d, $^1J_{C,P}$ 51 Hz, *C*$^{1''}$), 76.3 (d, $^2J_{C,P}$ 13 Hz, *C*$^{2'/5'}$), 74.7 (d, $^2J_{C,P}$ 13 Hz, *C*$^{2''/5''}$), 74.5 (d, $^3J_{C,P}$ 8 Hz, *C*$^{5''/2''}$), 72.9 (d, $^3J_{C,P}$ 3 Hz, *C*$^{5'/2'}$), 71.5 (d, $^2J_{C,P}$ 7 Hz, *C*$^{3'/4'}$), 71.2 (d, $^3J_{C,P}$ 4 Hz, *C*$^{4''/3''}$), 70.1 (d, $^2J_{C,P}$ 6 Hz, *C*$^{3''/4''}$), 69.9 (d, $^3J_{C,P}$ 3 Hz, *C*$^{4'/3'}$), 37.1 (d, $^1J_{C,P}$ 26 Hz, *C*Me$_3$), 29.7 (d, $^2J_{C,P}$ 6 Hz, C*Me*$_3$). **^{31}P{^{1}H} NMR (C_6D_6, 243 MHz, 298 K):** δ 50.8 (d, $^1J_{P,Pt}$ 5651 Hz, $^2J_{P,P}$ 56 Hz, C_5H_4P(^{t}Bu)Ar), 28.5 (d, $^1J_{P,Pt}$ 4183 Hz, $^2J_{P,P}$ 56 Hz, C_5H_4PPh$_2$). **^{31}P{^{1}H} NMR (CD_2Cl_2, 203 MHz, 298 K):** δ 51.3 (d, $^1J_{P,Pt}$ 5657 Hz, $^2J_{P,P}$ 55 Hz, C_5H_4P(^{t}Bu)Ar), 28.4 (d, $^1J_{P,Pt}$ 4157 Hz, $^2J_{P,P}$ 55 Hz, C_5H_4PPh$_2$). **^{11}B NMR (CD_2Cl_2, 161 MHz, 298 K):** δ 21 (broad s, $\omega_{1/2}$ = 1400 Hz). **^{195}Pt{^{1}H} NMR (CD_2Cl_2, 128 MHz, 298 K):** δ –4934 (dd, ^1JPt,P 5654 Hz, ^1JPt,P 4138 Hz). **Elemental Analysis Calcd (%)** for $C_{45.8}H_{44.2}BFeP_2Pt$: C, 59.84, H, 4.96. Found: C, 59.93, H, 5.27.

***In situ* Generation of [Ni(μ-dba)(TXPB)] (31):** [Ni(cod)$_2$] (6.1 mg, 2.2×10^{-2} mmol) and TXPB (15 mg, 2.2×10^{-2} mmol) were dissolved in C_6D_6 (0.6 mL) in an NMR tube and left at room temperature for 2 hours. One equivalent of dba (5.2 mg, 2.2×10^{-2} mmol) was then added to the [Ni(TXPB)] solution, resulting in a colour change from cherry red to black with a slight red tinge. The reaction solution was left at room temperature for 30 minutes before NMR spectroscopy was utilized to determine successful coordination of dba to [Ni(TXPB)] had occurred. Key NMR data: **^{1}H NMR (C_6D_6, 500 Hz, 298 K):** δ 1.65 (s, 6H, C*Me*$_2$), 1.27, 1.03 (2×s, 18H, 2×C*Me*$_3$). **^{31}P{^{1}H} NMR (C_6D_6, 203 MHz, 298 K):** δ 34.1 (s). **^{11}B NMR (C_6D_6, 298 K, 161 MHz):** δ 5 ppm (broad s, $\omega_{1/2}$ ~ 1300 Hz).

"Ni(FcPPP)" (32): Toluene (10 mL) was condensed into a 50 mL round bottom flask containing [Ni(cod)$_2$] (50.4 mg, 0.183 mmol) and FcPPP (132 mg, 0.183 mmol) through the use of a dry ice/acetone bath, and the reaction was left to stir for three hours at room temperature. The ruby red reaction solution was evaporated to dryness *in vacuo* to yield a dark red oily residue. Hexamethyldisiloxane (20 mL) was added to the crude oil and the slurry was sonicated for 15 minutes, resulting in precipitation of a red/orange solid. The O(SiMe$_3$)$_2$ solution was filtered and the collected red/orange solid was washed with O(SiMe$_3$)$_2$ (10 mL) then dried *in vacuo*. Yield = 124 mg (87 %). **^{31}P{^{1}H} NMR (Toluene-d$_8$, 203 MHz, 298 K):** δ 59.8 (appt. t, $^2J_{P,P}$ 40 Hz), 55.1 (broad s, $\omega_{1/2}$ ~100 Hz), 53.0 (broad s, $\omega_{1/2}$ ~100 Hz), 40.3 (broad s, $\omega_{1/2}$ ~100 Hz), 21.9 (broad s, $\omega_{1/2}$ ~100 Hz), 21.3 (broad s, $\omega_{1/2}$ ~100 Hz), 19.0 (broad s, $\omega_{1/2}$ ~100 Hz), 17.7 (broad s, $\omega_{1/2}$ ~100 Hz). **Elemental Analysis Calcd (%)** for $C_{44}H_{41}FeNiP_3$: C, 67.99; H, 5.32%. Found: C, 67.97; H, 5.37%.

***rac*-[{Ni(FcPPP)}$_2$(μ-N$_2$)] (33):** "Ni(FcPPP)" (**32**) (118 mg, 0.151 mmol) was dissolved in a mixture of benzene (3 mL) and hexanes (10 mL) in a 50 mL Schlenk tube. The resulting solution was subjected to three freeze/pump/thaw cycles before the introduction of 1 atm of N_2. The Schlenk tube was sealed and the solution was maintained under N_2 at room temperature for 7 days, resulting in crystallization of *rac*-[{Ni(FcPPP)}$_2$(μ-N$_2$)] as

ruby red crystals. The mother liquors were decanted, and the remaining crystalline material was dried *in vacuo*. Yield = 76.7 mg (64 %). X-ray quality crystals of *rac*-[{Ni(FcPPP)}$_2$(μ-N$_2$)]·(C$_6$H$_6$)(C$_6$H$_{14}$) were obtained by slow diffusion of hexanes (~10 mL) into a solution of "Ni(FcPPP)" (~30 mg) in benzene (3 mL) at room temperature under an argon atmosphere. **^{1}H NMR (THF-d$_8$, 600 MHz, 298 K):** δ 8.13 (broad s, 2H, C*H*^{6}), 8.05 (t, $^3J_{H,H}$ 7 Hz, 4H, *o*-P*Ph*$_2^{Ar}$ A), 7.69–7.64 (broad m, 6H, C*H*^{3}, *o*-P*Ph*$_2^{Cp}$ A), 7.48–7.36 (m, 10H, C*H*^{4}, C*H*^{5}, *m*,*p*-P*Ph*$_2^{Ar}$ A), 6.97 (t, $^3J_{H,H}$ 7 Hz, 2H, *p*-P*Ph*$_2^{Cp}$ A), 6.85 (broad s, 4H, *o*-P*Ph*$_2^{Cp}$ B), 6.70 (t, $^3J_{H,H}$ 7 Hz, 2H, *p*-P*Ph*$_2^{Ar}$ B), 6.67–6.61 (m, 6H, *p*-P*Ph*$_2^{Cp}$ B, *o*-P*Ph*$_2^{Ar}$ B), 6.46 (t, $^3J_{H,H}$ 7 Hz, 4H, *m*-P*Ph*$_2^{Ar}$ B), 6.42 (t, $^3J_{H,H}$ 6 Hz, 4H, *m*-P*Ph*$_2^{Cp}$ A), 6.16 (broad s, 4H, *m*-P*Ph*$_2^{Cp}$ B), 4.77 (s, 2H, C*H*$^{2'/5'}$), 4.37 (s, 2H, C*H*$^{5'/2'}$), 4.12 (s, 2H, C*H*$^{3'/4'}$), 4.11 (s, 2H, C*H*$^{4'/3'}$), 3.95 (s, 2H, C*H*$^{3''/4''}$), 3.89 (s, 2H, C*H*$^{4''/3''}$), 3.38 (s, 2H, C*H*$^{2''/5''}$), 3.22 (s, 2H, C*H*$^{5''/2''}$), 1.50 (d, $^3J_{H,P}$ 13 Hz, 18H, C*Me*$_3$). **^{13}C NMR (THF-d$_8$, 151 MHz, 298 K):** δ 149.2 (dd, $^1J_{C,P}$ 49 Hz, $^2J_{C,P}$ 35 Hz, *C*$^{1/2}$), 145.0 (dd, $^1J_{C,P}$ 45 Hz, $^2J_{C,P}$ 29 Hz, *C*$^{1/2}$), 144.2–144.0 (m, *ipso*-P*Ph*$_2^{Ar}$ A), 141.8–141.5 (m, *ipso*-P*Ph*$_2^{Cp}$ A/B), 139.7–139.4 (m, *ipso*-P*Ph*$_2^{Cp}$ A/B), 138.0–137.7 (m, *ipso*-P*Ph*$_2^{Ar}$ B), 136.3 (d, $^2J_{C,P}$ 15 Hz, *o*-P*Ph*$_2^{Cp}$ A), 134.6 (d, $^2J_{C,P}$ 13 Hz, *C*^{3}), 134.4 (d, $^2J_{C,P}$ 16 Hz, *o*-P*Ph*$_2^{Ar}$ A), 133.3 (d, $^2J_{C,P}$ 11 Hz, *C*^{6}), 131.8 (d, $^2J_{C,P}$ 12 Hz, *o*-P*Ph*$_2^{Ar}$ B), 129.4 (s, *C*^{4}), 129.1 (s, *C*^{5}), 128.5 (d, $^3J_{C,P}$ 8 Hz, *m*-P*Ph*$_2^{Ar}$ A, *p*-P*Ph*$_2^{Cp}$ A), 128.3 (d, $^3J_{C,P}$ 8 Hz, *m*-P*Ph*$_2^{Cp}$ A), 127.9 (broad s, *o*/*m*-P*Ph*$_2^{Cp}$ B), 127.8 (s, *p*-P*Ph*$_2^{Ar}$ A), 127.6 (broad s, *o*/*m*-P*Ph*$_2^{Cp}$ B), 127.1 (d, $^3J_{C,P}$ 6 Hz, *m*-P*Ph*$_2^{Ar}$ B), 126.7 (s, *p*-P*Ph*$_2^{Cp}$ B), 126.2 (s, *p*-P*Ph*$_2^{Ar}$ B), 84.7 (dd, $^1J_{C,P}$ 35 Hz, $^3J_{C,P}$ 4 Hz, *C*$^{1''}$), 83.4 (m, *C*$^{1'}$), 75.9 (d, $^2J_{C,P}$ 24 Hz, *C*$^{2'/5'}$), 74.7 (d, $^2J_{C,P}$ 23 Hz, *C*$^{2''/5''}$), 73.3 (s, *C*$^{5''/2''}$), 72.8 (s, *C*$^{5'/2'}$), 72.4, 72.3 (2×s, *C*$^{3'/4'}$, *C*$^{3''/4''}$), 69.0 (s, *C*$^{4'/3'}$, *C*$^{4''/3''}$), 35.7 (s, *C*Me$_3$), 29.7 (d, $^2J_{C,P}$ 10 Hz, C*Me*$_3$). **^{31}P{^{1}H} NMR (THF-d$_8$, 203 MHz, 298 K):** δ 51.6 (broad d, $^2J_{P,P}$ ~ 84 Hz, C$_5$H$_4$*P*^{t}BuAr), 35.6 (broad dd, $^2J_{P,P}$ ~ 87 Hz, $^2J_{P,P}$ ~ 64 Hz, Ar*P*Ph$_2$), 19.2 (broad d, $^2J_{P,P}$ ~ 59 Hz, C$_5$H$_4$*P*Ph$_2$). Raman: ν(N≡N) = 2006 cm^{-1}. **Elemental Analysis Calcd (%)** for C$_{88}$H$_{82}$Fe$_2$N$_2$Ni$_2$P$_6$: C, 66.78; H, 5.22; N, 1.78%. Found: C, 66.44; H, 5.07; N, 1.72%.

[Pd(η^2-dba)(FcPPP)] (34): Toluene (25 mL) was condensed into a 50 mL round bottom flask containing [$Pd_2(dba)_3$] (235 mg, 0.257 mmol) and FcPPP (369 mg, 0.513 mmol) through the use of a dry ice/acetone bath, and the reaction was left to stir overnight at room temperature. The black/yellow reaction solution was filtered to remove any unreacted [$Pd_2(dba)_3$], the residue was washed with toluene (2 × 10 mL), and the resulting clear, blood orange filtrate was evaporated to dryness *in vacuo* to afford a red/orange, oily residue. Hexanes (30 mL) were added to the crude oil and the resulting mixture was sonicated for 15 minutes, allowing for [Pd(η^2-dba)(FcPPP)] to precipitate from solution as a bright orange powder. The hexanes solution was filtered and the collected product was washed with hexanes (3 × 10 mL) then dried *in vacuo*. Yield = 412 mg (76 %). X-ray quality crystals of [Pd(η^2-dba)(FcPPP)]·CH_2Cl_2 were obtained by slow diffusion of hexanes (~10 mL) into a solution of [Pd(η^2-dba)(FcPPP)] (~30 mg) in CH_2Cl_2 (~3 mL) at –30 °C. **^{31}P{^{1}H} NMR (C_6D_6, 203 MHz, 298 K):** δ 60.2 (broad s, $\omega_{1/2}$ ~190 Hz), 57.3 (broad s, $\omega_{1/2}$ ~190 Hz), 55.7 (broad s, $\omega_{1/2}$ ~190 Hz), 38.9 (broad s, $\omega_{1/2}$ ~190 Hz), –16.7 (broad s, $\omega_{1/2}$ ~110 Hz). **^{1}H NMR (Toluene-d_8, 500 MHz, 230 K; selected data):** δ 1.06 (d, $^3J_{H,P}$ 12 Hz, C*Me*$_3$), 0.99 (d, $^3J_{H,P}$ 14 Hz, C*Me*$_3$), 0.69 (d, $^3J_{H,P}$ 15 Hz, C*Me*$_3$), 0.40 (d, $^3J_{H,P}$ 15 Hz, C*Me*$_3$). **Elemental Analysis Calcd (%)** for $C_{61}H_{55}FeOP_3Pd$: C, 69.17; H, 5.23%. Found: C, 69.07; H, 5.45%.

***In situ* generation of [Ni(η^2-dba)(FcPPP)]: Method A:** "Ni(FcPPP)" (**32**) (12 mg, 1.5×10^{-2} mmol) and dba (3.6 mg, 1.5×10^{-2} mmol) were dissolved in C_6D_6 (0.6 mL) in an NMR tube at room temperature, causing the previously orange/red solution to become cherry red. The NMR scale reaction was maintained at room temperature for 2 hours. **Method B:** [{Ni(FcPPP)}$_2$(μ-N_2)] (**33**) (7.9 mg, 5.0×10^{-3} mmol) and dba (2.3 mg, 9.8×10^{-3} mmol) were dissolved in C_6D_6 (0.6 mL) in an NMR tube at room temperature. The NMR scale reaction was maintained at room temperature for 1 hour. Key NMR data: **^{1}H NMR (C_6D_6, 500 MHz, 298 K):** δ 7.82 (s), 7.71 (s), 7.59 (s), 7.48 (broad s), 7.37 (broad s), 7.27–7.24 (m), 7.05 (s), 7.02 (s), 6.94–6.88 (m), 6.69 (broad s), 5.30 (s), 4.91 (s), 4.79 (s), 4.30 (s), 4.26 (s), 4.20 (s), 4.13 (s), 3.97 (s), 3.59 (s), 3.55 (s), 3.37 (s), 0.95

(d, $^{3}J_{H,P}$ 14 Hz, C*Me*$_3$), 0.71 (d, $^{3}J_{H,P}$ 14 Hz, C*Me*$_3$). **^{31}P{^{1}H} NMR (C_6D_6, 203 MHz, 298 K):** δ 65.4 (d, $^{2}J_{P,P}$ 54 Hz, $C_5H_4P^t$BuAr), 50.2 (d, $^{2}J_{P,P}$ 54 Hz, Ar*P*Ph$_2$), –16.7, –16.9 (2×s, C_5H_4*P*Ph$_2$).

[Pt(CO)(FcPPB)] (35): A solution of [Pt(FcPPB)] · 0.3hexanes (**30**·0.3hexanes) (64.7 mg, 7.04×10^{-2} mmol) in CH_2Cl_2 (5 mL) was subject to three freeze/pump/thaw cycles before being cooled to –140 °C, at which point CO was added. The reaction mixture was stirred for one hour at room temperature before being evaporated to dryness *in vacuo* to yield a brown/yellow oily residue. Hexanes (20 mL) were added to the crude product and the resulting solution was sonicated for 15 minutes, after which point the resulting solution was evaporated to dryness *in vacuo* to yield a mustard yellow solid. Yield = 38 mg (58 %). X-ray quality crystals of [Pt(CO)(FcPPB)]·2CH_2Cl_2 were obtained by slow diffusion of hexanes (~10 mL) into a solution of [Pt(CO)(FcPPB)] in CH_2Cl_2 (~3 mL) at –30 °C. **^{1}H NMR (C_6D_6, 600 MHz, 298 K):** δ 8.12 (d, $^{3}J_{H,H}$ 7 Hz, 2H, *o*-B*Ph*$_2$ A), 7.83–7.80 (m, 2H, *o*-P*Ph*$_2$ A), 7.66 (d, $^{3}J_{H,P}$ 8 Hz, 1H, C*H*^{6}), 7.47 (t, $^{3}J_{H,H}$ 8 Hz, 2H, *m*-B*Ph*$_2$ A), 7.35 (t, $^{3}J_{H,H}$ 7 Hz, 1H, C*H*^{3}), 7.30–7.28 (m, 3H, *o*-B*Ph*$_2$ B, *p*-B*Ph*$_2$ A), 7.18–7.12 (m, 3H, C*H*^{5}, *o*-P*Ph*$_2$ B), 7.08–7.05 (m, 1H, C*H*^{4}), 7.04–7.00 (m, 3H, *m*,*p*-P*Ph*$_2$ A), 6.89–6.83 (m, 4H, *p*-B*Ph*$_2$ B, *m*,*p*-P*Ph*$_2$ B), 6.64 (t, $^{3}J_{H,H}$ 8 Hz, 2H, *m*-B*Ph*$_2$ B), 4.51 (s, 1H, C*H*$^{5'/2'}$), 4.49 (d, $^{3}J_{H,H}$ 1 Hz, 1H, C*H*$^{2'/5'}$), 4.03–4.01 (m, 1H, C*H*$^{2''/5''}$), 4.01–4.00 (m, 1H, C*H*$^{5''/2''}$), 3.91 (sextet, $^{3}J_{H,H}$ 1 Hz, 1H, C*H*$^{3''/4''}$), 3.85 (sextet, $^{3}J_{H,H}$ 1 Hz, 1H, C*H*$^{4'/3'}$), 3.81 (q, $^{3}J_{H,H}$ 2 Hz, 1H, C*H*$^{3'/4'}$), 3.73 (sextet, $^{3}J_{H,H}$ 1 Hz, 1H, C*H*$^{4''/3''}$), 1.31 (d, $^{3}J_{H,P}$ 15 Hz, 9H, C*Me*$_3$). **^{13}C{^{1}H} NMR (C_6D_6, 151 MHz, 298 K):** δ 193.6 (dd, $^{2}J_{C,P}$ 87 Hz, $^{2}J_{C,P}$ 9 Hz, Pt-*C*O), 165.5 (broad d, $^{2}J_{C,P}$ 45 Hz, *C*^{2}), 153.0 (broad s, *ipso*-B*Ph*$_2$ A), 140.1 (s, *o*-B*Ph*$_2$ B), 138.9 (dd, $^{1}J_{C,P}$ 49 Hz, $^{3}J_{C,P}$ 11 Hz, *C*^{1}), 138.4 (d, $^{1}J_{C,P}$ 32 Hz, *ipso*-P*Ph*$_2$ B), 136.9 (s, *o*-B*Ph*$_2$ A), 136.2 (d, $^{1}J_{C,P}$ 36 Hz, *ipso*-P*Ph*$_2$ A), 135.2 (d, $^{2}J_{C,P}$ 15 Hz, *o*-P*Ph*$_2$ A), 134.5 (d, $^{2}J_{C,P}$ 26 Hz, *C*^{6}), 132.9 (d, $^{2}J_{C,P}$ 14 Hz, *o*-P*Ph*$_2$ B), 130.9 (s, *C*^{3}), 130.5 (d, $^{2}J_{C,P}$ 9 Hz, *m*-P*Ph*$_2$ A), 130.3 (broad s, *ipso*-B*Ph*$_2$ B), 129.0 (s, *p*-P*Ph*$_2$ B), 128.2 (s, *C*^{5}, *p*-P*Ph*$_2$ A), 128.1 (s, *p*-B*Ph*$_2$ B), 127.7 (d, $^{3}J_{C,P}$ 10 Hz, *m*-P*Ph*$_2$ B), 127.3 (s, *m*-B*Ph*$_2$ A), 126.0 (s, *m*-B*Ph*$_2$ B), 125.7 (s, *p*-B*Ph*$_2$ A), 125.3 (d, $^{4}J_{C,P}$ 7 Hz, *C*^{4}), 86.9 (dd, $^{1}J_{C,P}$ 36 Hz, $^{3}J_{C,P}$ 6 Hz, *C*$^{1'}$), 86.0

(d, $^{1}J_{C,P}$ 41 Hz, *C*$^{1''}$), 75.4 (d, $^{2}J_{C,P}$ 7 Hz, *C*$^{5'/2'}$), 75.0 (s, *C*$^{3''/4''}$), 74.8 (d, $^{2}J_{C,P}$ 20 Hz, *C*$^{2''/5''}$), 72.1 (d, $^{2}J_{C,P}$ 8 Hz, *C*$^{5''/2''}$), 71.5 (d, $^{2}J_{C,P}$ 7 Hz, *C*$^{2'/5'}$), 70.1 (d, $^{3}J_{C,P}$ 4 Hz, *C*$^{3'/4'}$), 69.2 (s, *C*$^{4''/3''}$), 69.0 (d, $^{3}J_{C,P}$ 4 Hz, *C*$^{4'/3'}$), 37.9 (d, $^{1}J_{C,P}$ 31 Hz, *C*Me$_3$), 29.4 (d, $^{2}J_{C,P}$ 6 Hz, C*Me*$_3$). **^{31}P{^{1}H} NMR (C_6D_6, 203 MHz, 298 K):** δ 59.4 (s, $^{1}J_{P,Pt}$ 4884 Hz, $C_5H_4P(^{t}Bu)Ar$), 22.8 (s, $^{1}J_{Pt,P}$ 2343 Hz, $C_5H_4PPh_2$). **^{11}B NMR (C_6D_6, 161 MHz, 298 K):** δ 21 (broad s, $\omega_{1/2}$ = 1550 Hz). **^{11}B NMR (CD_2Cl_2, 161 MHz, 298 K):** δ 19 (broad s, $\omega_{1/2}$ = 1550 Hz). **^{195}Pt{^{1}H} NMR (CD_2Cl_2, 128 MHz, 298 K):** *δ* –4422 (dd, $^{1}J_{Pt,P}$ 4820 Hz, $^{1}J_{Pt,P}$ 2223 Hz). **IR:** ν(CO) = 1994, 1968 cm^{-1} (nujol); 1982 cm^{-1} (CH_2Cl_2). **Elemental Analysis Calcd (%)** for $C_{45}H_{41}BFeOP_2Pt$: C, 58.65, H, 4.49. Found: C, 57.94, H, 4.68.

[Pt(CNXyl)(FcPPB)] (36): A solution of XylNC (15.4 mg, 0.118 mmol) in CH_2Cl_2 (3 mL) was added dropwise at room temperature to a solution of [Pt(FcPPB)]·0.3hexanes (**30**·0.3hexanes) (105 mg, 0.114 mmol) in CH_2Cl_2 (10 mL). The transparent, orange/red solution was left to stir for one hour at room temperature before being evaporated to dryness *in vacuo*. Hexanes (20 mL) were added to the remaining orange/red oily residue and the resulting solution was sonicated for 15 minutes, which resulted in the precipitation of [Pt(CNXyl)(FcPPB)] as a yellow powder. The hexanes solution was filtered and the collected product was washed with hexanes (2 × 10 mL). Yield = 101 mg (87 %). X-ray quality crystals of [Pt(CNXyl)(FcPPB)]·CH_2Cl_2 were obtained by slow diffusion of hexanes (~10 mL) into a solution of [Pt(CNXyl)(FcPPB)] in CH_2Cl_2 (~3 mL) at –30 °C. **^{1}H NMR (C_6D_6, 600 MHz, 298 K):** δ 8.26 (d, $^{3}J_{H,H}$ 7 Hz, 2H, *o*-B*Ph*$_2$ A), 8.01 (dt, $^{3}J_{H,P}$ 10 Hz, $^{3}J_{H,H}$ 1 Hz, 2H, *o*-P*Ph*$_2$ A), 7.73 (d, $^{3}J_{H,P}$ 8 Hz, 1H, C*H*^{6}), 7.54 (d, $^{3}J_{H,H}$ 7 Hz, 2H, *o*-B*Ph*$_2$ B), 7.30 (t, $^{3}J_{H,H}$ 8 Hz, 2H, *m*-B*Ph*$_2$ A), 7.22–7.13 (m, 6H, C*H*^{3}, C*H*^{5}, *o*-P*Ph*$_2$ B, *m*-B*Ph*$_2$ B), 7.08–7.03 (m, 5H, C*H*^{4}, *m*-P*Ph*$_2$ A, *p*-B*Ph*$_2$ A and B), 7.00–6.96 (m, 3H, *m*-P*Ph*$_2$ B, *p*-P*Ph*$_2$ A), 6.91 (tq, $^{3}J_{H,H}$ 7 Hz, $^{4}J_{H,H}$ 1 Hz, 1H, *p*-P*Ph*$_2$ B), 6.65 (t, $^{3}J_{H,H}$ 8 Hz, 1H, *p*-Xyl), 6.55 (d, $^{3}J_{H,H}$ 8 Hz, 2H, *m*-Xyl), 4.79 (septet, $^{3}J_{H,H}$ 1 Hz, 1H, C*H*$^{2'/5'}$), 4.52 (s, 1H, C*H*$^{5'/2'}$), 4.22 (sextet, $^{3}J_{H,H}$ 1 Hz, 1H, C*H*$^{5''/2''}$), 3.95 (t, $^{3}J_{H,H}$ 2 Hz, 1H, C*H*$^{3'/4'}$), 3.89 (sextet, $^{3}J_{H,H}$ 1 Hz, 1H, C*H*$^{4''/3''}$), 3.87 (sextet, $^{3}J_{H,H}$ 1 Hz, 1H, C*H*$^{4'/3'}$), 3.81 (sextet, $^{3}J_{H,H}$ 1 Hz, 1H, C*H*$^{3''/4''}$), 3.77 (septet, $^{3}J_{H,H}$ 1 Hz, 1H, C*H*$^{2''/5''}$), 1.89 (s, 6H, Xyl-C*H*$_3$), 1.47 (d,

$^{3}J_{H,P}$ 15 Hz, 9H, C*Me*$_3$). **^{13}C{^{1}H} NMR (C_6D_6, 151 MHz, 298 K):** δ 170.3 (broad d, $^{2}J_{C,P}$ 58 Hz, *C*^{2}), 163.9 (d, $^{1}J_{C,P}$ 112 Hz, *C*^{1}), 158.7 (broad s, *ipso*-B*Ph*$_2$ A), 149.5 (broad s, *ipso*-B*Ph*$_2$ B), 138.6 (d, $^{1}J_{C,P}$ 30 Hz, *ipso*-P*Ph*$_2$ B), 138.0 (s, *o*-B*Ph*$_2$ B), 137.0 (s, *o*-B*Ph*$_2$ A), 136.6 (d, $^{1}J_{C,P}$ 27 Hz, *ipso*-P*Ph*$_2$ A), 135.6 (d, $^{2}J_{C,P}$ 15 Hz, *o*-PPh$_2$ A), 134.7 (dd, $^{2}J_{C,P}$ 27 Hz, $^{4}J_{C,P}$ 5 Hz, *C*^{6}), 134.1 (s, *o*-Xyl), 133.4 (d, $^{2}J_{C,P}$ 15 Hz, *o*-P*Ph*$_2$ B), 131.1 (s, *C*^{5}), 130.4 (s, *C*^{3}), 130.4 (s, *p*-P*Ph*$_2$ A), 129.1 (s, *p*-P*Ph*$_2$ B), 128.8 (s, *ipso*-Xyl), 128.2 (s, *C*^{4}), 128.1 (d, $^{3}J_{C,P}$ 9 Hz, *m*-PPh$_2$ A), 127.9 (d, $^{3}J_{C,P}$ 10 Hz, *m*-P*Ph*$_2$ B), 127.6 (s, *m*-Xyl), 127.4 (s, *p*-Xyl), 126.8 (s, *m*-B*Ph*$_2$ A), 126.6 (s, *m*-B*Ph*$_2$ B), 124.6 (s, *p*-B*Ph*$_2$ B), 124.0 (s, *p*-B*Ph*$_2$ A), 86.1 (d, $^{1}J_{C,P}$ 36 Hz, *C*$^{1''}$), 85.7 (d, $^{1}J_{C,P}$ 8 Hz, *C*$^{1'}$), 75.4 (d, $^{2}J_{C,P}$ 13 Hz, *C*$^{2''/5''}$), 75.0 (d, $^{2}J_{C,P}$ 13 Hz, *C*$^{2'/5'}$), 74.4 (d, $^{3}J_{C,P}$ 5 Hz, *C*$^{5''/2''}$), 73.4 (s, *C*$^{5'/2'}$), 71.0 (d, $^{2}J_{C,P}$ 7 Hz, *C*$^{3'/4'}$), 70.2 (d, $^{2}J_{C,P}$ 5 Hz, *C*$^{3''/4''}$), 69.8 (d, $^{3}J_{C,P}$ 2 Hz, *C*$^{4''/3''}$), 69.7 (d, $^{3}J_{C,P}$ 2 Hz, *C*$^{4'/3'}$), 36.8 (d, $^{1}J_{C,P}$ 34 Hz, *C*Me$_3$), 30.4 (d, $^{2}J_{C,P}$ 5 Hz, C*Me*$_3$), 18.5 (s, Xyl-*C*H$_3$). **^{31}P{^{1}H} NMR (C_6D_6, 203 MHz, 298 K):** δ 62.7 (d, $^{1}J_{P,Pt}$ 4549 Hz, $^{2}J_{P,P}$ 11 Hz, $C_5H_4P(^{t}Bu)Ar$), 21.8 (d, $^{1}J_{Pt,P}$ 1381 Hz, $^{2}J_{P,P}$ 11 Hz, $C_5H_4PPh_2$). **^{11}B NMR (C_6D_6, 161 MHz, 298 K):** δ 13 (broad s, $\omega_{1/2}$ = 800 Hz). **^{11}B NMR (CD_2Cl_2, 161 MHz, 298 K):** δ 10 (broad s, $\omega_{1/2}$ = 800 Hz). **^{195}Pt{^{1}H} NMR (C_6D_6, 128 MHz, 298 K):** δ –4486 (broad dd, $^{1}J_{Pt,P}$ 4632 Hz, $^{1}J_{Pt,P}$ 1430 Hz, $\omega_{1/2}$ = 300 Hz). **IR:** ν(CN) = 2122 cm^{-1} (nujol); 2128 cm^{-1} (CH_2Cl_2). **Elemental Analysis Calcd (%)** for $C_{53}H_{50}BFeNP_2Pt$: C, 62.12; H, 4.92; N, 1.37. Found: C, 62.52, H, 5.07, N, 1.20.

[PtH(μ-H)(FcPPB)] (37): A solution of [Pt(FcPPB)] · 0.3hexanes (**30**·0.3hexanes) (25.0 mg, 2.72×10^{-2} mmol) in C_6D_6 (1 mL) was subject to three freeze/pump/thaw cycles; H_2 was then added to the reaction mixture at room temperature, which resulted in the *in situ* generation of [PtH(μ-H)(FcPPB)]. **^{1}H NMR (C_6D_6, 600 MHz, 298 K):** δ 8.21 (d, $^{3}J_{H,H}$ 7 Hz, 2H, *o*-B*Ph*$_2$ A), 8.09 (dd, $^{3}J_{H,P}$ 11 Hz, $^{3}J_{H,H}$ 7 Hz, 2H, *o*-P*Ph*$_2$ A), 7.72 (d, $^{3}J_{H,H}$ 7 Hz, 1H, C*H*^{6}), 7.61 (d, $^{3}J_{H,H}$ 7 Hz, 2H, *o*-B*Ph*$_2$ B), 7.48 (t, $^{3}J_{H,H}$ 7 Hz, 2H, *m*-B*Ph*$_2$ A), 7.31 (t, $^{3}J_{H,H}$ 7 Hz, 1H, *p*-B*Ph*$_2$ A), 7.29–7.24 (m, 3H, *m,p*-B*Ph*$_2$ B), 7.08 (t, $^{3}J_{H,H}$ 7 Hz, 1H, C*H*^{5}), 7.04 (t, $^{3}J_{H,H}$ 7 Hz, 1H, C*H*^{4}), 7.01–6.95 (m, 6H, *m,p*-P*Ph*$_2$ A and B), 6.91 (t, $^{3}J_{H,H}$ 7 Hz, 1H, C*H*^{3}), 6.87 (dd, $^{3}J_{H,P}$ 13 Hz, $^{3}J_{H,H}$ 7 Hz, 2H, *o*-P*Ph*$_2$ B), 4.76 (s, 1H, C*H*$^{2'/5'}$), 4.45 (s,

1H, C*H*$^{2''/5''}$), 4.37 (s, 1H, C*H*$^{5'/2'}$), 3.96 (s, 1H, C*H*$^{3''/4''}$), 3.94 (s, 1H, C*H*$^{3'/4'}$), 3.75 (s, 1H, C*H*$^{4'/3'}$), 3.59 (s, 1H, C*H*$^{4''/3''}$), 3.56 (s, 1H, C*H*$^{5''/2''}$), 1.30 (d, $^{3}J_{H,P}$ 14 Hz, 9H, C*Me*$_3$), –2.76 (dd, $^{1}J_{H,Pt}$ 792 Hz, $^{2}J_{H,P}$ 95 Hz, $^{2}J_{H,P}$ 10 Hz, 1H, Pt–*H*–B), –5.19 (ddd, $^{1}J_{H,Pt}$ 905 Hz, $^{2}J_{H,P}$ 177 Hz, $^{2}J_{H,P}$ 24 Hz, $^{2}J_{H,H}$ 2 Hz, 1H, Pt–*H*). **^{13}C{^{1}H} NMR (C_6D_6, 151 MHz, 298 K):** δ 165.0 (broad s, *C*^{2}), 154.6 (broad s, *ipso*-B*Ph*$_2$ A), 148.8 (broad s, *ipso*-B*Ph*$_2$ B), 138.5 (d, $^{1}J_{C,P}$ 48 Hz, *C*^{1}), 138.5 (s, *o*-B*Ph*$_2$ B), 136.6 (s, *o*-B*Ph*$_2$ A), 135.8 (d, $^{2}J_{C,P}$ 13 Hz, *o*-P*Ph*$_2$ A), 135.8 (d, $^{1}J_{C,P}$ 60 Hz, *ipso*-P*Ph*$_2$ A), 135.0 (d, $^{2}J_{C,P}$ 18 Hz, *C*^{6}), 134.1 (d, $^{1}J_{C,P}$ 60 Hz, *ipso*-P*Ph*$_2$ B), 133.6 (d, $^{2}J_{C,P}$ 14 Hz, *o*-P*Ph*$_2$ B), 132.5 (s, *C*^{4}), 131.2 (s, *p*-P*Ph*$_2$ A), 130.4 (s, *C*^{5}), 130.1 (s, *p*-P*Ph*$_2$ B), 128.1 (d, $^{3}J_{C,P}$ 11 Hz, *m*-P*Ph*$_2$ A), 127.8 (d, $^{3}J_{C,P}$ 12 Hz, *m*-P*Ph*$_2$ B), 127.6 (s, *m*-B*Ph*$_2$ A), 127.1 (s, *m*-B*Ph*$_2$ B), 125.7 (s, *p*-B*Ph*$_2$ A and B), 124.9 (d, $^{3}J_{C,P}$ 6 Hz, *C*^{3}), 88.3 (dd, $^{1}J_{C,P}$ 58 Hz, $^{3}J_{C,P}$ 7 Hz, *C*$^{1''}$), 80.7 (d, $^{1}J_{C,P}$ 40 Hz, *C*$^{1'}$), 77.1 (d, $^{3}J_{C,P}$ 10 Hz, *C*$^{5''/2''}$), 75.0 (d, $^{3}J_{C,P}$ 10 Hz, *C*$^{2''/5''}$), 74.8 (s, *C*$^{2'/5'}$), 74.7 (s, *C*$^{5'/2'}$), 73.3 (d, $^{2}J_{C,P}$ 8 Hz, *C*$^{3'/4'}$), 70.4 (d, $^{2}J_{C,P}$ 6 Hz, *C*$^{3''/4''}$), 69.6 (s, *C*$^{4'/3'}$), 68.7 (d, $^{2}J_{C,P}$ 6 Hz, *C*$^{4''/3''}$), 35.0 (d, $^{1}J_{C,P}$ 30 Hz, *C*Me$_3$), 29.7 (d, $^{2}J_{C,P}$ 5 Hz, C*Me*$_3$). **^{31}P{^{1}H} NMR (C_6D_6, 242 MHz, 298 K):** δ 64.3 (dd, $^{1}J_{P,Pt}$ 2123 Hz, $^{2}J_{P,H}$ 19 Hz, $^{2}J_{P,P}$ 10 Hz, $C_5H_4P(^{t}Bu)Ar$), 24.1 (d, $^{1}J_{Pt,P}$ 3721 Hz, $^{2}J_{P,P}$ 10 Hz, $C_5H_4PPh_2$). **^{11}B NMR (C_6D_6, 161 MHz, 298 K):** δ 6 (broad s, $\omega_{1/2}$ = 1200 Hz). **^{11}B NMR (CD_2Cl_2, 161 MHz, 298 K):** δ 5 (broad s, $\omega_{1/2}$ = 1200 Hz). **^{195}Pt{^{1}H} NMR (CD_2Cl_2, 128 MHz, 298 K):** δ –4980 (dd, $^{1}J_{Pt,P}$ 3753 Hz, $^{1}J_{Pt,P}$ 2130 Hz). **IR (CH_2Cl_2):** ν(Pt–H) = 2020 cm^{-1} (broad); ν(Pt–H–B) = 1822 cm^{-1} (very broad). Elemental analysis could not be obtained due to the instability of [PtH(μ-H)(FcPPB)] under dynamic vacuum.

[PtD(μ-D)(FcPPB)] (37-D): This compound was generated by the same method as described for compound **37**, however using D_2 instead of H_2. IR (CH_2Cl_2): ν(Pt–D) = 1478 cm^{-1} (broad). The Pt–D–B stretch was not located due to broadness combined with spectral overlap [predicted 1428 cm^{-1} (Pt–D) and 1288 cm^{-1} (Pt–D–B) by Hooke's Law].

Spectroscopic data for [Pt(C_2Ph)(μ-H)(FcPPB)] (38): NMR data was collected via *in situ* generation of compound **38**; IR data was collected following evaporation of the

reaction solvent *in vacuo*, thus isolating a sample that contained compounds **38** and **39A** in an approximate 1:1 ratio. The IR data was collected in nujol. **^{1}H NMR (C_6D_6, 500 MHz, 298 K):** δ 8.40 (q, $^{3}J_{H,P}$ 11 Hz, $^{3}J_{H,H}$ 8 Hz, 2H, phenyl-C*H*), 7.80 (d, $^{3}J_{H,H}$ 7 Hz, 2H, phenyl-C*H*), 7.75 (d, $^{3}J_{H,H}$ 7 Hz, 1H, phenyl-C*H*), 7.53–7.49 (m, 3H, phenyl-C*H*), 7.34–7.30 (m, 5 H, phenyl-C*H*), 7.01–6.96 (m, 6H, phenyl-C*H*), 6.85–6.84 (m, 4H, phenyl-C*H*), 4.88 (s, 1H, C_5H_4), 4.33 (s, 1H, C_5H_4), 4.27 (s, 1H, C_5H_4), 3.96 (s, 1H, C_5H_4), 3.85 (s, 1H, C_5H_4), 3.76 (s, 1H, C_5H_4), 3.71 (s, 1H, C_5H_4), 3.55 (s, 1H, C_5H_4), 1.29 (d, $^{3}J_{H,P}$ 15 Hz, 9H, C*Me*$_3$), –3.69 (dd, $^{1}J_{H,Pt}$ 760 Hz, $^{2}J_{H,P}$ 115 Hz, $^{2}J_{H,P}$ 12 Hz, 1H, Pt–*H*–B). **^{31}P{^{1}H} NMR (C_6D_6, 203 MHz, 298 K):** δ 62.9 (d, $^{1}J_{P,Pt}$ 2594 Hz, $^{2}J_{P,P}$ 12 Hz, $C_5H_4P(^{t}Bu)Ar$), 27.8 (d, $^{1}J_{Pt,P}$ 3252 Hz, $^{2}J_{P,P}$ 12 Hz, $C_5H_4PPh_2$). **^{11}B NMR (C_6D_6, 161 MHz, 298 K):** δ 11 (broad s, $\omega_{1/2}$ ~ 1500 Hz). **IR:** ν(C≡C) = 2126 cm^{-1}(nujol).

[Pt(FcPPB')] (39A/39B): A solution of [Pt(FcPPB)] · 0.3hexanes (**30**·0.3hexanes) (78.9 mg, 8.58×10^{-2} mmol) and PhC_2H (9.0 mg, 8.81×10^{-2} mmol) in benzene (10 mL) was allowed to stir for 6 days at room temperature. The reaction mixture was then evaporated to dryness *in vacuo* to yield a yellow/brown oily residue. Hexanes (20 mL) were added to the crude product and the resulting solution was sonicated for 15 minutes, after which point the resulting solution was evaporated to dryness *in vacuo* to yield a beige solid, which consisted of [Pt(FcPPB')] (Isomers A and B) in a 45:55 ratio. Yield = 65 mg (76 %). Single crystals of [Pt(FcPPB')] (Isomer A)·4C_6H_6 were obtained by dissolving [Pt(FcPPB')] (Isomers A and B) in benzene/hexanes and cooling to –30 °C. **NMR data for [Pt(FcPPB')] (Isomer A)**: **^{1}H NMR (C_6D_6, 600 MHz, 298 K):** δ 8.32 (d, $^{3}J_{H,H}$ 8 Hz, 2H, *o*-B*Ph*), 8.11 (dd, $^{3}J_{H,P}$ 11 Hz, $^{3}J_{H,H}$ 8 Hz, 2H, *o*-P*Ph*$_2$ A), 7.72 (d, $^{3}J_{H,H}$ 8 Hz, 1H, C*H*^{6}), 7.51 (t, $^{3}J_{H,H}$ 8 Hz, 2H, *m*-B*Ph*), 7.32 (t, $^{3}J_{H,H}$ 7 Hz, 1H, *p*-B*Ph*), 7.22 (dd, $^{3}J_{H,P}$ 11 Hz, $^{3}J_{H,H}$ 8 Hz, 2H, *o*-P*Ph*$_2$ B), 7.14 (d, $^{3}J_{H,H}$ 8 Hz, 2H, *o*-*Ph*$^{\alpha}$), 7.08–7.03 (m, 3H, C*H*^{5}, *m*-P*Ph*$_2$ A), 6.98 (dt, $^{3}J_{H,H}$ 7 Hz, $^{5}J_{H,P}$ 1 Hz, 1H, *p*-P*Ph*$_2$ A), 6.91–6.87 (m, 6H, C*H*^{4}, *m*,*p*-*Ph*$^{\alpha}$, *o*-*Ph*$^{\beta}$), 6.78 (t, $^{3}J_{H,H}$ 7 Hz, 1H, C*H*^{3}), 6.63 (dt, $^{3}J_{H,H}$ 7 Hz, $^{5}J_{H,P}$ 1 Hz, 1H, *p*-P*Ph*$_2$ B), 6.60–6.56 (m, 3H, *m*,*p*-*Ph*$^{\beta}$), 6.54 (dt, $^{3}J_{H,H}$ 8 Hz, $^{4}J_{H,P}$ 2 Hz, 2H, *m*-P*Ph*$_2$ B), 5.86 (dd, $^{2}J_{H,Pt}$ 46 Hz, $^{3}J_{H,P}$ 10 Hz, $^{3}J_{H,P}$ 5 Hz, 1H, vinylC$^{\beta}$–*H*), 4.99 (s, 1H, C*H*$^{2'/5'}$), 4.65 (s, 1H,

C*H*$^{2''/5''}$), 4.45 (s, 1H, C*H*$^{5'/2'}$), 4.43 (s, 1H, C*H*$^{5''/2''}$), 4.05 (s, 1H, C*H*$^{3'/4'}$), 4.04 (s, 1H, C*H*$^{4''/3''}$), 4.03 (s, 1H, C*H*$^{3''/4''}$), 3.91 (s, 1H, C*H*$^{4'/3'}$), 0.97 (d, $^{3}J_{H,P}$ 15 Hz, 9H, C*Me*$_3$). **^{13}C{^{1}H} NMR (C_6D_6, 151 MHz, 298 K):** δ 165.7 (broad s, *C*^{2}), 151.4 (broad s, *ipso*-B*Ph*), 147.4 (d, $^{1}J_{C,P}$ 46 Hz, *C*^{1}), 145.9 (d, $^{3}J_{C,P}$ 3 Hz, *ipso*-*Ph*$^{\alpha}$), 142.7 (s, *ipso*-*Ph*$^{\beta}$), 138.6 (d, $^{1}J_{C,P}$ 44 Hz, *ipso*-P*Ph*$_2$ A), 135.6 (d, $^{2}J_{C,P}$ 15 Hz, *o*-P*Ph*$_2$ A), 134.6 (appt. d, *J* 27 Hz, C^{6}, *ipso*-P*Ph*$_2$ B), 134.2 (s, *o*-B*Ph*), 132.7 (s, *p*-*Ph*$^{\alpha}$), 131.5 (s, *o*-*Ph*$^{\beta}$), 131.4 (d, $^{2}J_{C,P}$ 13 Hz, *o*-P*Ph*$_2$ B), 130.6 (s, *p*-P*Ph*$_2$ A, *o*-*Ph*$^{\alpha}$), 129.7 (s, *C*^{5}), 128.4 (s, *o*-*Ph*$^{\alpha}$), 128.3 (d, $^{3}J_{C,P}$ 11 Hz, *m*-P*Ph*$_2$ A), 128.2 (s, *p*-P*Ph*$_2$ B), 127.6 (d, $^{3}J_{C,P}$ 10 Hz, *m*-P*Ph*$_2$ B), 127.3 (s, *m*-B*Ph*), 126.7 (s, *m*-*Ph*$^{\beta}$), 126.6 (s, *m*-*Ph*$^{\alpha}$), 125.7 (s, *p*-B*Ph*), 124.7 (d, $^{4}J_{C,P}$ 6 Hz, *C*^{4}), 124.3 (s, *p*-*Ph*$^{\beta}$), 123.7 (s, *C*^{3}), 114.0 (broad s, vinyl*C*$^{\alpha}$), 85.9 (d, $^{1}J_{C,P}$ 51 Hz, *C*$^{1''}$), 82.4 (d, $^{1}J_{C,P}$ 40 Hz, *C*$^{1'}$), 77.7 (dd, $^{2}J_{C,P}$ 34 Hz, $^{2}J_{C,P}$ 4 Hz, vinyl*C*$^{\beta}$), 75.0 (d, $^{2}J_{C,P}$ 13 Hz, *C*$^{2'/5'}$), 74.6 (d, $^{2}J_{C,P}$ 6 Hz, *C*$^{5'/2'}$), 74.5 (s, *C*$^{2''/5''}$), 73.7 (s, *C*$^{5''/2''}$), 71.7 (d, $^{3}J_{C,P}$ 6 Hz, *C*$^{3'/4'}$), 70.2 (d, $^{3}J_{C,P}$ 7 Hz, *C*$^{3''/4''}$), 69.7 (s, *C*$^{4'/3'}$), 69.2 (s, *C*$^{4''/3''}$), 35.5 (d, $^{1}J_{C,P}$ 24 Hz, *C*Me$_3$), 29.1 (d, $^{2}J_{C,P}$ 5 Hz, C*Me*$_3$). **^{31}P{^{1}H} NMR (C_6D_6, 203 MHz, 298 K):** δ 50.3 (d, $^{1}J_{P,Pt}$ 3695 Hz, $^{2}J_{P,P}$ 19 Hz, C_5H_4*P*(^{t}Bu)Ar), 27.6 (d, $^{1}J_{Pt,P}$ 3937 Hz, $^{2}J_{P,P}$ 19 Hz, C_5H_4*P*Ph$_2$). **^{11}B NMR (C_6D_6, 161 MHz, 298 K):** δ 24 (broad s, $\omega_{1/2}$ = 1200 Hz). **^{11}B NMR (CD_2Cl_2, 161 MHz, 298 K):** δ 24 (broad s, $\omega_{1/2}$ = 1200 Hz). **^{195}Pt{^{1}H} NMR (CD_2Cl_2, 128 MHz, 298 K):** *δ* –5117 (dd, $^{1}J_{Pt,P}$ 3950 Hz, $^{1}J_{Pt,P}$ 3689 Hz). **NMR Data for [Pt(FcPPB')] (Isomer B): ^{1}H NMR (C_6D_6, 500 MHz, 298 K):** δ 7.88 (dq, $^{3}J_{H,P}$ 11 Hz, $^{3}J_{H,H}$ 8 Hz, $^{4}J_{H,H}$ 2 Hz, 2H, *o*-P*Ph*$_2$ A or B), 7.84 (d, $^{3}J_{H,H}$ 7 Hz, 2H, *o*-B*Ph*), 7.73–7.70 (m, 3H, *o*-Ph$^{\alpha}$, aryl-C*H*), 7.28–7.21 (m, 4H, aryl-C*H*), 7.14–6.96 (m, 11H, aryl-C*H*), 6.85–6.84 (m, 5H, aryl-C*H*), 6.81–6.75 (m, 2H, aryl-C*H*), 5.20 (dd, $^{2}J_{H,Pt}$ 55 Hz, $^{3}J_{H,P}$ 15 Hz, $^{3}J_{H,P}$ 5 Hz, 1H, vinylC$^{\beta}$-*H*), 4.88 (s, 1H, C_5H_4), 4.41 (s, 1H, C_5H_4), 4.23 (s, 1H, C_5H_4), 4.18 (s, 1H, C_5H_4), 3.95 (s, 1H, C_5H_4), 3.91 (s, 1H, C_5H_4), 3.84 (s, 1H, C_5H_4), 3.81 (s, 1H, C_5H_4), 1.01 (d, $^{3}J_{H,P}$ 15 Hz, 9H, C*Me*$_3$). **^{13}C{^{1}H} NMR (C_6D_6, 151 MHz, 298 K):** δ 162.9 (broad s, aryl-*C*), 152.1 (broad s, *ipso*-B*Ph*), 147.5 (d, $^{1}J_{C,P}$ 47 Hz, *ipso*-aryl-*C*), 145.5 (dd, $^{1}J_{C,P}$ 45 Hz, $J_{C,P}$ 9 Hz, aryl-*C*), 144.1 (d, $J_{C,P}$ 6 Hz, aryl-*C*), 143.8 (d, $J_{C,P}$ 4 Hz, aryl-*C*), 138.6 (d, $^{1}J_{C,P}$ 42 Hz, *ipso*-aryl-*C*), 137.2 (d, $J_{C,P}$ 17 Hz, *o*-P*Ph*$_2$ A or B), 135.8 (d, $J_{C,P}$ 24 Hz, aryl-*C*), 135.6 (s, *o*-B*Ph*), 134.0 (d, $^{1}J_{C,P}$ 39 Hz, aryl-*C*), 133.5 (d, $^{3}J_{C,Pt}$ 24 Hz, $^{4}J_{C,P}$ 4 Hz, *o*-Ph$^{\alpha}$), 133.1 (s, aryl-*C*),

132.6 (d, $J_{C,P}$ 6 Hz, aryl-*C*), 132.0 (d, $J_{C,P}$ 13 Hz, aryl-*C*), 131.2 (s, aryl-*C*), 130.2 (s, aryl-*C*), 129.2 (s, aryl-*C*), 128.3 (s, aryl-*C*), 128.0 (d, $J_{C,P}$ 10 Hz, aryl-*C*), 127.4 (s, aryl-*C*), 127.1 (s, aryl-*C*), 126.8 (s, aryl-*C*), 125.4 (s, aryl-*C*), 125.2 (d, $J_{C,P}$ 6 Hz, aryl-*C*), 124.4 (s, aryl-*C*), 93.8 (broad s, vinylC^{α}), 89.5 (dd, $^{1}J_{C,P}$ 51 Hz, $^{3}J_{C,P}$ 4 Hz, $C^{1"}$), 85.5 (d, $^{1}J_{C,P}$ 36 Hz, $C^{1'}$), 75.7 (d, $J_{C,P}$ 12 Hz, C_5H_4), 74.5 (d, $J_{C,P}$ 13 Hz, C_5H_4), 74.1 (d, $J_{C,P}$ 7 Hz, C_5H_4), 73.7 (d, $J_{C,P}$ 3 Hz, C_5H_4), 73.1 (d, $J_{C,P}$ 4 Hz, C_5H_4), 71.6 (dd, $^{2}J_{C,P}$ 37 Hz, $^{2}J_{C,P}$ 5 Hz, vinylC^{β}), 71.3 (d, $J_{C,P}$ 7 Hz, C_5H_4), 69.9 (d, $J_{C,P}$ 3 Hz, C_5H_4), 69.7 (s, C_5H_4), 69.2 (d, $J_{C,P}$ 4 Hz, C_5H_4), 35.2 (d, $^{1}J_{C,P}$ 66 Hz, *C*Me$_3$), 30.3 (d, $^{2}J_{C,P}$ 7 Hz, C*Me*$_3$). **^{31}P{^{1}H} NMR (C_6D_6, 203 MHz, 298 K):** δ 55.7 (d, $^{1}J_{P,Pt}$ 3449 Hz, $^{2}J_{P,P}$ 20 Hz, $C_5H_4P(^{t}Bu)Ar$), 23.3 (d, $^{1}J_{Pt,P}$ 4090 Hz, $^{2}J_{P,P}$ 20 Hz, $C_5H_4PPh_2$). **^{11}B NMR (C_6D_6, 161 MHz, 298 K):** δ 32 (broad s, $\omega_{1/2}$ = 1500 Hz). **^{11}B NMR (CD_2Cl_2, 161 MHz, 298 K):** δ 30 (broad s, $\omega_{1/2}$ = 1500 Hz). **^{195}Pt{^{1}H} NMR (CD_2Cl_2, 128 MHz, 298 K):** δ –4840 (dd, $^{1}J_{Pt,P}$ 4097 Hz, $^{1}J_{Pt,P}$ 3440 Hz). **Elemental Analysis Calcd (%)** for $C_{52}H_{47}BFeNP_2Pt$ ([Pt(FcPPB'] A/B): C, 62.73; H, 4.76. Found: C, 62.48, H, 4.73.

[D_5]-[Pt(FcPPB')] (39A/639-D): This compound was generated by the same method as described for [Pt(FcPPB')] (Isomers A/B), however using $HC_2(C_6D_5)$ instead of $HC_2(C_6H_5)$. The NMR spectra were identical to that of a mixture of [Pt(FcPPB')] (Isomers A/B), however with the C_6H_5 resonances from the activated HC_2Ph unit missing from the ^{1}H and ^{13}C{^{1}H} NMR spectra.

10.7 – Synthetic Procedures and Characterization Pertaining to Chapter 7

[{Au(FcPPB)}$_2$][GaCl$_4$]$_2$ (40): Toluene (30 mL) was condensed into a 100 mL round bottom flask containing [AuCl(PPh_3)] (177 mg, 0.358 mmol) and $GaCl_3$ (63.0 mg, 0.358 mmol) through the use of a dry ice/acetone bath. The reaction mixture was stirred for 1 hour at room temperature, at which point a solution of FcPPB (250 mg, 0.358 mmol) in toluene (10 mL) was added; the resulting reaction mixture was stirred overnight at room temperature. After stirring overnight, a dark orange oil had precipitated from solution; the

solvent was removed *in vacuo* and hexanes (~30 mL) were added to the crude material. The hexanes slurry was sonicated for 15 minutes, resulting in the precipitation of an orange solid, which was then filtered through the use of a swivel frit. The collected orange solid was washed with hexanes (2 × 10 mL) and dried *in vacuo*. Yield = 355 mg (90 %). [{Au(FcPPB)}$_2$][GaCl$_4$]$_2$ was isolated as a diasteromeric mixture in a 65:35 ratio; the NMR signals corresponding to the diastereomer of highest concentration are denoted as "A". X-ray quality crystals of *meso*-[{Au(FcPPB)}$_2$][GaCl$_4$]$_2$·2(C$_6$H$_{14}$) were obtained by slow diffusion of hexanes into a solution of [{Au(FcPPB)}$_2$][GaCl$_4$]$_2$ in CH$_2$Cl$_2$ at –30 °C. **^{1}H NMR (CD$_2$Cl$_2$, 600 MHz, 298 K):** δ 8.06–7.99 (m, aryl-C*H*), 7.90 (t, *J* 7 Hz, aryl-C*H*), 7.86–7.71 (m, aryl-C*H*), 7.69–7.54 (m, aryl-C*H*), 7.45 (dt, *J* 8 Hz, *J* 2 Hz, aryl-C*H*), 7.41 (t, *J* 7 Hz, aryl-C*H*), 7.34–7.28 (m, aryl-C*H*), 7.22 (t, *J* 8 Hz, aryl-C*H*), 7.13 (t, *J* 8 Hz, aryl-C*H*), 6.96–6.88 (m, aryl-C*H*), 6.83 (d, *J* 7 Hz, aryl-C*H*), 6.61 (dd, *J* 13 Hz, *J* 8 Hz, aryl-C*H*), 5.31 (s, 1H, C$H^{2'/5'}$ B), 5.05 (s, 1H, C$H^{5'/2'}$ B), 5.00 (s, 2H, C$H^{2'/5'}$ A, C$H^{5'/2'}$ A), 4.71 (s, 1H, C$H^{2''/5''}$ A), 4.63 (s, 2H, C$H^{2''/5''}$ B, C$H^{4''/3''}$ B), 4.60 (s, 1H, C$H^{5''/2''}$ A), 4.52 (s, 1H, C$H^{3'/4'}$ B), 4.44 (s, 1H, C$H^{4''/3''}$ A), 4.20 (s, 1H, C$H^{4'/3'}$ B), 4.17 (s, 1H, C$H^{3'/4'}$ A), 3.99 (s, 1H, C$H^{3''/4''}$ A), 3.96 (s, 1H, C$H^{5''/2''}$ B), 3.76 (s, 1H, C$H^{3''/4''}$ B), 3.66 (s, 1H, C$H^{4'/3'}$ A), 0.94 (d, $^3J_{H,P}$ 18 Hz, 9H, CMe_3 A), 0.75 (d, $^3J_{H,P}$ 18 Hz, 9H, CMe_3 B). **^{13}C{^{1}H} NMR (CD$_2$Cl$_2$, 151 MHz, 298 K):** δ 155.2 (d, *J* 32 Hz, aryl-*C* A), 154.8 (d, *J* 31 Hz, aryl-*C* B), 143.2 (s, aryl-*C*), 142.5 (s, aryl-*C*), 142.4 (s, aryl-*C*), 140.4 (s, aryl-*C*), 140.0 (s, aryl-*C*), 139.4 (s, aryl-*C*), 138.3 (s, aryl-*C*), 136.4 (s, aryl-*C*), 135.9 (s, aryl-*C*), 135.5 (d, *J* 14 Hz, aryl-*C*), 134.6–134.4 (m, aryl-*C*), 134.4 (s, aryl-*C*), 134.3 (s, aryl-*C*), 133.9 (s, aryl-*C*), 133.4 (s, aryl-*C*), 133.2 (s, aryl-*C*), 132.9 (s, aryl-*C*), 132.6 (d, *J* 13 Hz, aryl-*C*), 132.4 (s, aryl-*C*), 132.2 (s, aryl-*C*), 132.0 (s, aryl-*C*), 131.4 (s, aryl-*C*), 131.2 (s, aryl-*C*), 131.1 (s, aryl-*C*), 131.0 (d, *J* 7 Hz, aryl-*C*), 130.7 (d, *J* 12 Hz, aryl-*C*), 130.6 (d, *J* 12 Hz, aryl-*C*), 130.4 (d, *J* 7 Hz, aryl-*C*), 130.2 (s, aryl-*C*), 130.1 (d, *J* 12 Hz, aryl-*C*), 129.9 (d, *J* 11 Hz, aryl-*C*), 129.5 (d, *J* 8 Hz, aryl-*C*), 129.4 (s, aryl-*C*), 128.9 (s, aryl-*C*), 128.7 (s, aryl-*C*), 126.6 (dd, *J* 57 Hz, *J* 4 Hz, aryl-*C*), 80.1 (d, $^2J_{C,P}$ 25 Hz, $C^{2'/5'}$ B), 80.0 (d, $^2J_{C,P}$ 24 Hz, $C^{2'/5'}$ A), 78.5 (d, $^2J_{C,P}$ 26 Hz, $C^{2''/5''}$ A), 77.1 (d, $^3J_{C,P}$ 7 Hz, $C^{4''/3''}$ A), 77.0 (d, $^3J_{C,P}$ 10 Hz, $C^{3''/4''}$ B), 76.4 (s, $C^{5''/2''}$ B), 75.8 (s, $C^{5'/2'}$ A), 75.6 (d, $^3J_{C,P}$ 7 Hz, $C^{4'/3'}$ B),

75.5 (d, $^{3}J_{C,P}$ 7 Hz, $C^{4''/3''}$ B), 75.4 (d, $^{3}J_{C,P}$ 5 Hz, $C^{4'/3'}$ A), 75.3 (s, $C^{5''/2''}$ A), 74.8 (s, $C^{5'/2'}$ B), 74.7 (s, $C^{3'/4'}$ B), 74.0 (d, $^{2}J_{C,P}$ 11 Hz, $C^{2''/5''}$ B), 73.9 (s, $C^{3'/4'}$ A), 72.6 (d, $^{3}J_{C,P}$ 11 Hz, $C^{3''/4''}$ A), 72.1 (d, $^{1}J_{C,P}$ 63 Hz, $C^{1'/1''}$ A/B), 70.3 (d, $^{1}J_{C,P}$ 65 Hz, $C^{1'/1''}$ A/B), 38.5 (d, $^{1}J_{C,P}$ 29 Hz, *C*Me$_3$ A), 38.4 (d, $^{1}J_{C,P}$ 31 Hz, *C*Me$_3$ B), 28.5 (d, $^{2}J_{C,P}$ 6 Hz, C*Me*$_3$ A), 28.4 (d, $^{2}J_{C,P}$ 6 Hz, C*Me*$_3$ B). **^{31}P{^{1}H} NMR (CD$_2$Cl$_2$, 203 MHz, 298 K):** δ 63.3 (d, $^{2}J_{P,P}$ 310 Hz, C$_5$H$_4$*P*(^{t}Bu)Ar B), 63.1 (d, $^{2}J_{P,P}$ 302 Hz, C$_5$H$_4$*P*(^{t}Bu)Ar A), 40.7 (d, $^{2}J_{P,P}$ 310 Hz, C$_5$H$_4$*P*Ph$_2$ B), 39.1 (d, $^{2}J_{P,P}$ 302 Hz, C$_5$H$_4$*P*Ph$_2$ A). **^{11}B NMR (CD$_2$Cl$_2$, 161 MHz, 298 K):** δ 68 (broad s, $\omega_{1/2}$ 3000 Hz). **Elemental Analysis Calcd (%)** for C$_{44}$H$_{41}$AuBCl$_4$FeGaP$_2$: C, 47.74; H, 3.73%. **Found:** C, 47.45; H, 3.94%.

[W(CO)$_4$(FcPPB*)] (41): A toluene solution (15 mL) of FcPPB (199 mg, 0.285 mmol) and [W(CO)$_6$] (100 mg, 0.285 mmol) in a 100 mL quartz flask equipped with a glass Schlenk adapter was irradiated under UV light for 24 hours. The bright orange solution was evaporated to dryness *in vacuo* and the resulting jack-o-lantern orange solid was brought into the dry box, washed with cold hexanes (~10 mL) and dried *in vacuo*. Yield = 214 mg (82 %). X-ray quality crystals of [W(CO)$_4$(FcPPB*)]·C$_6$H$_6$ were grown by slow diffusion of hexanes (~10 mL) into a solution of [W(CO)$_4$(FcPPB*)] in benzene (~3 mL) at room temperature. **^{1}H NMR (CD$_2$Cl$_2$, 600 MHz, 298 K):** δ 8.17 (dd, $^{3}J_{H,P}$ 13 Hz, $^{3}J_{H,H}$ 8 Hz, 1H, C*H*^{6}), 8.02 (dt, $^{3}J_{H,H}$ 7 Hz, $^{4}J_{H,P}$ 1 Hz, 1H, C*H*^{3}), 7.74–7.71 (m, 2H, *o*-P*Ph*$_2$ A), 7.67–7.66 (m, 3H, C*H*^{3}, *o*-B*Ph*), 7.51 (tt, $^{3}J_{H,H}$ 7 Hz, $^{3}J_{H,H}$ 1 Hz, 1H, C*H*^{4}), 7.49–7.47 (m, 6H, *m*,*p*-P*Ph*$_2$ A, *m*,*p*-B*Ph*), 7.25–7.23 (m, 1H, *p*-P*Ph*$_2$ B), 7.22–7.18 (m, 5H, *o*,*m*-P*Ph*$_2$ B), 5.42 (s, 1H, C*H*$^{5'}$), 4.94 (s, 1H, C*H*$^{4'}$), 4.50 (s, 1H, C*H*$^{3'}$), 4.45 (s, 1H, C*H*$^{5''/2''}$), 4.23 (s, 1H, C*H*$^{3''/4''}$), 3.99 (s, 1H, C*H*$^{4''/3''}$), 3.66 (s, 1H, C*H*$^{2''/5''}$), 1.07 (d, $^{3}J_{H,P}$ 14 Hz, 9H, C*Me*$_3$). **^{13}C{^{1}H} NMR (CD$_2$Cl$_2$, 151 MHz, 298 K):** δ 208.4 (dd, $^{2}J_{C,P}$ 26 Hz, $^{2}J_{C,P}$ 6 Hz, W-*C*O), 205.8 (appt. t, $^{2}J_{C,P}$ 7 Hz, W-*C*O), 204.8 (dd, $^{2}J_{C,P}$ 24 Hz, $^{2}J_{C,P}$ 5 Hz, W-*C*O), 203.0 (appt. t, $^{2}J_{C,P}$ 7 Hz, W-*C*O), 143.1 (broad s, *ipso*-B*Ph*), 142.0 (d, $^{1}J_{C,P}$ 31 Hz, C^{1}), 140.6 (broad s, C^{2}), 140.3 (d, $^{3}J_{C,P}$ 6 Hz, C^{3}), 139.9 (d, $^{1}J_{C,P}$ 42 Hz, *ipso*-P*Ph*$_2$ B), 137.7 (d, $^{2}J_{C,P}$ 25 Hz, C^{6}), 136.2 (d, $^{1}J_{C,P}$ 39 Hz, *ipso*-P*Ph*$_2$ A), 134.4 (d, $^{2}J_{C,P}$ 13 Hz, *o*-P*Ph*$_2$ A), 133.7 (s, *o*-B*Ph*), 132.8 (d, $^{2}J_{C,P}$ 11 Hz, *o*-P*Ph*$_2$ B), 130.9 (s, C^{5}), 130.8 (s, *p*-P*Ph*$_2$ A), 129.8 (s, *p*-

P*Ph*$_2$ B), 129.7 (s, *C*^{4}), 129.4 (s, *p*-B*Ph*), 128.8 (d, $^3J_{C,P}$ 10 Hz, *m*-P*Ph*$_2$ A), 128.2 (d, $^3J_{C,P}$ 9 Hz, *m*-P*Ph*$_2$ B), 128.1 (s, *m*-B*Ph*), 86.1 (d, $^2J_{C,P}$ 19 Hz, *C*$^{5'}$), 84.5 (dd, $^1J_{C,P}$ 38 Hz, $^3J_{C,P}$ 3 Hz, *C*$^{1'}$), 83.8 (d, $^1J_{C,P}$ 38 Hz, *C*$^{1''}$), 80.0 (d, $^3J_{C,P}$ 8 Hz, *C*$^{4'}$), 79.8 (s, *C*$^{3'}$), 78.6 (d, $^2J_{C,P}$ 18 Hz, *C*$^{2''/5''}$), 75.1 (d, $^2J_{C,P}$ 7 Hz, *C*$^{5''/2''}$), 73.4 (s, *C*$^{4''/3''}$), 72.9 (d, $^3J_{C,P}$ 3 Hz, *C*$^{3''/4''}$), 38.3 (d, $^1J_{C,P}$ 21 Hz, *C*Me$_3$), 27.7 (d, $^2J_{C,P}$ 5 Hz, C*Me*$_3$); *C*$^{2'}$ could not be located. **^{31}P{^{1}H} (CD_2Cl_2, 203 MHz, 298 K):** δ 19.7 (d, $^1J_{P,W}$ 233 Hz, $^2J_{P,P}$ 24 Hz, $C_5H_4P(^t$Bu)Ar), 14.2 (d, $^1J_{P,W}$ 236 Hz, $^2J_{P,P}$ 24 Hz, C_5H_4PPh$_2$). **^{11}B NMR (CD_2Cl_2, 161 MHz, 298 K):** δ 57 (broad s, $\omega_{1/2}$ ~ 1200 Hz). **IR (nujol):** ν(CO) = 2014, 1907, 1889, 1851, 1846 cm^{-1}. **IR (CH_2Cl_2):** 2015, 1934, 1910, 1892, 1868 cm^{-1}. **Elemental Analysis Calcd (%)** for $C_{42}H_{35}BFeO_4P_2W$: C, 55.06; H, 3.85%. **Found:** C, 55.22; H, 4.24%.

[Ru_3(μ-H)(CO)$_{10}$(FcPPB'')] (42): Toluene (10 mL) was condensed into a 50 mL Schlenk flask containing FcPPB (109 mg, 0.156 mmol) and [$Ru_3(CO)_{12}$] (101 mg, 0.156 mmol) through the use of a dry ice/acetone bath. The reaction mixture was heated to 85 °C, which resulted in immediate formation of a deep, blood red solution accompanied by evolution of CO. The reaction was heated for 5 days, after which point the reaction solution was evaporated to dryness *in vacuo*. Hexanes (~20 mL) were condensed into the flask via a dry ice/acetone bath, and the slurry was sonicated for 10 minutes before filtering away the precipitate; the precipitate was washed with hexanes (2 × 10 mL). Yield = 115 mg (58 %). The collected material contained ~20 % of unidentified impurities, which could be removed by sequential recrystallization processes from hexanes at –30 °C, which resulted in precipitation of the impurities. Yields following this process were ~20–30 mg. X-ray quality crystals of [Ru_3(μ-H)(CO)$_{10}$(FcPPB**)]·1.3(C_6H_{14}) were obtained by cooling a solution of [Ru_3(μ-H)(CO)$_{10}$(FcPPB**)] in hexanes to –30 °C for several days. **Note:** the ^{31}P and ^{11}B NMR data given below are unreferenced. **^{1}H NMR (C_6D_6, 600 MHz, 298 K):** δ 8.23 (dd, *J* 13 Hz, *J* 8 Hz, 1H, aryl-C*H*), 8.09–8.02 (m, 3H, aryl-C*H*), 7.61–7.59 (m, 2H, aryl-C*H*), 7.33–7.32 (m, 4H, aryl-C*H*), 7.25 (t, *J* 7 Hz, 2H, aryl-C*H*), 7.14 (t, *J* 8 Hz, 1H, aryl-C*H*), 7.05 (td, *J* 7 Hz, *J* 2 Hz, 2H, aryl-C*H*), 7.00 (t, *J* 7 Hz, 2H, aryl-C*H*), 6.82 (m, 1H, aryl-

C*H*), 6.75–6.70 (m, 4H, aryl-C*H*), 5.57 (s, 1H, Cp-*H*), 4.35 (s, 2H, Cp-*H*), 4.33 (s, 1H, Cp-*H*), 4.21 (d, *J* 2 Hz, 1H, Cp-*H*), 3.63 (s, 1H, Cp-*H*), 3.49 (s, 1H, Cp-*H*), 1.10 (d, *J* 14 Hz, $^{3}J_{H,P}$ 9 Hz, C*Me*$_3$). **^{31}P{^{1}H} NMR (C_6D_6, 203 MHz, 298 K):** δ 42.6 (d, $^{2}J_{P,H}$ 22 Hz, $C_5H_4P(^{t}Bu)Ar$), 41.3 (d, $^{2}J_{P,H}$ 22 Hz, $C_5H_4PPh_2$). **^{11}B NMR (C_6D_6, 161 MHz, 298 K):** δ –11.4 (d, $^{3}J_{B,P}$ 29 Hz). **IR:** ν(CO) = 2059, 2044, 2030, 2005, 1987, 1955, 1934, 1912 cm^{-1} (nujol).

FcPPB{B(C_6F_5)$_3$} (43): Benzene (10 mL) was condensed into a 50 mL round bottom flask containing FcPPB (75.9 mg, 0.114 mmol) and B(C_6F_5)$_3$ (55.6 mg, 0.114 mmol) through the use of a dry ice/acetone bath, and the reaction mixture was stirred overnight at room temperature. The reaction solution was then evaporated to dryness *in vacuo* to yield a tangarine solid. Yield = 95.0 mg (69 %). **^{1}H NMR (CD_2Cl_2, 600 MHz, 298 K):** 7.94 (broad s, 2H, *o*-B*Ph*$_2$ A), 7.88 (broad s, 2H, *o*-B*Ph*$_2$ B), 7.68–7.66 (m, 3H, C*H*^{3}, *o*-P*Ph*$_2$ A), 7.48 (broad s, 2H, *m*-B*Ph*$_2$ A), 7.42–7.38 (m, 2H, C*H*^{4}, *p*-B*Ph*$_2$ A), 7.29 (t, $^{3}J_{H,H}$ 9 Hz, 2H, *o*-P*Ph*$_2$ B), 7.26 (broad s, 2H, *m*-B*Ph*$_2$ B), 7.16 (app. s, 2H, C*H*^{5}, *p*-B*Ph*$_2$ B), 7.11 (t, $^{3}J_{H,H}$ 7 Hz, 1H, C*H*^{6}), 7.05 (t, $^{3}J_{H,H}$ 7 Hz, 1H, *p*-P*Ph*$_2$ A), 7.00 (t, $^{3}J_{H,H}$ 7 Hz, 1H, *p*-P*Ph*$_2$ B), 6.95 (td, $^{3}J_{H,H}$ 7 Hz, $^{4}J_{H,P}$ 2 Hz, 2H, *m*-P*Ph*$_2$ A), 6.80 (td, $^{3}J_{H,H}$ 8 Hz, $^{4}J_{H,P}$ 2 Hz, 2H, *m*-P*Ph*$_2$ B), 4.29 (s, 1H, C*H*$^{2'/5'}$), 3.78 (s, 1H, C*H*$^{5'/2'}$), 3.69 (s, 1H, C*H*$^{3'/4'}$), 3.56 (s, 1H, C*H*$^{4'/3'}$), 3.40 (s, 1H, C*H*$^{3''/4''}$), 3.29 (s, 1H, C*H*$^{2''/5''}$), 3.25 (s, 1H, C*H*$^{4''/3''}$), 2.97 (s, 1H, C*H*$^{5''/2''}$), 0.69 (d, $^{3}J_{H,P}$ 14 Hz, 9H, C*Me*$_3$). **^{13}C{^{1}H} NMR (CD_2Cl_2, 151 MHz, 298 K:** 163.9 (broad d, $^{2}J_{C,P}$ 42 Hz, *C*^{2}), 148.8 (d, $^{1}J_{C,F}$ 241 Hz, *o*-B(*C*$_6$F$_5$)$_3$), 146.8 (broad s, *ipso*-B*Ph*$_2$ A and B), 140.7 (broad d, $^{1}J_{C,F}$ 253 Hz, *p*-B(*C*$_6$F$_5$)$_3$), 137.4 (ddd, $^{1}J_{C,F}$ 248 Hz, $^{2}J_{C,F}$ 19 Hz, $^{4}J_{C,P}$ 12 Hz, *m*-B(*C*$_6$F$_5$)$_3$), 135.3 (s, *o*-B*Ph*$_2$ B), 134.4 (d, $^{2}J_{C,P}$ 9 Hz, *o*-P*Ph*$_2$ A), 133.9 (d, $^{2}J_{C,P}$ 9 Hz, *o*-P*Ph*$_2$ B, *o*-B*Ph*$_2$ A), 132.1 (s, *C*^{4}), 131.7 (s, *C*^{3}), 131.7 (s, *p*-P*Ph*$_2$ B), 131.5 (s, *p*-P*Ph*$_2$ A), 129.5 (s, *C*^{6}), 128.4 (s, *p*-B*Ph*$_2$ B), 128.2 (d, $^{3}J_{C,P}$ 10 Hz, *m*-P*Ph*$_2$ B), 127.9 (d, $^{3}J_{C,P}$ 10 Hz, *m*-P*Ph*$_2$ A), 127.9 (s, *m*-B*Ph*$_2$ A and B), 127.7 (s, *p*-B*Ph*$_2$ A), 127.6 (d, $^{3}J_{C,P}$ 6 Hz, *C*^{5}), 116.1 (broad s, *ipso*-B(*C*$_6$F$_5$)$_3$), 77.1 (d, $^{2}J_{C,P}$ 19 Hz, *C*$^{2'/5'}$), 76.8 (d, $^{3}J_{C,P}$ 5 Hz, *C*$^{4''/3''}$), 75.5 (d, $^{2}J_{C,P}$ 12 Hz, *C*$^{2''/5''}$), 75.1 (dd, $^{1}J_{C,P}$ 118 Hz, $^{3}J_{C,P}$ 11 Hz, *C*$^{1'/1''}$), 75.0 (d, $^{2}J_{C,P}$ 10 Hz, *C*$^{5''/2''}$), 74.0 (d, $^{3}J_{C,P}$ 7 Hz, *C*$^{3'/4'}$), 73.1 (d, $^{2}J_{C,P}$ 3 Hz, *C*$^{5'/2'}$),

72.5 (d, $^{3}J_{C,P}$ 7 Hz, $C^{3''/4''}$), 72.0 (s, $C^{4'/3'}$), 71.5 (dd, $^{1}J_{C,P}$ 53 Hz, $^{3}J_{C,P}$ 8 Hz, $C^{1'/1''}$), 34.1 (d, $^{1}J_{C,P}$ 3 Hz, *C*Me$_3$), 27.4 (d, $^{2}J_{C,P}$ 5 Hz, C*Me*$_3$). **^{19}F NMR (CD_2Cl_2, 188 MHz, 298 K):** δ –125.1 (s, *o*-B(C_6F_5)$_3$), –156.7 (s, *p*-B(C_6F_5)$_3$), –164.3 (s, *m*-B(C_6F_5)$_3$). **^{31}P{^{1}H} NMR (CD_2Cl_2, 203 MHz, 298 K):** δ 20.0 (broad s, $\omega_{1/2}$ ~ 93 Hz, $C_5H_4PPh_2$), 15.1 (s, $C_5H_4P(^{t}Bu)Ar$). **^{11}B NMR (CD_2Cl_2, 161 MHz, 298 K):** δ 25 (broad s, $\omega_{1/2}$ ~ 2300 Hz, Ar*B*Ph$_2$), –4 (broad s, $\omega_{1/2}$ ~ 1200 Hz, *B*(C_6F_5)$_3$).

[FcPPB^{-Ph}][BF_4] (44): Benzene (15 mL) was condensed into a 50 mL Schlenk flask containing FcPPB (108 mg, 0.155 mmol) and $BF_3{\cdot}OEt_2$ (22.0 mg, 0.155 mmol) through the use of a dry ice/acetone bath. The reaction solution was stirred for 3 days at 70 °C, after which point the precipitated pale orange solid was isolated by centrifugation and dried *in vacuo*. Yield = 69.9 mg (64 %). X-ray quality crystals of [FcPPB^{-Ph}][BF_4] precipitated from a solution of FcPPB (14.8 mg, 2.12×10^{-2} mmol) and $BF_3{\cdot}OEt_2$ (6.00 mg, 2.12×10^{-2} mmol) in benzene at room temperature. **^{1}H NMR (CD_2Cl_2, 600 MHz, 298 K):** δ 7.86–7.83 (m, 1H, *p*-P*Ph*$_2$ A), 7.80 (t, $^{3}J_{H,H}$ 9 Hz, 1H, C*H*^{3}), 7.77–7.71 (m, 5H, *o*,*m*-P*Ph*$_2$ A, C*H*^{4}), 7.68–7.65 (m, 2H, *p*-P*Ph*$_2$ B, C*H*^{5}), 7.41 (dt, $^{3}J_{H,H}$ 8 Hz, $^{4}J_{H,P}$ 3 Hz, 4H, *m*-P*Ph*$_2$ B, *o*-B*Ph*), 7.29 (tp, $^{3}J_{H,H}$ 7 Hz, $^{4}J_{H,H}$ 2 Hz, 1H, *p*-B*Ph*), 7.23 (t, $^{3}J_{H,H}$ 7 Hz, 2H, *m*-B*Ph*), 7.03 (ddd, $^{3}J_{H,P}$ 12 Hz, $^{3}J_{H,H}$ 8 Hz, $^{4}J_{H,H}$ 1 Hz, 2H, *o*-P*Ph*$_2$ B), 6.76 (d, $^{3}J_{H,H}$ 8 Hz, 1H, C*H*^{6}), 5.03 (sextet, $^{3}J_{H,H}$ 1 Hz, 1H, C*H*$^{2'/5'}$), 4.83 (septet, $^{3}J_{H,H}$ 1 Hz, 1H, C*H*$^{3'/4'}$), 4.72 (dt, $^{3}J_{H,H}$ 3 Hz, $^{4}J_{H,H}$ 1 Hz, 1H, C*H*$^{4'/3'}$), 4.63 (septet, $^{3}J_{H,H}$ 1 Hz, 1H, C*H*$^{4''/3''}$), 4.60 (septet, $^{3}J_{H,H}$ 1 Hz, 1H, C*H*$^{5'/2'}$), 4.57 (septet, $^{3}J_{H,H}$ 1 Hz, 1H, C*H*$^{3''/4''}$), 3.69 (septet, $^{3}J_{H,H}$ 1 Hz, 1H, C*H*$^{2''/5''}$), 3.17 (s, 1H, C*H*$^{5''/2''}$), 1.12 (d, $^{3}J_{H,P}$ 16 Hz, 9H, C*Me*$_3$). **^{13}C{^{1}H} NMR (CD_2Cl_2, 151 MHz, 298 K):** δ 155.5 (broad s, C^{2}), 135.8 (t, $^{3}J_{C,P}$ 6 Hz, *o*-B*Ph*), 135.4 (s, C^{5}), 134.8 (d, $^{2}J_{C,P}$ 10 Hz, *o*-P*Ph*$_2$ A), 134.5 (s, *p*-P*Ph*$_2$ A), 134.1 (d, $^{2}J_{C,P}$ 9 Hz, *o*-P*Ph*$_2$ B), 133.9 (s, *p*-P*Ph*$_2$ B), 133.5 (dd, $^{1}J_{C,P}$ 61 Hz, $^{3}J_{C,P}$ 13 Hz, C^{1}), 132.9 (d, $^{2}J_{C,P}$ 31 Hz, C^{6}), 131.9 (d, $^{4}J_{C,P}$ 8 Hz, C^{4}), 130.4 (d, $^{3}J_{C,P}$ 11 Hz, *m*-P*Ph*$_2$ A), 129.9 (s, C^{3}), 129.8 (d, $^{3}J_{C,P}$ 11 Hz, *m*-P*Ph*$_2$ B), 129.0 (s, *m*-B*Ph*), 129.0 (s, *p*-B*Ph*), 123.1 (d, $^{1}J_{C,P}$ 64 Hz, *ipso*-P*Ph*$_2$ A), 122.3 (dd, $^{1}J_{C,P}$ 64 Hz, $^{3}J_{C,P}$ 9 Hz, *ipso*-P*Ph*$_2$ B), 78.7 (s, $C^{5'/2'}$), 77.4 (appt t, $J_{C,P}$ 8 Hz, $C^{3'/4'}$, $C^{2''/5''}$), 77.0 (d, $^{3}J_{C,P}$ 8 Hz, $C^{4''/3''}$), 75.0 (d, $^{2}J_{C,P}$ 15 Hz, $C^{2'/5'}$), 74.7 (d, $^{3}J_{C,P}$ 6 Hz, $C^{4'/3'}$), 74.6 (d, $^{2}J_{C,P}$ 11 Hz, $C^{5''/2''}$), 74.4 (d, $^{3}J_{C,P}$ 8 Hz, $C^{3''/4''}$), 65.0 (d, $^{1}J_{C,P}$ 76 Hz, $C^{1''}$), 62.7 (d,

$^{1}J_{C,P}$ 43 Hz, $C^{1'}$), 36.1 (d, $^{1}J_{C,P}$ 16 Hz, CMe$_3$), 26.1 (s, CMe_3). **^{19}F NMR (CD_2Cl_2, 188 MHz, 298 K):** δ –152.9 (s, BF_4). **^{31}P{^{1}H} NMR (CD_2Cl_2, 203 MHz, 298 K):** δ 27.8 (broad s, $\omega_{1/2}$ ~ 65 Hz, C_5H_4P(^{t}Bu)Ar), 1.0 (broad s, $\omega_{1/2}$ ~ 150 Hz, C_5H_4PPh$_2$). **^{11}B NMR (CD_2Cl_2, 161 MHz, 298 K):** δ –1.4 (s, BF$_4$), –2.0 (broad s, $\omega_{1/2}$ ~ 250 Hz, FcPPB^{-Ph}).

10.8 – Synthetic Procedures and Characterization Pertaining to Chapter 8

[Pt(η^2-nb)(FcPPAl)] (45): Benzene (30 mL) was condensed into a 100 mL round bottom flask containing [Pt(nb)$_3$] (232 mg, 0.486 mmol) and FcPPAl (287 mg, 0.486 mmol) through the use of a dry ice/acetone bath. The fawn yellow reaction solution was left to stir for 3 hours at room temperature before being evaporated to dryness *in vacuo*, providing a brown, oily residue. Hexanes (60 mL) were condensed into the reaction flask and the oily suspension was sonicated for 15 minutes, after which the hexanes solution was filtered. The undesired reaction byproducts collected on the frit were washed with hexanes (2 × 15 mL), and the filtrate was evaporated to dryness *in vacuo*, providing a light yellow solid. Yield = 283 mg (66 %). **^{1}H NMR (C_6D_6, 600 MHz, 298 K):** δ 7.84 (d, $^{3}J_{H,H}$ 7 Hz, 1H, CH^{6}), 7.71 (dd, $^{3}J_{H,H}$ 8 Hz, $^{4}J_{H,P}$ 5 Hz, 1H, CH^{3}), 7.68 (broad t, $^{3}J_{H,H}$ 8 Hz, 2H, *o*-PPh_2 A), 7.47 (broad t, $^{3}J_{H,H}$ 9 Hz, 2H, *o*-PPh_2 B), 7.29 (ddt, $^{3}J_{H,H}$ 7 Hz, $^{4}J_{H,P}$ 3 Hz, $^{4}J_{H,H}$ 1 Hz, 1H, CH^{5}), 7.20 (qt, $^{3}J_{H,H}$ 8 Hz, $^{4}J_{H,H}$ 1 Hz, 1H, CH^{4}), 7.09 (t, $^{3}J_{H,H}$ 7 Hz, 2H, *m*-PPh_2 A), 7.04 (dt, $^{3}J_{H,H}$ 7 Hz, $^{4}J_{H,H}$ 1 Hz, 1H, *p*-PPh_2 A), 6.95 (dt, $^{3}J_{H,H}$ 7 Hz, $^{4}J_{H,H}$ 1 Hz, 1H, *p*-PPh_2 B), 7.90 (t, $^{3}J_{H,H}$ 7 Hz, 2H, *m*-PPh_2 B), 4.58 (d, $^{3}J_{H,P}$ 1 Hz, 1H, C$H^{2'/5'}$), 4.49 (d, $^{3}J_{H,P}$ 1 Hz, 1H, C$H^{5'/2'}$), 4.06 (s, 1H, C$H^{2''/5''}$), 3.96 (s, 1H, C$H^{3''/4''}$), 3.91 (s, 1H, C$H^{3'/4'}$), 3.88 (s, 1H, C$H^{5''/2''}$), 3.85 (d, $^{4}J_{H,P}$ 1Hz, 1H, C$H^{4'/3'}$), 3.75 (s, 1H, C$H^{4''/3''}$), 3.75 (s, $^{2}J_{H,Pt}$ 58 Hz, 1H, CH^{α}), 3.14 (s, 1H, CH^{β}), 2.89 (q, $^{2}J_{H,Pt}$ 53 Hz, $^{3}J_{H,P}$ 7 Hz, 1H, CH^{α}), 2.32 (s, 1H, CH^{β}), 1.65–1.52 (m, 2H, Endo/Exo–CH_2), 1.35 (d, $^{3}J_{H,P}$ 14 Hz, 9H, CMe_3), 1.30–1.22 (m, 2H, Endo/Exo–CH_2), 1.10 (d, $^{2}J_{H,H}$ 9 Hz, 1H, Bridgehead–CH), 0.48 (d, $^{2}J_{H,H}$ 9 Hz, 1H, Bridgehead−CH), –0.06, −0.54 (2×s, 6H, AlMe_2). **^{13}C{^{1}H} NMR (C_6D_6, 151 MHz, 298 K):** δ 170.9 (broad s, C^{2}), 140.7 (d, $^{1}J_{C,P}$ 46 Hz, C^{1}), 137.5 (dd, $^{1}J_{C,P}$ 40 Hz, $^{3}J_{C,P}$ 4 Hz, *ipso*-PPh_2 A), 136.4 (appt. s, *ipso*-PPh_2 B), 136.0 (d, $^{2}J_{C,P}$ 29 Hz, C^{6}), 134.5 (d,

$^{2}J_{C,P}$ 12 Hz, *o*-P*Ph*$_2$ B), 134.0 (d, $^{2}J_{C,P}$ 10 Hz, *o*-P*Ph*$_2$ A), 131.9 (d, $^{3}J_{C,P}$ 4 Hz, C^{3}), 129.9 (s, *p*-P*Ph*$_2$ B), 129.8 (s, *p*-P*Ph*$_2$ A), 129.4 (s, C^{5}), 127.9 (d, $^{3}J_{C,P}$ 5 Hz, *m*-P*Ph*$_2$ B), 127.9 (d, $^{3}J_{C,P}$ 5 Hz, *m*-P*Ph*$_2$ A), 125.4 (d, $^{4}J_{C,P}$ 5 Hz, C^{4}), 83.9 (d, $^{1}J_{C,P}$ 32 Hz, $C^{1'}$), 81.2 (d, $^{1}J_{C,P}$ 45 Hz, $C^{1''}$), 75.2 (s, $C^{5'/2'}$), 74.9 (d, $^{2}J_{C,P}$ 9 Hz, $C^{5''/2''}$), 73.8 (d, $^{2}J_{C,P}$ 11 Hz, $C^{2''/5''}$), 73.6 (d, $^{2}J_{C,P}$ 12 Hz, $C^{2'/5'}$), 72.0 (d, $^{3}J_{C,P}$ 5 Hz, $C^{3''/4''}$), 71.6 (d, $^{3}J_{C,P}$ 4 Hz, $C^{4''/3''}$), 71.2 (d, $^{3}J_{C,P}$ 5 Hz, $C^{3'/4'}$), 70.0 (d, $^{3}J_{C,P}$ 2 Hz, $C^{4'/3'}$), 62.1 (dd, $^{1}J_{C,Pt}$ 37 Hz, $^{2}J_{C,P}$ 6 Hz, C^{α}), 59.8 (dd, $^{1}J_{C,Pt}$ 37 Hz, $^{2}J_{C,P}$ 7 Hz, C^{α}), 45.7 (s, $^{2}J_{C,Pt}$ 18 Hz, C^{β}), 44.7 (s, $^{2}J_{C,Pt}$ 17 Hz, C^{β}), 40.3 (s, $^{3}J_{C,Pt}$ 41 Hz, Bridgehead−*C*H$_2$), 35.5 (dd, $^{1}J_{C,P}$ 20 Hz, $^{3}J_{C,P}$ 7 Hz, *C*Me$_3$), 31.8–31.5 (m, Endo/Exo−*C*H$_2$), 28.1 (d, $^{2}J_{C,P}$ 7 Hz, C*Me*$_3$), −1.8, −2.4 (2×broad s, Al*Me*$_2$). **^{31}P{^{1}H} NMR (C$_6$D$_6$, 203 MHz, 298 K):** δ 66.5 (d, $^{1}J_{P,Pt}$ 3050, $^{2}J_{P,P}$ 40 Hz, C$_5$H$_4$*P*(^{t}Bu)Ar), 26.2 (broad d, $^{1}J_{P,Pt}$ 2654, $^{2}J_{P,P}$ 40 Hz, C$_5$H$_4$*P*Ph$_2$). **^{31}P{^{1}H} NMR (Toluene-d$_8$, 203 MHz, 298 K):** δ 66.9 (d, $^{1}J_{P,Pt}$ 3060 Hz, $^{2}J_{P,P}$ 40 Hz, C$_5$H$_4$*P*(^{t}Bu)Ar), 26.5 (broad d, $^{1}J_{P,Pt}$ 2657 Hz, $^{2}J_{P,P}$ 40 Hz, C$_5$H$_4$*P*Ph$_2$); **171 K:** δ 66.7 (appt t, $^{1}J_{P,Pt}$ 2949 Hz, $^{1}J_{P,Pt}$ 3024 Hz, $^{2}J_{P,P}$ 38 Hz, C$_5$H$_4$*P*(^{t}Bu)Ar), 31.3 (d, $^{1}J_{P,Pt}$ 2746 Hz, $^{2}J_{P,P}$ 38 Hz, C$_5$H$_4$*P*Ph$_2$), 22.4 (d, $^{1}J_{P,Pt}$ 2576 Hz, $^{2}J_{P,P}$ 38 Hz, C$_5$H$_4$*P*Ph$_2$). **^{195}Pt{^{1}H} NMR (Toluene-d$_8$, 128 MHz, 298 K):** δ –4615 (broad dd, $^{1}J_{Pt,P}$ 3100 Hz, $^{1}J_{Pt,P}$ 2800 Hz, $\omega_{1/2}$ 400 Hz). **Elemental Analysis Calcd (%)** for C$_{41}$H$_{47}$AlFeP$_2$Pt: C, 55.98; H, 5.39. Found: C, 55.96; H, 5.60.

[{Pt(FcPPAl)}$_2$] (46): A solution of [Pt(η^2-nb)(FcPPAl)] (**45**) (61.2 mg, 6.96×10^{-2} mmol) in toluene (5 mL) in a 50 mL Schlenk flask was heated to 80 °C for 48 hours, which resulted in the precipitation of a yellow solid. The toluene solution was filtered, and the collected product was washed with toluene (2 × 5 mL) and dried *in vacuo*. Yield = 35 mg (65 %). X-ray quality crystals of [{Pt(FcPPAl)}$_2$] precipitated from a C$_6$D$_6$ solution heated to 80 °C for 24 hours. [{Pt(FcPPAl)}$_2$] was characterized using PXRD, however, a small fraction of [{Pt(FcPPAl)}$_2$] remained in solution during the course of the reaction (in the presence of unreacted [Pt(η^2-nb)(FcPPAl)]) allowing for tentative identification of the corresponding ^{1}H and ^{31}P NMR signals. **^{1}H NMR (C$_6$D$_6$, 500 MHz, 298 K):** δ 8.03–7.99 (m, 2H, phenyl-C*H*), 7.93 (d, *J* 7 Hz, 1H, phenyl-C*H*), 7.55 (t, *J* 7 Hz, 1H, phenyl-C*H*), 7.37 (dt, *J* 7 Hz, *J* 3 Hz, 1H, phenyl-C*H*), 7.25–7.22 (m, 2H, phenyl-C*H*), 5.92 (s,

1H, C_5H_4), 5.70 (s, 1H, C_5H_4), 4.95 (s, 1H, C_5H_4), 4.58 (s, 1H, C_5H_4), 4.04 (s, 1H, C_5H_4), 3.81 (s, 1H, C_5H_4), 3.44 (s, 1H, C_5H_4), 2.96 (s, 1H, C_5H_4), 1.36 (d, $^3J_{H,H}$ 15 Hz, 9H, CMe_3), –0.14, –0.32 (2×s, 6H, AlMe_2). **^{31}P{^{1}H} NMR (C_6D_6, 203 MHz, 298 K):** δ 74.9 (d, $^2J_{P,P}$ 356 Hz, C_5H_4P(*t*Bu)Ar), 40.7 (d, $^2J_{P,P}$ 356 Hz, C_5H_4PPh$_2$). **Elemental Analysis Calcd (%)** for $C_{68}H_{74}Al_2Fe_2P_4Pt_2$: C, 51.99; H, 4.75. Found: C, 51.65; H, 4.76.

[Pt(η^2-C_2H_4)(FcPPAl)] (47): A solution of [Pt(η^2-nb)(FcPPAl)] (**45**) (63.3 mg, 7.20×10^{-2} mmol) in benzene (5 mL) in a 50 mL Schlenk flask was subjected to three freeze/pump/thaw cycles before warming to room temperature, at which point C_2H_4 was added. The bright orange reaction mixture was stirred for one hour at room temperature before being brought into the glove box, at which point the benzene solution was layered with hexanes (~10-15 mL), stored at room temperature for two days to allow the hexanes to diffuse into the benzene solution, then at –30 °C for recrystallization. After two days at –30 °C, the benzene/hexanes mother liquors were decanted and the remaining light yellow, crystalline solid was collected and dried under an atmosphere of argon. Yield = 49 mg (84 %). X-ray quality crystals of [Pt(η^2-C_2H_4)(FcPPAl)] were obtained by slow diffusion of hexanes (~3 mL) into a solution of [Pt(η^2-C_2H_4)(FcPPAl)] in C_6D_6 (~1 mL) at room temperature. **^{1}H NMR (C_6D_6, 600 MHz, 298 K):** δ 7.87 (dd, $^3J_{H,H}$ 8 Hz, $^4J_{H,P}$ 5 Hz, 1H, CH^3), 7.86 (d, $^3J_{H,H}$ 8 Hz, 1H, CH^6), 7.58 (ddd, $^3J_{H,P}$ 11 Hz, $^3J_{H,H}$ 8 Hz, $^4J_{H,H}$ 1 Hz, 2H, *o*-PPh$_2$ A), 7.44 (ddd, $^3J_{H,P}$ 10 Hz, $^3J_{H,H}$ 8 Hz, $^4J_{H,H}$ 2 Hz, 2H, *o*-PPh$_2$ B), 7.30 (ddt, $^3J_{H,H}$ 7 Hz, $^4J_{H,P}$ 3 Hz, $^4J_{H,H}$ 1 Hz, 1H, CH^5), 7.22 (ddt, $^3J_{H,H}$ 8 Hz, $^5J_{H,P}$ 3 Hz, $^4J_{H,H}$ 1 Hz, 1H, CH^4), 7.03–6.96 (m, 6H, *m*,*p*-PPh$_2$ A and B), 4.55 (s, 1H, C$H^{2''/5''}$), 4.53 (d, $^3J_{H,P}$ 1 Hz, 1H, C$H^{2'/5'}$), 4.43 (s, 1H, C$H^{5'/2'}$), 3.88 (d, $^4J_{H,P}$ 1 Hz, 1H, C$H^{3'/4'}$), 3.86 (d, $^4J_{H,P}$ 1 Hz, 1H, C$H^{4''/3''}$), 3.81–3.79 (m, 2H, C$H^{3''/4''}$, C$H^{5''/2''}$), 3.77 (s, 1H, C$H^{4'/3'}$), 3.68–3.60 (m, 1H, C_2H_4), 2.90–2.84 (m, $^2J_{H,Pt}$ 63 Hz, 1H, C_2H_4), 2.80–2.73 (m, $^2J_{H,Pt}$ 63 Hz, 1H, C_2H_4), 2.48–2.42 (m, $^2J_{H,Pt}$ 69 Hz, 1H, C_2H_4), 1.24 (d, $^3J_{H,P}$ 14 Hz, 9H, CMe_3), –0.16 (s, 3H, Al*Me*), –0.71 (d, $^4J_{H,P}$ 1 Hz, 3H, Al*Me*). **^{13}C{^{1}H} NMR (C_6D_6, 151 MHz, 298 K):** δ 171.5 (broad d, $^2J_{C,P}$ 54 Hz, C^2), 140.0 (dd, $^1J_{C,P}$ 40, $^3J_{C,P}$ 3 Hz, *ipso*-PPh$_2$ A/B), 138.6 (dd, $^1J_{C,P}$ 44 Hz, $^3J_{C,P}$ 3 Hz, *ipso*-PPh$_2$ A/B), 138.4 (d, $^1J_{C,P}$ 54 Hz, C^1), 136.2 (d, $^2J_{C,P}$ 30

Hz, C^6), 134.7 (d, $^2J_{C,P}$ 13 Hz, *o*-PPh_2 B), 133.1 (d, $^2J_{C,P}$ 12 Hz, *o*-PPh_2 A), 131.2 (d, $^3J_{C,P}$ 5 Hz, C^3), 130.5 (s, *p*-PPh_2 B), 129.9 (s, C^5), 129.6 (s, *p*-PPh_2 A), 128.2 (d, $^3J_{C,P}$ 11 Hz, *m*-PPh_2 A/B), 128.1 (d, $^3J_{C,P}$ 10 Hz, *m*-PPh_2 A/B), 125.6 (d, $^4J_{C,P}$ 5 Hz, C^4), 80.2 (d, $^1J_{C,P}$ 35 Hz, $C^{1'}$), 79.1 (d, $^1J_{C,P}$ 47 Hz, $C^{1''}$), 76.6 (d, $^2J_{C,P}$ 21 Hz, $C^{2''/5''}$), 75.3 (d, $^2J_{C,P}$ 17 Hz, $C^{5'/2'}$), 74.7 (s, $C^{2'/5'}$), 74.1 (s, $C^{3''/4''}$), 74.0 (d, $^2J_{C,P}$ 10 Hz, $C^{5''/2''}$), 72.8 (d, $^3J_{C,P}$ 7 Hz, $C^{4'/3'}$), 71.2 (d, $^3J_{C,P}$ 4 Hz, $C^{4''/3''}$), 70.4 (d, $^3J_{C,P}$ 3 Hz, $C^{3'/4'}$), 42.0 (dd, $^2J_{C,P}$ 31 Hz, 6 Hz, C_2H_4), 37.7 (dd, $^2J_{C,P}$ 29 Hz, 7 Hz, C_2H_4), 36.1 (dd, $^1J_{C,P}$ 22 Hz, $^3J_{C,P}$ 6 Hz, CMe$_3$), 27.6 (d, $^2J_{C,P}$ 6 Hz, C*Me*$_3$), –2.0 (d, $^3J_{C,P}$ 9 Hz, Al*Me*), –3.4 (s, Al*Me*). **^{31}P{^{1}H} NMR (C_6D_6, 203 MHz, 298 K):** δ 67.2 (d, $^1J_{P,Pt}$ 3270 Hz, $^2J_{P,P}$ 43 Hz, $C_5H_4P(^t$Bu)Ar), 27.9 (d, $^1J_{P,Pt}$ 2979 Hz, $^2J_{P,P}$ 43 Hz, C_5H_4PPh$_2$). **^{195}Pt{^{1}H} NMR (C_6D_6, 128 MHz, 298 K):** δ –4734 (dd, $^1J_{Pt,P}$ 3278 Hz, $^1J_{Pt,P}$ 2983 Hz). **Raman:** ν(C=C) = 1156 cm^{-1}. **Elemental Analysis Calcd (%)** for $C_{36}H_{41}AlFeP_2Pt$: C, 53.15; H, 5.08. Found: C, 53.41; H, 5.08.

[Pt(η^2-C_2Ph_2)(FcPPAl)] (48): Toluene (5 mL) was condensed into a 25 mL round bottom flask containing [Pt(η^2-nb)(FcPPAl)] (**45**) (76.1 mg, 8.65×10^{-2} mmol) and C_2Ph_2 (15.4 mg, 8.65×10^{-2} mmol) through the use of a dry ice/acetone bath. The fawn yellow reaction mixture was left to stir overnight at room temperature before being evaporated to dryness *in vacuo*. Hexanes (10 mL) were condensed into the reaction flask and the crude product was sonicated for 15 minutes; the translucent hexanes solution was then brought into the glove box and stored at –30 °C for recrystallization. After two days, the hexanes mother liquors were decanted and the remaining fawn yellow crystalline solid was collected and dried *in vacuo*. Yield = 54 mg (65 %). X-ray quality crystals of [Pt(η^2-C_2Ph_2)(FcPPAl)] were obtained by slow diffusion of hexanes (~3 mL) into a solution of [Pt(η^2-C_2Ph_2)(FcPPAl)] in C_6D_6 (~1 mL) at room temperature. **^{1}H NMR (C_6D_6, 600 MHz, 298 K):** δ 8.04 (d, $^3J_{H,H}$ 7 Hz, 1H, CH^6), 7.93–7.89 (m, 2H, *o*-PPh_2 A), 7.86 (dd, $^3J_{H,H}$ 8 Hz, $^4J_{H,P}$ 5 Hz, 1H, CH^3), 7.67 (d, $^3J_{H,H}$ 8 Hz, 2H, *o-Ph* A), 7.62 (dd, $^3J_{H,P}$ 12 Hz, $^3J_{H,H}$ 8 Hz, 2H, *o*-PPh_2 B), 7.35 (dt, $^3J_{H,H}$ 7 Hz, $^4J_{H,P}$ 4 Hz, 1H, CH^5), 7.24 (d, $^3J_{H,H}$ 8 Hz, 2H, *o-Ph* B), 7.19 (t, $^3J_{H,H}$ 8 Hz, 1H, CH^4), 7.05–7.02 (m, 5H, *m*,*p*-PPh_2 A, *m-Ph* A), 6.93 (t, $^3J_{H,H}$ 7 Hz, 3H, *p-Ph* A, *m-Ph* B), 6.89 (t, $^3J_{H,H}$ 7 Hz, 2H, *p*-PPh_2 B, *p-Ph* B), 6.84 (dt,

$^{3}J_{H,H}$ 8 Hz, $^{4}J_{H,P}$ 1 Hz, 2H, *m*-P*Ph*$_2$ B), 4.77 (s, 1H, C*H*$^{2''/5''}$), 4.56 (s, 1H, C*H*$^{2'/5'}$), 4.35 (s, 1H, C*H*$^{5'/2'}$), 3.86 (s, 1H, C*H*$^{4'/3'}$), 3.83 (s, 1H, C*H*$^{4''/3''}$), 3.82 (s, 1H, C*H*$^{3'/4'}$), 3.73 (s, 1H, C*H*$^{3''/4''}$), 3.72 (s, 1H, C*H*$^{5''/2''}$), 1.21 (d, $^{3}J_{H,P}$ 14 Hz, 9H, C*Me*$_3$), 0.18, −0.54 (2×s, 6H, Al*Me*$_2$). **^{13}C{^{1}H} NMR (C$_6$D$_6$, 151 MHz, 298 K):** δ 173.2 (d, $^{2}J_{C,P}$ 73 Hz, *C*^{2}), 139.4 (d, $^{1}J_{C,P}$ 54 Hz, *C*^{1}), 138.0 (d, $^{1}J_{C,P}$ 43 Hz, $^{2}J_{C,Pt}$ 18 Hz, *ipso*-P*Ph*$_2$ A), 136.6 (d, $^{2}J_{C,P}$ 30 Hz, *C*^{6}), 136.3–136.0 (m, *ipso-Ph* A and B), 135.7 (dd, $^{1}J_{C,P}$ 46 Hz, $^{3}J_{C,P}$ 2 Hz, *ipso*-P*Ph*$_2$ B), 135.0 (appt. t, $^{2}J_{C,P}$ 12 Hz, *o*-P*Ph*$_2$ A and B), 132.3 (dd, $^{2}J_{C,P}$ 73 Hz, $^{2}J_{C,P}$ 8 Hz, *C*$^{\alpha}$ A), 131.8 (dd, $^{2}J_{C,P}$ 77 Hz, $^{2}J_{C,P}$ 7 Hz, *C*$^{\alpha}$ B), 131.0 (d, $^{3}J_{C,P}$ 5 Hz, *C*^{3}), 130.6 (s, *p*-P*Ph*$_2$ A), 130.2 (s, *p*-P*Ph*$_2$ B, *C*^{5}), 130.0 (d, $^{3}J_{C,Pt}$ 24 Hz, $^{4}J_{C,P}$ 4 Hz, *o-Ph* A), 129.4 (d, $^{3}J_{C,Pt}$ 23, $^{4}J_{C,P}$ 3 Hz, *o-Ph* B), 128.6 (s, *m-Ph* B), 128.3 (d, $^{3}J_{C,P}$ 8 Hz, *m*-P*Ph*$_2$ A), 128.0 (s, *m-Ph* A), 128.0 (d, $^{3}J_{C,P}$ 11 Hz, *m*-P*Ph*$_2$ B), 127.0 (2 × s, *p-Ph* A and B), 125.7 (d, $^{4}J_{C,P}$ 5 Hz, *C*^{4}), 82.2 (dd, $^{1}J_{C,P}$ 37 Hz, $^{3}J_{C,P}$ 2 Hz, *C*$^{1'}$), 80.3 (d, $^{1}J_{C,P}$ 51 Hz, *C*$^{1''}$), 75.0 (2 × s, *C*$^{5''/2''}$, *C*$^{5'/2'}$), 74.2 (d, $^{3}J_{C,P}$ 6 Hz, *C*$^{3''/4''}$), 74.1 (s, *C*$^{2''/5''}$), 72.7 (d, $^{3}J_{C,P}$ 6 Hz, *C*$^{3'/4'}$), 72.3 (d, $^{2}J_{C,P}$ 13 Hz, *C*$^{2'/5'}$), 71.0 (d, $^{2}J_{C,P}$ 4 Hz, *C*$^{4''/3''}$), 70.5 (s, *C*$^{4'/3'}$), 36.5 (dd, $^{1}J_{C,P}$ 26, $^{3}J_{C,P}$ 3 Hz, *C*Me$_3$), 29.2 (d, $^{2}J_{C,P}$ 6 Hz, C*Me*$_3$), 1.3 (d, $^{3}J_{C,P}$ 6 Hz, Al*Me*), −1.3 (s, $^{2}J_{C,Pt}$ 21 Hz, Al*Me*). **^{31}P{^{1}H} NMR (C$_6$D$_6$, 203 MHz, 298 K):** δ 59.1 (d, $^{1}J_{P,Pt}$ 2961 Hz, $^{2}J_{P,P}$ 24 Hz, C$_5$H$_4$*P*(^{t}Bu)Ar), 20.6 (d, $^{1}J_{P,Pt}$ 2933 Hz, $^{2}J_{P,P}$ 24 Hz, C$_5$H$_4$*P*Ph$_2$). **^{195}Pt{^{1}H} NMR (C$_6$D$_6$, 128 MHz, 298 K):** δ –4443 (appt t, $^{1}J_{Pt,P}$ 2941 Hz). **Raman:** ν(C≡C) = 1735 cm^{-1}. **Elemental Analysis Calcd (%)** for C$_{48}$H$_{47}$AlFeP$_2$Pt: C, 59.82; H, 4.92. Found: C, 59.95; H, 5.30.

[PtH$_2$(FcPPAl)] (49): A solution of [Pt(η^2-nb)(FcPPAl)] (**45**) (56.4 mg, 6.41×10^{-2} mmol) in benzene (5 mL) in a 50 mL Schlenk flask was subjected to three freeze/pump/thaw cycles before being cooled to –140 °C, at which point H$_2$ was added. The reaction mixture was stirred overnight at room temperature before being evaporated to dryness *in vacuo*. Hexanes (5 mL) were added to the crude product and the resulting slurry was sonicated for 15 minutes and then brought into the glove box; the precipitated product (yellow/orange solid) was isolated by centrifugation and dried *in vacuo*. Yield = 28 mg (56 %). X-ray quality crystals of [PtH$_2$(FcPPAl)] were obtained by slow diffusion of hexanes (~3 mL) into a solution of [PtH$_2$(FcPPAl)] in C$_6$D$_6$ (~1 mL) at room temperature.

^{1}H NMR (C_6D_6, 600 MHz, 298 K): δ 8.06 (d, $^{3}J_{H,H}$ 7 Hz, 1H, C*H*^{6}), 7.77–7.68 (m, 4H, C*H*^{3}, *o*-P*Ph*$_2$ A and B), 7.31 (dt, $^{3}J_{H,H}$ 7 Hz, $^{4}J_{H,P}$ 3 Hz, 1H, C*H*^{5}), 7.16 (appt. s, 1H, C*H*^{4}), 7.03–7.02 (m, 3H, *m*,*p*-P*Ph*$_2$ A), 6.96–6.92 (m, 3H, *m*,*p*-P*Ph*$_2$ B), 4.52 (s, 1H, C*H*$^{2'/5'}$), 4.50 (s, 1H, C*H*$^{2''/5''}$), 4.44 (s, 1H, C*H*$^{5'/2'}$), 3.92 (s, 1H, C*H*$^{5''/2''}$), 3.84 (s, 1H, C*H*$^{3'/4'}$), 3.82 (s, 1H, C*H*$^{4''/3''}$), 3.76 (s, 2H, C*H*$^{4'/3'}$, C*H*$^{3''/4''}$), 1.22 (d, $^{3}J_{H,P}$ 14 Hz, 9H, C*Me*$_3$), 0.30 (s, $^{3}J_{H,Pt}$ 18 Hz, 3H, Al*Me*), −0.40 (s, $^{3}J_{H,Pt}$ 11 Hz, 3H, Al*Me*), −2.44 (dd, $^{1}J_{H,Pt}$ 1002 Hz, $^{2}J_{H,P}$ 177 Hz, $^{2}J_{H,P}$ 18 Hz, 1H, Pt*H*), −3.31 (dd, $^{1}J_{H,Pt}$ 993 Hz, $^{2}J_{H,P}$ 159 Hz, $^{2}J_{H,P}$ 18 Hz, 1H, Pt*H*). **^{13}C{^{1}H} NMR (C_6D_6, 151 MHz, 298 K):** δ 173.5 (broad d, $^{2}J_{C,P}$ 64 Hz, *C*^{2}), 137.4 (d, $^{2}J_{C,P}$ 27 Hz, *C*^{6}), 137.0 (d, $^{1}J_{C,P}$ 53 Hz, *C*^{1}), 136.5 (d, $^{1}J_{C,P}$ 59 Hz, *ipso*-P*Ph*$_2$ B), 135.7 (d, $^{1}J_{C,P}$ 49 Hz, *ipso*-P*Ph*$_2$ A), 135.6 (d, $^{3}J_{C,Pt}$ 36 Hz, $^{2}J_{C,P}$ 14 Hz, *o*-P*Ph*$_2$ A), 133.4 (d, $^{3}J_{C,Pt}$ 31 Hz, $^{2}J_{C,P}$ 11 Hz, *o*-P*Ph*$_2$ B), 131.3 (s, *p*-P*Ph*$_2$ A), 131.1 (d, $^{3}J_{C,P}$ 5 Hz, *C*^{3}), 130.2 (s, *p*-P*Ph*$_2$ B), 130.0 (s, *C*^{5}), 128.8 (d, $^{3}J_{C,P}$ 11 Hz, *m*-P*Ph*$_2$ A), 128.2 (d, $^{3}J_{C,P}$ 10 Hz, *m*-P*Ph*$_2$ B), 125.5 (d, $^{4}J_{C,P}$ 6 Hz, *C*^{4}), 77.4 (d, *J* 4 Hz, *C*$^{1'}$), 77.1 (d, $^{2}J_{C,P}$ 20 Hz, *C*$^{2''/5''}$), 76.2 (dd, $^{1}J_{C,P}$ 55 Hz, $^{3}J_{C,P}$ 5 Hz, *C*$^{1''}$), 75.1 (s, *C*$^{2'/5'}$), 74.7 (s, *C*$^{3''/4''}$), 74.7 (d, $^{2}J_{C,P}$ 27 Hz, *C*$^{5'/2'}$), 74.3 (s, *C*$^{5''/2''}$), 73.3 (d, $^{3}J_{C,P}$ 7 Hz, *C*$^{4'/3'}$), 71.2 (d, $^{3}J_{C,P}$ 4 Hz, *C*$^{4''/3''}$), 70.5 (s, *C*$^{3'/4'}$), 36.3 (d, $^{1}J_{C,P}$ 26 Hz, *C*Me$_3$), 27.9 (d, $^{2}J_{C,P}$ 5 Hz, C*Me*$_3$), −1.5 (s, $^{2}J_{C,Pt}$ 50 Hz, Al*Me*), −3.0 (s, $^{2}J_{C,Pt}$ 45 Hz, Al*Me*). **^{31}P{^{1}H} NMR (C_6D_6, 243 MHz, 298 K):** δ 64.1 (d, $^{1}J_{P,Pt}$ 1891 Hz, $^{2}J_{P,P}$ 15 Hz, $C_5H_4P(^{t}Bu)Ar$), 34.1 (d, $^{1}J_{P,Pt}$ 2374 Hz, $^{2}J_{P,P}$ 15 Hz, $C_5H_4PPh_2$). **^{195}Pt{^{1}H} NMR (C_6D_6, 128 MHz, 298 K):** δ –5001 (dd, $^{1}J_{Pt,P}$ 2384 Hz, $^{1}J_{Pt,P}$ 1899 Hz). **IR:** ν(Pt–H) = 2101, 2049 cm^{-1} (nujol). **Elemental Analysis Calcd (%)** for $C_{34}H_{39}AlFeP_2Pt$: C, 51.85; H, 4.99. Found: C, 51.50; H, 4.75.

[Pt(CO)(FcPPAl)] (50): A solution of [Pt(η^{2}-nb)(FcPPAl)] (**45**) (60.3 mg, 6.86×10^{-2} mmol) in benzene (5 mL) in a 50 mL Schlenk flask was subjected to three freeze/pump/thaw cycles before being cooled to –140 °C, at which point CO was added. The reaction mixture was stirred overnight at room temperature before being evaporated to dryness *in vacuo*. Hexanes (10 mL) were added to the crude product and the resulting slurry was sonicated for 15 minutes and then brought into the glove box; the resulting translucent, orange solution was stored at –30 °C for recrystallization. After one hour, the

hexanes mother liquors were decanted and the remaining yellow, crystalline solid was dried *in vacuo*. Yield = 34 mg (61 %). X-ray quality crystals of [Pt(CO)(FcPPAl)] were obtained by slow diffusion of hexanes (~3 mL) into a solution of [Pt(CO)(FcPPAl)] in C_6D_6 (~1 mL) at room temperature. **^{1}H NMR (C_6D_6, 600 MHz, 298 K):** δ 8.12 (d, $^3J_{H,H}$ 7 Hz, 1H, C*H*^{6}), 7.69–7.64 (m, 4H, *o*-P*Ph*$_2$ A and B), 7.28 (dt, $^3J_{H,H}$ 7 Hz, $^4J_{H,P}$ 4 Hz, 1H, C*H*^{5}), 7.13 (t, $^3J_{H,H}$ 7 Hz, 1H, C*H*^{3}), 7.08–7.00 (m, 4H, *m*,*p*-P*Ph*$_2$ A, C*H*^{4}), 6.95–6.93 (m, 3H, *m*,*p*-P*Ph*$_2$ B), 4.34 (s, 1H, C*H*$^{2'/5'}$), 4.27 (s, 1H, C*H*$^{2''/5''}$), 4.22 (s, 1H, C*H*$^{5'/2'}$), 4.04 (s, 1H, C*H*$^{3''/4''}$), 3.83 (s, 1H, C*H*$^{3'/4'}$), 3.79 (s, 1H, C*H*$^{5''/2''}$), 3.77 (s, 1H, C*H*$^{4''/3''}$), 3.73 (s, 1H, C*H*$^{4'/3'}$), 1.25 (d, $^3J_{H,P}$ 15 Hz, 9H, C*Me*$_3$), 0.38, 0.17 (2×s, 6H, Al*Me*$_2$). **^{13}C{^{1}H} NMR (C_6D_6, 151 MHz, 298 K):** δ 204.6 (dd, $^2J_{C,P}$ 94 Hz, $^2J_{C,P}$ 12 Hz, Pt*C*O), 171.1 (broad d, $^2J_{C,P}$ 68 Hz, *C*^{2}), 139.5 (dd, $^1J_{C,P}$ 60 Hz, $^3J_{C,P}$ 8 Hz, *C*^{1}), 137.6 (d, $^1J_{C,P}$ 32 Hz, *ipso*-P*Ph*$_2$ A), 137.0 (d, *J* 32 Hz, *ipso*-P*Ph*$_2$ B, *C*^{6}), 134.1 (d, $^2J_{C,P}$ 14 Hz, *o*-P*Ph*$_2$ B), 133.6 (d, $^2J_{C,P}$ 14 Hz, *o*-P*Ph*$_2$ A), 131.8 (d, $^3J_{C,P}$ 7 Hz, *C*^{3}), 130.7 (s, *p*-P*Ph*$_2$ B), 130.4 (s, *p*-P*Ph*$_2$ A), 130.0 (s, *C*^{5}), 128.9 (d, $^3J_{C,P}$ 10 Hz, *m*-P*Ph*$_2$ A), 128.7 (d, $^3J_{C,P}$ 10 Hz, *m*-P*Ph*$_2$ B), 126.2 (d, $^4J_{C,P}$ 6 Hz, *C*^{4}), 84.2 (dd, $^1J_{C,P}$ 41 Hz, $^3J_{C,P}$ 7 Hz, *C*$^{1'}$), 79.1 (d, $^1J_{C,P}$ 41 Hz, *C*$^{1''}$), 75.9 (d, $^2J_{C,P}$ 7 Hz, *C*$^{5''/2''}$), 75.6 (d, $^3J_{C,P}$ 14 Hz, *C*$^{2''/5''}$), 75.4 (d, $^2J_{C,P}$ 13 Hz, *C*$^{5'/2'}$), 74.3 (d, $^2J_{C,P}$ 4 Hz, *C*$^{2'/5'}$), 72.5 (d, $^3J_{C,P}$ 6 Hz, *C*$^{3''/4''}$), 71.6 (d, $^3J_{C,P}$ 7 Hz, *C*$^{4'/3'}$), 71.2 (d, $^3J_{C,P}$ 4 Hz, *C*$^{4''/3''}$), 70.5 (d, $^3J_{C,P}$ 3 Hz, *C*$^{3'/4'}$), 37.1 (d, $^1J_{C,P}$ 28 Hz, *C*Me$_3$), 29.9 (d, $^2J_{C,P}$ 6 Hz, C*Me*$_3$), −2.56, −4.03 (2×broad s, Al*Me*$_2$). **^{31}P{^{1}H} NMR (C_6D_6, 203 MHz, 298 K):** δ 73.8 (d, $^1J_{P,Pt}$ 4089 Hz, $^2J_{P,P}$ 18 Hz, $C_5H_4P(^t$Bu)Ar), 41.1 (d, $^1J_{P,Pt}$ 2191 Hz, $^2J_{P,P}$ 18 Hz, C_5H_4PPh$_2$). **^{195}Pt{^{1}H} NMR (C_6D_6, 128 MHz, 298 K):** δ –4413 (dd, $^1J_{Pt,P}$ 4094 Hz, $^1J_{Pt,P}$ 2194 Hz). **IR:** ν(C≡O) = 1982 cm^{-1} (nujol). **Elemental Analysis Calcd (%)** for $C_{35}H_{37}AlFeOP_2Pt$: C, 51.67; H, 4.58. Found: C, 51.65; H, 4.79.

References

(1) Oakley, S. R.; Parker, K. D.; Emslie, D. J. H.; Vargas-Baca, I.; Robertson, C. M.; Harrington, L. E.; Britten, J. F. *Organometallics* **2006**, *25*, 5835.

(2) Green, M. L. H. *J. Organomet. Chem.* **1995**, *500*, 127.

(3) Parkin, G. *Organometallics* **2006**, *25*, 4744.

(4) Burlitch, J. M.; Leonowicz, M. E.; Petersen, R. B.; Hughes, R. E. *Inorg. Chem.* **1979**, *18*, 1097.

(5) Mayer, J. M.; Calabrese, J. C. *Organometallics* **1984**, *3*, 1292.

(6) Bauer, J.; Braunschweig, H.; Radacki, K. *Chem. Commun.* **2012**, *48*, 10407.

(7) Bauer, J.; Braunschweig, H.; Damme, A.; Gruß, K.; Radacki, K. *Chem. Commun.* **2011**, *47*, 12783.

(8) Bauer, J.; Braunschweig, H.; Brenner, P.; Kraft, K.; Radacki, K.; Schwab, K. *Chem. -Eur. J.* **2010**, *16*, 11985.

(9) (a) Bauer, J.; Bertermann, R.; Braunschweig, H.; Gruss, K.; Hupp, F.; Kramer, T. *Inorg. Chem.* **2012**, *51*, 5617. (b) Braunschweig, H.; Gruss, K.; Radacki, K. *Angew. Chem. Int. Ed.* **2007**, *46*, 7782.

(10) Fischer, R. A.; Miehr, A.; Hoffmann, H.; Rogge, W.; Boehme, C.; Frenking, G.; Herdtweck, E. *Z. Anorg. Allg. Chem.* **1999**, *625*, 1466.

(11) Cokoja, M.; Gemel, C.; Steinke, T.; Schröder, F.; Fischer, R. A. *Dalton Trans.* **2005**, 44.

(12) Steinke, T.; Gemel, C.; Cokoja, M.; Winter, M.; Fischer, R. A. *Dalton Trans.* **2005**, 55.

(13) Leiner, E.; Hampe, O.; Scheer, M. *Eur. J. Inorg. Chem.* **2002**, 584.

(14) Bunn, N. R.; Aldridge, S.; Kays, D. L.; Coombs, N. D.; Day, J. K.; Ooi, L.-l.; Coles, S. J.; Hursthouse, M. B. *Organometallics* **2005**, *24*, 5879.

(15) Aldridge, S.; Kays, D. L.; Bunn, N. R.; Coombs, N. D.; Ooi, L.-l. *Main Group Met. Chem.* **2005**, *28*, 201.

(16) Braunschweig, H.; Gruss, K.; Radacki, K. *Inorg. Chem.* **2008**, *47*, 8595.

(17) Nuber, B.; Schatz, W.; Ziegler, M. L. *Z. Naturforsch.***1990**, *B45*, 508.

(18) Esser, M.; Neumüller, B.; Petz, W.; Uddin, J.; Frenking, G. *Z. Anorg. Allg. Chem.* **2000**, *626*, 915.

(19) Rutsch, P.; Renner, G.; Huttner, G.; Sandhöfner, S. *Z. Naturforsch.* **2002**, *B57*, 757.

(20) (a) Shriver, D. F. *J. Am. Chem. Soc.* **1963**, *85*, 3509. (b) Johnson, M. P.; Shriver, D. F. *J. Am. Chem. Soc.* **1966**, *88*, 301.

(21) Parshall, G. W. *J. Am. Chem. Soc.* **1964**, *86*, 361.

(22) Burlitch, J. M.; Burk, J. H.; Leonowicz, M. E.; Hughes, R. E. *Inorg. Chem.* **1979**, *18*, 1702.

(23) Braunschweig, H.; Wagner, T. *Chem. Berichte* **1994**, *127*, 1613.

(24) Braunschweig, H.; Wagner, T. *Z. Naturforsch.* **1996**, *B51*, 1618.

(25) Braunschweig, H.; Kollann, C. *Z. Naturforsch.* **1999**, *B54*, 839.

(26) Bonanno, J. B.; Henry, T. P.; Wolczanski, P. T.; Pierpont, A. W.; Cundari, T. R. *Inorg. Chem.* **2007**, *46*, 1222.

(27) Thibault, M. H.; Boudreau, J.; Mathiotte, S.; Drouin, F.; Sigouin, O.; Michaud, A.; Fontaine, F.-G. *Organometallics* **2007**, *26*, 3807.

(28) Boudreau, J.; Fontaine, F.-G. *Organometallics* **2011**, *30*, 511.

(29) Sircoglou, M.; Bouhadir, G.; Saffon, N.; Miqueu, K.; Bourissou, D. *Organometallics* **2008**, *27*, 1675.

(30) Sircoglou, M.; Saffon, N.; Miqueu, K.; Bouhadir, G.; Bourissou, D. *Organometallics* **2013**, *32*, 6780.

(31) Devillard, M.; Nicolas, E.; Appelt, C.; Backs, J.; Mallet-Ladeira, S.; Bouhadir, G.; Slootweg, J. C.; Uhl, W.; Bourisou, D. *Chem. Commun.* **2014**, *50*, 14805.

(32) Fontaine, F.-G.; Zargarian, D. *J. Am. Chem. Soc.* **2004**, *126*, 8786.

(33) Beachley, O. T.; Banks, M. A.; Kopasz, J. P.; Rogers, R. D. *Organometallics* **1996**, *15*, 5170.

(34) Labinger, J. A.; Miller, J. S. *J. Am. Chem. Soc.* **1982**, *104*, 6856.

(35) Grimmett, D. L.; Labinger, J. A.; Bonfiglio, J. N.; Masuo, S. T.; Shearin, E.; Miller, J. S. *J. Am. Chem. Soc.* **1982**, *104*, 6858.

(36) Labinger, J. A.; Bonfiglio, J. N.; Grimmett, D. L.; Masuo, S. T.; Shearin, E.; Miller, J. S. *Organometallics* **1983**, *2*, 733.

(37) Grimmett, D. L.; Labinger, J. A.; Bonfiglio, J. N.; Masuo, S. T.; Shearin, E.; Miller, J. S. *Organometallics* **1983**, *2*, 1325.

(38) Rudd, P. A.; Liu, S.; Gagliardi, L.; Young, V. G.; Lu, C. C. *J. Am. Chem. Soc.* **2011**, *133*, 20724.

(39) Rudd, P. A.; Planas, N.; Bill, E.; Gagliardi, L.; Lu, C. C. *Eur. J. Inorg. Chem.* **2013**, 3898.

(40) Harman, W. H.; Lin, T.-P.; Peters, J. C. *Angew. Chem. Int. Ed.* **2014**, *53*, 1081.

(41) (a) Lin, T.-P.; Nelson, R. C.; Wu, T.; Miller, J. T.; Gabbaï, F. P. *Chem. Sci.* **2012**, *3*, 1128. (b) Fontaine, F.-G.; Boudreau, J.; Thibault, M.-H. *Eur. J. Inorg. Chem.* **2008**, 5439.

(42) Kameo, H.; Hashimoto, Y.; Nakazawa, H. *Organometallics* **2012**, *31*, 3155.

(43) Zhao, X.; Otten, E.; Song, D.; Stephan, D. W. *Chem. -Eur. J.* **2010**, *16*, 2040.

(44) Sircoglou, M.; Bontemps, S.; Mercy, M.; Saffon, N.; Takahashi, M.; Bouhadir, G.; Maron, L.; Bourissou, D. *Angew. Chem. Int. Ed.* **2007**, *46*, 8583.

(45) Amgoune, A.; Bourissou, D. *Chem. Commun.* **2011**, *47*, 859.

(46) Moret, M.-E.; Peters, J. C. *Angew. Chem. Int. Ed.* **2011**, *50*, 2063.

(47) Bontemps, S.; Bouhadir, G.; Miqueu, K.; Bourissou, D. *J. Am. Chem. Soc.* **2006**, *128*, 12056.

(48) Vergnaud, J.; Ayed, T.; Hussein, K.; Vendier, L.; Grellier, M.; Bouhadir, G.; Barthelat, J.-C.; Sabo-Etienne, S.; Bourissou, D. *Dalton Trans.* **2007**, 2370.

(49) Bontemps, S.; Bouhadir, G.; Apperley, D. C.; Dyer, P. W.; Miqueu, K.; Bourissou, D. *Chem. Asian J.* **2009**, *4*, 428.

(50) Pang, K.; Tanski, J. M.; Parkin, G. *Chem. Commun.* **2008**, 1008.

(51) Figueroa, J. S.; Melnick, J. G.; Parkin, G. *Inorg. Chem.* **2006**, *45*, 7056.

(52) (a) Crossley, I. R.; Hill, A. F. *Dalton Trans.* **2008**, 201. (b) Podiyanachari, S. K.; Fröhlich, R.; Daniliuc, C. G.; Petersen, J. L.; Mück-Lichtenfeld, C.; Kehr, G.; Erker, G. *Angew. Chem. Int. Ed.* **2012**, *51*, 8830. (c) Podiyanachari, S. K.; Kehr, G.; Mück-Lichtenfeld, C.; Daniliuc, C. G.; Erker, G. *J. Am. Chem. Soc.* **2013**, *135*, 17444. (d) Cowie, B. E.; Emslie, D. J. H.; Jenkins, H. A.; Britten, J. F. *Inorg. Chem.* **2010**, *49*, 4060.

(53) Turculet, L.; Feldman, J. D.; Tilley, T. D. *Organometallics* **2004**, *23*, 2488.

(54) Fischbach, A.; Bazinet, P. R.; Waterman, R.; Tilley, T. D. *Organometallics* **2008**, *27*, 1135.

(55) Khaskin, E.; Zavalij, P. Y.; Vedernikov, A. N. *J. Am. Chem. Soc.* **2008**, *130*, 10088.

(56) Fromel, S.; Kehr, G.; Fröhlich, R.; Daniliuc, C. G.; Erker, G. *Dalton Trans.* **2013**, *42*, 14531.

(57) (a) Pal, S.; Vedernikov, A. N. *Dalton Trans.* **2012**, *41*, 8116. (b) Khaskin, E.; Zavalij, P. Y.; Vedernikov, A. N. *Angew. Chem. Int. Ed.* **2007**, *46*, 6309.

(58) (a) Zhu, J.; Mukherjee, D.; Sadow, A. D. *Chem. Commun.* **2012**, *48*, 464. (b) Dunne, J. F.; Manna, K.; Wiench, J. W.; Ellern, A.; Pruski, M.; Sadow, A. D. *Dalton Trans.* **2010**, *39*, 641.

(59) Emslie, D. J. H.; Blackwell, J. M.; Britten, J. F.; Harrington, L. E. *Organometallics* **2006**, *25*, 2412.

(60) Fong, H.; Moret, M.-E.; Lee, Y.; Peters, J. C. *Organometallics* **2013**, *32*, 3053.

(61) Crossley, I. R.; Hill, A. F.; Willis, A. C. *Organometallics* **2007**, *26*, 3891.

(62) Miller, A. J. M.; Labinger, J. A.; Bercaw, J. E. *Organometallics* **2011**, *30*, 4308.

(63) Miller, A. J. M.; Labinger, J. A.; Bercaw, J. E. *Organometallics* **2010**, *29*, 4499.

(64) Miller, A. J. M.; Labinger, J. A.; Bercaw, J. E. *J. Am. Chem. Soc.* **2008**, *130*, 11874.

(65) Hill, A. F.; Owen, G. R.; White, A. J. P.; Williams, D. J. *Angew. Chem. Int. Ed.* **1999**, *38*, 2759.

(66) Brown, H. C.; Fletcher, E. A. *J. Am. Chem. Soc.* **1951**, *73*, 2808.

(67) Garner, M.; Reglinski, J.; Cassidy, I.; Spicer, M. D.; Kennedy, A. R. *Chem. Commun.* **1996**, 1975.

(68) Cordero, B.; Gómez, V.; Platero-Prats, A. E.; Revés, M.; Echeverría, J.; Cremades, E.; Barragán, F.; Alvarez, S. *Dalton Trans.* **2008**, 2832.

(69) Braunschweig, H.; Koster, M.; Wang, R. *Inorg. Chem.* **1999**, *38*, 415.

(70) Crossley, I. R.; Foreman, M.; Hill, A. F.; Owen, G. R.; White, A. J. P.; Williams, D. J.; Willis, A. C. *Organometallics* **2008**, *27*, 381.

(71) Foreman, M. R. St.-J.; Hill, A. F.; White, A. J. P.; Williams, D. J. *Organometallics* **2004**, *23*, 913.

(72) Crossley, I. R.; Foreman, M. R. St.-J.; Hill, A. F.; White, A. J. P.; Williams, D. J. *Chem. Commun.* **2005**, 221.

(73) Crossley, I. R.; Hill, A. F.; Humphrey, E. R.; Willis, A. C. *Organometallics* **2005**, *24*, 4083.

(74) Crossley, I. R.; Hill, A. F.; Willis, A. C. *Organometallics* **2006**, *25*, 289.

(75) Crossley, I. R.; Hill, A. F.; Willis, A. C. *Organometallics* **2010**, *29*, 326.

(76) Crossley, I. R.; Hill, A. F.; Willis, A. C. *Organometallics* **2008**, *27*, 312.

(77) Kimblin, C.; Hascall, T.; Parkin, G. *Inorg. Chem.* **1997**, *36*, 5680.

(78) Crossley, I. R.; Hill, A. F.; Willis, A. C. *Organometallics* **2005**, *24*, 1062.

(79) Pang, K.; Quan, S. M.; Parkin, G. *Chem. Commun.* **2006**, 5015.

(80) Landry, V. K.; Melnick, J. G.; Buccella, D.; Pang, K.; Ulichny, J. C.; Parkin, G. *Inorg. Chem.* **2006**, *45*, 2588.

(81) Senda, S.; Ohki, Y.; Hirayama, T.; Toda, D.; Chen, J.-L.; Matsumoto, T.; Kawaguchi, H.; Tatsumi, K. *Inorg. Chem.* **2006**, *45*, 9914.

(82) Mihalcik, D. J.; White, J. L.; Tanski, J. M.; Zakharov, L. N.; Yap, G. P. A.; Incarvito, C. D.; Rheingold, A. L.; Rabinovich, D. *Dalton Trans.* **2004**, 1626.

(83) López-Gómez, M. J.; Connelly, N. G.; Haddow, M. F.; Hamilton, A.; Orpen, A. G. *Dalton Trans.* **2010**, *39*, 5221.

(84) Blagg, R. J.; Connelly, N. G.; Haddow, M. F.; Hamilton, A.; Lusi, M.; Orpen, A. G.; Ridgway, B. M. *Dalton Trans.* **2010**, *39*, 11616.

(85) Blagg, R. J.; Adams, C. J.; Charmant, J. P. H.; Connelly, N. G.; Haddow, M. F.; Hamilton, A.; Knight, J.; Orpen, A. G.; Ridgway, B. M. *Dalton Trans.* **2009**, 8724.

(86) Blagg, R. J.; Charmant, J. P. H.; Connelly, N. G.; Haddow, M. F.; Orpen, A. G. *Chem. Commun.* **2006**, 2350.

(87) López-Gómez, M. J.; Connelly, N. G.; Haddow, M. F.; Hamilton, A.; Lusi, M.; Baisch, U.; Orpen, A. G. *Dalton Trans.* **2011**, *40*, 4647.

(88) Tsoureas, N.; Haddow, M. F.; Hamilton, A.; Owen, G. R. *Chem. Commun.* **2009**, 2538.

(89) Tsoureas, N.; Kuo, Y.-Y.; Haddow, M. F.; Owen, G. R. *Chem. Commun.* **2011**, *47*, 484.

(90) Tsoureas, N.; Bevis, T.; Butts, C. P.; Hamilton, A.; Owen, G. R. *Organometallics* **2009**, *28*, 5222.

(91) Zech, A.; Haddow, M. F.; Othman, H.; Owen, G. R. *Organometallics* **2012**, *31*, 6753.

(92) Tsoureas, N.; Hamilton, A.; Haddow, M. F.; Harvey, J. N.; Orpen, A. G.; Owen, G. R. *Organometallics* **2013**, *32*, 2840.

(93) Owen, G. R.; Gould, P. H.; Charmant, J. P. H.; Hamilton, A.; Saithong, S. *Dalton Trans.* **2010**, *39*, 392.

(94) Dyson, G.; Zech, A.; Rawe, B. W.; Haddow, M. F.; Hamilton, A.; Owen, G. R. *Organometallics* **2011**, *30*, 5844.

(95) Nuss, G.; Saischek, G.; Harum, B. N.; Volpe, M.; Gatterer, K.; Belaj, F.; Mösch-Zanetti, N. C. *Inorg. Chem.* **2011**, *50*, 1991.

(96) Nuss, G.; Saischek, G.; Harum, B. N.; Volpe, M.; Belaj, F.; Mösch-Zanetti, N. C. *Inorg. Chem.* **2011**, *50*, 12632.

(97) (a) Pang, K.; Quan, S. M.; Parkin, G. *Chem. Commun.* **2006**, 5015. (b) Landry, V. K.; Melnick, J. G.; Buccella, D.; Pang, K.; Ulichny, J. C.; Parkin, G. *Inorg. Chem.* **2006**, *45*, 2588.

(98) Pearson, R. G. *Science* **1966**, *151*, 172.

(99) Blagg, R. J.; Charmant, J. P. H.; Connelly, N. G.; Haddow, M. F.; Orpen, A. G. *Chem. Commun.* **2006**, 2350.

(100) Careri, M.; Elviri, L.; Lanfranchi, M.; Marchiò, L.; Mora, C.; Pellinghelli, M. A. *Inorg. Chem.* **2003**, *42*, 2109.

(101) Song, D.; Jia, W. L.; Wu, G.; Wang, S. *Dalton Trans.* **2005**, 433.

(102) Dyson, G.; Hamilton, A.; Mitchell, B.; Owen, G. R. *Dalton Trans.* **2009**, 6120.

(103) Bontemps, S.; Gornitzka, H.; Bouhadir, G.; Miqueu, K.; Bourissou, D. *Angew. Chem. Int. Ed.* **2006**, *45*, 1611.

(104) Bontemps, S.; Bouhadir, G.; Dyer, P. W.; Miqueu, K.; Bourissou, D. *Inorg. Chem.* **2007**, *46*, 5149.

(105) Sircoglou, M.; Bontemps, S.; Mercy, M.; Miqueu, K.; Ladeira, S.; Saffon, N.; Maron, L.; Bouhadir, G.; Bourissou, D. *Inorg. Chem.* **2010**, *49*, 3983.

(106) Smirnova, E. S.; Echavarren, A. M. *Angew. Chem. Int. Ed.* **2013**, *52*, 9023.

(107) Son, J.-H.; Pudenz, M. A.; Hoefelmeyer, J. D. *Dalton Trans.* **2010**, *39*, 11081.

(108) Vergnaud, J.; Grellier, M.; Bouhadir, G.; Vendier, L.; Sabo-Etienne, S.; Bourissou, D. *Organometallics* **2008**, *27*, 1140.

(109) Spies, P.; Erker, G.; Kehr, G.; Bergander, K.; Fröhlich, R.; Grimme, S.; Stephan, D. W. *Chem. Commun.* **2007**, 5072.

(110) Miller, A. J. M.; Labinger, J. A.; Bercaw, J. E. *J. Am. Chem. Soc.* **2010**, *132*, 3301.

(111) Ostapowicz, T. G.; Merkens, C.; Hölscher, M.; Klankermayer, J.; Leitner, W. *J. Am. Chem. Soc.* **2013**, *135*, 2104.

(112) Baker, R. T.; Calabrese, J. C.; Westcott, S. A.; Marder, T. B. *J. Am. Chem. Soc.* **1995**, *117*, 8777.

(113) Jana, R.; Blacque, O.; Jiang, Y.; Berke, H. *Eur. J. Inorg. Chem.* **2013**, 3155.

(114) Greenacre, V. K.; Ansell, M. B.; Roe, S. M.; Crossley, I. R. *Eur. J. Inorg. Chem.* **2014**, 5053.

(115) Emslie, D. J. H.; Cowie, B. E.; Kolpin, K. B. *Dalton Trans.* **2012**, *41*, 1101.

(116) Barnett, B. R.; Moore, C. E.; Rheingold, A. L.; Figueroa, J. S. *J. Am. Chem. Soc.* **2014**, *136*, 10262.

(117) Bebbington, M. W. P.; Bontemps, S.; Bouhadir, G.; Hanton, M. J.; Tooze, R. P.; Rensburg, H. v.; Bourissou, D. *New J. Chem.* **2010**, *34*, 1556.

(118) Malacea, R.; Saffon, N.; Gómez, M.; Bourissou, D. *Chem. Commun.* **2011**, *47*, 8163.

(119) Malacea, R.; Chahdoura, F.; Devillard, M.; Saffon, N.; Gómez, M.; Bourissou, D. *Adv. Synth. Catal.* **2013**, *355*, 2274.

(120) Bontemps, S.; Sircoglou, M.; Bouhadir, G.; Puschmann, H.; Howard, J. A. K.; Dyer, P. W.; Miqueu, K.; Bourissou, D. *Chem. -Eur. J.* **2008**, *14*, 731.

(121) Carvajal, M. A.; Novoa, J. J.; Alvarez, S. *J. Am. Chem. Soc.* **2004**, *126*, 1465.

(122) Emslie, D. J. H.; Harrington, L. E.; Jenkins, H. A.; Robertson, C. M.; Britten, J. F. *Organometallics* **2008**, *27*, 5317.

(123) Emslie, D. J. H.; Cowie, B. E.; Oakley, S. R.; Huk, N. L.; Jenkins, H. A.; Harrington, L. E.; Britten, J. F. *Dalton Trans.* **2012**, *41*, 3523.

(124) Kameo, H.; Nakazawa, H. *Organometallics* **2012**, *31*, 7476.

(125) Conifer, C. M.; Law, D. J.; Sunley, G. J.; White, A. J. P.; Britovsek, G. J. P. *Organometallics* **2011**, *30*, 4060.

(126) Boone, M. P.; Stephan, D. W. *J. Am. Chem. Soc.* **2013**, *135*, 8508.

(127) Boone, M. P.; Stephan, D. W. *Chem. -Eur. J.* **2014**, *20*, 3333.

(128) Harman, W. H.; Peters, J. C. *J. Am. Chem. Soc.* **2012**, *134*, 5080.

(129) MacMillan, S. N.; Harman, W. H.; Peters, J. C. *Chem. Sci.* **2014**, *5*, 590.

(130) Suess, D. L. M.; Peters, J. C. *J. Am. Chem. Soc.* **2013**, *135*, 4938.

(131) Suess, D. L. M.; Peters, J. C. *J. Am. Chem. Soc.* **2013**, *135*, 12580.

(132) Bontemps, S.; Bouhadir, G.; Gu, W.; Mercy, M.; Chen, C.-H.; Foxman, B. M.; Maron, L.; Ozerov, O. V.; Bourissou, D. *Angew. Chem. Int. Ed.* **2008**, *47*, 1481.

(133) Sircoglou, M.; Bontemps, S.; Bouhadir, G.; Saffon, N.; Miqueu, K.; Gu, W.; Mercy, M.; Chen, C.-H.; Foxman, B. M.; Maron, L.; Ozerov, O. V.; Bourissou, D. *J. Am. Chem. Soc.* **2008**, *130*, 16729.

(134) Moret, M.-E.; Peters, J. C. *J. Am. Chem. Soc.* **2011**, *133*, 18118.

(135) (a) Chatt, J.; Dilworth, J. R.; Richards, R. L. *Chem. Rev.* **1978**, *78*, 589. (b) Hendrich, M. P.; Gunderson, W.; Behan, R. K.; Green, M. T.; Mehn, M. P.; Betley, T. A.; Lu, C. C.; Peters, J. C. *Proc. Natl Acad. Sci. USA* **2006**, *103*, 17107.

(136) Anderson, J. S.; Moret, M.-E.; Peters, J. C. *J. Am. Chem. Soc.* **2013**, *135*, 534.

(137) Anderson, J. S.; Rittle, J.; Peters, J. C. *Nature* **2013**, *501*, 84.

(138) Moret, M.-E.; Zhang, L.; Peters, J. C. *J. Am. Chem. Soc.* **2013**, *135*, 3792.

(139) Suess, D. L. M.; Tsay, C.; Peters, J. C. *J. Am. Chem. Soc.* **2012**, *134*, 14158.

(140) Tutusaus, O.; Ni, C.; Szymczak, N. K. *J. Am. Chem. Soc.* **2013**, *135*, 3403.

(141) Courtemanche, M.-A.; Larouche, J.; Légaré, M.-A.; Bi, W.; Maron, L.; Fontaine, F.-G. *Organometallics* **2013**, *32*, 6804.

(142) (a) Fryzuk, M. D.; McManus, N. T.; Rettig, S. J.; White, G. S. *Angew. Chem. Int. Ed. Engl.* **1990**, *29*, 73. (b) Fryzuk, M. D.; Huang, L.; McManus, N. T.; Paglia, P.; Rettig, S. J.; White, G. S. *Organometallics* **1992**, *11*, 2979.

(143) Karsch, H. H.; Appelt, A.; Kohler, F. H.; Muller, G. *Organometallics* **1985**, *4*, 231.

(144) Appelt, C.; Westenberg, H.; Bertini, F.; Ehlers, A. W.; Slootweg, J. C.; Lammertsma, K.; Uhl, W. *Angew. Chem. Int. Ed.* **2011**, *50*, 3925.

(145) Lancaster, S. J.; Al-Benna, S.; Thornton-Pett, M.; Bochmann, M. *Organometallics* **2000**, *19*, 1599.

(146) Crevier, T. J.; Bennett, B. K.; Soper, J. D.; Bowman, J. A.; Dehestani, A.; Hrovat, D. A.; Lovell, S.; Kaminsky, W.; Mayer, J. M. *J. Am. Chem. Soc.* **2001**, *123*, 1059.

(147) Languérand, A.; Barnes, S. S.; Bélanger-Chabot, G.; Maron, L.; Berrouard, P.; Audet, P.; Fontaine, F.-G. *Angew. Chem. Int. Ed.* **2009**, *48*, 6695.

(148) Antiñolo, A. C.-H., F.; Fernández-Baeza, J.; García-Yuste, S.; Otero, A.; Sánchez-Prada, J.; Villaseñor, E. *J. Organomet. Chem.* **2000**, *609*, 123.

(149) (a) Frech, C. M.; Shimon, L. J. W.; Milstein, D. *Organometallics* **2009**, *28*, 1900. (b) Tkach, V. S.; Myagmarsuren, G.; Suslov, D. S.; Darjaa, T.; Dorj, D.; Shmidt,

F. K. *Cat. Comm.* **2008**, *9*, 1501. (c) Majumdar, M.; Patra, S. K.; Kannan, M.; Dunbar, K. R.; Bera, J. K. *Inorg. Chem.* **2008**, *47*, 2212. (d) Feller, M.; Ben-Ari, E.; Gupta, T.; Shimon, L. J. W.; Leitus, G.; Diskin-Posner, Y.; Weiner, L.; Milstein, D. *Inorg. Chem.* **2007**, *46*, 10479. (e) Drabent, K.; Clunlk, Z.; Ozarowskl, A. *Inorg. Chem.* **2008**, *47*, 3358.

(150) Fischer, E. O.; Bock, M. *J. Organomet. Chem.* **1985**, *287*, 279.

(151) (a) Kiplinger, J. L.; Richmond, T. G.; Osterberg, C. E. *Chem. Rev.* **1994**, *94*, 373. (b) Grushin, V. V.; Alper, H. *Chem. Rev.* **1994**, *94*, 1047. (c) Torrens, H. *Coord. Chem. Rev.* **2005**, *249*, 1957. (d) Murphy, E. F.; Murugavel, R.; Roesky, H. W. *Chem. Rev.* **1997**, *97*, 3425. (e) Amii, H.; Uneyama, K. *Chem. Rev.* **2009**, *109*, 2119. (f) Perutz, R. N.; Braun, T. Chapter 1.26: Transition Metal-mediated C-F Bond Activation. In *Comprehensive Organometallic Chemistry III*; Parkin, G., Ed.; Elsevier Ltd.: Oxford, 2007; Vol. 3. Compounds of Groups 13-15, p. 725. (g) Watson, D. A.; Su, M.; Teverovskiy, G.; Zhang, Y.; García-Fortanet, J.; Kinzel, T.; Buchwald, S. L. *Science* **2009**, *325*, 1661.

(152) Burdeniuc, J.; Jedlicka, B.; Crabtree, R. H. *Chem. Ber.* **1997**, *130*, 145.

(153) Doherty, N. M.; Hoffman, N. W. *Chem. Rev.* **1991**, *91*, 553.

(154) (a) Baker, M. J.; Giles, M. F.; Orpen, A. G.; Taylor, M. J.; Watt, R. J. *J. Chem. Soc., Chem. Commun.* **1995**, 197. (b) Steeg, N.; Kramolowsky, R. *Z. Kristallogr. - New Cryst. Struct.* **1997**, *212*, 273. (c) Raghuraman, K.; Krishnamurthy, S. S.; Nethaji, M. *J. Organomet. Chem.* **2003**, *669*, 79.

(155) Brauer, D. J.; Bürger, H.; Chebude, Y.; Pawelke, G. *Inorg. Chem.* **1999**, *38*, 3972.

(156) (a) Cross, W. I.; Lightfoot, M. P.; Mair, F. S.; Pritchard, R. G. *Inorg. Chem.* **2000**, *39*, 2690. (b) Narula, C. K.; Nöth, H. *Inorg. Chem.* **1984**, *24*, 2532.

(157) Gunther, H. *NMR Spectroscopy*, Thieme Verlag: Stuttgart, 1992.

(158) Weller, F.; Mohlen, M.; Dehnicke, K. *Z. Kristallogr. - New Cryst. Struct.* **1997**, *212*, 159.

(159) Lijima, K.; Oonishi, I.; Shibata, S. *Chem. Lett.* **1983**, 251.

(160) Brown, D. S.; Carmalt, C. J.; Cowley, A. H.; Decken, A.; Isom, H. S. *Heteroatom Chem.* **1998**, *9*, 79.

(161) Steyl, G.; Kirsten, L.; Muller, A.; Roodt, A. *Acta Cryst.* **2006**, *E62*, m1127.

(162) Thomas, C. M.; Peters, J. C. *Inorg. Chem.* **2004**, *43*, 8.

(163) César, V.; Bellemin-Laponnaz, S.; Gade, L. H. *Eur. J. Inorg. Chem.* **2004**, 3436.

(164) Willems, S. T. H.; Budzelaar, P. H. M.; Moonen, N. N. P.; Gelder, R. D.; Smits, J. M. M.; Gal, A. W. *Chem. -Eur. J.* **2002**, *8*, 1310.

(165) Kranich, R.; Eis, K.; Geis, O.; Mühle, S.; Bats, J. W.; Schmalz, H.-G. *Chem. -Eur. J.* **2000**, *6*, 2874.

(166) Dilworth, J. R.; W, C. A. M. v. B.; Pascu, S. I. *Dalton Trans.* **2005**, 2151.

(167) Aarset, K.; Shen, Q.; Thomassen, H.; Richardson, A. D.; Hedberg, K. *J. Phys. Chem.* **1999**, *A103*, 1644.

(168) Housecroft, C. E.; Sharpe, A. G. *Inorganic Chemistry*, 2nd ed.; Pearson Education Limited: London, 2005.

(169) Brunner, H.; Zettler, C.; Zabel, M. *Z. Anorg. Allg. Chem.* **2003**, *629*, 1131.

(170) Lamb, G.; Clarke, M.; Slawin, A. M. Z.; Williams, B.; Key, L. *Dalton Trans.* **2007**, 5582.

(171) Corey, E. J.; Rohde, J. J.; Fischer, A.; Mihai D, A. *Tetrahedron Lett.* **1997**, *38*, 33.

(172) Nie, Y.; Schwiegk, S.; Pritzkow, H.; Siebert, W. *Eur. J. Inorg. Chem.* **2004**, 1630.

(173) Black, D. L.; Taylor, R. C. *Acta Crystallogr.* **1975**, *B31*, 1116.

(174) Tsao, F. A.; Stephan, D. W. *Dalton Trans.* **2015**, *44*, 71.

(175) Jimenez-Rodriguez, C.; Pogorzelec, P. J.; Eastham, G. R.; Slawin, A. M. Z.; Cole-Hamilton, D. J. *Dalton Trans.* **2007**, 4160.

(176) Welch, G. C.; Cabrera, L.; Chase, P. A.; Hollink, E.; Masuda, J. D.; Wei, P.; Stephan, D. W. *Dalton Trans.* **2007**, 3407.

(177) Agou, T.; Kobayashi, J.; Kim, Y.; Gabbaï, F. P.; Kawashima, T. *Chem. Lett.* **2007**, *36*, 976.

(178) Yamaguchi, S.; Akiyama, S.; Tamao, K. *J. Am. Chem. Soc.* **2001**, *123*, 11372.

(179) Hannant, M. H.; Wright, J. A.; Lancaster, S. J.; Hughes, D. L.; Horton, P. N.; Bochmann, M. *Dalton Trans.* **2006**, 2415.

(180) Chiu, C.-W.; Gabbaï, F. P. *J. Am. Chem. Soc.* **2006**, *128*, 14248.

(181) Brauer, D. J.; Burger, H.; Hubinger, R.; Pawelke, G. *Z. Anorg. Allg. Chem.* **2001**, *627*, 679.

(182) (a) Bondi, A. *J. Phys. Chem.* **1964**, *68*, 441. (b) Nag, S.; Banerjee, K.; Datta, D. *New J. Chem.* **2007**, *31*, 832.

(183) Kuznetsov, V. F.; Facey, G. A.; Yap, G. P. A.; Alper, H. *Organometallics* **1999**, *18*, 4706.

(184) Zhao, P.; Incarvito, C. D.; Hartwig, J. F. *J. Am. Chem. Soc.* **2006**, *128*, 3124.

(185) (a) Grushin, V. V.; Marshall, W. J. *J. Am. Chem. Soc.* **2004**, *126*, 3068. (b) Macgregor, S. A.; Roe, D. C.; Marshall, W. J.; Bloch, K. M.; Bakhmutov, V. I.; Grushin, V. V. *J. Am. Chem. Soc.* **2005**, *127*, 15304. (c) Marshall, W. J.; Aullón, G.; Alvarez, S.; Dobbs, K. D.; Grushin, V. V. *Eur. J. Inorg. Chem.* **2006**, 3340.

(186) Mallory, F. B.; Mallory, C. W. Coupling Through Space in Organic Chemistry. In *An Encyclopedia of Nuclear Magnetic Resonance*; Grant, D. M.; Harris, R. K., Eds.; Wiley: Chichester, 1996; Vol. 3, p. 1495.

(187) Hierso, J.-C.; Fihri, A.; Ivanov, V. V.; Hanquet, B.; Pirio, N.; Donnadieu, B.; Rebière, B.; Amardeil, R.; Meunier, P. *J. Am. Chem. Soc.* **2004**, *126*, 11077.

(188) Thomas, D. A.; Ivanov, V. V.; Butler, I. R.; Horton, P. N.; Meunier, P.; Hierso, J.-C. *Inorg. Chem.* **2008**, *47*, 1607.

(189) Arnold, W. D.; Mao, J.; Sun, H.; Oldfield, E. *J. Am. Chem. Soc.* **2000**, *122*, 12164.

(190) Kruck, M.; Munoz, M. P.; Bishop, H. L.; Frost, C. G.; Chapman, C. J.; Kociok-Köhn, G.; Butts, C. P.; Lloyd-Jones, G. C. *Chem. -Eur. J.* **2008**, *14*, 7808.

(191) Tuttle, T.; Gräfenstein, J.; Cremer, D. *Chem. Phys. Lett.* **2004**, *394*, 5.

(192) Miller, G. R.; Yankowsky, A. W.; Grim, S. O. *J. Chem. Phys.* **1969**, *51*, 3185.

(193) Jonáš, J.; Gutowsky, H. S. *J. Chem. Phys.* **1965**, *42*, 140.

(194) Iwaoka, M.; Komatsu, H.; Katsuda, T.; Tomoda, S. *J. Am. Chem. Soc.* **2002**, *124*, 1902.

(195) Benson, J. W. *Organometallics* **1998**, *17*, 4275.

(196) Thomas, J. C.; Peters, J. C. *Inorg. Chem.* **2003**, *42*, 5055.

(197) Sonoda, A.; Bailey, P. M.; Maitlis, P. M. *J. Chem. Soc., Dalton Trans.* **1979**, 346.

(198) Hitchcock, P. B.; Khvostov, A. V.; Lappert, M. F.; Protchenko, A. V. *Dalton Trans.* **2009**, 2383.

(199) Akagi, F.; Matsuo, T.; Kawaguchi, H. *J. Am. Chem. Soc.* **2005**, *127*, 11936.

(200) Cook, K. S.; Piers, W. E.; Woo, T. K.; McDonald, R. *Organometallics* **2001**, *20*, 3927.

(201) Cook, K. S.; Piers, W. E.; Rettig, S. J. *Organometallics* **1999**, *18*, 1575.

(202) Zettler, F.; Hausen, H. D.; Hess, H. *J. Organomet. Chem.* **1974**, *72*, 157.

(203) Goldman, A. S.; Krogh-Jespersen, K. *J. Am. Chem. Soc.* **1996**, *118*, 12159.

(204) Crossley, I. R.; Hill, A. F.; Humphrey, E. R.; Smith, M. K. *Organometallics* **2006**, *25*, 2242.

(205) Tsoureas, N.; Owen, G. R.; Hamilton, A.; Orpen, A. G. *Dalton Trans.* **2008**, 6039.

(206) Herberhold, M.; Eibl, S.; Milius, W.; Wrackmeyer, B. *Z. Anorg. Allg. Chem.* **2000**, *626*, 552.

(207) (a) Barybin, M. V.; Meyers J. J., Jr.; Neal, B. M. Renaissance of Isocyanoarenes as Ligands in Low-Valent Organometallics. In *Isocyanide Chemistry*; Nenajdenko, V., Ed.; Wiley: Hoboken, NJ, 2012; p. 493. (b) Hahn, E. E. *Angew. Chem. Int. Ed. Engl.* **1993**, *32*, 650.

(208) Cronin, D. L.; Wilkinson, J. R.; Todd, L. J. *J. Mag. Res.* **1975**, *17*, 353.

(209) (a) Yamamoto, Y. *Coord. Chem. Rev.* **1980**, *32*, 193. (b) Lazar, M.; Angelici, R. J. Isocyanide Binding Modes on Metal Surfaces and in Metal Complexes. In *Mondern Surface Organometallic Chemistry*; Basset, J.-M.; Psaro, R.; Roberto, D.; Ugo, R., Eds.; Wiley-VCH: Weinheim, Germany, 2009; p. 513. (c) Vogler, A. Coordinated Isonitriles. In *Isonitrile Chemistry*; Ugi, I., Ed.; Academic Press: New York 1971; p. 217.

(210) Fehlhammer, W. P.; Schrölkamp, S.; Sperber, W. *Inorg. Chim. Acta* **1993**, *212*, 207.

(211) Wu, J.; Fanwick, P. E.; Kubiak, C. P. *J. Am. Chem. Soc.* **1989**, *111*, 7812.

(212) Watanabe, T.; Kurogi, T.; Ishida, Y.; Kawaguchi, K. *Dalton Trans.* **2011**, *40*, 7701.

(213) Albano, V. G.; Busetto, L.; Cassani, M. C.; Sabatino, P.; Schmitz, A.; Zanotti, V. *J. Chem. Soc., Dalton Trans.* **1995**, 2087.

(214) Albano, V. G.; Bordoni, S.; Busetto, L.; Camiletti, C.; Monari, M.; Palazzi, A.; Prestopino, F.; Zanotti, V. *J. Chem. Soc., Dalton Trans.* **1997**, 4665.

(215) Knorr, M.; Strohmann, C. *Eur. J. Inorg. Chem.* **1998**, 495.

(216) Goswami, A.; Maier, C.-J.; Pritzkow, H.; Siebert, W. *J. Organomet. Chem.* **2005**, *690*, 3251.

(217) Pombeiro, A. J. L.; da Silva, M. F. C. G.; Michelin, R. A. *Coord. Chem. Rev.* **2001**, *218*, 43.

(218) Lutz, M.; Haukka, M.; Pakkanen, T. A.; Gade, L. H. *Organometallics* **2001**, *20*, 2631.

(219) Fukumoto, K.; Sakai, A.; Oya, T.; Nakazawa, H. *Chem. Commun.* **2012**, *48*, 3809.

(220) Hunt, I. D.; Mills, O. S. *Acta Cryst.* **1977**, *B33*, 2432.

(221) Akita, M.; Kato, S.-i.; Terada, M.; Masaki, Y.; Tanaka, M.; Moro-oka, Y. *Organometallics* **1997**, *16*, 2392.

(222) Werner, H.; Schwab, P.; Bleuel, E.; Mahr, N.; Windmüller, B.; Wolf, J. *Chem. - Eur. J.* **2000**, *6*, 4461.

(223) Werner, H.; Schwab, P.; Bleuel, E.; Mahr, N.; Steinert, P.; Wolf, J. *Chem. -Eur. J.* **1997**, *3*, 1375.

(224) Jones, W. D.; Duttweiler, R. P., Jr.; Feher, F. J. *Inorg. Chem.* **1990**, *29*, 1505.

(225) Herrmann, W. A.; Weber, C.; Ziegler, M. L.; Serhadli, O. *J. Organomet. Chem.* **1985**, *297*, 245.

(226) Esteruelas, M. A.; Lahoz, F. J.; Oñate, E.; Oro, L. A.; Rodríguez, L. *Organometallics* **1993**, *12*, 4219.

(227) Kiviniemi, S.; Nissinen, M.; Alaviuhkola, T.; Rissanen, K.; Pursiainen, J. *J. Chem. Soc., Perkin Trans. 2* **2001**, 2364.

(228) (a) Abdalla, J. A. B.; Riddlestone, I. M.; Tirfoin, R.; Phillips, N.; Bates, J. I.; Aldridge, S. *Chem. Commun.* **2013**, *49*, 5547. (b) Conway, A. J.; Gainsford, G. J.; Schrieke, R. R.; Smith, J. D. *J. Chem. Soc., Dalton Trans.* **1975**, 2499. (c) McDade, C.; Gibson, V. C.; Santarsiero, B. D.; Bercaw, J. E. *Organometallics* **1988**, *7*, 1. (d) Baibich, I. M.; Parlier, A.; Rudler, H. *J. Mol. Catal.* **1988**, *53*, 193.

(229) Kubo, K.; Nakazawa, H.; Nakahara, S.; Yoshino, K.; Mizuta, T.; Miyoshi, K. *Organometallics* **2000**, *19*, 4932.

(230) (a) Colacot, T. J.; Teichman, R. A.; Cea-Olivares, R.; Alvarado-Rodríguez, J.-G.; Toscano, R. A.; Boyko, W. J. *J. Organomet. Chem.* **1998**, *557*, 169. (b) Grice, K. A.; Kaminsky, W.; Goldberg, K. I. *Inorg. Chim. Acta* **2011**, *369*, 76. (c) Romeo, R.; Scolaro, L. M.; Plutino, M. R.; Romeo, A.; Nicolo', F.; Zotto, A. D. *Eur. J. Inorg. Chem.* **2002**, 629. (d) Jamali, S.; Nabavizadeh, S. M.; Rashidi, M. *Inorg. Chem.* **2008**, *47*, 5441. (e) Rashidi, M.; Nabavizadeh, S. M.; Zare, A.; Jamali, S.; Puddephatt, R. J. *Inorg. Chem.* **2010**, *49*, 8435.

(231) (a) Muller, P.; Huck, S.; Koppel, H.; Pritzkow, H.; Siebert, W. *Z. Naturforsch.* **1995**, *B50*, 1476. (b) Hoefelmeyer, J. D.; Gabbaï, F. *Organometallics* **2002**, *21*, 982.

(232) Pregosin, P. S. Chapter 7 - Coupling Constants. In *NMR in Organometallic Chemistry*, Wiley-VCH: Weinheim, 2012; p. 207.

(233) Bauer, J.; Braunschweig, H.; Dewhurst, R. D.; Radacki, K. *Chem. -Eur. J.* **2013**, *19*, 8797.

(234) (a) Crumpton-Bregel, D. M.; Goldberg, K. I. *J. Am. Chem. Soc.* **2003**, *125*, 9442. (b) Bayler, A.; Canty, A. J.; Edwards, P. G.; Skelton, B. W.; White, A. H. *J. Chem. Soc., Dalton Trans.* **2000**, 3325. (c) Still, B. M.; Kumar, P. G. A.; Aldrich-Wright, J. R.; Price, W. S. *Chem. Soc. Rev.* **2007**, *36*, 665.

(235) Kays, D. L.; Aldridge, S. Transition Metal Boryl Complexes. In *Structure & Bonding*; Mingos, D. M. P.; Marder, T. B.; Lin, Z., Eds.; Springer-Verlag: Berlin, Heidelberg, 2008; p. 29.

(236) (a) Laidler, K. J. *Chemical Kinetics*, 3rd ed.; Harper & Row: New York, 1987. Doherty, S.; Newman, C. R.; Rath, R. K.; van den Berg, J.-A.; Hardacre, C.; Nieuwenhuyzen, M.; Knight, J. G. *Organometallics* **2004**, *23*, 1055. (b) Leigh, W. J.; Arnold, D. R. *Can. J. Chem.* **1981**, *59*, 609.

(237) (a) Jordan, R. B. *Reaction Mechanisms of Inorganic and Organometallic Systems*, 3rd ed.; Oxford University Press: New York, 2007. (b) Crabtree, R. H. *The Organometallic Chemistry of the Transition Metals*, 5 ed.; John Wiley & Sons: Hoboken, New Jersey, 2009.

(238) (a) Vicente, J.; Arcas, A.; Fernández-Hernández, J. M.; Aullón, G.; Bautista, D. *Organometallics* **2007**, *26*, 6155. (b) Vicente, J.; Arcas, A.; Gálvez-López, M.-D.; Jones, P. G. *Organometallics* **2006**, *25*, 4247.

(239) (a) Fujita, M.; Kim, W. H.; Sakanishi, Y.; Fujiwara, K.; Hirayama, S.; Okuyama, T.; Ohki, Y.; Tatsumi, K.; Yoshioka, Y. *J. Am. Chem. Soc.* **2004**, *126*, 7548. (b) Hinkle, R. J.; Stang, P. J.; Arif, A. M. *Organometallics* **1993**, *12*, 3510.

(240) Bandoli, G.; Dolmella, A. *Coord. Chem. Rev.* **2000**, *209*, 161.

(241) Bishop, J. J.; Davison, A.; Katcher, M. L.; Lichtenberg, D. W.; Merrill, R. E.; Smart, J. C. *J. Organomet. Chem.* **1971**, *27*, 241.

(242) Shafir, A.; Power, M. P.; Whitener, G. D.; Arnold, J. *Organometallics* **2000**, *19*, 3978.

(243) Butler, I. R.; Davies, R. L. *Synthesis* **1996**, 1350.

(244) Brown, H. C.; Racherla, U. S. *J. Org. Chem.* **1986**, *51*, 427.

(245) Eisch, J. J.; Kaska, W. C. *J. Am. Chem. Soc.* **1966**, *88*, 2976.

(246) Boudreau, J.; Courtemanche, M.-A.; Fontaine, F.-G. *Chem. Commun.* **2011**, *47*, 11131.

(247) Shatunov, V. V.; Korlyukov, A. A.; Lebedev, A. V.; Sheludyakov, V. D.; Kozyrkin, B. I.; Orlov, V. Y. *J. Organomet. Chem.* **2011**, *696*, 2238.

(248) Hierso, J.-C.; Evrard, D.; Lucas, D.; Richard, P.; Cattey, H.; Hanquet, B.; Meunier, P. *J. Organomet. Chem.* **2008**, *693*, 574.

(249) Ziebart, C.; Federsel, C.; Anbarasan, P.; Jackstell, R.; Baumann, W.; Spannenberg, A.; Beller, M. *J. Am. Chem. Soc.* **2012**, *134*, 20701.

(250) Lee, Y.; Mankad, N. P.; Peters, J. C. *Nature Chem.* **2010**, *2*, 558.

(251) Zank, J.; Schier, A.; Schmidbaur, H. *Dalton Trans.* **1999**, 415.

(252) Lee, Y.; Peters, J. C. *J. Am. Chem. Soc.* **2011**, *133*, 4438.

(253) Kim, Y.-E.; Kim, J.; Lee, Y. *Chem. Commun.* **2014**, *50*, 11458.

(254) Crociani, B.; Benetollo, F.; Bertani, R.; Bombieri, G.; Meneghetti, F.; Zanotto, L. *J. Organomet. Chem.* **2000**, *605*, 28.

(255) Kolpin, K. B.; Emslie, D. J. H. *Angew. Chem. Int. Ed.* **2010**, *49*, 2716.

(256) Cook, K. S.; Piers, W. E.; Rettig, S. J. *Organometallics* **1999**, *18*, 1575.

(257) Kim, Y.-E.; Oh, S.; Kim, S.; Kim, O.; Kim, J.; Han, S. W.; Lee, Y. *J. Am. Chem. Soc.* **2015**, *137*, 4280.

(258) Holland, P. L. *Dalton Trans.* **2010**, *39*, 5415.

(259) Majchrzak, M.; Kostera, S.; Kubicki, M.; Kownacki, I. *Dalton Trans.* **2013**, *42*, 15535.

(260) Comanescu, C. C.; Iluc, V. M. *Inorg. Chem.* **2014**, *53*, 8517.

(261) (a) Astruc, D. Metal Carbonyls and Complexes of Other Monohapto L Ligands. In *Organometallic Chemistry and Catalysis*, Springer: New York, 2007; p. 151. (b) Carlton, L.; Mokoena, L. V.; Fernandes, M. A. *Inorg. Chem.* **2008**, *47*, 8696. (c) Misumi, Y.; Seino, H.; Mizobe, Y. *J. Organomet. Chem.* **2006**, *691*, 3157. (d) Brennessel, W. W.; Ellis, J. E. *Angew. Chem. Int. Ed.* **2007**, *46*, 598. (e) Vincente, J.; Chicote, M. T.; Vincente-Hernández, I.; Bautista, D. *Inorg. Chem.* **2007**, *46*, 8939.

(262) Nakata, N.; Ikeda, T.; Ishii, A. *Inorg. Chem.* **2010**, *49*, 8112.

(263) Itazaki, M.; Nishihara, Y.; Osakada, K. *Organometallics* **2004**, *23*, 1610.

(264) Li, H.; Aquino, A. J. A.; Cordes, D. B.; Hung-Low, F.; Hase, W. L.; Krempner, C. *J. Am. Chem. Soc.* **2013**, *135*, 16066.

(265) Berenguer, J. R.; Bernechea, M.; Lalinde, E. *Organometallics* **2007**, *26*, 1161.

(266) Crabtree, R. H. Allyl Complexes. In *The Organometallic Chemistry of the Transition Metals*, Fifth ed.; John Wiley & Sons, Inc.: Hoboken, New Jersey, 2009; p. 128.

(267) El-Amouri, H.; Bahsoun, A. A.; Fischer, J.; Osborn, J. A.; Youinou, M.-T. *Organometallics* **1991**, 3582.

(268) McWhannell, M. A.; Rosair, G. M.; Welch, A. J.; Teixidor, F.; Viñas, C. *J. Organomet. Chem.* **1999**, *573*, 165.

(269) (a) Barranco, E. M.; Crespo, O.; Gimeno, M. C.; Laguna, A.; Jones, P. G.; Ahrens, B. *Inorg. Chem.* **2000**, *39*, 680. (b) Less, R. J.; Guan, B.; Muresan, N. M.; McPartlin, M.; Reisner, E.; Wilson, T. C.; Wright, D. S. *Dalton Trans.* **2012**, *41*, 5919. (c) Bayler, A.; Schier, A.; Bowmaker, G. A.; Schmidbaur, H. *J. Am. Chem. Soc.* **1996**, *118*, 7006. (d) Deák, A.; Megyes, T.; Tárkányi, G.; Király, P.; Biczók, L.; Pálinkás, G.; Stang, P. J. *J. Am. Chem. Soc.* **2006**, *128*, 12668.

(270) Schmidbaur, H. *Chem. Soc. Rev.* **1995**, 391.

(271) Inagaki, F.; Matsumoto, C.; Okada, Y.; Maruyama, N.; Mukai, C. *Angew. Chem. Int. Ed.* **2015**, *54*, 818.

(272) Kaufmann, L.; Breunig, J.-M.; Vitze, H.; Schödel, F.; Nowik, I.; Pichlmaier, M.; Bolte, M.; Lerner, H.-W.; Winter, R. F.; Herber, R. H.; Wagner, M. *Dalton Trans.* **2009**, 2940.

(273) Siewert, I.; Fitzpatrick, P.; Broomsgrove, A. E. J.; Kelly, M.; Vidovic, D.; Aldridge, S. *Dalton Trans.* **2011**, *40*, 10345.

(274) Appel, A.; Jäkle, F.; Priermeier, T.; Schmid, R.; Wagner, M. *Organometallics* **1996**, *15*, 1188.

(275) Scheibitz, M.; Bolte, M.; Bats, J. W.; Lerner, H.-W.; Nowik, I.; Herber, R. H.; Krapp, A.; Lein, M.; Holthausen, M. C.; Wagner, M. *Chem. -Eur. J.* **2005**, *11*, 584.

(276) Carpenter, B. E.; Piers, W. E.; Parvez, M.; Yap, G. P. A.; Rettig, S. J. *Can. J. Chem.* **2001**, *79*, 857.

(277) Cabeza, J. A.; Pruneda, V. *Dalton Trans.* **2012**, *41*, 7249.

(278) Ang, H.-G.; Ang, S.-G.; Du, S. *J. Organomet. Chem.* **1999**, *590*, 1.

(279) Batsanov, A. S.; Hérault, D.; Howard, J. A. K.; Patrick, L. G. F.; Probert, M. R.; Whiting, A. *Organometallics* **2007**, *26*, 2414.

(280) Aldridge, S.; Bresner, C. *Coord. Chem. Rev.* **2003**, *244*, 71.

(281) Jacobsen, H.; Berke, H.; Döring, S.; Kehr, G.; Erker, G.; Fröhlich, R.; Meyer, O. *Organometallics* **1999**, *18*, 1724.

(282) Shuttleworth, T. A.; Huertos, M. A.; Pernik, I.; Young, R. D.; Weller, A. S. *Dalton Trans.* **2013**, *42*, 12917.

(283) Westcott, S. A.; Blom, H. P.; Marder, T. B.; Baker, R. T.; Calabrese, J. C. *Inorg. Chem.* **1993**, *32*, 2175.

(284) Devillard, M.; Brousses, R.; Miqueu, K.; Bouhadir, G.; Bourissou, D. *Angew. Chem. Int. Ed.* **2015**, *54*, 5722.

(285) Hodgkins, T. G.; Powell, D. R. *Inorg. Chem.* **1996**, *35*, 2140.

(286) Biani, F. F. d.; Gmeinwieser, T.; Herdtweck, E.; Jäkle, F.; Laschi, F.; Wagner, M.; Zanello, P. *Organometallics* **1997**, *16*, 4776.

(287) Dureen, M. A.; Lough, A.; Gilbert, T. M.; Stephan, D. W. *Chem. Commun.* **2008**, 4303.

(288) (a) Amgoune, A.; Bouhadir, G.; Bourissou, D. *Top. Curr. Chem.* **2013**, *334*, 281. (b) Bouhadir, G.; Amgoune, A.; Bourissou, D. *Adv. Organomet. Chem.* **2010**, *58*, 1, and references therein.

(289) Golden, J. T.; Peterson, T. H.; Holland, P. L.; Bergman, R. G.; Andersen, R. A. *J. Am. Chem. Soc.* **1998**, *120*, 223.

(290) Hoyte, S. A.; Spencer, J. L. *Organometallics* **2011**, *30*, 5415.

(291) Michalak, A.; DeKock, R. L.; Ziegler, T. *J. Phys. Chem.* **2008**, *A112*, 7256.

(292) Sircoglou, M.; Mercy, M.; Saffon, N.; Coppel, Y.; Bouhadir, G.; Maron, L.; Bourissou, D. *Angew. Chem. Int. Ed.* **2009**, *48*, 3454.

(293) Gualco, P.; Lin, T.-P.; Sircoglou, M.; Mercy, M.; Ladeira, S.; Bouhadir, G.; Pérez, L. M.; Amgoune, A.; Maron, L.; Gabbaï, F. P.; Bourissou, D. *Angew. Chem. Int. Ed.* **2009**, *48*, 9892.

(294) Derrah, E. J.; Sircoglou, M.; Mercy, M.; Ladeira, S.; Bouhadir, G.; Miqueu, K.; Maron, L.; Bourissou, D. *Organometallics* **2011**, *30*, 657.

(295) Jones, J. S.; Wade, C. R.; Gabbaï, F. P. *Angew. Chem. Int. Ed.* **2014**, *53*, 8876.

(296) Ke, I.-S.; Jones, J. S.; Gabbaï, F. P. *Angew. Chem. Int. Ed.* **2014**, *53*, 2633.

(297) Wade, C. R.; Gabbaï, F. P. *Angew. Chem. Int. Ed.* **2011**, *50*, 7369.

(298) Ke, I.-S.; Gabbaï, F. P. *Inorg. Chem.* **2013**, *52*, 7145.

(299) Lin, T.-P.; Ke, I.-S.; Gabbaï, F. P. *Angew. Chem. Int. Ed.* **2012**, *51*, 4985.

(300) Tschersich, C.; Limberg, C.; Roggan, S.; Herwig, C.; Ernsting, N.; Kovalenko, S.; Mebs, S. *Angew. Chem. Int. Ed.* **2012**, *51*, 4989.

(301) (a) Bennett, M. A.; Contel, M.; Hockless, D. C. R.; Welling, L. L.; Willis, A. C. *Inorg. Chem.* **2002**, *41*, 844. (b) Bennett, M. A.; Contel, M.; Hockless, D. C. R.; Welling, L. L. *Chem. Commun.* **1998**, 2401.

(302) López-de-Luzuriaga, J. M.; Monge, M.; Olmos, M. E.; Pascual, D. *Inorg. Chem.* **2014**, *53*, 1275.

(303) Hupf, E.; Lork, E.; Mebs, S.; Beckmann, J. *Inorg. Chem.* **2015**, *54*, 1847.

(304) Burger, B. J.; Bercaw, J. E. Vacuum Line Techniques for Handling Air-Sensitive Organometallic Compounds. In *Experimental Organometallic Chemistry - A Practicum in Synthesis and Characterization*, American Chemical Society: Washington D.C., 1987; Vol. 357, p. 79.

(305) Yamashita, M.; Vicario, J. V. C.; Hartwig, J. F. *J. Am. Chem. Soc.* **2003**, *125*, 16347.

(306) Tollefson, M. B.; Li, J. J.; Beak, P. *J. Am. Chem. Soc.* **1996**, *118*, 9052.

(307) Plotkin, J. S.; Shore, S. G. *Inorg. Chem.* **1981**, *20*, 284.

(308) Eisch, J. J.; King, R. B. Organometallic Syntheses. In *Nontransition metal-compounds*; Eisch, J. J., Ed.; Academic Press: New York, 1981; Vol. 2, p. 121.

(309) Punji, B.; Mague, J. T.; Balakrishna, M. S. *Inorg. Chem.* **2007**, *46*, 10268.

(310) Crascall, L. E.; Spencer, J. L. *Inorg. Synth.* **1990**, *28*, 126.

(311) Costa, E.; Pringle, P. G.; Ravetz, M. *Inorg. Synth.* **1997**, *31*, 284.

(312) McDermott, J. X.; White, J. F.; Whitesides, G. M. *J. Am. Chem. Soc.* **1976**, *98*, 6521.

(313) Pohlmann, J. L. W.; Brinckmann, F. E. *Z. Naturforsch.* **1965**, *B20*, 5.

(314) Rudie, A. W.; Lichtenberg, D. W.; Katcher, M. L.; Davison, A. *Inorg. Chem.* **1978**, *17*, 2859.

(315) Tyburn, J.-M., Bruker Variable Temperature Unit User Manual. In Wissembourg, France, 1998; Vol. 1, p. 35.

(316) Sluis, P. V. D.; Spek, A. L. *Acta Crystallogr.* **1990**, *A46*, 194.

(317) Morse, P. M.; Spencer, M. D.; Wilson, S. R.; Girolami, G. S. *Organometallics* **1994**, *13*, 1646.

(318) (a) ADF2010, SCM, Theoretical Chemistry, Vrije Universiteit, Amsterdam, The Netherlands, http://www.scm.com. (b) te Velde, G.; Bickelhaupt, F. M.; van Gisbergen, S. J. A.; Fonseca Guerra, C.; Baerends, E. J.; Snijders, J. G.; Ziegler, T. *J. Comput. Chem.* **2001**, *22*, 931. (c) Fonseca Guerra, C.; Snijders, J. G.; te Velde, G.; Baerends, E. J. *Theor. Chem. Acc.* **1998**, *99*, 391.

(319) (a) van Lenthe, E.; Baerends, E. J.; Snijders, J. G. *J. Chem. Phys.* **1993**, *99*, 4597. (b) van Lenthe, E.; Baerends, E. J.; Snijders, J. G. *J. Chem. Phys.* **1994**, *101*, 9783. (c) van Lenthe, E.; Ehlers, A.; Baerends, E. J. *J. Chem. Phys.* **1999**, *110*, 8943. (d) van Lenthe, E.; Leeuwen, R. v.; Baerends, E. J.; Snijders, J. G. *Int. J. Quantum Chem.* **1996**, *57*, 281. (e) van Lenthe, E.; Snijders, J. G.; Baerends, E. J. *J. Chem. Phys.* **1996**, *105*, 6505.

(320) Perdew, J. P.; Burke, K.; Ernzerhof, M. *Phys. Rev. Lett.* **1996**, *77*, 3865.

(321) (a) Grimme, S.; Anthony, J.; Ehrlich, S.; Krieg, H. *J. Chem. Phys.* **2010**, *132*, 154104. (b) Grimme, S.; Ehrlich, S.; Goerigk, L. *J. Comput. Chem.* **2011**, *32*, 1457.

(322) (a) Bridgeman, A. J.; Cavigliasso, G.; Ireland, L. R.; Rothery, J. *J. Chem. Soc., Dalton Trans.* **2001**, 2095. (b) Mayer, I. *Chem. Phys. Lett.* **1983**, *97*, 270. (c) Mayer, I. *Int. J. Quantum Chem.* **1986**, *29*, 73. (d) Sannigrahi, A. B.; Kar, T. *Chem. Phys. Lett.* **1990**, *173*, 569.

(323) Gopinathan, M. S.; Jug, K. *Theor. Chim. Acta* **1983**, *63*, 497.

(324) (a) Mrozek, J.; Nalewajski, R. F.; Michalak, A. *Pol. J. Chem.* **1998**, *72*, 1779. (b) Nalewajski, R. F.; Mrozek, J.; Michalak, A. *Int. J. Quantum Chem.* **1997**, *61*, 589. (c) Nalewajski, R. F.; Mrozek, J.; Mazur, G. *Can. J. Chem.* **1996**, *74*, 1121. (d) Nalewajski, R. F.; Mrozek, J. *Int. J. Quantum Chem.* **1994**, *51*, 187.

(325) NBO 6.0. Glendening, E. D.; Badenhoop, J. K.; Reed, A. E.; Carpenter, J. E.; Bohmann, J. A.; Morales, C. M.; Landis, C. R.; Weinhold, F. Theoretical Chemistry Institute, University of Wisconsin: Madison, 2013.

(326) (a) Bickelhaupt, F. M.; Baerends, E. J. In *Reviews in Computational Chemistry*; Lipkowitz, K. B.; Boyd, D. B., Eds.; Wiley -VCH: New York, 2000; Vol. 15, p. 1. (b) Ziegler, T.; Rauk, A. *Inorg. Chem.* **1979**, *18*, 1755. (c) Ziegler, T.; Rauk, A. *Inorg. Chem.* **1979**, *18*, 1558.

Appendix 1

For complete crystallographic data tables, atomic coordinates, anisotropic displacement parameters and metrical data, see the .docx files and cifs in the attached flash drive. Also included are the published and accepted works arising from this thesis.